Design Considerations For An Electron Energy Loss Spectroscopy Parallel Recording System.

by Colin P Scott

submitted for the degree of Doctor of Philosophy in the University of Glasgow.

May 1988

". . . . . get the shooters out, George . . . ."

Jack Regan

"The Sweeney"

ITV circa 1976.

Declaration

This thesis is a report of work which I have undertaken in the Department of Physics and Astronomy at the University of Glasgow. The work described is my own, apart from the design and construction of the digital timing / interface circuits, the analogue - digital conversion unit, and the construction of the RL128S preamplifier board, all of which were carried out by Mr R. Pallister. Some of the results contained in this thesis are published in the following papers:

"The Influence of Magnetic Sector Aberrations in the Design of Parallel Recording Systems for EELS", A J Craven and C P Scott (1986), in Proc. XIth ICEM (eds. T Imura, S Maruse and T Suzuki, Japanese Society of Electron Microscopy), p 517

"Electron Detection in the Analytical Electron Microscope", J N Chapman, A J Craven and C P Scott (1988), Ultramicroscopy (to be published).

"A Quadrupole Lens System for use in a Parallel Recording System for Electron Energy Loss Spectroscopy", C P Scott and A J Craven (1988), Ultramicroscopy (to be published).

"The Design of A Parallel Recording System For EELS", C P Scott and A J Craven (1988) submitted to EUREM, York.

This thesis has not been submitted in any previous application for a degree.

Contents

Acknowledgements

This work would not have been possible without the help and assistance of a large number of people. I would especially like to thank my supervisor Dr A J Craven for his invaluable guidance and encouragement throughout the project, and Professor R P Ferrier for provision of research facilities within the Solid State Physics Group. Thanks also to Dr A M McLeod for the use of computing facilities and Dr S Beaumont for his original Monte Carlo program. I am grateful to Miss M Cluckie for provision of the vanadium carbide spectrum shown in chapter 1, and also to Dr M Drummond for the use of his beam blank unit and endless supply of life stories.

In any instrumentation project technicians play a vital part; - I am indebted to Mr R Pallister for designing, building and maintaining most of the digital electronics used in the detector, Mr K Piechowsiak for polishing the YAG crystals, and Mr D Blackwell and Mr J Richardson for their help in the mechanical workshop. Thanks also to Mr J Sims for maintaining the TEM, and Miss M Low and Mr I McVicar for photographic aid.

I am grateful to Mullard PLC for the supply of fibre optic faceplates and to Collimated Holes Inc. for the terbium scintillator plate. Finally, I would like to thank the Science and Engineering Research Council and VG Scientific Ltd for the provision of a CASE award.

Summary

This thesis describes the results of an investigation into the design of a parallel recording system for electron energy loss spectroscopy (EELS). The motivation behind the construction of such a system is the greatly enhanced detection efficiency which can be achieved, as compared to conventional serial recording systems. This is of great benefit in experimental situations where specimen drift, radiation damage, or signal to noise ratio are limiting factors.

Chapter 1 provides a brief introduction to the method of EELS analysis in the transmission electron microscope (TEM) and discusses the instrumentation required to generate and record EELS spectra. Chapter 2 contains a detailed review of the theory of homogeneous field magnetic sector spectrometers, following the work of Enge, Brown, and Heighway. The matrix method used to calculate the optical properties of such spectrometers is introduced, and the focussing coefficients for an arbitrary magnetic sector are derived to second order. A spectrometer analysis program based on the theory of chapter 2 is described in chapter 3. The program is used to calculate the aberration coefficients of two well known 2nd order corrected spectrometer designs [Shuman 1983, Scheinfein and Isaacson 1984] and hence determine the nature of the electron intensity distribution at their dispersion planes.

Post-spectrometer magnification of the dispersion plane is required in parallel EELS in order to overcome the resolution limiting effects of electron scatter within the detector. The requirement that the magnifications in the dispersive and non-dispersive planes be independent indicates the use of quadrupole lenses as the magnifying elements. Chapter 4 reviews the theory of quadrupoles and extends the matrix transfer method of chapters 2 and 3 to quadrupole lenses. The design of a four lens quadrupole system suitable for post-spectrometer magnification in EELS is described in chapter 5. The system can vary the magnification in the dispersive direction from 5x to 97x (at 100 keV), while maintaining an almost constant magnification in the non-dispersive direction.

Chapter 6 considers the types of multielement detectors which could be applied to parallel EELS, and discusses the advantages of using wide aperture linear photodiode arrays operating in the indirect mode as detection elements. The design and construction of the instrumentation required to operate two such arrays, manufactured by Reticon and Hamamatsu, is also reported in this chapter. Experiments on the electrical and optical performance of both these arrays are described in chapter 7. The results of these experiments

indicate that the Hamamatsu device is the more suitable for detection of EELS spectra. Chapter 8 contains experimental results on the evaluation of various scintillator screens laid on fibre-optic plates directly coupled to the fibre-optic input window of the Hamamatsu array. The most suitable of the scintillators tested was a screen made from a single crystal of yttrium aluminium garnet (YAG) polished down to a thickness of 30μm. The detective quantum efficiency of a prototype detector consisting of the Hamamatsu photodiode array fibre-optically coupled to such a screen is shown to be greater than 0.25 for a range of input electron doses varying from 40 electrons / channel-second to greater than 10^8 electrons / channel-second.

Finally, chapter 9 discusses the implications of the results obtained in this work and considers improvments that could be made to the prototype detector to form an operational system.

CHAPTER 1

Electron Energy Loss Spectroscopy and Parallel Detection

Introduction

Electron energy loss spectroscopy (EELS) is a powerful technique for gaining chemical and structural information from the thin solid specimens used in transmission electron microscopy (TEM). The general method of EELS is quite simple - a beam of monoenergetic electrons is incident upon a thin sample, some of the electrons lose energy in traversing the specimen and the resultant energy loss distribution (spectrum) is obtained by passing the transmitted electrons through a momentum analysing device (spectrometer). The energy loss spectrum is characteristic of the area being irradiated and so the elemental composition of the specimen can be identified. This chapter gives a brief discussion of the physical principles of electron energy loss spectroscopy and outlines the information that can be obtained from an EELS spectrum by quantitative analysis. Further, the necessary instrumentation for generating and recording the spectrum is described along with factors which affect the performance of an EELS system. The advantages of recording the spectrum in parallel as opposed to the more usual serial recording technique are considered, and the difficulties to be overcome in designing a successful parallel recording system are discussed.

1.1 ELECTRON SCATTERING WITHIN A SOLID

When a fast electron beam enters a specimen, which is thin enough so that most of the beam is not absorbed, the transmitted electrons can be classified into three main groups:- electrons that pass straight through the specimen without collision, electrons that undergo elastic scattering and electrons that are inelastically scattered. The first group of undeviated electrons can give information only upon the scattering power (and hence thickness) of the specimen and contains no other useful information, whereas the second two classes are of much more interest from an analytical point of view.

1.1.1 Elastic scattering

Elastic scattering occurs when an incident electron is deflected by the internal electrostatic field of an atom i.e. the nuclear field modified by the screening effect of the surrounding electrons. The mass of the nucleus is very much greater than that of the electron and consequently the latter loses a negligible amount of energy in the collision. Isaacson [1978]

gives an approximate expression for the angular distribution of electrons elastically scattered through small angles from free atoms :

$$\frac{I_{EL}(\theta)}{I_{EL}(0)} = \frac{1}{(\theta^2 + \theta_0^2)^2}$$

where - $I_{EL}(0)$ is the intensity of electrons which are undeviated in scattering
$I_{EL}(\theta)$ is the intensity of electrons elastically scattered through angle θ
θ_0 is the characteristic screening angle = $\lambda/2\pi a$

λ is the incident electron wavelength, a is the characteristic atomic radius given by:

$$a = 0.9\, a_0 Z^{-1/4}$$

where a_0 is the Bohr radius of the atom and Z is the atomic number. For 100keV incident electrons a typical scattering angle of ~ 20 mrads per elastic collision is quoted by Egerton [1982]. If the specimen is crystalline, the angular distribution is peaked at angles satisfying the Bragg condition, $\theta=\lambda d$ where d is the lattice spacing. Elastic scattering is represented in the energy loss spectrum by a sharp peak at zero energy loss (Figure 1.1).

1.1.2 Inelastic scattering

Inelastic scattering occurs when an electron interacts directly with one or more atomic electrons, and since the masses are comparable appreciable energy transfer can occur. If the scattering takes place from valence electrons the energy transfer is typically 10-100eV per collision. Valence electron scattering is observed in the energy loss spectrum in the form of one or more peaks in the 10-100eV range as illustrated in figure 1.1. The probability for valence electron scattering is comparable to that for elastic scattering, but there is also a smaller probability that the incident electron may be scattered by an inner shell electron. The inner shell electron can make a transition to the vacuum continuum or to a vacant energy level only if the energy transferred exceeds the ionisation energy of that particular shell. Such events are characterised in the energy loss spectrum by a sharp rise in intensity at an energy loss equal to the inner shell ionisation energy (Figure 1.1). These sharp rises in the spectrum are referred to as ionisation edges, and the energy at which the edge occurs is dependent upon the type of shell (K,L,etc.) and the atomic number of the atom involved. The energy values are well known for every element and are not greatly affected by the chemical environment of the atom. Detection of the ionisation edges in an energy loss

Figure 1.1 EELS Spectrum of Vanadium Carbide

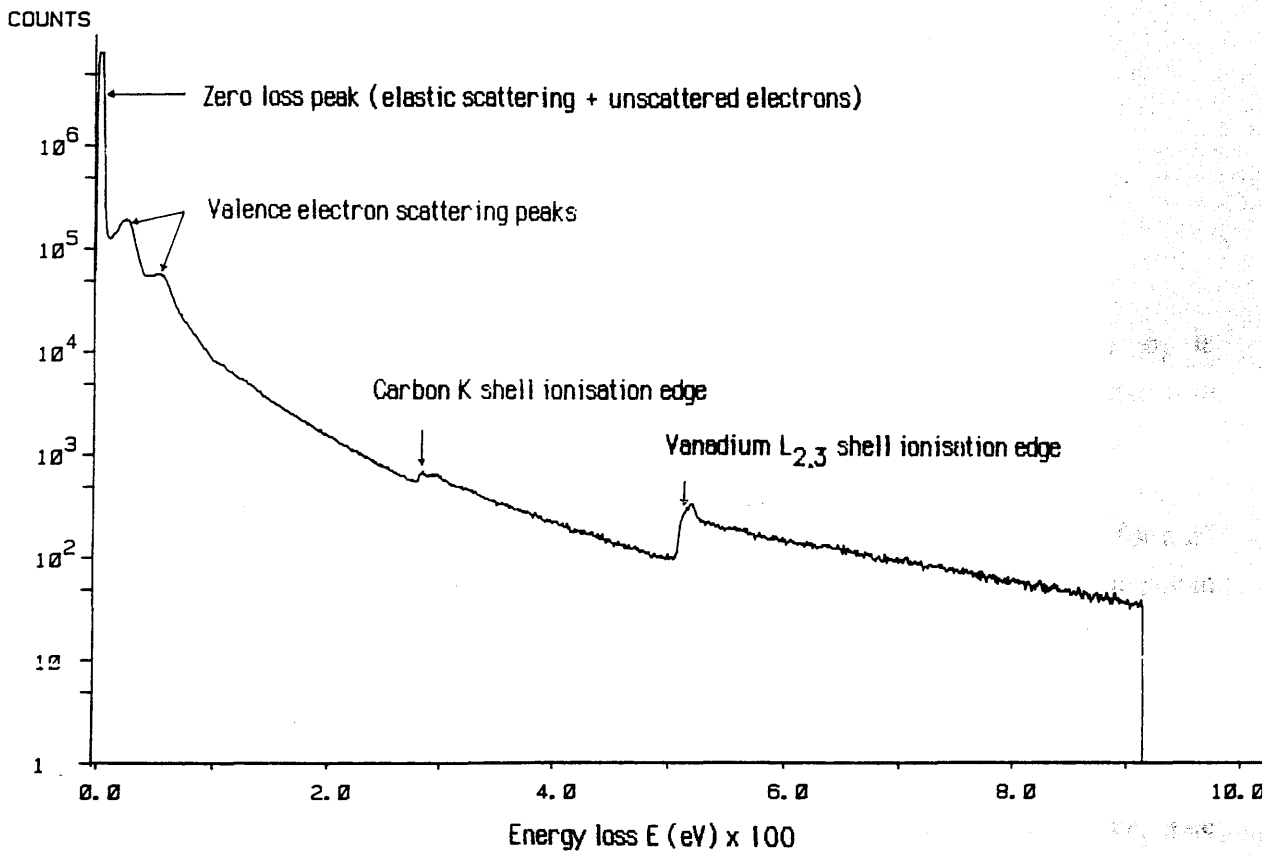

spectrum enables the constituent elements to be identified.

The angle of inelastic scattering is, in general, less than that for elastic scattering and depends upon the energy lost by the incident electron. Isaacson [1978] gives an approximate expression for the angular distribution which is valid for small scattering angles:

$$\frac{I_{IN}(\theta)}{I_{IN}(0)} = \frac{1}{(\theta^2 + \theta_E^2)}$$

where $I_{IN}(0)$ is the intensity of electrons inelastically scattered but undeviated
$I_{IN}(\theta)$ is the intensity of electrons inelastically scattered through angle θ
and $\theta_E = E/pv$.

where E is the energy lost by the incident electron of velocity v and momentum p. θ_E is related to the minimum momentum which must be transferred by an incident electron in losing an amount of energy E through the expression:

$$p_{min} = p\,\theta_E$$

For incident electrons of 100keV energy Isaacson [1978] gives $\theta_E = 0.137$ mrad for a 25 eV loss and 1.37 mrad for a 250 eV energy loss. Thus electrons which lose more energy in the collision are scattered through larger angles.

1.1.3 Quantitative analysis of EELS spectra

The information present in an energy loss spectra is sufficient to provide absolute (standardless) quantitation of the elemental constitution of the sampled area. The concentration N of a measured element, in atoms per unit area of the specimen is given by Egerton [1982] as:

$$N \sim \frac{1}{G\,\sigma_i(\alpha,\Delta)} \left[\frac{I_i(\alpha,\Delta)}{I_l(\alpha,\Delta)} \right]$$

where α is the maximum angle of scattering accepted by the spectrometer, Δ is an energy range of integration within the spectrum (Figure 1.2), and G is a gain change factor between the low loss and high loss regions of the spectrum. The parameter $\sigma_i(\alpha,\Delta)$ is an ionisation partial cross-section for the edge in question (K or L) which can be calculated knowing the experimental conditions. $I_l(\alpha,\Delta)$ is the integrated energy loss intensity over an energy range

Figure 1.2 Quantitative Analysis of EELS Spectrum

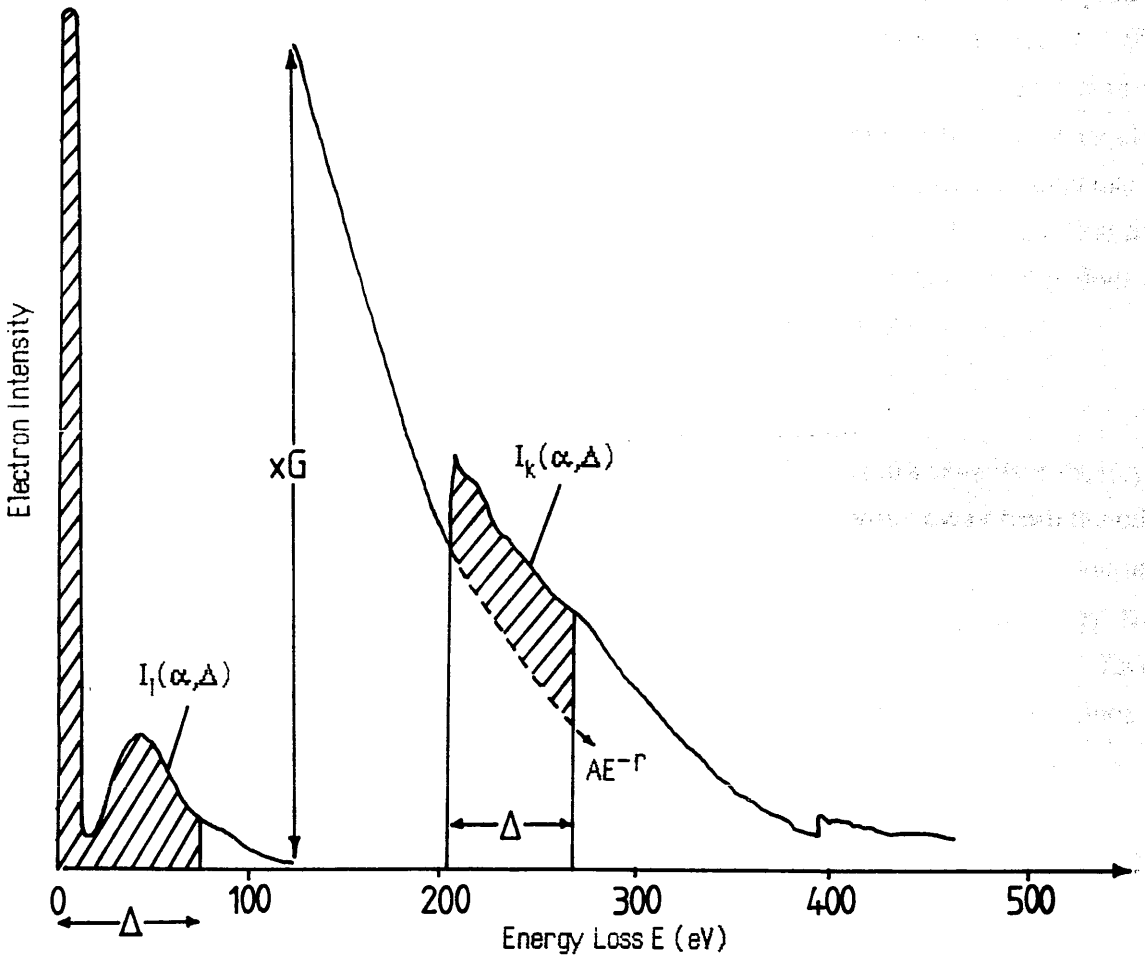

Δ, starting at the zero loss peak. $I_i(\alpha,\Delta)$ is the integrated intensity under the ionisation edge over the same range Δ, after subtraction of the background intensity (Figure 1.2). For the simple case of thin specimens, where there is no multiple scattering, the background under an isolated ionisation edge can be modelled by a power law decay function AE^{-r} where E is the energy loss, and A and r are constants which can be calculated by sampling the background prior to the edge. This type of analysis depends crucially on achieving a good pre-edge fit, which means that detection noise and artefacts must be kept to a minimum. Moreover, the problem is exacerbated if the sample is thicker than the mean free path for valence electron scattering (~100 nm for 100keV electrons) as multiple valence scattering causes the background shape to deviate from the AE^{-r} form, as well as reducing the ionisation edge height. Another difficulty occurs if two ionisation edges lie very close together, in which case background subtraction becomes more complicated because the second pre-edge region is perturbed by the post edge region of the first. Thus the first edge can be fitted with a normal background, but the background of the following edge does not follow a simple power law decay as discussed by Chapman et al. [1985].

1.1.4 Other information present in EELS spectra

A detailed inspection of the ionisation edges present in EELS spectra reveals a variety of structures close to the edge and as far as several hundred electron volts away from the edge. Figure 1.3 shows that the fine structure near the edge (energy loss near edge structure - ELNES) has peaks seperated by 1eV or less whereas the oscillatory structure away from the edge (extended energy loss fine structure - EXELFS) varies on a 3 -30 eV level. The ELNES contains information about the local chemical bonding in the specimen, since the peaks correspond (approximately) to the excitation of an inner shell electron to a bound excited state rather than the continuum, and the energy levels of the bound states are influenced by the chemical bonding present. The extended oscillatory structure away from the edge occurs when an inner shell electron is ejected from an atom with some kinetic energy such that it experiences elastic collisions with neighbouring atoms, and inelastic collisions with their electrons. Thus the EXELFS structure gives information about the short range order around the excited atom.

The book by Egerton [1986] provides a useful introduction to the theory of ELNES and EXELFS

1.2 INSTRUMENTAL CONSIDERATIONS

In any EELS experiment the characteristics of the incident electron probe are of great importance since they influence the information content of the recorded spectrum. Generally

Figure 1.3 Schematic Energy Loss Spectrum Around An Ionisation Edge

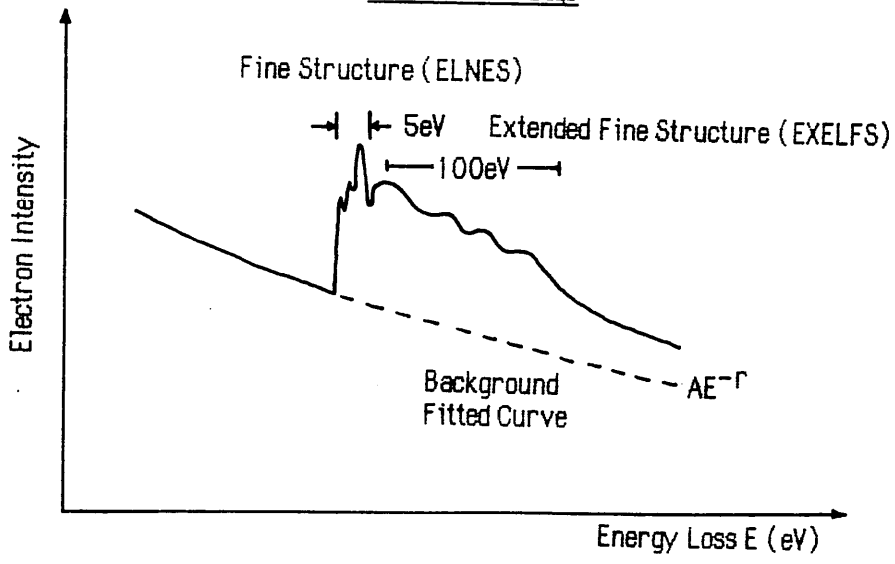

Figure 1.4 General First Order Spectrometer

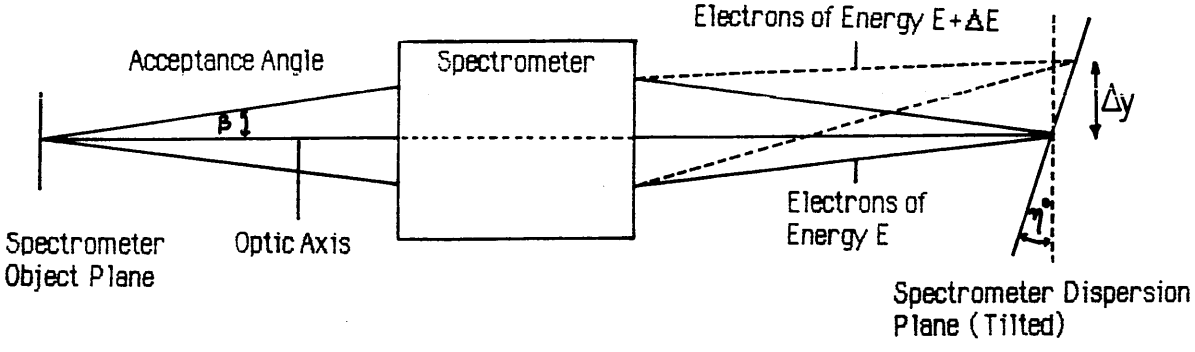

Figure 1.5 Spectrometer Energy Resolution

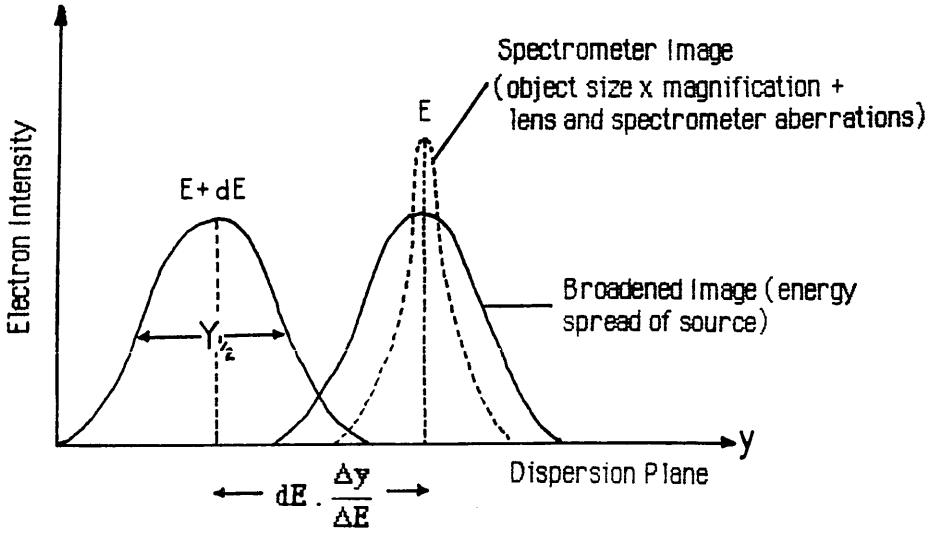

speaking probe conditions must be optimised in order to obtain the best results. An important parameter is the probe accelerating voltage - as mentioned before if the specimen is thicker than the mean free path for valence electron scattering the signal to background ratio decreases due to multiple scattering events. For this reason EELS analysis is usually done at the highest accelerating voltage possible, ~100keV for most microscopes. Higher accelerating voltages are now becoming available on new machines (200-400keV) allowing thicker samples to be analysed. This is especially useful for EELS analysis of biological specimens, where preparing sufficiently thin specimens is often difficult.

Other important considerations are factors such as the probe diameter and convergence angle which influence the spatial resolution and angular distribution of the scattered electrons respectively. High spatial resolution EELS requires the smallest possible probe diameter at the specimen. However, obtaining a small probe size generally requires the use of large convergence angles which increase the angular distribution of the scattered electrons. Thus, in general, for a fixed spectrometer collection angle the collection efficiency falls as the spatial resolution is increased.

The amount of time required to collect enough electrons to obtain a good signal to noise ratio in an EELS experiment is directly proportional to the probe current. Minimising the collection time is important in high spatial resolution EELS where specimen drift can be a problem. The maximum probe current which can be used may be limited by the gun brightness, or the appearance of secondary effects such as specimen contamination or even specimen damage. As regards the energy resolution of the recorded spectrum the fundamental limit is the inherent energy spread in the electron probe - this is discussed in the next section.

1.2.1 The electron source

The energy spread in the electron beam is dependent upon the type of electron gun used in the microscope and also on the operating conditions, such as the amount of current drawn from the filament. For microscopes using standard directly heated tungsten filament guns this is ~ 1-2eV, lanthanum hexaboride (LaB_6) filaments have a spread of ~1eV, whilst cold field emission guns have a spread of ~ 0.25 eV. Of course these figures are dependent upon the stability of the microscope accelerating voltage supply. It is clear that unless some form of monochromator is placed between the gun and the specimen the 1 eV or better resolution required for ELNES studies suggests the use of a cold field emission gun. This is the type of electron source used in the Vacuum Generators HB5 analytical scanning transmission

electron microscope (STEM) used for EELS experiments at Glasgow. Field emission guns have the further advantage that they produce the highest brightness of any of the three emitters i.e. a field emission gun can produce the highest current densities at the specimen. Field emission guns also produce the smallest apparent source size, e.g. the 100keV field emission gun in the HB5 has ~5nm diameter apparent source diameter compared with ~25μm for a typical conventional tungsten filament. This places great demands upon the mechanical and electrical stability of the gun because the effect of spatial fluctuations cannot be reduced by using a strongly demagnifying illumination system as in standard microscopes. Probe diameters of <1nm at the specimen are possible with this machine, allowing EELS analysis to be done at very high spatial resolution. The main disadvantage of using field emission guns is the very high vacuum required ($<1x10^{-10}$ torr at the gun) to prevent positively charged contaminants from being accelerated into the tip and ultimately destroying it. This means that microscopes using this kind of illumination system must have their gun sections built to UHV standard which is very expensive. A bonus point is that the ultra clean vacuum system tends to reduce the amount of contamination occuring at the specimen. The article by Le Poole [1983] gives a good introduction to electron sources in the electron microscope.

1.2.2 The spectrometer

The spectrometer is a device which accepts a given angular distribution β of electrons scattered by a point on the specimen, and produces a first order (at least) image of this point at some dispersion plane, with chromatic aberration producing an image shift Δy for an energy difference ΔE (Figure 1.4). In general the dispersion plane is tilted by other aberrations to some angle η to the optic axis. Depending upon the design of the spectrometer, the first order focus achieved may be single (point source is imaged to a line) or double (point source is imaged to a point). The ratio Δy/ΔE is known as the dispersion and is generally of the order of 1-5μm/eV for simple spectrometers. It is possible to obtain larger values of the dispersion by using electrostatic lenses to decelerate the electron beam before the spectrometer entrance, but this is not often done due to the difficulty of shielding the required high voltages. The energy resolution of the spectrometer is determined by the ratio of the dispersion to the full width at half maximum ($Y_{1/2}$) of the image of the probe formed at the dispersion plane (Figure 1.5). $Y_{1/2}$ is determined by the combined effects of:

1) The object size (probe diameter) at the specimen multiplied by the magnification of the spectrometer and any intervening post specimen lenses.

2) Broadening of the image caused by the inherent energy spread of the incident electron

probe.

3) Contributions from any aberrations present in the spectrometer and intervening lenses.

In the case of microanalysis in the electron microscope the probe diameter can be considered to be negligible (~ 1nm for VG HB5) and it can be assumed that the spectrometer images a point source, thus only 2) and 3) above need give concern. The broadening caused by 2) is just the dispersion multiplied by the energy spread of the probe and is a fundamental resolution limit for any spectrometer. The contribution of 3) is generally more significant and is discussed in the next section.

1.2.3 Spectrometer aberrations and collection efficiency.

Most spectrometers in use are non-cylindrically symmetric devices and therefore contain aberrations of all orders. Assuming a first order focus has been achieved then the dominant aberrations will be of second order. Using the point source assumption the most important resolution limiting aberrations are proportional to β^2 (assuming a circular entrance aperture), since aberration terms proportional to off-axis distance are negligible (see Chapter 2). This means that high angular collection efficiency and high energy resolution are generally incompatible.

The situation is modified in the case of microscopes where the specimen is immersed in the objective lens field. In this case the portion of field after the specimen can be considered to act as a separate lens which supplies some favourable degree of angular compression to the scattered electrons. Of course it is not possible to vary the strength of this 'post-field lens' without changing the focus of the 'pre-field' or probe forming lens. Some degree of freedom is possible if, as in the HB5, the height of the specimen in the lens can be varied using a z lift stage. In this manner the lens strength can be varied and the probe refocussed by changing the position of the specimen, allowing some control over the post-field compression and hence the angular distribution of the scattered electrons. Naturally, changing the lens excitation moves image position, hence defocussing the object for the spectrometer and reducing the energy resolution, so that this method of varying the angular distribution of the scattered electrons has very limited use.

In order to improve the collection efficiency without sacrificing energy resolution it is often possible to provide some limited form of second order aberration correction to the

spectrometer thus allowing larger collection angles to be used. Another solution to the same problem is to interpose one or more post specimen lenses (PSLs) between the specimen and the spectrometer. This technique has been developed by Buggy and Craven [1981] on the Glasgow HB5 where there are three post-specimen lenses between the objective lens and the spectrometer. By varying the strength of these lenses a large angular distribution from the specimen can be compressed to match a smaller spectrometer collection angle (Figure 1.6). Further, the effective object position for the spectrometer is controlled by the strength of the lenses, and the effective source size is determined by the spherical and chromatic aberrations of the post specimen lenses (assuming the combined magnification is small). If these lens aberrations are too large the performance of the spectrometer will suffer, as the effective source size may become large enough so that the uncorrected axial aberrations of the spectrometer become dominant. The combination of a large angular acceptance second order corrected spectrometer along with two post specimen lenses seems to provide an optimum solution to the problem of obtaining good collection efficiency along with high energy resolution in EELS experiments.

1.2.4 Recording the energy loss spectrum

The spectrometer forms an energy loss spectrum at a dispersion plane some distance from its exit face. This dispersion plane will in general be oriented at some angle η to the optic axis, as shown in figure 1.4. Physically, the spectrum is a distribution of electron intensity vs distance (α energy) which varies on a scale of $\sim 10^9$ electrons/sec at the zero loss peak down to ~10 electrons/sec at the far energy loss end (Figure 1.1). This means that any detection system must be capable of recording signals with a dynamic range $\sim 10^8$.

The most common method of recording the spectrum is to scan the spectrometer exit beam across a slit placed at the dispersion plane, behind the slit lies the electron detector - generally a block of scintillator placed in front of a photomultiplier tube (Figure 1.7). This technique is known as serial collection and is the method currently used at Glasgow. It has the advantages of simplicity, low detector noise, sensitivity independent of energy loss (since each data channel is sampled by the same detector), and large dynamic range.

There are two methods of scanning the electron beam across the slits. Scanning can be done either using scan coils after the spectrometer or, in the case of a magnetic sector, by changing the excitation of the magnet itself. The former technique is used at Glasgow, with the advantage that scanning is fast and hysteresis free. Unfortunately the tilted dispersion plane of the Glasgow spectrometer (Figure 1.4) means that the spectrum becomes

Figure 1.6 Post Specimen Optics In The HB5

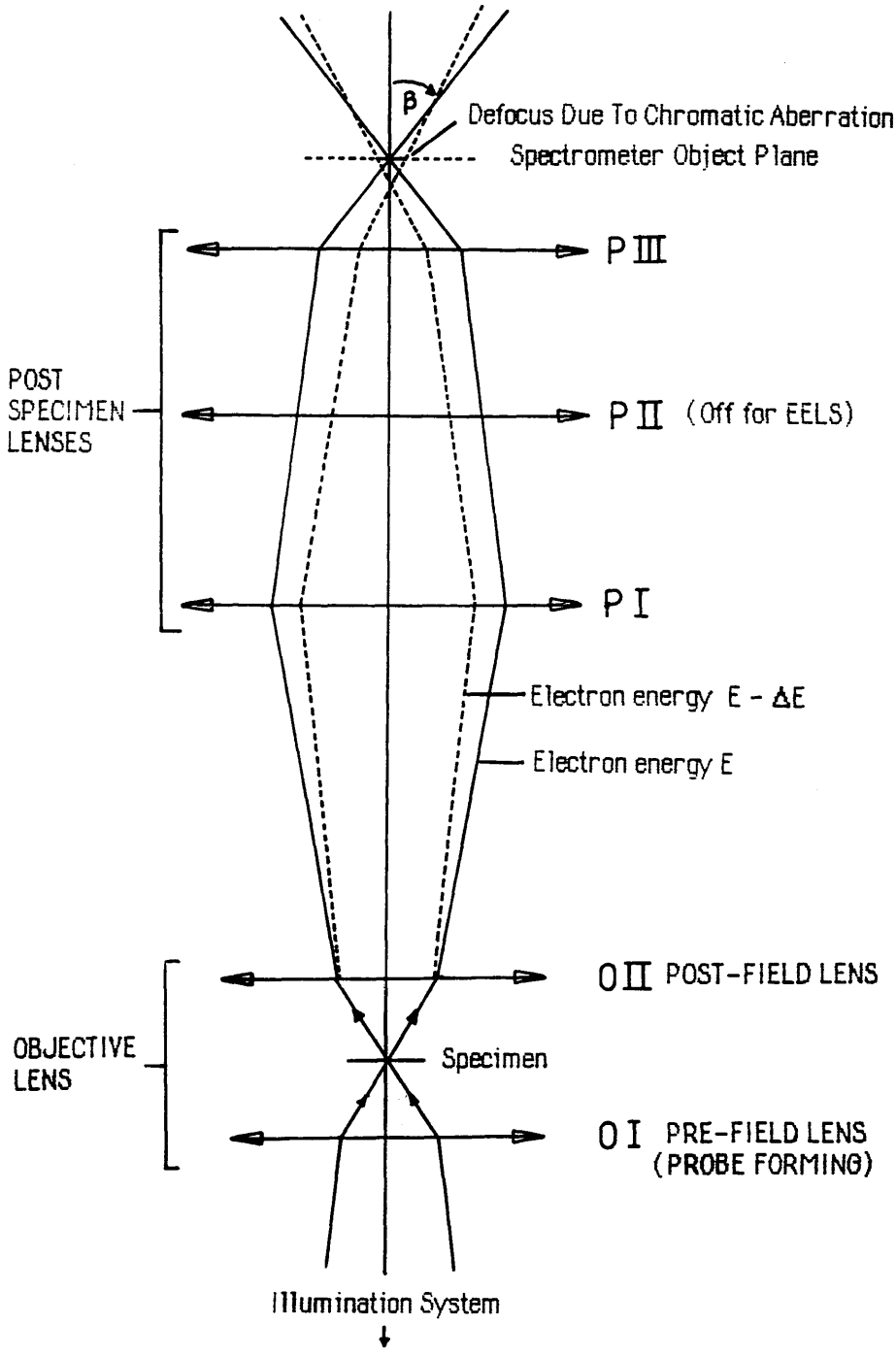

Figure 1.7 Serial Collection System

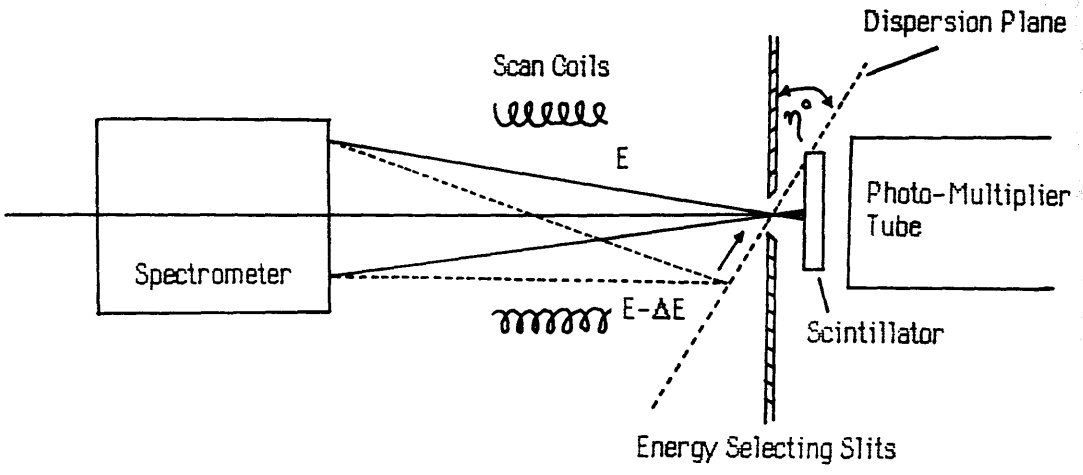

defocussed as the scan moves away from the central ray, and consequently it is necessary to refocus the spectrum to compensate. Changing the spectrometer excitation, although slower, has a great advantage - aberrations which are proportional to the energy difference from the central ray, such as the dispersion plane tilt, are nullified so that the spectrometer image is always focussed in the plane of the slits.

It is usual to record the high signal intensities present in the low loss region of the spectrum by digitising the analogue output of the photomultiplier. The much smaller signal levels present in the far energy loss can be recorded using an increased photomultiplier gain G controlled by the high voltage bias applied to the tube, or alternatively the photomultiplier gain can be left constant and the far energy loss signal detected using a digital pulse counting system, with pulse height discriminators to eliminate spurious counts due to dark noise in the photomultiplier tube. The latter allows single electron detection for far energy loss signals and is the method used at Glasgow. Both signals (analogue counts and digital counts) are then combined using an algorithm developed by Craven and Buggy [1984] in such a way as to produce the complete spectrum.

The major drawback of serial collection is its inherently low collection efficiency. For example in a spectrum consisting of 1000 data channels each channel contains only 0.1% of the total available signal. If the spectrum could be recorded in a parallel manner (ie. all channels simultaneously) by some multielement detector, the collection efficiency could be improved by up to 1000 times, thus an equivalent spectrum could theoretically be recorded 1000 times faster with the specimen receiving only 1/1000 of the total electron dose. This would be of enormous benefit in cases where radiation damage, specimen contamination, stage drift or signal to noise ratio are the limiting factors.

1.2.5 Design specifications of a parallel detection system.

There are many technical difficulties to be overcome in designing a high performance parallel recording system, and the major requirements of such a system are outlined below:

1) High dynamic range and linear response to cope with the rapid change of signal intensity with energy loss.

2) Good energy resolution to make use of ELNES information.

3) Low noise detection system. A suitable detector will have many hundreds of individual

detection elements so that channel to channel variations in sensitivity and linearity must be kept to a minimum.

The dynamic range of a typical EELS spectrum is ~10^8; no solid state detector currently available is capable of this level of performance, so that the spectrum has to be recorded in discrete sections - the number of which depends upon the maximum dynamic range of the device. A major problem concerning energy resolution is the scattering of 100keV electrons as they strike the solid material of the detector. Lateral spreading is of the order of 10-50μm depending upon the elemental composition (eg. the spread in silicon is ~30μm). Therefore the energy resolution of a solid state detector placed directly at the dispersion plane would be limited to between 5 and 25 eV, assuming a spectrometer dispersion of 2μm/eV.

One solution to this problem is to provide some form of post spectrometer electron optical magnification of the dispersion. Such an optical system should not introduce any significant aberrations or artefacts into the spectrum, and should be capable of varying the dispersion over a wide range to suit the geometry of the detector used. Another difficulty encountered with parallel detection has already been mentioned - for a typical first order focussing spectrometer, such as the magnetic sector spectrometer currently installed on the HB5, the dispersion plane is not perpendicular to the optic axis of the spectrometer but is tilted by the second order aberrations to some angle η (Figure 1.4). This makes any post spectrometer magnification of the dispersion plane very difficult, so it is desirable that the second order aberrations can be corrected so that $\eta=0^o$.

At the time of writing there are several prototype parallel detection systems operating in different laboratories, [Egerton and Crozier 1987, Monson et al. 1982, Shuman 1981, McMullan et al. 1985, Bourdillon et al. 1985] and one system is soon to be commercially available [Krivanek et al. 1987]. All of these designs are different and it is clear that much work remains to be done to arrive at the optimum detection system. The following chapters identify the problems encountered in the design of parallel recording systems for EELS and hopefully provide some insight into the most practical solutions.

CHAPTER 2

Homogeneous field magnetic sector spectrometers - theory

Introduction

The design of a successful parallel recording system for EELS requires calculation of the optical properties of the spectrometer, in order to determine the electron intensity distribution at the spectrometer dispersion plane. Knowledge of this distribution is essential to optimise both post-spectrometer coupling optics and the geometry of the detector used. This chapter is mainly a review of the theory of homogeneous field magnetic sector spectrometers based on the work of Brown, Enge, Penner, and Heighway, and is included in order to provide a background and a consistent notation for the equations used later in the thesis. In particular the treatment draws heavily on the articles by Enge [1964,1967] and figures 2.8, 2.9, 2.10, 2.12, 2.13, 2.14 and 2.18 are essentially taken from these papers.

2.1 SPECTROMETER TYPES

The two types of energy analyser most commonly considered in electron energy loss spectroscopy are the homogeneous field magnetic sector (Figure 2.1) and the Wien filter (Figure 2.2). Other types are discussed in the review article by Pearce-Percy [1978].

2.1.1 The Wien Filter

In its simplest form the Wien filter consists of uniform electric $\underline{E}$ and magnetic $\underline{B}$ fields crossed perpendicularly. The particle beam to be analysed is injected along the normal to the $\underline{E}$ - $\underline{B}$ plane so that the force on an electron moving with velocity v is the Lorentz force:

$$\underline{F} = -e[\underline{E} + (\underline{v} \times \underline{B})] \qquad (2.1)$$

For a particle moving along the x axis with velocity v_0 such that $v_0=|E/B|$ the net force is zero and there is no deflection. All other velocities will be deflected to form an energy spectrum, or more accurately a momentum spectrum. Note that focussing only occurs in the horizontal (x-y) plane so that a point source forms a line image. In order to achieve stigmatic focussing the electrostatic plates can be curved to introduce a component of $\underline{E}$ in the z direction. This

Figure 2.1 Simple Magnetic Sector Analyser

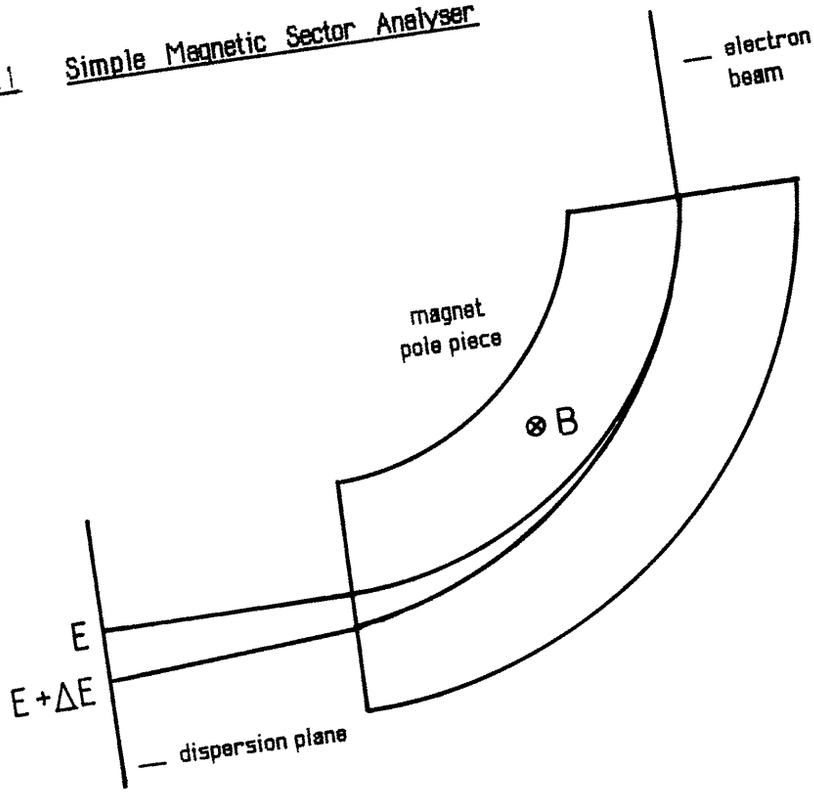

Figure 2.2 Wien Filter

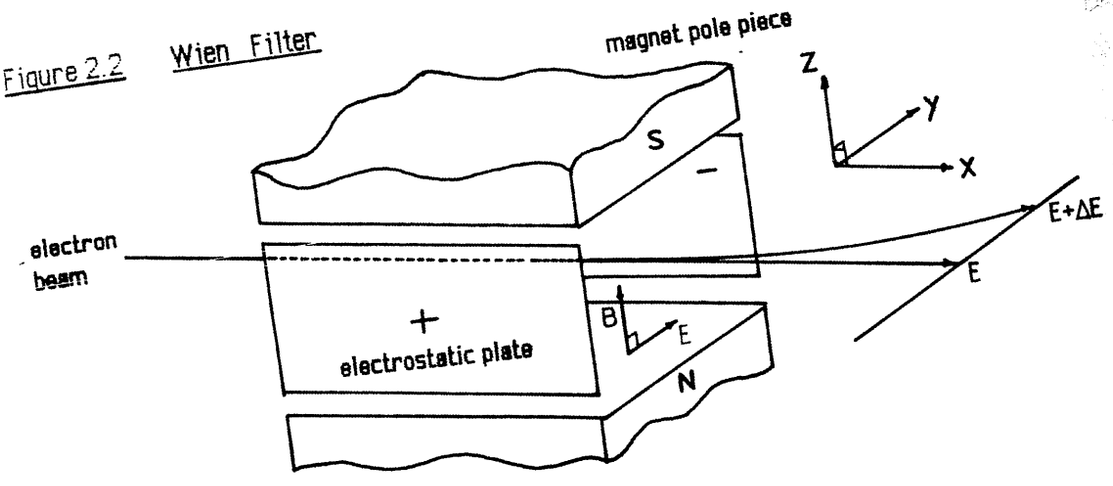

component will cause vertical focussing to occur, allowing point to point imaging. The main disadvantage of the Wien filter is the complication of generating two separate fields, especially at higher beam voltages where electrical breakdown may occur.

2.1.2 The magnetic sector

The optical properties of magnetic sectors have been studied in great detail, principally because of their use in high energy particle accelerators. The theoretical studies are more complete than those of the Wien filter and this, allied to a simpler construction, has led to a wide acceptance of the design - particularly in commercial applications. This is the type of spectrometer which will be considered in detail here.

2.2 MATRIX FORMALISM

Prior to a discussion of the optical properties of magnetic sectors it will be useful to introduce the matrix method of calculation first used in ray optics and later introduced to charged particle optics by Penner [1961]. The advantage of this approach is that complex transport systems consisting of many elements can be analysed simply, with clear reference to the physical parameters involved.

2.2.1 Transfer matrix of a drift space

Consider a field free region of length D (Figure 2.3). A particle enters the region at position (x_0,z_0) with gradient x_0'. As there are no forces acting in this region the particle gradient will be unchanged at z_1 and the equations describing its position are:

$$x_1 = x_0 + Dx_0'$$

$$x_1' = x_0'$$

These linear equations can be conveniently expressed in matrix form as:

$$\begin{bmatrix} x_1 \\ x_1' \end{bmatrix} = \begin{bmatrix} 1 & D \\ 0 & 1 \end{bmatrix} \begin{bmatrix} x_0 \\ x_0' \end{bmatrix}$$

where the 2x2 matrix is known as the transfer matrix of a drift space of length D.

Figure 2.3 **Drift Space**

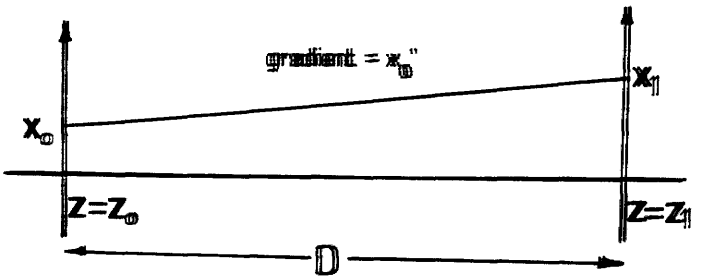

Figure 2.4 **Thin Lens**

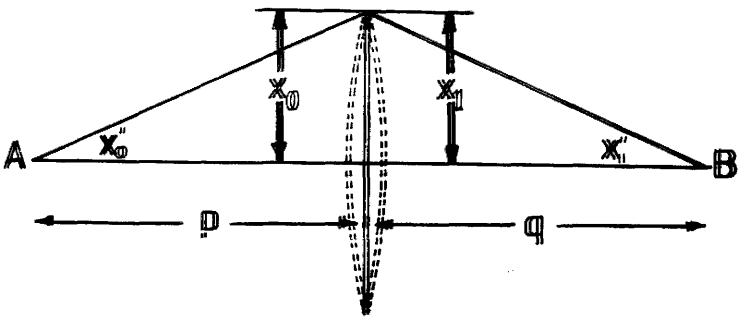

Figure 2.5 **Thick Lens**

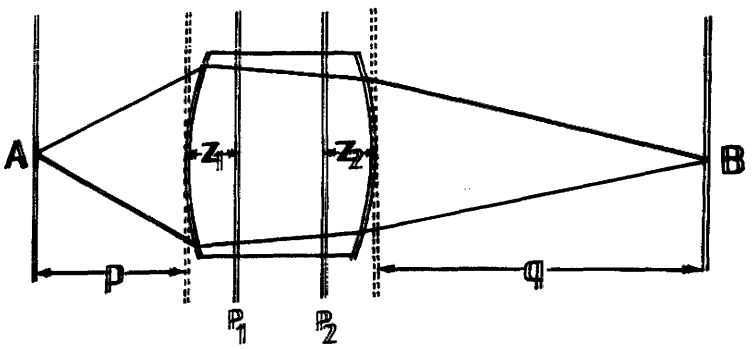

2.2.2 Transfer matrix of a thin lens

A thin lens is a focussing device such that the gradient of a ray or particle entering the lens is altered whilst the position measured from the optic axis is unchanged. This requires that the principal planes are coincident at the centre of the lens. Of course, for true lens action the change in gradient must be proportional to the distance off axis at which the ray enters the lens. Figure 2.4 shows a particle entering a thin lens with coordinates (x_0,x_0') and leaving with coordinates (x_1,x_1') where $x_1 = x_0$. The equation of a thin lens is:

$$1 / p + 1 / q = 1 / f \tag{2.2}$$

where p and q are the object and image distances respectively, and f is the focal length. The trajectory equations are simply:

$$x_1 = x_0$$

$$x_1' = - x_0 / f + x_0'$$

So that the transfer matrix for the lens action between the princip planes is thus:

$$\begin{bmatrix} x_1 \\ x_1' \end{bmatrix} = \begin{bmatrix} 1 & 0 \\ -\frac{1}{f} & 1 \end{bmatrix} \begin{bmatrix} x_0 \\ x_0' \end{bmatrix} \tag{2.3}$$

Note that in both the above cases the determinant of the transfer matrix is unity. This is true generally and is a manifestation of Liouville's theorem of conservation of phase space area. For a proof of the above see Brown [1967].

2.2.3 Transfer matrix of a thick lens

The focussing elements of electron optical systems cannot in general be considered to act as thin lenses. Figure 2.5 is a schematic of a thick lens, in this case equation (2.3) above does not hold. However, if two planes P_1 and P_2 located at distances z_1 and z_2 from the lens boundaries are introduced, it is always possible to find values for z_1 and z_2 such that:

$$1 / (p + z_1) + 1 / (q + z_2) = 1 / f$$

When this equation holds P_1 and P_2 are known as the principal planes. The matrix formulation for a thick lens becomes:

$$\begin{bmatrix} x_1 \\ x_1' \end{bmatrix} = \begin{bmatrix} A & B \\ C & D \end{bmatrix} \begin{bmatrix} x_0 \\ x_0' \end{bmatrix} \tag{2.4}$$

where:

$$\begin{bmatrix} A & B \\ C & D \end{bmatrix} = \begin{bmatrix} 1 & z_2 \\ 0 & 1 \end{bmatrix} \begin{bmatrix} 1 & 0 \\ -\frac{1}{f} & 1 \end{bmatrix} \begin{bmatrix} 1 & z_1 \\ 0 & 1 \end{bmatrix} \tag{2.5}$$

i.e. the thick lens is equivalent to a thin lens flanked by two drift spaces, and again the determinant is unity.

2.2.4 Transfer matrix of an optical system

Now consider the simplest optical system (Figure 2.6) of two drift spaces of length p and q, separated by some focussing element - the complete transfer from object to image is obtained by multiplying together the respective transfer matrices.

$$\begin{bmatrix} x_1 \\ x_1' \end{bmatrix} = \begin{bmatrix} 1 & q \\ 0 & 1 \end{bmatrix} \begin{bmatrix} A & B \\ C & D \end{bmatrix} \begin{bmatrix} 1 & p \\ 0 & 1 \end{bmatrix} \begin{bmatrix} x_0 \\ x_0' \end{bmatrix} \tag{2.6}$$

Assuming that the two planes of interest Z_0 and Z_i are conjugate (see below) then p is the object distance, counted positive towards the left starting from the entrance plane, and q is the image distance counted positive towards the right starting from the exit plane. It is important to note the order in which the matrices are multiplied together - starting from the image point and working back towards the object.

2.2.5 Optical characteristics

Multiplying out equation (2.6) gives:

$$x_1 = (A + Cq)\,x_0 + [Ap + B + q(Cp + D)]\,x_0' \tag{2.7a}$$

$$x_1' = C\,x_0 + (Cp + D)\,x_0' \tag{2.7b}$$

These relations reveal all the first order characteristics of the system :

1) Object / Image Conjugation - point to point focussing requires that image position x_1 is independent of the initial gradient x_0'. From equation (2.7a) the condition is:

$$C p q + A p + D q + B = 0 \qquad (2.8)$$

2) Image Position - if the object position is known then (2.8) gives:

$$q = -(A p + B) / (C p + D) \qquad (2.9)$$

3) Magnification . Assuming the conjugation relation (2.9) is satisfied then:

$$M = x_1 / x_0 = A + C q$$

i.e. $$M = A - C[(A p + B) / (C p + D)]$$

or $$M = (AD - BC) / (C p + D)$$

but (AD-BC) is simply the determinant of the focussing element transfer matrix and from before must be unity. Therefore:

$$M = 1 / (C p + D) \qquad (2.10)$$

Complex systems with more than one element are handled in exactly the same manner by multiplication of the appropriate transfer matrices.

2.3 OPTICAL PROPERTIES OF MAGNETIC SECTORS

The literature contains many studies of the optical properties of magnetic sectors, eg. Penner [1961], Brown [1967,1980] one of the clearest and most comprehensive being that by Enge [1967]. This section essentially follows his treatment.

2.3.1 General representation of sector properties

Figure 2.7 represents an arbitrary magnetic sector which is mirror symmetric about a horizontal plane - i.e. the plane of the paper. For convenience this plane is known as the median plane and the direction of the field B is perpendicular to the median plane, in what is known as the vertical plane. An arbitrary median plane ray, called the central ray, is chosen to define the origin of the coordinate systems, having a given position and direction at the input and a given momentum. The entrance coordinate system (x_0,y_0,z_0) is constructed as shown with the x direction perpendicular to the median plane, while the exit coordinate system (x_1,y_1,z_1) has the z axis displaced such that it coincides with the central ray after its deflection through the magnet. Given the entrance coordinates (x_0,y_0,z_0), the slopes x_0'=

Figure 2.6 Simple Optical System

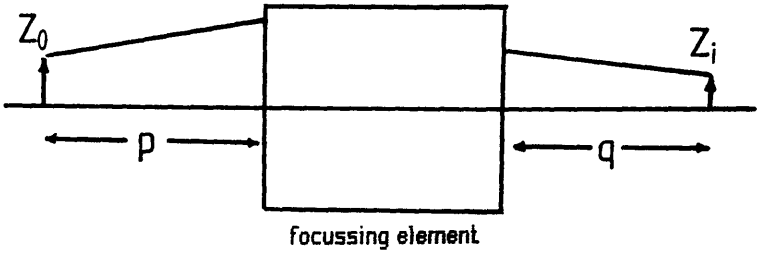

Figure 2.7 Magnetic Sector Coordinate Systems

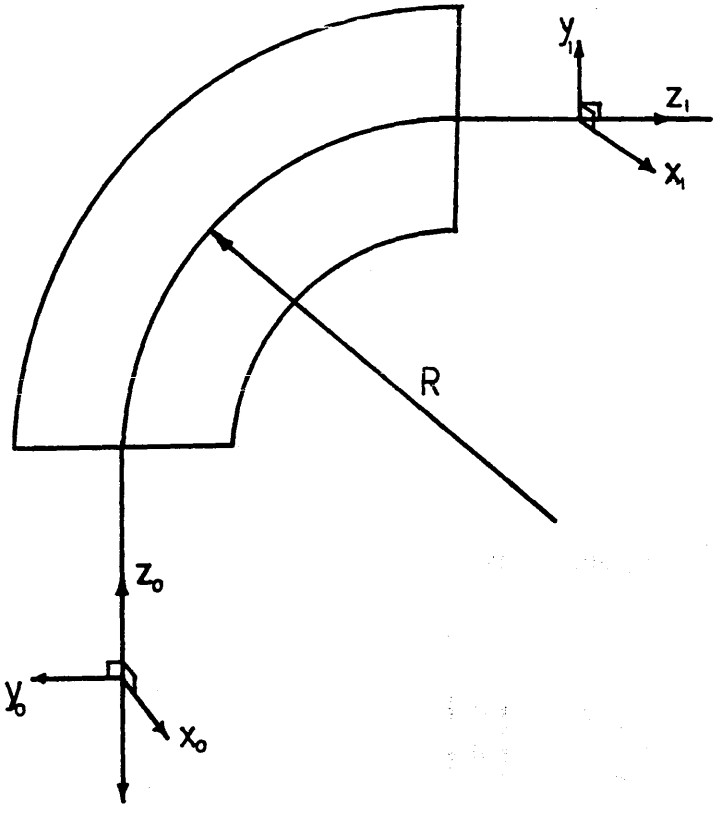

dx_0/dz_0, $y_0' = dy_0/dz_0$ and the momentum deviation $\delta = \Delta p/p$ of an arbitrary ray, the problem is to determine the exit position (x_1,y_1,z_1) and gradients x_1', y_1'. That is to obtain functions f_n such that at $z_1 = 0$:

$$y_1 / R = f_1 (y_0 / R,\ y_0',\ x_0 / R,\ x_0',\ \delta) \qquad (2.11a)$$

$$y_1' = f_2 (y_0 / R,\ y_0',\ x_0 / R,\ x_0',\ \delta) \qquad (2.11b)$$

$$x_1 / R = f_3 (y_0 / R,\ y_0',\ x_0 / R,\ x_0',\ \delta) \qquad (2.11c)$$

$$x_1' = f_4 (y_0 / R,\ y_0',\ x_0 / R,\ x_0',\ \delta) \qquad (2.11d)$$

where y_0, y_0', x_0, x_0' are specified at $z_0 = 0$. Note that in order to make the above equations dimensionless all lengths (x,y) have been divided by the orbit radius of the central ray, R (Figure 2.7). It is reasonable, in electron microscopy, to assume that the parameters y_0/R, x_0/R, y_0', x_0', and δ are all very much smaller than unity. For example in STEM the diameter of the probe which forms the object for the spectrometer may be as small as 1nm and the collection angle is normally < 5 mrads. The entire electron energy loss spectrum covers ~ 2000 eV, so that at an operating voltage of 100kV δ_{max} is of the order of 0.01. It is therefore feasible to expand equations (2.11) in a Taylor series about the central ray :

$$\frac{y_1}{R} = \left[\frac{\partial y_1}{\partial y_0}\left[\frac{y_0}{R}\right] + \frac{1}{R}\frac{\partial y_1}{\partial y_0'}\left[y_0'\right] + \frac{\partial y_1}{\partial x_0}\left[\frac{x_0}{R}\right] + \frac{1}{R}\frac{\partial y_1}{\partial x_0'}\left[x_0'\right] + \frac{1}{R}\frac{\partial y_1}{\partial \delta}\left[\delta\right] \right]$$

$$+ \frac{1}{2!}\left[\text{2nd order terms} \right] + \frac{1}{3!}\left[\text{3rd order terms} \right] + \ldots\ldots \qquad (2.12a)$$

$$y_1' = \left[R\frac{\partial y_1'}{\partial y_0}\left[\frac{y_0}{R}\right] + \frac{\partial y_1'}{\partial y_0'}\left[y_0'\right] + R\frac{\partial y_1'}{\partial x_0}\left[\frac{x_0}{R}\right] + \frac{\partial y_1'}{\partial x_0'}\left[x_0'\right] + \frac{\partial y_1'}{\partial \delta}\left[\delta\right] \right]$$

$$+ \frac{1}{2!}\left[\text{2nd order terms} \right] + \frac{1}{3!}\left[\text{3rd order terms} \right] + \ldots\ldots \qquad (2.12b)$$

$$\frac{x_1}{R} = \left[\frac{\partial x_1}{\partial y_0}\left[\frac{y_0}{R}\right] + \frac{1}{R}\frac{\partial x_1}{\partial y_0'}\left[y_0'\right] + \frac{\partial x_1}{\partial x_0}\left[\frac{x_0}{R}\right] + \frac{1}{R}\frac{\partial x_1}{\partial x_0'}\left[x_0'\right] + \frac{1}{R}\frac{\partial x_1}{\partial \delta}\left[\delta\right] \right]$$

$$+ \frac{1}{2!}\left[\text{2nd order terms} \right] + \frac{1}{3!}\left[\text{3rd order terms} \right] + \ldots\ldots \qquad (2.12c)$$

$$x_1' = \left[R\frac{\partial x_1'}{\partial y_0}\left[\frac{y_0}{R}\right] + \frac{\partial x_1'}{\partial y_0'}\left[y_0'\right] + R\frac{\partial x_1'}{\partial x_0}\left[\frac{x_0}{R}\right] + \frac{\partial x_1'}{\partial x_0'}\left[x_0'\right] + \frac{\partial x_1'}{\partial \delta}\left[\delta\right]\right]$$

$$+ \frac{1}{2!}\left[\text{ 2nd order terms }\right] + \frac{1}{3!}\left[\text{ 3rd order terms }\right] + \ldots\ldots \qquad (2.12d)$$

where all partial derivatives are evaluated at $x_0 = y_0 = x_0' = y_0' = \delta = 0$. Now the median plane symmetry of the magnet places some restrictions upon the allowable Taylor coefficients i.e.

$$y_1/R = f_1(y_0/R, y_0', x_0/R, x_0', \delta) = f_1(y_0/R, y_0', -x_0/R, -x_0', \delta) \qquad (2.13a)$$

$$x_1/R = f_3(y_0/R, y_0', x_0/R, x_0', \delta) = -f_3(y_0/R, y_0', -x_0/R, -x_0', \delta) \qquad (2.13b)$$

Expanding equations (2.12a-d) to second order and eliminating all terms which do not satisfy the symmetry conditions (2.13a,2.13b) gives :

$$\frac{y_1}{R} = \left[\frac{\partial y_1}{\partial y_0}\left[\frac{y_0}{R}\right] + \frac{1}{R}\frac{\partial y_1}{\partial y_0'}\left[y_0'\right] + \frac{1}{R}\frac{\partial y_1}{\partial \delta}\left[\delta\right]\right] \qquad (2.14a)$$

$$+\left[\frac{R}{2}\frac{\partial^2 y_1}{\partial y_0^2}\left[\frac{y_0}{R}\right]^2 + \frac{1}{2R}\frac{\partial^2 y_1}{\partial y_0'^2}\left[y_0'\right]^2 + \frac{R}{2}\frac{\partial^2 y_1}{\partial x_0^2}\left[\frac{x_0}{R}\right]^2 + \frac{1}{2R}\frac{\partial^2 y_1}{\partial x_0'^2}\left[x_0'\right]^2 + \frac{1}{2R}\frac{\partial^2 y_1}{\partial \delta^2}\left[\delta\right]^2\right]$$

$$+\left[\frac{\partial^2 y_1}{\partial y_0 \partial y_0'}\left[\frac{y_0}{R}y_0'\right] + \frac{\partial^2 y_1}{\partial x_0 \partial x_0'}\left[\frac{x_0}{R}x_0'\right] + \frac{\partial^2 y_1}{\partial y_0 \partial \delta}\left[\frac{y_0}{R}\delta\right] + \frac{1}{R}\frac{\partial^2 y_1}{\partial y_0' \partial \delta}\left[y_0'\delta\right]\right]$$

$$y_1' = \left[R\frac{\partial y_1'}{\partial y_0}\left[\frac{y_0}{R}\right] + \frac{\partial y_1'}{\partial y_0'}\left[y_0'\right] + \frac{\partial y_1'}{\partial \delta}\left[\delta\right]\right] \qquad (2.14b)$$

$$+\left[\frac{R^2}{2}\frac{\partial^2 y_1'}{\partial y_0^2}\left[\frac{y_0}{R}\right]^2 + \frac{1}{2}\frac{\partial^2 y_1'}{\partial y_0'^2}\left[y_0'\right]^2 + \frac{R^2}{2}\frac{\partial^2 y_1'}{\partial x_0^2}\left[\frac{x_0}{R}\right]^2 + \frac{1}{2}\frac{\partial^2 y_1'}{\partial x_0'^2}\left[x_0'\right]^2 + \frac{1}{2}\frac{\partial^2 y_1'}{\partial \delta^2}\left[\delta\right]^2\right]$$

$$+\left[R\frac{\partial^2 y_1'}{\partial y_0 \partial y_0'}\left[\frac{y_0}{R}y_0'\right] + R\frac{\partial^2 y_1'}{\partial x_0 \partial x_0'}\left[\frac{x_0}{R}x_0'\right] + R\frac{\partial^2 y_1'}{\partial y_0 \partial \delta}\left[\frac{y_0}{R}\delta\right] + \frac{\partial^2 y_1'}{\partial y_0' \partial \delta}\left[y_0'\delta\right]\right]$$

$$\frac{x_1}{R}=\left[\frac{\partial x_1}{\partial x_0}\left[\frac{x_0}{R}\right]+\frac{1}{R}\frac{\partial x_1}{\partial x_0'}\left[x_0'\right]\right]+\left[\frac{\partial^2 x_1}{\partial x_0\partial\delta}\left[\frac{x_0}{R}\delta\right]+\frac{1}{R}\frac{\partial^2 x_1}{\partial x_0'\partial\delta}\left[x_0'\,\delta\right]\right] \tag{2.14c}$$

$$+\left[R\frac{\partial^2 x_1}{\partial y_0\partial x_0}\left[\frac{y_0}{R}\frac{x_0}{R}\right]+\frac{\partial^2 x_1}{\partial y_0\partial x_0'}\left[\frac{y_0}{R}x_0'\right]+\frac{\partial^2 x_1}{\partial y_0'\partial x_0}\left[y_0'\frac{x_0}{R}\right]+\frac{1}{R}\frac{\partial^2 x_1}{\partial y_0'\partial x_0'}\left[y_0'\,x_0'\right]\right]$$

$$x_1'=\left[R\frac{\partial x_1'}{\partial x_0}\left[\frac{x_0}{R}\right]+\frac{\partial x_1'}{\partial x_0'}\left[x_0'\right]\right]+\left[R\frac{\partial^2 x_1'}{\partial x_0\partial\delta}\left[\frac{x_0}{R}\delta\right]+\frac{\partial^2 x_1'}{\partial x_0'\partial\delta}\left[x_0'\,\delta\right]\right] \tag{2.14d}$$

$$+\left[R^2\frac{\partial^2 x_1'}{\partial y_0\partial x_0}\left[\frac{y_0}{R}\frac{x_0}{R}\right]+R\frac{\partial^2 x_1'}{\partial y_0\partial x_0'}\left[\frac{y_0}{R}x_0'\right]+R\frac{\partial^2 x_1'}{\partial y_0'\partial x_0}\left[y_0'\frac{x_0}{R}\right]+\frac{\partial^2 x_1'}{\partial y_0'\partial x_0'}\left[y_0'\,x_0'\right]\right]$$

2.3.2 First order matrix transformations

Considering the first order coefficients only, equations (2.14 a-d) are linear and can be rewritten in matrix form:

$$\begin{bmatrix}\frac{y_1}{R}\\ y_1'\\ \delta\end{bmatrix}=\begin{bmatrix}\frac{y}{y}&\frac{y}{y'}&\frac{y}{\delta}\\ \frac{y'}{y}&\frac{y'}{y'}&\frac{y'}{\delta}\\ 0&0&1\end{bmatrix}\begin{bmatrix}\frac{y_0'}{R}\\ y_0'\\ \delta\end{bmatrix} \tag{2.15}$$

and similarly for the vertical plane:

$$\begin{bmatrix}\frac{x_1}{R}\\ x_1'\end{bmatrix}=\begin{bmatrix}\frac{x}{x}&\frac{x}{x'}\\ \frac{x'}{x}&\frac{x'}{x'}\end{bmatrix}\begin{bmatrix}\frac{x_0}{R}\\ x_0'\end{bmatrix} \tag{2.16}$$

The partial derivatives that appear in the Taylor expansion have been written in abbreviated form and are known as 'focussing coefficients'. For example:

$$\frac{y}{y'} = \frac{1}{R}\frac{\partial y_1}{\partial y_0'} \qquad \frac{y'}{y} = R\frac{\partial y_1'}{\partial y_0} \qquad \frac{y}{\delta} = \frac{1}{R}\frac{\partial y_1}{\partial \delta}$$

$$\frac{x}{x'} = \frac{1}{R}\frac{\partial x_1}{\partial x_0'} \qquad \frac{x'}{x} = R\frac{\partial x_1'}{\partial x_0}$$

Note that to first order the motions in the x and y planes are independent of each other. The values in the third row of equation (2.15) reflect the fact that static magnetic fields cannot alter the scalar momentum of charged particles.

2.4 DERIVATION OF MATRIX COEFFICIENTS FOR HOMOGENEOUS FIELD MAGNETIC SECTORS

There are two methods to obtain analytical expressions for the focussing coefficients (y/y) etc. The simplest calculation, as carried out by Penner [1961], is a geometrical analysis based on the fact that all trajectories within a sector are arcs of circles. This procedure is not capable of handling the effects of extended fringe fields however, and it is more useful to solve the trajectory equations for the motion of an electron through a sector magnet. Figure 2.8 shows a typical magnet with entrance and exit faces normal to the central ray and constant field $|B|=B_0$. R is the bending radius of the central ray and r (=R+y) describes the position of an arbitrary ray. As before it is assumed that the deviations from the central ray are small ie. $y/R << 1$.

2.4.1 Derivation of equations of motion

Using the cylindrical coordinate system (r,θ,x) defined in Figure 2.8 consider motion in the median plane. The Lorentz force is:

$$\underline{F} = -e(\underline{v} \times \underline{B}) \qquad \text{where}$$

$$B(r, \theta, x) = B(0, 0, B_0)$$

carrying out the vector product gives the components of the force acting:

$$F_r = -e r \dot{\theta} B_0$$

Figure 2.8 Simple Magnetic Sector

After Enge [1967]

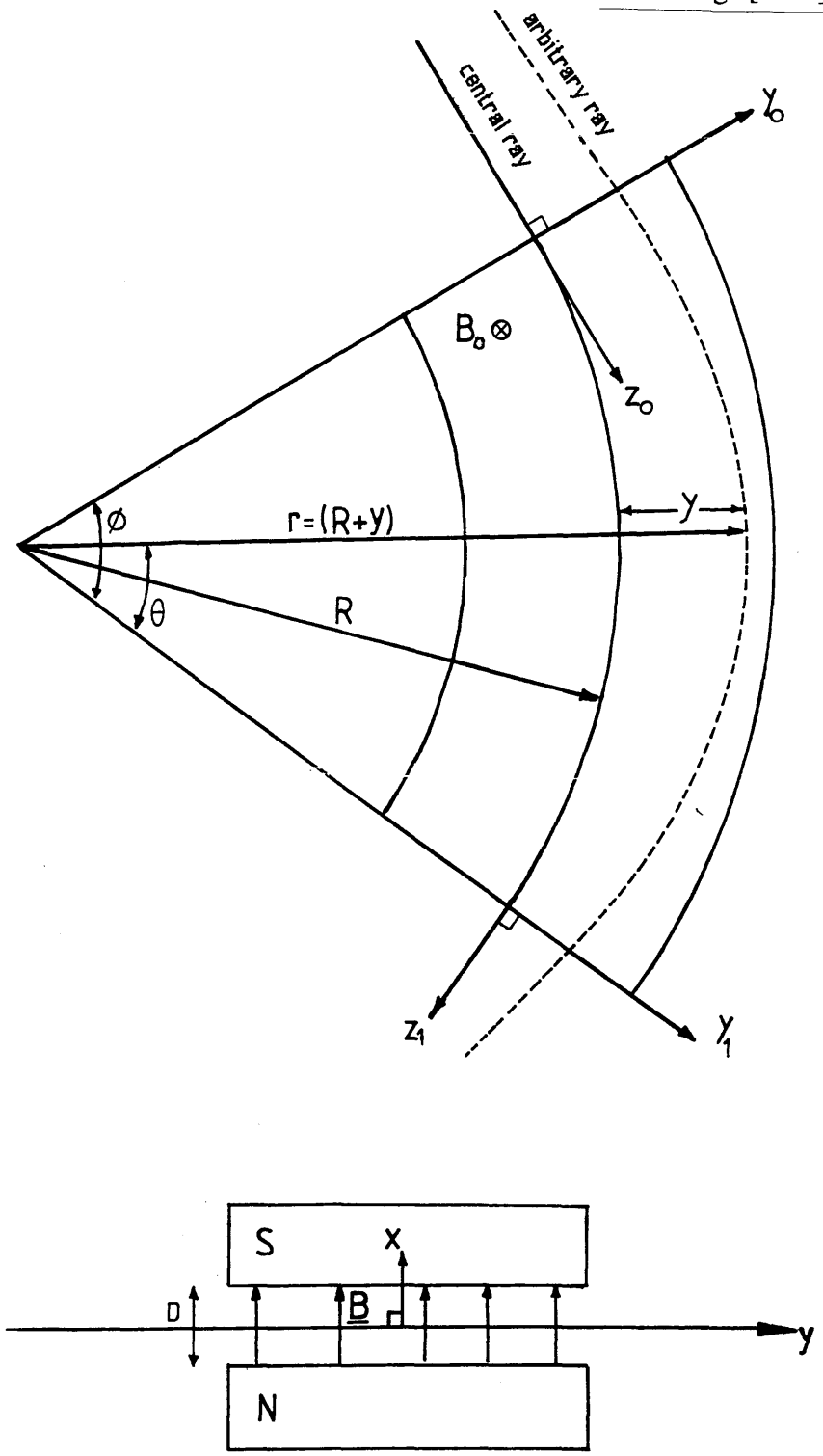

$$F_\theta = e\dot{r}B_0$$

$$F_x = 0$$

where the dot stands for time derivative and - e is the charge on an electron. Now from Newton's second law:

$$\frac{d}{dt}(m\dot{r}) = mr\dot{\theta}^2 - er\dot{\theta}B_0 \qquad (2.17)$$

ie. mass x radial acceleration = mass x centripetal acceleration - Lorentz force . Equating the rate of change of angular momentum to the moment of the angular force gives:

$$\frac{d}{dt}(mr^2\dot{\theta}) = r F_\theta = er\dot{r}B_0 \qquad (2.18)$$

Rewrite (2.17) as:

$$\ddot{r} = r\dot{\theta}^2 - \frac{e}{m}r\dot{\theta}B_0$$

$$\ddot{r} = r\dot{\theta}^2 + \omega r\dot{\theta} \qquad (2.19)$$

where $\omega = -eB_0/m$ is the 'cyclotron' frequency of a particle in the central orbit. Rewrite (2.18) as:

$$\frac{d}{dt}(r^2\dot{\theta}) = -\omega r\dot{r}$$

$$\frac{d}{dt}(r^2\dot{\theta}) = -\frac{\omega}{2}\frac{d}{dt}\left[r^2 + c\right]$$

$$\dot{\theta} = -\frac{\omega}{2}\left[1 + \frac{c}{r^2}\right]$$

Now when r = R, the radius of the central ray then:

$$\dot{\theta} = -\omega$$

$$c = R^2$$

substituting r = (R+y) :

$$\dot{\theta} = -\frac{\omega}{2}\left[1 + \frac{1}{\left[1+\frac{y}{R}\right]^2}\right]$$

Assuming $y << R$ gives to first order :

$$\dot{\theta} = -\omega \left[1 - \frac{y}{R} \right]$$

which is inserted into equation (2.19) together with $r = R + y$ to give:

$$\frac{d^2y}{dt^2} + \omega^2 y = 0 \qquad (2.20)$$

This is the Kerst - Serber equation governing the excursion of a particle from the central ray in the median plane. The particle executes harmonic motion in the radial direction about the central ray, so it can be said that the magnet has a positive focussing action in the median plane. Motion in the x direction is dependent upon the r component of the magnetic field $B(r,\theta,x)$, for the case of a homogeneous field sector this is, of course, zero (Figure 2.8). Thus the simple sector discussed has no focussing properties in the x direction and would image a point source to a line, however it is quite possible to introduce a component of B_r by tapering the polefaces of the magnet - and indeed this is a common approach in high energy particle accelerators. However, there are simpler ways of introducing a vertical focus which are discussed in later sections.

2.4.2 The matrix coefficients

The time dependence can be eliminated from equation (2.20) by introducing a new independent variable $z = R\omega t$ where z is the distance along the central ray from the entrance of the magnet.

$$z = R\omega t$$

$$dz = R\omega\, dt$$

$$dz^2 = R^2\omega^2 dt^2$$

substituting in (2.20) gives :

$$R^2\omega^2 \frac{d^2y}{dz^2} + \omega^2 y = 0 \qquad \text{or :}$$

$$\frac{d^2y}{dz^2} + \frac{y}{R^2} = 0 \qquad (2.21)$$

The solution of equation (2.21) is:

$$y = y_A \sin\left(\frac{z}{R} + \gamma\right)$$

Which has a derivative with respect to z :

$$y' = \frac{y_A}{R} \cos\left(\frac{z}{R} + \gamma\right)$$

Now at the magnet entrance z=0 so :

$$y_0 = y_A \sin(\gamma)$$

$$y_0' = \frac{y_A}{R} \cos(\gamma)$$

Also at the exit $z = \Phi R$, where Φ is the spectrometer bend angle so :

$$y_1 = y_A \sin\left(\frac{\Phi R}{R} + \gamma\right)$$

$$= y_A \sin\gamma \cos\Phi + y_A \sin\Phi \cos\gamma$$

$$= y_0 \cos\Phi + y_0' R \sin\Phi$$

$$y_1' = \frac{y_A}{R} \cos\left(\frac{\Phi R}{R} + \gamma\right)$$

$$= \frac{y_A}{R} \cos\Phi \cos\gamma - \frac{y_A}{R} \sin\Phi \sin\gamma$$

$$= y_0' \cos\Phi - \frac{y_0}{R} \sin\Phi$$

These expressions can now be written in simple matrix form :

$$\begin{bmatrix} \frac{y_1}{R} \\ y_1' \end{bmatrix} = \begin{bmatrix} \cos\Phi & \sin\Phi \\ -\sin\Phi & \cos\Phi \end{bmatrix} \begin{bmatrix} \frac{y_0}{R} \\ y_0' \end{bmatrix} \qquad (2.22)$$

The equivalent transfer matrix for the vertical or x plane is of course that of a drift space of length $L = \Phi R$:

$$\begin{bmatrix} \frac{x_1}{R} \\ x_1' \end{bmatrix} = \begin{bmatrix} 1 & \Phi \\ 0 & 1 \end{bmatrix} \begin{bmatrix} \frac{x_0}{R} \\ x_0' \end{bmatrix} \qquad (2.23)$$

Notice that the determinants of (2.22) and (2.23) are unity. Equation (2.22) shows that the magnet is behaving as a thick lens in the median plane and, referring back to section 2.2.3, the distances of the principal planes from the sector boundaries, z_1 and z_2 are found to be :

$$\frac{z_1}{R} = \frac{z_2}{R} = -\frac{(1 - \cos\Phi)}{\sin\Phi}$$

and the focal length is :

$$\frac{R}{f} = \sin\Phi$$

2.4.3 The effects of momentum variation

The coefficients (y/δ) and (y'/δ) of equation (2.6) still remain to be calculated. To find the effect of a momentum change Δp, notice that this new momentum must correspond to a new equilibrium orbit with radius :

$$r_\delta = R + y_\delta$$

For the central ray :

$$\frac{m v^2}{R} = -e v B_0 \qquad \text{therefore} \qquad p_0 = -e B_0 R$$

Now :

$$\begin{aligned} p_0 + \Delta p &= -e B_0 r_\delta \\ &= -e B_0 (R + y_\delta) \\ &= -e B_0 R (1 + y_\delta / R) \end{aligned}$$

so :

$$\delta = \frac{\Delta p}{p_0} = \frac{y_\delta}{R} \quad \text{or} \quad y_\delta = R\delta \qquad (2.24)$$

This new momentum causes the particle to exhibit harmonic motion about the new equilibrium orbit (Figure 2.9). For the particle with initial conditions $y_0 = 0$, $y_0' = 0$,

$p=p_0+\Delta p$, the new orbit can be found from the transfer matrix (2.22). With respect to the new equilibrium orbit the particle enters the sector at $y_0'^* = 0$, $y_0^* = -y_\delta = -R\delta$. The transfer matrix describing the position of this particle at the magnet exit with respect to the new equilibrium orbit is :

$$\begin{bmatrix} \frac{y_1^*}{R} \\ y_1'^* \end{bmatrix} = \begin{bmatrix} \cos\Phi & \sin\Phi \\ -\sin\Phi & \cos\Phi \end{bmatrix} \begin{bmatrix} \frac{-y_\delta}{R} \\ 0 \end{bmatrix}$$

so :

$$\frac{y_1^*}{R} = -\frac{y_\delta}{R}\cos\Phi$$

$$y_1'^* = \frac{y_\delta}{R}\sin\Phi$$

Now comparing the displacements y^* with the central ray :

$$\frac{y_1}{R} = \frac{y_1^*}{R} + \frac{y_\delta}{R} \qquad \text{i.e.} \qquad \frac{y_1}{R} = -\frac{y_\delta}{R}\cos\Phi + \frac{y_\delta}{R}$$

$$\frac{y_1}{R} = \frac{y_\delta}{R}(1 - \cos\Phi)$$

$$= \delta(1 - \cos\Phi)$$

$$y_1' = y_1'^* \qquad \text{i.e.} \qquad y_1' = \frac{y_\delta}{R}\sin\Phi$$

$$= \delta \sin\Phi$$

so the complete first order horizontal transfer matrix becomes :

$$\begin{bmatrix} \frac{y_1}{R} \\ y_1' \\ \delta \end{bmatrix} = \begin{bmatrix} \cos\Phi & \sin\Phi & 1-\cos\Phi \\ -\sin\Phi & \cos\Phi & \sin\Phi \\ 0 & 0 & 1 \end{bmatrix} \begin{bmatrix} \frac{y_0}{R} \\ y_0' \\ \delta \end{bmatrix} \qquad (2.25)$$

Figure 2.9 Folded Out Motion Of Particle With Momentum $P_0 + \Delta P$ With Reference To The Central Ray After Enge [1967]

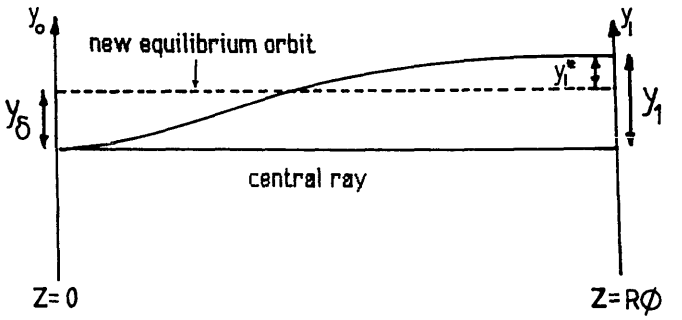

Figure 2.10a Magnet With Non-Zero Entrance And Exit Angles After Enge [1967]

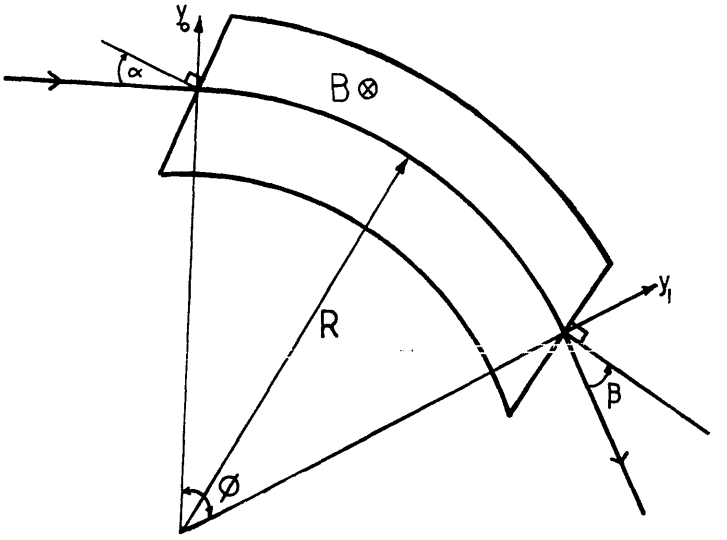

Figure 2.10b

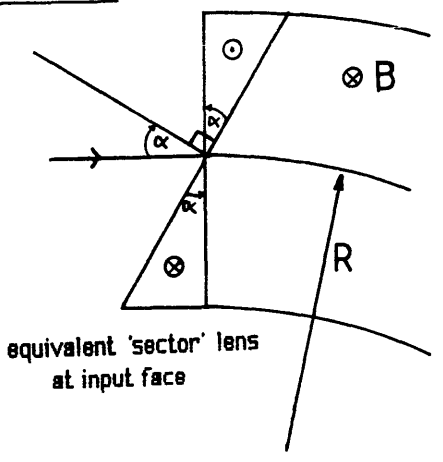

Figure 2.10c.

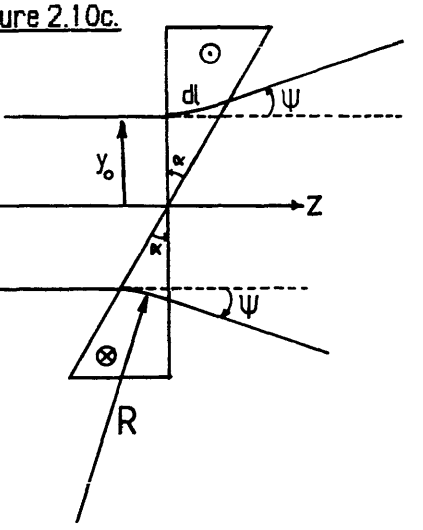

2.5 THE EFFECTS OF TILTED ENTRANCE AND EXIT PLANES

Figure 2.10a shows a magnet where the central ray does not enter and exit normal to the pole boundaries. The entrance angle α is the angle between the normal to the pole boundary and the central ray in entrance space, and β is the corresponding angle at the exit side. Both α and β are defined as positive when the normals are on the outside of the beam with respect to the centre of curvature.

2.5.1 The median plane.

The effect of positive angles α and β on median plane focussing is to reduce the overall focussing strength. Looking at the entrance side, figure 2.10a shows that positive α tends to remove some of the field traversed by particles with positive y, and to add more field for the inside rays - obviously this is a defocussing effect. Tilting the poleface is equivalent to superimposing a double sector magnet (Figure 2.10b) at the entrance, with the field direction reversed above and below the central ray as shown. This field is of the same strength as the main field and the radius of curvature of the particle is therefore the same as before (Figure 2.10c). If y_0 is small, i.e. small deviation from the central ray, arc dl is short so that the particle y component is approximately unchanged upon traversing the magnet. Thus the entrance sector,and hence the tilted poleface acts as a thin divergent lens. From Figure 2.10c:

$$dl \sim y_0 \tan\alpha$$

The radius of curvature of the trajectory is R since $|B| = B_0$. Hence :

$$dl = R\Psi \sim y_0 \tan\alpha$$

$$\Psi = \frac{y_0}{R}\tan\alpha$$

where Ψ is the angle of deflection. Now if Ψ is small then $\tan\Psi \sim \Psi = y_1'$ so that the transfer matrix for the thin lens can be written as :

$$\begin{bmatrix} \frac{y_1}{R} \\ y_1' \\ \delta \end{bmatrix} = \begin{bmatrix} 1 & 0 & 0 \\ \tan\alpha & 1 & 0 \\ 0 & 0 & 1 \end{bmatrix} \begin{bmatrix} \frac{y_0}{R} \\ y_0' \\ \delta \end{bmatrix} \qquad (2.26)$$

The non-zero exit angle has an identical effect except α is replaced by β in the transfer

matrix. The complete transfer matrix in the median plane is found by multiplying together the three individual matrices starting from the exit face i.e. :

$$\begin{bmatrix} \frac{y_1}{R} \\ y_1' \\ \delta \end{bmatrix} = \begin{bmatrix} 1 & 0 & 0 \\ \tan\beta & 1 & 0 \\ 0 & 0 & 1 \end{bmatrix} \begin{bmatrix} \cos\Phi & \sin\Phi & 1-\cos\Phi \\ -\sin\Phi & \cos\Phi & \sin\Phi \\ 0 & 0 & 1 \end{bmatrix} \begin{bmatrix} 1 & 0 & 0 \\ \tan\alpha & 1 & 0 \\ 0 & 0 & 1 \end{bmatrix} \begin{bmatrix} \frac{y_0}{R} \\ y_0' \\ \delta \end{bmatrix}$$

Which gives for the first order median plane matrix :

$$\begin{bmatrix} \frac{y_1}{R} \\ y_1' \\ \delta \end{bmatrix} = \begin{bmatrix} \frac{\cos(\Phi - \alpha)}{\cos\alpha} & \sin\Phi & 1 - \cos\Phi \\ \frac{-\sin(\Phi - \alpha - \beta)}{\cos\alpha \cos\beta} & \frac{\cos(\Phi - \beta)}{\cos\beta} & \sin\Phi + (1 - \cos\Phi)\tan\beta \\ 0 & 0 & 1 \end{bmatrix} \begin{bmatrix} \frac{y_0}{R} \\ y_0' \\ \delta \end{bmatrix} \qquad (2.27)$$

2.5.2 Motion in the vertical plane

It has been shown that a simple sector with straight edge polefaces normal to the direction of the central ray acts as a drift space in the vertical plane and a thick lens in the median plane. Figure 2.11a shows a vertical plane cross-section through the magnet poles at the exit face. The field well inside the magnet is constant , B_0. However, at the polefaces the field cannot rise instantaneously from zero and there exists a region known as the fringing field zone where $\underline{B}$ is not constant. Outside the prism the field lines are curved and lie in planes perpendicular to the polefaces (Figure 2.11b) and a component of $\underline{B}$ in the z direction appears. This component affects the second order focussing properties in the median plane . For $\beta = 0$ however, B_r must still be zero because the field lines lie in planes perpendicular to the r direction. In the case of non-zero β the magnetic lines of force in the fringe field lie in planes perpendicular to the tilted poleface, so that B_z can be further resolved into components B_s and B_r, where s is the direction normal to the poleface (Figure 2.11c). The vertical motion is determined by the x component of Newtons' second law :

$$F_x = \frac{d}{dt}(m\dot{x}) = e\,r\,\dot{\theta}\,B_r \qquad \text{(see 2.4.1)}$$

Figure 2.11a Fringe Field In The Vertical (z-x) Plane At Exit Face

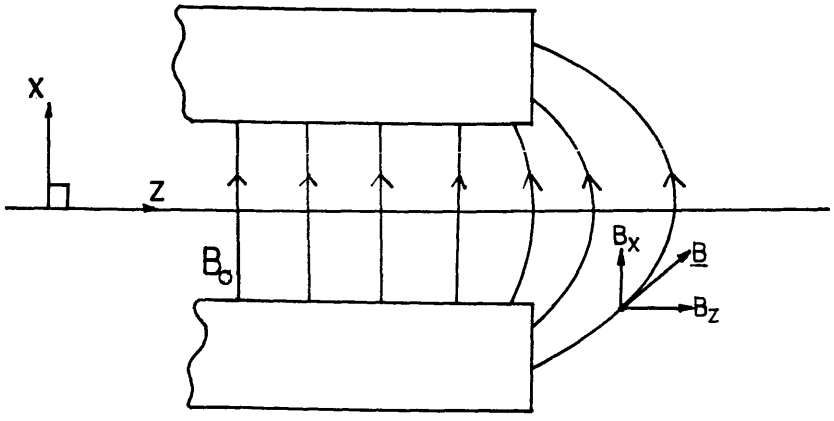

Figure 2.11b Fringe Field At Exit Face Of Magnet With No Poleface Rotation

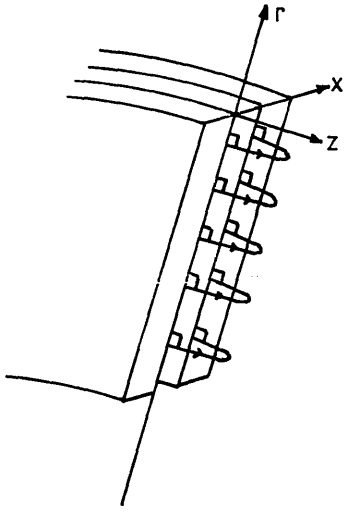

Figure 2.11c Fringe Field In Median Plane Of Magnet With Rotated Poleface

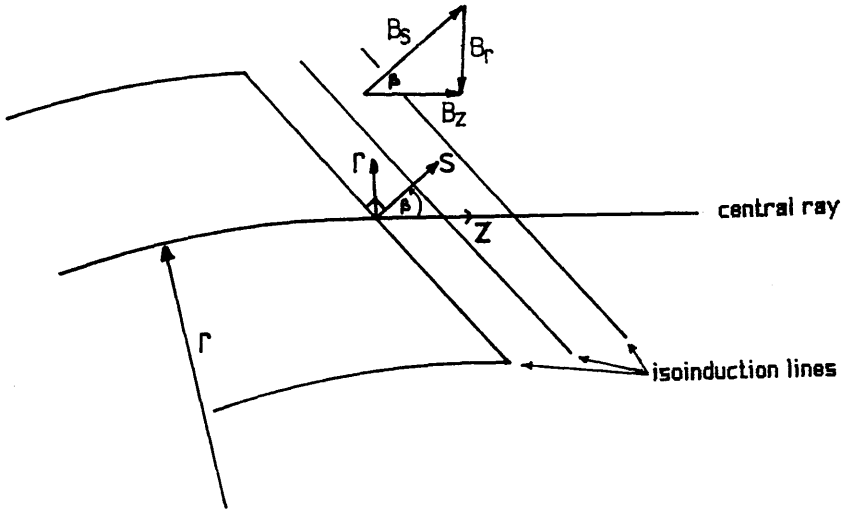

Now since the motion is mainly in the z direction $v \sim r\, d\theta/dt$ so :

$$\ddot{x} = \frac{e}{m} v\, B_r$$

Remembering that :

$$B_0 = -\frac{m v}{e R}$$

gives :

$$\ddot{x} = -\frac{B_r}{B_0}\frac{v^2}{R}$$

and eliminating the time dependence as before gives :

$$\frac{d^2x}{dz^2} = -\frac{B_r}{B_0 R}$$

$$\Delta\left[\frac{dx}{dz}\right] = -\frac{1}{B_0 R}\int_z B_r\, dz \qquad (2.28a)$$

B_r can be found from Maxwells' equation Curl $\underline{B} = 0$ which gives :

$$\frac{\partial B_r}{\partial x} = \frac{\partial B_x}{\partial r}$$

$$\frac{\partial}{\partial x}\int B_r\, dz = \frac{\partial}{\partial r}\int B_x\, dz \qquad \text{and from Fig.2.10c}$$

$$\int B_x\, dz \sim y_0 B_0 \tan\alpha = (r - R) B_0 \tan\alpha$$

$$\frac{\partial}{\partial r}(r - R) B_0 \tan\alpha = B_0 \tan\alpha$$

to first order. It is now possible to write :

$$\frac{\partial}{\partial x}\int B_r\, dz = B_0 \tan\alpha$$

$$\int B_r\, dz = x B_0 \tan\alpha + C$$

The field symmetry about the median plane means that at $x = 0$ (i.e. on the median plane) the component B_r must be zero so that the constant $C = 0$. Now using equation (2.28a) :

$$\Delta\left[\frac{dx}{dz}\right] = -\frac{1}{B_0 R} B_0 x \tan\alpha$$

$$\Delta[x'] = -\frac{x \tan\alpha}{R} \qquad (2.28b)$$

This shows that the tilted entrance face behaves like a thin lens, which is focussing when $\alpha > 0$ and defocussing when $\alpha < 0$ - the opposite to the horizontal plane case. The effect of the exit angle β is identical. The total transfer matrix for vertical plane focussing is found by multiplying equation (2.23) by the appropriate thin lens matrices :

$$\begin{bmatrix} \frac{x_1}{R} \\ x_1' \end{bmatrix} = \begin{bmatrix} 1 & 0 \\ -\tan\beta & 1 \end{bmatrix} \begin{bmatrix} 1 & \Phi \\ 0 & 1 \end{bmatrix} \begin{bmatrix} 1 & 0 \\ -\tan\alpha & 1 \end{bmatrix} \begin{bmatrix} \frac{x_0}{R} \\ x_0' \end{bmatrix}$$

$$\begin{bmatrix} \frac{x_1}{R} \\ x_1' \end{bmatrix} = \begin{bmatrix} 1-\Phi\tan\alpha & \Phi \\ -\tan\alpha-\tan\beta+\Phi\tan\alpha\tan\beta & 1-\Phi\tan\beta \end{bmatrix} \begin{bmatrix} \frac{x_0}{R} \\ x_0' \end{bmatrix} \qquad (2.29)$$

Note that the tilted polefaces correspond to the introduction of a quadrupole component to the entrance field (see chapter 4).

2.6 THE EFFECTS OF EXTENDED FRINGING FIELDS

All of the first order calculations in the previous sections assumed that the electron beam moves from a field free region to a region of constant field B_0 over a very short distance. In this way the effects of tilting the polefaces could be examined by considering the equivalent thin lens properties. These calculations are known as SCOFF (sharp cut off fringing field) calculations. In this type of calculation the effect of the fringing field is approximated by displacing the magnetic field boundary from the poleface edge. There are empirical methods for determining the approximate distance between the polepiece edge and the effective field boundary, but the essential thing about SCOFF calculations is that the transition from constant field to zero field is considered to occur over a vanishingly small distance. This is, of course, only an approximation as real sector magnets have fringe fields where $\underline{B}$ rises

from zero to its constant value over a considerable distance - comparable to the polepiece gap. The influence of this extended fringing field (EFF) upon the optical properties of the sector is not negligible and must be considered in any accurate design.

2.6.1 Field curves and semiempirical approximations

The shape and extent of the fringing field depends upon the geometry of the sector in question, the shape and position of the field producing coils, and the presence of any external field clamping devices. As such it is obvious that to develop a general theory to cover all possible situations would be very difficult; consequently semiempirical methods of calculation are usually adopted. Figure 2.12 shows a typical fringing field curve plotted against s', the distance from the pole edges in units of the gap width D. The field $B_{x,0}$ is the x component of the magnetic field measured in the median plane normal to the polepiece boundary and midway between the corners of the polepieces. Enge [1967] provides an analytical expression for this type of curve :

$$h(s) = B_{x,0} / B_0 = 1 / (1 + \exp(S)) \qquad (2.31)$$

where :

$$S = c_0 + c_1 s + c_2 s^2 + c_3 s^3 \qquad (2.32)$$

The constants c_n have to be determined for each particular case. The variable s in equation (2.31) is again the distance along the normal in units of D, but the origin for s has been placed at the 'virtual field boundary' (vfb) i.e. the point where :

$$\int_0^{vfb} B_{x,0}(\text{SCOFF})\, ds' = \int_0^{\infty} B_{x,0}(\text{EFF})\, ds'$$

(Figure 2.12). This means that the pole edges are at negative s. The ratio $B_{x,0} / B_0$ can be expressed by a function h(s) where :

$$\lim_{s \to \infty} h(s) = 0 \quad \text{and} \quad \lim_{s \to -\infty} h(s) = 1$$

$$\text{i.e.} \int_{-s_1}^{\infty} h(s)\, ds \sim s_1 \quad \text{for large } s_1$$

This means that the angle of deflection of particles going through this fringing field is nearly identical to that of a SCOFF field terminating at s=0. Off the median plane, the x component of the field is modified, and there will also be a y and z component. Figure 2.13 defines the coordinate systems. The dimensionless coordinate s is found by noting :

Figure 2.12 Example Fringe Field Curve Taken From Enge [1967]

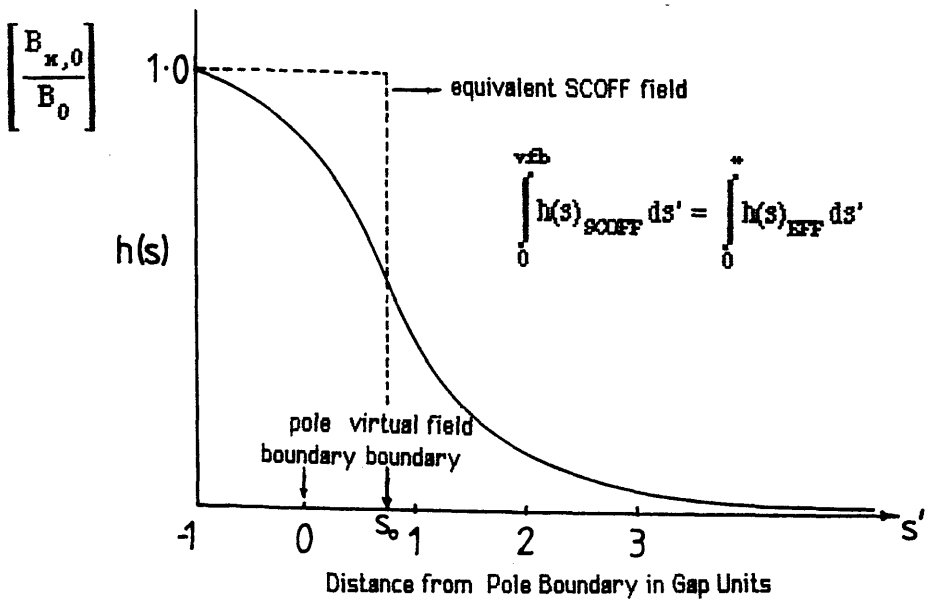

Figure 2.13 Coordinate Systems For EFF Calculations After Enge [1967]

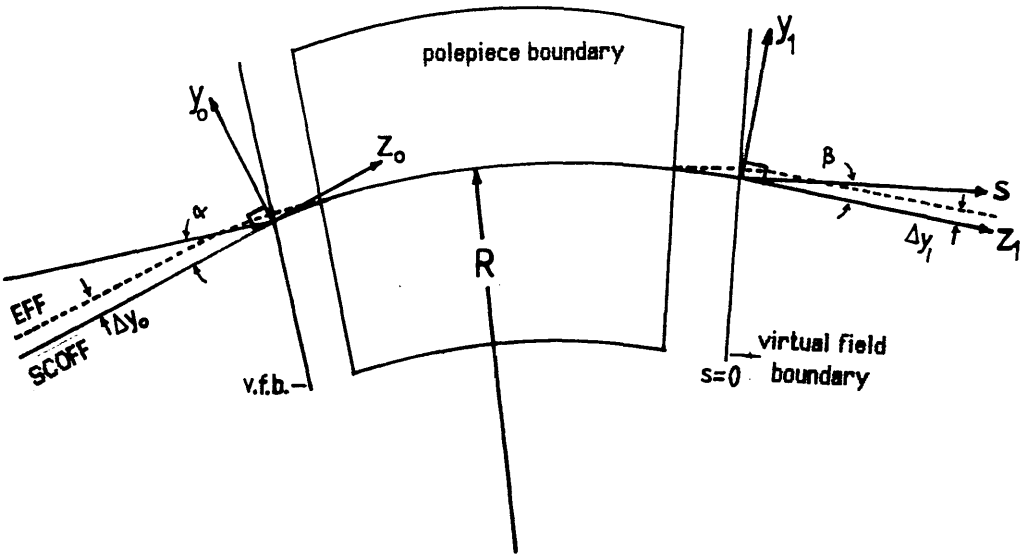

Figure 2.14 Defining Angle γ Between Velocity Vector And Normal To The Field Boundary

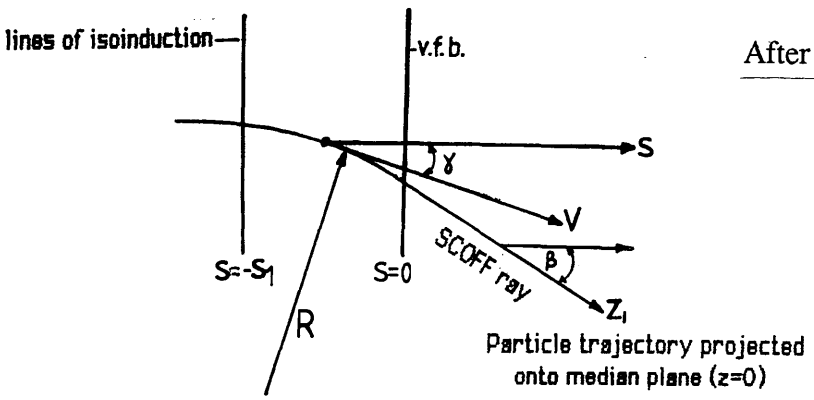

After Enge [1967]

$$z\cos\beta + y\sin\beta = \left[\frac{z^2}{Ds} + \frac{y^2}{Ds}\right]$$

$$(Ds)^2 = z^2 + y^2$$

$$\frac{z\cos\beta + y\sin\beta}{D} = s$$

in the exit coordinate system (subscripts 1 have been dropped). Off the median plane, the field components can be expressed in the form of a Taylor series in x. Symmetry conditions imply that $B_x(x) = B_x(-x)$, so the expansion for B_x can contain only even powers of x (Figure 2.11a). Similarly $B_y(x) = -B_y(-x)$ and $B_z(x) = -B_z(-x)$ so that B_y and B_z expansions contain only odd powers of x. To first order :

$$B_x = B_{x,0} \qquad (2.33a)$$

$$B_z = x\left[\frac{\partial B_z}{\partial x}\right]_{x=0} \qquad (2.33b)$$

$$B_z = x\left[\frac{\partial B_{x,0}}{\partial z}\right] \qquad (2.33c)$$

where (2.33c) is obtained from (2.33b) using curl $\underline{B}$=0. From the definition of h(s) :

$$B_{x,0} = B_0 h(s)$$

$$\frac{\partial B_{x,0}}{\partial z} = B_0 \frac{dh(s)}{ds}\frac{ds}{dz}$$

$$B_z = x B_0 \frac{dh(s)}{ds}\frac{\cos\beta}{D} \qquad (2.34)$$

where B_z was obtained using equation (2.33c). In a similar manner it can be shown that :

$$B_y = \frac{x}{D} B_0 \sin\beta \frac{dh(s)}{ds} \qquad (2.35)$$

2.6.2 Calculation of trajectories (median plane)

For the purposes of calculation it can be assumed that the EFF trajectory well inside the magnet coincides with that of the SCOFF central ray which is a circle segment inside the virtual field boundaries (Figure 2.13) and straight lines, tangents to the circle, outside these boundaries. The radius of curvature in the EFF fringing field is larger than that for the

SCOFF case (as $B_{x,0}(EFF) < B_0$ for $s > 0$), so the real (EFF) trajectory will start to diverge from the SCOFF line when the field begins to decrease (exit side). It will still be curving towards the SCOFF ray after the virtual field boundary and will eventually leave the fringing field parallel to the SCOFF ray, as both particles will have traversed the same field integral. The entrance trajectories obey similar restrictions. Since, to first order, the ray gradients remain unchanged the only effect to calculate is the entrance and exit displacements Δy_0 and Δy_1. Field symmetry about the median plane implies that any differences between median plane motion and motion in any y-z plane off the median plane must be of second and higher even orders in x. Such factors can be neglected at present by assuming that x=0 always. Now on the median plane :

$$F_y = e v_z B_x = m \frac{d^2 y}{dt^2}$$

eliminating the time dependence gives:

$$v_z^2 \frac{d^2 y}{dz^2} = \frac{e v_z}{m} B_x$$

writing :

$$\frac{m v^2}{R} = - e v B_0$$

it is possible to write $v \sim v_z$ as the motion under consideration is very largely in the z direction. Substituting this expression in above gives :

$$\frac{d^2 y}{dz^2} = \frac{e B_x}{- e R B_0} = - \frac{h}{R} \qquad (2.36)$$

From equation (2.31) h is a function of s and :

$$dz = \frac{D}{\cos\beta} ds \qquad (2.37)$$

so integrating (2.36) gives :

$$\int_{-s_1}^{s} \frac{d^2 y}{dz^2} dz = - \int_{-s_1}^{s} \frac{h(s)}{R} \frac{D}{\cos\beta} ds$$

$$\left.\frac{dy}{dz}\right|_s - \left.\frac{dy}{dz}\right|_{-s_1} = - \frac{D}{R \cos\beta} \int_{-s_1}^{s} h(s) ds$$

where the gradient dy/dz at $-s_1$ is the slope of both the EFF and SCOFF trajectories at the position $s = -s_1$, inside the magnet where the rays coincide. The SCOFF fringing field function can be written as :

$$h_0(s) = 1 \qquad \text{for } s < 0$$

$$h_0(s) = 0 \qquad \text{for } s > 0$$

and the difference in slopes between the EFF and SCOFF rays is :

$$\left[\frac{dy}{dz}\right]_{EFF} - \left[\frac{dy}{dz}\right]_{SCOFF} = -\frac{D}{R\cos\beta}\int_{-s_1}^{s}(h_0 - h)\,ds$$

and remembering that :

$$\int_{-s_1}^{\infty} h(s)\,ds = s_1$$

it is obvious that for $s = \infty$ the difference in slope is zero. Integrating again :

$$\int_{-s_1}^{s} dz \int_{-s_1}^{s} \frac{d^2y}{dz^2} dz = \int_{-s_1}^{s}\left[\frac{-D}{R\cos\beta}\int_{-s_1}^{s} h(s)\,ds\right]dz$$

$$y\,|_s - y\,|_{s_1} = \frac{D^2}{R\cos^2\beta}\int_{-s_1}^{s} ds \int_{-s_1}^{s}(h_0 - h)\,ds$$

substituting for dz. The left hand term $y_{|s1}$ is the position of both the EFF and SCOFF trajectories at $s = -s_1$. The difference in position between the EFF and SCOFF rays after they have passed through the fringing field is :

$$y_{EFF} - y_{SCOFF} = \frac{D^2}{R\cos^2\beta} I_1 = \Delta y_1 \quad \text{where :}$$

$$I_1 = \int_{-s_1}^{\infty} ds \int_{-s_1}^{s}(h_0 - h)\,ds$$

Similarly at the entrance :

$$\Delta y_0 = \frac{D^2 I_1}{R \cos^2\alpha}$$

The integral I_1 should be obtained experimentally for each sector under consideration. Enge[1967] gives some values for typical sector designs of the order of 0.4 - 0.9. The effect of the extended fringing field on the horizontal plane focussing is to produce a zeroth order (i.e. independent of y,z,y',z',δ) displacement to the beam. Thus, if the sector is aligned with respect to this new centre line all the first order horizontal plane matrix coefficients calculated before are valid.

2.6.3 Vertical (x) plane motion

Vertical focussing effects occur because of the existence of a component of B_y in the fringing field, i.e. the region where dh/ds is non-zero. The focussing force is proportional to (dh/ds)tan γ where γ is the angle between the normal to the field boundary and the velocity vector of the particle (Figure 2.14). Therefore the focussing forces are largest in the region where dh/ds is greatest. The SCOFF approximation has h(s) as a step like function at the virtual field boundary, so dh/ds is non-zero over a very localised region. For the SCOFF exit fringing field $\gamma = \beta$ in the region of maximum dh/ds - i.e. the virtual field boundary (Figure 2.13). The extended fringing field is different, however, as when the particle passes through maximum dh/ds it has not yet experienced the full angle of deflection, so that $\gamma < \beta$ and consequently the focussing force is less. There is no change to first order in the exit coordinates for the EFF and SCOFF rays in the vertical plane if the fringe field is still considered to be a thin lens for z focussing (see section 2.6.4). Let γ describe the direction of the beam as projected down on the median plane, and z describe the length of path along this projection (Figure 2.14). Consider a particle moving parallel to the median plane outside the exit field i.e. at $z = \infty$, $x = x_1$, $dx/dz = 0$. Equations (2.36) and (2.37) can be rewritten as :

$$\frac{d\gamma}{dz} = -\frac{h(s)}{R}$$

$$dz = \left[\frac{D}{\cos\gamma}\right] ds$$

Integrate this last equation once through the fringe field region :

$$\int_s^\infty \cos\gamma \, d\gamma = -\frac{D}{R} \int_s^\infty h(s) \, ds$$

Now for $s = \infty$, $\gamma = \beta$ so :

$$\sin\gamma = \sin\beta - \frac{D}{R} \int_s^\infty h(s) \, ds \qquad (2.37a)$$

Replace β by γ in equation (2.35) to give :

$$B_y = \frac{x}{D} B_0 \sin\gamma \frac{dh}{ds}$$

Newtons' Law for motion in the x direction is :

$$v_z^2 m \frac{d^2x}{dz^2} = -\frac{e v_z B_0 x}{mD} \sin\gamma \frac{dh}{ds}$$

Now substitute $mv_z \sim mv = -e B_0 R$:

$$\frac{d^2x}{dz^2} = \frac{x}{DR} \sin\gamma \frac{dh}{ds}$$

and integrating this expression through the fringing field using the previous expression for dz :

$$\frac{dx}{dz} = \int_s^\infty \frac{x}{R} \tan\gamma \, dh \qquad (2.38)$$

solve this by successive approximation by writing $x = x_1$ and $\gamma = \beta$ at large s :

$$\int_s^\infty dx = \int_s^\infty \frac{D}{\cos\beta} ds \int_s^\infty \frac{x_1}{R} \tan\beta \, dh$$

$$x_1 - x = x_1 \frac{D}{R} \frac{\tan\beta}{\cos\beta} \int_s^\infty h \, ds$$

$$x = x_1 \left[1 - \frac{D \tan\beta}{R \cos\beta} \int_s^\infty h \, ds \right]$$

Substitute this expression into (2.38) together with an expression for tan γ obtained from equation (2.37a) :

$$\tan\gamma = \tan\beta - \frac{1}{\cos^3\beta}\left[\frac{D}{R}\int_s^\infty h\,ds\right]$$

$$\frac{dx}{dz} = \frac{x_1}{R}\int_s^\infty\left[1 - \frac{D\tan B}{R\cos\beta}\int_s^\infty h\,ds\right]\left[\tan\beta - \frac{D}{R\cos^3\beta}\int_s^\infty h\,ds\right]$$

and it can be shown that the total change in slope through the exit fringing field is :

$$\Delta\left[\frac{dx}{dz}\right] = -\frac{x_1}{R}\left[\tan\beta - \frac{D}{R}\left[\frac{1+\sin^2\beta}{\cos^3\beta}\right]\int_{-s_1}^\infty dh\int_s^\infty h\,ds\right]$$

to first order. The reduction in vertical focussing implied by the above equation is small when D/R is small, and can be expressed as a decrease in the exit angle β so that the effective exit angle is written as :

$$\tan\beta_v = \tan\beta - \frac{D\,I_2\,(1+\sin^2\beta)}{R\cos^3\beta}$$

where I_2 is given by :

$$I_2 = \int_{-s_1}^\infty dh\int_s^\infty h\,ds$$

Assuming that the fractional term above is small it is possible to simplify the equation to :

$$\beta_v = \beta - \frac{D\,I_2\,(1+\sin^2\beta)}{R\cos\beta} \qquad (2.39)$$

and similarly for the entrance side :

$$\alpha_v = \alpha - \frac{D\,I_2\,(1+\sin^2\alpha)}{R\cos\alpha} \qquad (2.40)$$

The reduction in vertical focussing is accounted for if the poleface rotation angles α and β in the vertical transfer matrix are replaced by the effective angles α_v and β_v.

2.6.4 Fringe field clamping

The previous section provides integral expressions for the effective entrance and exit angles α, β which are used to account for the loss in vertical focussing caused by the presence of extended fringing fields. Enge[1964] has calculated values of the integrals I_1 and I_2 pertaining to specific pole geometries and coil arrangements. However, it is clear that precise determination of the position of the virtual field boundaries and evaluations of the integral equations (2.39),(2.40) for an arbitrary design requires experimental measurement of the fringe field component $B_{x,0}$. Another problem is that realistic fringe fields have a long tail at low field strength which extends far out from the magnet. The vertical focussing occurs through the action of the component of B_y in the fringing field (section 2.6.3) and from equation (2.35) B_y is proportional to dh(s)/ds. Thus, if dh(s)/ds is non-zero over an extended region then so is B_y and the fringe field cannot be considered to act as a thin lens for vertical focussing. To overcome these problems it has become common practice to employ a technique known as 'field clamping' first developed in high energy physics. The clamp is a piece of high permeability material placed near the edge of the magnet with a hole to allow passage of the beam (Figure 2.15a). Such a clamp behaves as a 'magnetic short circuit' and acts to terminate the fringe field in a shorter distance. Figure 2.15b illustrates the action of the field clamp in 'collecting' field lines. As can be seen from figure 2.15b the clamp tends to extract field lines from the pole gap and the field strength between the poles falls off earlier causing the virtual field boundary to move closer to the mechanical boundary.

Investigations of the design of field clamps have been carried out with reference to sector magnets used in particle accelerators by many authors, including Hübner and Wollnik [1970]. Generally, it must be pointed out that many of the factors considered in these papers are concerned with saturation effects due to the high magnetic fields used in these machines (i.e. ~ 10000 gauss). Some designers, such as Crewe et al. [1971] and Egerton [1980], have applied these designs directly to EELS spectrometers, even following the high energy practice of rounding the edges of the sector polefaces. It has been shown by Braams [1964] that this practice causes the field inside the magnet to fall off even sooner. The theory is that by constructing the correct curvature [Steffen 1965] the virtual field boundary can be made coincident with the mechanical boundary thus simplifying the calculations. In practice the required hyperbolic surface is approximated by a 45^o taper of the pole edges. There are two objections to this:

1) By reducing the field in the gap the integral I_2 is increased and h(s) is made to vary over a

Figure 2.15a Magnetic Fringe Field Clamp (After Heighway)

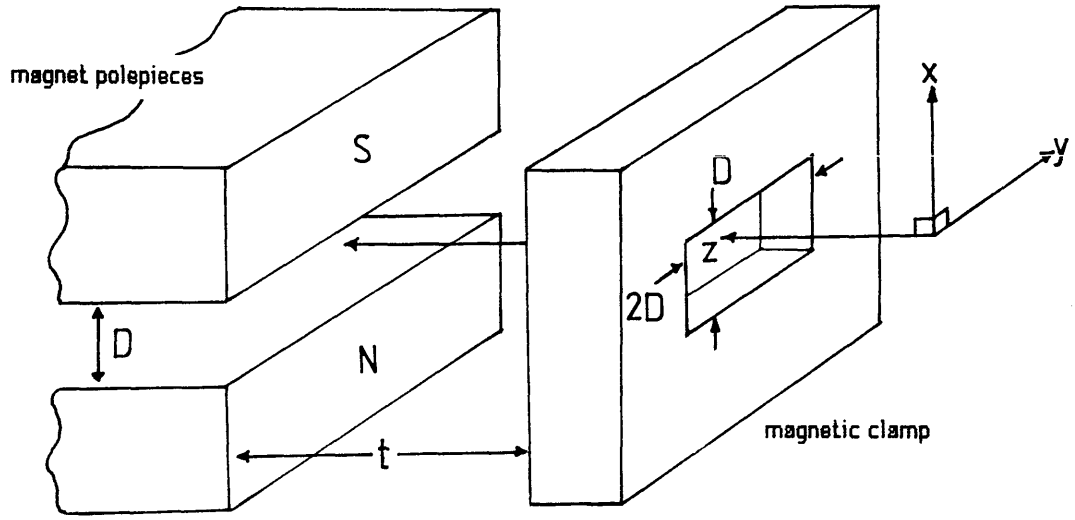

Figure 2.15b Action Of Fringe Field Clamp (After Hubner And Wollnik)

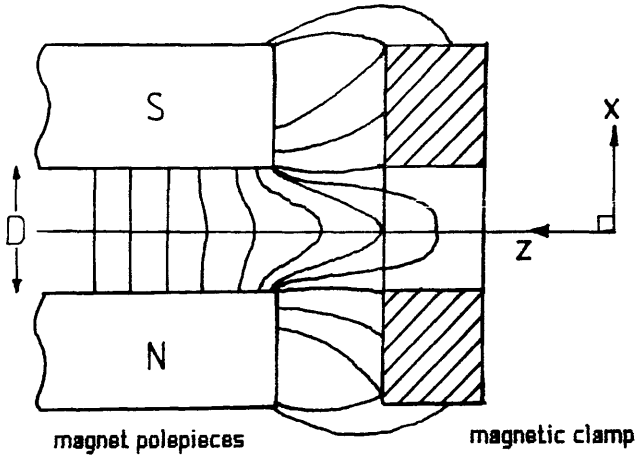

larger distance - thus violating the thin lens criterion of the fringe field calculations.

2) Secondly, the original purpose of rounding the polefaces was to remove edge effects whereby the shape of the fringe field was altered by local saturation near the sharp edge of the pole corner [Braams 1964]. It is true that these local saturations occur at fields very much smaller than that required to saturate the main body of the spectrometer, but even so they are very unlikely to occur in microscopy where the main field is so weak (~100 gauss). Also it is not clear that replacing one 90^{o} edge with two 45^{o} corners gives much improvement.

2.6.5 Empirical methods for determining fringe field integrals.

Heighway [1975] has provided semiempirical expressions for evaluating fringe field effects in clamped dipole magnets with pole gap to bending radius ratios $D/R \leq 0.55$ and poleface rotations $-45^{o} \leq \alpha \leq 45^{o}$. The geometry of the clamp is as shown in Figure 15a. Integral equations (2.39)and (2.40) are replaced by:

$$\beta_v = \beta - C\,k\,\frac{D}{R}\,\frac{(1+\sin^2\beta)}{\cos\beta} \qquad (2.41)$$

with a similar expression for α_v. The coefficient k replaces the integral I_2 of Enge and the coefficient C is a correction factor. Both C and k are experimentally determined parametric functions of β, D/R, and t/D where t is the clamp to poleface distance. Heighway gives the expression for k as:

$$k = 0.1326 + 0.0842\left[\frac{t}{D}\right] + 0.00805\left[\frac{t}{D}\right]^2 \qquad (2.42)$$

The equivalent expression for the correction coefficient C has eighteen terms, which are listed in the above reference, however the value of C is of the order unity. The location of the virtual field boundary is described by:

$$\frac{e}{D} = \left[0.386 + 0.324\left[\frac{D}{R_n}\right]\right]\left[\frac{t}{D}\right] - \left[0.0455 + 0.0930\left[\frac{D}{R_n}\right]\right]\left[\frac{t}{D}\right]^2 \qquad (2.43)$$

where R_n is the radius of curvature of the poleface. In the case of the straight edge magnets considered up to now $R_n \rightarrow \infty$. For the curved faces described in section 2.7.2 the field clamp is curved also, so that its center of curvature coincides with that of the poleface.

The above equations were derived using sector magnet fields varying between 8000 and 15000 gauss. How well they apply to the low field conditions of EELS is open to question,

however several successful spectrometers have been designed using these results [Shuman 1980, Scheinfein and Isaacson 1984].

2.7 SECOND ORDER COEFFICIENTS.

The previous sections have derived expressions for the first order focussing coefficients including the effects of tilted polefaces and extended fringe fields. The remaining thirty second order coefficients in equations (2.14 a-d) must now be considered. There are twelve median plane coefficients (i.e. independent of x and x'), and eighteen others concerned with motion off the median plane. A brief outline of the calculations will be given in the next sections, based on the derivations of Brown [1964] and Enge [1967].

2.7.1 Median plane coefficients of second order

These coefficients can most readily be derived from geometrical considerations. Figure 2.16 shows the trajectory of the central ray in the median plane of a sector magnet with no rotation of the polefaces. Also shown is an arbitrary ray, A with entrance coordinates (y_1, y_1', δ). It is assumed that the trajectory of the central ray is an arc of radius R centre O, and the trajectory of the arbitrary ray is also an arc, of radius $R(1+\delta)$ (see equation (2.24)) centre P. In the following calculations all quantities y, y', δ are considered small as before. It is convenient to replace the ray gradient y' used in the previous sections with an equivalent small angle θ and use the relation $y' = \tan\theta \sim \theta$. The bend radius R is normalised to unity for convenience. Applying the sine rule to triangles OPQ and OPR gives:

$$\frac{1+y_1}{\sin(\omega+\theta_1)} = \frac{a}{\sin\theta_1} = \frac{1+\delta}{\sin\omega} \qquad (2.44a)$$

$$\frac{1+y_2}{\sin(\omega-\phi+\theta_2)} = \frac{1+\delta}{\sin(\omega-\phi)} = \frac{a}{\sin\theta_2} \qquad (2.44b)$$

Solving these equations together with expressions obtained using the cosine rule:

$$[a]^2 = (1+\delta)^2 + (1+y_1)^2 - 2(1+\delta)(1+y_1)\cos\theta_1 \qquad (2.44c)$$

$$\cos\omega = \frac{(1+\delta)^2 - (1+y_1)^2 - a^2}{-2a(1+x_1)} \qquad (2.44d)$$

gives the required expressions for y_2 and θ_2 to second order in the terms y_1, θ_1, and δ.

Figure 2.16 Simple Magnetic Sector Magnet

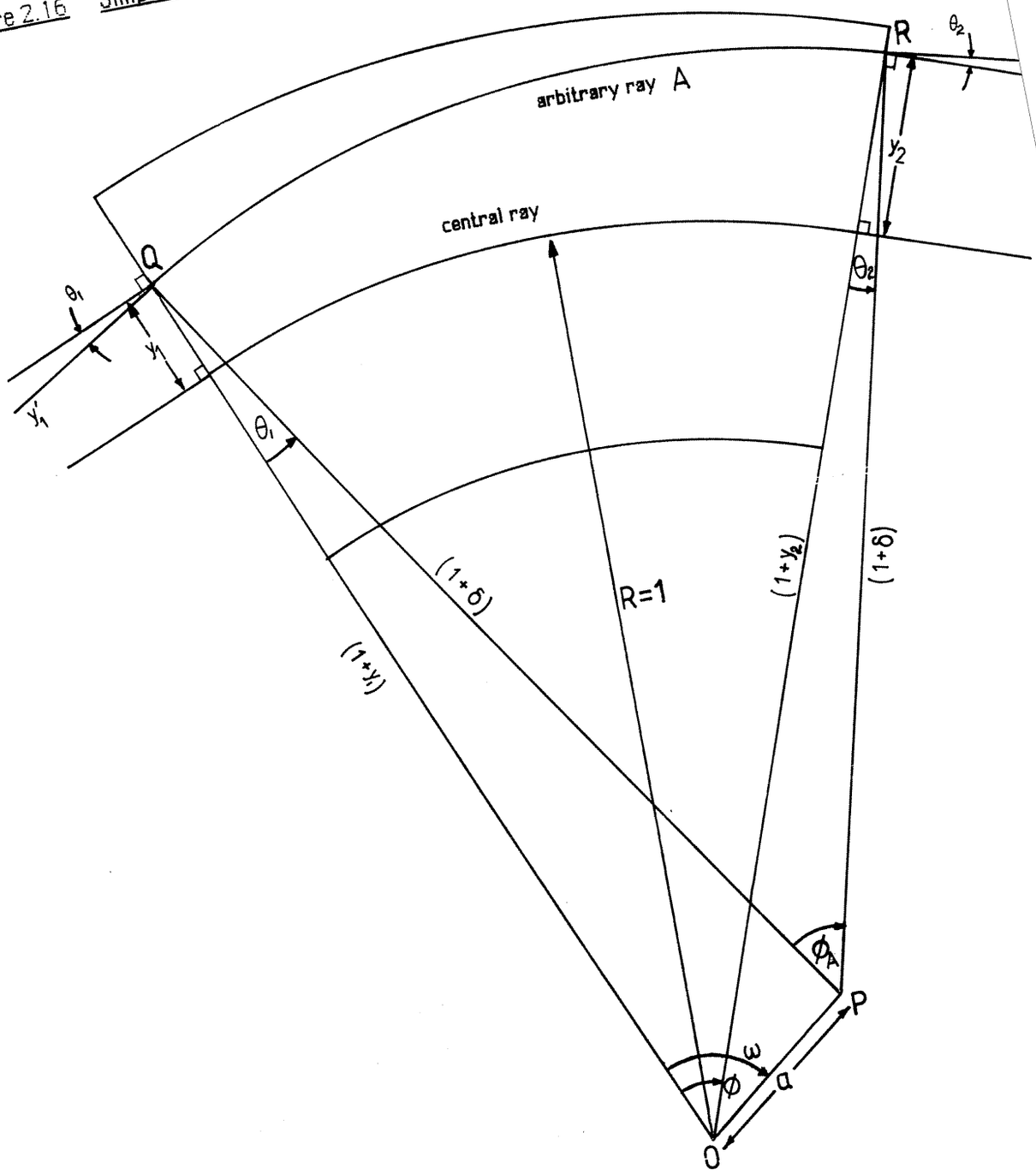

$$y_2 = y_1 \cos\phi + \theta_1 \sin\phi + \delta(1 - \cos\phi) - \frac{1}{2} y_1^2 \sin^2\phi + \frac{1}{2}\theta^2 \cos\phi (1 - \cos\phi)$$

$$- \frac{1}{2}\delta^2 \sin^2\phi + y_1 \theta \sin\phi \cos\phi + y_1 \delta \sin^2\phi + \theta\delta \sin\phi (1 - \cos\phi) \quad (2.45a)$$

$$\theta_2 = - y_1 \sin\phi + \theta_1 \cos\phi + \delta \sin\phi - \frac{1}{2}\theta_1^2 \sin\phi - \delta^2 \sin\phi + y_1 \delta \sin\phi \quad (2.45b)$$

The three remaining focussing coefficients y_1^2, $y_1\theta$, and $\theta\delta$ in the expansion for θ_2 are all identically zero. The above equations (2.45a,b) describe the first and second order optical properties in the median plane of the simple magnet shown in figure 2.16. Note that the first order coefficients are the same as those in equation (2.25).

2.7.2 Coefficients of General Sector Magnets.

As described before the provision of a vertical focus requires that the polefaces of figure 2.16 be rotated at angles α and β. This modifies some of the first order median plane coefficients (see equation (2.27)) and the second order coefficients derived above will also be changed. In order to obtain the best performance from a spectrometer, it is desirable to have some degree of control over the magnitude of the second order focussing coefficients (see chapter 3). This can be done either by placing multipole corrector lenses before and after the magnet [Tang 1981] or by curving the poleface boundaries to the appropriate arcs of circles [Kerwin 1949]. Figure 2.17a depicts the entrance side of such a magnet. The input face is rotated at an angle α to provide vertical focussing and has a radius of curvature R_1 which is defined as positive as shown. The centre of curvature is at point (Z_{c1}, Y_{c1}). The Y axis is coincident with the poleface of the equivalent straight edge sector with no poleface tilt (Figure 2.16.).

The modified first and second order median plane coefficients can be derived by calculating a transformation which transforms the initial conditions (y,θ,δ) of a ray entering the magnet of figure 2.17a at position (y_0,θ_0) to an equivalent input condition (y_1,θ_1) which results in the ray following an identical trajectory inside the magnet of figure 2.16 (see Figure 2.17b.). A similar approach calculates the transformation at the output face (Figure 2.17c.). Here the problem is to transform from coordinates (y_2,θ_2) for a ray exiting from the magnet of Figure 2.16 to the coordinates (y_3,θ_3) corresponding to the actual exit conditions as shown. Combining the three solutions gives the first and second order median plane focussing coefficients for an arbitrary sector magnet with curved and rotated polefaces.

2.7.3 Entrance and exit transformations.

Figure 2.17a shows an arbitrary ray intersecting the curved poleface at position (Z_A, Y_A).

Figure 2.17a Geometry Of Curved And Rotated Entrance Face

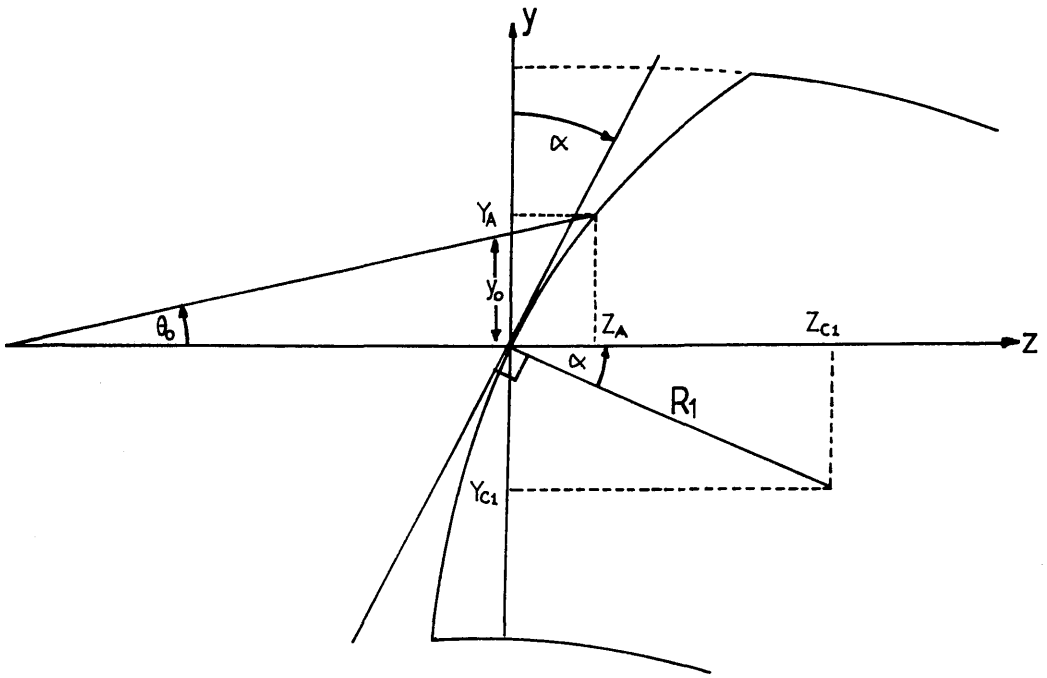

Figure 2.17b Transform From Straight Entrance Face To Curved Face

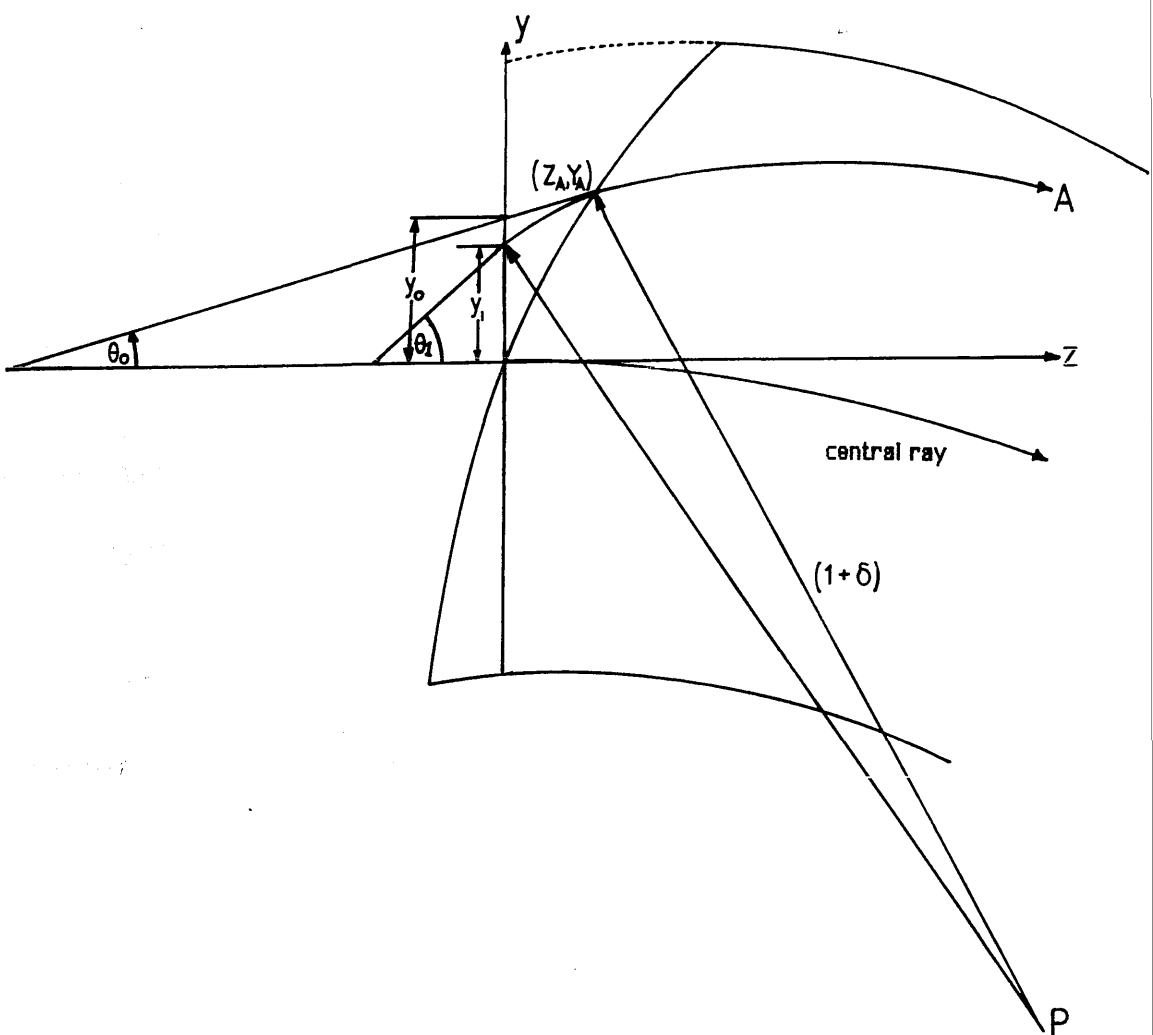

The linear equation of the trajectory before it crosses the magnet boundary is :

$$y = z\,\theta_0 + y_0 \qquad \text{(for small } \theta_0\text{)} \tag{2.46}$$

The equation of the poleface is:

$$(y + R_1 \sin\alpha)^2 + (z - R_1 \cos\alpha)^2 = R_1^2 \tag{2.47}$$

The simultaneous solution of (2.46) and (2.47) gives the intersection point (Z_A, Y_A). The equation of the circular trajectory A inside the magnet is :

$$\left[y - (Y_A - (1+\delta)\cos\theta_0)\right]^2 + \left[z - (Z_A + (1+\delta)\sin\theta_0)\right]^2 = \left[1+\delta\right]^2 \tag{2.48}$$

i.e. a circle of radius $(1+\delta)$ intersecting the poleface at (Z_A, Y_A). Solving equation (2.48) for y at z=0 gives the expansion for y_1 in terms of Y_A, Z_A, δ and θ_0. Substitution of the equations for Y_A and Z_A obtained from the simultaneous solution of (2.46) and (2.47) gives the required expansion for y_1 in terms of y_0, θ_0 and δ. The expansion for θ_1 can be obtained in a similar manner using $\tan\theta_1 = dz/dx$ at z=0. The results are:

$$y_1 = y_0 - \frac{1}{2} y_0^2 \tan^2\alpha \tag{2.49a}$$

$$\theta_1 = y_0\tan\alpha + \theta_0 + \frac{1}{2}\left[\frac{y_0^2}{R_1}\right]\sec^3\alpha + y_0\theta_0\tan^2\alpha - y_0\delta\tan\alpha \tag{2.49b}$$

Similarly for the exit side (Figs. 2.17c, 2.17d), the equations to be solved are:

$$y_3 = Y_B - Z_B\,\theta_3 \tag{2.50a}$$

$$(z + R_2\cos\beta)^2 + (y + R_2\sin\beta)^2 = R_2^2 \tag{2.50b}$$

$$(z - (1+\delta)\sin\theta_2)^2 + (y - (y_2 - (1+\delta)\cos\theta_2))^2 = (1+\delta)^2 \tag{2.50c}$$

The solutions are:

$$y_3 = y_2 + \frac{1}{2} y_2^2 \tan^2\beta \tag{2.51a}$$

$$\theta_3 = y_2\tan\beta + \theta_2 - \frac{1}{2} y_2^2\tan^3\beta + \frac{1}{2}\left[\frac{y_2^2}{R_2}\right]\sec^3\beta - y_2\theta_2\tan^2\beta - y_2\delta\tan\beta \tag{2.51b}$$

Three transformations have been derived:

$$y_1 = y_1(x_0,\theta_0,\delta) \qquad \theta_1 = \theta_1(x_0,\theta_0,\delta)$$
$$y_2 = y_2(x_0,\theta_0,\delta) \qquad \theta_2 = \theta_2(x_0,\theta_0,\delta)$$
$$y_3 = y_3(x_0,\theta_0,\delta) \qquad \theta_3 = \theta_3(x_0,\theta_0,\delta)$$

Figure 2.17c Geometry Of Curved And Rotated Exit Face

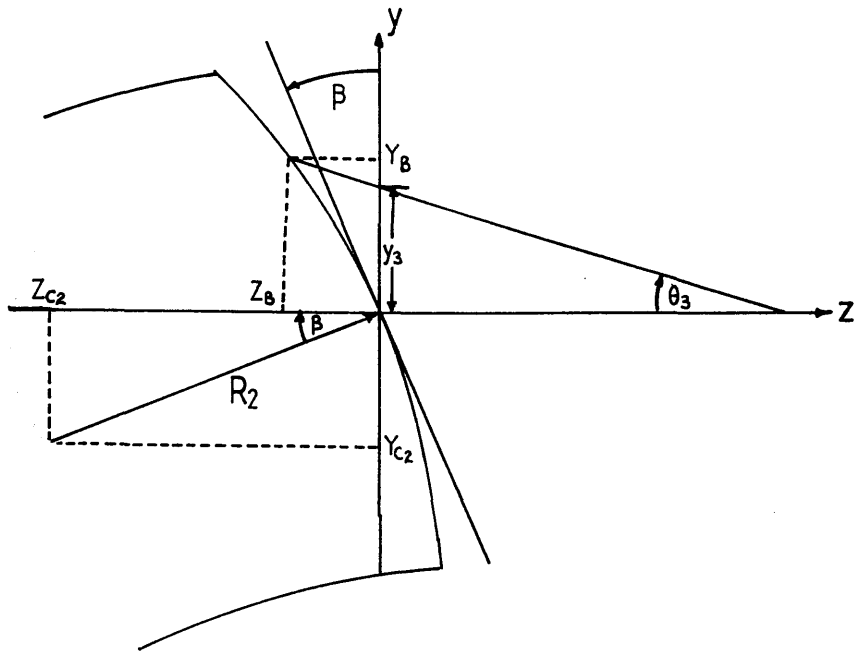

Figure 2.17d Transform From Straight Exit Face To Curved Exit Face

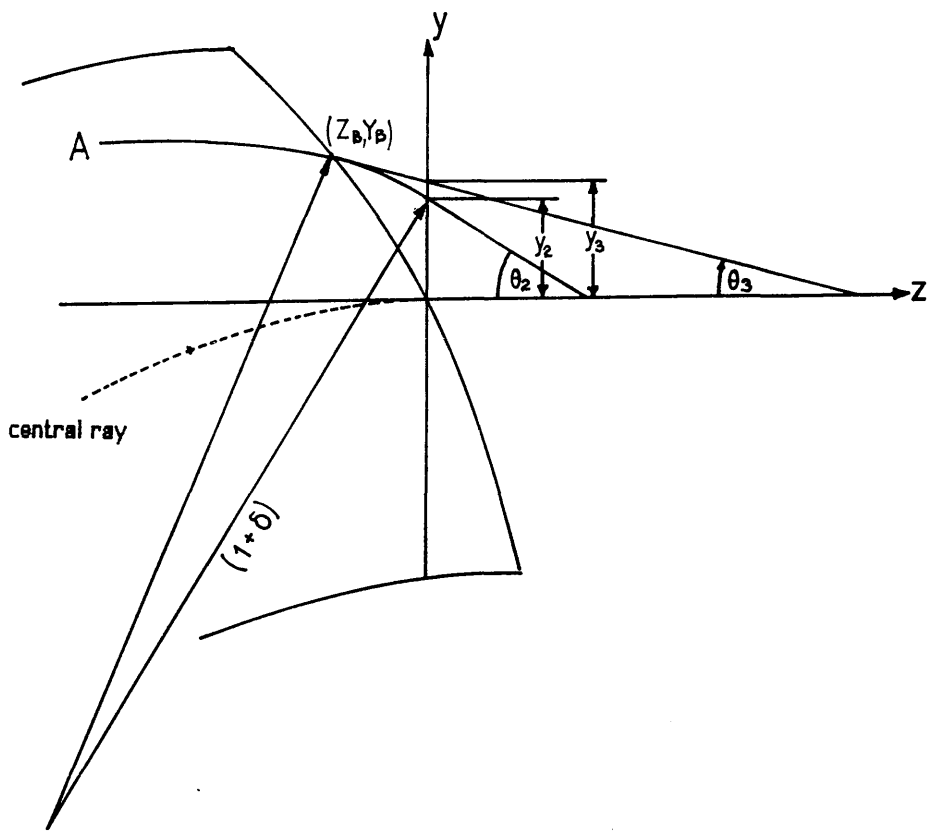

The required transform is:

$$y_3 = y\ (x_0,\theta_0,\delta) \qquad \theta_3 = \theta\ (x_0,\theta_0,\delta)$$

which is obtained by the following procedure - substitute equations (2.49a,b) into equations (2.45a,b) giving y_2, θ_2 in terms of y_0 and θ_0. Substitution of the resultant expressions into equations (2.51a,b) provides the complete first and second order median plane focussing coefficients as listed in appendix 1. The first order coefficients are identical to those given in equation (2.27) for a straight edge sector with poleface tilts α and β. This implies that curvature of the polefaces does not alter the first order focussing properties of the magnet-an important property for correction of second order aberrations.

2.7.4 Cross terms affecting median plane focussing

As shown in section 2.3.2 motions in the median and vertical planes are independent to first order. This is not the case for second order terms of the type (y_1/x_0^2), $(y_1/x_0'^2)$, (y_1'/x_0x_0') etc. seen in equations (2.14a,b). The effect of these terms is to introduce changes in the y position and slope of a ray at the exit of the magnet due to variations in the x position and slope at the entrance . There are three perturbations to be considered:

1) The x component of the magnetic field off the median plane (B_x)is not the same as the x component on the median plane ($B_{x,0}$) in the fringe field zones.

2) The coupling between the vertical velocity v_x and the horizontal component of the magnetic field B_z which appears off the median plane in the fringe field zones.

3) The reduction in median plane velocity v_z in the whole magnet when the particle has an x component of velocity.

The first effect was mentioned in section (2.6.2) and is shown in figure 2.11a. The component of the Lorentz force involved was written in section (2.6.2) as:

$$F_y = e\, v_z B_x$$

It is necessary to modify the Taylor expansion for B_x (eqn.(2.33a)) to include the second order effects due to motion in y-z planes off the median plane. This is done by adding another term to equation (2.33a):

$$B_x = B_{x,0} + \frac{x^2}{2!}\frac{\partial^2 B_{x,0}}{\partial x^2} \qquad (2.52)$$

The last term in equation (2.52)produces second order perturbations in the velocity and displacement of the particle in the y direction. The corresponding expressions for the changes in gradient and position of the entrance and exit rays- $\Delta(dy/dx)_1$, $\Delta(dy/dz)_2$, Δy_1 and Δy_2 are given in Enge [1967].

To consider the second effect figure 2.11a. shows that a horizontal component of the magnetic field B_Z appears off the median plane in the fringe field zones. This component couples with the vertical velocity v_X giving an acceleration in the y direction caused by the force $-ev_xB_z$. The equation of motion is :

$$v_z^2 \frac{d^2y}{dz^2} = -\frac{e}{m} v_x B_z$$

where from equation (2.34):

$$B_z = \frac{x}{D} B_0 \cos\beta \frac{dh(s)}{ds}$$

The solution of the above two equations gives the resulting changes in gradient in the fringe field zones - $\Delta(dy/dz)_1$ and $\Delta(dy/dz)_2$ caused by this effect. There are no contributions to the second order term for Δy.

For the third case, the calculations of previous sections have assumed that the particle velocity $v\,(x,y,z) \sim v_z$. When the particle has an x component of velocity, the projected velocity on the median plane is:

$$v_m = v\,(1 - x_i'^2)^{\frac{1}{2}} \sim v\,(1 - \frac{x_i'^2}{2})$$

where x_i' is the vertical slope measured inside the magnet i.e. from equation (2.28a):

$$x_i' = x_1' - [(x_1 \tan\alpha) / R]$$

where x_1 and x_1' are the vertical plane entrance coordinates. The equation for v_m shows that the particle has a reduced median plane velocity throughout the whole magnet. The corresponding effect on the y direction slope and position at the exit is the same as if the particle had a reduced momentum with $\Delta p/p = \delta = -x_i'^2/2$. The perturbations are simply:

$$\Delta y_2' = -\left[\frac{y'}{\delta}\right]\frac{x_i^{\,2}}{2} = -\left[\frac{y'}{\delta}\right]\left[\frac{x_i'^2}{2} - \frac{x_1 x_1'}{R}\tan\alpha + \frac{x_1^2\tan^2\alpha}{2R^2}\right]$$

$$\frac{\Delta y_2}{R} = -\left[\frac{y}{\delta}\right]\frac{x_i^{\,2}}{2} = -\left[\frac{y}{\delta}\right]\left[\frac{x_i'^2}{2} - \frac{x_1 x_1'}{R}\tan\alpha + \frac{x_1^2\tan^2\alpha}{2R^2}\right]$$

The total effects on y displacement and slope at the exit are found by combining the effects from the above three causes in the appropriate manner to yield the six second order median plane cross coefficients $(y/x^2),(y/xx'),(y/x'^2),(y'/x^2),(y'/xx'),(y'/x'^2)$ as given in appendix 1.

2.7.5 Second order effects on vertical focussing.

The second order coefficients for vertical focussing can be found by a matrix calculation similar to equation (2.29). Referring to figure 18 the angle of deflection ϕ_A for the arbitrary ray A can be found by noting that:

$$(\omega - \phi) = 180^o - (\phi_A + \chi + y_2')$$

where

$$\chi = 180^o - (y_1' + \omega)$$

Solution of the above two equations gives:

$$\phi_A = \phi + y_1' - y_2'$$

Figure 19 shows the arbitrary ray A at the entrance face. The effective entrance angle α_A for this ray is:

$$\alpha_A = y_1' + \theta_A = y_1' + \alpha + \sigma$$

Now $R_1\sigma \sim x$ so :

$$\sigma \sim y_1/R_1\cos\alpha \quad \text{and} \quad \alpha_A = \alpha + y_1' + (y_1/R_1\cos\alpha)$$

Similarly:

$$\beta_A = \beta - y_2' + (y_2/R_2\cos\beta)$$

The effective vertical plane lens strength at the entrance is from equation (2.28b):

$$\frac{1}{f_1} = \frac{\tan\alpha_A}{R(1+\delta)} \sim \frac{1}{R}\tan\left[\alpha + y_1' + \frac{y_1}{R_1\cos\alpha}\right](1-\delta)$$

Figure 2.18 Aid For Calculation Of Second Order Vertical Focussing

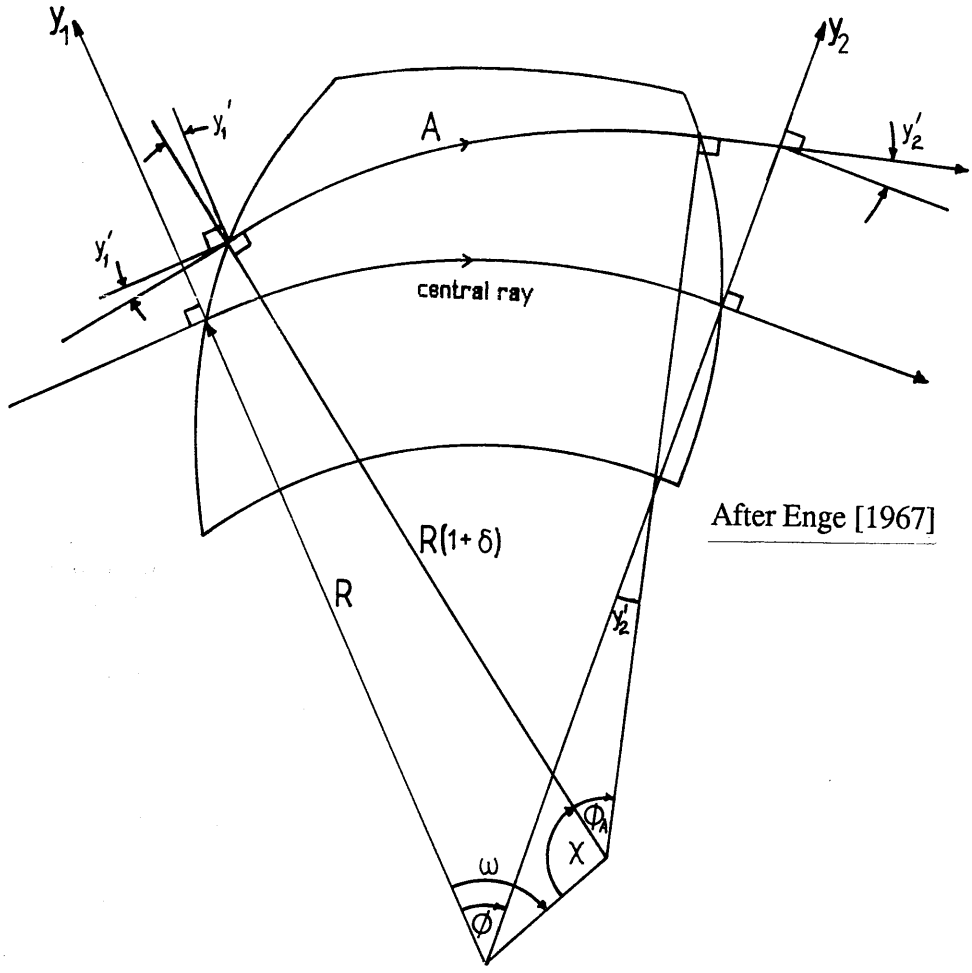

After Enge [1967]

Figure 2.19 Calculating Effective Entrance Angle Of An Arbitrary Ray

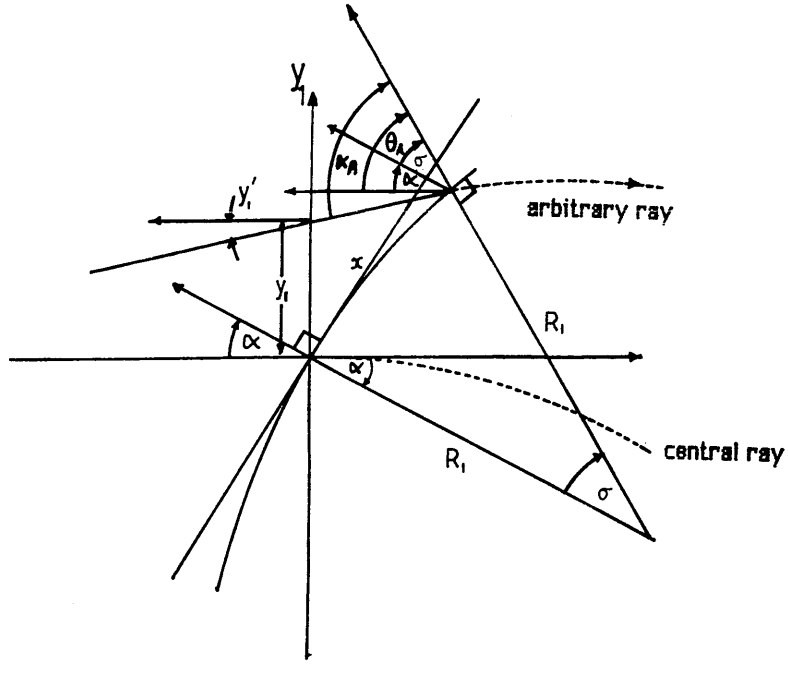

The tangent in the above equation can be expanded in a Taylor series about α to give:

$$\frac{1}{f_1} = \frac{1}{R}\left[\tan\alpha + \frac{1}{\cos^2\alpha}\left[y_1' + \frac{y_1}{R_1\cos\alpha}\right]\right](1-\delta)$$

$$= \frac{1}{R}\left[\tan\alpha + \frac{y_1'}{\cos^2\alpha} + \frac{y_1}{R_1\cos^3\alpha} - \delta\tan\alpha\right]$$

Similarly for the exit side:

$$\frac{1}{f_2} = \frac{\tan\beta_A}{R(1+\delta)} \sim \frac{1}{R}\left[\tan\beta - \frac{y_2'}{\cos^2\beta} + \frac{y_2}{R_2\cos^3\beta} - \delta\tan\beta\right]$$

The arc length of trajectory A between the polefaces is:

$$L = R(1+\delta)(\phi + y_1' - y_2') \sim R(\phi + y_1' - y_2' + \phi\delta)$$

There are also small flight paths between the y axes and the pole boundaries (Figure 2.19). For small displacements y_1 and small angles y_1' these approximate to $y_1\tan\alpha$ and $y_2\tan\beta$ so that the complete matrix equation for the x direction motion is therefore:

$$\begin{bmatrix} x_1 \\ x_1' \end{bmatrix} = \begin{bmatrix} 1 & y_2\tan\beta \\ 0 & 1 \end{bmatrix}\begin{bmatrix} 1 & 0 \\ \frac{1}{f_2} & 1 \end{bmatrix}\begin{bmatrix} 1 & L \\ 0 & 1 \end{bmatrix}\begin{bmatrix} 1 & 0 \\ \frac{1}{f_1} & 1 \end{bmatrix}\begin{bmatrix} 1 & y_1\tan\alpha \\ 0 & 1 \end{bmatrix}\begin{bmatrix} x_0 \\ x_0' \end{bmatrix}$$

Multiplying this equation out and retaining only first and second order terms gives the twelve second order coefficients for vertical focussing given in appendix 1.

2.7.6 Second order effects of extended fringe fields

The preceding second order calculations take no account of any second order effects of extended fringe fields. Enge [1967] has calculated the magnitude of these effects by comparing the results from ray tracing computer calculations using an extended fringe field with those obtained using a very sharp cutoff fringe field (D/R = 0.04). The latter results compared well with coefficients calculated analytically using the expressions in appendix 1 as should be expected. Enge showed that changes (in going from SCOFF to EFF calculations) in the second order median plane coefficients were small. However changes in the second order cross terms and some of the second order vertical terms were of the same order of magnitude as those of the first order coefficients for z direction focussing, i.e. of the order

(D/R).

In an attempt to improve the accuracy of the cross terms (which are more important than the vertical plane coefficients from the point of view of energy resolution) the values of α and β used in section 2.7.4. can be replaced by the effective entrance angles for vertical focussing α_V and β_V [Shuman 1980]. Clearly for magnets with extended fringe fields (large pole gap to bend radius ratio) the second order vertical plane coefficients will be in error by some amount of the order of D/R. In practice the second order error introduced by the fringe fields will be dominated by machining and alignment tolerances, inhomogeneity of the iron polepieces and the effects of third and higher order aberrations. For these reasons most spectrometer designs utilise external multipole corrector lenses for trimming the residual aberrations of the sector.

CHAPTER 3

Calculation of Spectrometer Aberration Coefficients

Introduction

The previous chapter introduced the matrix multiplication method for calculating the optical properties of beam transport systems and the first and second order focussing coefficients for a general homogeneous field magnetic sector spectrometer were derived. This chapter shows how the spectrometer aberration coefficients, and hence the optical properties, are generated from the resulting transfer matrices. The influence of each aberration coefficient upon the electron intensity distribution at the dispersion plane is discussed with particular regard to parallel detection. As explained in the previous chapter it is possible to correct for some of the second order median plane aberrations by choosing appropriate curvatures for the entrance and exit polefaces. It is shown by reference to calculations for two such second order corrected designs [Scheinfein and Isaacson 1984, Shuman 1980] that the effect of the uncorrected vertical plane aberrations must be considered in any parallel detection system.

3.1 EXPANSION OF TRANSFER MATRICES TO SECOND ORDER

The first order median plane and vertical plane transfer matrices developed in the previous chapter (equations 2.15 and 2.16) can be expanded to second order to include the focussing coefficients derived in section 2.7. The complete second order median plane transfer matrix is of order 12 (i.e. 12 x12 coefficients) and the complete vertical transfer matrix is of order 8. Equations (3.1) and (3.2) show the median and vertical plane matrices respectively. The focussing coefficients are written in the abbreviated Taylor notation - the analytical expressions for each coefficient are listed in appendix 1.

3.1.1 The transfer matrix coefficients

Equations (3.1) and (3.2) show the transfer matrices divided into four quadrants. The top left hand quadrant contains the first order focussing coefficients which are independent in the median and vertical planes, and the top right hand quadrant contains the second order coefficients. The bottom left hand quadrant is uniformly zero and the bottom right hand quadrant contains coefficients which are products of the first order terms. These terms are necessary if the calculation involves more than one focussing element, and describe the coupling of aberrations through the system. The derivation of these terms is very straightforward. For example, the second order component $(y_1 y_1'/R)$ is found by

multiplying together the expansions for the first order quantities y_1/R and y_1'.

$$\left[\frac{y_1}{R}\, y_1'\right] = \left[\left[\frac{y}{y}\right]\frac{y_0}{R} + \left[\frac{y}{y'}\right] y_0' + \left[\frac{y}{\delta}\right]\delta + {}^{2^{nd}\text{order}}_{\text{terms}}\right]\left[\left[\frac{y'}{y}\right]\frac{y_0}{R} + \left[\frac{y'}{y'}\right] y_0' + \left[\frac{y'}{\delta}\right]\delta + {}^{2^{nd}\text{order}}_{\text{terms}}\right]$$

Multiplying this equation out and excluding all terms higher than second order yields the sixth row of the median plane transfer matrix below (equation 3.1).

Equation (3.1) - Second order median plane transfer matrix.

$$\begin{array}{|c|}\frac{y_1}{R}\\ y_1'\\ \delta\\ \frac{y_1^2}{R^2}\\ y_1'^2\\ \frac{y_1}{R}y_1'\\ \frac{y_1}{R}\delta\\ y_1'\delta\\ \delta^2\\ \frac{x_1^2}{R^2}\\ x_1'^2\\ \frac{x_1}{R}x_1'\end{array} = \left|\begin{array}{cccc|cccccccccc} \frac{y}{y} & \frac{y}{y'} & \frac{y}{\delta} & & \frac{y}{y^2} & \frac{y}{y'^2} & \frac{y}{yy'} & \frac{y}{y\delta} & \frac{y}{y'\delta} & \frac{y}{\delta^2} & \frac{y}{x^2} & \frac{y}{x'^2} & \frac{y}{xx'} & \\ \frac{y'}{y} & \frac{y'}{y'} & \frac{y'}{\delta} & & \frac{y'}{y^2} & \frac{y'}{y'^2} & \frac{y'}{yy'} & \frac{y'}{y\delta} & \frac{y'}{y'\delta} & \frac{y'}{\delta^2} & \frac{y'}{x^2} & \frac{y'}{x'^2} & \frac{y'}{xx'} & \\ 0 & 0 & 1 & & 0 & 0 & 0 & 0 & 0 & 0 & 0 & 0 & 0 & \\ \hline 0 & 0 & 0 & & \frac{yy}{yy} & \frac{yy}{y'y'} & \frac{yy}{yy'} & \frac{yy}{y\delta} & \frac{yy}{y'\delta} & \frac{yy}{\delta\delta} & 0 & 0 & 0 & \\ 0 & 0 & 0 & & \frac{y'y'}{yy} & \frac{y'y'}{y'y'} & \frac{y'y'}{yy'} & \frac{y'y'}{y\delta} & \frac{y'y'}{y'\delta} & \frac{y'y'}{\delta\delta} & 0 & 0 & 0 & \\ 0 & 0 & 0 & & \frac{yy'}{yy} & \frac{yy'}{y'y'} & \frac{yy'}{yy'} & \frac{yy'}{y\delta} & \frac{yy'}{y'\delta} & \frac{yy'}{\delta\delta} & 0 & 0 & 0 & \\ 0 & 0 & 0 & & 0 & 0 & 0 & \frac{y}{y} & \frac{y}{y'} & \frac{y}{\delta} & 0 & 0 & 0 & \\ & & & & & & & \text{etc} & & & & & & \\ & & & & & & & & & & & & & \\ & & & & & & & & & & & & & \\ & & & & & & & & & & & & & \\ & & & & & & & & & & & & & \end{array}\right| \begin{array}{|c|}\frac{y_0}{R}\\ y_0'\\ \delta\\ \frac{y_0^2}{R^2}\\ y_0'^2\\ \frac{y_0}{R}y_0'\\ \frac{y_0}{R}\delta\\ y_1'\delta\\ \delta^2\\ \frac{x_0^2}{R^2}\\ x_0'^2\\ \frac{x_0}{R}x_0\end{array}$$

The second order vertical transfer matrix is constructed in a similar way :

Equation (3.2) - Second order vertical plane transfer matrix.

$$\begin{vmatrix} \frac{x_1}{R} \\ x_1' \\ \frac{x_1 y_1}{R^2} \\ \frac{x_1}{R} y_1' \\ x_1' \frac{y_1}{R} \\ x_1' y_1' \\ \frac{x_1}{R}\delta \\ x_1'\delta \end{vmatrix} = \left[\begin{array}{cc|cccccc} \frac{x}{x} & \frac{x}{x'} & \frac{x}{xy} & \frac{x}{xy'} & \frac{x}{x'y} & \frac{x}{x'y'} & \frac{x}{x\delta} & \frac{x}{x'\delta} \\ \frac{x'}{x} & \frac{x'}{x'} & \frac{x'}{xy} & \frac{x'}{xy'} & \frac{x'}{x'y} & \frac{x'}{x'y'} & \frac{x'}{x\delta} & \frac{x'}{x'\delta} \\ \hline 0 & 0 & \frac{xy}{xy} & \frac{xy}{xy'} & \frac{xy}{x'y} & \frac{xy}{x'y'} & \frac{xy}{x\delta} & \frac{xy}{x'\delta} \\ 0 & 0 & \frac{xy'}{xy} & \frac{xy'}{xy'} & \frac{xy'}{x'y} & \frac{xy'}{x'y'} & \frac{xy'}{x\delta} & \frac{xy'}{x'\delta} \\ 0 & 0 & \frac{x'y}{xy} & \frac{x'y}{xy'} & \frac{x'y}{x'y} & \frac{x'y}{x'y'} & \frac{x'y}{x\delta} & \frac{x'y}{x'\delta} \\ 0 & 0 & \frac{x'y'}{xy} & \frac{x'y'}{xy'} & \frac{x'y'}{x'y} & \frac{x'y'}{x'y'} & \frac{x'y'}{x\delta} & \frac{x'y'}{x'\delta} \\ 0 & 0 & 0 & 0 & 0 & 0 & \frac{x}{x} & \frac{x}{x'} \\ 0 & 0 & 0 & 0 & 0 & 0 & \frac{x'}{x} & \frac{x'}{x'} \end{array}\right] \begin{vmatrix} \frac{x_0}{R} \\ x_0' \\ \frac{x_0 y_0}{R^2} \\ \frac{x_0}{R} y_0' \\ x_0' \frac{y_0}{R} \\ x_0' y_0' \\ \frac{x_0}{R}\delta \\ x_0'\delta \end{vmatrix}$$

The quantities of most interest in many calculations are the first order positions and slopes y_1/R, x_1/R, y_1', x_1' at the exit of the spectrometer. Thus in many simple cases it is sufficient to work with only the first two quadrants of the above transfer matrices-the extra terms in the fourth quadrant are unnecessary.

3.1.2 Second order drift matrices.

The optical properties of an arbitrary homogeneous field magnetic sector spectrometer can be derived by multiplying the above transfer matrices by the appropriate drift matrices. In order to do this the first order transfer matrices for a drift space, developed in section 2.2.1, must also be expanded to second order. The complete median plane and vertical plane transfer matrices for a drift space are given in equations (3.3) and (3.4). As before the matrices are divided into four quadrants. The top left hand quadrants contain the first order terms and are identical to the first order matrices of section 2.2.1. The top right hand quadrants are

identically zero, as there are no second order contributions to the trajectory of a ray in a drift space. The lower left hand quadrants are zero as before and the bottom right hand quadrant is obtained by multiplication of the appropriate first order terms exactly as described previously.

Equation (3.3) - Second order transfer matrix of a horizontal plane drift space.

$$
\begin{vmatrix} y_1 \\ y'_1 \\ \delta \\ y_1^2 \\ y_1'^2 \\ y_1 y'_1 \\ y_1 \delta \\ y'_1 \delta \\ \delta^2 \\ x_1^2 \\ x_1'^2 \\ x_1 x'_1 \end{vmatrix} =
\left|\begin{array}{ccc|cccccccccc}
1 & L & 0 & 0 & 0 & 0 & 0 & 0 & 0 & 0 & 0 & 0 \\
0 & 1 & 0 & 0 & 0 & 0 & 0 & 0 & 0 & 0 & 0 & 0 \\
0 & 0 & 1 & 0 & 0 & 0 & 0 & 0 & 0 & 0 & 0 & 0 \\
\hline
0 & 0 & 0 & 1 & L^2 & 2L & 0 & 0 & 0 & 0 & 0 & 0 \\
0 & 0 & 0 & 0 & 1 & 0 & 0 & 0 & 0 & 0 & 0 & 0 \\
0 & 0 & 0 & 0 & L & 1 & 0 & 0 & 0 & 0 & 0 & 0 \\
0 & 0 & 0 & 0 & 0 & 0 & 1 & L & 0 & 0 & 0 & 0 \\
0 & 0 & 0 & 0 & 0 & 0 & 0 & 1 & 0 & 0 & 0 & 0 \\
0 & 0 & 0 & 0 & 0 & 0 & 0 & 0 & 1 & 0 & 0 & 0 \\
0 & 0 & 0 & 0 & 0 & 0 & 0 & 0 & 0 & 1 & L^2 & 2L \\
0 & 0 & 0 & 0 & 0 & 0 & 0 & 0 & 0 & 0 & 1 & 0 \\
0 & 0 & 0 & 0 & 0 & 0 & 0 & 0 & 0 & 0 & L & 1
\end{array}\right|
\begin{vmatrix} y_0 \\ y'_0 \\ \delta \\ y_1^2 \\ y_0'^2 \\ y_0 y'_0 \\ y_0 \delta \\ y'_0 \delta \\ \delta^2 \\ x_0^2 \\ x_0'^2 \\ x_0 x'_0 \end{vmatrix}
$$

Equation (3.4)- Second order transfer matrix for a vertical plane drift space:

$$\begin{vmatrix} x_1 \\ x_1' \\ x_1 y_1 \\ x_1 y_1' \\ x_1' y_1 \\ x_1' y_1' \\ x_1 \delta \\ x_1' \delta \end{vmatrix} = \left|\begin{array}{cc|cccccc} 1 & L & 0 & 0 & 0 & 0 & 0 & 0 \\ 0 & 1 & 0 & 0 & 0 & 0 & 0 & 0 \\ \hline 0 & 0 & 1 & L & L & L^2 & 0 & 0 \\ 0 & 0 & 0 & 1 & 0 & L & 0 & 0 \\ 0 & 0 & 0 & 0 & 1 & L & 0 & 0 \\ 0 & 0 & 0 & 0 & 0 & 1 & 0 & 0 \\ 0 & 0 & 0 & 0 & 0 & 0 & 1 & L \\ 0 & 0 & 0 & 0 & 0 & 0 & 0 & 1 \end{array}\right| \begin{vmatrix} x_0 \\ x_0' \\ x_0 y_0 \\ x_0 y_0' \\ x_0' y_0 \\ x_0' y_0' \\ x_0 \delta \\ x_0' \delta \end{vmatrix}$$

3.2 TOTAL TRANSFER MATRICES + ABERRATION COEFFICIENTS

Following the simple procedure described in section 2.2 it is possible to obtain the total transfer matrices for an arbitrary homogeneous magnetic sector spectrometer. These are calculated by multiplying the second order transfer matrices (equations 3.1 and 3.2) by the appropriate second order transfer matrices for a drift space (equations 3.3 and 3.4). Referring to figure 3.1 the correct order of multiplication is :

$$\left[T_M \right] = \left[Q_M \right] \left[M \right] \left[P_M \right] \tag{3.5}$$

$$\left[T_V \right] = \left[Q_V \right] \left[V \right] \left[P_V \right] \tag{3.6}$$

Figure 3.1 Definition of Median and Vertical Plane Object and Image Distances

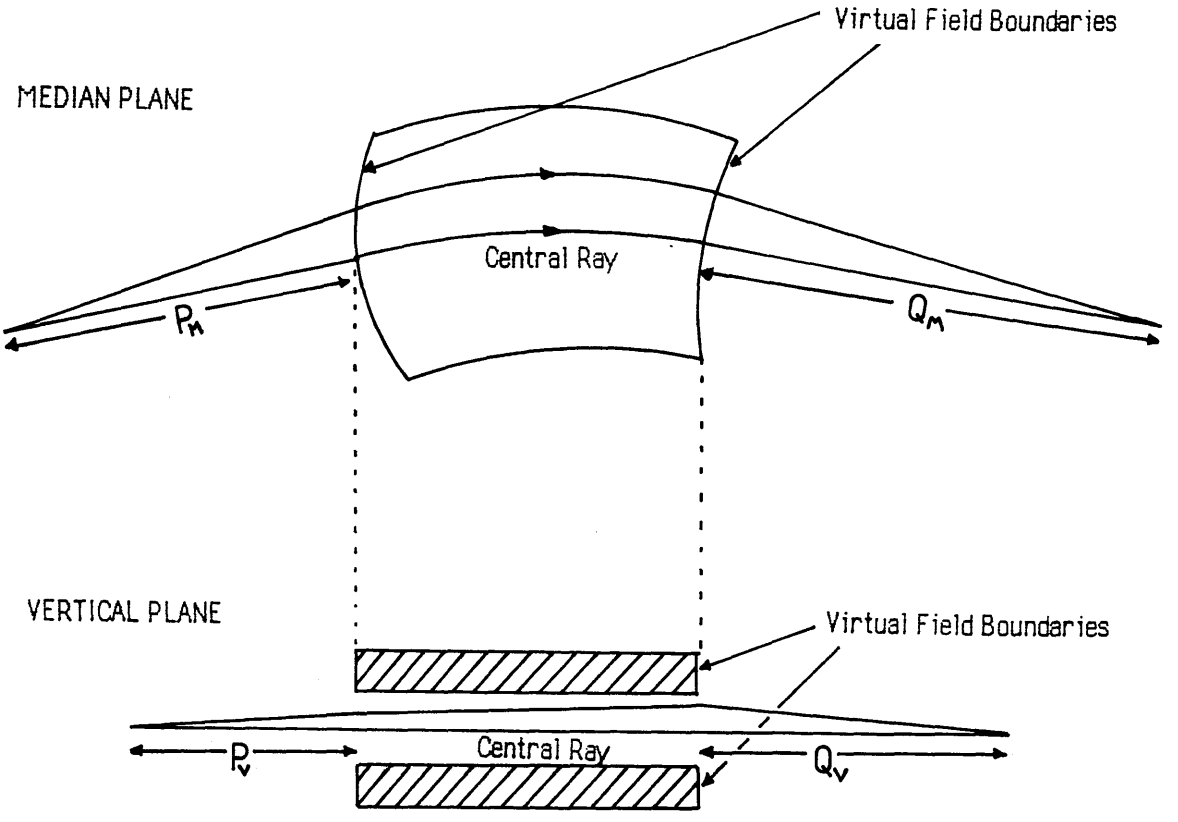

Figure 3.2 Definition of Coordinate Systems

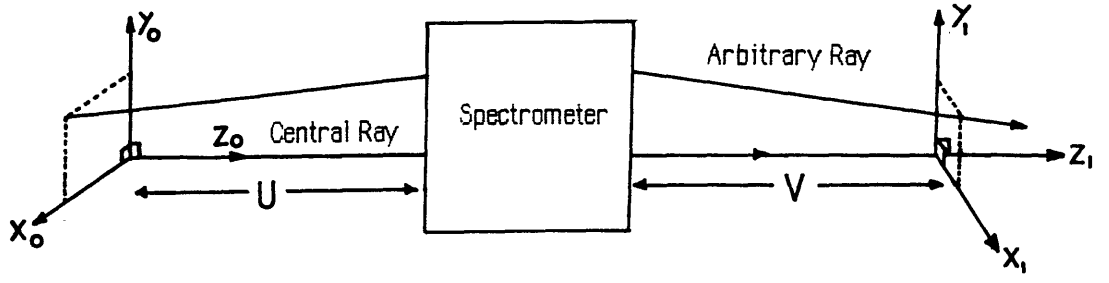

where $[T_M]$ and $[T_V]$ are the total median and vertical plane matrices respectively, and matrices [M] and [V] are the transfer matrices of equations (3.1) and (3.2). $[Q_M]$ is the second order median plane drift matrix for an image distance Q_M and $[P_M]$ is the associated drift matrix for an object distance P_M. $[Q_V]$ and $[P_V]$ are the corresponding drift matrices in the vertical plane (see Figure 3.1). Equations (3.5) and (3.6) describe the optical properties of the spectrometer for given object distances P_M, P_V, and given image distances Q_M, Q_V in the median and vertical planes respectively.

The first order coefficients of the first row of the resulting total transfer matrices $[T_M]$ and $[T_V]$ describe the basic focussing properties of the spectrometer, whereas the second order coefficients in the first row are known as the aberration coefficients - they describe the departures from perfect focussing of trajectories other than that of the central ray. All the aberration coefficients are functions of the object and image distances, as well as the focussing coefficients.

The total transfer matrices are easily calculated but the expressions involved for all the individual elements are lengthy and are not given here. It is sufficient to develop the equations describing the optical properties of an arbitrary spectrometer imaging a point source a distance U (U=P/R) from the entrance face and forming an image at some plane a distance V (V=Q/R) from the exit face. In this case the object and image distances are the same in both planes i.e. $P_M=P_V$ and $Q_M=Q_V$ which is the most common situation in simple systems. The quantities of most interest are the first order positions y_1 and x_1 of a trajectory as it crosses the image plane (Figure 3.2), and also the first order slopes y_1', x_1'.

3.2.1 Aberration equations

The expansions for the first order properties obtained from the first and second quadrants of the total transfer matrices can be written as:

$$y_1/R = Y_0(y_0/R) + Y_1(y_0') + Y_2(\delta) + Y_3(y_0'\delta) + Y_4(y_0')^2 + Y_5(\delta)^2 + Y_6(x_0')^2 + Y_7(y_0/R)^2 + Y_8(y_0y_0'/R) + Y_9(y_0\delta/R) + Y_{10}(x_0/R)^2 + Y_{11}(x_0x_0'/R) \quad (3.7a)$$

$$y_1' = Y_0'(y_0/R) + Y_1'(y_0') + Y_2'(\delta) + \ldots\ldots \quad (3.7b)$$

$$x_1/R = X_0(x_0/R) + X_1(x_0') + X_2(x_0'y_0') + X_3(x_0'\delta) + X_4(x_0y_0/R^2) + X_5(x_0y_0'/R) + X_6(x_0'y_0/R) + X_7(x_0\delta/R) \quad (3.7c)$$

$$x_1' = X_0'(x_0/R) + X_1'(x_0') + X_2'(x_0'y_0') + \ldots\ldots \quad (3.7d)$$

where Y_3-Y_{11} are the median plane aberration coefficients and X_2-X_7 are the vertical plane aberration coefficients. The ordering of the terms has been changed slightly to make the notation consistent with that of Shuman [1980]. Equations (3.7 a-d) above can be simplified in the case of a point source (as in EELS) where all terms containing the quantities y_0 and x_0 must disappear, thus the twelve terms in each of equations (3.7 a,b) are reduced to six terms, and the eight terms of equations (3.7 c,d) are reduced to three. Expressions for the remaining terms in equations (3.7a) and (3.7c), as functions of the focussing coefficients and the normalised object and image distances U and V, are given below along with expressions for the first order Y_0 and X_0 terms. Other elements of the total transfer matrices can readily be deduced from equations (3.5) and (3.6).

$$Y_0 = \frac{y}{y} + \frac{y'}{y}V_M \quad (3.8a)$$

$$Y_1 = \frac{y}{y}U + \frac{y}{y'} + \left[\frac{y'}{y'} + U\frac{y'}{y}\right]V_M \quad (3.8b)$$

$$Y_2 = \frac{y}{\delta} + \frac{y'}{\delta}V_M \quad (3.8c)$$

$$Y_3 = \frac{y}{y\delta}U + \frac{y}{y'\delta} + \left[\frac{y'}{y'\delta} + U\frac{y'}{y\delta}\right]V_M \quad (3.8d)$$

$$Y_4 = \frac{y}{y^2}U^2 + \frac{y}{yy'}U + \frac{y}{y'^2} + \left[\frac{y'}{y'^2} + U\frac{y'}{yy'} + U^2\frac{y'}{y^2}\right]V_M \quad (3.8e)$$

$$Y_5 = \frac{y}{\delta^2} + \frac{y'}{\delta^2}V_M \quad (3.8f)$$

$$Y_6 = \frac{y}{x^2}U^2 + \frac{y}{xx'}U + \frac{y}{x'^2} + \left[\frac{y'}{x'^2} + U\frac{y'}{xx'} + U^2\frac{y'}{x^2}\right]V_M \quad (3.8g)$$

$$X_0 = \frac{x}{x} + \frac{x'}{x} V_M \tag{3.8h}$$

$$X_1 = \frac{x}{x} U + \frac{x}{x'} + \left[\frac{x'}{x'} + U \frac{x'}{x} \right] V_M \tag{3.8i}$$

$$X_2 = \frac{x}{xy} U^2 + \left[\frac{x}{xy'} + \frac{x}{x'y} \right] U + \frac{x}{x'y'} + \left[\frac{x'}{x'y'} + U \left[\frac{x'}{x'y} + \frac{x'}{xy'} \right] + U^2 \frac{x'}{xy} \right] V_M \tag{3.8j}$$

$$X_3 = \frac{x}{x\delta} U + \frac{x}{x'\delta} + \left[\frac{x'}{x'\delta} + U \frac{x'}{x\delta} \right] V_M \tag{3.8k}$$

3.2.2 First order parameters

Reducing equations (3.7a) and (3.7c) to first order gives:

$$\frac{y_1}{R} = Y_0 (y_0/R) + Y_1 (y_0') + Y_2 (\delta) \tag{3.9a}$$

$$\frac{x_1}{R} = X_0 (x_0/R) + X_1 (x_0') \tag{3.9b}$$

The condition for a first order focus in the median plane is clearly $Y_1 = 0$, i.e. the position at which a ray strikes the image plane is independent of its direction when leaving the object. The image plane which satisfies this condition is known as the dispersion plane. From the expression for Y_1 given in equation (3.8b) this occurs at an image distance V_M given by:

$$V_M = -\left[\frac{y}{y} U + \frac{y}{y'} \right] / \left[\frac{y'}{y} U + \frac{y'}{y'} \right] \tag{3.10}$$

For the vertical plane the equivalent expression is obviously $X_1 = 0$. From equation (3.8i):

$$V_V = -\left[\frac{x}{x} U + \frac{x}{x'} \right] / \left[\frac{x'}{x} U + \frac{x'}{x'} \right] \tag{3.10a}$$

In general $V_M \neq V_V$ so that point source is imaged to a line at the dispersion plane, and the system is said to be single focussing. Setting $V_V = V_M = V$ gives a quadratic equation in U which may or may not have any real solutions depending upon the values of the focussing coefficients. If it does then, for that particular object and image plane only, the system is said to be double focussing.

Assuming that a first order focus has been achieved, the median plane magnification is given by the value of Y_0 at $V = V_M$. The appropriate expression for Y_0 is given in equation (3.8a). Similarly, the vertical plane magnification is given by the value of X_0 when $X_1 = 0$ i.e. $V = V_V$. For the condition of a real object and real image the magnifications are always

negative, showing that the image is inverted. In general, the values of Y_0 and X_0 are different for a given focus position, which means that the focussing is not truly stigmatic even when $V_V=V_M$, as the magnifications are different in the median and vertical planes. Such pseudostigmatic imaging is not important in the case of EELs where the object is a point source.

The remaining first order median plane term is Y_2 - the dispersion, defined in section 1.2.2. It is always positive and describes the shift in median plane image position with change in electron momentum. From equation (3.9a):

$$\Delta y_1 = R\, Y_2 \frac{\Delta p}{p_0}$$

where p_0 is the momentum of the central ray. The relativistic kinetic energy of the electron can be written in terms of the momentum as:

$$\frac{\Delta p}{p_0} = \frac{\Delta E}{E_0}\left[\frac{E_0 + m_0c^2}{E_0 + 2m_0c^2}\right]$$

where E_0 is the kinetic energy of the central ray and m_0c^2 is the electron rest mass energy. Substituting this in the above equation gives:

$$\Delta y_1 = R Y_2 \frac{\Delta E}{E_0}\left[\frac{E_0 + m_0c^2}{E_0 + 2m_0c^2}\right] \qquad (3.11)$$

3.2.3 Second order parameters

The reduced forms of equations (3.7a) and (3.7c) for the simplified case of a point source are:

$$y_1/R = Y_1(y_0') + Y_2(\delta) + Y_3(y_0'\delta) + Y_4(y_0')^2 + Y_5(\delta)^2 + Y_6(x_0')^2 \qquad (3.12)$$

$$x_1/R = X_1(x_0') + X_2(x_0'y_0') + X_3(x_0'\delta) \qquad (3.13)$$

The first order terms were discussed in the previous section, but there remain four second order median plane aberrations (Y_3-Y_6) and two second order vertical plane aberrations (X_2,X_3) to be considered. The combined effect of these aberrations is to cause the image of a point source to be broadened and defocussed at the dispersion plane, thus reducing the spectrometer energy resolution.

The most important resolution limiting terms for serial collection are the median plane aberrations Y_4 and Y_6. Expressions for these coefficients are given in equations (3.8e) and (3.8g) respectively. Effectively, these aberrations cause an electron leaving a point object

with slopes (y_0',x_0') to be imaged to a position y_1, in the dispersion plane, different to that of the central ray. In the absence of other aberrations a point source is defocussed into a line image in the dispersion direction. The magnitude of this effect is proportional to the square of the spectrometer acceptance angle, so that for a given energy resolution the magnitudes of Y_4 and Y_6 determine the maximum useful collection angle. It is obvious that similar considerations apply to any parallel recording system.

The aberration term Y_3 (equation 3.8d) introduces a defocus with energy loss in the dispersion direction which is equivalent to tilting the dispersion plane at some angle η to the central ray (see Figure 1.4). This aberration is most important for parallel detection systems for the reason already discussed in chapter 1 - it makes magnification of the dispersion plane very difficult to achieve. In addition, in serial collection systems where the spectrum is scanned across the energy selecting slits by auxiliary coils placed after the spectrometer, Y_3 causes a loss of energy resolution as the spectrum moves away from the central ray. However, if the scanning is done by varying the excitation of the spectrometer then Y_3 has no effect, as in this case δ is effectively zero always.

The remaining median plane aberration term is Y_5 (equation 3.8f), which is the dispersion nonlinearity. This term systematically reduces or increases the dispersion as $|\delta|$ increases, i.e. $\Delta y/\Delta E$ is not constant. Again this aberration is not important in the case of serial collection where the main field is varied; however in the case of parallel detection or post spectrometer scanning in serial detection, the non-linear dispersion could introduce artefacts into the recorded spectrum.

In the vertical plane there are only two second order aberrations to consider. The first is X_2 (equation 3.8j) which is a defocussing term analogous to Y_4 and Y_6. In the absence of other aberrations, this term causes a point source to be imaged to a line perpendicular to the dispersion direction. X_2 is not so important for serial detection as long as the alignment of the energy selecting slits is sufficiently parallel to the direction of defocus, otherwise signal intensity can be lost. If X_2 is very large then the multielement detector used in a parallel recording system will need careful alignment, and also should be wider than the defocus so as not to lose signal.

The last aberration to consider is X_3 (equation 3.8k). This aberration is similar to Y_3 and causes a defocus in the non dispersion plane with energy loss, which is equivalent to tilting the X focal plane. Again X_3 is not so important for serial detection when the spectrometer

main field is varied, but must be considered when post spectrometer scanning is used. As far as parallel collection systems are concerned, large values of X_3 influence the width and shape of the spectrum in the non-dispersion direction, and this must be taken into account in designing a magnification system and also when deciding the geometry of the detector to be used. In any real spectrometer design, all the above aberrations will exist to some degree. The corresponding effect upon the image will be determined by the relative magnitudes and the signs of the various coefficients. As mentioned in the previous chapter, it is possible to provide some limited form of second order aberration correction for the median plane of homogeneous field magnetic sector spectrometers by curving the input and output polefaces to the appropriate shape. This is discussed in the following section.

3.2.4 Aberration correction

For an ideal (to second order) spectrometer all the coefficients in equations (3.12) and (3.13) should be set to zero except Y_2, the first order dispersion. There are altogether eight coefficients to be made zero and eight sector parameters which can be varied - U, V, R, ϕ, α, β, R_1, R_2 and D. Unfortunately the coefficients are not linearly related to the sector parameters and no ideal solutions have yet been found so that compromise solutions have to be adopted. The conditions usually required for serial recording are:

1) First order double focussing ($Y_1 = X_1 = 0$).
   The advantage of this condition is that the detector slit does not have to be carefully aligned with respect to the x axis at the dispersion plane.

2) Second order median plane focussing ($Y_4 = Y_6 = 0$).
   Enables good energy resolution to be obtained at large spectrometer collection angles.

3) Median focal plane perpendicular to the central ray ($Y_3 = 0$).
   This correction allows post spectrometer scanning of the spectrum in serial detection without loss of energy resolution.

Several spectrometer designs exist which satisfy the above criteria. [Shuman 1980, Scheinfein and Isaacson 1984, Krivanek and Swann 1981]. The solution of the simultaneous equations involved requires numerical analysis techniques, particularly when the calculations are of the extended fringe field type. A concise algorithm for deriving the values of the sector parameters required to correct the above aberrations is described in the paper by Shuman [1980].

3.3 EVALUATION OF EXISTING SPECTROMETER DESIGNS

The spectrometers mentioned in the previous section are typical of the best designs currently available using homogeneous field magnetic sectors. The performance of these magnets is well characterised for serial detection techniques, where they have been applied with success. However, transferring from serial to parallel detection methods requires a careful study of the electron intensity distribution at the spectrometer dispersion plane, so that both post spectrometer coupling optics and the geometry of the detector used can be optimised to suit a given spectrometer. To this end two Fortran computer programs were written, one to analyse the performance of any arbitrary magnetic sector spectrometer and the other to provide a graphical display of the electron intensity distribution at the dispersion plane.

3.3.1 Spectrometer analysis program

The analysis program is called FSPECT and was written on an IBM 370 mainframe computer running under the CMS operating system. The program requires as data the magnetic sector parameters, together with information describing the position of the fringe field clamps if such devices are used. The output consists of the first two quadrants of the second order median and vertical plane transfer matrices (equations 3.1 and 3.2), followed by the first two quadrants of the total transfer matrices (equations 3.7 a-d). Also calculated are the first order image positions and magnifications in the median and vertical planes. A listing of the code is contained in appendix 2.

The input data includes the sector parameters and information describing the presence and position of fringe field clamps. It is assumed that the parameters entered are those of the virtual field boundaries, which diverge from the mechanical boundaries as the polepiece gap increases from zero. If data concerning the polepiece boundaries is not available, the program can calculate the location of the virtual field boundary for clamped magnets using equation (2.43). This gives the displacement of the effective edge from the mechanical edge and allows the values of ϕ, R_1, R_2, U and V to be recalculated with respect to the virtual field boundaries; and the program can then be rerun using the new values. If the magnet has no field clamps and there is no information concerning the virtual field boundary then an estimate must be made concerning its position. Approximately 0.6 times the pole gap is a reasonable assumption for the distance between the mechanical boundaries and the virtual field position for unclamped magnets [Enge 1967]. Of course, accurate analysis of the sector properties requires a careful determination of the position of the virtual field boundaries.

Assuming that the virtual field boundaries have been obtained, the program calculates the effective poleface tilts for vertical focussing. If the magnet has field clamps then Heighway's expression (equation 2.41) is evaluated for the entrance and exit faces. If there are no field clamps a value of the integral coefficient I_2 (see section 2.6.3) must be supplied - e.g. for an unclamped magnet with square pole edges Enge [1967] estimates that $I_2 = 0.475$.

The next step is to calculate the first and second order focussing coefficients of equations (3.1) and (3.2) using the analytical expressions given in appendix 1. These coefficients are multiplied by the second order drift matrices, corresponding to the reduced object and image distances U and V (equations 3.3 and 3.4), in the manner shown in equations (3.5) and (3.6). The multiplication is done using expressions (3.8 a-k) and similar relations derived for the other terms. The resulting coefficients form the first two quadrants of the total transfer matrices and characterise the optical performance of the spectrometer.

All of the calculations are done using double precision arithmetic to minimise rounding errors. The accuracy of the program was checked by comparing the output with the values of analytical focussing coefficients derived for a straight edge sector magnet in Enge [1967]. Good agreement was found for all the terms.

3.3.2 Spectrum plotting program

Once the spectrometer aberration coefficients have been derived, it is useful to obtain a quick display of the resultant aberration figure for a particular spectrometer acceptance angle β. A second Fortran program called SPECTRUM was written to plot the electron distribution at the dispersion plane using the aberration coefficients calculated by FSPECT. SPECTRUM assumes the spectrometer has a circular entrance aperture with a point source producing an equal number of incident electrons per unit solid angle. The program is looped to allow the energy of the incident electrons to vary by discrete intervals. SPECTRUM is also capable of producing a plot of the spectrometer alignment figure [Egerton 1981, Jeanguillame et al. 1981], which is the image that is displayed on the CRT of a serial collection system in a STEM when the entrance aperture of the spectrometer is systematically explored by the electron beam. The alignment figure differs from the aberration figure in that only trajectories which pass through the energy selecting slits at the dispersion plane are displayed.

The plots obtained from SPECTRUM do not strictly correspond to those that would be obtained in practice as the point source/equal number of electrons per unit solid angle model is only an approximation to the real conditions. A more accurate algorithm would be to

model the spectrometer object using a Monte-Carlo simulation, however the results obtained from FSPECT and SPECTRUM are adequate to provide a good description of the performance of current spectrometer designs.

3.4 RESULTS OF CALCULATIONS ON REAL SPECTROMETERS

Two well known spectrometer designs [Shuman 1980, Scheinfein and Isaacson 1984] were analysed using program FSPECT and the resulting electron distributions at the dispersion plane were obtained using program SPECTRUM. The influence of the calculated aberration patterns for each spectrometer on the design of a parallel detection system is discussed in the following sections.

3.4.1 Shuman spectrometer

This spectrometer has a large bending radius and a corresponding value of D/R ~ 0.14, which is small for a typical energy loss spectrometer, with the advantage that the effects of extended fringe fields are lessened. Moreover, the complete system includes two external quadrupole lenses before and after the spectrometer [Shuman et al. 1986], which can be used to trim the first order focussing properties, but there are no correction lenses for second or higher order aberrations. The quoted energy resolution is 0.5 eV at 1 mrad acceptance angle, showing that good second order correction is achieved by the sector alone.

The physical parameters of the virtual field boundaries of the Shuman spectrometer were obtained from two papers [Shuman 1980,1983], and are listed below. The value of the polepiece gap is not given explicitly, but can be calculated knowing the value of I_2 (k in Heighway notation) which is given as 0.174. The distance from poleface to field clamps is given as t=D/2. However, substitution of this value in equation (2.42) gives a value for k of 0.177. Forcing k to be 0.174 gives a value for t of 0.47D, which is the value used in the calculations. (Using t=0.5D gave higher residual values for some of the corrected aberrations).

Bending Angle	ϕ	70 ^{o}
Bending Radius	R	165.1 mm
Pole Gap	D	22.68 mm
Pole-Clamp Gap	t	10.67 mm
Entrance Tilt	α	11.744 ^{o}
Exit Tilt	β	28.785 ^{o}

Entrance Radius	R_1	116.72 mm
Exit Radius	R_2	-99.55 mm
Object Distance	UR	594.36 mm
Image Distance	VR	393.59 mm

Figure 3.3 is the output from program FSPECT given the above parameters for the virtual field boundaries. As can be seen, the calculated values of the effective entrance and exit tilts for vertical focussing are 10.26 ^{o} and 26.83 ^{o} respectively. These should be compared with the mechanical values of 11.744 ^{o} and 28.785 ^{o} showing the influence of the extended fringe fields. The values of Y_1 and X_1 in the total transfer matrices are effectively zero, implying that the spectrometer is double focussing at the given image plane, however the magnifications in the median and vertical planes are not equal - the imaging is said to be pseudostigmatic. The notation of Figure 3.3 is explained on the page preceding it.

The value of the dispersion coefficient Y_2 is 3.76 which, substituted into equation (3.11), gives a dispersion of 3.4μm/eV at a primary beam energy of 100keV. The energy resolution limiting aberrations Y_4 and Y_6 are well corrected, allowing large collection angles to be used. For the Shuman spectrometer, the blurring at the dispersion plane caused by these two aberrations for a 5 mrad circular spectrometer acceptance angle β can be written:

$$\Delta y_{max} = R\beta^2\left[\,|Y_4| + |Y_6|\,\right] \qquad \text{giving}$$

$$\Delta y_{max} = 0.33\ \mu m$$

corresponding to an energy resolution of ~0.1 eV. The aberration describing the dispersion plane tilt, Y_3 is reduced to -0.0031, which ensures that the dispersion plane is normal to the central ray.

The dispersion nonlinearity Y_5 is calculated to be -5.8583 for this spectrometer. The total first and second order dispersion terms can be written:

$$\Delta y \sim R\left[\, Y_2\frac{\Delta E}{2E} + Y_5\left[\frac{\Delta E}{2E}\right]^2\right]$$

As can be seen from figure 3.3 Y_2 and Y_5 are of opposite sign, so that in moving away from the central ray in increasing energy (ΔE positive), the dispersion tends to decrease as energy increases. Conversely, for electrons with energy less than the central ray , (ΔE negative) the dispersion increases with energy loss. However, for a 2000eV spectrum the maximum value

Figure 3.3

OPTICAL PROPERTIES OF HOMOGENOUS MAGNETIC FIELD
SECTOR MAGNET USING FRINGING FIELD APPROXIMATION.

SHUMAN SPECTROMETER

VIRTUAL FIELD BOUNDARIES

BENDING ANGLE OF CENTRAL RAY = 70.00 Degrees

BENDING RADIUS OF CENTRAL RAY = 165.10 mm.

ENTRANCE POLEFACE TILT = 11.744 Degrees

EXIT POLEFACE TILT = 28.785 Degrees

OBJECT POSITION = 594.36 mm.

POLEPIECE SEPARATION = 22.68 mm.

ENTRANCE FIELD RADIUS OF CURVATURE = 116.73 mm.

EXIT FACE RADIUS OF CURVATURE = -99.55 mm.

DISTANCE FROM ENTRANCE CLAMP TO POLE = 10.67 mm.

DISTANCE FROM EXIT CLAMP TO POLE = 10.67 mm.

ENTRANCE FRINGING FIELD PROPERTIES.

INTEGRAL COEFFICIENT K = 0.1740

CORRECTION COEFFICIENT C = 1.0147

EFFECTIVE VERTICAL POLEFACE TILT = 10.2660 Degrees

EXIT FRINGING FIELD PROPERTIES.

INTEGRAL COEFFICIENT K = 0.1740

CORRECTION COEFFICIENT C = 1.0141

EFFECTIVE VERTICAL POLEFACE TILT = 26.8333 Degrees

Figure 3.3 Calculation of the Aberration Coefficients of the Shuman Spectrometer Using FSPECT.

The output of the program consists of the first three rows of the horizontal and vertical total transfer matrices, corresponding to the position, slope, and momentum of the electrons as described in matrix equations (3.1) and (3.2). The ordering of the terms has been changed slightly from that expressed in equations 3.7a-d. In terms of the Shuman notation the first row of the horizontal total transfer matrix corresponds to:

$Y_0, Y_1, Y_2, Y_4, Y_6, Y_5, Y_3, Y_7, Y_{10}, Y_8, Y_{11}, Y_9$

The ordering of the vertical matrix is:

$X_0, X_1, X_2, X_3, X_4, X_5, X_7, X_6$

The values calculated agree well with those published by Shuman [1983] except for X_2. The discrepancy is due to an error in Shuman's calculations which has since been resolved [Shuman 1986]. The coefficients Y_7-Y_{11} and X_4-X_7 have not previously been published.

Figure 3.3

ELEMENTS OF HORIZONTAL TRANSFER MATRIX

y/y	y/y'	y/d	y/y'2	y/x'2	y/d2
0.5374	0.9397	0.6580	0.2458	-1.3006	-0.3762
-0.5733	0.8583	1.3012	-1.6659	1.4525	-2.2995
0.0000	0.0000	1.0000	0.0000	0.0000	0.0000

y/y'd	y/y2	y/x2	y/yy'	y/xx'	y/yd
0.8049	0.3745	-0.8291	0.5612	-1.1600	0.9229
-2.1367	0.2008	-0.3013	-1.0927	2.5777	0.1122
0.0000	0.0000	0.0000	0.0000	0.0000	0.0000

ELEMENTS OF VERTICAL TRANSFER MATRIX

x/x	x/x'	x/y'x'	x/x'd
0.7787	1.2217	0.3389	0.0586
-0.5750	0.3820	4.1154	4.7647

x/yx	x/y'x	x/xd	x/yx'
-2.1302	-1.6009	0.0626	0.8480
-0.0606	2.2904	3.0077	0.2708

ELEMENTS OF THE TOTAL HORIZONTAL TRANSFER MATRIX

y/y	y/y'	y/d	y/y'2	y/x'2	y/d2
-0.8295	-0.0003	3.7600	-0.0266	0.0542	-5.8583
-0.5733	-1.2058	1.3012	-7.3287	10.6036	-2.2995
0.0000	0.0000	1.0000	0.0000	0.0000	0.0000

y/y'd	y/y2	y/x2	y/yy'	y/xx'	y/yd
-0.0031	0.8532	-1.5474	4.0989	-6.1563	1.1905
-1.7326	0.2008	-0.3013	0.3530	0.4083	0.1122
0.0000	0.0000	0.0000	0.0000	0.0000	0.0000

ELEMENTS OF THE TOTAL VERTICAL TRANSFER MATRIX

x/x	x/x'	x/y'x'	x/x'd
-0.5922	0.0005	-0.0593	37.4568
-0.5750	-1.6882	12.5504	15.5926

x/yx	x/y'x	x/xd	x/yx'
-2.2747	-4.3295	7.2331	-6.6954
-0.0606	2.0723	3.0077	0.0526

SPECTROMETER IS DOUBLE FOCUSSING AT OBJECT POSITION 594.36 mm

HORIZONTAL MAGNIFICATION = -0.8295 AT IMAGE POSITION = 393.5980 m

VERTICAL MAGNIFICATION = -0.5922 AT IMAGE POSITION = 393.5980 mm

DISPERSION = 3.7600 AT HORIZONTAL IMAGE POSITION

Figure 3.4 Theoretical Electron Intensity Distribution at the Dispersion Plane of the Shuman Spectrometer for a Monochromatic On-Axis Point Source

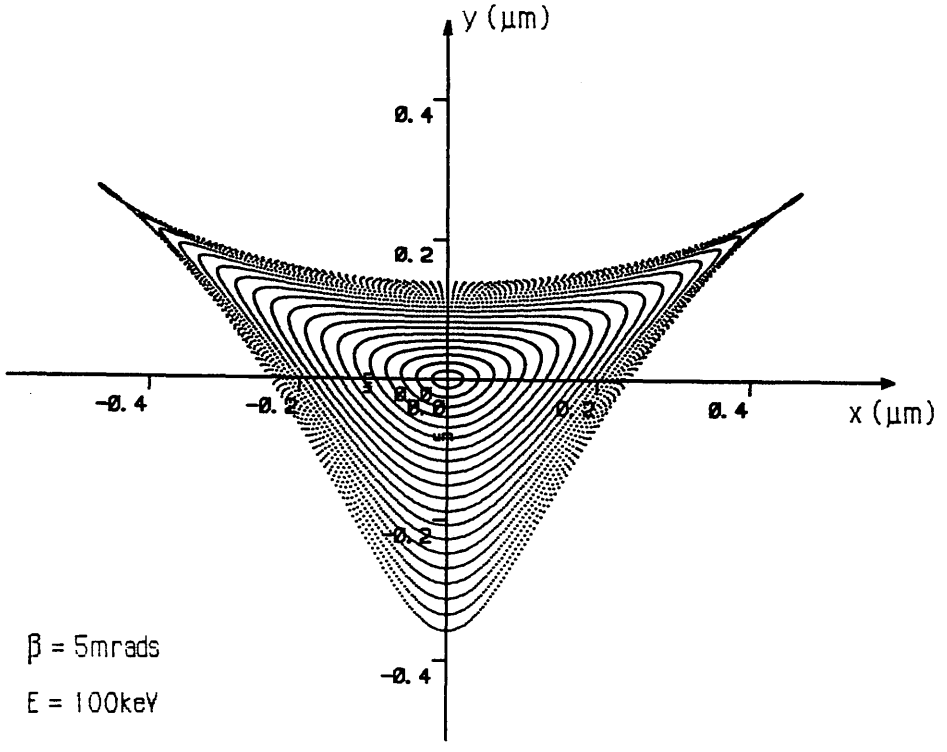

Figure 3.5 Theoretical Electron Intensity Distribution - 2000 eV Range

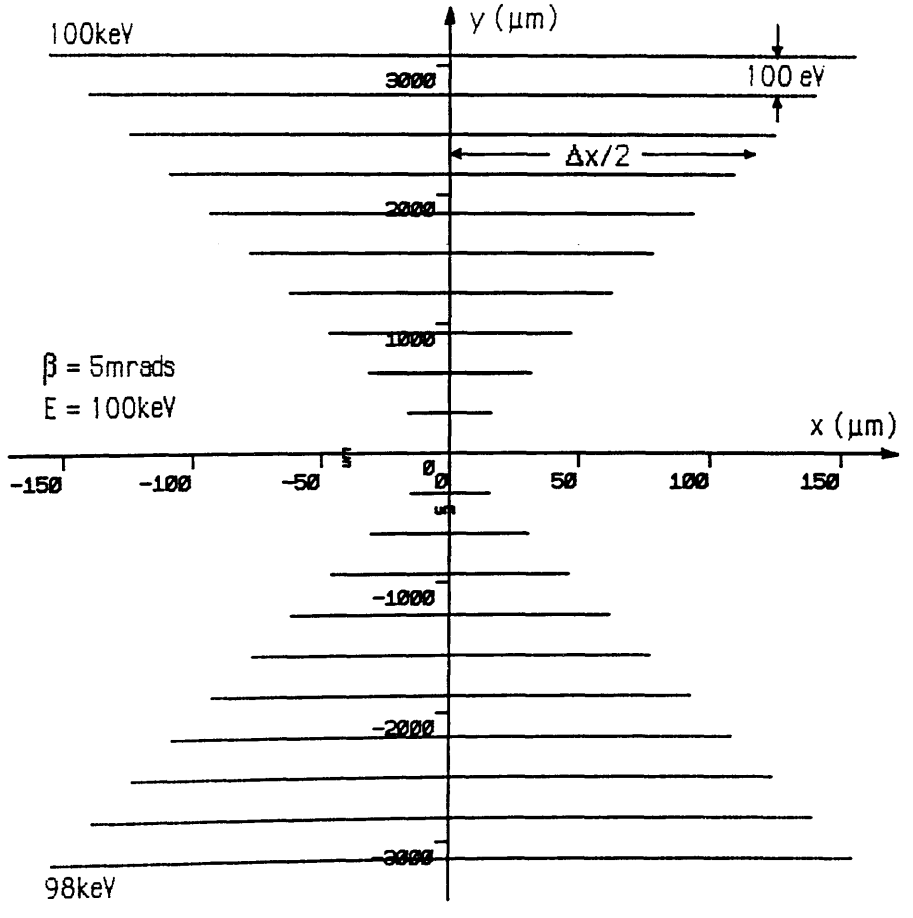

of the second term in brackets is approximately 1.5% of the first order term at 100keV. This means that the variation in dispersion over an entire spectrum is only ~1.5% which is negligible, especially when it is very unlikely that such a wide energy range would be recorded simultaneously.

The two vertical plane aberrations X_2 and X_3 have values of -0.0593 and 37.4568 respectively. The first term is small enough to be neglected even though it was not specifically corrected for in the original design. However, the second term is large and causes a defocus with energy loss in the x direction given by:

$$\Delta x \sim 2 R X_3 \beta \left[\frac{\Delta E}{2E} \right]$$

For the Shuman spectrometer Δx=0.34 μm/eV at 100 keV , assuming an entrance angle β of 5 mrads. Thus electrons with an energy difference of 1000 eV from the central ray are defocussed to a line extending 340 μm in the x direction. This has obvious repercussions on both the design of the post-spectrometer magnification system and the detector width. The defocus increases linearly with acceptance angle β, which must also be taken into account when deciding the maximum entrance angle to the spectrometer.

The final aberration figure is a complex pattern influenced by all the component aberrations. Figure 3.4 is a plot produced by SPECTRUM of the electron intensity at the dispersion plane of the Shuman spectrometer assuming a monoenergetic point source (δ=0) and a circular acceptance angle β of 5 mrads. As can be seen the extent of the defocus in the dispersion direction is ~0.6 μm, which implies an intrinsic spectrometer resolution of 0.2 eV at this acceptance angle. Figure 3.5 shows the image of a complete spectrum assuming the same entrance angle. The electron energy is varied in discrete steps of 100 eV, so that the energy spectrum covers 2000 eV. Each 'bar' on the figure consists of monochromatic electrons - in a real spectrum the top bar would correspond to electrons of energy 100 keV, the next bar down to 99.9 keV and so on, down to 98 keV at the bottom (the sector would have to be adjusted so that the energy of the central ray was 99 keV). Clearly illustrated is the defocussing effect of the X_3 aberration. The thickness of each bar is constant owing to the good correction of the Y_3 aberration.

3.4.2 Scheinfein and Isaacson spectrometer

The Scheinfein and Isaacson spectrometer [1984] is a more compact design than the Shuman spectrometer, and consequently has a much larger value of D/R=0.25. The fringe fields will

therefore play a bigger part in the optical performance. The complete system contains external quadrupole lenses, a sextupole lens and an octupole corrector lens to eliminate residual second order and reduce third order aberrations. The quoted energy resolution is 0.5 eV at 7.8 mrad acceptance, angle using the external corrector lenses. The sector parameters are listed below:

Bending Angle	ϕ	80 ^{o}
Bending Radius	R	100.0 mm
Pole Gap	D	25.00 mm
Pole-Clamp Gap	t	9.50 mm
Entrance Tilt	α	14.61 ^{o}
Exit Tilt	β	35.05 ^{o}
Entrance Radius	R_1	72.80 mm
Exit Radius	R_2	-57.607 mm
Object Distance	UR	350.00 mm
Image Distance	VR	182.17 mm

Figure 3.6 is the output from program FSPECT. The effective entrance and exit tilts for vertical focussing are 11.95 ^{o} and 31.12 ^{o} respectively, compared with mechanical values of 14.61 ^{o} and 35.05 ^{o}. The difference is larger than that of the Shuman spectrometer because of the more extended fringe fields.

The total transfer matrices indicate that the spectrometer is not perfectly double focussing (X_1=0.0863) and that the vertical focus lies some 4 mm behind the horizontal focus. This could be corrected using the external quadrupole lenses, but is unnecessary for serial detection. On its own, the defocus is small enough to be ignored for parallel detection systems. The dispersion term Y_2 is calculated to be 3.6764 giving a dispersion of 2.0μm/eV at 100 keV. The aberration Y_3 is very well corrected so that the dispersion plane is not tilted, similarly Y_5 is of the same order as the Shuman spectrometer and can be neglected for the reasons given previously. Of the two median plane aperture aberrations Y_4 is corrected but Y_6 is 0.3647 which will limit the energy resolution - i.e for an entrance angle β = 5 mrads:

$$\Delta y_{max} = R\beta^2 Y_6 \qquad \text{giving}$$

$$\Delta y_{max} = 0.91\ \mu m$$

which gives an energy resolution of 0.5eV. It may be possible to reduce this value using the

Figure 3.6 Calculation of the Aberration Coefficients of the Scheinfein and Isaacson Spectrometer Using FSPECT.

The output of the program consists of the first three rows of the horizontal and vertical total transfer matrices, corresponding to the position, slope, and momentum of the electrons as described in matrix equations (3.1) and (3.2). The ordering of the terms has been changed slightly from that expressed in equations 3.7a-d. In terms of the Shuman notation the first row of the horizontal total transfer matrix corresponds to:

$Y_0, Y_1, Y_2, Y_4, Y_6, Y_5, Y_3, Y_7, Y_{10}, Y_8, Y_{11}, Y_9$

The ordering of the vertical matrix is:

$X_0, X_1, X_2, X_3, X_4, X_5, X_7, X_6$

The values calculated have not previously been published.

Figure 3.6

OPTICAL PROPERTIES OF HOMOGENOUS MAGNETIC FIELD
SECTOR MAGNET USING FRINGING FIELD APPROXIMATION.

SCHEINFEIN AND ISAACSON DESIGN

VIRTUAL FIELD BOUNDARIES

BENDING ANGLE OF CENTRAL RAY = 80.00 Degrees

BENDING RADIUS OF CENTRAL RAY = 100.00 mm.

ENTRANCE POLEFACE TILT = 14.610 Degrees

EXIT POLEFACE TILT = 35.050 Degrees

OBJECT POSITION = 350.00 mm.

POLEPIECE SEPARATION = 25.00 mm.

ENTRANCE FIELD RADIUS OF CURVATURE = 72.80 mm.

EXIT FACE RADIUS OF CURVATURE = -57.61 mm.

DISTANCE FROM ENTRANCE CLAMP TO POLE = 9.50 mm.

DISTANCE FROM EXIT CLAMP TO POLE = 9.50 mm.

ENTRANCE FRINGING FIELD PROPERTIES.

INTEGRAL COEFFICIENT K = 0.1658

CORRECTION COEFFICIENT C = 1.0194

EFFECTIVE VERTICAL POLEFACE TILT = 11.9497 Degrees

EXIT FRINGING FIELD PROPERTIES.

INTEGRAL COEFFICIENT K = 0.1658

CORRECTION COEFFICIENT C = 1.0181

EFFECTIVE VERTICAL POLEFACE TILT = 31.1235 Degrees

Figure 3.6

ELEMENTS OF HORIZONTAL TRANSFER MATRIX

y/y	y/y'	y/d	y/y'2	y/x'2	y/d2
0.4304	0.9848	0.8264	0.3104	-1.8677	-0.3169
-0.6376	0.8645	1.5645	-2.2279	2.7462	-3.5033
0.0000	0.0000	1.0000	0.0000	0.0000	0.0000

y/y'd	y/y2	y/x2	y/yy'	y/xx'	y/yd
1.2143	0.3507	-0.8967	0.4839	-1.3598	1.1003
-3.5236	0.2197	-0.3732	-1.1204	3.3409	0.2123
0.0000	0.0000	0.0000	0.0000	0.0000	0.0000

ELEMENTS OF VERTICAL TRANSFER MATRIX

x/x	x/x'	x/y'x'	x/x'd
0.7045	1.3963	0.2439	-0.0773
-0.6370	0.1569	6.0566	8.0075

x/yx	x/y'x	x/xd	x/yx'
-2.4752	-1.9665	0.0385	0.8687
0.1677	2.9611	3.8374	-0.0406

ELEMENTS OF THE TOTAL HORIZONTAL TRANSFER MATRIX

y/y	y/y'	y/d	y/y'2	y/x'2	y/d2
-0.7312	0.0003	3.6764	-0.0004	0.3647	-6.6988
-0.6376	-1.3673	1.5645	-9.0281	16.7336	-3.5033
0.0000	0.0000	1.0000	0.0000	0.0000	0.0000

y/y'd	y/y2	y/x2	y/yy'	y/xx'	y/yd
-0.0001	0.7509	-1.5765	3.6988	-6.3095	1.4870
-2.7806	0.2197	-0.3732	0.4173	0.7287	0.2123
0.0000	0.0000	0.0000	0.0000	0.0000	0.0000

ELEMENTS OF THE TOTAL VERTICAL TRANSFER MATRIX

x/x	x/x'	x/y'x'	x/x'd
-0.4559	0.0863	-0.5253	39.1123
-0.6370	-2.0726	18.3318	21.4386

x/yx	x/y'x	x/xd	x/yx'
-2.1698	-4.1668	7.0292	-6.7998
0.1677	3.5478	3.8374	0.5461

SPECTROMETER IS NOT DOUBLE FOCUSSING AT OBJECT POSITION 350.00 mm

HORIZONTAL MAGNIFICATION = -0.7314 AT IMAGE POSITION = 182.1928m

VERTICAL MAGNIFICATION = -0.4825 AT IMAGE POSITION = 186.3355 mm

DISPERSION = 3.6768 AT HORIZONTAL IMAGE POSITION

Figure 3.7 Theoretical Electron Intensity Distribution at the Dispersion Plane of the Scheinfein + Isaacson Spectrometer for a Monochromatic On-Axis Point Source

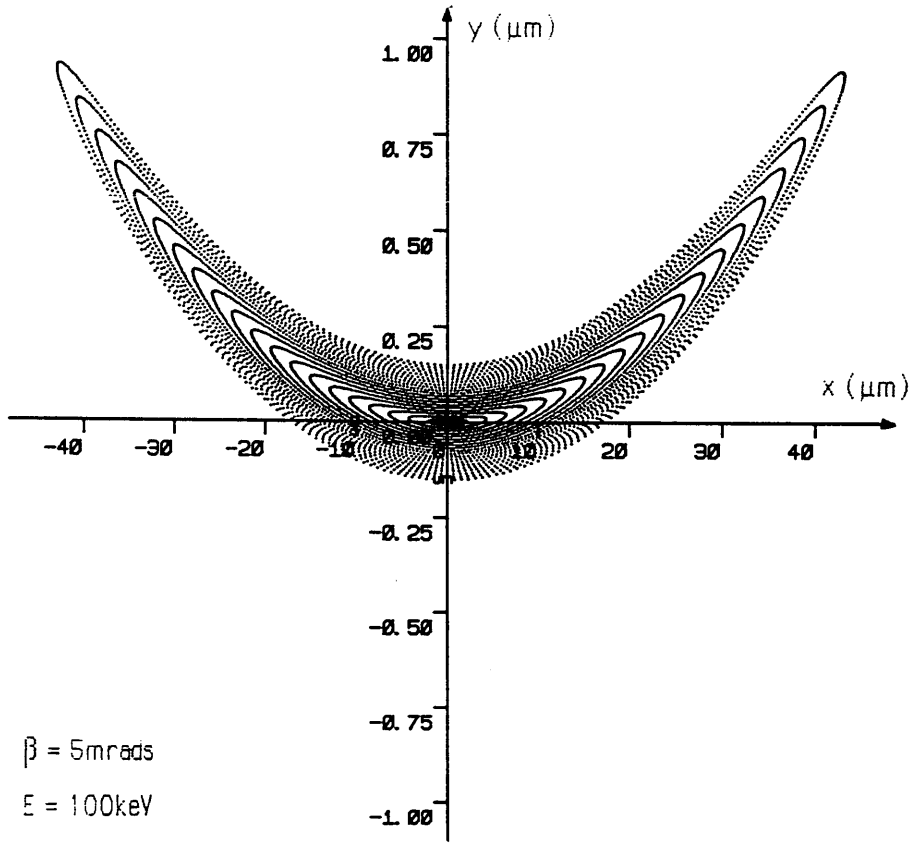

Figure 3.8 Theoretical Electron Intensity Distribution - 2000 eV Range

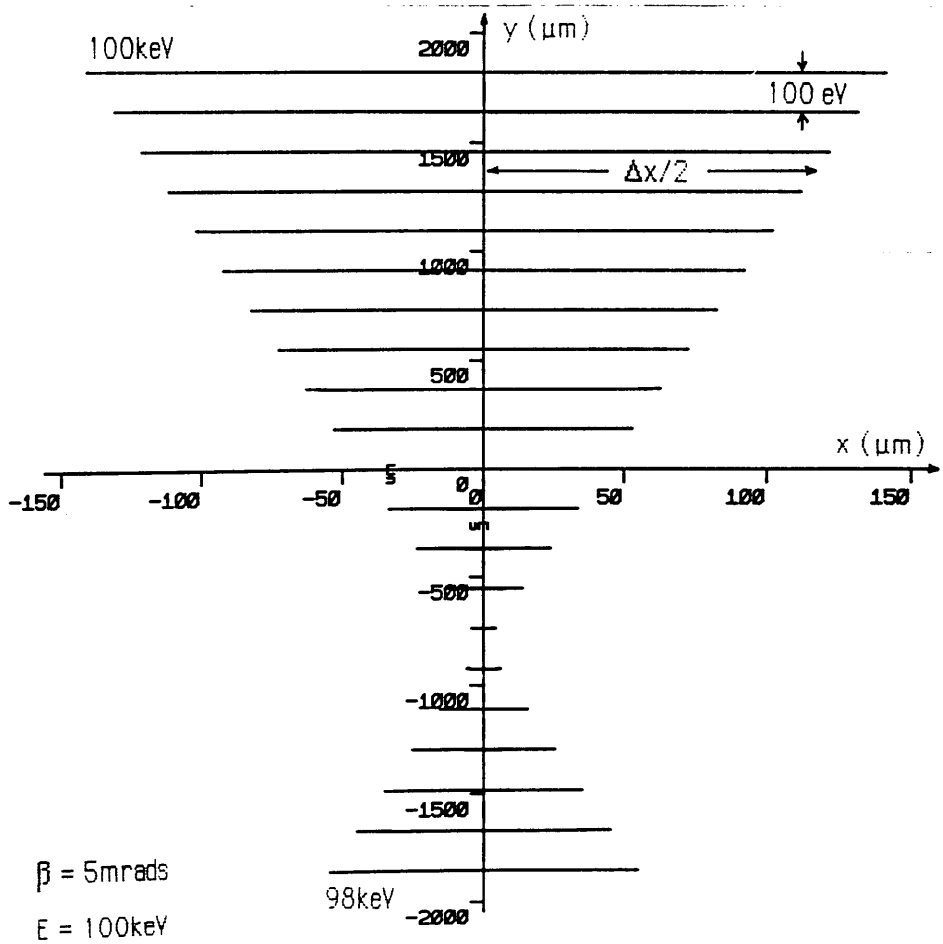

external sextupole lens, however it is likely that altering Y_6 will introduce an undesirable change in Y_4. The vertical aberration X_2 is ten times larger than that of the Shuman spectrometer (-0.5253 vs -0.0593), however at β = 5 mrads, for example, X_2 contributes only 1 μm to the defocus in x and can be neglected. The value of X_3 is 39.1123 which is very similar to the Shuman value so that the defocussing effect is very similar, i.e. for a 5 mrad acceptance angle the defocus in x with energy loss is 0.2 μm/eV.

Figure 3.7 shows the electron intensity at the dispersion plane of the Scheinfein and Isaacson spectrometer for an on axis point source and β = 5 mrads. All the electrons have the same energy as the central ray (δ=0). As can be seen, the defocus in x is much larger than for the Shuman spectrometer (~80 μm vs 1 μm), due to the residual uncorrected first order focussing term X_1. In the dispersion (y) direction the figure extends ~ 1 μm giving an energy resolution of ~ 0.55 eV for this acceptance angle. The blurring in the y direction is mainly due to the Y_6 term.

Figure 3.8 shows the image of a complete spectrum assuming β = 5 mrads. As before each 'bar' consists of monochromatic electrons and the energy increment between each bar is 100 eV, so that the entire spectrum encompasses 2000 eV. From the figure it can be seen that the spectrum is not symmetrical about y=0. The reason can easily be seen by writing the equation for the defocus in x as:

$$\Delta x = R\left[X_1 (x') + X_3 (x'\delta) \right]$$

The coefficients X_1 (=0.0863) and X_3 (=39.1123) have the same sign, so that when δ is positive (y>0) the two components add, and when δ is negative (y<0) the two components subtract to give the pattern shown in figure 3.8. Consequently, the x defocus is at a minimum at some non-zero value of δ corresponding to an energy difference of -441.3 eV from the central ray. The same effect occurs in the Shuman spectrometer but to a much smaller degree, as X_1 is close to zero.

Figure 3.9 shows the electron intensity distribution at the dispersion plane for monochromatic electrons which have an energy 441.3 eV less than that of the central ray. As can be seen, the defocus in the dispersion direction is the same as for the central ray, ~1μm, but the defocus in the x direction is reduced to ~1.2 μm. Referring back to figure 3.8 it is as though the spectrometer had an effective bending angle slightly greater than 70^{o}. In practice, for serial collection, the energy selecting slits could be displaced from the position of the central ray (y = 0 mm) by -0.81mm so that the 'effective central ray', (i.e. ray with minimum

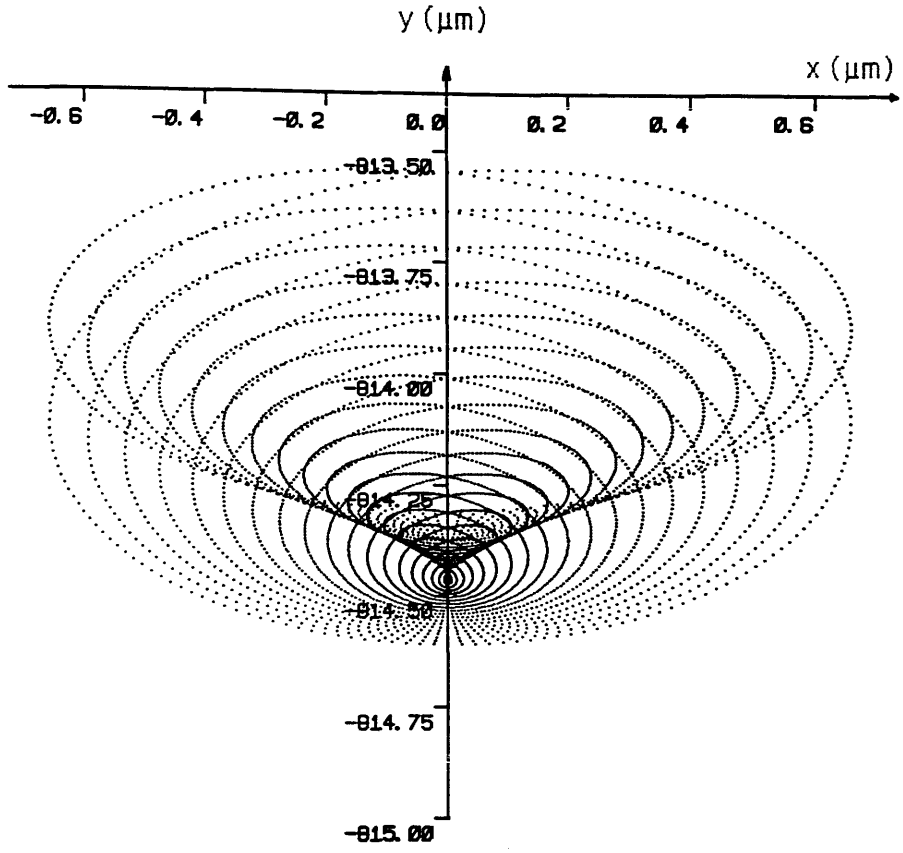

Figure 3.9 Theoretical Electron Intensity Distribution at the Dispersion Plane of the Scheinfein + Isaacson Spectrometer for an On-Axis Point Source With Energy 441 eV Less Than The Central Ray - Minimum Defocus in x

defocus in x) could be recorded. However, as there is no real difference in the energy resolution between the two rays there is limited advantage in doing so.

3.4.3 Investigating the cause of the large X_3 aberration.

An expression for calculating the value of the X_3 aberration is given in equation (3.8k). As can be seen the magnitude of X_3 depends upon the values of four focussing coefficients, $x/x\delta$, $x/x'\delta$, $x'/x\delta$, $x'/x'\delta$. An examination of the appropriate transfer matrices (Figures 3.3 and 3.6) firstly shows that the coefficients are of similar signs and magnitudes for each spectrometer, and secondly that the values of the last two coefficients are the most significant, being two orders of magnitude larger than those of the first two in each case. Analytical expressions for these two coefficients are given in appendix 1. These can be written:

$$\frac{x'}{x'\delta} = F_1(\phi, \alpha, \beta, D) - F_2(\phi, \alpha, \beta, D)\, C_2$$

$$\frac{x'}{x\,\delta} = F_3(\phi, \alpha, \beta, D) - F_4(\phi, \alpha, \beta, D)\, C_2$$

where C_2 is the exit curvature ($C_2 = R/R_2\cos^3\beta$) and the functions F_j depend upon the sector parameters. For both spectrometers, the values of the first terms on the right hand side of the above equations are approximately equal in magnitude to those of the second terms, but of opposite sign as the exit face radius of curvature R_2 is negative in each case. If R_2 were positive then the magnitudes of the $x'/x'\delta$ and $x'/x\delta$ focussing coefficients would be much smaller, and consequently the value of the X_3 aberration much reduced. Egerton [1980] has shown that correction of the median plane aberrations Y_4 and Y_6 requires R_1 and R_2 to be of opposite sign, and that designs with a negative entrance curvature tend to have lower values of first order dispersion. For this reason most second order spectrometer designs have a positive entrance curvature and negative exit curvature. From the above it can be inferred that, at least in part, a negative curvature on the exit poleface coupled with positive values of α and β tends to increase the value of the X_3 aberration.

3.4.4 Higher order aberrations

Sector spectrometers produce aberrations of all orders. There is some evidence to suggest that correction of second order aberrations can increase the values of third order aberrations, to the point that these become resolution limiting even at moderate acceptance angles [Tang 1982]. Scheinfein and Isaacson [1984] noted that third order aberrations began to dominate the residual second order aberrations for acceptance angles > 5 mrads. Derivation of third and higher order aberrations by the matrix method is possible [Fujita et al 1977, Matsuda

and Wollnik 1970], but the calculations involved are extremely lengthy and require an accurate determination of the fringe field profiles. The paper by Tang outlined a method whereby these fringe field profiles could be calculated using the finite element analysis programs developed by Munro [1973] for analysing round lenses. Correction of third order aberrations using shaped polepieces is likely to be almost impossible due to the machining tolerances required. External multipole lenses could possibly be used, however each new element adds further cost and complexity to a detection system. At present, it seems that obtaining good energy resolution with high collection efficiency is best accomplished using the combination of a second order corrected spectrometer with post specimen lenses to compress the angular distribution of the scattered electrons before the spectrometer.

3.4.5 Conclusions from spectrometer calculations

The two spectrometers analysed are typical of second order corrected homogeneous field magnetic sector designs. It has been shown that correction of the median plane aberrations tends to increase the value of the vertical plane aberration coefficient X_3 to ~40, causing a considerable vertical defocus with energy loss. It is very likely that other such spectrometers behave similarly, and that the vertical defocus is a general property for spectrometers with median plane aberrations corrected. It is obvious that careful calculations of the type shown in this chapter are necessary to design a parallel collection system that successfully matches an existing spectrometer.

CHAPTER 4

Post-spectrometer magnification: quadrupole optics

Introduction

Parallel detection in electron energy loss spectroscopy requires that the dispersion plane of the spectrometer be magnified to overcome the resolution limiting effects of electron scattering within the detector, and that the shape of the magnified spectrum should match the geometry of the particular detector used. This chapter describes the properties required of such post-spectrometer magnification systems and discusses the advantages of using combinations of quadrupole lenses as the magnifying elements. A review of the theory of the focussing properties of multipole lenses is given and the transfer matrix for a magnetic quadrupole lens is developed to second order. The optical properties of single quadrupoles and quadrupole pairs are discussed, and the relevant matrix equations are developed.

4.1 POST SPECTROMETER MAGNIFICATION

The need for post spectrometer magnification has already been discussed in chapter 1 (section 1.2.4). A successful magnification system should be able to couple the spectrometer dispersion plane to the detector with minimum loss of signal, and ideally no loss of resolution. The magnification should be variable over a wide range allowing collection of whole spectra at low energy resolution, and also detailed high energy resolution images of ionisation edges and fine structure. Furthermore, it is desirable that the magnifications in the median and vertical planes be independent, so that the dispersion of a spectrum can be increased without changing its width in the nondispersive direction. Thus by adjusting the non-dispersive magnification the width of the spectrum could be made to match exactly that of the detector at every magnification. The choice of magnifying elements is discussed below.

4.1.1 Advantages of quadrupole lenses over round lenses

There are two types of electron lens which can be used for magnifying the dispersion plane- round lenses or quadrupole lenses. These lenses can be either magnetic or electrostatic, however electrostatic lenses are less practical as they must be contained within the vacuum system, whereas magnetic lenses can be external to a vacuum flight tube. This difficulty, allied to problems of shielding the high voltages required suggests that magnetic lenses are

more suitable for this application. The properties of round lenses and quadrupoles compare as follows:

	Quadrupoles	Round Lenses
1)	Low power, no cooling required.	High power, must be cooled.
2)	No image rotation.	Image rotation unless paired.
3)	Short working distance.	Long working distance.
4)	Psuedostigmatic focussing if paired.	Stigmatic focussing only.
5)	Four second order chromatic aberrations.	No second order aberrations.

The first point is important from a constructional point of view - water cooling of lenses is best avoided if possible as it involves extra expense and complexity. Image rotation is obviously undesirable as the detector would have to be rotated into a new alignment every time the magnification was changed. Also it is advantageous to have as short a working distance as possible between the spectrometer exit plane and the detector, both from a mechanical point of view and also to limit the effects of external electromagnetic fields. The advantage of psuedostigmatic focussing is that it is possible to make the magnifications in the dispersive and non-dispersive planes independent. This feature is impossible to achieve using round lenses. The rotational symmetry of round lenses excludes all aberrations of second and higher even orders. Quadrupole lenses also have no second order aperture or geometric aberrations, but do possess four second order chromatic aberrations which must be considered.

Magnification systems using two and three post spectrometer quadrupoles have been constructed [Egerton and Crozier 1987, Krivanek et al. 1987] and a system using four round lenses configured as two anti-rotation pairs has been reported [Shuman and Kruit 1985]. The latter system has a very long flight path and suffers from electromagnetic interference, to the extent that a feedback system designed to reduce the effects of the external a.c. fields is necessary [Kruit and Shuman 1985]. It seems that quadrupole lens systems offer much more flexibility and ease of construction than equivalent round lens configurations, and can form the basis of a more efficient magnification system. The following sections outline the theory of magnetic multipole lenses, and quadrupole lenses in particular.

Figure 4.1 Particle Trajectory In Generalised Multipole Lens

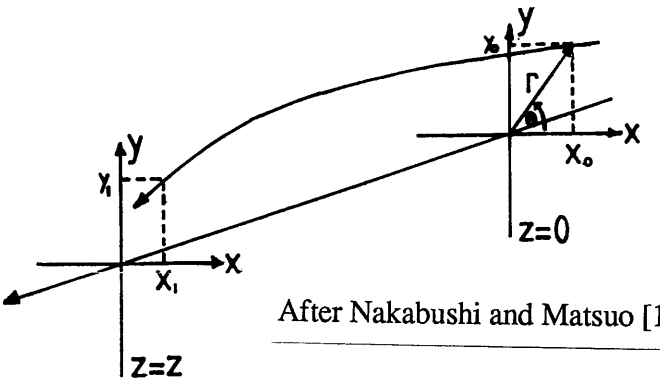

After Nakabushi and Matsuo [1982]

Figure 4.2 Idealised Quadrupole Lens

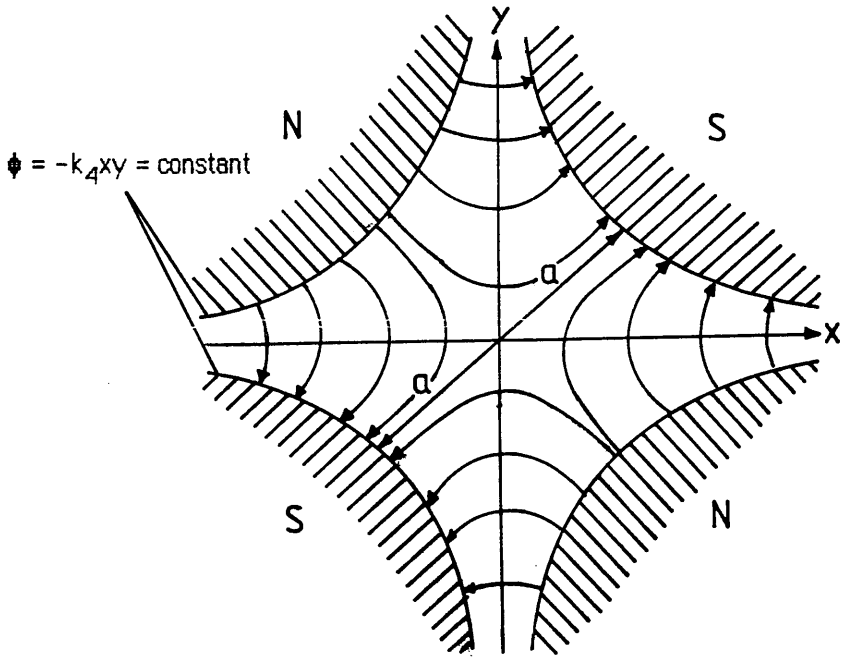

Figure 4.3 Aid For Calculation Of k_4

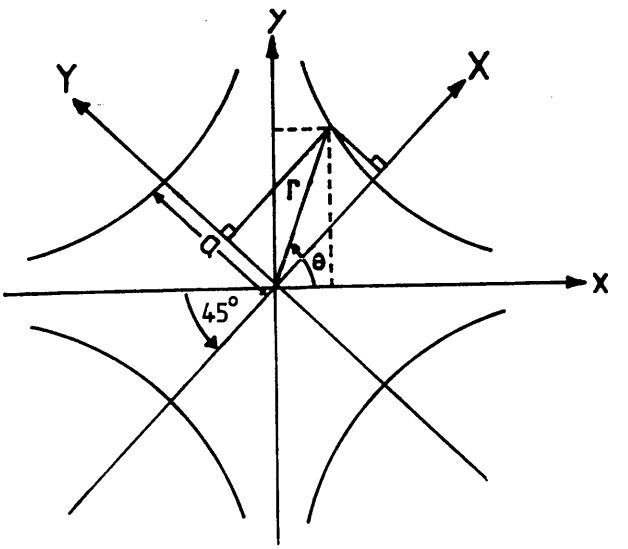

4.2 MAGNETIC MULTIPOLE LENSES - THEORY

The electron-optical properties of any multipole lens can be derived using the matrix multiplication method described in the previous chapters. An ideal magnetic multipole lens produces a field which is transverse to the optic axis of the lens and possesses one or more rotational symmetry planes. In the next sections the generalised form of the magnetic field of a multipole lens is derived and the trajectory equations for the motion of electrons in such a field are developed. Solution of these equations gives the transfer matrix focussing coefficients for the particular multipole field of interest. The first and second order focussing coefficients for a pure quadrupole field are used to form the quadrupole transfer matrix. The derivations assume sharp cutoff (SCOFF) fringe fields, and follow the method of Steffen (1965) and Nakabushi and Matsuo (1982).

4.2.1 The magnetic field of a multipole lens

Figure 4.1 shows an arbitrary trajectory of an electron in a generalised multipole lens. The electron enters the lens with coordinates (x_0,y_0) at position z=0, and exits at position z=z with coordinates (x_1,y_1). The magnetic field is assumed to be transverse and unsaturated, so that the magnetic scalar potential ϕ has no z dependence, and the only symmetry condition is that the scalar magnetic potential be an odd function of y:

$$\phi(x, -y) = -\phi(x, y) \tag{4.1}$$

ϕ must satisfy the Laplace equation which can be written in cylindrical polar coordinates :

$$\nabla^2\phi(r, \theta) = \frac{1}{r}\frac{\partial}{\partial r}\left[r\frac{\partial\phi}{\partial r}\right] + \frac{1}{r^2}\frac{\partial^2\phi}{\partial\theta^2} = 0 \tag{4.2}$$

This equation can be solved using the method of separation of variables [Nakabushi and Matsuo 1982] to give using (4.1):

$$\phi(r, \theta) = -\sum_n \frac{k_{2n}}{n} r^n \sin n\theta \qquad n = 1,2,3,4.... \tag{4.3}$$

where r and θ are the plane polar coordinates in the x-y plane. Expanding equation (4.3):

$$\phi(r, \theta) = -k_2 r\sin\theta - \frac{k_4}{2}r^2\sin2\theta - \frac{k_6}{3}r^3\sin3\theta - \frac{k_8}{4}r^4\sin4\theta - ... \tag{4.4}$$

It is easy to identify the individual multipole components from equation (4.4). For example the term containing sin2θ has two maxima and two minima as θ rotates from 0 to 2π radians about the z axis, suggesting a four pole or quadrupole type symmetry. Similarly the sin3θ term is a sextupole field and the sin4θ term represents an octupole field. The constants k_4, k_6 and k_8 are the field strength parameters of the quadrupole, sextupole and octupole field

components respectively, whereas the k_2 term represents a dipole field (such as a sector) and is not considered further. Equation (4.4) can be expressed in cartesian form by substituting $\sin\theta = y/r$ and $\cos\theta = x/r$ to give:

$$\phi(x, y) = -k_4 xy - k_6\left(x^2 y - \frac{1}{3}y^3\right) - k_8\left(x^3 y - xy^3\right) - \ldots. \qquad (4.5)$$

The magnetic field components can be now obtained using $B = \nabla\phi$ i.e.

$$B_x = k_4 y + 2k_6 x y + k_8(3x^2 y - y^3) \qquad (4.6a)$$

$$B_y = k_4 x + k_6(x^2 - y^2) + k_8(x^3 - 3xy^2) \qquad (4.6b)$$

$$B_z = 0 \qquad (4.6c)$$

4.2.2 The trajectory equations

The equations of motion for an electron in a multipole lens field are obtained by combining the Lorentz equation together with equations (4.6 a-c) to give:

$$m\ddot{x} = e\dot{z}B_y \qquad (4.7a)$$

$$m\ddot{y} = -e\dot{z}B_x \qquad (4.7b)$$

$$m\ddot{z} = -e(\dot{x}B_y - \dot{y}B_x) \qquad (4.7c)$$

where the dot stands for time derivative as before. In order to change the independent variable from time to z the differentials can be rewritten as follows:

$$\dot{x} = x'\dot{z} \qquad \text{so} \qquad \ddot{x} = x'\ddot{z} + z\dot{x}'$$

where the dash stands for derivative with respect to z. Expanding the last term gives:

$$\dot{z}\dot{x}' = \dot{z}\frac{d}{dz}(x'\dot{z}) = \dot{z}(x'\ddot{z} + \dot{z}x'') = \dot{z}^2 x'' \quad (\text{as } \ddot{z} = 0)$$

Substituting back gives the following transformations:

$$\ddot{x} = x'\ddot{z} + \dot{z}^2 x'' \qquad (4.8a)$$

$$\ddot{y} = y'\ddot{z} + \dot{z}^2 y'' \qquad (4.8b)$$

The velocity of the electron is:

$$v^2 = \dot{x}^2 + \dot{y}^2 + \dot{z}^2$$

$$v^2 = (x'\dot{z})^2 + (y'\dot{z})^2 + \dot{z}^2$$

$$v^2 = \dot{z}^2(1 + x'^2 + y'^2) \qquad (4.9)$$

where v is particle velocity and dz/dt is the velocity component of the electron parallel to the optic axis. From equation (4.8a):

$$x'' = \frac{1}{\dot{z}^2}(\ddot{x} - x'\ddot{z})$$

Substituting in the above equation for $\dot{z}^2$ using equation (4.9), $\ddot{x}$ using equation (4.7a) and $\ddot{z}$ using equation (4.7c) gives:

$$x'' = \frac{e}{mv}(1+x'^2+y'^2)^{\frac{1}{2}}\left[B_y + (x' B_y - y' B_x)\, x' \right] \qquad (4.10a)$$

A similar procedure gives for the y direction:

$$y'' = \frac{e}{mv}(1+x'^2+y'^2)^{\frac{1}{2}}\left[-B_x + (x' B_y - y' B_x)\, y' \right] \qquad (4.10b)$$

To consider chromatic aberrations a momentum deviation is defined as before:

$$p = p_0(1+\delta) \quad \text{and} \quad \frac{1}{p} = \frac{1}{p_0}\left[1 - \delta + \delta^2 - \ldots \right] \qquad (4.11)$$

Equation (4.10a) can be written:

$$x'' = \frac{e}{p}\left[B_y\left(1+\frac{3}{2}x'^2+\frac{1}{2}y'^2\right) - B_x(x'y') \right]$$

Where terms of greater than third order in x', y' have been neglected. Substituting for B_x and B_y using equations (4.6 a,b) and including chromatic terms through equation (4.11) yields, again to third order:

$$x'' = \frac{e}{p_0}\left[k_4\left[x+\frac{3}{2}xx'^2+\frac{1}{2}xy'^2-yy'x'\right]+k_6\left[x^2-y^2\right]+k_8\left[x^3-3xy^2\right]-k_4x\delta+k_6\left[y^2\delta-x^2\delta\right]+k_4x\delta^2\right]$$

which can be rewritten as:

$$x''+qx = qx\delta + h(y^2-x^2) - qx\delta^2 - h\delta(y^2-x^2) + q(xyy' - \frac{3}{2}xx'^2 - \frac{1}{2}xy'^2) + p(3xy^2-x^3) \qquad (4.12)$$

where:

$$q = -\frac{e\,k_4}{p_0} = \text{quadrupole strength}$$

$$h = -\frac{e\,k_6}{p_0} = \text{sextupole strength}$$

$$p = -\frac{e\,k_8}{p_0} = \text{octupole strength}$$

A similar method develops the trajectory equation for y:

$$y'' - qy = -qy\,\delta + 2hxy \tag{4.13}$$

where only terms of first and second order have been carried. Equations (4.12) and (4.13) are the trajectory equations describing the motion of an electron through a general multipole lens.

4.2.3 First order solution of the trajectory equations - quadrupole field

In the case of a pure quadrupole field the sextupole and octupole terms k_6 and k_8 must be zero and the trajectory equations (4.12, 4.13) can be written to first order in x, y and δ:

$$x'' - qx = 0 \tag{4.14}$$

$$y'' + qy = 0 \tag{4.15}$$

The solutions to these equations are:

$$x = x_0 \cos\sqrt{q}\,z + x_0' \frac{1}{\sqrt{q}} \sin\sqrt{q}\,z \tag{4.16}$$

$$y = y_0 \cosh\sqrt{q}\,z + y_0' \frac{1}{\sqrt{q}} \sinh\sqrt{q}\,z \tag{4.17}$$

where x_0, y_0, x_0', y_0' are the initial values of the coordinates and gradients of the electron at z=0. The form of equations (4.16) and (4.17) suggests that a pure quadrupole field is convergent in one plane and divergent in the other. For positive q as above the x plane is convergent and the y plane is divergent. Thus, particles travelling in the x0z plane experience a focussing action whilst particles travelling in the y0z plane are defocussed, which implies that a single quadrupole field images a point source to a line.

Equations (4.16) and (4.17) are linear and can be expressed in matrix form exactly as in the case of the magnetic sector equations of chapter 2. Once more motions in the two orthogonal planes are independent to first order. The first order transfer matrices for the x and y planes of a pure quadrupole field are given below in equations (4.18) and (4.19), where the focussing coefficients for the second row are found by differentiating the approriate first row coefficients with respect to z.

First order transfer matrix for quadrupole convergent plane:

$$\begin{bmatrix} x_1 \\ x_1' \end{bmatrix} = \begin{bmatrix} \cos\sqrt{q}\, z & \frac{1}{\sqrt{q}} \sin\sqrt{q}\, z \\ -\sqrt{q} \sin\sqrt{q}\, z & \cos\sqrt{q}\, z \end{bmatrix} \begin{bmatrix} x_0 \\ x_0' \end{bmatrix} \qquad (4.18)$$

First order transfer matrix for quadrupole divergent plane:

$$\begin{bmatrix} y_1 \\ y_1' \end{bmatrix} = \begin{bmatrix} \cosh\sqrt{q}\, z & \frac{1}{\sqrt{q}} \sinh\sqrt{q}\, z \\ \sqrt{q} \sinh\sqrt{q}\, z & \cosh\sqrt{q}\, z \end{bmatrix} \begin{bmatrix} y_0 \\ y_0' \end{bmatrix} \qquad (4.19)$$

4.2.4 Quadrupole lenses

This section describes how a quadrupole field can be generated in practice. From equations (4.6 a-c) a pure quadrupole field has $B_y=k_4x$, $B_x=k_4y$ and $B_z=0$, where k_4 is the field strength gradient, which should be constant. The quadrupole field $\underline{B}$ may be derived from a potential:

$$\phi = -k_4xy \qquad \text{as} \qquad \underline{B} = -\nabla\phi \qquad (4.20)$$

The equipotential lines $\phi = -k_4xy$ = constant form a set of symmetric hyperbolae in the x-y plane. Figure 4.2 shows four such hyperbolae which represent the contour lines of the four magnetic poles of an ideal lens. For the polarity shown the lens is focussing in the y direction and defocussing in the x direction. In practical terms real polepieces can only approximate to the infinite hyperbolae required. Further modifications to the contours may be necessary to make room for coil windings. Deviations from the ideal pole shape will introduce higher order field components (hexapole, octupole etc.) into the field expansion, but in general the magnitude of these higher terms is small, and Grivet [1972] has shown that hyperbolic polepieces can be approximated by circular polepieces without introducing any significant departures from an ideal quadrupole field.

4.2.5 Calculation of the quadrupole field gradient k_4

The equation of a hyperbola such as depicted in figure 4.3 is:

$$X^2 - Y^2 = a^2$$

with respect to the X-Y coordinate system. However the principal axes of the lens x,y are rotated at 45^o to this system. The equation of the hyperbola, with respect to the x-y axes, can

be found by noting:

$$X = r\cos(\theta - 45^0) \qquad Y = r\sin(\theta - 45^0)$$

Where r and θ are polar coordinates as shown. The sine and cosine terms can be expanded and written in terms of coordinate axes x and y as:

$$X = \frac{1}{\sqrt{2}}(x+y) \qquad Y = \frac{1}{\sqrt{2}}(y-x)$$

substituting these expressions into the original equation gives:

$$\frac{1}{2}\left[(x+y)^2 - (y-x)^2 \right] = a^2$$

$$\text{i.e.} \qquad xy = \frac{a^2}{2}$$

If the polefaces are assumed to be equipotential surfaces the magnetic scalar potential is:

$$\phi = \mu_0 NI$$

where NI is the number of amp-turns per pole. Substituting for ϕ in equation (4.20):

$$\mu_0 NI = -k_4 xy$$

$$k_4 = \frac{-2\mu_0 NI}{a^2} \qquad (4.21)$$

where a is the radius of the largest circle that can be inscribed inside the polepieces.

4.2.6 Higher order solutions of the trajectory equations

Solutions of equation (4.12) are given to third order by Nakabushi and Matsuo [1982] in the form of matrix coefficients. The same authors also present solutions of equation (4.13) to second order. It is interesting to note that pure sextupole fields (k_4=k_8=0) have no non-zero first order focussing coefficients and hence do not affect first order focussing properties. For this reason sextupole corrector lenses are often used to correct for residual second order aberrations of magnetic sectors. Pure octupole lenses have no first or second order coefficients so that they can be used to correct for third order aberration effects. Field symmetry limits quadrupole lenses to eight non-zero second order chromatic focussing coefficients in each plane - analytical expressions for these are given in appendix 3;and the second order transfer matrices for the convergent and divergent planes of a quadrupole lens can be constructed in an identical manner to those given in chapter 3 for a magnetic sector. The transfer matrix for the x plane is given below in terms of the abbreviated Taylor coefficient notation of chapter 2. The y plane transfer matrix is identical in form simply

requiring substitution of the appropriate focussing coefficients.

Second order quadrupole transfer matrix (x plane):

$$\begin{bmatrix} x_1 \\ x_1' \\ x_1\delta \\ x_1'\delta \end{bmatrix} = \left[\begin{array}{cc|cc} \frac{x}{x} & \frac{x}{x'} & \frac{x}{x\delta} & \frac{x}{x'\delta} \\ \frac{x'}{x} & \frac{x'}{x'} & \frac{x'}{x\delta} & \frac{x'}{x'\delta} \\ \hline 0 & 0 & \frac{x}{x} & \frac{x}{x'} \\ 0 & 0 & \frac{x'}{x} & \frac{x'}{x'} \end{array}\right] \begin{bmatrix} x_0 \\ x_0' \\ x_0\delta \\ x_0'\delta \end{bmatrix} \qquad (4.22)$$

Unlike the magnetic sector there are no second order cross terms in a quadrupole lens, so that motions in the horizontal and vertical planes are independent to second order.

4.2.7 Effects of extended fringe fields

The magnetic field in any real quadrupole lens does not disappear abruptly at the end planes of the magnet. As in the case of a magnetic sector there exist fringe field zones outside the magnet where B_x and B_y are non-zero, and the fringe field does not have a pure quadrupole configuration, as k_4 is not constant and also a component of B_z appears. To account for this effect it is usual to represent the lens by three transfer matrices, one for the idealised main field (i.e. equation 4.22), and two others to represent the actions of the entrance and exit fringe fields.

The principal effect of extended fringe fields is to shorten the focal length of the lens and hence change the first order focussing properties. Expressions for the focussing coefficients of the fringe field matrices have been determined [Lee-Whiting 1970, Smith 1970, Matsuda and Wollnik 1972] however the calculations require experimental measurements of the fringe field profiles. Smith [1972] has shown that a SCOFF type calculation, where the constant interior field is extended a distance beyond the mechanical edges to a virtual field boundary, (Figure 4.4) can give a good approximation to the first order focussing properties of a real lens. An expression for the 'effective length' L of the lens is given by Grivet [1972] as:

$$L = L' + 1.1\,a \qquad (4.23)$$

where L' is the mechanical length and a is the radius of the quadrupole aperture.

Figure 4.4 Defining The Effective Length Of A Quadrupole Lens

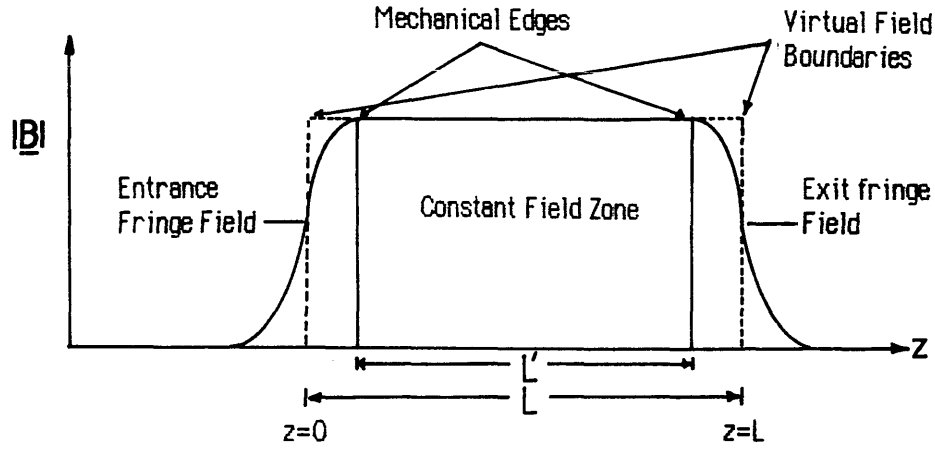

Figure 4.5 Quadrupole Pair Imaging

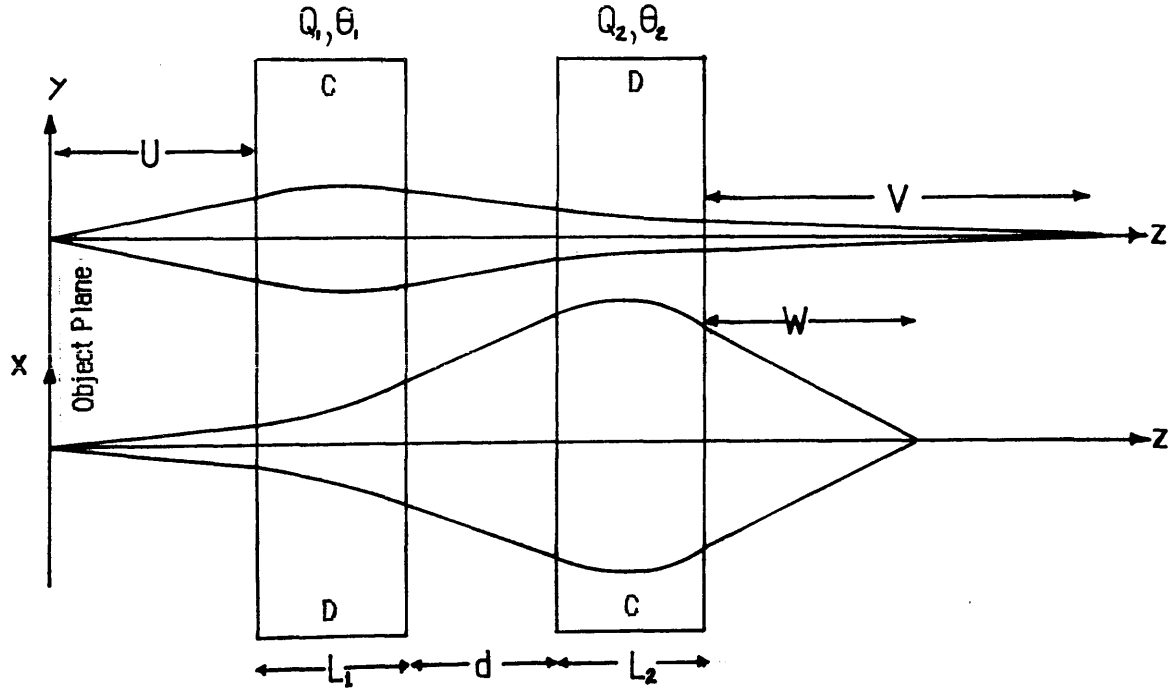

4.2.8 Drift matrices and the total transfer matrix

As in the case of the magnetic sector the optical properties of a quadrupole lens are obtained from the total transfer matrices for each plane. The second order drift matrix for a length U is determined in exactly the same manner as for the magnetic sector i.e.

$$\begin{bmatrix} x_1 \\ x_1' \\ x_1\delta \\ x_1'\delta \end{bmatrix} = \begin{bmatrix} 1 & U & 0 & 0 \\ 0 & 1 & 0 & 0 \\ 0 & 0 & 1 & U \\ 0 & 0 & 0 & 1 \end{bmatrix} \begin{bmatrix} x_0 \\ x_0' \\ x_0\delta \\ x_0'\delta \end{bmatrix} \tag{4.24}$$

with an identical matrix for the y plane. The total transfer matrices are then given by:

$$[T_x] = [Q_x][X][P_x] \tag{4.25}$$

$$[T_y] = [Q_y][Y][P_y] \tag{4.26}$$

where $[T_X]$ and $[T_y]$ are the x and y plane total transfer matrices. [X] and [Y] are the transfer matrices corresponding to equation (4.22). $[Q_X]$ is the second order x plane drift matrix for an image distance Q_X and $[P_X]$ is the associated drift matrix for an object distance P_X. $[Q_y]$ and $[P_y]$ are the corresponding drift matrices in the y plane. As mentioned before single quadrupole lenses are incapable of stigmatic focussing, and as such are of limited practical use for the magnification of an EELS spectrum. Obtaining any form of stigmatism requires the use of a second lens.

4.3 QUADRUPOLE PAIRS

Starting from a real object, a single quadrupole gives a real image point in its convergent plane and a virtual image in its divergent plane. Producing a real image in both planes requires a pair of quadrupoles, Q_1,Q_2 rotated at 90^0 to each other as shown in figure 4.5. Thus the focussing plane of the second quadrupole is aligned with the defocussing plane of the first and the overall effect can be to produce focussing in both planes. Quadrupole pairs are basic focussing elements in particle transport systems, and the next sections describe some of their optical properties.

4.3.1 Transfer matrices of quadrupole pairs

From figure 4.5 the distance between the effective ends of the quadrupoles is d. L_1 and L_2 are the effective lengths of the quadrupoles and the respective excitations θ_1 and θ_2 are:

$$\theta_1 = \sqrt{q_1}\, L_1 = \sqrt{\frac{-e k_{4_1}}{p_0}}\, L_1 = \sqrt{\frac{2 e \mu_0 (NI)_1}{p_0}}\, \frac{L_1}{a_1} \qquad (4.27)$$

$$\theta_2 = \sqrt{q_2}\, L_2 = \sqrt{\frac{-e k_{4_2}}{p_0}}\, L_2 = \sqrt{\frac{2 e \mu_0 (NI)_2}{p_0}}\, \frac{L_2}{a_2} \qquad (4.28)$$

where subscript 1 refers to the first quadrupole and 2 refers to the second. It is interesting to note that the quadrupole strength is directly proportional to the quantity L/a. Figure 4.5 shows typical trajectories in each plane. In general, the image position in the convergent-divergent (CD) plane is different from that in the divergent-convergent (DC) plane, but by varying θ_1 and θ_2 it is possible to produce a psuedo-stigmatic image (V=W) for any given object distance U. The choice of θ_1 and θ_2 is fixed by the required object and image positions. The magnifications are then completely determined and are unequal, in general the magnification is greatest in the CD plane.

The equations for the combined transfer matrices of a quadrupole pair such as shown in figure 4.5 can be written :

$$[YCD] = [X2][d][Y1] \qquad (4.29)$$

$$[XDC] = [Y2][d][X1] \qquad (4.30)$$

The notation can be explained as follows:
Both quadrupoles are assumed to be convergent in their y-planes and divergent in their x-planes. The x-y coordinate axes of Q_2 are rotated at 90^o to those of Q_1 so that a particle leaving Q_1 in its convergent y-plane enters Q_2 in its divergent x-plane. Thus [X2] is the transfer matrix for the divergent plane of quadrupole 2, [Y1] is the convergent transfer matrix of quadrupole 1. Similarly [X1] is the divergent transfer matrix for Q_1 and [Y2] is the convergent transfer matrix for Q_2. The transfer matrix for the drift space between the lenses is [d]. [YCD] is the combined transfer matrix for the CD direction, [XDC] is the corresponding combined transfer matrix for the DC direction. The total transfer matrices for

the two directions are given by:

$$[TYCD] = [V][YCD][U] \tag{4.31}$$

$$[TXDC] = [W][XDC][U] \tag{4.32}$$

where [U],[V],[W] are the transfer matrices for the appropriate drift spaces of the object and image planes.

The total transfer matrices are the products of five individual transfer matrices, so the expressions for each coefficient are extremely lengthy and are not listed here, but are quite straightforward to derive. The conditions for a pseudo-stigmatic image (V=W) can easily be obtained from equations (4.31) and (4.32) in a manner similar to that used in section 3.2.2 for a magnetic sector. Again the equations are very lengthy and are not listed here.

4.3.2 Quadrupole pair calculations

A Fortran computer program, QPAIR*, was written to calculate the first order optical properties of quadrupole pairs. The program requires as data the effective lengths L_1,L_2 of each lens and the distance d between them, along with data describing the range of excitations θ_1 and θ_2 to be considered. The desired ratio of the image distances W/V should also be supplied. For pseudo-stigmatic imaging W/V=1, however other values can be useful (see chapter 5). The program calculates the the combined transfer matrices (equations 4.29,4.30) for each value of θ_1 and θ_2 , and then solves the appropriate equations to find the object and image distances that correspond to the required conditions. For example, if psuedo-stigmatic imaging is required the program calculates, for each θ_1, θ_2 pair, the unique value of object distance U such that the image distance is equal in both planes i.e. W=V. Also calculated are the associated magnifications in each plane.

The results of a calculation for the case where L_1=L_2 =L and d=L/2 are shown in figures 4.6 a,b and c. The imaging condition imposed is that W=V i.e. pseudo-stigmatic imaging, and θ_1 and θ_2 are constrained to vary between 1.0 and 1.7. Figure 4.6a shows the universal curves for this quadrupole pair, where the object and image distances have been normalised by dividing by L. The vertical curves are for θ_1 constant whilst the horizontal curves are for θ_2 constant. The graph can be used to predict the values of θ_1 and θ_2 which will produce a pseudo-stigmatic focus for a given object and image distance. The example shown is the

* Listing in Appendix 4

Figure 4.6a

Universal Curves For Quadrupole Pair

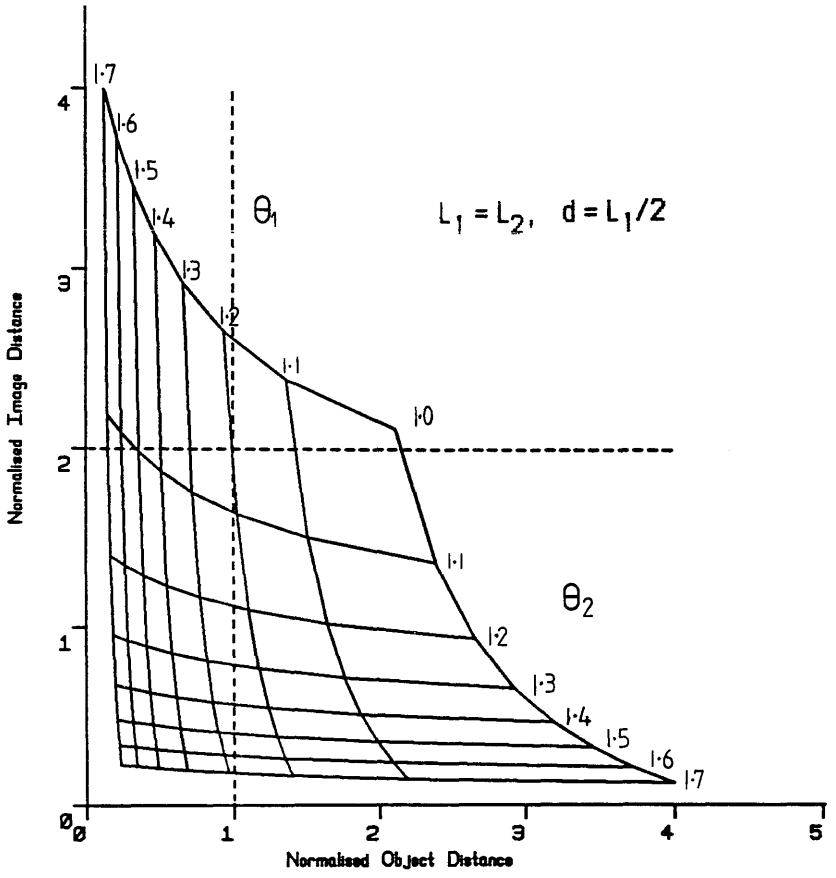

Figure 4.6b

Magnification Curves For The Convergent-Divergent Plane

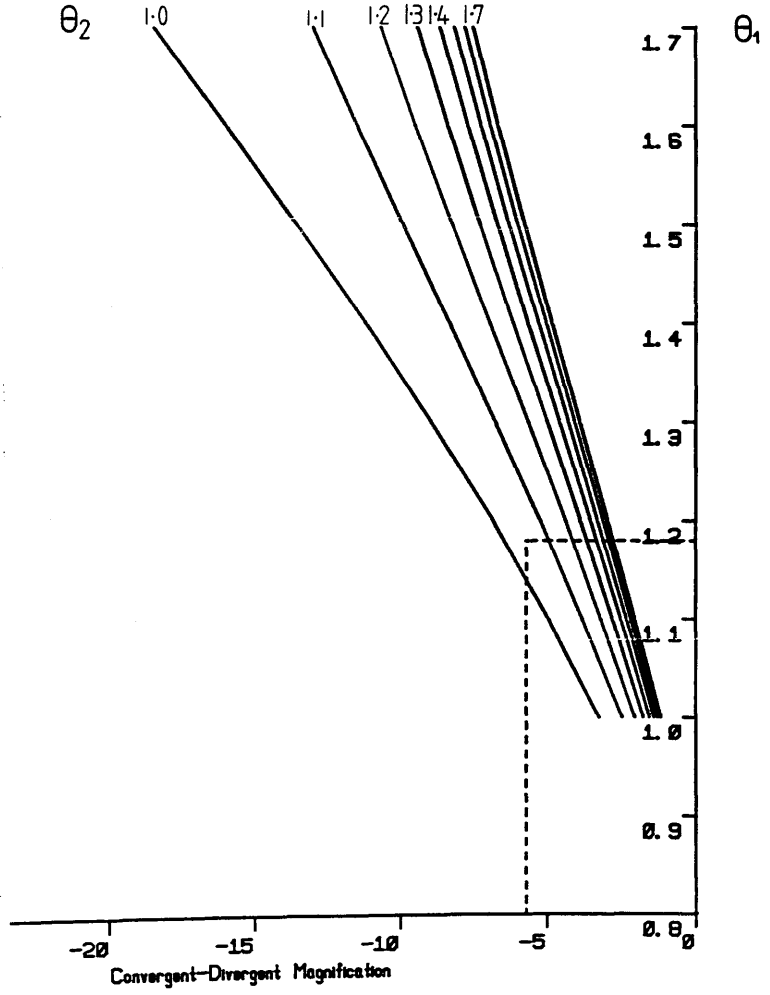

Figure 4.6c Magnification Curves For The Divergent-Convergent Plane

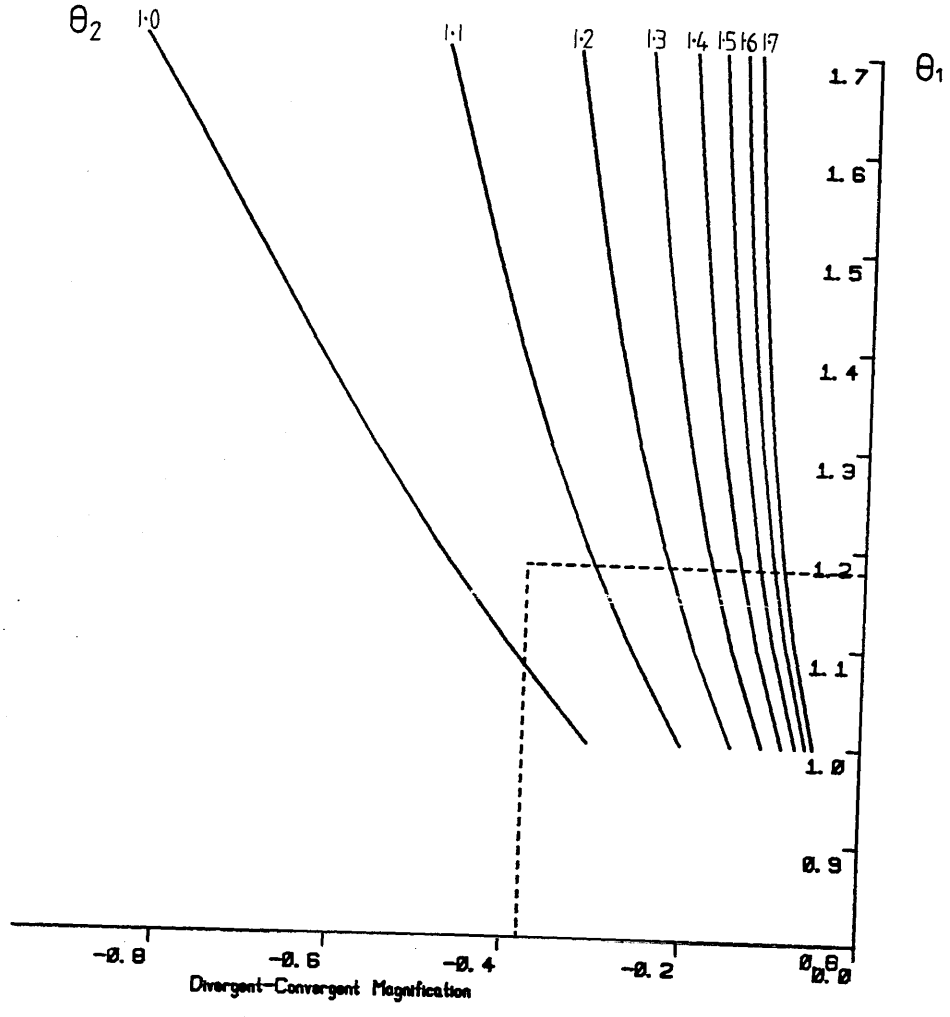

case where U/L=1 and V/L=2. The intersection of the two lines U/L=1 and V/L=2 occurs at θ_1 ~1.18, θ_2 ~1.05. Figure 4.6b shows the corresponding magnification curves for the CD plane as a function of θ_1, for θ_2 constant. The associated magnification in the DC plane is shown in figure 4.6c. As can be seen, the magnification curves in both planes are negative so that the doublet produces an inverted image. In figure 4.6c the DC magnification is always less than unity which means that the quadrupole pair is actually demagnifying in this plane, over the given range of θ_1 and θ_2. From figures 4.6b and c the magnifications associated with the pseudostigmatic focus above are: M_{CD}=-5.70, M_{DC}=-0.38.

The choice of object and image planes completely determines the values of θ_1 and θ_2 and therefore the magnifications in each plane. It is however, possible to change the optical properties by varying the distance d between the lenses - the effect of increasing the distance d from zero is, for fixed values of θ_1 and θ_2 , to decrease the object and image distances and to decrease the magnifications in each plane. In practical terms d can never be made to be zero, as there must be a finite transition region where the field gradient is reversing. Also it is likely that the physical gap between the lenses is determined by the dimensions of the coil windings.

4.3.3 Towards a magnification system

It is clear that obtaining variable magnification with fixed object and image planes requires another degree of freedom i.e. another quadrupole lens. The properties of quadrupole triplets are well known from high energy physics where they are used extensively in beam transport systems. With a triplet it is possible to vary the magnification in both directions over a wide range while maintaining the same conjugate planes. It is even possible to arrange that the imaging is truly stigmatic (magnifications equal in both planes) as in a round lens. Unfortunately it is not possible to hold the magnification in one plane constant while varying the other as is required in EELS. In order to make the magnifications in each plane independent another lens is needed. The properties of quadrupole triplets and the design of a suitable quadruplet magnification system are discussed in the next chapter.

CHAPTER 5

A Post-Spectrometer Quadrupole Magnification System

Introduction

This chapter describes the design of a four lens quadrupole system suitable for use in post-spectrometer magnification in EELS. The configuration is basically an astigmatic quadrupole pair running at fixed excitation, with two external 'thin' quadrupole lenses - one to vary the magnification in the dispersion direction and the other to refocus the spectrum at the specified image plane. A real object configuration is used in preference to a virtual object, both for ease of alignment and elimination of stray electron scattering. A further advantage of this mode is that the spectrum can be recorded in a serial manner if required. The theoretical magnification range is from ~-5x to ~-97x at 100 keV, assuming a maximum lens excitation of 200 amp-turns per pole. Chromatic aberrations of second order in the quadrupoles are calculated (in a SCOFF approximation) within the given magnification range, and their effect on the energy resolution is discussed. Methods of reducing stray electron scattering within the flight tube are considered, and to this effect the optimum placement of slits and spray apertures in the optical system is investigated. The effects of external a.c. magnetic fields are an important consideration in any electron imaging system, especially as the flight path increases in length. Systems using a real object configuration are especially sensitive in this respect, as the flight path is extended beyond the spectrometer dispersion plane - in this case by 22.5 cm. Calculations of the reduction in resolution caused by the presence of an a.c. magnetic field of 1milligauss were carried out for a range of magnifications (using a thin lens model), and the results are reported. The following sections and illustrations explain the various procedures involved in the design process and outline the operating modes of the system.

5.1 SYSTEM CONSIDERATIONS

The principal requirement of any post-spectrometer magnification system is to provide suitable magnification of the dispersion plane, in order to overcome the effects of electron scatter in the detection system, and thus produce the desired energy resolution. The geometry of the magnified spectrum should match, as closely as possible, that of the detector used, to avoid loss of signal and make for ease of alignment. From this it is obvious that the detector geometry and magnification system are closely linked, each influencing the other.

The proposed detection element for the parallel EELS system is a linear photodiode array described in chapter 6. The array consists of 512 individual elements 25μm wide and 2.5mm long, making the total active detector area 12.8mm by 2.5mm. These figures therefore mark the maximum useful dimensions of the image produced by the magnification system. It is assumed that the object for the magnification system is the spectrum produced by the Scheinfein and Isaacson spectrometer discussed previously, since this spectrometer is one of those which are commercially available and can be interfaced to the HB5.

5.1.1 Discussion of a suitable optical configuration

As mentioned in the previous chapter, maintaining fixed object and image planes with independent magnifications in the dispersive and non-dispersive directions requires the use of four quadrupole lenses. The requirement that the post spectrometer flight path be kept as short as possible suggests the use of a virtual object. This approach was followed by Krivanek et al [1987] who used one pre and three post-spectrometer quadrupoles in their system. The quadrupole before the magnet performs two functions; firstly it compensates for a varying object position and secondly it produces a pair of line foci one on either side of the midplane of the first post-spectrometer quadrupole. In addition to coupling the pre and post-spectrometer optics, this system must also affect the aberration correction of the spectrometer, since exciting the pre-spectrometer quadrupole causes the object point for the analyser to become astigmatic.

A simpler approach by Egerton and Crozier [1987] consisted of two post-spectrometer quadrupoles in a virtual object configuration. The magnification and focus of the spectrum are varied by altering the lens excitations and also by physically changing the relative positions of each lens. This system is not capable of independent control of the dispersive and non-dispersive magnifications, thus the width of the spectrum at the detector is a function of the magnification selected.

There are two disadvantages to working with a virtual object - the first is the alignment problem. In the case of the above designs no readily detectable real image from the spectrometer is available even when the magnification system is off, and so the sector alignment and aberration correction cannot be done independently of the alignment of the magnification system. The second difficulty is that of multiple backscattering of electrons which strike the walls of the flight tube. Some of these reach the detector, forming an instrumental background signal which can degrade the recorded spectra. Elimination of this stray scattering is usually accomplished with combinations of slits and spray apertures,

Figure 5.1 Quadrupole Post-Spectrometer Magnification System

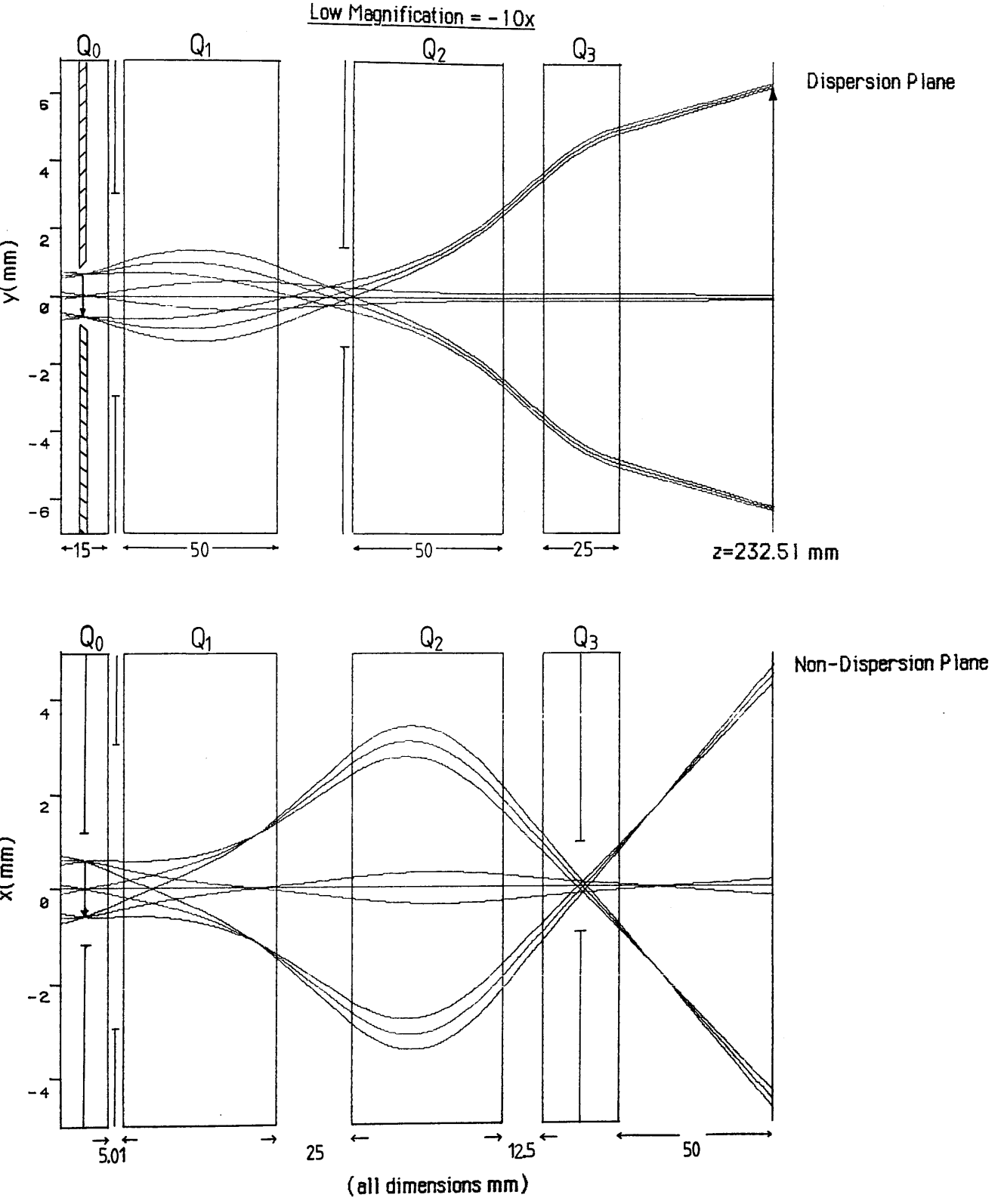

however the virtual object mode means that, especially in the dispersion direction, there are no obvious positions to place the apertures without obstructing some signal electrons. For these reasons, the system described in the following sections uses a real object, and is correspondingly longer than an equivalent virtual object design. All the results presented refer to the focussing of 100keV electrons.

Figure 5.1 shows the entire four lens system operating in low magnification mode with a dispersion plane gain of ~-10x. The position of the various spray apertures and slits discussed in section 5.2.2 is indicated. Some ray bunches have been traced through the system to illustrate the imaging operation in the dispersive and non-dispersive planes. (For the purpose of clarity, these rays are more divergent and further off axis than would normally be expected, and the lack of apparent focus is due to a plotting artefact). For simplicity the lens combination is designed to operate with the central quadrupoles , Q_1 and Q_2, running at fixed excitation. Changing the excitation of Q_3 alters the magnification in the dispersion plane, whilst Q_0 is used to refocus the spectrum at the image plane - essentially a two control system. The optical properties in the non-dispersive plane are largely independent of Q_0 and Q_3, because of the particular optical configuration chosen.

5.1.2 The quadrupole pair - Q_1 and Q_2

The operation of the central quadrupole pair in isolation is shown in figure 5.2. The lens orientation is convergent-divergent (CD) in the dispersion plane and divergent-convergent (DC) in the non-dispersive plane, and the bores of all the lenses to be described are 2cm, allowing for a flight tube to match the 2cm gap of the Scheinfein and Isaacson spectrometer. The gap between lenses Q_1 and Q_2 is 25mm, and the effective length L of each lens is 50mm, giving an L/a ratio of 5. Q_1 and Q_2 are operated in an astigmatic imaging condition at fixed excitation, where the ratio of the non-dispersive focal distance W to the dispersion direction focal distance V has been chosen to be 1:2 (fig.5.2). The Fortran programme QPAIR, described previously, was used to produce the universal curves of figure 5.3a. Choosing the object and image distances to be U=0.25 and V=1 (W=0.5) respectively, where U, V and W have been normalised to L, gives from figure 5.3a excitation values θ_1 and θ_2 of 1.651 and 1.486. Using equations (4.27) and (4.28) these values correspond to 44.5 and 36 amp-turns per pole respectively. The resultant magnifications are obtained from figures 5.3b and 5.3c as -11.05x in the CD (dispersive) and -0.18x in the DC (non-dispersive)planes.

Figure 5.2 The Quadrupole Pair

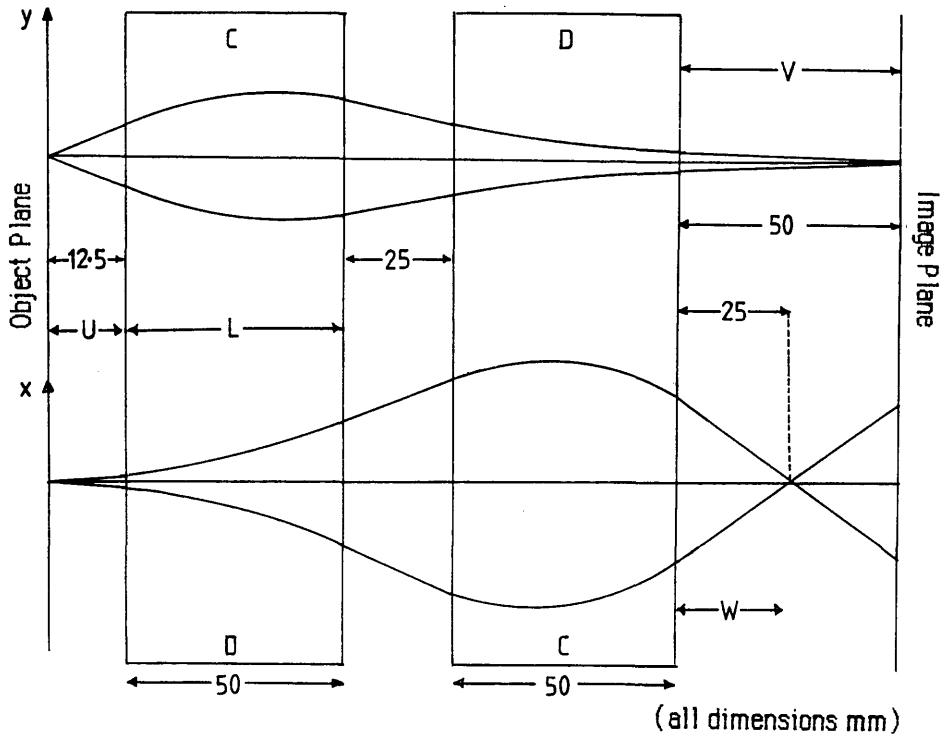

Figure 5.3a Universal Curves For Figure 5.2

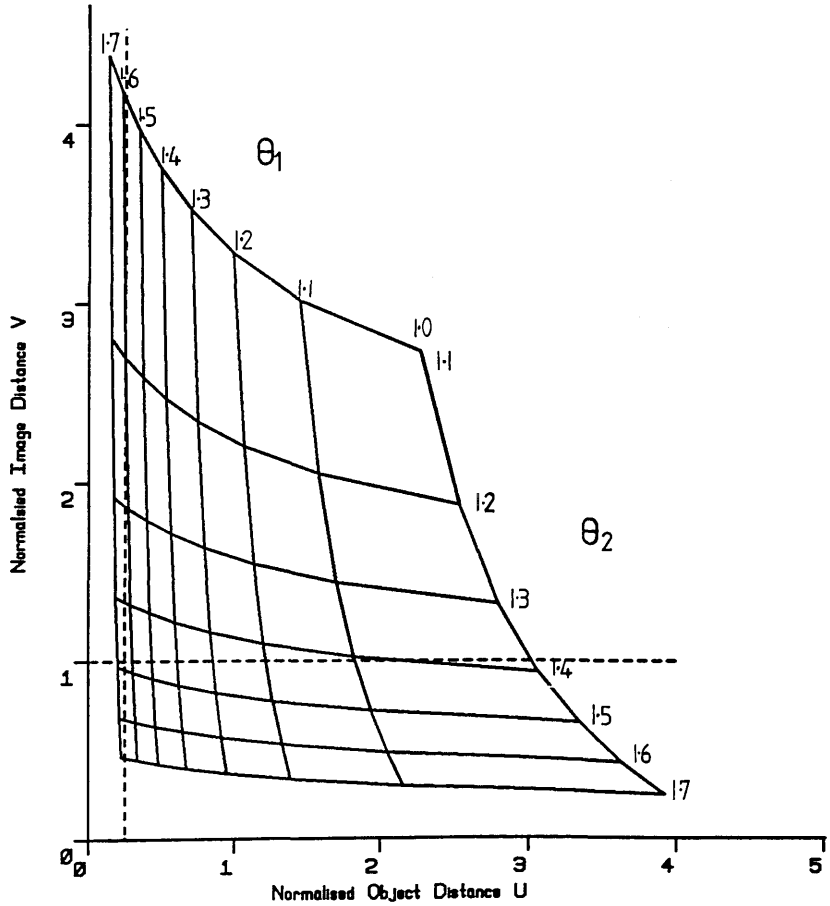

Figure 5.3b Dispersion Plane (C-D)Magnification Curves

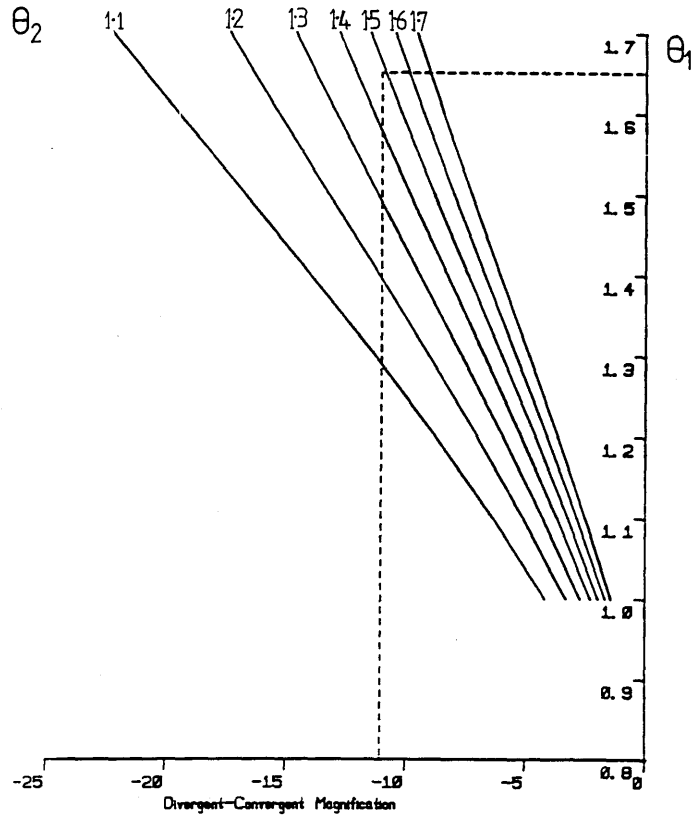

Figure 5.3c Non-Dispersion Plane (D-C)Magnification Curves

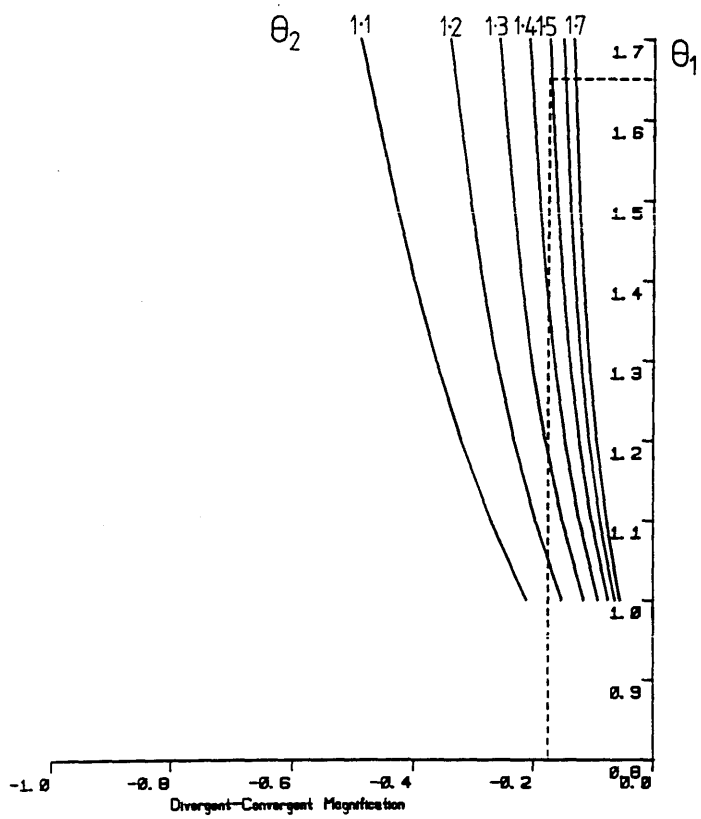

5.1.3 Varying the magnification - Q_3

As mentioned in the previous chapter, the quadrupole pair excitations θ_1 and θ_2 are completely determined by the chosen object and image planes. In order to provide variable magnification a third quadrupole lens is necessary. This lens, Q_3 is positioned so that the non-dispersive focus occurs at its centre (fig 5.4). Thus, if Q_3 is considered a 'thin' lens, it will have no effect on the position and magnification of the non-dispersive focus.

The design of Q_3 requires some compromise, due to the different tasks required of it in each plane. In order to provide high magnification in the dispersion plane the lens excitation should be strong, however the length L_3 cannot be made large as the lens would behave as a thick lens, causing the non-dispersive focus position to vary. Simply using a large number of amp-turns per pole is not the ideal solution as the excitation $\theta \propto \sqrt{(NI)}$, and heating effects will limit the maximum value of NI. Accordingly, as the bore is 20mm the effective length L_3 was chosen to be 25mm, i.e. L/2.

A Fortran program QTRIP4, was written to calculate the optical properties of systems containing up to four quadrupoles. It is essentially an extended version of QPAIR and uses the same matrix calculations. Figures 5.5 a,b show the optical properties of the quadrupole triplet configuration described above, as a function of the third lens excitation θ_3, for θ_1 and θ_2 constant. In this case the action of Q_3 is diverging in the dispersion (CDD) plane and converging in the non-dispersion (DCC) plane. The object position is referenced to the entrance face of Q_1 while the image positions are referenced to the exit face of Q_2. As expected, for θ_3=0 the optical properties are identical to those of Q_1 and Q_2 alone. Increasing θ_3 causes the dispersive focus and magnification to increase, whilst the corresponding quantities in the non-dispersive plane remain relatively constant. This configuration is called the high magnification mode. Reversing the polarity of Q_3 causes the opposite effect, as shown in figures 5.6 a, b. Now an increase in θ_3 causes the dispersion plane focus position and magnification to decrease, so that this configuration is known as the low magnification mode. Again the non-dispersive properties remain largely constant.

5.1.4 Refocussing the spectrum - Q_0

In order to position the dispersion plane focus at the required image plane a fourth lens is necessary. If this lens, Q_0 is positioned so that the spectrometer dispersion plane is located at its centre, then relatively coarse changes in the lens excitation will effect only small changes in the effective object position as seen by the following lens Q_1, producing a fine focussing action. Again the construction of this lens requires a compromise between short length and

Figure 5.4 Quadrupole Triplet Showing Position Of Q_3 Relative To Q_1 And Q_2

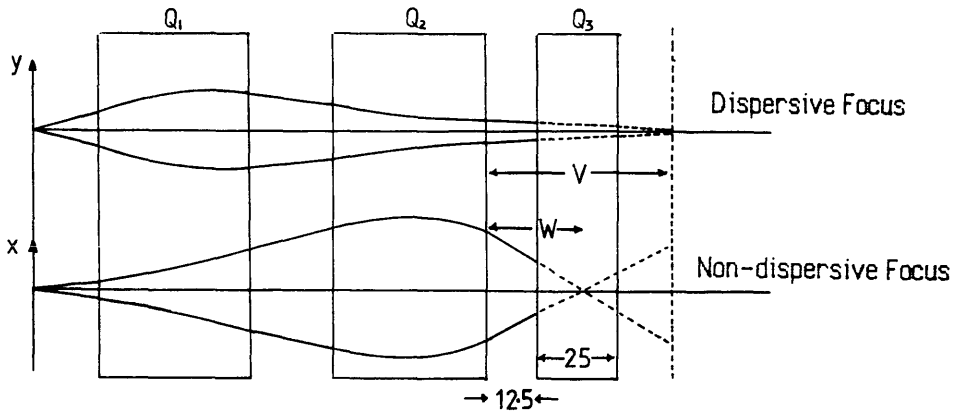

Figure 5.5a Imaging Properties Of Figure 5.4 (High Mag Mode)

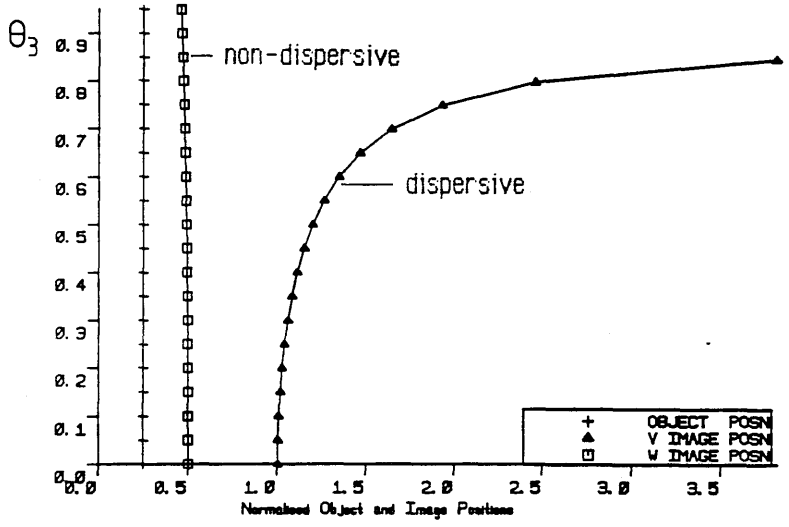

Figure 5.5b Magnification Properties Of Figure 5.4 (High Mag Mode)

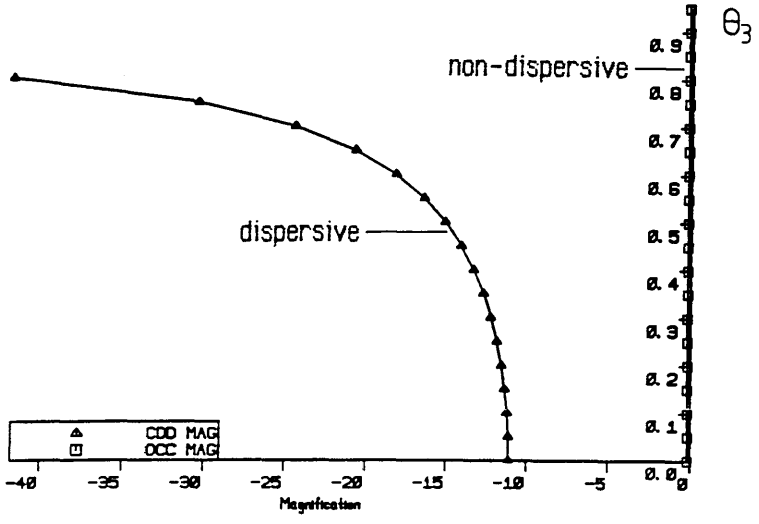

Figure 5.6a Imaging Properties Of Figure 5.4 (Low Mag Mode)

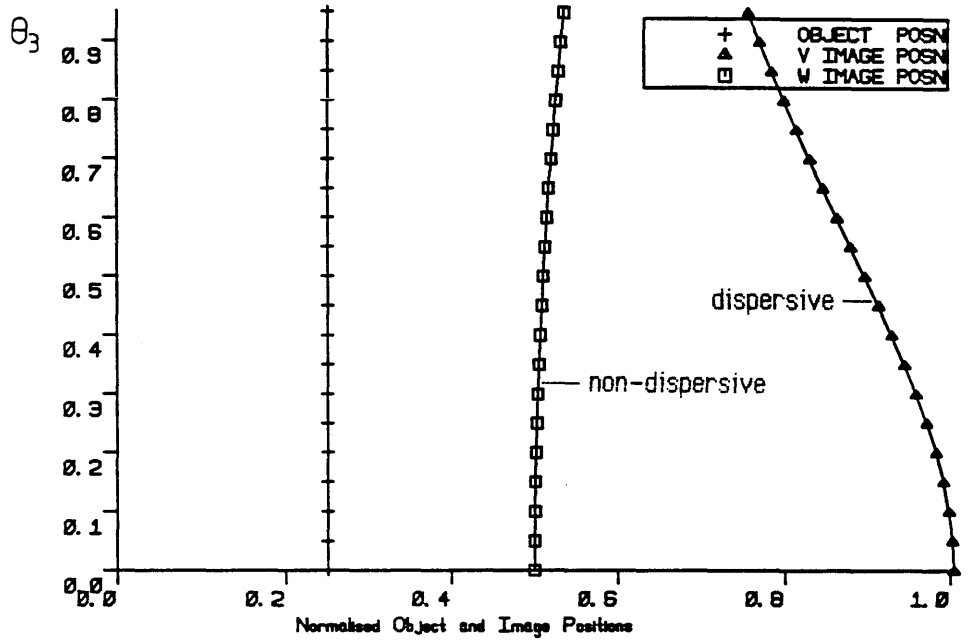

Figure 5.6b Magnification Properties Of Figure 5.4 (Low Mag Mode)

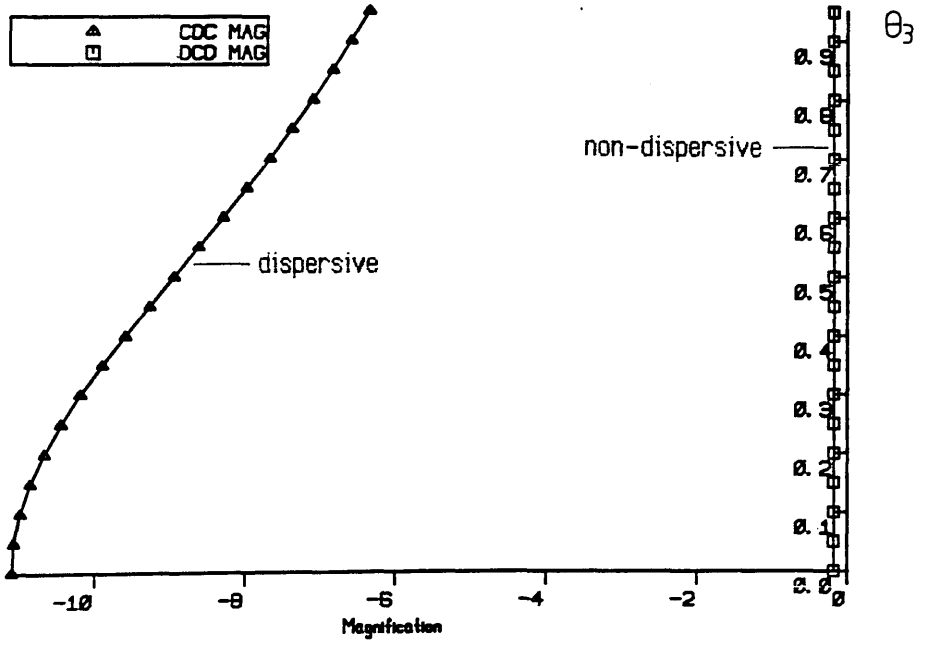

maximum excitation. The effective length is chosen to be 15mm (i.e. 0.3L) and the lens is positioned as shown in figure 5.1.

Figures 5.7a,b are the optical properties as calculated by QTRIP4 for the high magnification mode, given the above configuration. Again θ_1 and θ_2 are held constant and the optical properties are plotted as a function of θ_3, for constant values of θ_0. In this case Q_0 is converging in the dispersion direction giving a CCDD arrangement, and diverging in the non-dispersion direction to give the complementary DDCC configuration in this plane. As can be seen, increasing θ_0 for constant θ_3 tends to reduce the dispersive focus and lowers the dispersive magnification. The corresponding effects on the non-dispersive plane focus and magnification are negligible, because of the demagnifying nature of this plane.

Figures 5.8 a,b show the associated results for the low magnification mode. In this configuration the polarities of Q_0 and Q_3 are reversed, so that the dispersion plane configuration is DCDC, and the non-dispersion plane configuration is therefore CDCD. Now increasing θ_0 for θ_3 constant results in an increase in the dispersion plane focal position. The effect on the magnification in this plane is more complex;- for $\theta_3 < 0.7$ the magnification increases, whereas for $\theta_3 > 0.7$ the magnification decreases with increasing θ_0. At the crossover point it is interesting to see that the magnification is independent of θ_0, however the image position is not. It is obvious from figures 5.7 and 5.8 that the excitations of Q_0 and Q_3 can be chosen so as to provide a variable magnification in the dispersion plane, at fixed object and image positions. This is discussed in the next section.

5.1.5 Final image plane and optical performance

The location of the final image plane is determined by the desire to keep the optical system as compact as possible, and yet provide large values of magnification in the dispersion plane, without recourse to unrealistically large excitations of Q_3. The chosen image position is 87.5mm (1.75L) after the exit of Q_2, which corresponds to a distance of 50mm (L) after the exit of Q_3. This gives a complete optical system length of 232.5mm (not including the drift space between the spectrometer exit and the dispersion plane), however since the object is at the centre of Q_0 the optical flight path is actually 225mm. A further Fortran program, QQUAD was written to calculate the correct focussing excitation θ_0, for each value of θ_3, which focusses the magnified dispersion plane at this image position.

The solution for the high magnification (CCDD) configuration is shown in figure 5.9a, along with the associated magnifications in each plane (fig.5.9b). As can be seen from figure 5.7a,

Figure 5.7a IMAGING PROPERTIES OF QUADRUPLET (HIGH MAG)

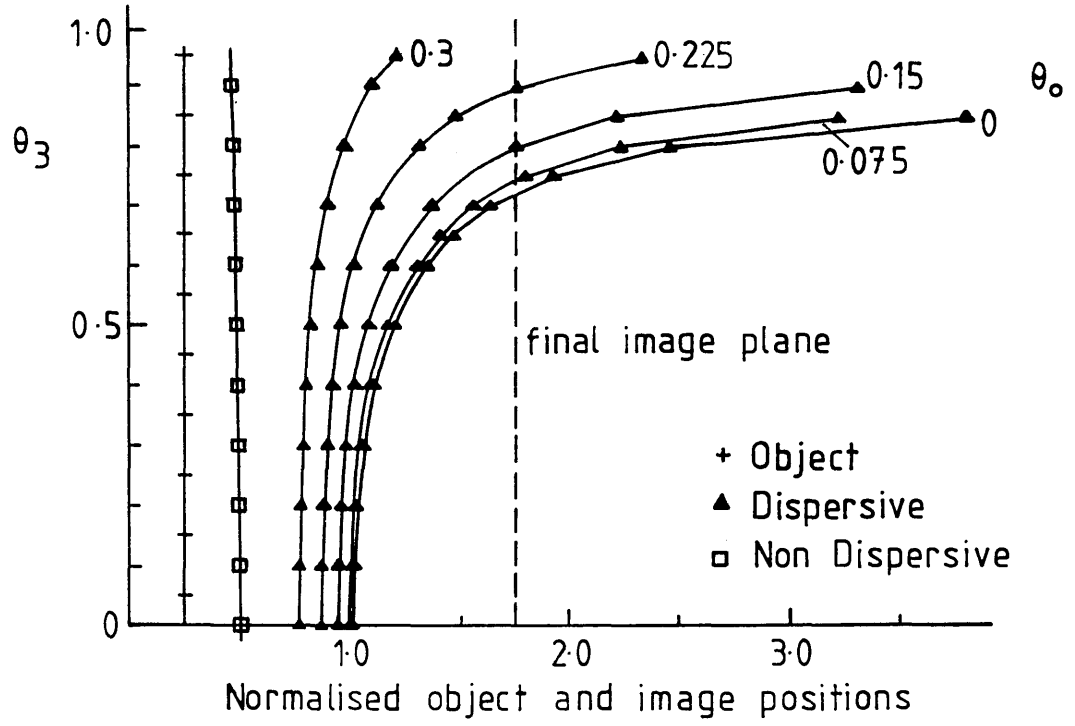

Figure 5.7b MAGNIFICATION OF QUADRUPLET (HIGH MAG)

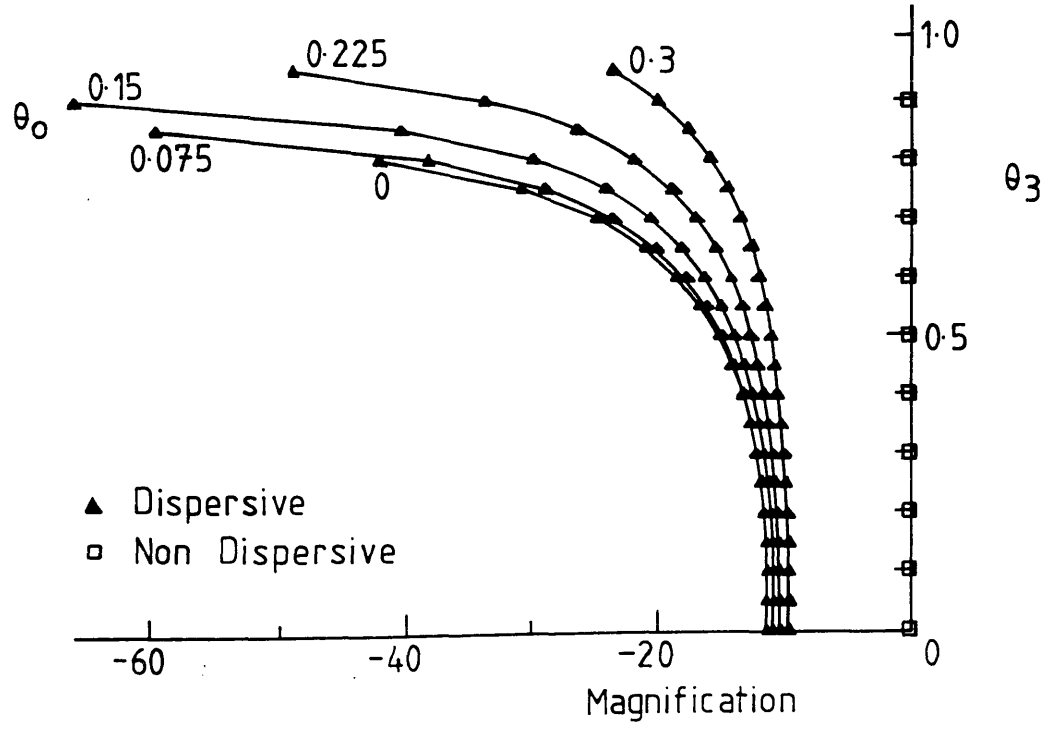

Figure 5.8a IMAGING PROPERTIES OF QUADRUPLET (LOW MAG)

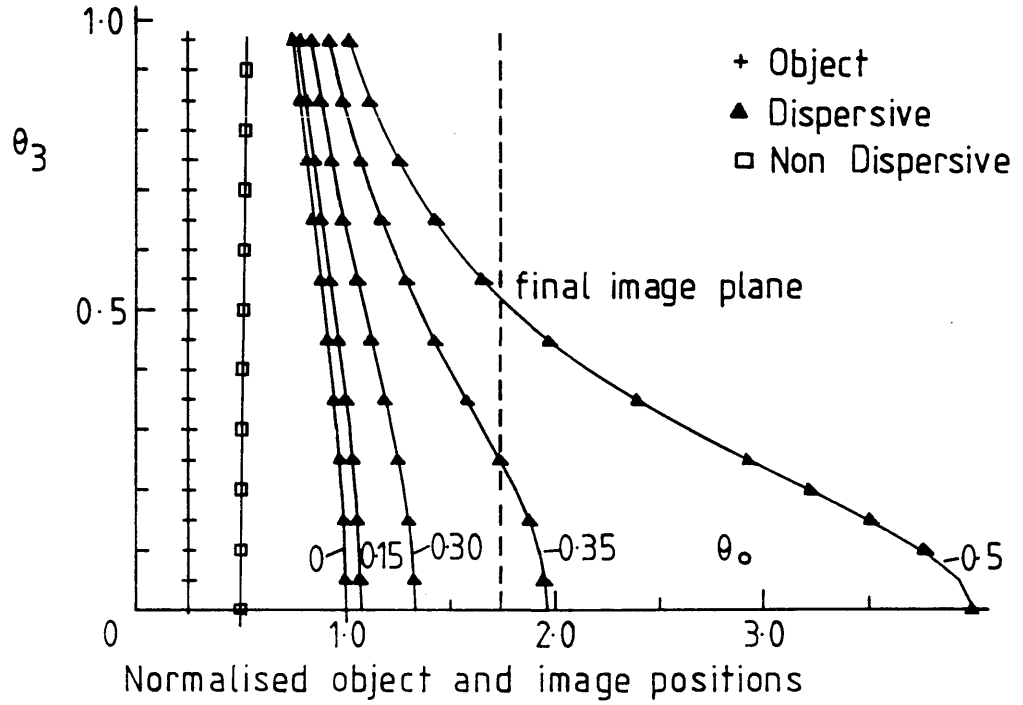

Figure 5.8b MAGNIFICATION PROPERTIES OF QUADRUPLET (LOW MAG)

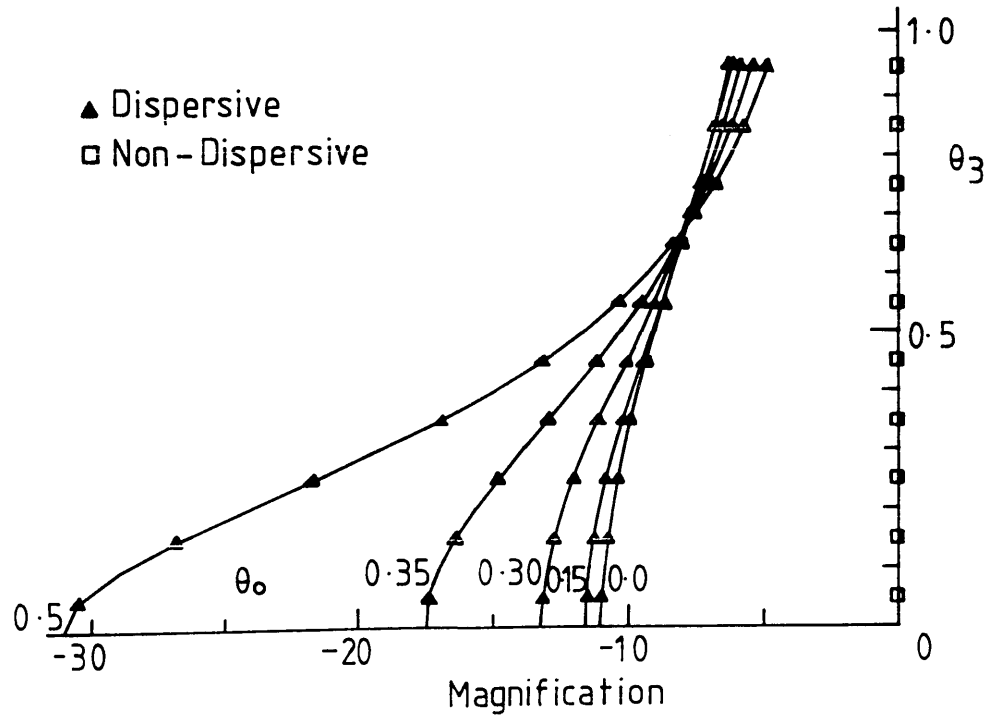

Figure 5.9a Focussing Excitations Of Quadruplet (High Mag)

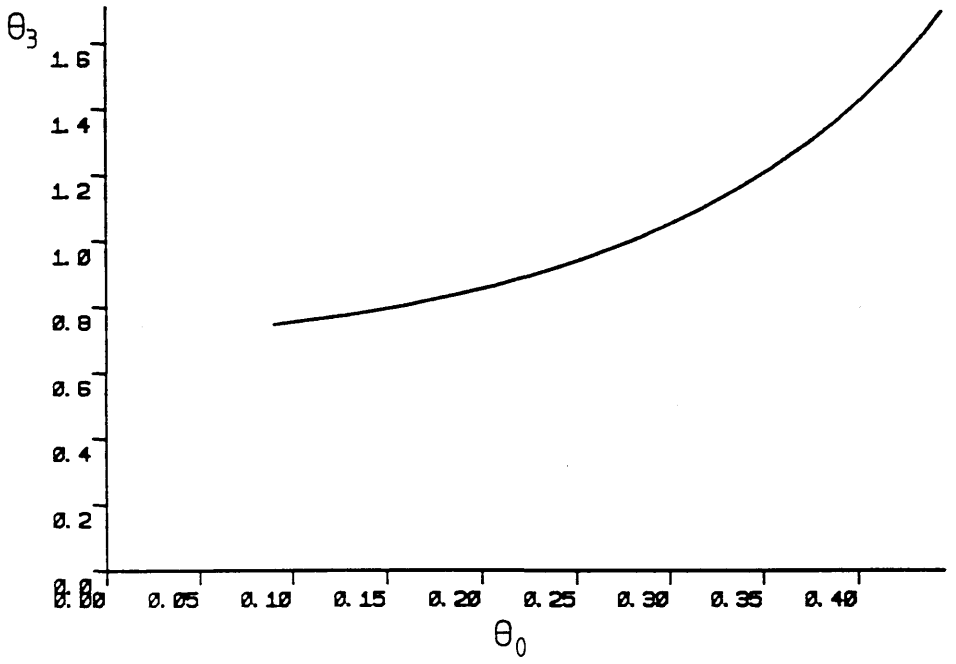

Figure 5.9b Magnification Range Of Quadruplet (High Mag)

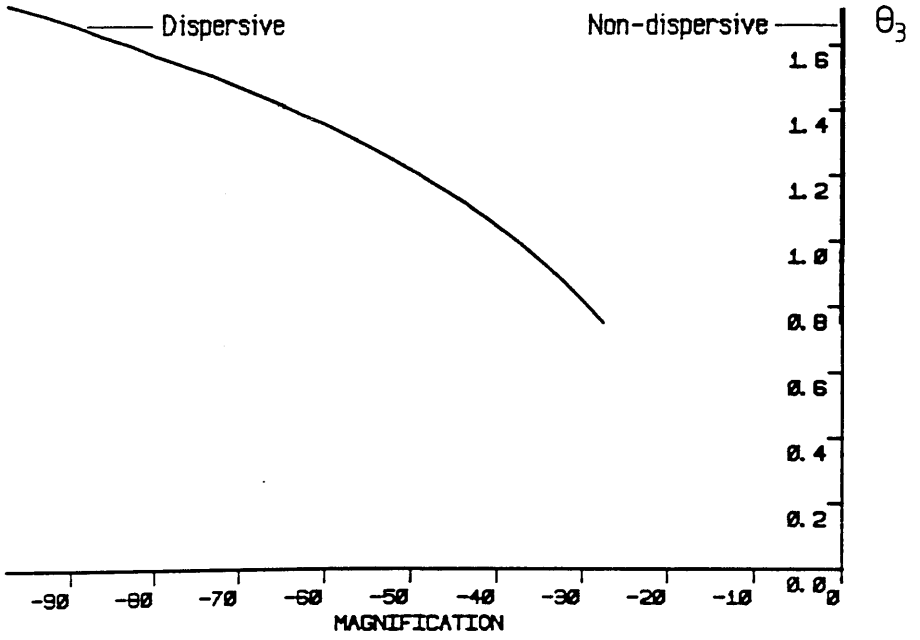

Figure 5.10a Focussing Excitations Of Quadruplet (Low Mag)

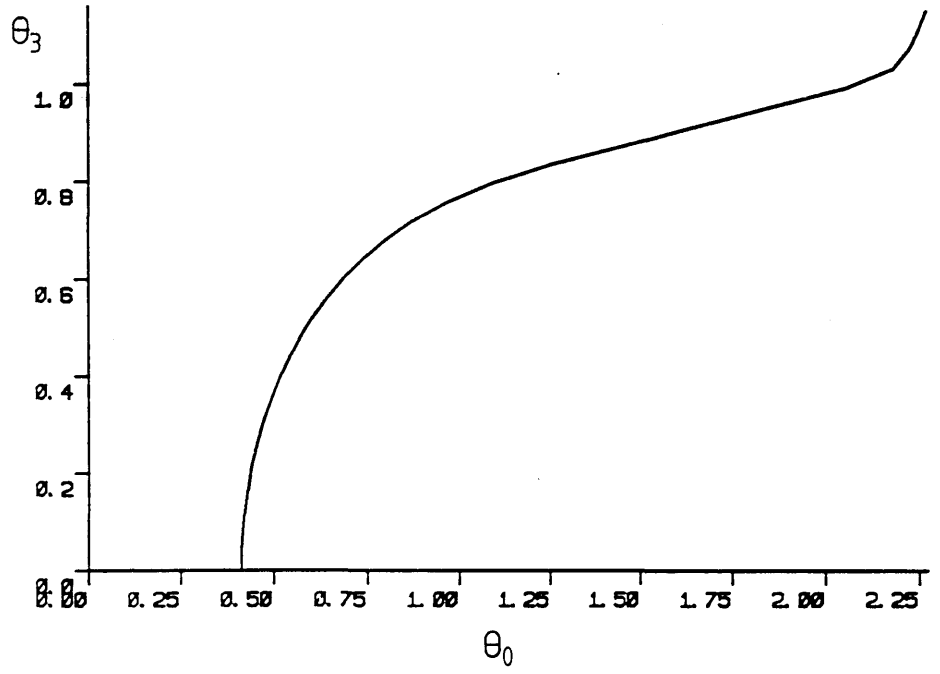

Figure 5.10b Magnification Range Of Quadruplet (Low Mag)

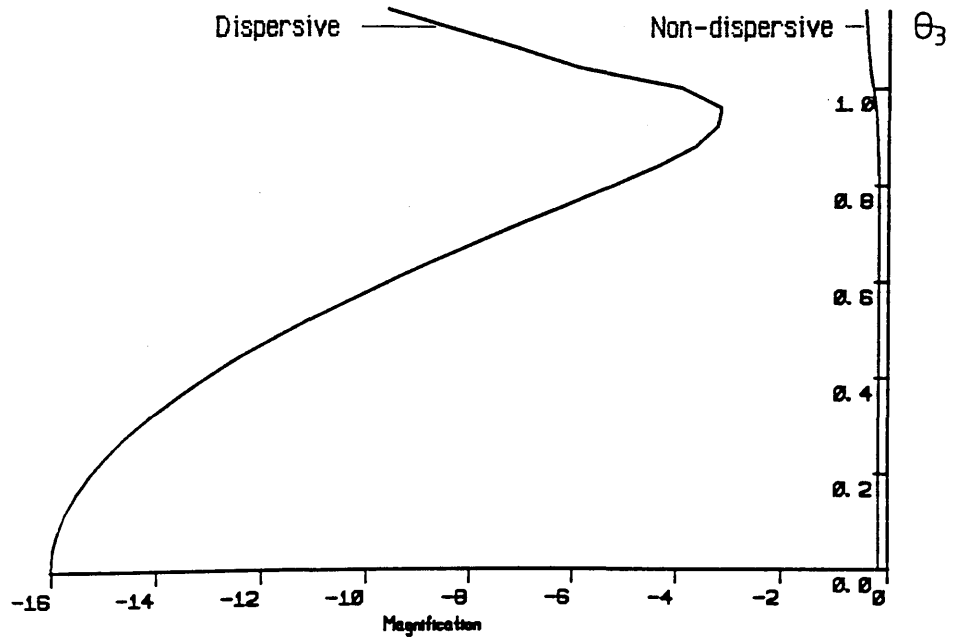

the smallest value of θ_3 for which a solution exists is $\theta_3 \sim 0.75$, which corresponds to an excitation of ~37 amp-turns per pole and gives a dispersion plane magnification of ~-27x. The highest attainable magnification is determined by the maximum excitation of Q_3. Assuming that the maximum value of NI is of the order of 200 amp-turns per pole [Hawkes 1970] then $\theta_{3\ max} \sim 1.7$, giving a magnification of ~-97x at $\theta_0 = 0.44$. The magnification in the non-dispersive plane remains constant at around -0.2x.

The solution for the low magnification (CDCD) configuration is shown in figures 5.10 a,b. The behaviour of the system is now slightly more complex, and the maximum magnification in this mode is -16x, occurring at $\theta_3 = 0$, $\theta_0 = 0.41$. The minimum obtainable magnification is determined by the maximum excitation of Q_0 - if θ_0 were unlimited the minimum magnification would be ~-3x. However, assuming $NI_{max} = 200$ amp-turns per pole, θ_0 max = 1.05 giving $\theta_3 = 0.8$ (42 amp-turns per pole) and a practical minimum magnification of ~ -5.2x. The magnification in the non-dispersive plane is invariant at -0.17x up to this point, and then slowly increases.

Combining the two optical modes above gives a magnification range of ~-5x to ~-97x. The dispersion of the Scheinfein and Isaacson spectrometer is 1.8μm/eV, so that the range of the magnified dispersion is ~ 9μm/eV up to ~ 175μm/eV, which is wide enough to cover most practical requirements.

5.2 RAY TRACING AND REDUCTION OF ELECTRON SCATTERING

It is most important, in any magnification system, to eliminate electrons which have been randomly scattered in the flight tube and which, if detected, would contribute to an instrumental background signal. The most efficient way to do this is by constructing a suitable series of spray apertures, fixed slits, and movable slits along the optical path. In order to optimise the position and apertures of these elements a Fortran program, QTRACE, was written to trace selected trajectories through the system. Trajectories of most interest are those of the extreme rays which can be imaged at each magnification by the 12.8 mm detector. The divergence of each ray bunch is calculated from the spectrum produced by the Scheinfein and Isaacson spectrometer, assuming an entrance angle β of 5mrads.

Output from QTRACE is displayed in graphical form in figures 5.11 to 5.16. The six figures cover the entire range of magnifications, and are useful in determining the most

efficient positions for the placement of slits and apertures. In all cases the maximum excursion of any trajectory from the optic axis does not exceed 9mm in the dispersion direction, and 5mm in the non-dispersive direction. It is also obvious from the figures that the width of the defocussed image in the non-dispersive plane is virtually independent of the dispersion plane magnification, being determined solely by the angular divergence of the electrons at the object plane. This angular distribution in turn is directly proportional to the entrance angle β, so that the width of the magnified spectrum in the non-dispersive direction can be controlled by varying the spectrometer collection angle. At the very lowest magnification the source size does contribute a small amount to the broadening of the defocus.

The position of the non-dispersive focus remains relatively close to the centre of lens Q_3, except at the higher magnifications when θ_3 becomes very strong. At this point the focus position is pulled towards the entrance face, however the defocus at the final image plane does not increase because the rest of the lens acts to compress the angular distribution of the electrons. For example, at a magnification of -51x the focus position is shifted ~4mm away from the centre of the lens. The entire shift over the whole magnification range is approximately 10mm.

5.2.1 Energy selecting slits.

Proper design of entrance slits is very important in order to reduce stray scattering effects. The purpose of these slits is to block out all the electrons with energy differences greater than the maximum range which can be detected at each magnification, and the optimium location is at the spectrometer dispersion plane, conjugate with the final image plane i.e. at the centre of Q_0. At the lowest magnification of -5.19x, the maximum object size which can be imaged onto the detector is 2.46 mm, corresponding to an energy range of 1369eV (for the Scheinfein and Isaacson spectrometer). Thus, to prevent electrons outside this range entering the magnification system the slits should be closed down to a gap of 2.46mm. At the highest magnification of -97x the slits should be closed down to 0.13mm, corresponding to an energy range of 73eV. If it is desired that the system be also capable of serial detection, then the entrance slits should close down to $< 1\mu m$.

In the non-dispersive plane a pair of fixed slits can be located anywhere inside the bore of Q_0, preferably after the energy selecting slits. The purpose of these fixed slits is to stop any electrons which have been scattered inside the spectrometer and managed to pass through the energy selecting slits. If the magnification system were perfectly aligned then these slits

could easily be made less than 1mm wide. However, this narrow gap could make initial setting up very difficult, so that a compromise gap of 2.5mm may be more convenient.

5.2.2 Spray apertures and fixed slits

After the energy selecting slits there is scope for the placement of a circular spray aperture of radius 3mm in the gap between Q_0 and Q_1. This aperture would help to stop any high angle electrons scattered off the edges of the energy selecting slits from progressing any further, especially at lower magnifications. There is a beam crossover point in the dispersive plane which is located after the exit of Q_1 and before the exit of Q_2, the exact position depending upon the magnification. A pair of fixed slits ~3mm wide placed at the entrance of Q_2 would pass all the signal trajectories and act as a further impediment to the progress of randomly scattered electrons. There are no further positions for the placement of slits or apertures in the dispersion plane.

The most obvious place for a pair of fixed slits in the non-dispersive plane is at the focus point at the centre of Q_3, unfortunately the slits cannot be made too narrow because of the slight movement of this focal point with change in magnification. However, a gap of 2mm should be narrow enough to help to eliminate any spurious electron trajectories at this point, without obstructing the signal path at even the most extreme magnifications. Figures 5.1 and 5.11 include schematic representations of the above mentioned apertures and slits. In the latter case the figure refers to the lowest attainable magnification, where the electrons are most displaced from the optic axis, and it can be seen that there is no obstruction to even the most extreme trajectories.

5.3 CHROMATIC ABERRATIONS AND IMAGING PROPERTIES

As described in chapter 4 quadrupole field symmetry excludes all second order aberrations except second order chromatic aberrations. There are eight second order focussing coefficients to be considered, four in each plane (the convergent and divergent planes are still independent to second order). In order to obtain values for these coefficients a Fortran program, QMATRIX was written to carry out the required second order matrix calculations using the SCOFF approximation. The results are discussed in the following sections.

Figure 5.11

Magnification = -5x

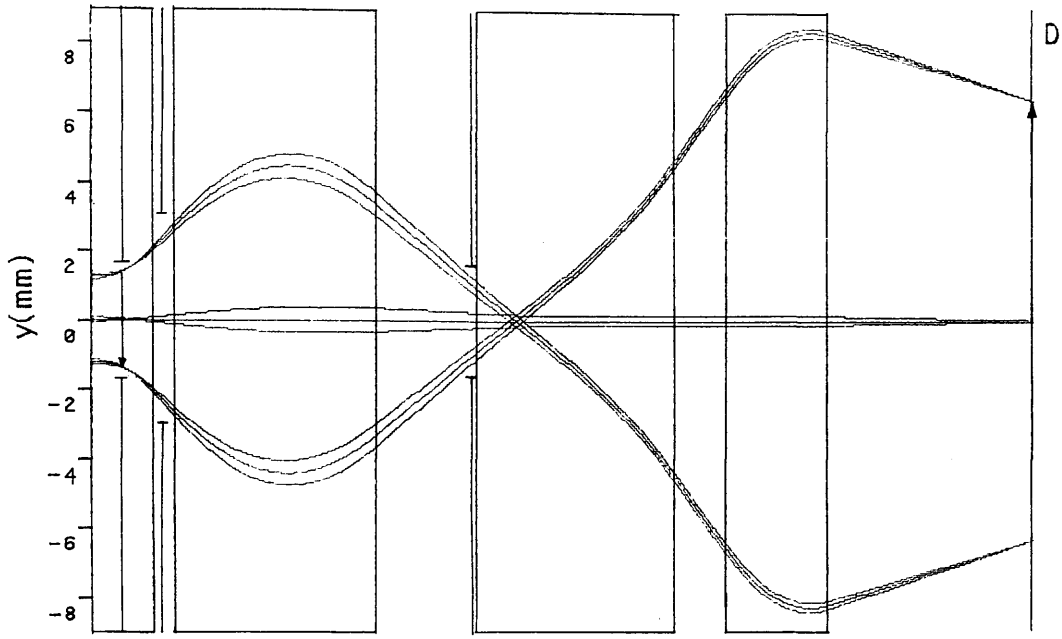

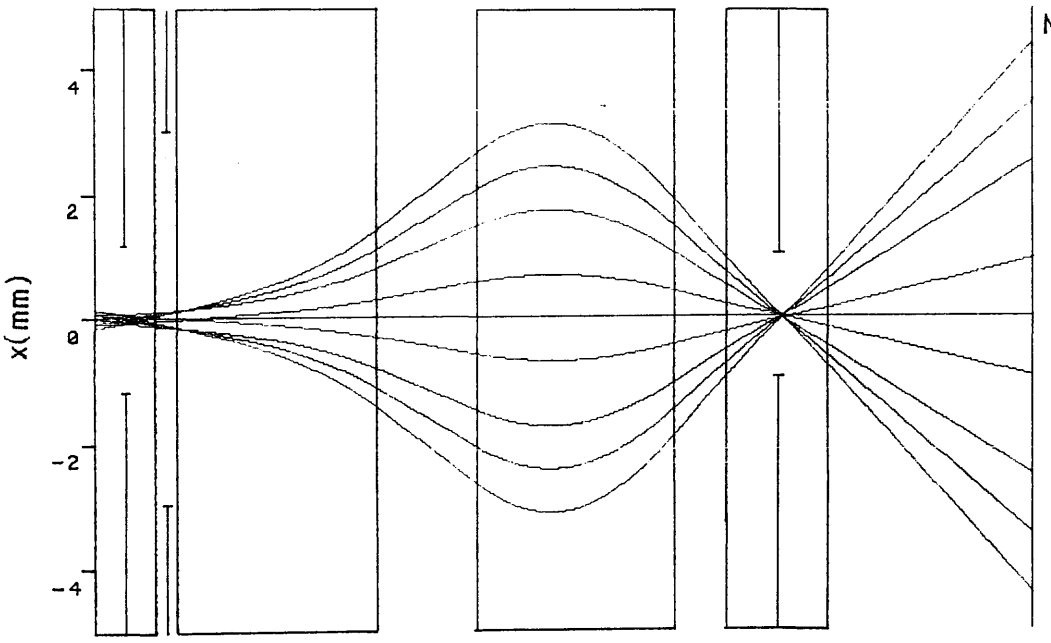

Figure 5.12

Magnification = -10x

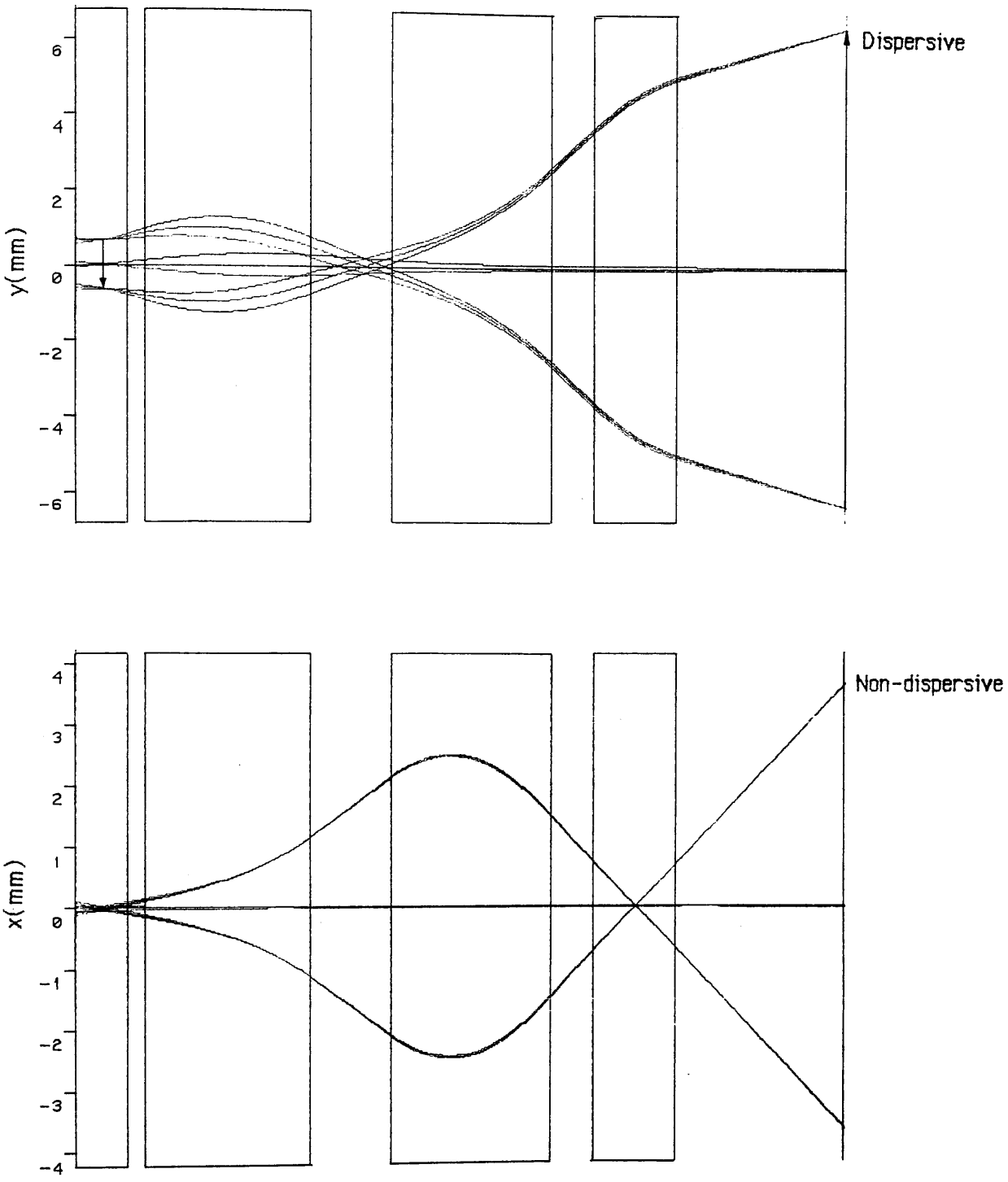

Figure 5.13

Magnification = -16x

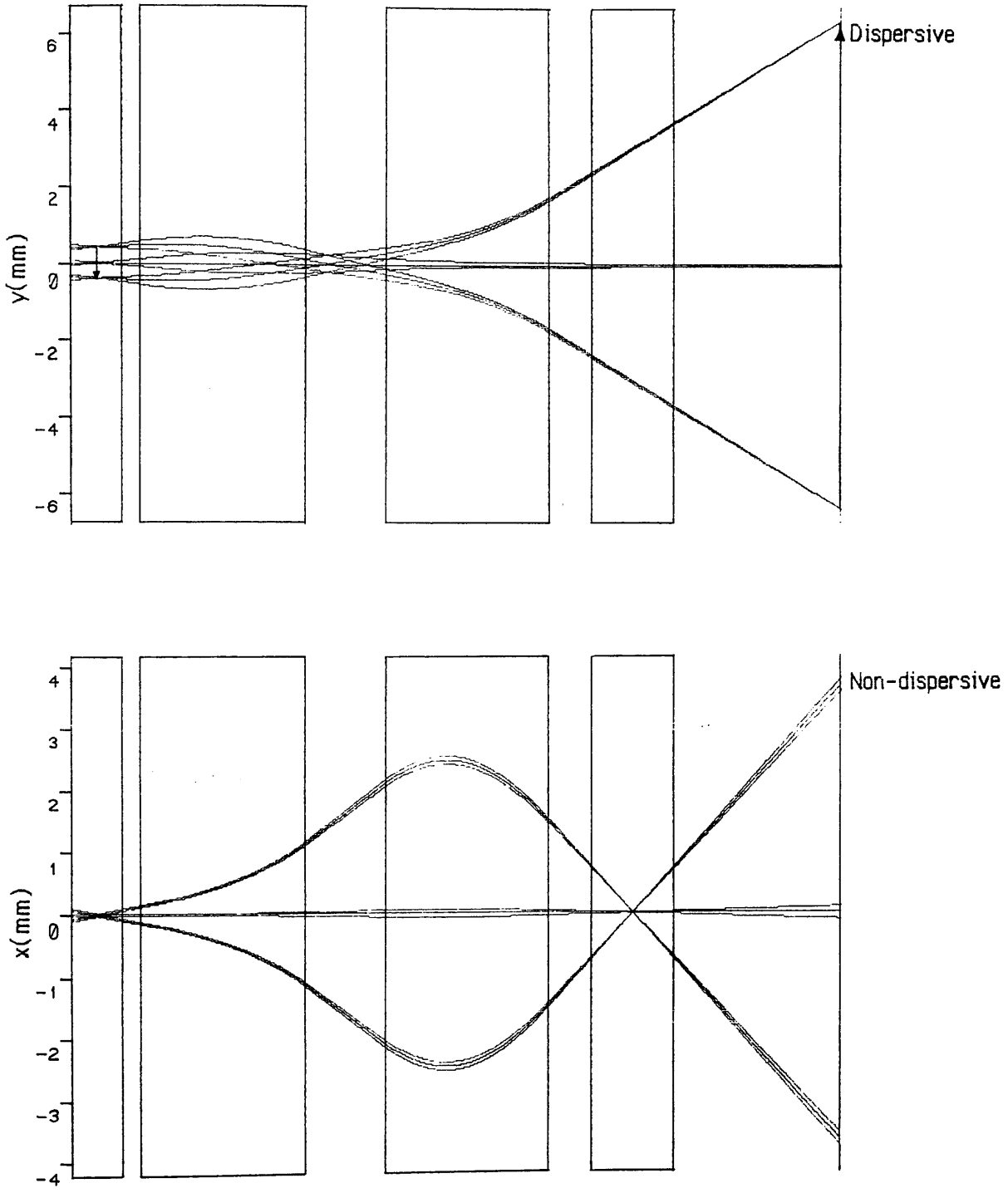

Figure 5.14

Magnification = -28x

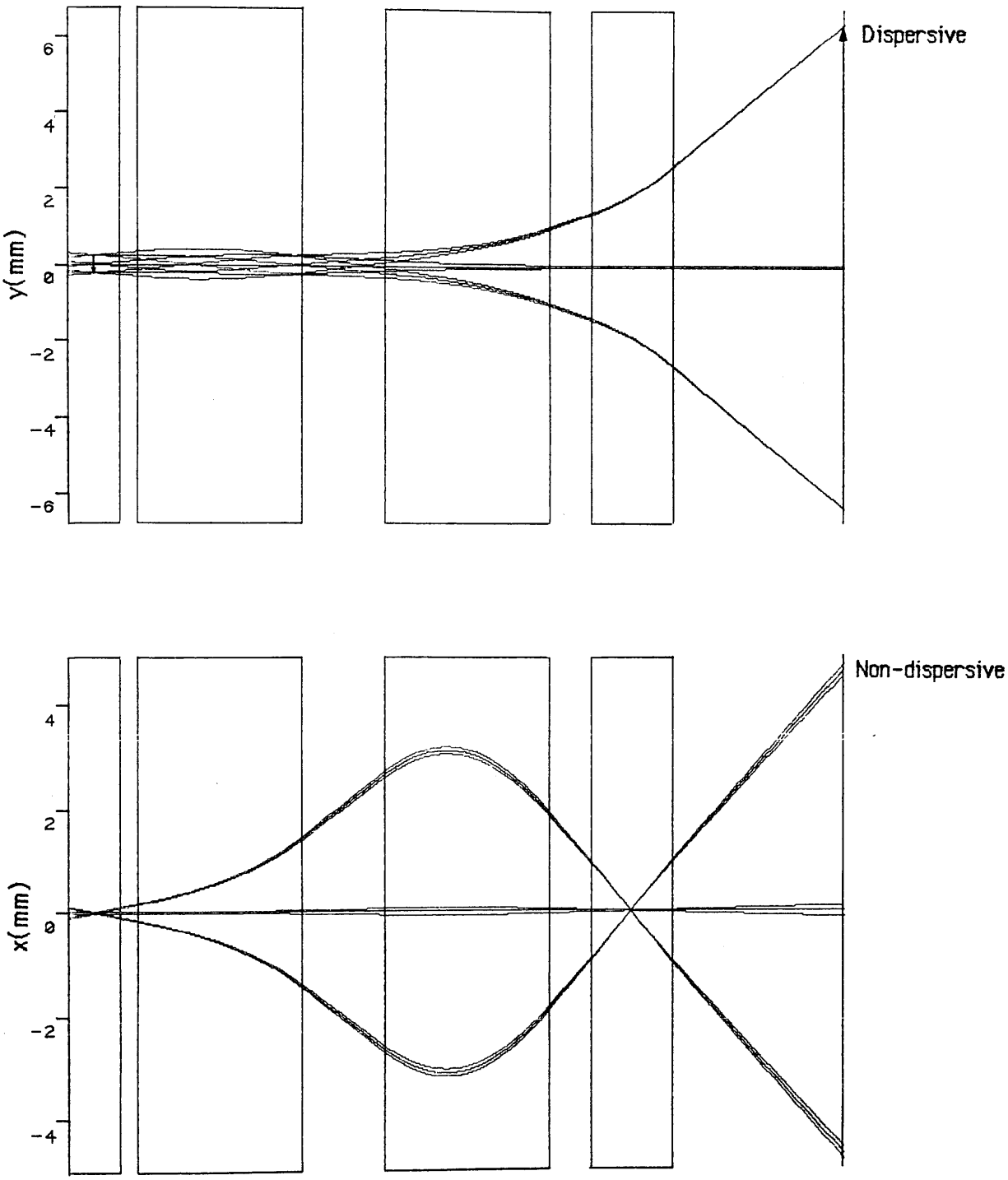

Figure 5.15

Magnification = -51x

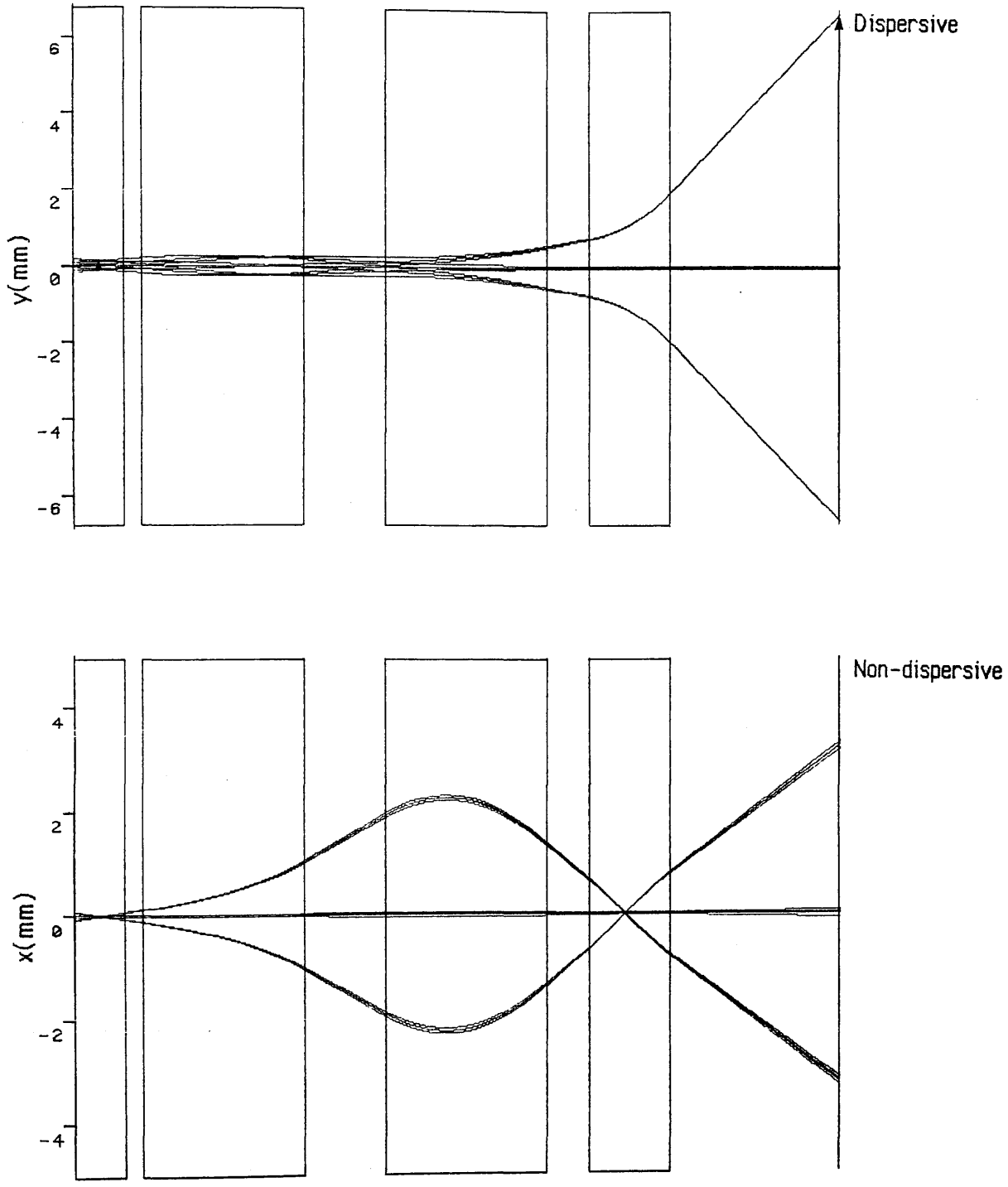

Figure 5.16

Magnification = -90x

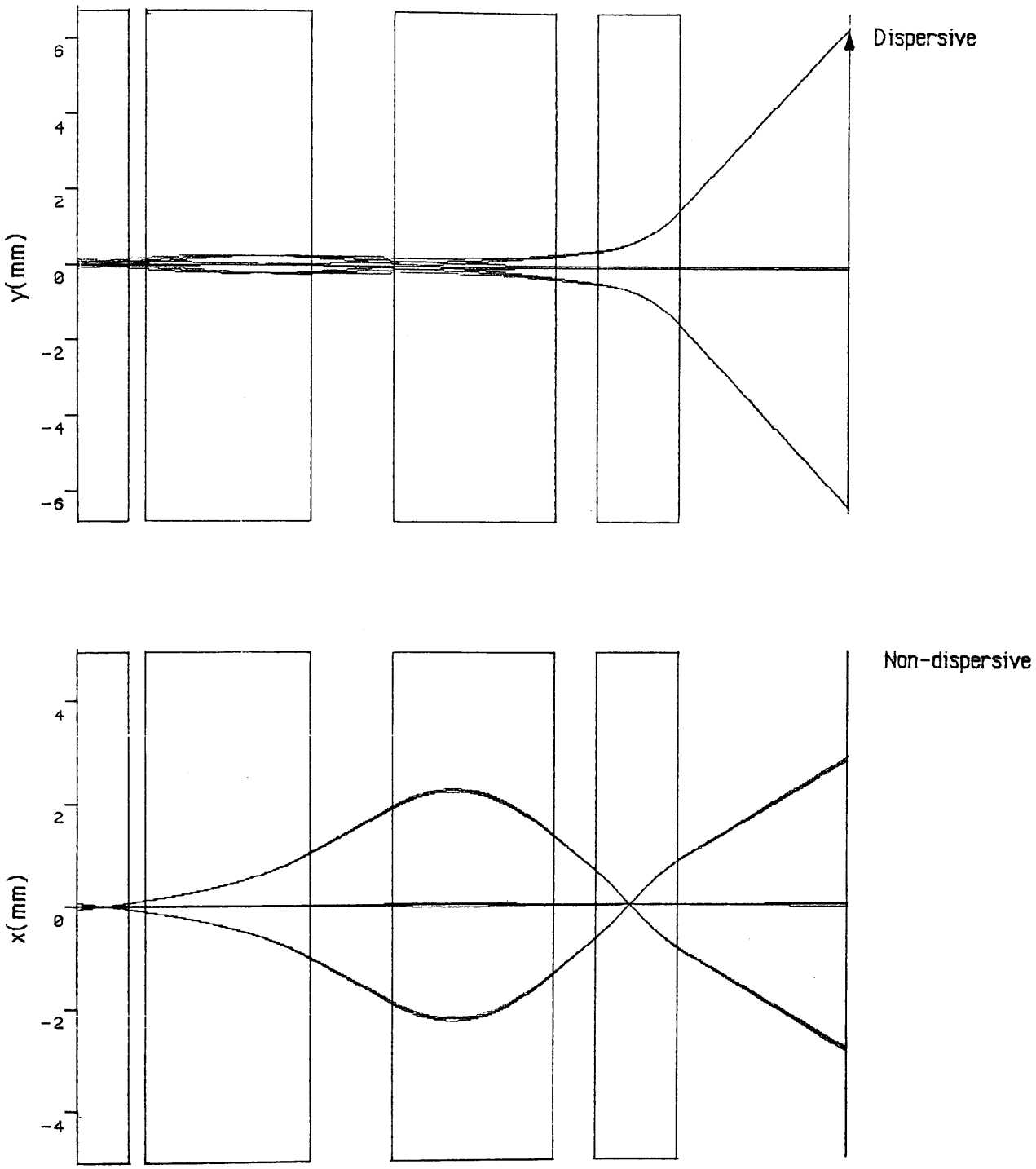

5.3.1 Calculation of chromatic aberration coefficients

Figure 5.17 is an example of the output of program QMATRIX given lens excitations corresponding to a magnification of -27.7x. Table 5.1 contains the results for other magnifications covering the available range. The second row aberrations y'/y δ, y'/y'δ, x'/xδ, x'/x'δ are not listed, as they do not affect the final image resolution. However, the corresponding focussing coefficients must, of course, be carried in the matrix calculation. The expressions for the transformation through the whole system from an object position (y_0,x_0), to the associated image position (y_1,x_1) are:

$$y_1 = \frac{y}{y}(y_0) + \frac{y}{y'}(y_0') + \frac{y}{y\delta}(y_0\delta) + \frac{y}{y'\delta}(y_0'\delta) \qquad (5.1)$$

$$x_1 = \frac{x}{x}(x_0) + \frac{x}{x'}(x_0') + \frac{x}{x\delta}(x_0\delta) + \frac{x}{x'\delta}(x_0'\delta) \qquad (5.2)$$

where the coefficients are obtained from the total transfer matrices for each plane (see fig.5.17). The values of the chromatic aberration terms are complex functions of the magnification and it is interesting to note from table 5.1 that the terms in the dispersion (y) direction are always positive, while those in the non-dispersion (x) direction tend to vary in sign. In practice only the terms in the dispersion plane are of importance.

Figure 5.18a shows a schematic spectrum from the Scheinfein and Isaacson spectrometer covering an energy range of 700 eV, at an accelerating voltage of 100 keV. The spectrometer acceptance angle β is 5 mrads, and it is assumed that the magnet excitation has been adjusted so that the central ray corresponds to an electron energy of 99.65 keV. Figure 5.18b shows an image of the spectrum magnified by -10.36x, produced by a Fortran program QPLOT, which calculates the position of each electron entering the magnification system as it crosses the final image plane. As can be seen the final image is magnified, inverted, and defocussed to a constant width in the non-dispersive direction.

The effect of the y/y δ term can be deduced using figure 5.18a and equation 5.1. For electrons with an energy greater than that of the central ray both y_0 and δ are positive, so that as y/y δ is always positive, the net effect of this aberration is to cause a positive y shift at the image plane. For electrons with less energy than the central ray δ and y_0 are both negative, so the aberration causes a y shift in the same sense at the image plane. The overall result is that a non-linearity in dispersion is introduced to the final image, as indicated in

figure 5.18b. Obviously this effect is greatest for large values of δ, and therefore most obvious at lower magnifications where the energy range accepted is at a maximum. For example, at the lowest magnification of ~-5.2x the energy range of interest is ~1369 eV, corresponding to a maximum axial displacement y_0 of 1.232mm. From table 5.1 the value of $y/y\,\delta$ at this magnification is 16.54, so that the image shift at the extremes of the spectrum is:

$$\Delta y_{max}(\text{shift}) = \frac{y}{y\delta}\,(\,y_{0\,max}\,)\,(\,\delta_{max}\,)$$

$$\Delta y_{max}(\text{shift}) = 16.54\ (1.232\text{x}10^{-3}\text{m}\,)\ (684.5\ \text{eV}/200000\text{eV})$$

$$\Delta y_{max}(\text{shift}) = 69.7\mu\text{m}$$

Compared with a detector channel width of 25μm. The magnified dispersion is 9.3μm/eV, so that this shift corresponds to a displacement of ~7.5 eV, or equivalently a non-linearity in dispersion of ~1%. This is, of course, an extreme case; at a magnification of -50x the corresponding non-linearity is reduced to 0.001% which is negligible.

The effect of the aberration $y/y'\delta$ is to cause a blurring of the magnified spectrum with energy loss i.e. it is analogous to the dispersion plane tilt aberration Y_3 of a sector spectrometer. If the assumption is made that the angular distribution of electrons entering the magnification system is approximately independent of energy loss, then this aberration will have the greatest effect at low magnifications where δ is largest. Using the data in table 5.1 for a magnification of -5.19x and assuming a spectrometer collection angle of 5 mrads, the magnitude of the defocus is:

$$\Delta y_{max}(\text{blur}) = \frac{y}{y'\delta}\,(\,y'_{0\,max}\,)\,(\,\delta_{max}\,)$$

$$\Delta y_{max}(\text{blur}) = 0.1633\text{m}\ (0.012\,)\ (684.5\ \text{eV}/200000\text{eV})$$

$$\Delta y_{max}(\text{blur}) = 6.7\mu\text{m}$$

[The maximum angular divergence for the extreme electrons is ~12 mrads calculated using equation 3.7b]. As before the magnified dispersion is 9.3μm/eV, so that this corresponds to a maximum defocus of ~0.72eV. The magnitude of the maximum defocus is relatively independent of the magnification, remaining around 6μm, so that the effect is negligible at higher magnifications.

Figure 5.17

QUADRUPOLE QUADRUPLET HIGH MAG MODE MAGNIFICATION = -27.67x

LENGTH OF FIRST LENS = 15.00 mm.

First quadrupole strength = 0.09001

LENGTH OF SECOND LENS = 50.00 mm.

Second quadrupole strength = 1.65100

LENGTH OF THIRD LENS = 50.00 mm.

Third quadrupole strength = 1.48600

LENGTH OF FOURTH LENS = 25.00 mm.

Fourth quadrupole strength = 0.75000

OBJECT POSITION = -7.50 mm.

NORMALISED IMAGE POSITION = 1.00

LENS 1-2 SEPARATION = 5.01 mm.

LENS 2-3 SEPARATION = 25.00 mm.

LENS 3-4 SEPARATION = 12.50 mm.

QUADRUPOLE 0 CONVERGENT TRANSFER MATRIX

y/y	y/y'	y/yd	y/y'd
0.9960	0.0150	0.0040	0.0000
-0.5394	0.9960	0.5387	0.0040
0.0000	0.0000	0.9960	0.0150
0.0000	0.0000	-0.5394	0.9960

QUADRUPOLE 0 DIVERGENT TRANSFER MATRIX

x/x	x/x'	x/xd	x/x'd
1.0041	0.0150	-0.0041	0.0000
0.5408	1.0041	-0.5416	-0.0041
0.0000	0.0000	1.0041	0.0150
0.0000	0.0000	0.5408	1.0041

QUADRUPOLE 1 CONVERGENT TRANSFER MATRIX

y/y	y/y'	y/yd	y/y'd
-0.0801	0.0302	0.8228	0.0171
-32.9139	-0.0801	14.2731	0.8228
0.0000	0.0000	-0.0801	0.0302
0.0000	0.0000	-32.9139	-0.0801

QUADRUPOLE 1 DIVERGENT TRANSFER MATRIX

x/x	x/x'	x/xd	x/x'd
2.7020	0.0760	-2.0721	-0.0295
82.8857	2.7020	-115.0946	-2.0721
0.0000	0.0000	2.7020	0.0760
0.0000	0.0000	82.8857	2.7020

QUADRUPOLE 2 CONVERGENT TRANSFER MATRIX

y/y	y/y'	y/yd	y/y'd
0.0847	0.0335	0.7403	0.0146
-29.6132	0.0847	16.6768	0.7403
0.0000	0.0000	0.0847	0.0335
0.0000	0.0000	-29.6132	0.0847

Figure 5.17

QUADRUPOLE 2 DIVERGENT TRANSFER MATRIX

x/x	x/x'	x/xd	x/x'd
2.3228	0.0705	-1.5577	-0.0228
62.3096	2.3228	-82.4474	-1.5577
0.0000	0.0000	2.3228	0.0705
0.0000	0.0000	62.3096	2.3228

QUADRUPOLE 3 CONVERGENT TRANSFER MATRIX

y/y	y/y'	y/yd	y/y'd
0.7317	0.0227	0.2556	0.0022
-20.4492	0.7317	18.4561	0.2556
0.0000	0.0000	0.7317	0.0227
0.0000	0.0000	-20.4492	0.7317

QUADRUPOLE 3 DIVERGENT TRANSFER MATRIX

x/x	x/x'	x/xd	x/x'd
1.2947	0.0274	-0.3084	-0.0025
24.6695	1.2947	-26.8999	-0.3084
0.0000	0.0000	1.2947	0.0274
0.0000	0.0000	24.6695	1.2947

ELEMENTS OF THE TOTAL C-C-D-D TRANSFER MATRIX

y/y	y/y'	y/yd	y/y'd
-27.6717	0.0000	55.7042	1.0626
-321.7547	-0.0361	715.9514	12.2829
0.0000	0.0000	-27.6717	0.0000
0.0000	0.0000	-321.7547	-0.0361

ELEMENTS OF THE TOTAL D-D-C-C TRANSFER MATRIX

x/x	x/x'	x/xd	x/x'd
-8.6307	-0.3602	15.6004	0.5395
-132.1037	-5.6294	120.7825	3.1234
0.0000	0.0000	-8.6307	-0.3602
0.0000	0.0000	-132.1037	-5.6294

OBJECT POSITION = -7.50000 mm.

CONV-CONV-DIV-DIV MAG = -27.67170 AT IMAGE POSITION = 50.23531 mm.

DIV-CONV-DIV-CONV MAG = -0.17764 AT IMAGE POSITION = -13.75264 mm.

Figure 5.18a

700eV Spectrum From Scheinfein + Isaacson Spectrometer

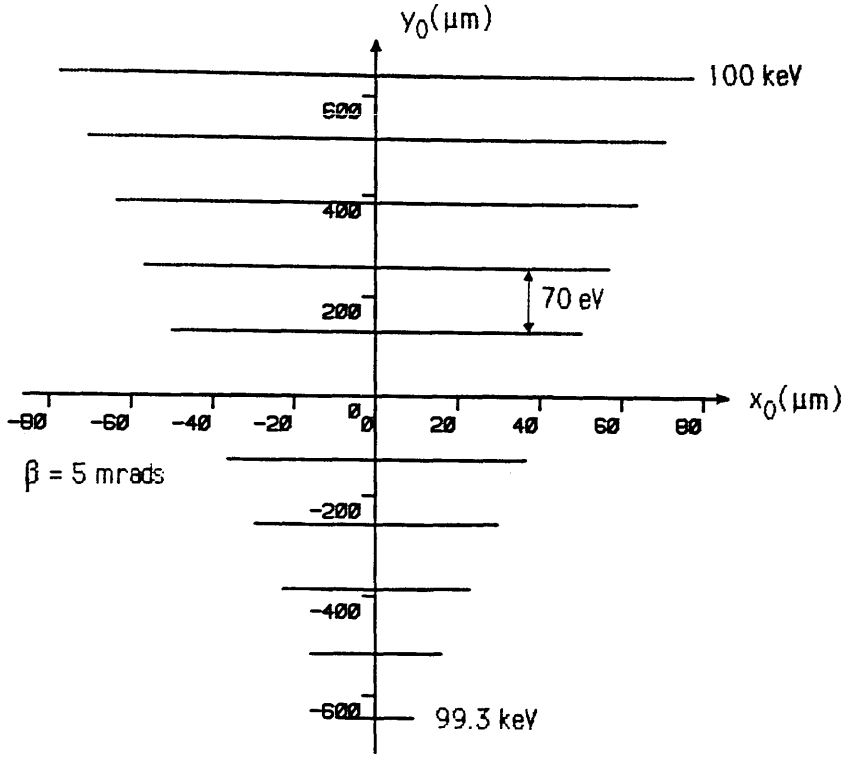

Figure 5.18b

Magnified Spectrum

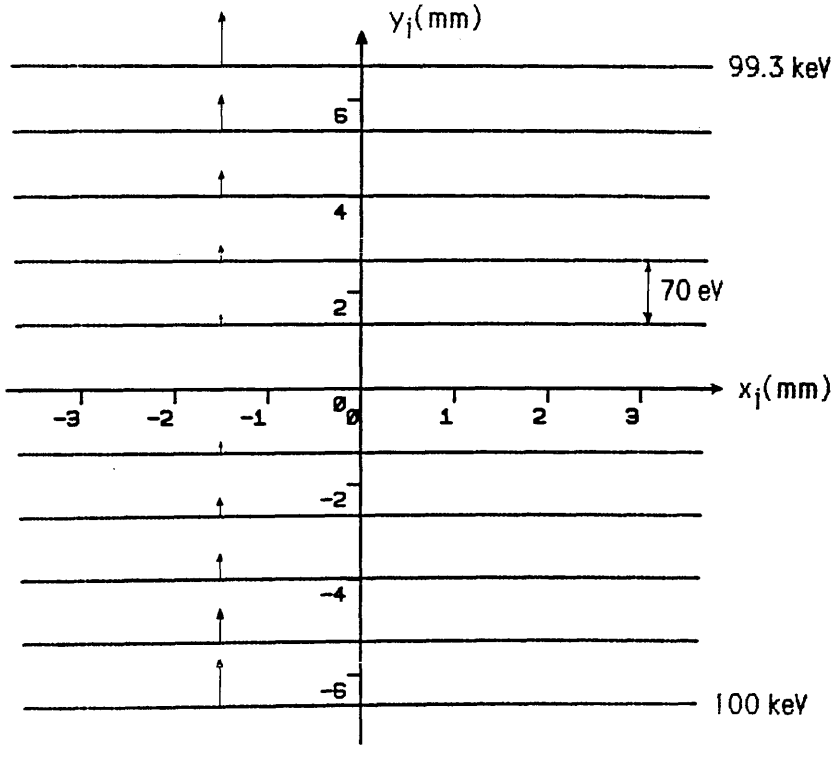

It should be pointed out that the values for the above aberration coefficients were calculated using the SCOFF approximation described in chapter 4. In practice real lenses have extended fringe fields, which tend to increase the magnitude of the aberrations. However, the previous calculations should be reliable enough to give a reasonable estimate of the chromatic aberrations in a real system.

5.4 EFFECTS OF A.C MAGNETIC FIELDS

Time varying magnetic fields are present in every experimental environment to a greater or lesser degree. It is possible to partially shield sensitive apparatus from these fields by enclosing the equipment in a material with a high magnetic permeability, for example 'mu-metal'. However, it is virtually impossible to suppress all the field, and very likely a small a.c. component ≤ 1 milligauss will remain in the system. These fields vary at mains and mains transformer frequencies i.e. 50-150 Hz, so that each electron traversing the optical system experiences essentially a static field. The effects of these stray fields are discussed in the following sections.

5.4.1 A.C. Field superimposed on a thin electron lens.

Figure 5.19 shows a schematic electron lens with an a.c. magnetic field B perpendicular to the plane of the paper. Consider an electron leaving the object point O and initially traveling along the optic axis. The effect of the stray field is to bend the trajectory away from the axis in the arc of a circle, in a positive or negative direction depending upon the direction of B. The radius R_s of this circle is just the cyclotron radius:

$$R_s = \frac{m v_z}{eB} \tag{5.3}$$

where the approximation that $v \sim v_z$ has been made. For a stray field of 1 milligauss $R_s \sim 10^4$m. The electron cuts the plane $z = 0$ at point $y = \Delta y$ at an angle ψ_s. The equation of the circular arc OP is:

$$(y - R_s)^2 + (z + U)^2 = R_s^2$$

Setting z=0 gives the intersection point P:

$$(\Delta y - R_s)^2 + U^2 = R_s^2$$

$$\cdot\ \Delta y^2 - 2R_s\Delta y + U^2 = 0$$

Figure 5.19 Thin Electron Lens With Stray Field

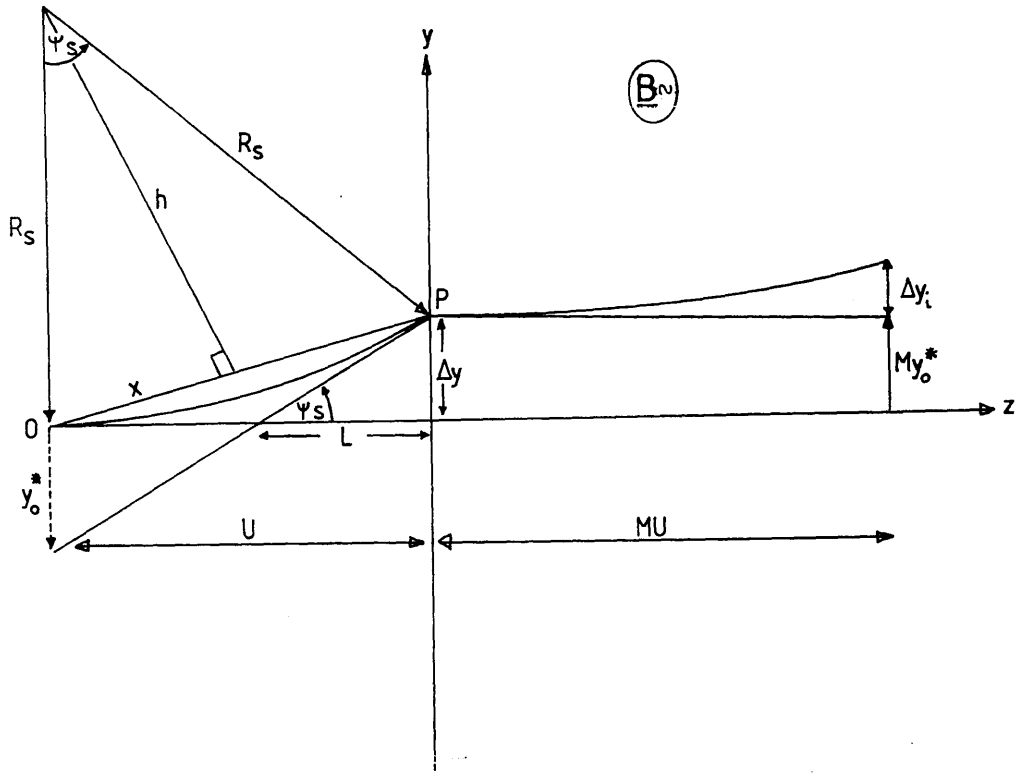

Figure 5.20 Equivalent Thin Lens System

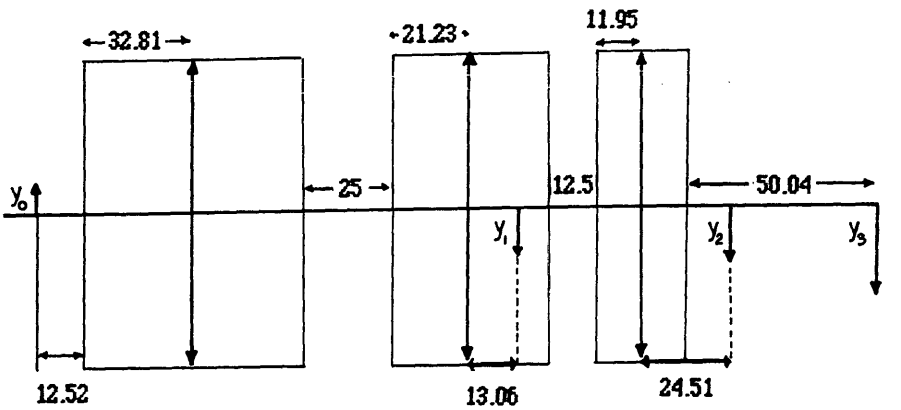

(all dimensions millimetres)

Solving this quadratic equation and choosing the smaller solution gives:

$$\Delta y = R_s \left(1 - \sqrt{1 - U^2/R_s^2} \right)$$

and as $R_s >> U$ the solution can be written:

$$\Delta y \sim U^2 / 2R_s \qquad (5.4)$$

Now referring to figure 5.19 the expression for the angle of deflection ψ_s can be found:

$$\tan(\psi_s/2) = x/h \quad \text{where } x = \frac{1}{2}\sqrt{U^2 + \Delta y^2} \sim \frac{1}{2}U$$

and $h \sim R_s$ so that :

$$\tan(\psi_s/2) \sim U/2R_s \text{ i.e. } \psi_s \sim U/R_s \qquad (5.5)$$

where ψ_s is assumed to be small. The effect of this displacement Δy and deflection ψ_s can be referred back to the object plane to produce an effective object y_o^* where:

$$y_0^* = (U - L)\tan\psi_s = U(\tan\psi_s - \Delta y)$$

$$= U(U/R_s - U/2R_s)$$

$$= U^2/2R_s$$

i.e. the effective object size y_o^* is equal to the displacement Δy. After the lens this effective object is magnified at the image plane, and there is also a contribution Δy_i from the curvature in image space. The size of the final image is thus:

$$y_i = M y_0^* + \Delta y_i$$

The displacement Δy_i in image space is found in exactly the same way as for the object space, so that the final image is just:

$$y_i = \frac{MU^2}{2R_s}\left[1 + M \right] \qquad (5.6)$$

Of course the magnetic field acts in both senses so that the final image size is twice this quantity.

5.4.2 Thin lens approximation for a quadrupole

The simplest way to estimate the effects of a small a.c. magnetic field on the whole system is to replace the quadrupole lenses by their equivalent thin lenses. Any quadrupole transfer

matrix can be replaced by an appropriate thin lens matrix with two drift matrices on either side; e.g. for the convergent plane:

$$\begin{bmatrix} \cos\theta & (1/\sqrt{q})\sin\theta \\ -\sqrt{q}\sin\theta & \cos\theta \end{bmatrix} = \begin{bmatrix} 1 & S_c \\ 0 & 1 \end{bmatrix}\begin{bmatrix} 1 & 0 \\ -1/f_c & 1 \end{bmatrix}\begin{bmatrix} 1 & S_c \\ 0 & 1 \end{bmatrix}$$

where:

$$1/f_c = \sqrt{q}\,\sin\theta \qquad S_c = \frac{1 - \cos\theta}{\sqrt{q}\,\sin\theta} \tag{5.7}$$

i.e. the focussing strength is the same, but the associated drift space is larger than L/2. A similar approach gives for the divergent plane:

$$1/f_d = \sqrt{q}\,\sinh\theta \qquad S_d = \frac{\cosh\theta - 1}{\sqrt{q}\,\sinh\theta} \tag{5.8}$$

In this way the entire magnification system can be represented by four thin lenses with the appropriate focal lengths. The influence of a.c. fields need only be considered in the dispersion plane, as the non-dispersive plane is not critical, and the overall demagnification of this plane will tend to reduce the effect. Referring back to figure 5.1 the object for the first quadrupole lens Q_0 is positioned at the centre of the lens, so that the object distance U in equation (5.6) is zero, and therefore the net effect of the stray field is negligible in a thin lens approximation. The purpose of this lens is to shift the object position for Q_1, so this must be taken into account in the optical calculation. The following sections carry out the necessary calculations for a system magnification of -27.7x, using the transfer matrices of figure 5.17, and assuming a stray field B~1milligauss, with a corresponding cyclotron radius R_s of 10^4m.

5.4.3 Calculation of the defocus at the final image plane

First of all the thin lens equivalents are calculated for each quadrupole using equations (5.7) and (5.8) and the data of figure 5.17. At the magnification of interest, -27.7x, the quadrupole configuration is CCDD i.e. the high magnification mode.The relevant parameters are:

f_1 = 30.38 mm S_1 = 32.81 mm
f_2 =-16.05 mm S_2 = 21.23 mm
f_3 =-40.54 mm S_3 = 11.95 mm

The mechanical object distance is U=12.51mm but this is modified by lens Q_0 to be 12.52mm (using equation 3.10). The equivalent thin lens system is shown in figure 5.20. Considering lens Q_1, the object distance is $U_1 = U+S_1 = 45.34$ mm. The image distance is found using the simple lens formula, and is 92.108 mm, thus the magnification is -2.032x. An on-axis point source will be imaged as a line, whose magnitude is given by equation (5.6) to be ~0.6 μm.

The following lens Q_2 is divergent in the dispersion plane, and the distance between Q_1 and Q_2 is :

$$d_{1\text{-}2} = S_1 + gap_{1\text{-}2} + S_2 = 79.05 \text{ mm.}$$

Thus the image produced by Q_1 acts as a virtual object for lens Q_2, where the object distance U_2=-13.06 mm. The focal length of Q_2 is -16.05 mm, so that the lens will produce a real magnified image at a position 70.18 mm to the right of Q_2. The magnification is therefore 5.37x. The size of the virtual object as seen by lens Q_2 is modified by the curvature of the trajectory in the drift space between lenses Q_1 and Q_2, however if $U_2^2 << V_1^2$ this effect can be neglected.

The size of the image produced by lens Q_2 is therefore:

$$y_2 = M_2 y_1 + (M_2 U_2)^2 / 2R_s$$

$$y_2 \sim 3 \text{ μm}$$

This image forms a virtual object for the final lens which is seperated from Q_2 by 45.68mm, making U_3 = -24.51 mm. The image formed by Q_3 is located at a position 61.98 mm to the right of Q_3 and the magnification of the final lens is therefore 2.53x. The final image size can be calculated as in the previous case:

$$y_3 = M_3 y_2 + (M_3 U_3)^2 / 2R_s$$

$$y_3 \sim 9 \text{ μm}$$

Thus the effect of an a.c. magnetic field of magnitude ~ 1 milligauss is to cause an axial point source to be imaged as a line of length $2y_3$ = 18 μm. The overall magnification of the thin lens equivalent system is the product of all the individual magnifications, which is -27.60x at

TABLE 5.1 Chromatic aberration coefficient values

Mag	x/xδ	x/x'δ (m)	y/yδ	y/y'δ(m)
-5.19	-78.94	1.44	16.54	0.163
-10.36	-8.88	1.22	23.38	0.376
-16.02	10.33	0.96	33.27	0.601
-27.67	15.60	0.53	55.70	1.063
-51.31	3.27	-0.08	105.05	1.999
-89.64	-18.33	-0.69	191.87	3.518

TABLE 5.2 Reduction in resolution introduced by 1 milligauss a.c. magnetic field.

Mag	f_0(cm)	f_1(cm)	f_2 (cm)	f_3 (cm)	M_1	M_2	M_3	Image(μm)	Resolution(eV)
-5.22	-1.05	3.04	-1.60	4.36	-2.24	-4.88	-0.45	3.84	0.41
-10.29	-3.43	3.04	-1.60	8.40	-2.10	19.22	0.26	8.64	0.47
-27.60	185.4	3.04	-1.60	-4.54	-2.03	5.37	2.52	18.80	0.38
-51.75	12.17	3.04	-1.60	-12.9	-2.01	4.46	5.58	33.84	0.36
-92.06	8.15	3.04	-1.60	-6.04	-2.00	4.08	11.27	60.42	0.36

Note that the image size is the diameter of the image disc formed from a point source.

a final image plane located 50.04 mm after the last drift space. Results from the corresponding matrix calculation are; magnification = -27.67x; final image plane 50.23mm after exit of lens Q_3. The small discrepancy is probably due to arithmetic rounding errors.

The calculated defocus can be referred back to the object plane by dividing by the magnification, to give an effective object size of ~0.7 μm. The dispersion of the Scheinfein and Isaacson spectrometer is 1.8μm/eV so that the effective object resolution is ~0.4eV. Table 5.2 gives results of calculations done at other magnifications throughout the available range. In each case the degradation in energy resolution is less than 0.5 eV, showing that a.c. fields of this magnitude do not significantly reduce the energy resolution of the magnification system.

The flight path from the spectrometer exit plane to the dispersion plane of the Scheinfein and Isaacson spectrometer is ~182mm. The effect of a 1 milligauss a.c. field can be estimated using equation (5.4), giving a value of Δy of 1.65mm. For the spectrometer alone, the corresponding degradation in energy resolution is :

$$\Delta E = 2\Delta y \,/\, \text{dispersion} = 1.84 \text{ eV}.$$

Thus in all cases the spectrometer itself is the limiting factor in determining the energy resolution, and not the post-spectrometer optics. In practice the resolution of this spectrometer operating in serial collection mode is known to be considerably better than the above figure, suggesting that a stray field remanent of 1 milligauss is a pessimistic estimate.

5.5 CONSTRUCTIONAL ABERRATIONS

Quadrupole lens systems are subject to defects arising from misalignment, inaccurate machining, inhomogeneity of magnetic materials, and asymmetries in the magnetic circuitry. These factors are of special importance as there is no simple device, such as a stigmator, to correct for them. A generalised study of the effects of aberrations resulting from these imperfections is not particularly feasible, because their relative importance varies widely with the lens design and application. The defects can be broadly classified into two separate types; cases where the quadrupole symmetry is maintained but the lens optic axis is shifted or rotated with respect to its ideal position (figure 5.21a,b), and instances where the planes of quadrupole symmetry are distorted by a displacement of one or more of the polepieces (figure 5.21c,d). Departures from quadrupole symmetry tend to introduce extra 'parasitic'

Figure 5.21 Quadrupole Constructional and Alignment Errors

a) Shifted and Rotated Axis

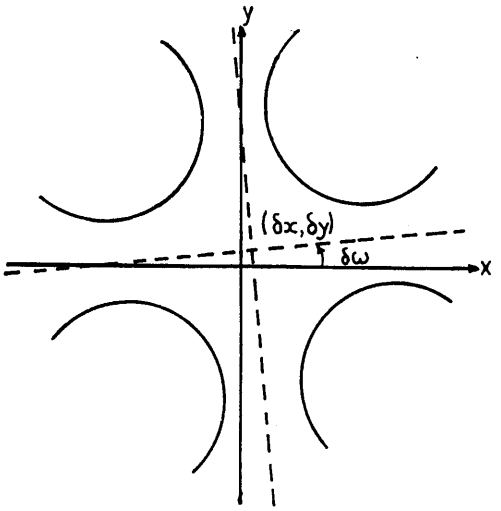

b) Tilted About Axis

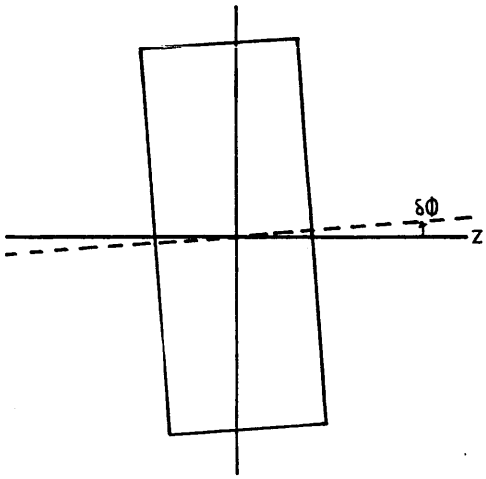

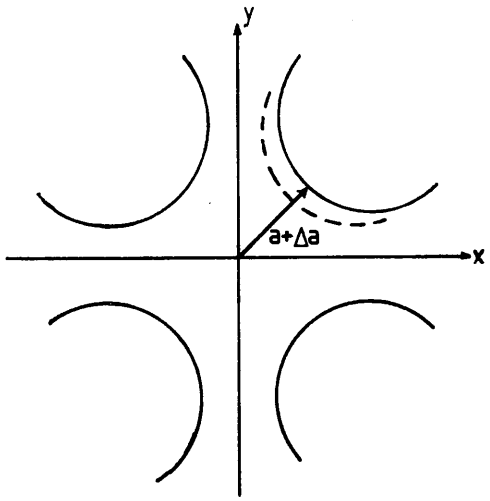

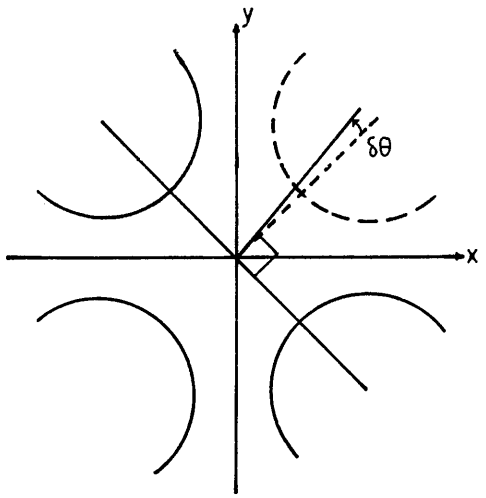

c) Radial Polepiece Error

d) Angular Polepiece Error

After Hawkes (1970)

terms [Hawkes 1970] into the magnetic field expansion of equation (4.5), and the net result is generally an introduction of second order aberrations to the image. Displacements and angular rotations of the lenses result in the formation of deflecting fields which cause a displacement in the image, and can also introduce second order aberrations.

Calculations of the required tolerances for the quadrupole system described in this chapter have not been carried out explicitly, however order of magnitude values for the various parameters involved can be estimated from the study of a symmetric quadruplet magnification system carried out by Kawakatsu et al. [1968]. This quadruplet was designed to act as the projection lens system for a microscope, so that the condition of stigmatic double focussing was required at all magnifications. Each lens had a mechanical length L' of 3cm, bore radius a of 1.5cm, separation d of 1.7cm, and the projector focal length was designed to vary between 0.75 and 3.6mm. Kawakatsu et al. found that the condition that the radial and rotational error in the magnification of the image be less than 3% at all magnifications gave tolerances for this system of:

1) Lens rotation $\delta\omega < \pm 1.7$ mrad
2) Individual Polepiece radial alignment $\Delta a/a < \pm 0.063$
3) Individual polepiece angular alignment $\delta\theta < \pm 13$ mrad
4) Axial Shifts $\delta x, \delta y < 0.5$mm
5) Lens tilt $\delta\phi < 10$ mrads

where the relevant parameters are defined in figure 5.21. To keep $\Delta M/M < \pm 10^{-4}$, where M is the magnification, fluctuations in the lens current must satisfy $\Delta I/I < \pm 8 \times 10^{-5}$. The authors found that the deflection introduced by tilt and displacement of the lenses was relatively harmless, hence the wide tolerances. In contrast, the quadrupole angular alignment $\delta\omega$ seems very critical; - as noted experimentally by Crewe et al. [1967] who used a weak quadrupole lens to correct for the aberrations arising when adjacent quadrupoles were twisted with respect to each other. This weak lens was placed between the quadrupoles of interest and its symmetry planes were oriented at 45^{o} to the others.

It is not clear exactly how appropriate the above calculations are to a post-spectrometer magnification system where the magnifications are greatly different in each plane; - at least an order af magnitude correlation should be expected, considering the similar dimensions of the components used. It is clear however, that constructional factors are extremely important in all quadrupole systems, and as such must be treated with the greatest of care.

Third Order Aberrations

The previous calculations do not include any effects caused by the third order geometrical aberrations of quadrupole lenses. In particular, at the lower magnifications (eg. Figure 5.11) the excursion of the extreme trajectories from the optic axis is very large, occupying almost all of the bore of the final quadrupole lens. Thus third order axial aberrations of this lens could introduce serious geometrical distortions to the magnified spectrum. Fortunately, for quantitative analysis of EELS spectra such wide energy ranges as Figure 5.11 (~1300eV) would not be required, and indeed dynamic range limitations of the detector (section 8.4) reduce the most practical energy range for parallel recording to a few hundred eV. Thus it is not anticipated that magnifications much lower than that of Figure 5.14 (~30x) would be required.

The effects of third order aperture aberrations can be reduced by restricting the angular divergence of the electrons at the dispersion plane. For example in the HB5 STEM equipped with post-specimen lenses the effective spectrometer collection angle β is ~2mrads giving a maximum angular divergence at the dispersion plane of ~6mrads using the Scheinfein and Isaacson spectrometer. Smaller divergence can be introduced by further restricting the spectrometer collection angle.

In principle, the matrix method used in all the previous calculations can be extended to third order by incorporating extra transfer matrices for the quadrupole entrance and exit fields. Analytical expressions for the third order aberrations of the central field regions of quadrupole lenses have been published by Smith [1969], and equivalent expressions for the third order aberrations of the fringing fields of such lenses are given in the paper by Matsuda and Wollnik [1972]. The latter are expressed in terms of the distribution function of the field gradient, which must be measured experimentally. The authors emphasise the fact that the focussing characteristics described apply to perfect lenses only, and that mechanical imperfections such as those described in section 5.5 must be considered.

It may be possible to reduce the effects of third order aberrations using suitably placed octupole corrector lenses [Scherzer 1947], but clearly further work would be required to determine the ultimate performance these aberrations would impose upon the optical system.

CHAPTER 6

A Prototype Acquisition System For Eels - Instrumentation

Introduction

The design and construction of a prototype parallel recording system for EELS is described in this chapter. The instrumentation was developed and tested in a vacuum chamber attached below the camera chamber of a JEOL JEM 100C transmission electron microscope, allowing irradiation of the detector by the electron beam. The performance of the detector under various conditions is reported in chapter 7; this chapter deals mainly with the design, construction and evaluation process of the detection system. The first section describes some of the multielement solid state detectors which can be applied to parallel EELS, and outlines the advantages of using wide aperture photodiode arrays in the indirect detection mode as the detection elements. The operation of two such arrays, manufactured by E G + G Reticon and Hamamatsu Photonics is described, along with the construction and function of the various electronic circuits necessary to drive the devices. The data output from both arrays is an analogue video signal, which must be digitised and processed. To this end, the design and evaluation of a sample and hold / analogue to digital conversion circuit is described, along with the digital electronics used to interface the output to a Motorola 68000 microprocessor monoboard, and hence to a VME minicomputer system for processing and display. As the photodiodes operated in the confined space of the microscope vacuum system, they were physically separated from some of their drive electronics. The effect of this separation on the electronic performance is reported, and the design of a suitable head amplifier for the Reticon array is given. In order to reduce the dark current generated in all photodiodes, the arrays were cooled in operation using a thermoelectric cooler chip, and the operation of this cooling system is also described.

6.1 ELECTRON DETECTORS

There are many different methods of recording, in parallel, the information present in an EELS spectrum. The most fundamental choice is whether to design a system relying on the direct detection of the electrons, for example in a semiconductor device, (direct detection) or whether to employ an intermediate conversion screen to convert the electrons to photons, and record the light signal generated (indirect detection). The latter method allows optional

intensification of the photon signal before detection. Applications of both recording methods are considered in the following sections, and the advantages of the indirect detection method are described.

6.1.1 Direct detection methods

The simplest method of direct detection is to place a photographic film at the spectrometer dispersion plane. After exposure to the electron beam the film is developed and digitised for quantitative analysis. Apart from dynamic range limitations imposed by over-exposure effects, the sheer inconvenience of this method makes it impractical for use in a modern detection system and it will not be discussed further.

An alternative solution is to detect the electrons directly using a solid state image sensor, such as a charge coupled device (CCD), photodiode array (PDA), or resistive strip position sensitive detector (PSD) located at the spectrometer dispersion plane, or preferably the final image plane of a post spectrometer magnification system. This configuration has the advantages of simplicity and very high detection efficiency at low beam currents, since each 100keV electron produces ~10^4 signal electrons in a silicon device. Single electron detection can therefore be achieved using this method and several investigations of this type of detection system have been carried out [McMullan et al 1985, Shuman 1981, Roberts 1980, Bourdillion et al 1985].

The following is a brief summary of the operation of the three types of sensor mentioned above;

1) Resistive strip (position sensitive) detectors.
   These detectors consist of a silicon p-n junction, on the surface of which is fabricated a resistive layer terminated by electrodes at each end. One contact is grounded, and the other is connected to a charge sensitive amplifier, the output of which is proportional to the distance from the grounded contact to the point of impact of the electron. The main problem with this device is that only one electron event can be handled at any one time.

2) Charge coupled device (CCD) image sensors.
   This device is basically an integrated circuit consisting of an oxide covered silicon substrate upon which is fabricated a linear or area array of closely spaced electrodes. Each electrode is equivalent to the 'gate' of a MOS transistor. Electrons or photons

absorbed in the silicon substrate produce a number of electron-hole pairs, proportional to energy. This charge is trapped in the 'potential wells' formed in depletion layers under electrodes supplied with an appropriate bias. After some period, known as the integration time, the potential on the electrodes is varied in such a way as to cause transfer of the accumulated packets of charge from one to the other, with very little loss of signal. By repeatedly pulsing the voltages on the electrodes between high and low levels the charge can be quickly transported to a shielded storage region, and hence to the readout register, where it is sequentially applied to a charge sensitive amplifier to form the video output. If the illumination is not blanked the charge transfer must be accomplished in an interval that is short compared to the integration time, otherwise light still incident upon the active area will cause image smearing to occur.

The main problem with direct exposure of a CCD is that the high gain involved ($\sim 10^4$ electrons produced per 100keV signal electron) soon causes the individual detection elements to saturate, resulting in low dynamic range.

3) Photodiode array (PDA) image sensors.
Photodiode arrays consist of one or more rows of silicon photodiodes each with an associated storage capacitance on which to integrate photocurrent, and a multiplex switch to connect the diode to a common video line. Incident photons or electrons generate charge (as in the CCD) which is stored on the diode capacitance. After an integration time the diodes are connected, in sequence, via the multiplex switches to the video line, and the charge pulse generated is converted to a video voltage output by a charge sensitive amplifier. Again the dynamic range is limited by cell saturation effects, although some diode arrays are constructed with large individual elements which can store more charge.

The problems associated with direct detection using any of the above devices are low dynamic range and, after prolonged exposure to 100 keV electrons, the occurrence of radiation damage effects (less so for PSD). Radiation damage is usually manifested in increased dark current, and a worsening of the device pixel to pixel response function. This problem can be mediated somewhat by annealing the devices at 400 ^{o}C [Roberts 1980], but not entirely removed. The construction of radiation hardened devices is a subject of current interest in military applications, but as yet no such devices are available in the civilian sector. In conclusion, direct detection is very attractive for recording weak signals where the high

electron gain is most useful. Unfortunately, EELS spectra contain intensities which tend to saturate currently available devices, and ultimately cause damage to occur. If, in future, radiation hard devices become available with higher cell capacities (or reduced gain) the merits of this form of detection will increase.

6.1.2 Indirect detection

Indirect detection of the spectrum has the advantage that radiation damage to the semiconductor detection element does not occur, and higher dynamic range is available because of the reduced gain. The penalty is that the system performance depends largely upon the properties of the conversion screen, and that single electron detection is not generally possible. This is discussed more fully in chapter 7.

The simplest method of recording the transmitted photons is using a commercial TV camera. Optical coupling between the conversion screen and the camera can be provided using glass lenses, or better still fibre-optic plates. In order to detect the low light levels generated at the far energy loss region of the spectrum, it is usually necessary to place some form of image intensifier between the screen and the camera. The literature available on image intensifying camera systems is vast, as is the number of designs. A useful review is given by Schlagen [1975]. Detection systems of this type have been constructed by Shuman [1984] and Egerton [1981] using silicon intensified target [SIT] vidicon cameras.

Systems using image intensified TV cameras as detectors can suffer from a number of disadvantages; the resolution of the camera itself is usually quite poor, and noise processes in the image intensification stage can limit the dynamic range. Apart from this, the gain of the image intensifier must be varied during the actual recording, in order to accommodate a reasonable dynamic range, and also to prevent overload damage occurring at high input intensities. Other drawbacks of traditional TV tube cameras include such undesirable properties as image lag and image distortion, both of which reduce the attractiveness of these devices for EELS applications. Recently low light level (LLL) cameras have become available using CCD arrays as detection elements. LLL cameras do not suffer from the same faults as electro-optic tubes, and are often used in TEM imaging systems. Their application to EELS may be considered if cost is a limiting factor and the highest performance is not required.

The preferred type of indirect detection system uses a solid state image sensor optically coupled to a transmission scintillator screen. Again the optical coupling can be achieved

using glass lenses [Monson et al 1982, Strauss et al 1987], or more efficiently by a fibre optic link [Krivanek et al 1987, Egerton and Crozier 1987]. This configuration does not suffer from the same kind of problems as the TV type systems. The detectors themselves are available with many different geometries, and generally feature improved performance as compared with those used in integrated camera systems. The choice of the most suitable detector is discussed in the next section.

6.1.3 Choice of imaging element

There are many factors to be considered when deciding upon the optimum imaging element for an indirect detection system. In practical terms, the types of sensor most suitable for this application are area CCD arrays and wide aperture linear photodiode arrays. CCD arrays are also available in linear form, but the element size is usually of the order of 25μm square which, from chapter 3, is much too narrow to image the full width of an EELS spectrum. Area photodiode arrays offer inferior performance to the equivalent CCD arrays, and are not considered further. The decision on whether to opt for an area CCD or a wide aperture linear photodiode array is not clear cut, as the electrical performance is equivalent, and each sensor has its own particular advantages. The important points are listed below:

1) The PDA cell capacity is ~ 100x larger than that of a CCD element, so that cell saturation is less of a problem at low energy losses.

2) CCD noise performance is much better than that of PDAs, partly because of the very much smaller source capacitance, however the dynamic ranges are roughly equivalent due to the higher cell capacity of the photodiode array.

3) If all the CCD elements are used for imaging, then the electron beam must be blanked during the CCD readout time, to prevent image smear.

4) Linear PDA readout time is very much faster than the time required to read out a whole two dimensional CCD array.

5) Linear photodiode arrays are available with up to 1024 elements in the dispersion direction, whereas the largest commercial CCD arrays are typically 512 x 512 elements.

6) CCD arrays can be used as two dimensional imaging devices e.g. for energy filtered

imaging studies [Shuman 1986].

7) Area CCDs with fibre optic windows are ~ 5x more expensive than an equivalent wide aperture photodiode array.

It is possible to improve points 3) and 4) by using only part of the CCD array to image the spectrum, and shielding the remainder from the beam. In the case of Strauss et al. [1987], a fractional area consisting of 5 x 512 elements is exposed to the spectrum. After an integration time this image is transferred under a shield (transfer time for 5 rows of cells ~ 5 μs) and another image is recorded. This is repeated until the array is full, by which time 100 consecutive images have been stored. Scan time is greatly reduced, since the CCD is only read out once every hundred acquisitions, and the need for beam blanking is also much reduced, as the charge packets need only be transferred across five elements each time. Disadvantages include the fact that the active area is only 150 μm wide, which is still too narrow to image the defocussed spectrum, and non-standard drive electronics must be used to control the charge transfer.

Taking all the above points into consideration, and noting that 2-dimensional imaging is not required in this application, it seems that the simplicity of application of the linear photodiode array tips the balance in favour of this sensor. Accordingly, the remainder of this chapter is concerned with the operation of two such devices, purchased from different manufacturers. The next sections describe the operation of the RL128S photodiode array manufactured by EG+G Reticon, and later sections deal with the S2304-512F sensor manufactured by Hamamatsu Photonics.

6.2 RETICON S SERIES PHOTODIODE ARRAYS

The Reticon S series (scientific) self scanned silicon photodiode arrays are specifically designed and optimised for applications in optical spectroscopy. The array under investigation is the RL128S which has 128 elements, but the operation is identical to larger arrays available with 512 or 1024 photodiodes. Each sensor element has a 100:1 aspect ratio (25μm x 2.5mm), and the maximum charge that can be stored on each diode is 14 pC i.e. 8.75×10^7 electrons. Normally light is incident on the photodiodes through a quartz window. The following sections describe in more detail the operation of these devices.

6.2.1 Principles of operation - RL 128 S

Each of the sensor elements in this device consists of a planar diode made by diffusing p-type bars in an n-type silicon substrate. Light incident on the sensing area generates charge, which is collected and stored on the p-type bars during the integration period. The n-type silicon surface is also photosensitive, charge generated here divides between the two adjacent p regions. Figure 6.1 shows a simplified equivalent circuit for the array. Each individual cell consists of a photodiode and a dummy diode, both with an associated storage capacitance. These diodes connect through MOS multiplex switches to video and dummy recharge lines; one pair of recharge lines is common to all the odd elements, and another pair is common to all the even elements.

The multiplex switches are turned on and off in sequence by two shift register scanning circuits, thereby periodically recharging each cell to 5 volts and storing charge Q_{sat} on its capacitance. After an integration time τ, the diodes have discharged by an amount proportional to the intensity of the incident light, and also an additional amount due to the dark leakage current. This charge must be replaced through the video line when the diode is sampled once each scan. Thus the output signal from each scan is a train of pulses each proportional to the light intensity on the corresponding photodiode. In addition to the signal charge, switching transients are capacitively coupled into the video lines by the multiplex switches. By differentially amplifying the dummy and active video lines these transients can be suppressed.

More detailed information on the operation and performance of these sensors has been published by Talmi and Simpson [1980] . Spectral response and responsivity information is also contained in 'Image Sensing Products' published by EG+G Reticon.

6.2.2 Drive electronics: RC-1024 SA evaluation board.

The electronic signals necessary to drive the array consist of timing circuitry to control the integration time and the scan speed, and a signal processing circuit to produce a sampled and held video output. Reticon supply an evaluation board, the RC-1024 SA which provides the above functions for all the S series arrays. The circuit is constructed on a standard 4.5" x 9" printed circuit card, and all the connections are made via a 22 pin edge connector.

Figure 6.2 is a block diagram representing the four major circuit sections. The logic section consists of TTL circuits which provide the program and control signals for clocking the arrays. It includes an oscillator clock circuit with a frequency variable between 150 kHz and

Figure 6.1 Equivalent Circuit For Reticon S Series Photodiode Arrays

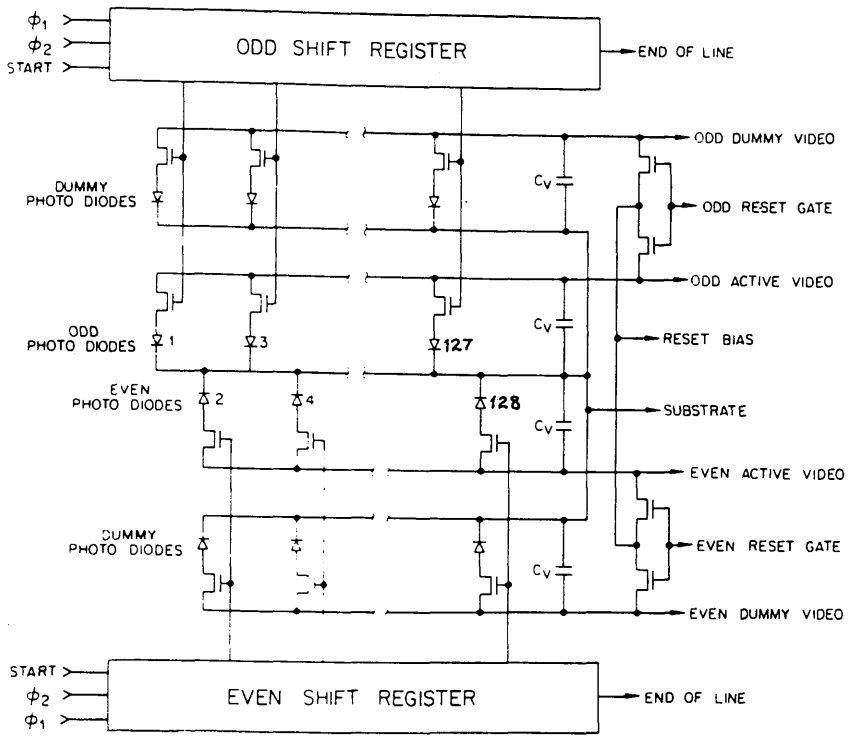

Figure 6.2 Block Diagram Of RC1024 SA Evaluation Board

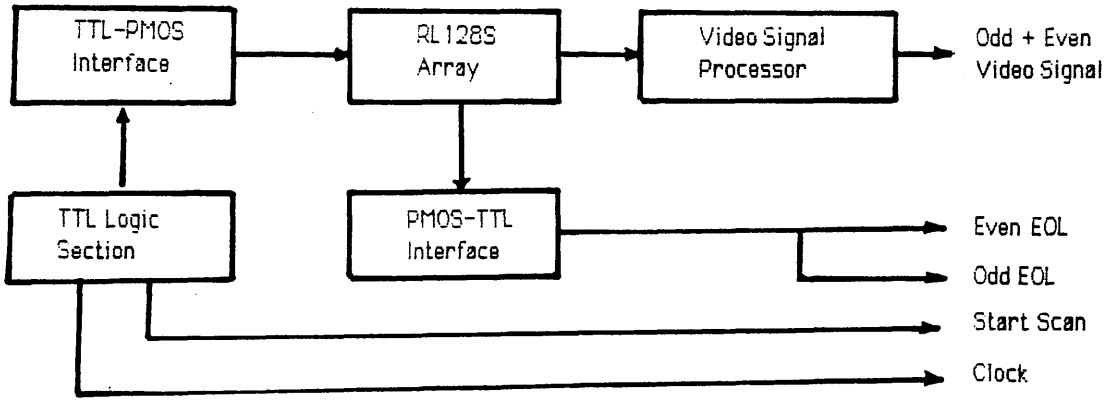

1.5 MHz. All subsequent timing signals, including the array integration time, are derived from this master clock. The diode sampling frequency operates at one quarter of the clock frequency, and is limited to a maximum of 300 kHz to optimise the low noise characteristics. The length of the integration time is varied using a preset binary counter, up to a maximum of 16384 sample periods (1 sample period = 4 clock periods), which corresponds to 0.4 seconds at the slowest clock rate. The minimum integration time is determined by the scan time (time required to read out all the elements) of the array and corresponds to an almost continuous video signal.

The signal processor is an analogue circuit which amplifies the video signal and enhances the signal to noise ratio using a double sampled auto-correlation technique (see chapter 7), after which the odd and even signals are combined in a sequential sample and held signal. The saturation video voltage is specified to be +3V, and the amplifier output impedance is 10 ohms. The gain of the video circuit is 2.14×10^{11} Volts/Coulomb or 3.42×10^{-8} Volts/electron.

The S series PDA is located in a DIL socket on the reverse side of the circuit board. The interface circuits simply provide the necessary voltage translation from TTL to MOS levels between the logic circuitry and the array inputs, and the reciprocal MOS to TTL transfer from the array output connections.

Apart from the video output signal the RC-1024 SA board also provides oscillator clock and start-of-scan output signals (positive TTL), and end-of-line (EOL) signals for the odd and even scans (negative TTL). From a constructional point of view, the board was shielded from external interference in a metal case, and all the output signals were carried on shielded coaxial cable using BNC connectors with the cable shields connected to the board earth and the case left floating. Further information, including detailed circuit and timing diagrams, is available in the Reticon publication 'Operational Instructions for RC-1024 SA Evaluation Board' [1978]. This publication also contains information concerning the setup procedure which is discussed later.

6.2.3 Power Supplies

The DC power supplies required for correct operation of the photodiode circuitry are ±15V at 75 mA and 175 mA respectively, and +5V at 500 mA. Obviously for the best performance the supplies should be regulated, low noise units. The components used were Powerail 23005A 5V/3A, and Powerail 23215A ±15V/0.8A supplies. The output ripple is specified

at 5mV pk-pk maximum, with a DC stability of ±0.3% over a 24hr period. Each supply was housed in a metal case to reduce external interference, and the output connections were made using RS 8-way sockets. All the output leads were contained in a multicore screened cable, which was mains earthed at the power supply end and left floating at the PDA end.

6.2.4 Alignment procedure - Reticon RL 128 S / RC 1024 SA

This section describes briefly the setup procedure for the RC 1024 SA evaluation board and the RL 128 S photodiode array. The signals illustrated in figures 6.3a-e were monitored using a Tektronix 7623A storage oscilloscope equipped with a 7A13 100MHz differential amplifier unit and a 7A22 10mV differential amplifier unit. The full alignment procedure, including the location of the relevant potentiometer controls, is described in the Reticon data sheet for the evaluation board, the purpose of this section being mainly to introduce the various waveforms involved.

For all experiments described in this work the oscillator clock frequency was set at 200kHz, as this was convenient for digitisation of the output signal and matched the highest available clock frequency on the Hamamatsu drive electronics (section 6.3.2). This sets the scan rate at 50 kHz i.e. a sample time of 20 μsec per diode. The maximum integration time is therefore 0.32 secs, and the minimum integration time is 2.56 msecs, which is the readout time for one complete scan.

Figure 6.3a shows part of the video output in the dark as might be seen after startup. The integration time is 2.56 msecs and the array temperature is ~30 ^{o}C. Clearly there is a 1,2,3,4 type fixed pattern noise to the dark signal. The first pixel is displaced from all the others and is ignored in this and later observations. The first step in aligning the board is to separate the odd and even video signals by 200 mV in the dark (fig 6.3b). By altering the capacitance, hence the signal coupling, between each pair of clock phases the imbalance in the odd and even signals can be independently reduced (Figure 6.3c). Figure 6.3d shows the odd and even signals correctly recombined to give a uniform dark signal. Note that the magnitude of the sampling pulse feedthrough is greater for the even scan. This is shown more clearly in figure 6.3e, which depicts the clock pulses superimposed upon the video output. Further alignment is concerned with optimising the video amplifier gain balance for each channel, and setting the retrace blank level coincident with the dark level at zero volts. This procedure is described in more detail in the relevant Reticon data sheets.

Dark Alignment Procedure For

Reticon RL1285 Linear Photodiode

Array On RC1024 SA Evaluation

Board

Figure 6.3a Unaligned Video Signal

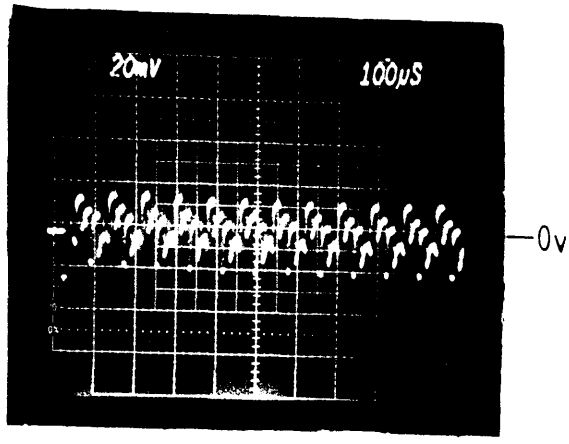

Figure 6.3b Separate Odd and Even Signals

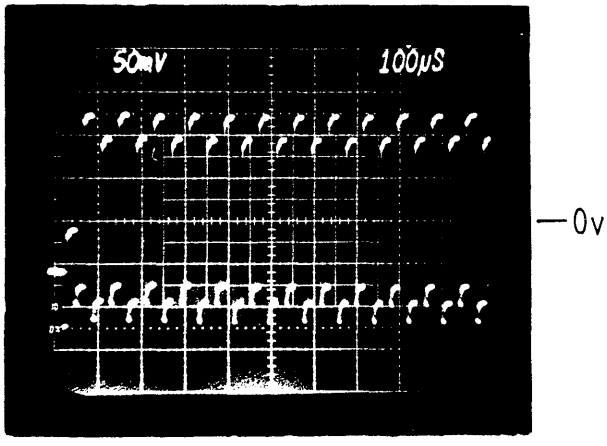

Figure 6.3c Balance Clock Phase Feedthrough

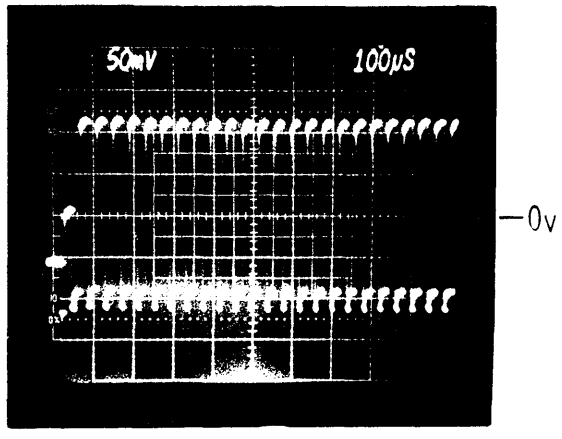

Figure 6.3d Odd + Even Correctly Recombined

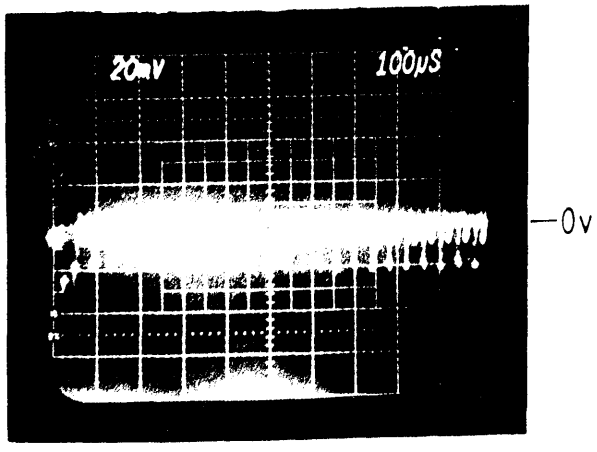

Figure 6.3e Video Output + Clock Pulses

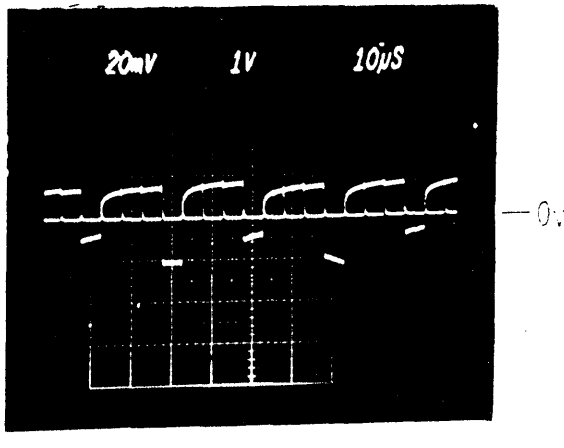

6.3 HAMAMATSU PCD LINEAR IMAGE SENSORS

The Hamamatsu S2304 series linear image sensors are monolithic self-scanning photodiode arrays designed specifically for applications in multichannel spectroscopy. The array under consideration is the S2304-512F, which has 512 elements of 25μmx2.5mm and is fitted with a fibre optic input window. The saturation charge for each diode is 7.5 pC, corresponding to an element capacity of $4.7x10^7$ electrons.

6.3.1 Principles of operation : S2304 - 512F

The actual construction and operation of the sensor elements in this photodiode array is extremely similar to that of the Reticon S series arrays, the main difference being in the readout circuitry. Figure 6.4 shows a simplified equivalent circuit for this sensor. As can be seen, there is only one video line, and the sampling switches are bipolar transistors compared with the MOS devices used in the Reticon arrays. The single bipolar static scanning shift register operates using three phase TTL compatible clocks. Advantages of this system include a much reduced sample pulse feedthrough, so that no dummy photodiodes are necessary, and the signal is available from only one row as a sequential output. This results in much simplified driver and readout electronics, with corresponding increases in reliability and ease of use. Further data is available in the Hamamatsu technical data publication, 'PCD Linear Image Sensors S2301, S2304 Series'.

6.3.2 Drive electronics : C2325 / C2335

The drive electronics for the Hamamatsu array are supplied on two separate PCBs with the PDA itself located on the C2325 driver/amplifier board, which generates the three clock phases necessary to drive the shift register and includes a low-noise video amplification system. The second board is the C2335 pulse generator, which provides the 'reference clock' and 'start' pulses for the C2325 board. Figure 6.5 shows a block diagram of the main circuit components.

The pulse generator board includes a quartz crystal oscillator 'master clock' at a frequency of 1MHz. The 'reference clock' applied to the C2325 board is obtained by dividing down the 'master clock' frequency using preset switches arranged in a 1-2-5 sequence. In this way the 'reference clock' frequency can be varied between 0.02Hz and 1MHz in discrete steps. The 'start' pulses control the integration time and are generated either from the 'master clock' or from the 'reference clock' depending upon the position of a circuit jumper. The maximum available integration time in the 'master clock' mode is 50 seconds, and the minimum usable

Figure 6.4 Equivalent Circuit For Hamamatsu Linear Photodiode Arrays

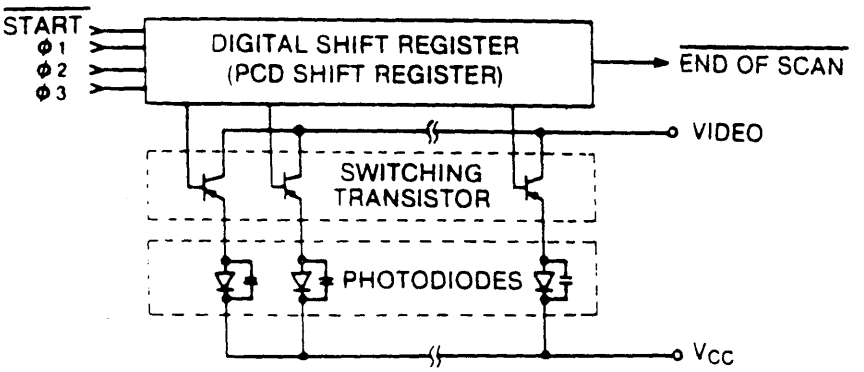

Figure 6.5 Block Diagram Of C2325 Driver/Amplifier Electronics

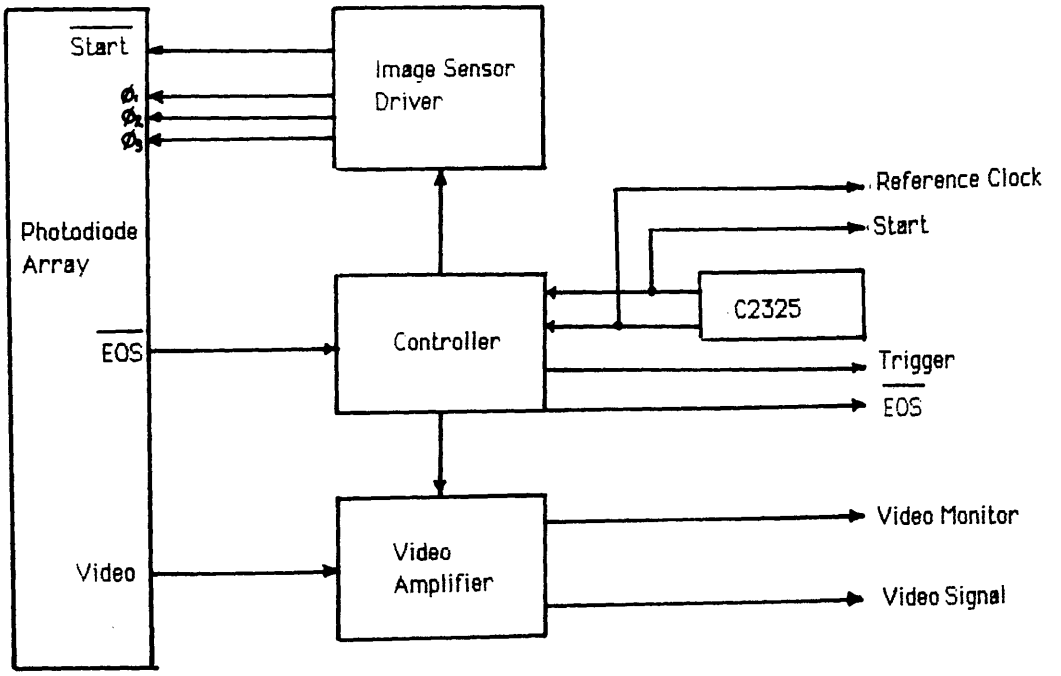

integration time is again determined by the array readout time.

The amplifier section of the C2325 board uses a low noise charge integrator to detect the diode output signal and a double sampling technique to reduce the reset or thermodynamic noise (see section 7.1.2). The maximum video rate is restricted to 62.5 kHz, and as the timing is identical to the Reticon diodes (i.e. one sample pulse every four clock periods) this corresponds to a maximum 'reference clock' frequency of 250 kHz. The closest clock frequency available from the C2335 board is 200kHz, giving a data rate of 50 kHz. With 512 elements the time taken to read out a complete scan of the S2304-512F array is therefore 10.2 msecs. The saturation video voltage is 3V, and the diode capacity is 7.5 pC, so that the amplifier gain is $4x10^{11}$ V/C or $6.4x10^{-8}$ V/electron.

Apart from the video signal, the C2325 board also provides 'reference clock', 'start', and 'trigger' outputs which are positive TTL signals. The 'trigger' pulse is used to provide the 'start convert' signal for the analogue to digital conversion board (section 6.4.2), and it occurs at the start of the fourth clock period in each sample pulse. Other outputs include an 'end of scan' (EOS) signal (negative LS-TTL compatible), and a 'video monitor' signal which is used in setting up the C2325 board.

The two driver boards were initially housed in one metal casing, and the input/output connections were constructed identically to those of the Reticon device described previously. The power supply requirements are ±15 V at 20mA each and +5V at 120mA, so that the power supplies of section 6.2.3 could be used to drive both the Reticon and Hamamatsu electronics.

6.3.3 Alignment procedure : S2304 -512F / C2325-C2335

This section gives a brief description of the setup procedure for the C2325 evaluation board and S2304-512F photodiode array. Further details are available in 'Operational Instructions for the C2325 Series Evaluation Board' published by Hamamatsu. The following images were obtained with the array in the dark, at a temperature of ~25°C.

The 'reference clock' frequency was set to 200 kHz, which is the maximum that the C2325-C2335 combination can achieve, giving a video rate of 50kHz. The integration time was set at 20 msec, which is the shortest usable value available on the C2335 board. Figure 6.6a shows the output of the 'video monitor' signal as displayed on the Tektronix oscilloscope. This signal corresponds to the integrated video current signal, and is used for

Figure 6.6a Unaligned Video Monitor Signal

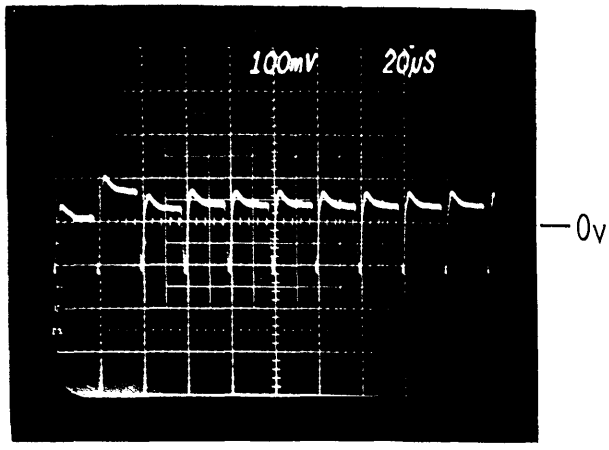

Figure 6.6b Zero Level Adjusted To Ground

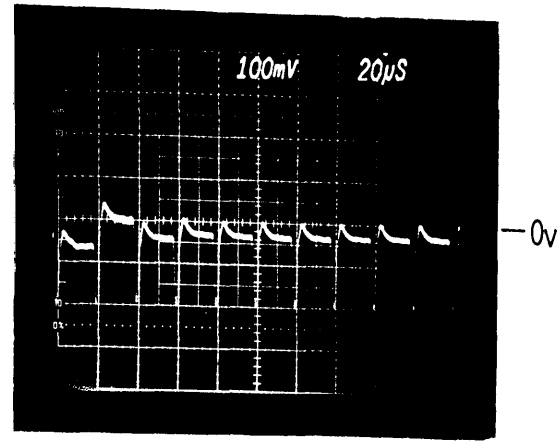

Figure 6.6c Reset Pulses Nulled

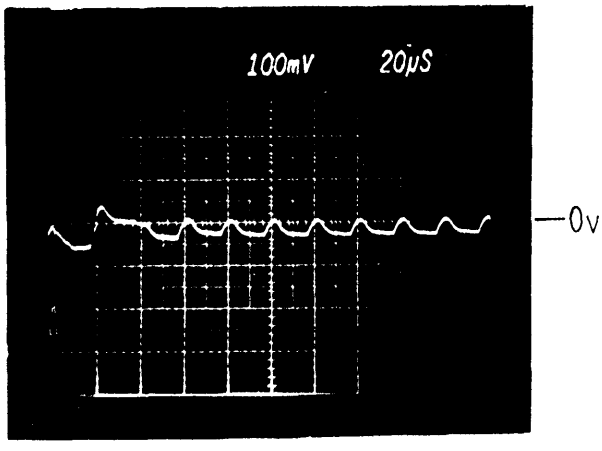

Figure 6.6d Correctly Aligned Video Signal

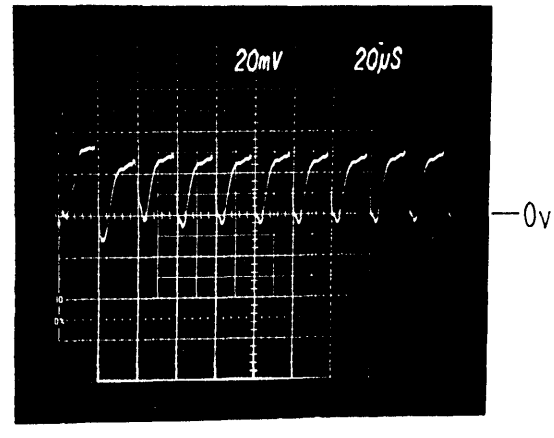

Figure 6.6 Alignment Procedure for Hamamatsu S2304-512F

Photodiode Array On C2325 Driver / Amplifier Board

adjusting the switching noise cancellation and setting the output zero level. Figure 6.6b shows the zero level adjusted to the oscilloscope ground, and figure 6.6c shows the 'video monitor' signal after the reset pulses have been nulled out. The resultant correctly adjusted video signal is shown in figure 6.6d. As can be seen there is no odd-even type pattern in the signal due to the single video line, and the output waveform is a pulse rather than a sampled and held type signal. The rounded edges and uneven tops of each pixel are probably due to the fact that the board is operating at near maximum speed. As the clock frequency is lowered, each pixel becomes more 'box like', however the rms noise is little altered, so that the dynamic range does not change.

6.4 DIGITISING THE VIDEO SIGNALS

For quantitative measurements the diode array video signals must be digitised and stored in computer memory for further processing. The actual conversion time must be fast enough to match the diode readout rate, and sufficiently precise to complement the dynamic range of the array. The following sections describe the digital timing / analogue-digital conversion electronics built to enable computer controlled acquisition of the video data from both diode arrays, via a 68000 microprocessor monoboard computer. Two circuits are required to cope with the different timing signals and number of pixels from each array. These circuits were constructed on the same PCB and shared some logic gates. Selection of the required circuit is by an external hardware switch.

6.4.1 Digital timing / interface circuits RL128S

The timing diagram for the output signals from the RC 1024S evaluation board and the interface circuit is shown in figure 6.7. As can be seen from this and figure 6.3e, the video signal is not constant over the four clock periods of each sample pulse. Obviously the digitisation point should be well away from the sample pulse feedthrough in the first clock period, and consequently it was decided to sample in the fourth clock period, where the signal changes least rapidly. Referring to figure 6.7 the first pixel occurs on the 10^{th} clock period after the positive edge of the 'start scan signal'. The preferred sampling point appears 3 clock periods later, and then every fourth subsequent clock period until the scan ends.

The digital timing circuit constructed to digitise the video signal is shown in figure 6.8. Some extra components are included as these form part of the equivalent timing circuit for the Hamamatsu array, the two circuits being combined on one board using some common

Figure 6.7 Timing Diagram For Reticon RL128S-RC1024S

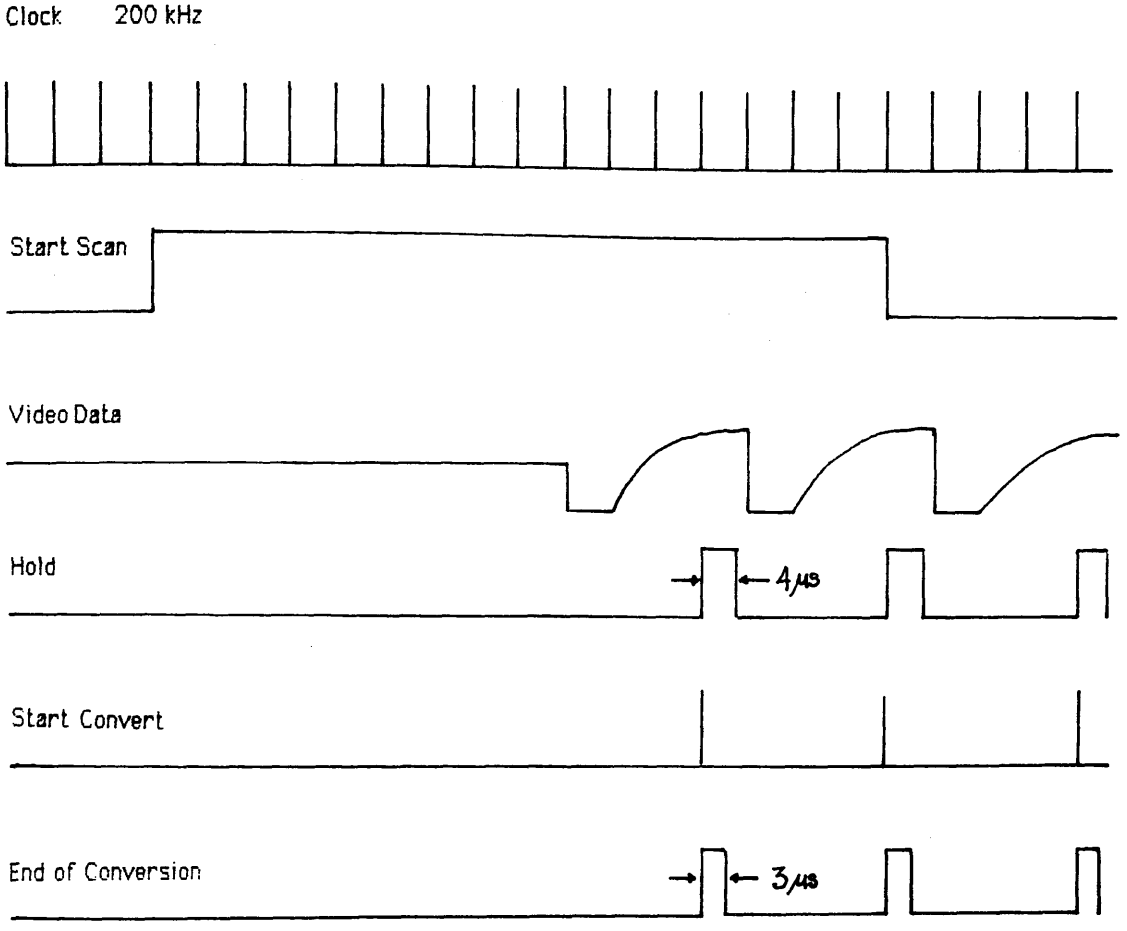

Figure 6.8 Digital Timing Circuit - Reticon RL128S / RC1024 SA

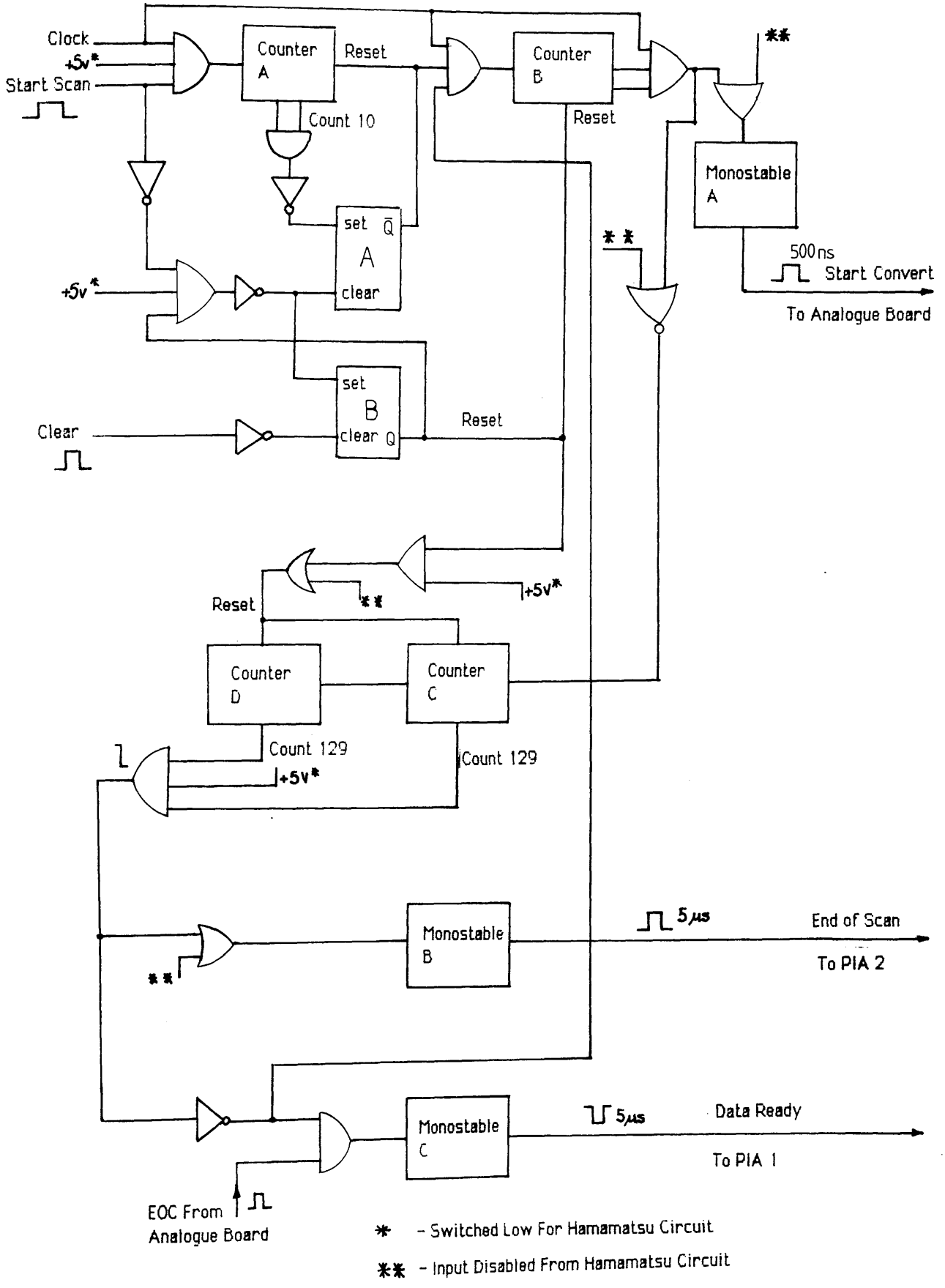

elements. The operation is as follows:

1) Initialisation is implemented by a 'clear' pulse from the microprocessor board. Prior to the 'clear' pulse, the output of flip-flop B is unchanged from its value at the end of the previous scan i.e. high (at power on the output is indeterminate, and one 'dummy' scan may be necessary to set up this gate), thus binary counter A is 'reset'.

2) The arrival of the 'clear' pulse sets the output of flip-flop A high, causing binary counters B, C, and D to be held in the 'reset' condition. If the 'start scan' input is low, the output of flip-flop B is set low, enabling counter A and disabling the clock input to counter B. The falling edge of the 'clear' pulse causes flip-flop A to reset to low, enabling counters B, C, and D.

3) The system now waits for the leading edge of the next 'start scan' pulse, which allows the diode clock pulses to trigger counter A. After 10 clock pulses (i.e.9 clock periods) the output of A is used to set flip-flop B output high, thus enabling the passage of clock pulses to counter B and putting counter A at 'reset'.

4) Counter B is wired as a divide by four gate, giving one sampling pulse for every four clock pulses, so that the first and subsequent pulses output from B coincide with the desired sampling points. These sampling pulses are used to trigger two monostable oscillators which provide the 'start convert' and 'hold' pulses for the analogue board, 500 nsecs for the former and 4 μsecs for the latter.

5) The signals from counter B are simultaneously applied to counters C and D, which are wired together to count 129 pulses. On the 129th pulse three things happen; the input to counter B is disabled until the next 'clear' pulse, thus inhibiting the 'start convert' pulses to the analogue board, the 'data ready' pulses described in section 6.4.3 are inhibited, and an 'end of scan' pulse is sent to interrupt the microprocessor and terminate the data transfer.

It is possible in step 2) above that the 'clear' pulse could arrive anywhere during the time when the 'start scan' pulse was high. In this case counter A is not enabled until the falling edge of the 'start scan' pulse, and the rest of the scan is ignored, as counter B cannot receive clock pulses until after the arrival of the next 'start scan' pulse.

The digital timing electronics were housed in a metal casing along with the analogue electronics described in section 6.4.3, on separate circuit boards. All external signal connections to the RL 1024 SA board were made by shielded coaxial cables using BNC connectors, and the regulated power supply used was a separate unit from the supplies used to drive the photodiode evaluation board.

6.4.2 Digital timing / interface circuits : S2304-512F

The timing diagram for the output signals from the C2325 driver/amplifier board is given in figure 6.9. The digitisation procedure is made simpler than that for the Reticon diode by the presence of the 'trigger' pulses, and the fact that the falling edge of the 'start' pulse corresponds with the start of the first pixel. The digital timing circuit constructed is shown in figure 6.10. As before, some of the components are shared with the Reticon circuit. The operation is as follows:

1) Initiation is implemented by a 'clear' pulse from the microprocessor board. Prior to the clear pulse, the output of flip-flops A, B, and C are unchanged from their values at the end of the previous scan (at power on the outputs are indeterminate, so a 'dummy' scan is sometimes necessary to set up the gates). The output Q of flip-flop A is low, inhibiting the 'start' pulse, the Q bar output of flip-flop B is high, such that the binary counters A,B,C are held at 'reset', while the complementary Q output being low inhibits the passage of 'trigger' pulses to monostable B. The Q output of flip-flop C is also low at this point.

2) The rising edge of the 'clear' pulse causes flip-flop A to change state, enabling the passage of the next 'start' pulse to flip-flop B.

3) Upon receipt of the rising edge of the 'start' pulse flip-flop B changes state. Output Q bar goes low, enabling counters A,B,C, and output Q goes high so that 'trigger' pulses are able to clock the counters. At the same time as B changes, the Q output of flip-flop C changes from low to high, enabling the passage of 'trigger' pulses to the analogue board via monostable B, which produces a 500nsec 'start' pulse for every 'trigger' pulse.

4) The operation continues until 512 'trigger' pulses have been counted by counters A,B,C, at which point the Q output of flip-flop C is set low, disabling the 'start convert' pulses.

Figure 6.9 Timing Diagram For Hamamatsu S2304-512F / C2325

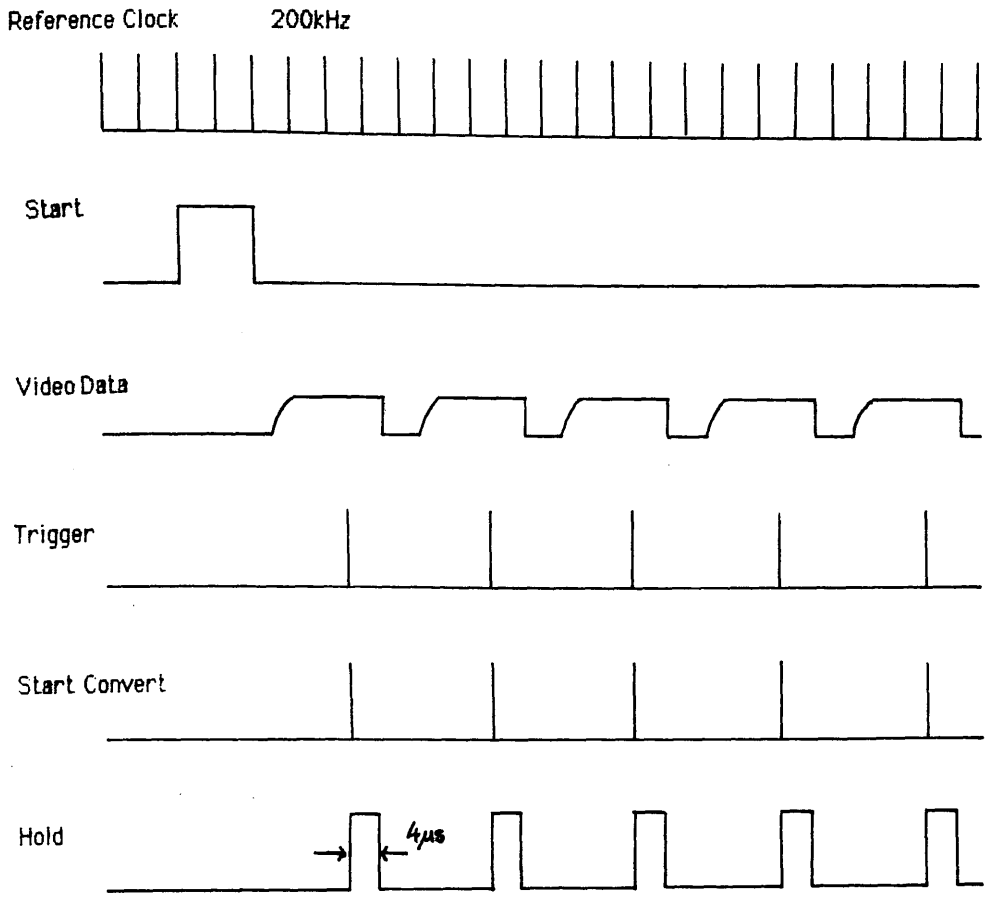

Figure 6.10 Digital Timing Circuit - Hamamatsu S2304-512F / C2325

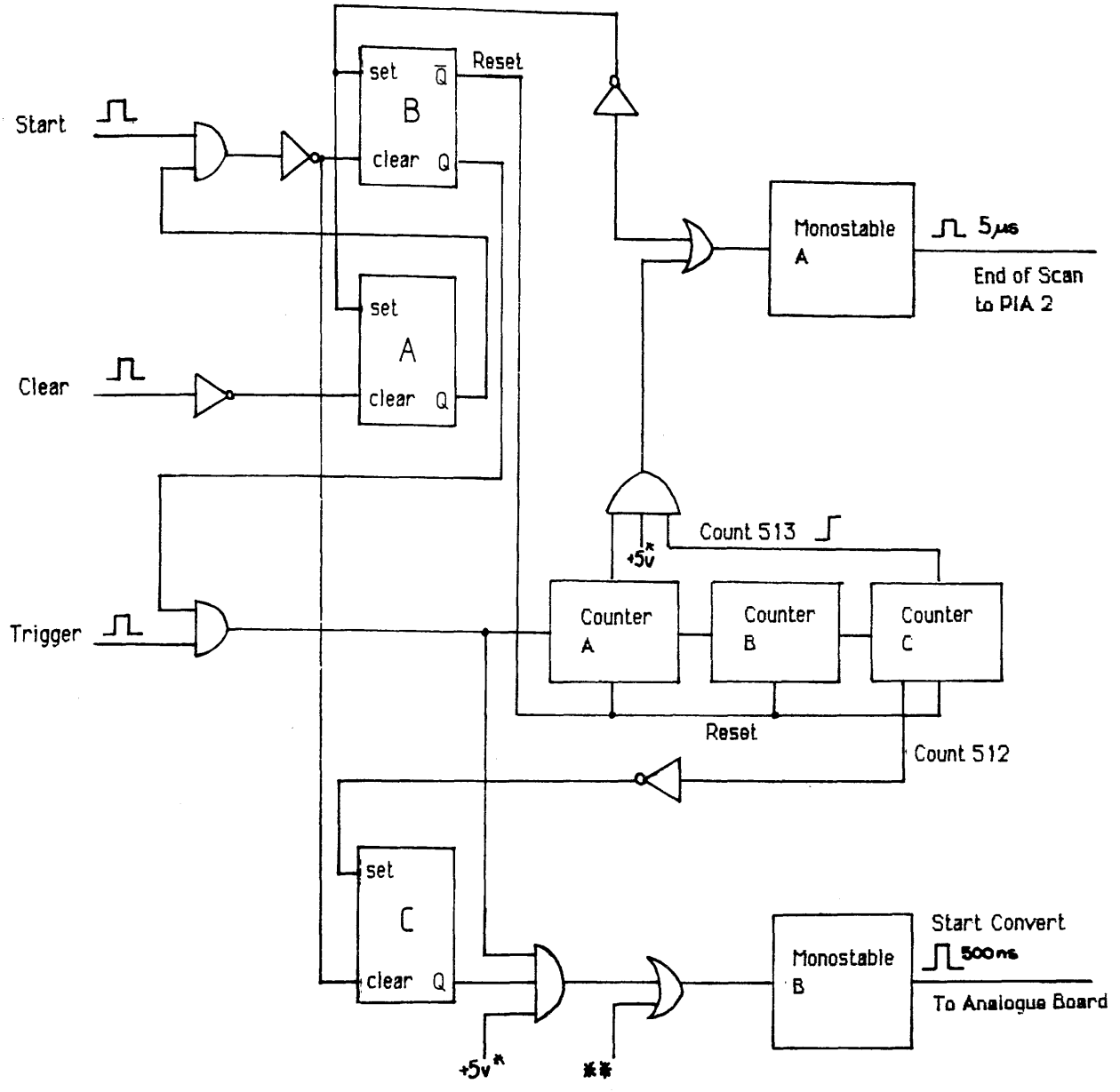

* - Switched Low For Reticon Circuit

** - Input Disabled From Reticon Circuit

5) On the 513th count an 'end of scan' pulse is sent to the microprocessor by monostable A, flip-flop B output changes state to 'reset' the counters and inhibit the 'trigger' signals, and flip-flop A output goes low to block any further 'start' pulses reaching flip-flop B. The circuit now waits for the next 'clear' pulse from the processor.

6.4.3 Analogue to digital conversion circuit : HTC 0300A / AD 578-L

The rms single pixel dynamic range of the RL 128 S array /RC 1024 SA evaluation board, defined as the ratio of the peak signal / rms noise on one pixel, is specified to be > 10000:1. This figure corresponds to ~9000 electrons rms noise. The equivalent figure quoted for the S2304-512F array /C2325 driver-amplifier is a dynamic range of 15000:1, corresponding to ~3100 rms electrons noise. Thus, it can readily be seen that for both these devices single electron detection in the indirect mode is not likely, unless an extremely efficient 100 keV electron-photon conversion efficiency can be achieved.

The above figure of 15000:1 dynamic range requires a conversion accuracy of 14 bits if the ADC is not to limit the dynamic range of the output. Conversion speed is also a critical factor; from the previous sections the digitisation and memory transfer cycle must be complete within four clock periods, i.e. with a clock frequency of 200 kHz 20μsecs. Unfortunately, the cost of ADCs rises rapidly with conversion speed and number of bits, so it was decided that, for the purposes of evaluation, the digital accuracy should be compromised slightly in favour of conversion speed. This allocated the maximum amout of time to the transfer of the digital information into memory, so that special high speed electronics, such as direct memory access (DMA) systems were not necessary.

The ADC chosen was an Analogue Devices AD578 L 12 bit successive approximation converter with a maximum conversion time of 3μsecs. The video signal was sampled using an Analogue Devices HTC 0300A track and hold amplifier, which can track a 10V step in input voltage to an accuracy of 0.01% in 300 nsecs. The layout of the analogue board is shown in figure 6.11. The op-amps are Analogue Devices AD711 units, which settle to an accuracy of 0.01% in 1μsec, with a slew rate of 18V/μsec at unity gain. Considerable care was exercised to obtain the best possible performance from the components used. All the analogue components were wire-wrapped onto an isolated circuit board, with an integral ground plane. The power supply lines were capacitively decoupled following the manufacturers advice, and solid state transient suppressors were used to protect the devices from power 'glitches'. The analogue circuit board was housed in the same casing as the digital timing circuits. Input and output connections to the microprocessor were made using

a standard 40 pin ribbon cable connector.

The principal operational difficulty was found to be the noise performance of the HTC-0300A track/hold amplifier, which proved to be ultra-sensitive to power supply variations and circuit layout. The final circuit design of figure 6.11 is the best of many different configurations tested, and is relatively noise free. Unfortunately there is no protection circuitry in the signal path, since any additional components (e.g. zener diodes etc) always seemed to degrade the performance, so great care has to be taken that the analogue input does not exceed ± 3V. The operation of the circuit is as follows:

1) The analogue video signal is amplified by -3.33x, to match the 0-3V signal from the evaluation board to the 0-10V signal required by the ADC. The HTC 0300A has a gain of -1x, so that the signal applied to the input of the AD 578 via the unity gain buffer amp has the correct polarity.

2) The 'start convert' pulse from the digital timing board is applied simultaneously to the ADC as a 500 nsec pulse, and to the HTC 0300 as a 4 μsec 'hold' command. At the instant the start convert pulse is applied, the end of conversion (EOC) output of the ADC goes high, and then 3 μsec later switches to low when the conversion is complete and the data is valid.

3) The negative going edge of the EOC signal from the ADC is used to trigger two 8 bit digital latches, causing the output of the ADC lines to be transferred to the output of the latches, where it can be read by the microprocessor. The latched output remains until the next conversion is complete. After every conversion the EOC signal triggers a monostable on the digital board to produce a negative edge on a control line which acts as a 'data ready' flag for the microprocessor. The operation of the microprocessor controller is discussed in more detail in section 6.5.1.

6.5 COMPUTER INTERFACING : Motorola 68000 monoboard - VME system

Once the video data has been digitised it must be read by a computer and stored in memory ready for processing. The computer must also provide and receive timing pulses, such as the 'clear' and 'data ready' signals mentioned in section 6.4. This section describes the operation of the Motorala 68000 microprocessor system used to provide the hardware

Figure 6.11 Analogue To Digital Conversion Circuit

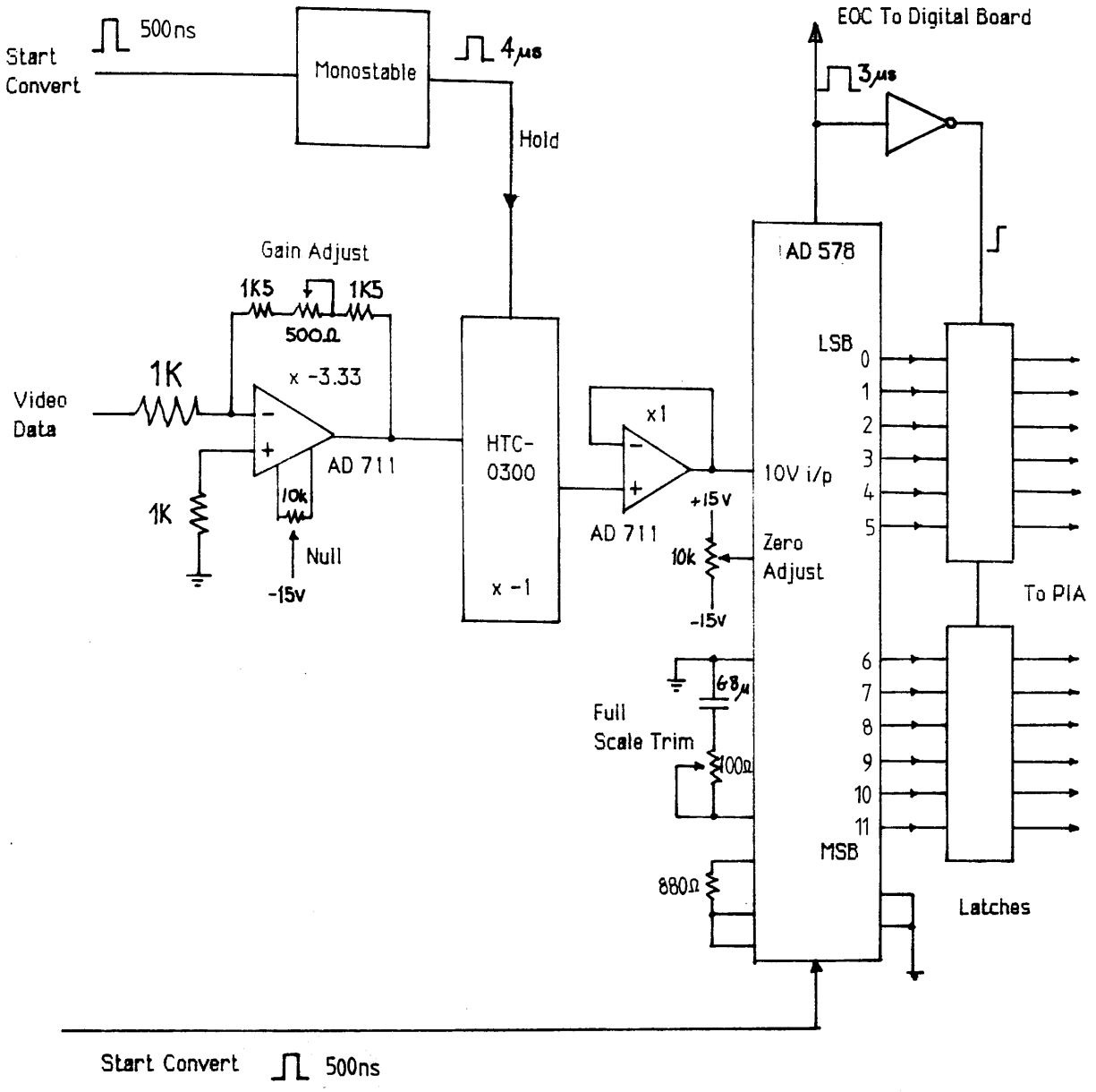

interfacing between the A-D / digital timing circuit, and a Motorola VME minicomputer system.

6.5.1 The microprocessor board: Motorola MC68000 KDM

The Motorola MC68000 KDM monoboard computer includes a 16 bit Motorola 68000 microprocessor with 32k bytes of dynamic RAM, two 16 bit peripheral interface adapter ports (PIA1,PIA2), along with other facilities such as 16 bit timers etc. Communication to the board is provided by two asynchronous communication ports (ACIAs). One ACIA is configured to be connected to a standard RS-232C data terminal, and the other is configured to simulate an RS-232C terminal, enabling communication with a host computer. Selection of a transparent mode allows the KDM board to be bypassed, so that a program can be directly created on the host computer and then downloaded into the microprocessor memory for execution. Similarly, the contents of the microprocessor memory can be uploaded into the host computer for processing and display.

Figure 6.12 shows the PIA input/output connections. The PIA ports are wired in such a way that the A peripheral data registers (PDRA1,PDRA2) from each port can be read simultaneously using one 16 bit read operation addressed to PDRA2. The system is configured so that the four most significant bits from the ADC are read by the A3 to A0 lines of PIA2, and the eight least significant bits are read by the A7-A0 lines of PIA1. Line A4 of PIA2 is used as an output line to provide the 'clear' pulse to initialise the timing circuit. All other data lines are grounded. Control line CA1 of PIA1 is an input line which registers the 'data ready' pulse generated by the end of conversion (EOC) signal from the ADC, and control line CA1 of PIA2 is used as an interrupt input which reads the 'end of scan' pulse from the timing circuit.

6.5.2 Acquisition software

The assembly language program which controls the data acquisition is listed in appendix 5. The program provides all the necessary instructions to acquire 10 consecutive digitised video scans from either the Hamamatsu or Reticon arrays, and store the data in memory. In practice, the program is stored on disk in the VME host computer system. The assembled machine code program is downloaded into the KDM board for execution, and the digitised video data is uploaded back to the VME system for processing. The program operation is as follows:

1) Assign various constants and address locations required in the program.

Figure 6.12 Microprocessor Interfacing Circuit

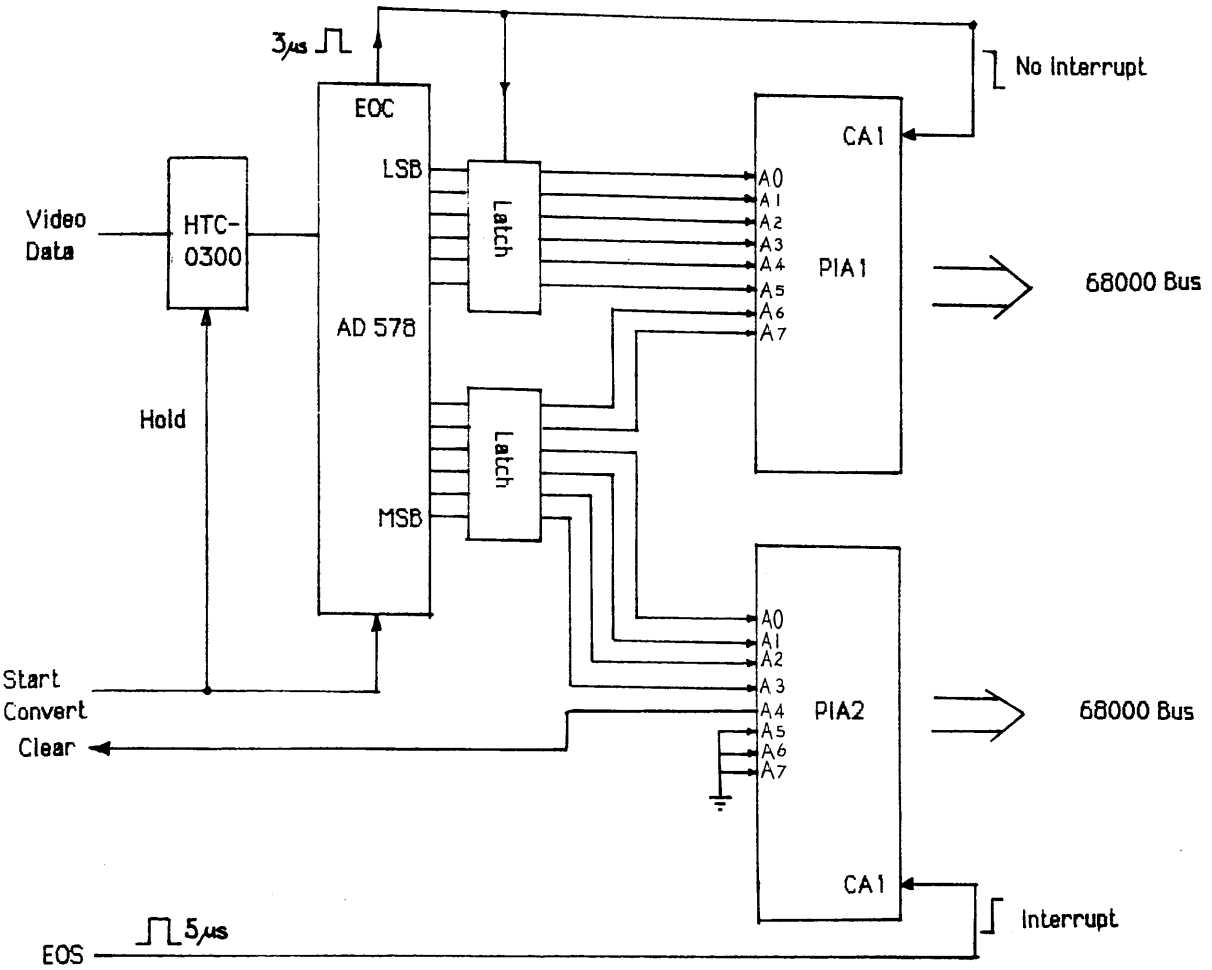

Figure 6.13 Testing The Acquisition System

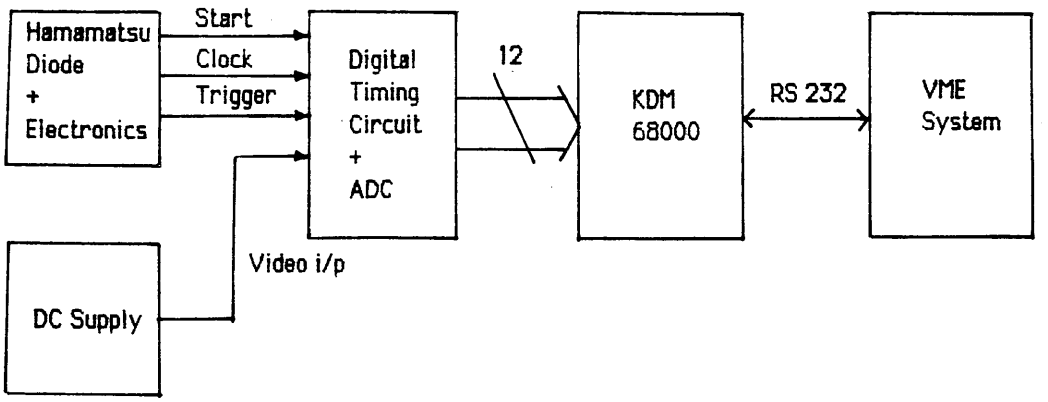

2) Clear a block of memory for the data.

3) Set up the PIA lines as inputs or outputs as described in the previous section. Line CA1 of PIA1 ('data ready') is initialised to respond to a falling edge, but the interrupt is masked. Line CA1 of PIA2 ('end of scan') provides a processor interrupt on receipt of a rising edge.

4) The main program firstly checks to see if all 10 scans are complete, if they are the program terminates. If there are still scans left to acquire a 'clear' pulse is sent out to the digital timing circuit.

5) The program enters a read loop which is only terminated upon receipt of the 'end of scan' interrupt. Inside the loop the program continuously polls the 'data ready' line. If the line is set, a 16 bit read takes place, transferring the data from the PIAs to memory.

6) When the 'end of scan' interrupt arrives the program control is transferred to an interrupt service routine. This routine firstly causes 16 blank bytes to be inserted in memory after the last received data byte, in order to serve as an end of scan marker. The interrupt flag is then cleared, control is returned to the main program and the cycle repeats until 10 scans have been completed.

The main difficulty the program must overcome is the relatively high data rate of the video signal i.e. 50kHz. Allowing at least 3 μsecs for the conversion, the time remaining for data detection, transfer and storage is <17 μsecs. This is not long enough for the standard handshaking/interrupt type interface between the processor and the ADC to be used. In order to speed up the transfer process the simple polling routine of step 5) is used. The actual loop consists of only four instructions, which take ~32 machine cycles to execute, i.e. at 8MHz clock rate the loop takes around 4 μsec. This time does not include overheads such as time spent refreshing the dynamic RAM, so that the actual average execution time is longer. Nevertheless this program enables data rates of up to ~75kHz to be acquired comfortably.

6.5.3 The VME host minicomputer system.

The Motorola VME host minicomputer system is a stand alone computer based on the 68000 microprocessor and running the VERSADOS operating system, which is compatible with the

KDM board. Data and programs are stored on an integral hard disk, or on 5 inch floppy disks. Serial ports are available for up to three terminals, and there is also a parallel printer port. Read/write communication with the KDM microprocessor board is via one of the terminal ports. The assembly language acquisition program described previously was written and debugged on this computer using the resident 68000 assembler.

At the start of an experiment the assembled code is downloaded to the KDM board as a series of 'S records' under VERSADOS control. After the microprocessor has finished the scans and stored all the video data in RAM, it is transferred back up to the VME system and stored in a data file again in 'S record' format. Each record consists of 8 identifier characters, 32 hexadecimal numbers corresponding to eight 16-bit conversions, followed by two checksum characters. An interactive Fortran program, NRUN, was written to read this data file and convert the hexadecimal numbers to decimal figures for further processing. This, and other such programs are described more fully in chapter 7.

6.5.4 Testing the acquisition system

A simple experiment was carried out to check the operation of the data acquisition system. The equipment was set up as in figure 6.13, with the video signal from the Hamamatsu array replaced by a DC voltage, from a Time Electronics Model 2004 DC precision voltage supply. The 'reference clock' frequency was set at 200 kHz, to give a sampling rate of 50 kHz. A series of complete scans, consisting of 512 conversions, were acquired and transferred to the host computer where the data was converted to decimal format and displayed on a monitor. The average value of each scan and the standard deviation about the mean σ were then calculated.

The AD 578 is a 12 bit converter, so that the digital output varies from 0 (all bits off) to 4095 (all bits on). The input voltage range is 10 volts, therefore one least significant bit (LSB) corresponds to 2.44 mV. However, in terms of the video output signal 1 LSB corresponds to 0.723 mV, because of the x3.33 gain introduced before the sample and hold amplifier. The continuous analogue signal is partitioned into 4096 discrete ranges for 12 bit conversion, so that all analogue values within a 1 bit range are represented by the same digital code which is nominally the midrange value. This implies a quantising uncertainty of $\pm$ 1/2 LSB, i.e. $\pm$ 0.366 mV.

The ADC was set up so that the transition from all bits off to LSB on ocurred at an input voltage of +1/2 LSB i.e. 0.366 mV, and the final transition to all bits on occurred at full scale

- 3/2 LSB i.e. 2.9989V. Having fixed the end points of the conversion, the input voltage was varied and the experimental conversion value was compared to the theoretical value. The purpose of averaging the 512 nominally identical readings in each scan was to reduce the effects of random electrical noise, so that a true measure of the system linearity could be obtained. Figure 6.14a is a plot of the absolute deviation from the theoretical conversion value, against the theoretical conversion value. As can be seen, the values are well within the ± 1/2 LSB quantisation error over the whole range, indicating that non-linearity effects are negligible. The corresponding plot of the standard deviation σ about the mean of each scan, against theoretical conversion value is shown in figure 6.14b. It can be seen that, for the most part, σ is less than 1/2 LSB indicating that the noise performance of the circuit is acceptable.

6.6 VACUUM CHAMBER AND COOLING SYSTEM

The experiments described in chapter 7 were carried out in the vacuum system of a JEOL JEM 100 C electron microscope. The vacuum chamber shown in figure 6.15 was attached below the microscope camera chamber in the position normally occupied by the STEM detector, so that the arrays could be exposed to the electron beam. The chamber is made of brass ~1.5 cm thick to absorb X-rays generated by the 100 keV electrons. Figure 6.16 is a photograph of the entire detection system in situ, showing the vacuum chamber, power supplies, and electronics used to drive the array

6.6.1 Mounting the photodiodes in the vacuum system

The Hamamatsu C2325 driver/amplifier board measures 10.6 cm by 6.3 cm so that it is small enough to fit inside the vacuum chamber. The RC 1024 SA evaluation board is much too large to do this, so that a special preamplifier board similar in size to the C2325 was constructed, to operate the Reticon array in vacuum. The C2325 board has a slot cut directly beneath the diode array, exposing the underside of the device for ease of cooling. A similar slot was cut in the preamp board built for the Reticon array.

Inside the vacuum chamber the circuit boards were sprung mounted on four insulating pillars, in order to force the back of the arrays into good thermal contact with the cold surface of a Peltier cooler, described in section 6.6.2. The Peltier cooler was mounted on a copper pillar attached to a copper vacuum flange, designed so that the entire cooling assembly could be removed independently from the baseplate. Electrical connections to the cooler were made

Figure 6.14a Linearity of Analogue - Digital Conversion System

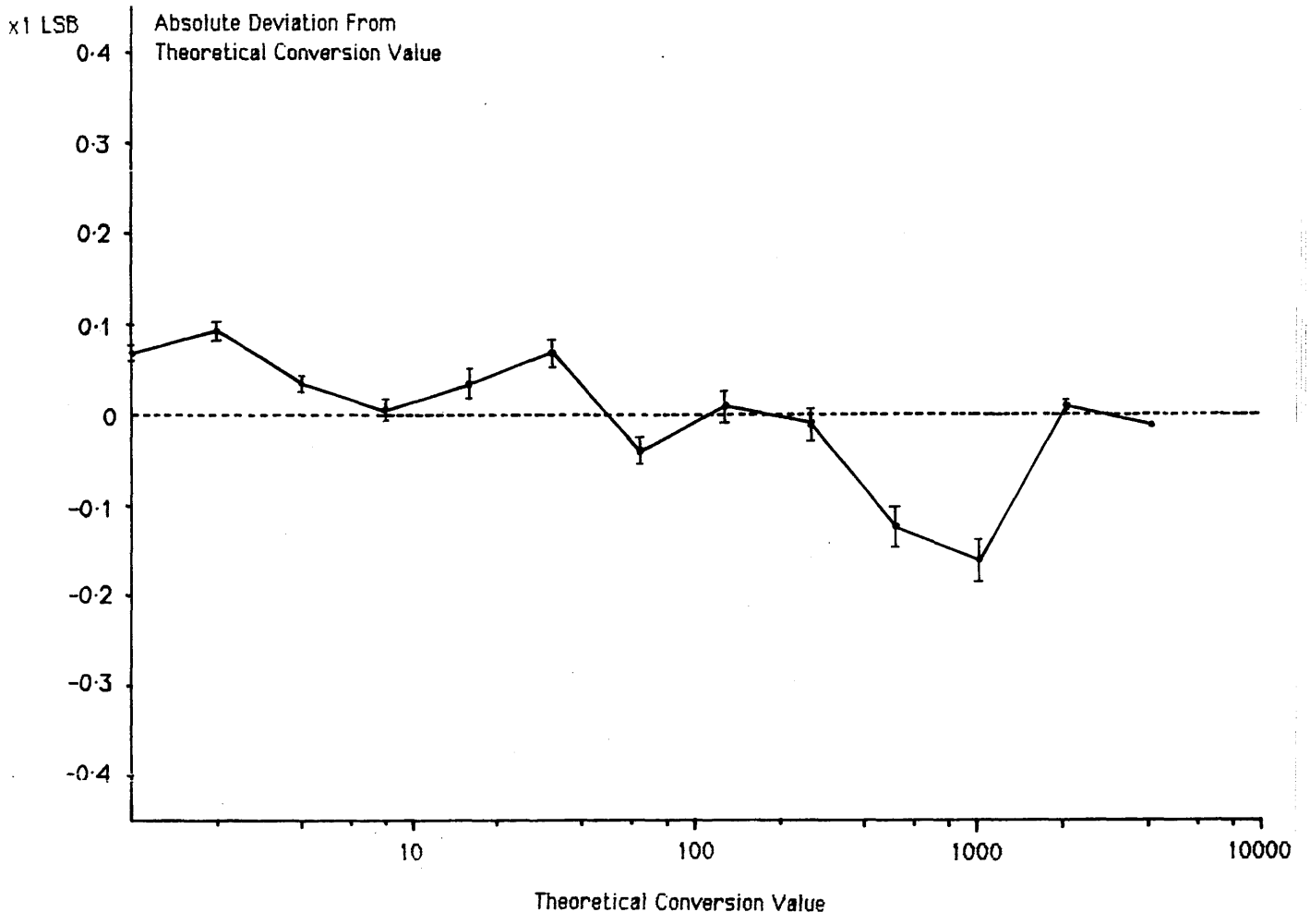

Figure 6.14b Noise Performance of Analogue - Digital Conversion System

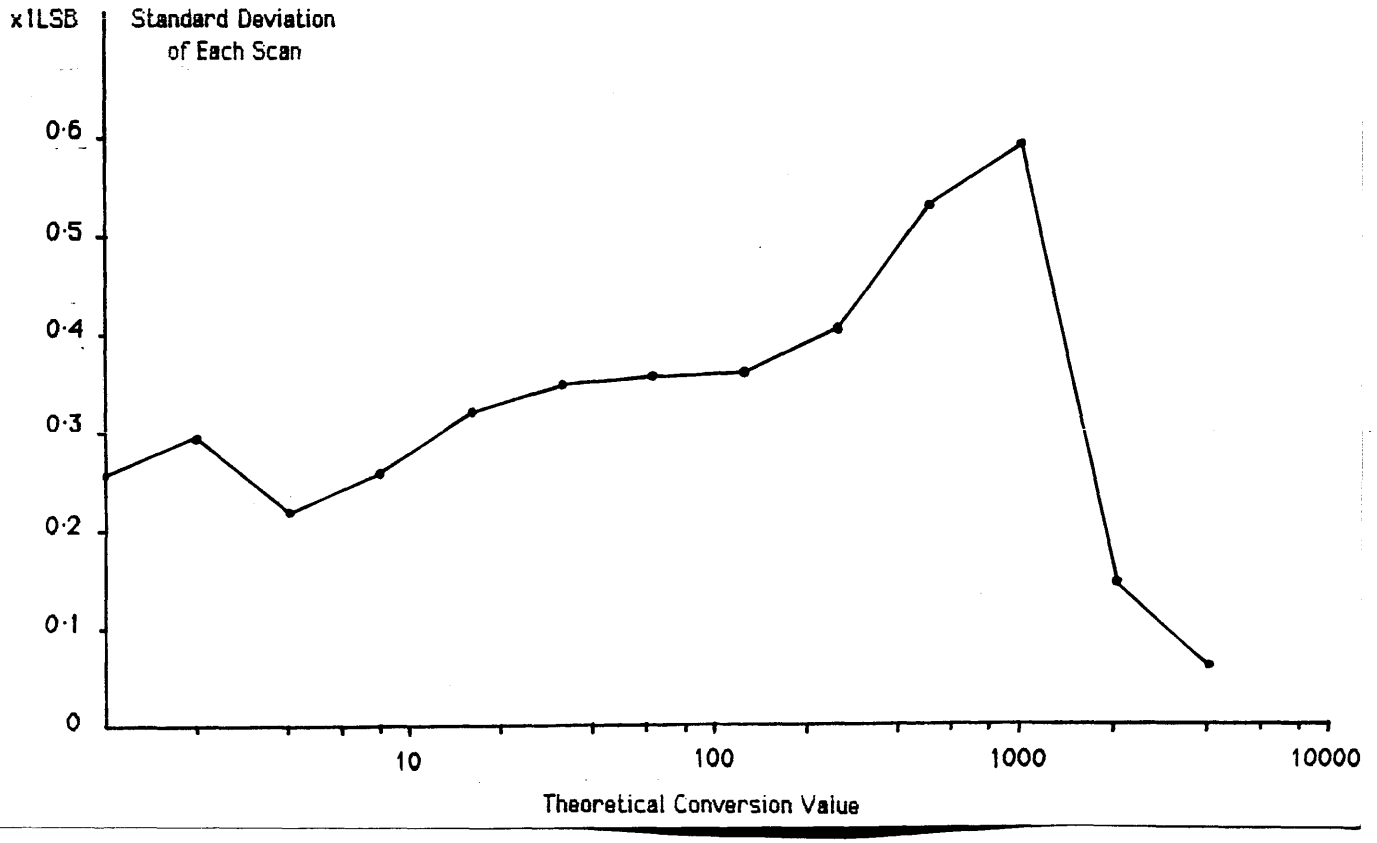

Figure 6.15 Vacuum Chamber, Diode Mounting and Cooling System

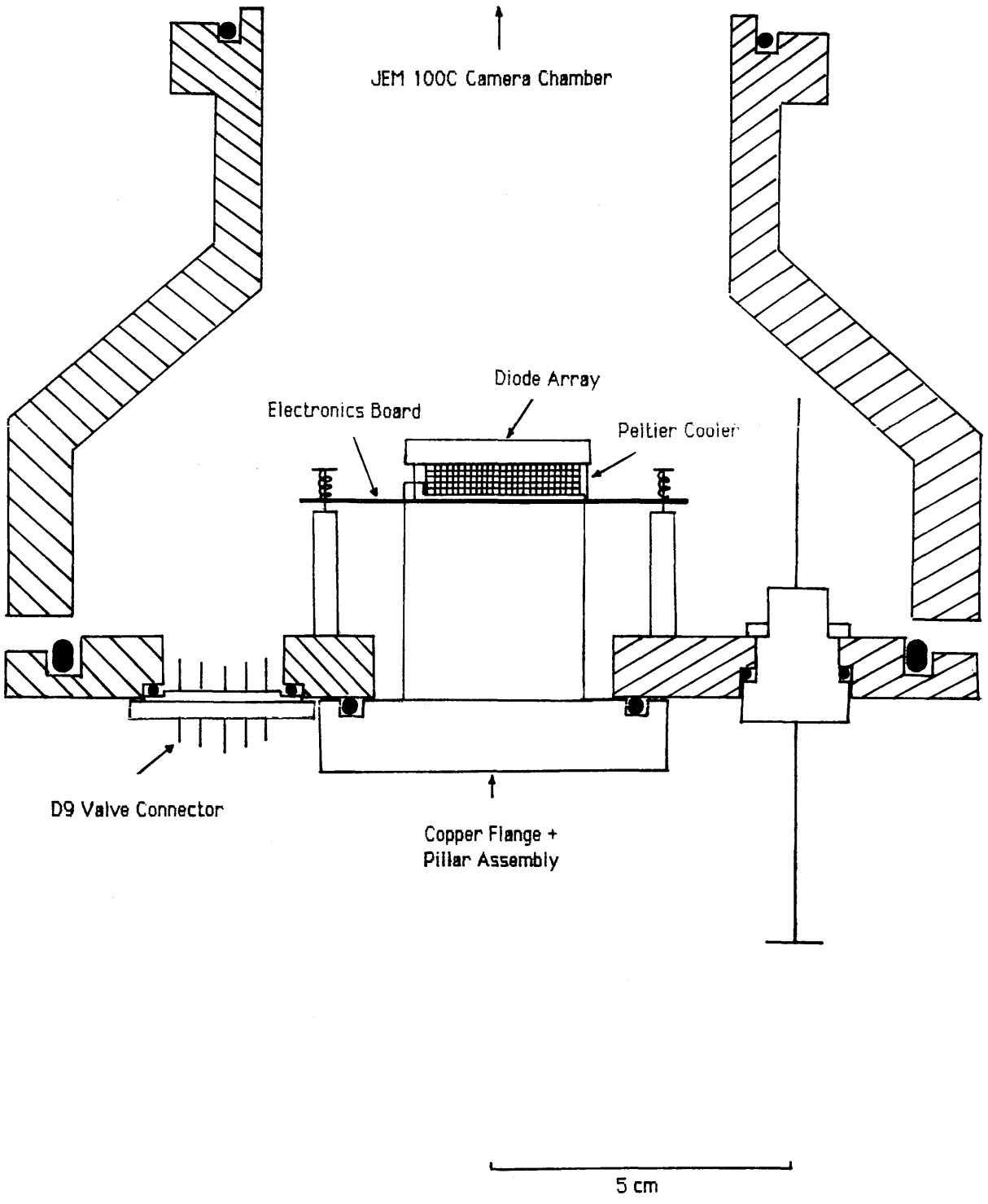

Figure 3.16 Prototype Detection System Attached to JEM 1000

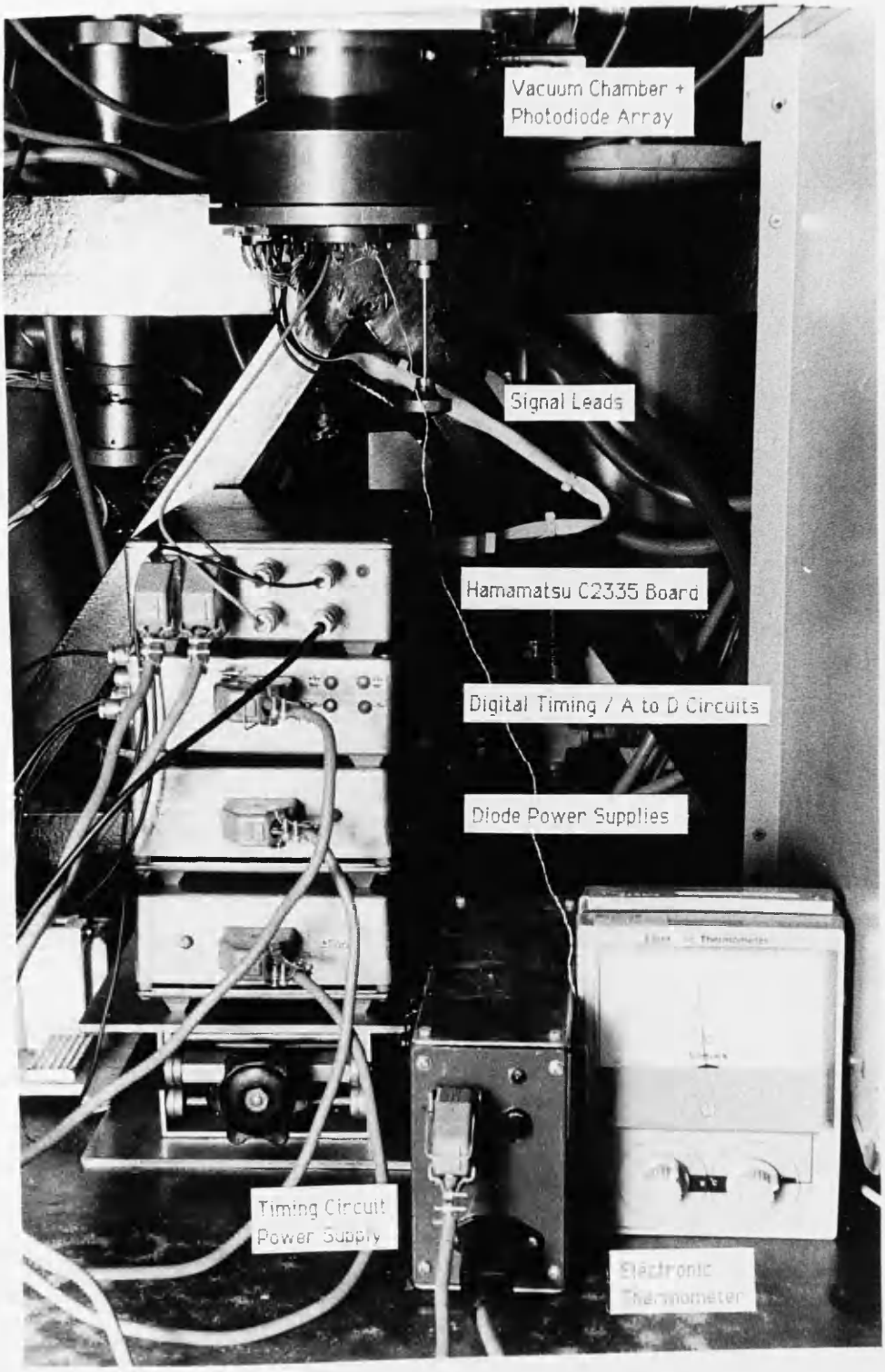

through two metal-to -glass seals hard soldered into the copper flange. A further metal-to -glass seal carried a pair of thermocouple wires, used for temperature monitoring.

The electrical signals used to drive the arrays were made via three D9 valve connectors which were vacuum sealed with O rings and a metal clamping plate. In this way up to 27 separate electrical connections could be made. The rotatable vacuum rod was originally included to enable a beam blanking plate to be positioned over the array, but was never used in practice.

6.6.2 The Peltier cooling system

At low light levels the maximum integration time that can be used in a photodiode array is limited by the build up of charge due to the dark leakage current. For example, at 25 ^{o}C the cells of the Reticon RL 128 S array are fully saturated in the dark after ~ 3 secs. In order to increase the integration time, and reduce the dark current shot noise, the array must be cooled. The most convenient method of cooling is to use a Peltier or thermoelectric cooler. The device employed was a single stage, 6 couple device manufactured by Midland Ross/Cambion for the purpose of cooling integrated circuits. The device number is 801-1029-01, the active area measures 26mm x 7.6mm, and the height is 5.3mm. The cooler is capable of maintaining a temperature difference of 60^{o}C between its hot and cold surfaces.

Silver loaded thermally conductive epoxy resin was used to bond the cooler directly to the copper pillar. The copper pillar and flange were designed to act as a heat sink by conducting the excess heat away to the main body of the chamber, and the temperature of the cold surface of the cooler was monitored using a Cu/Ni thermocouple connected to a Comark electronic thermometer. Good thermal contact between the cold surface and the photodiode array was ensured by the mechanical action of the spring loading, and some thermal paste applied to the junction. Power for the Peltier cooler was supplied using a Powerline LAB 515 10 amp regulated d.c. power supply.

Figure 6.17a is a plot of the Peltier temperature as a function of the applied current. The experiment was performed in the vacuum chamber attached to the microscope, one curve represents the response with no heat load, and the other curve the response when cooling the Hamamatsu photodiode. The start temperatures differ due to the heat generated by the diode and surrounding electronics. As can be seen, with no load the temperature of the cold surface can be varied over a range $\Delta T \sim 60^{o}$C. The initial variation is roughly linear, and then the response starts to level off. The effect is more obvious in the curve with the heat

Figure 6.17a Peltier Temperature v Applied Current

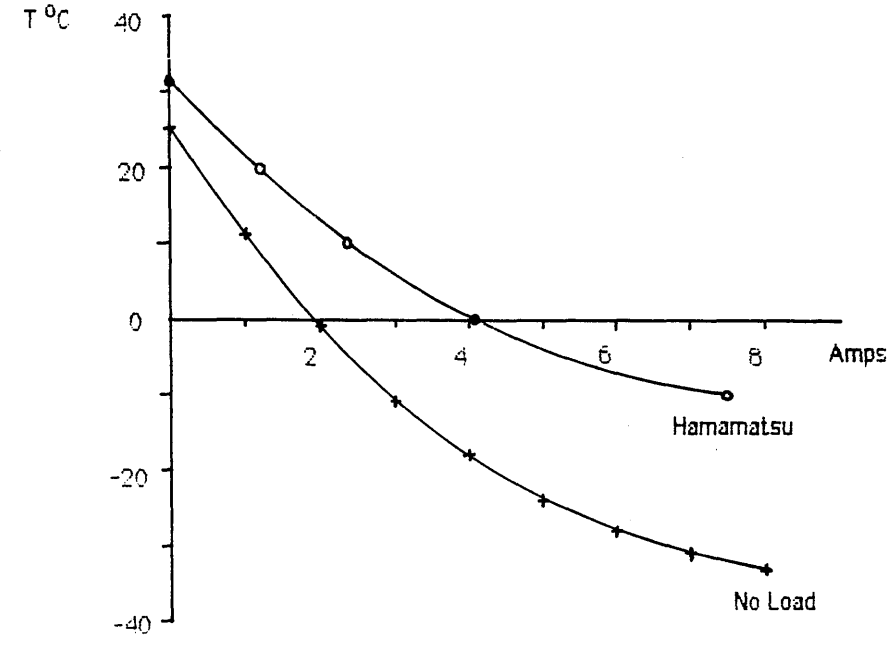

Figure 6.17b Temperature Stability of Cooling System I = 6 Amps

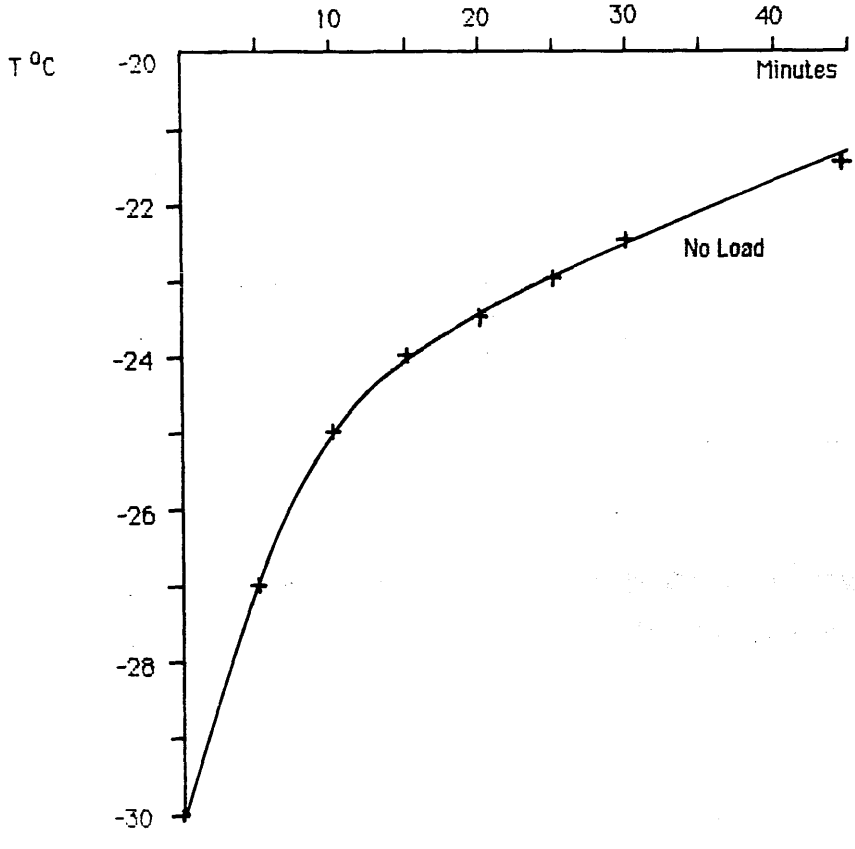

load. In this case the temperature range ΔT is reduced to ~ 40°C, mostly because the copper heatsink does not dissipate the excess heat efficiently enough. With more efficient heatsinking ΔT could be made larger, and lower operating temperatures could be maintained.

The temperature stability was examined and the results for no heatload are given in figure 6.17b. Initially the Peltier current was fixed at 6A, giving a cold surface temperature of -30°C. This temperature tends to increase with time as the heat removed from the cold surface is transferred to the copper flange, causing the hot surface temperature of the cooler to rise. The flange gradually heats up until some equilibrium point is reached, when the heat extracted from the cold surface is just balanced by the heat dissipated from the flange. In an attempt to measure the time constant of this thermal drift the temperature was monitored (for a fixed Peltier Current of 6A) every 5 minutes up to 30 minutes, and then again at 45 minutes. After ~ 10 minutes, the change in temperature with time becomes roughly linear, with a gradient of ~ 0.08°C/min. As can be seen from figure 6.17b the temperature was still rising at this rate after 45 minutes, indicating the presence of a very long equilibrium time constant, or possibly an external effect such as room heating. In comparison the longest integration time used in these experiments was 10 secs, so that this level of temperature stability was acceptable. Again, better heatsinking would decrease the drift rate.

6.7 OPERATION OF THE PHOTODIODE ARRAYS IN VACUUM

In order to operate the photodiode arrays in the vacuum system certain electrical modifications had to be made. As the Hamamatsu driver-amplifier board fitted inside the vacuum chamber, the only difference here was the increased separation of the C2335 and C2325 boards. On the other hand, the Reticon RL 128S array had to be completely removed from the RC 1024 SA evaluation board, and placed on a specially constructed preamplifier board. The design of this board, and the effects of vacuum operation on both arrays are discussed in the following sections.

6.7.1 Operating the Reticon RL 128S array in vacuum

Operating the RL 128 S array away from the RC 1024 SA board is not an entirely straightforward task, due to the sensitive nature of the device and its drive electronics. Special attention must be paid to the effects imposed by the increased capacitance associated with lengthy cable connections, both analogue and digital. The diode array must be physically close to the video signal preamplifier for successful operation; it cannot simply be

removed from the board on extended signal leads. Reticon have recently introduced a new satellite preamplifier board for S series photodiode arrays, which measures 11.4 cm x 5.1cm, and comes complete with a mother board containing the drive electronics. Unfortunately this was not available to be tested at the time of these experiments.

The preamplifier board constructed to operate the diode array in the vacuum system measured 10.9 cm x 6.8 cm, and was made from copper strip board with a top surface ground plane. Input and output connections were made using the three D9 valve base connections. External to the vacuum system, the digital connections were made using low-capacitance ribbon cable, whilst the two video outputs (odd and even) were carried by shielded coaxial cable to reduce noise pickup. The 40 cm long signal cable terminates in a standard RS 25 pin D connector socket, which plugs into the box containing the RC 1024 SA board.

The circuit diagram for the preamp board is shown in figures 6.18, and is virtually identical to the preamplifier stage of the RC1024 SA circuit. Certain modifications to the Reticon circuit were necessary; the capacitive coupling for the odd-even clock adjust is provided by the proximity of two PC tracks on the RC 1024 SA board. This was replaced on the preamp board by the capacitive coupling obtained by twisting together two short lengths of insulated wire connected to the relevant circuit points. Another difficulty was that the capacitance of the coaxial cables carrying the video signals is 44pF to ground, as shown in figure 6.18. This acted as a potential divider, reducing the overall gain of the amplifier circuit. In order to restore the gain to the correct value, the gain of op-amps U21 and U28 was increased by replacing their feedback resistors with 5k variable resistors. It was also found that the last two diodes in the scan, 127 and 128, would only operate in a linear fashion if the EOS (odd) line was grounded, and the EOS (even) line was loaded with 560 ohms to ground.

Figures 6.19 a and b show two dark scans, the first obtained with the photodiode array on the RC 1024 SA board, and the second obtained with the array on the preamplifier board. The integration time for both scans was 0.32 secs; the average values differ because the operating temperature of the RC 1024 SA board was ~ 40 ^{o}C, whilst the preamp board ran at ~ 27 ^{o}C. Clearly, the fixed pattern is essentially unchanged, except for diode 1 which is discounted anyway.

In order to examine the noise performance of the two configurations the reproducibility of dark scans was investigated, as a function of integration time. Figures 6.20 a ,b are graphs showing the results in each case, after subtraction of two consecutive dark scans. The video

Figure 6.18 Circuit Diagram for Reticon Preamplifier Board

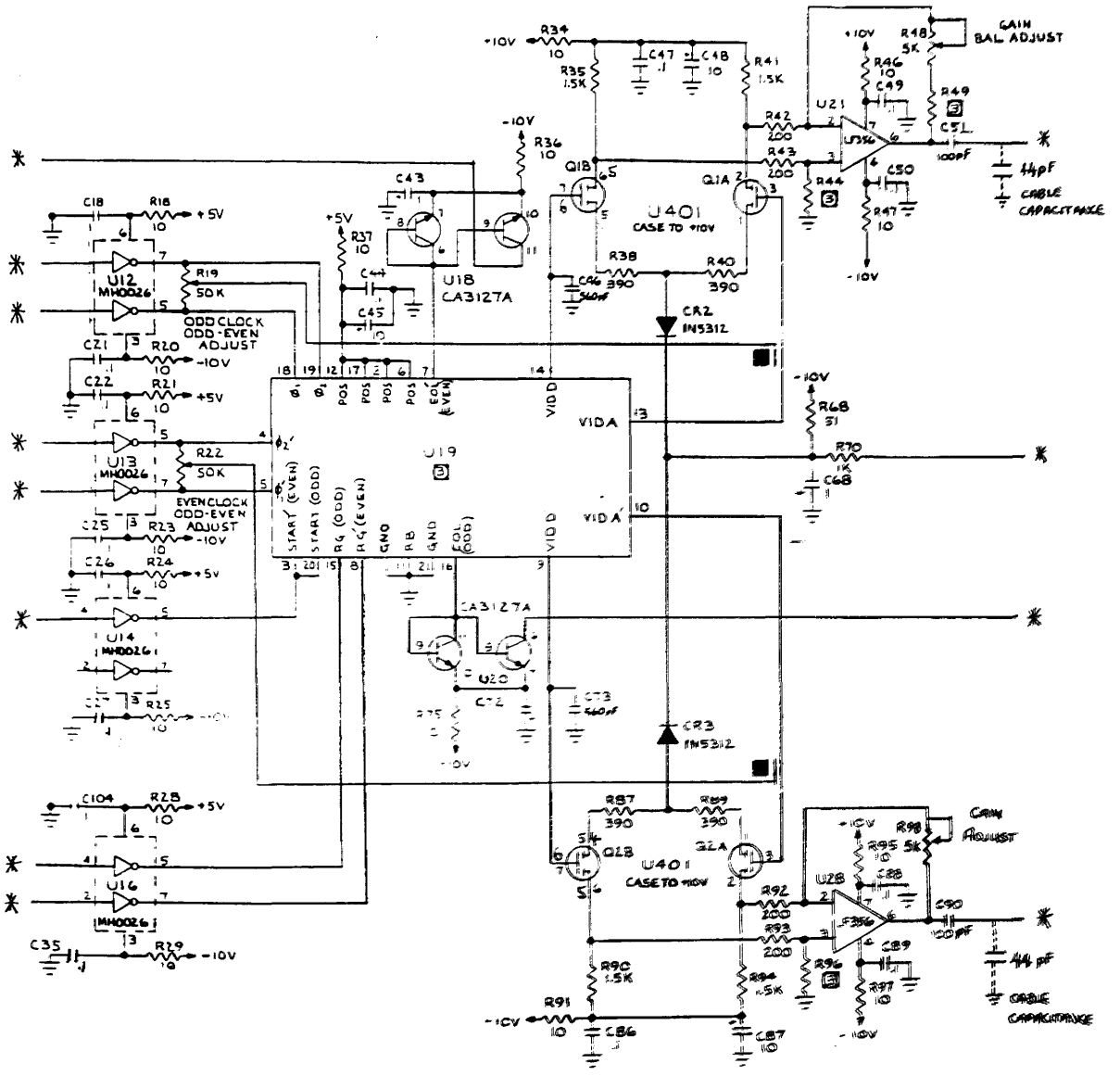

* - To Reticon RC1024 SA Evaluation Board

■ - Capacitive Coupling Provided By Short Twisted Wires

Figure 6.19a Reticon Dark Scan, Integration Time 0.32 sec, T= 40°C

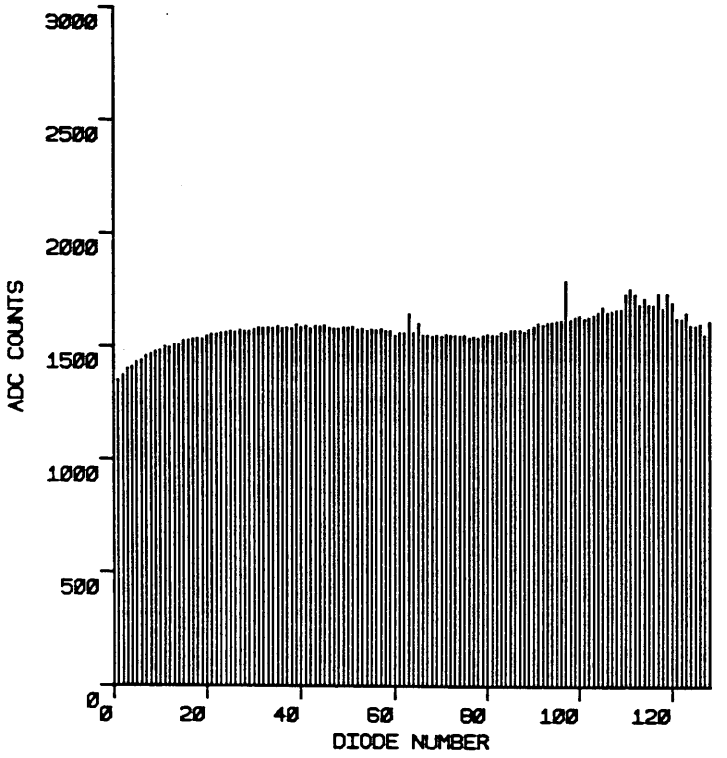

Reticon RL128S RC1024SA Board

Figure 6.19b Reticon Dark Scan, Integration Time 0.32 sec, T= 27°C

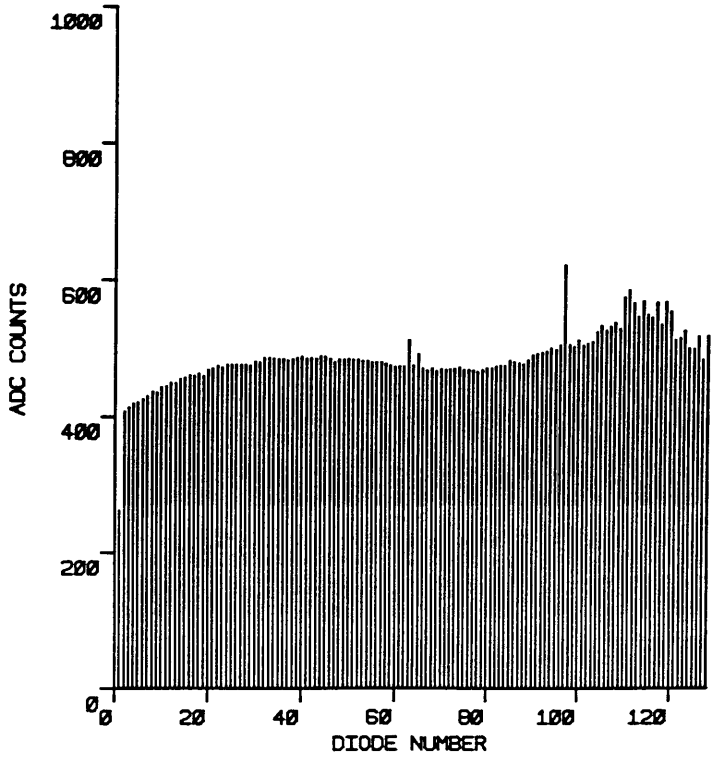

Reticon RL128S Preamp Board

Figure 6.20a Reproducibility of Dark Scans - Reticon RL128S

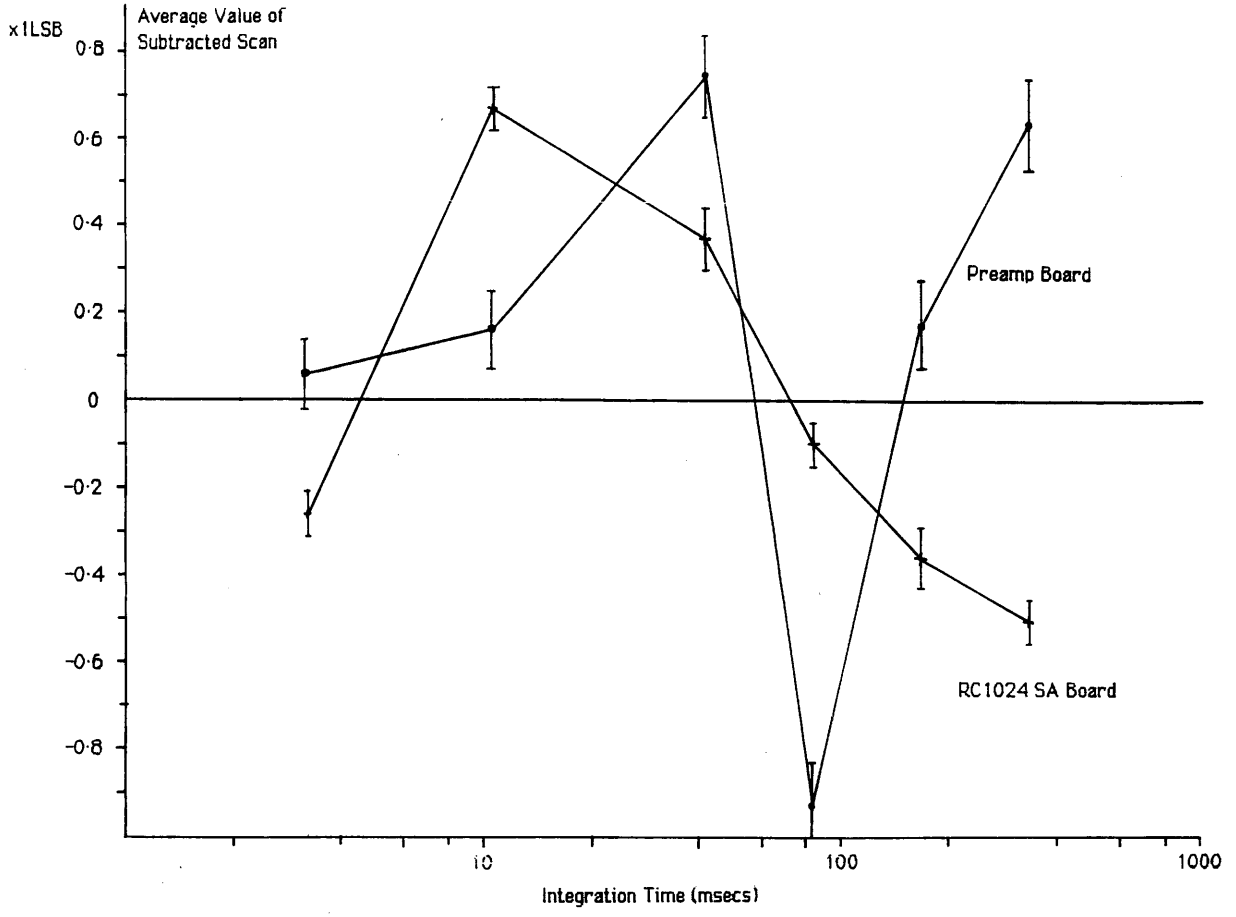

Figure 6.20b Noise Level In Subtracted Dark Scans - Reticon RL 128S

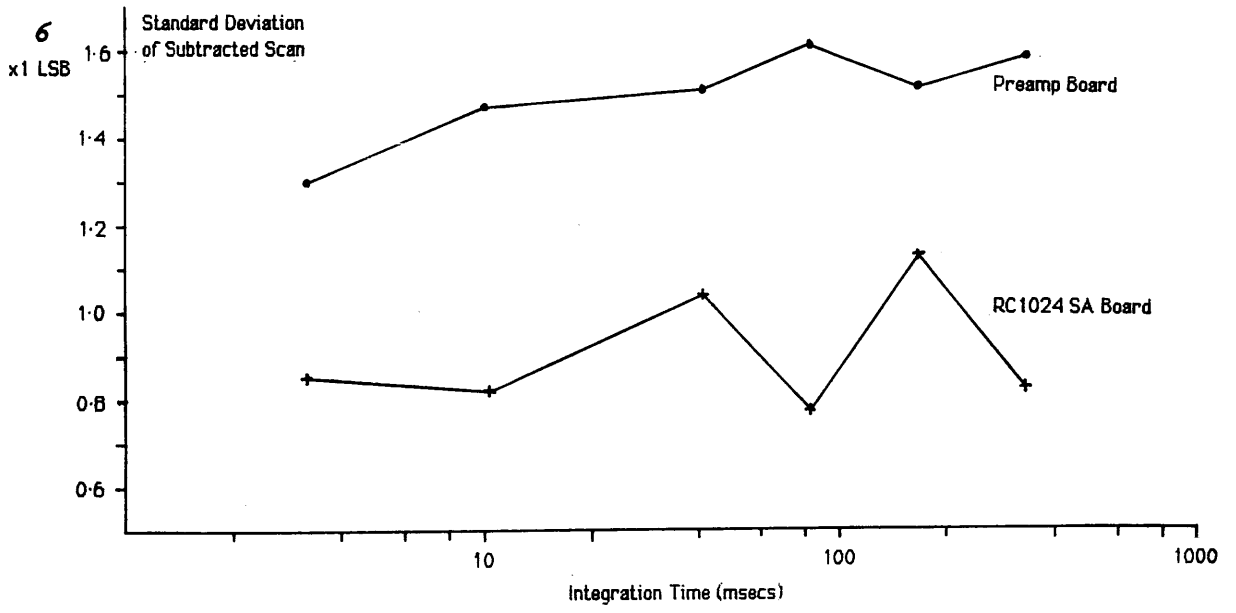

Figure 21a Reproducibility of Dark Scans - Hamamatsu S2304-512F

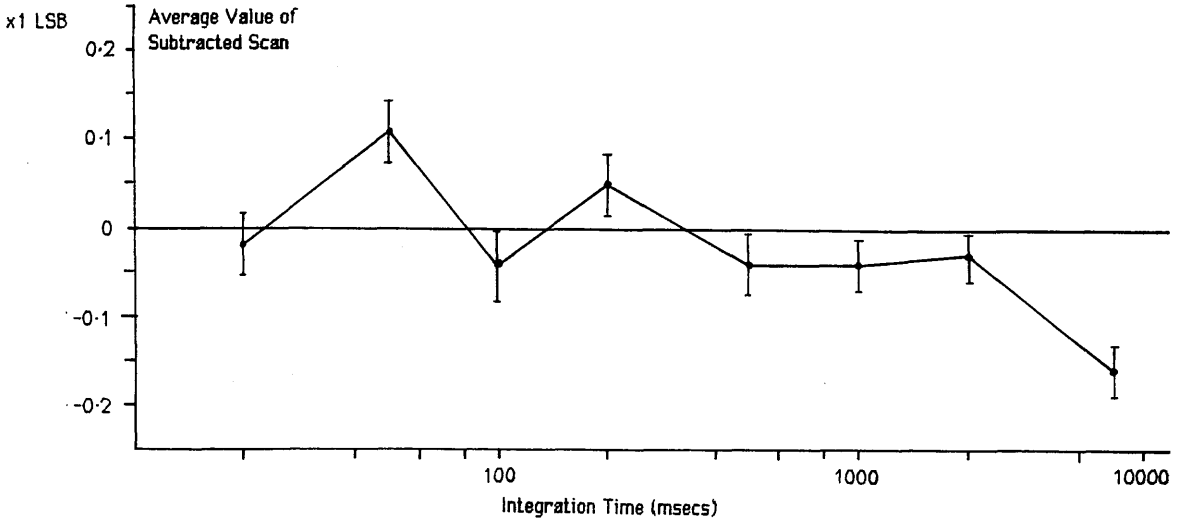

Figure 21b Noise Level In Subtracted Dark Scans - Hamamatsu S2304-512F

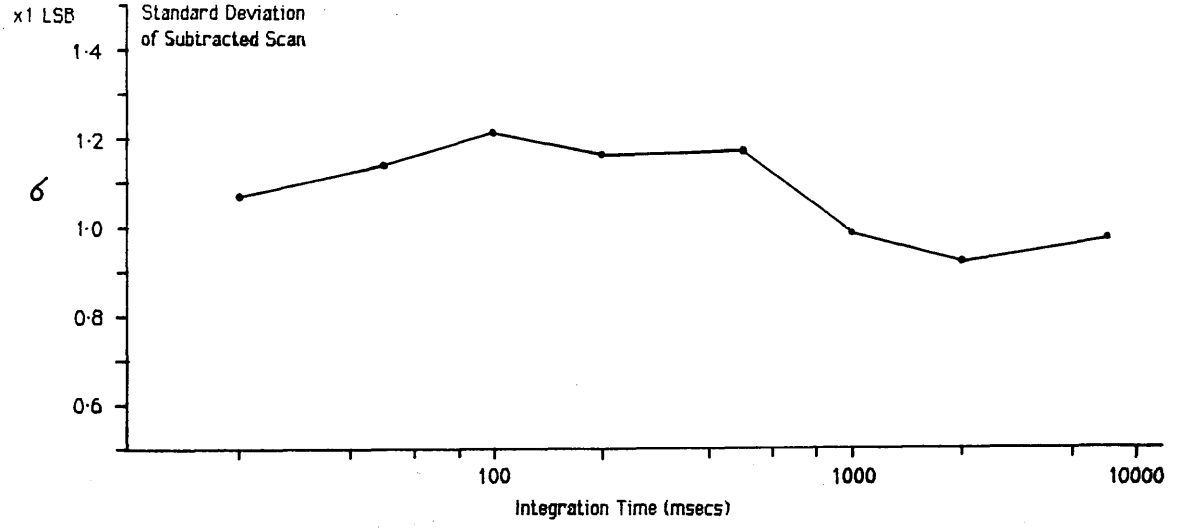

rate was 50 kHz. If the two consecutive scans were identical, the average value of the subtracted scan would be zero; any deviation from this value, greater than the inherent uncertainty introduced by the presence of readout and digitisation noise, indicates the presence of 'flicker' noise. The standard deviation about the mean of the subtracted scan gives some indication of the magnitude of other noise sources, such as the readout and digitisation noise mentioned above. Figure 6.20 a indicates that, not surprisingly, removing the diode from the RC 1024 SA evaluation board does increase the 'flicker' noise in the video signal. Figure 6.20b shows the standard deviation about the mean of the subtracted scans. Clearly the noise here has increased by almost a factor of two.

These results imply that removing the diode from the evaluation board degrades the electrical performance. Much of the increased noise seems to be picked up on the extended signal leads, as the video signal was very sensitive to movements of these connections. Indeed, setting up the preamplifier board correctly was almost impossible, as any movement of the cables connecting the preamp board to the RC 1024 SA board disturbed the fixed pattern shape of the scan. Further artefacts discovered in operating the Reticon arrays are discussed in chapter 7.

6.7.2 Operating the Hamamatsu S2304-512F array in vacuum

The fact that the C2325 driver/amplifier board was small enough to fit inside the vacuum chamber made this task relatively simple. Electrically, the only difference is that the signal connections between the C2325 and C2335 boards were lengthened. Figure 6.21 plots the average value of two consecutive dark scans after subtraction, with the array operating in the vacuum system at video rate of 50 kHz. As can be seen, this average is very much less than that for the Reticon array, showing that 'flicker' type noise is much reduced. The standard deviation is also slightly lower than that displayed by the Reticon array on the preamp board. From a practical point of view, the sensitivity of the Hamamatsu device to movements of the connecting cables was very much less than that for the Reticon array, and there was little difficulty involved in correctly setting up the C2325 board in the vacuum chamber. Further details concerning the operation of both arrays are given in chapter 7.

CHAPTER 7

Experiments on Photodiode Array Imaging Performance

Introduction

The previous chapter was concerned with the technical aspects involved in operating the Reticon and Hamamatsu photodiode arrays as detectors in the electron microscope. This chapter presents experimental results on the noise performance of these arrays, and the optical performance under indirect detection conditions. A brief review of the main sources of electrical noise generation in photodiode arrays is given, followed by experimental results obtained from series of dark scans, taken under various operating conditions. The response of the photodiodes to various levels of uniform illumination is reported, and the effectiveness of digital signal processing techniques is described. The performance of both types of array was slightly marred by artefacts in the video output signal, the importance and possible causes of these effects is also discussed.

7.1 DARK CURRENT AND NOISE SOURCES IN PHOTODIODES

This section gives a brief account of the sources of electrical noise generation characteristic to photodiode arrays in general, with specific reference to the Reticon and Hamamatsu devices of interest. The theoretical figures calculated are later compared with experimental values.

7.1.1 Dark current

All silicon photodiodes have a thermal leakage current which is independent of illumination and is a strong function of temperature. The specification for the Reticon S-series arrays is that the dark current i_d is $\leq$ 5pA at 25 ^{o}C, and halves for every 7^{o}C decrease in temperature. The corresponding figure for the Hamamatsu S2304 series arrays is less; i_d < 1pA at 25^{o}C. The integrated dark leakage current, at temperature T, from each diode can be expressed in terms of electrons as:

$$N_d = i_d(T)\tau / e \qquad (7.1)$$

where τ is the integration time and e is the electronic charge. For example, after a dark scan of one second at T=25 ^{o}C $N_d = 3.125 \times 10^7$ electrons for the Reticon S series, which is 36% of the saturation output ($Q_{sat} = 8.75 \times 10^7$ electrons). Of course, each individual diode element has a slightly different value of i_d, so that the resultant video scan will contain a

characteristic dark pattern superimposed upon the average signal. This dark pattern is constant for constant conditions and can be removed by subtraction (section 7.4). By cooling the device the magnitude of the dark signal can be reduced greatly, allowing longer integration times to be used.

7.1.2 Noise sources

The output signal from a photodiode array in the dark contains five components:

(1) The integrated dark leakage current N_d.
(2) Shot noise in the dark current n_d.
(3) Fixed pattern noise.
(4) Preamplifier noise n_a.
(5) Reset (thermodynamic) noise of the array diodes n_r.

Dark current noise n_d is caused by the shot noise in the dark current. Applying Poisson statistics to equation (7.1) it can be seen that:

$$n_d = (i_d(T)\,\tau / e)^{\frac{1}{2}} \qquad (7.2)$$

Applying this equation to the conditions used in section 7.1.1. gives a value for n_d of 5590 electrons for the Reticon array. This figure can be arbitrarily reduced by cooling the array.

Fixed pattern noise is a pixel output pattern in the dark which is the same from scan to scan under constant conditions. It is composed of the dark scan pattern mentioned previously and there are also effects dependent upon clock signal feedthrough, such as the odd/even variations between adjacent pixels described in the previous chapter. The essential consideration here is that fixed pattern noise can be removed by subtracting a dark scan from the scan containing the optical information of interest, and therefore does not directly affect the dynamic range.

Preamplifier noise is the electronic noise introduced to the signal by the video preamplifier and is obviously dependent upon the type of detection circuit used. Simpson [1979] gives an expression for amplifiers using an FET input :

$$n_a = (C/e)\left[4kTBR_c\right]^{\frac{1}{2}} \qquad (7.3)$$

where k = Boltzmanns constant, B = bandwidth, R_c = the channel resistance of the input FET, and C is the total capacitance at the input node including the video line capacitance C_v. Values of the order of $n_a \sim 1000$ electrons can be obtained with proper amplifier design [Talmi and Simpson 1980].

Reset noise or thermodynamic noise has basically two components - diode reset noise and video line reset noise. Of these diode reset noise is the most important, as it cannot be corrected by any form of signal processing and is relatively insensitive to temperature, so that it forms the ultimate limiting noise source in photodiode arrays [Walker et al. 1985]. Video line reset noise can be reduced by special signal processing known as correlated double sampling.

When the reset voltage is applied to each diode through the shift register switch S_n (see figure 7.1), Johnson noise in the switch resistance introduces an uncertainty in the actual value of the applied bias. An expression for this diode reset noise in terms of signal electrons is given by Simpson [1979] for the Reticon S series arrays as:

$$n_r = (1/e) [kT (2C_p + 2C_{vc})]^{\frac{1}{2}} \qquad (7.4)$$

where C_p is the pixel capacitance, and C_{vc} is the video line to clock line capacitance. At 25°C, n_r is ~ 1000 electrons rms for the Reticon arrays [Talmi and Simpson 1980]. An equivalent figure is not available for Hamamatsu devices, however as the diode capacitances are very similar (1.8pF against 2pF), n_r is likely to take a similar value. This figure is therefore the very best noise value which can be achieved with conventional photodiode arrays.

The video line reset noise occurs because the capacitance C_p of each photodiode is connected in parallel with the video line capacitance C_v, which can be very much larger for long arrays. From figure 7.1 it can be seen that this extra capacitance adds into equation (7.4) to increase the value of n_r. For example, C_v for the Hamamatsu S2304-512F array is 25pF, which increases the value of n_r at 25°C to ~2200 electrons. The Reticon RL128S array has C_v of only 3pF, because of the twin video line construction and smaller number of photodiode elements; in this case n_r is increased to ~1200 electrons. The video line reset noise can fortunately be reduced by using a correlated double sampling readout technique.

The operation of the correlated double sampling technique is as follows (see figure 7.1): initially assume that switches S_1 and S_0 are closed and S_2 is open so that diode 1 is biased to

Figure 7.1 Correlated Double Sampling

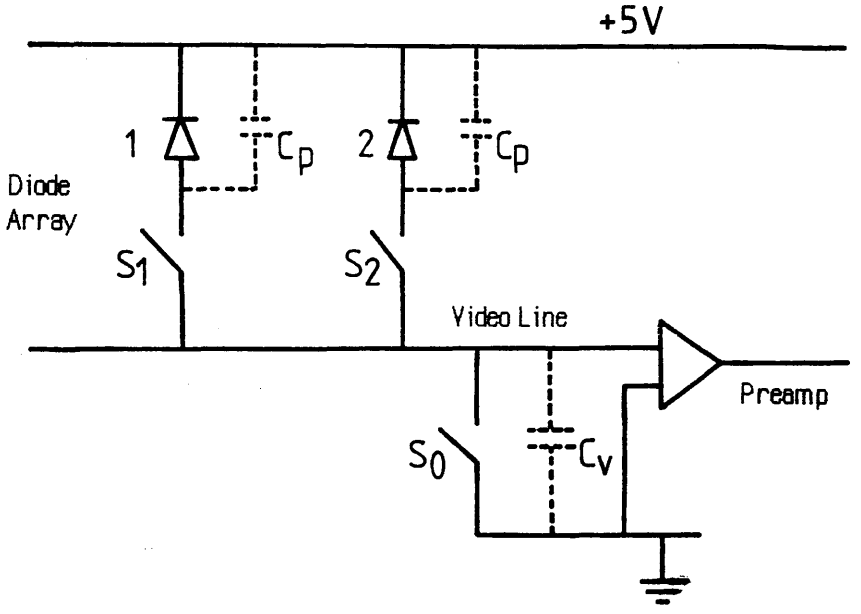

5v (+reset noise) while diode 2 is integrating; now switch S_0 is opened and the video line zero reference voltage v_0 is sampled; switch S_1 is then opened and S_2 closed, allowing the voltage V_2 on diode 2 to be sampled; closing S_2 causes diode 2 to be reset and the cycle repeats. The difference signal V_2-v_0 gives the video signal from diode 2 without any video line reset noise, since this is common to both samples. The main difficulty with correlated double sampling is that it cannot be successfully implemented at higher frequencies, hence the clock limitation on the RL1024 SA and C2325 boards.

7.1.3 Total readout noise and inherent dynamic range

The total readout noise can be expressed as the sum, in quadrature, of the individual noise components. Fixed pattern noise is ignored as this can be digitally removed from the signal.

$$n_t^2 = n_d^2 + n_r^2 + n_a^2 \qquad (7.5)$$

n_t increases with integration time τ, through equation (7.2), and is decreased with drop in temperature through equations (7.2) and (7.3). The inherent dynamic range of the array is defined as the maximum detectable signal divided by the minimum detectable signal. This can be expressed as [Egerton 1984]:

$$DR = \frac{S_{min}}{S_{max}} = \frac{Q_{sat} - i_d\tau}{e\, n_t F} \qquad (7.6)$$

where F represents the minimum signal/noise ratio acceptable in the output - often F is taken to be 5. It is possible to increase this inherent dynamic range by using a multiple scan technique [Egerton 1984], whereby each exposure time τ is divided into m periods and m separate readouts are digitally summed in memory. In this case the accumulated readout noise is:

$$n_t^2 = i_d\tau/e + m(n_r^2 + n_a^2) \qquad (7.7)$$

i.e. n_t increases by a factor slightly less than $\sqrt{m}$. However, the maximum recordable signal S_{max} increases by a factor of m, so that the overall dynamic range increases by a factor of at least $\sqrt{m}$. In practice the success of this technique can to be limited by any low frequency or flicker noise present in the video signal [Talmi and Simpson 1980] as described in section 7.2.2.

The theoretical noise value for a Reticon RL128S array at 25°C ignoring dark current noise but inclusive of video line reset noise is n_t ~1600 electrons, giving a theoretical inherent dynamic range of $5.5\text{x}10^4$ for F=1. The corresponding figure for the Hamamatsu S2304-512F array is n_t ~2400 electrons, or a dynamic range of $1.95\text{x}10^4$. Of course, these

figures are ideal and are unlikely to be achieved in practice due to the presence of noise sources external to the diode array.

7.2 DARK CURRENT AND NOISE EXPERIMENTS: RL128S array

The results of a series of dark scan experiments on two Reticon RL128S arrays are presented in this section. The dark scan response as a function of integration time and temperature is examined for each diode, and the results are compared with the theoretical values of the previous section. Some measure of the video noise level was obtained by examining the degree of reproducibility of these dark scans under identical conditions. The presence of two artefacts in the video signal is also reported, and the importance of the respective faults is considered.

7.2.1 Variation of dark current - Reticon RL128S array

Figures 7.2a and 7.2b illustrate dark scans for the two Reticon RL128S photodiodes under consideration, both operated on the external preamplifier board at a temperature of 27^{o}C. The integration time was 0.327 secs, which is the maximum available when using a 200kHz clock. As can be seen, the dark patterns are very different, with Reticon 1 having a much more uniform response than Reticon 2. The peak to peak non-uniformity in dark pattern (excluding diode 1) is 5.4% of the saturation output for Reticon 1, and 13.7% of saturation for Reticon 2. These figures are not constants however, as they vary with temperature and integration time. Using the average values for the dark signals of 491 ADC counts for Reticon 1, and 424 ADC counts for Reticon 2, it can be seen that both diodes would be completely saturated at this temperature in ~ 3 secs.

Equation (7.1) predicts that the average value of the dark signal should increase linearly with integration time. Figure 7.3 is a graph showing the average dark signal as a function of integration time for Reticon 1 on the RC1024 SA evaluation board, at a temperature of 44^{o}C. Clearly, for integration times longer than ~100 msecs the relationship is not linear. Figures 7.4a and 7.4b show similar graphs for Reticon 1 and Reticon 2 respectively, operating at various temperatures from -10^{o}C to +25^{o}C on the external preamplifier board. Again the dark current/integration time relationship becomes non-linear above 100msecs. The non-linearity becomes more pronounced as the temperature is decreased, until at a temperature of -10^{o}C, the integrated dark current actually appears to decrease with time, from 100 msecs onward.

Figure 7.2a Dark Signal τ=327msecs T=27^{0}C

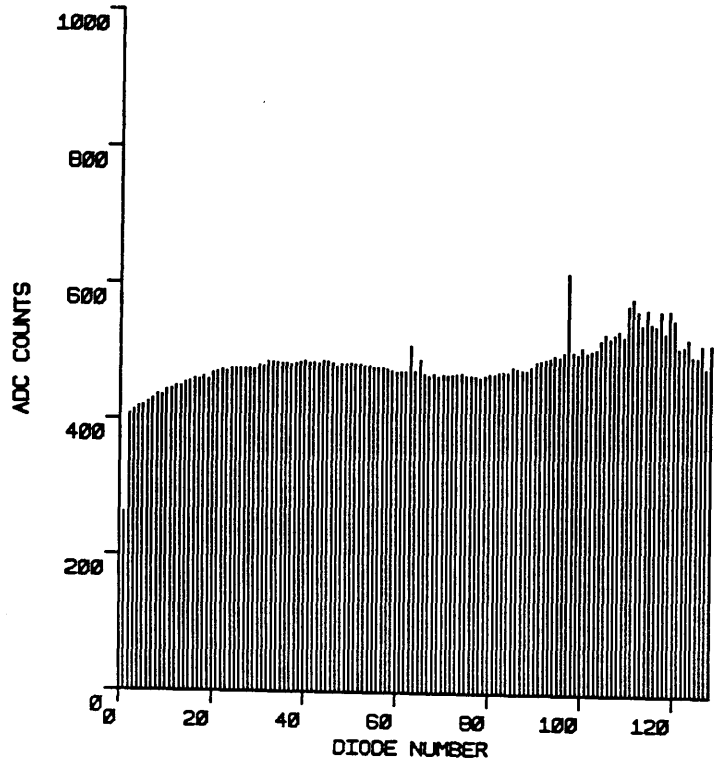

Reticon 1 on Preamp Board

Figure 7.2b Dark Signal τ=327msecs T=27^{0}C

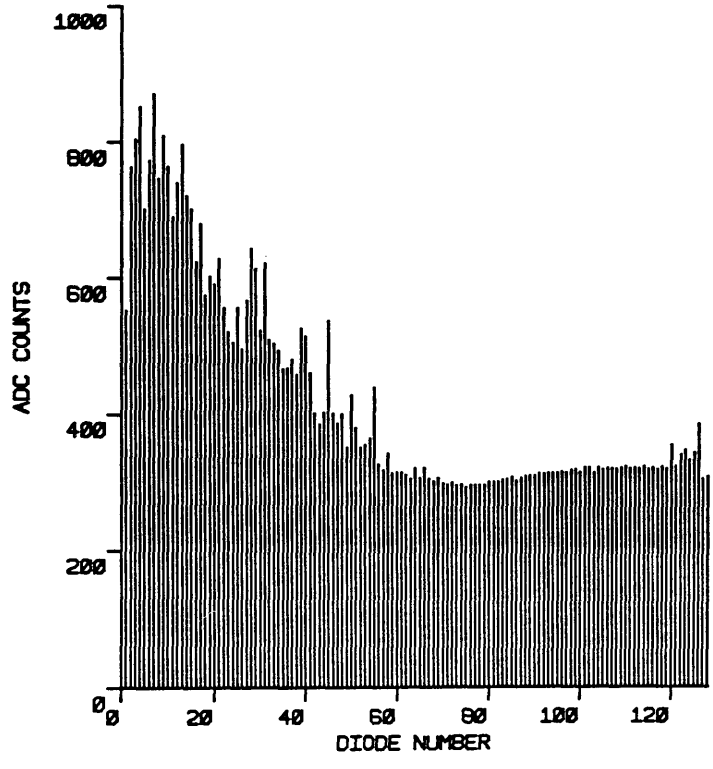

Reticon 2 on Preamp Board

Figure 7.3 Average Dark Signal v Integration Time Reticon 1 on RC1024 SA Board T=44°C

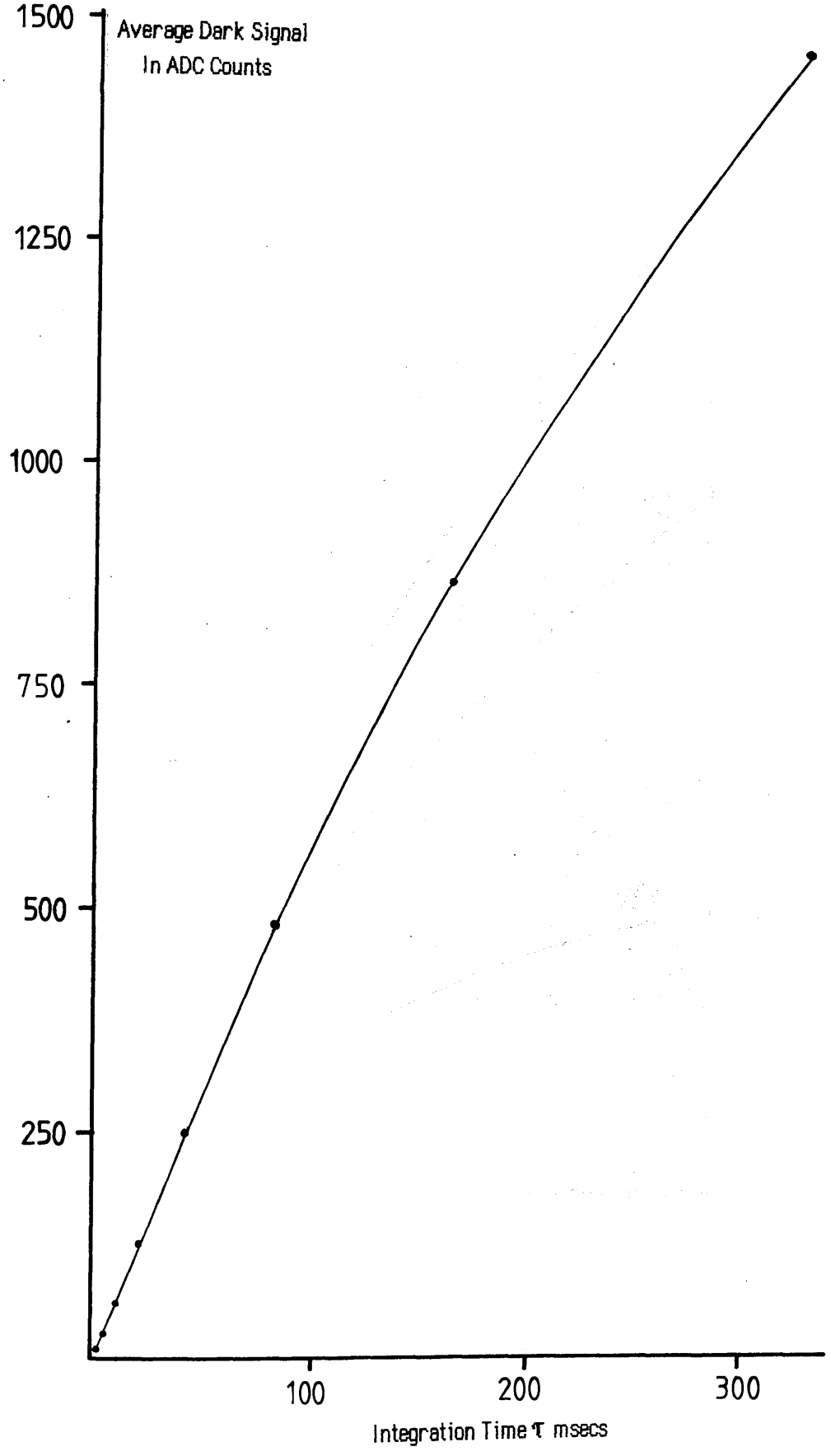

Figure 7.4a Average Dark Signal v Integration Time
Reticon 1 on Preamp Board

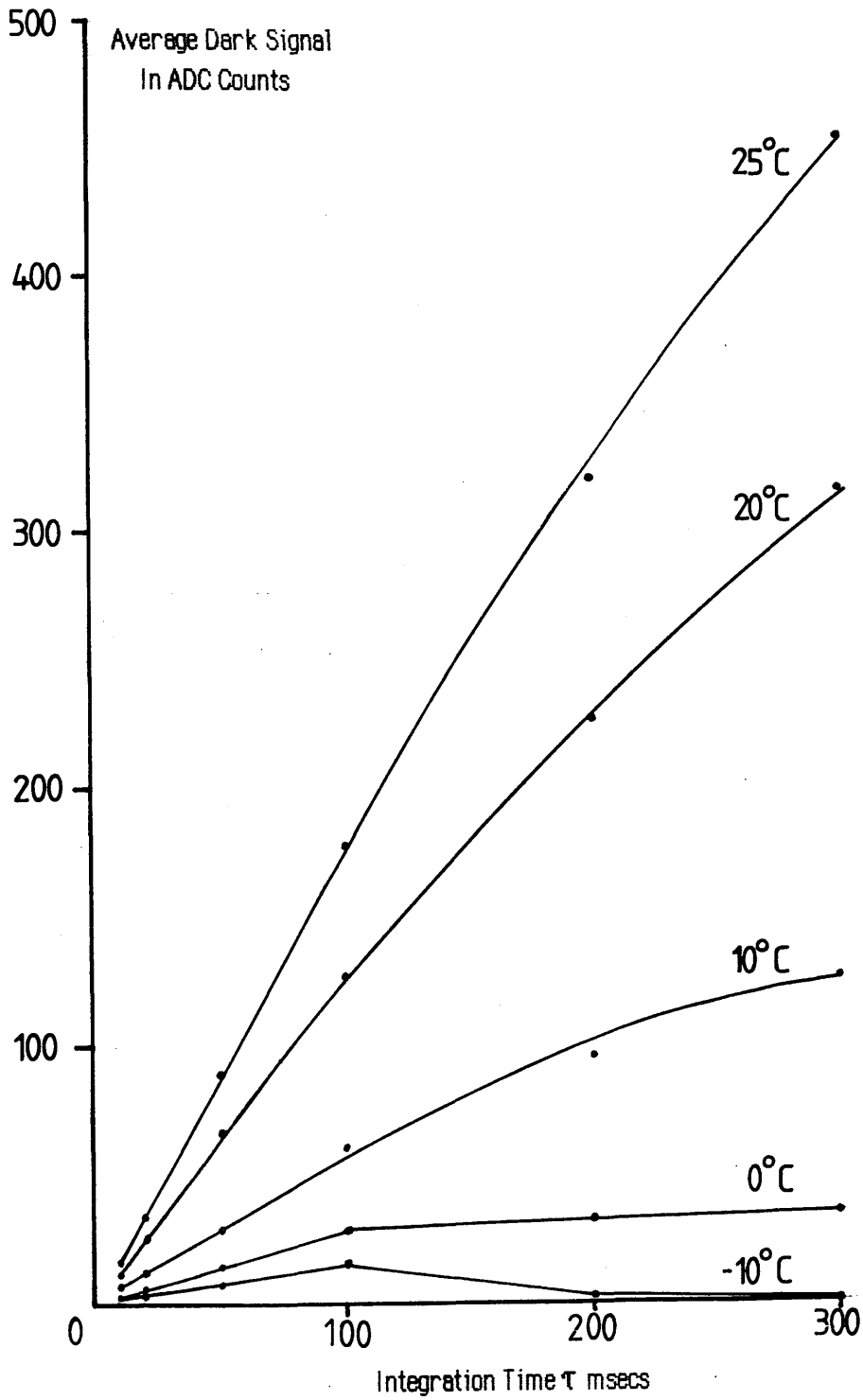

Figure 7.4b Average Dark Signal v Integration Time
Reticon 2 on Preamp Board

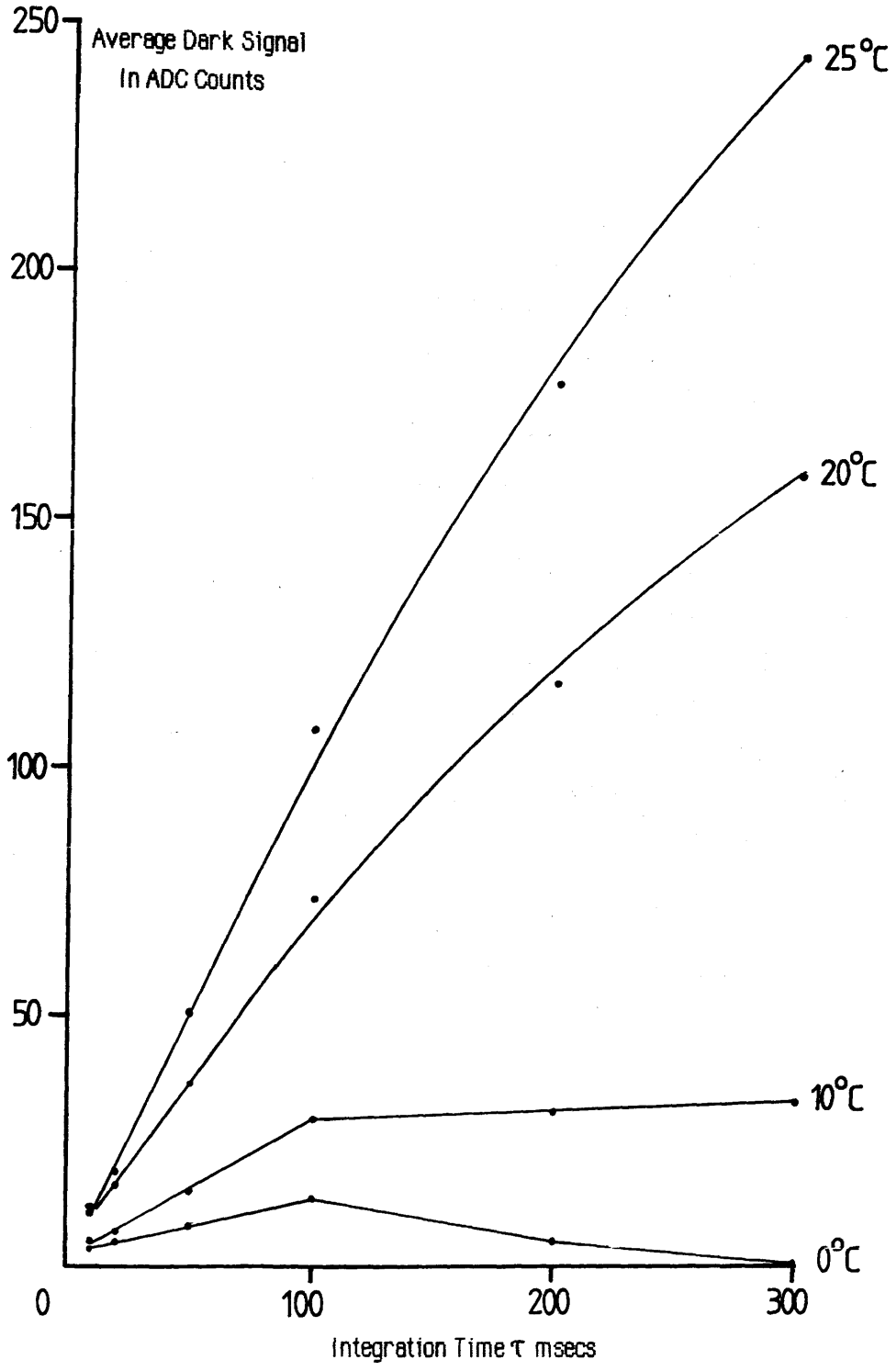

Clearly, this behaviour is incompatible with the expected relationship of equation (7.1). A closer examination of the waveforms revealed two possible causes of non-linearity. The first artefact discovered was a variation of the video signal retrace blank level with integration time. Figure 7.5a shows the dark scan of Reticon 2 at a temperature of -10^{o}C, with an integration time of 2.56 msecs. The 1-2-3-4 type fixed pattern noise is caused by the sensitivity of the diode alignment to movements of the electrical connections between the preamplifier board in the vacuum system, and the RC1024 SA evaluation board outside. External adjustment was not possible, as all the relevant potentiometer controls had to be located on the preamplifier board. Aside from this, the retrace blank level between the two scans is correctly set at zero volts. Figure 7.5b shows what happens when the integration time is increased to 50 msecs (T=20^{o}C), i.e. the retrace blank level drops to ~-6mV. This effect occured for both Reticons 1 and 2, and was independent of temperature. The retrace level remained constant up to 20 msec integration time, dropped to -6mV at this point, and varied between -4mV and -6mV at integration times above this. As this variation was repeatable from scan to scan, and occurred for both diodes, a fault on either the preamplifier board or the RC1024 SA board is suspected.

The magnitude of the D.C shifts from this effect are not enough to account for the non-linear behaviour of figures 7.4a and 7.4b. The strange results occurring at longer integration times may possibly be explained by the effect shown in figure 7.5 c. This shows sequential dark scans from Reticon 2, at a temperature of 10^{o}C and an integration time of 89 msecs. The negative signal is an artefact, which seems to breakthrough after ~80 msecs of integration. The magnitude of the breakthrough was independent of the diode examined or the operating temperature, and varied from ~-40 mV to ~-80mV as the integration time increased from 100 msecs to 327 msecs. The source of this signal could not be traced to any external influence, and the regular timing of the breakthrough suggests an internal electronic fault. Unfortunately, it was not possible to check the RC1024 SA board in isolation, as the effect was only discovered after the preamplifier section had been removed. However, the similarity in the shape of the dark response of figure 7.3 to those of figures 7.4a and 7.4b suggests that the fault was endemic to the evaluation board.

Figure 7.6 is a graph showing the average dark current i_d as a function of temperature for both the photodiodes. The values plotted were obtained using the gradients of the linear regions of figures 7.4a and 7.4b. As can be seen, the dark current for Reticon 1 is consistently higher than that of Reticon 2, by almost a factor of 2. The graphs show the exponential relationship of i_d with temperature, and indicate that the dark current is roughly

Figure 7.5a Reticon 2 (τ = 2.56 msecs)

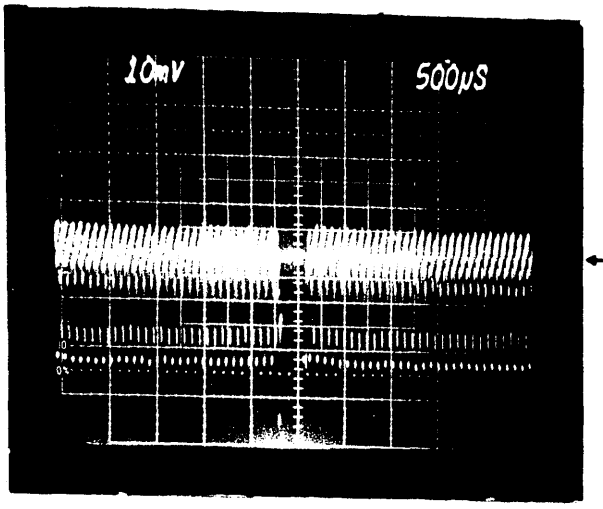

Figure 7.5b Reticon 2 (τ = 50 msecs)

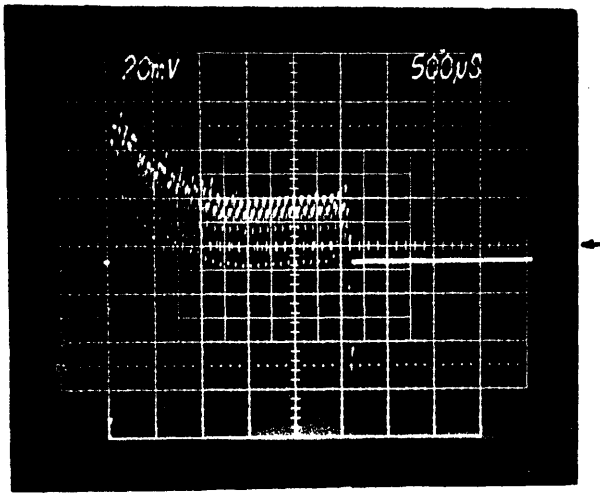

Figure 7.5c Reticon 2 (τ = 89 msecs)

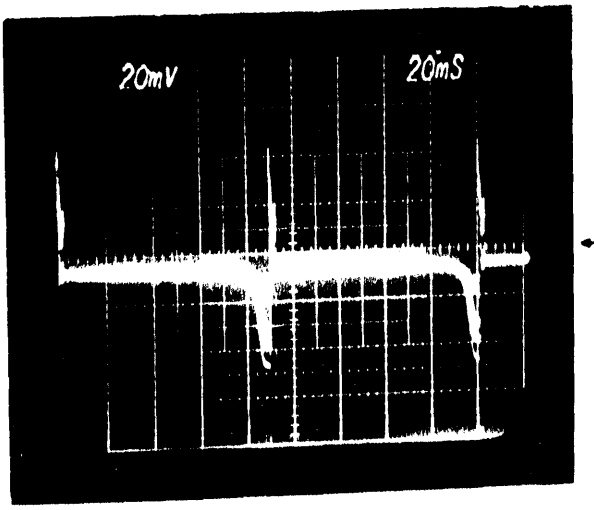

Figure 7.6 Average Dark Current v Temperature

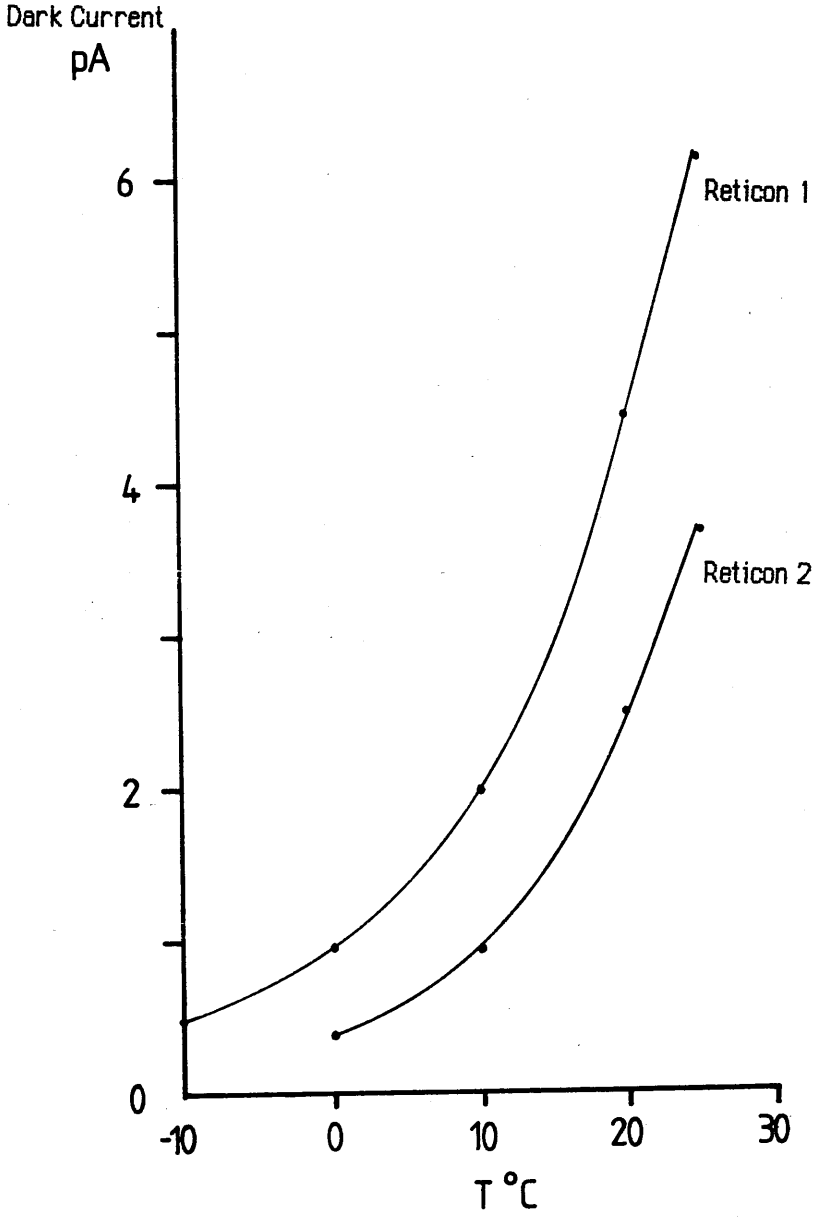

halved for every 9°C drop in temperature rather than the 7°C drop quoted by Reticon. Thus, at a temperature of 0°C the maximum integration time of Reticon 1 is increased to 15 secs, and that of Reticon 2 to 36 secs. Longer integration times than this can be obtained by further cooling.

7.2.2 Dark current noise - Reticon RL128S

Section 6.7.1 showed that the dark noise levels in the RL128S array were increased when the photodiode was transferred from the RC1024 SA board to the preamplifier board, in spite of the fact that the operating temperature was reduced by ~20°C. In this section the response of noise levels to variations in integration time and diode temperature is reported, using a similar dark scan subtraction technique.

Figure 7.7a shows the normalised distribution of ADC counts in a difference scan (subtraction of two consecutive dark scans), obtained using Reticon 1 on the RC1024 SA evaluation board at 40°C, with an integration time of 163 msec. As can be seen, the distribution is of a Gaussian form, with a mean value S of -0.35 LSB, and a standard deviation about this mean σ_1= 1.13 LSB, which can be compared to $\sigma < 0.5$ LSB for the amplifier/sample-hold/ADC system on its own (see section 6.5.4). Values of σ can be used to give some indication of the magnitude of readout noise present in the dark signals. Figures 7.7b and 7.7c plot the difference scan standard deviations σ_1 and σ_2 obtained from both Reticon photodiodes operating on the preamplifier board in vacuum, as a function of integration time. As can be seen, the performance of Reticon 1 is better than that of Reticon 2, with the magnitude of σ_1 typically 1.1 LSB, compared to σ_2 at typically 1.5 LSB.

There does not seem to be any clear relationship between the readout noise level and integration time, for either photodiode array, at any of the operating temperatures used, suggesting that the non-linear dark signals described previously are consistent from scan to scan, and that the signal artefacts do not introduce any significant extra noise to the video signal. No sensible data was obtained using Reticon 1 at -10°C for integration times longer than 100 msecs, as the signal artefacts reduced the average dark scan value to < 2 ADC counts, with most pixels giving a zero signal. Similarly, the limit for Reticon 2 was 100 msecs integration time at 0°C.

Some information about the presence of low frequency or flicker noise can be derived from an examination of the average value S of each difference scan. If there were no flicker noise, S would be zero, within an uncertainty ΔS introduced by the presence of readout noise.

Figure 7.7a Normalised Distribution Of Conversion Values In Difference Scan Reticon 1 on RC1024 SA board T=40°C, τ=163 msec

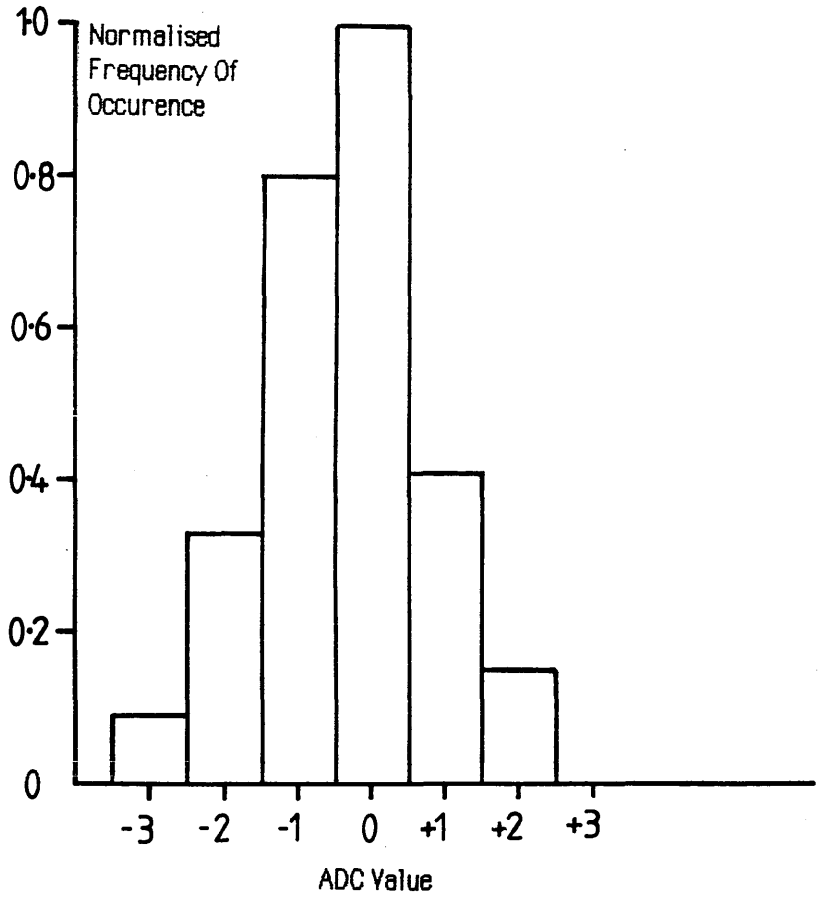

Figure 7.7b Standard Deviation in Difference Scans
Reticon 1 On Preamp Board

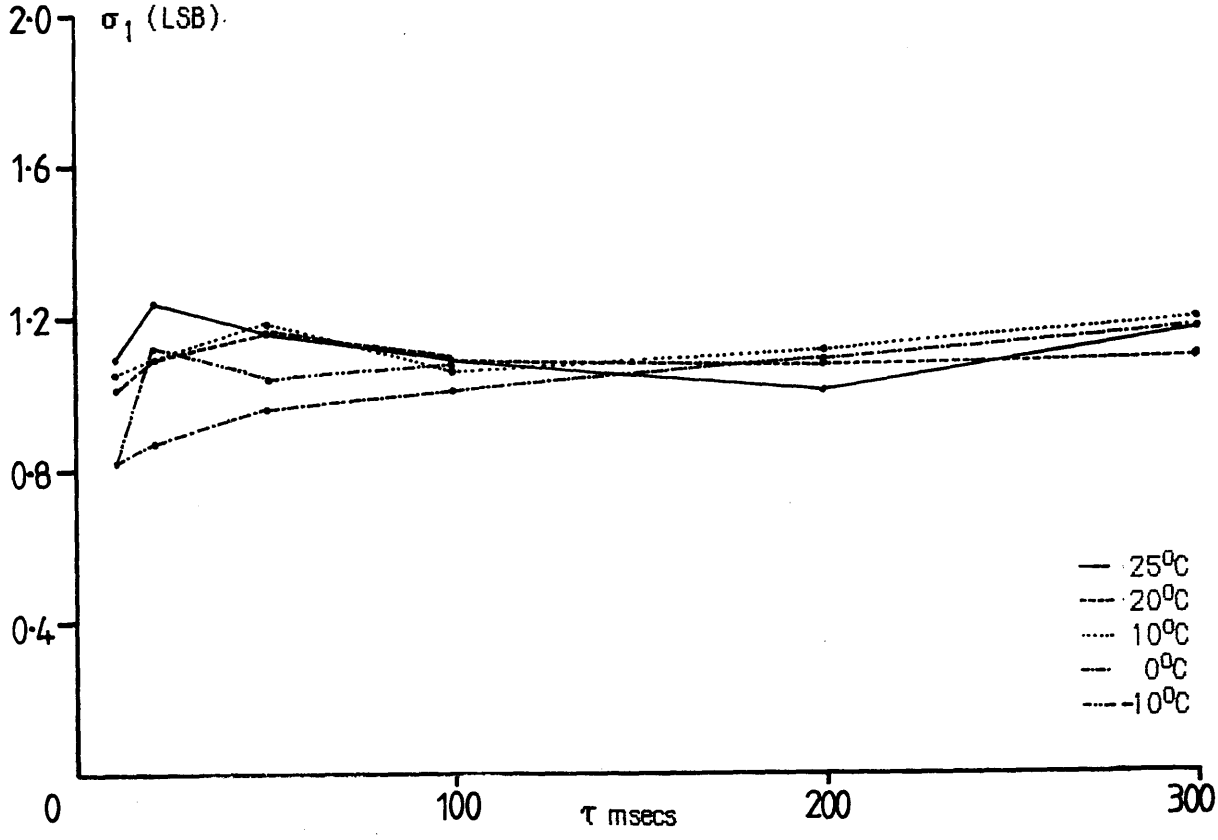

Figure 7.7c Standard Deviation in Difference Scans
Reticon 2 On Preamp Board

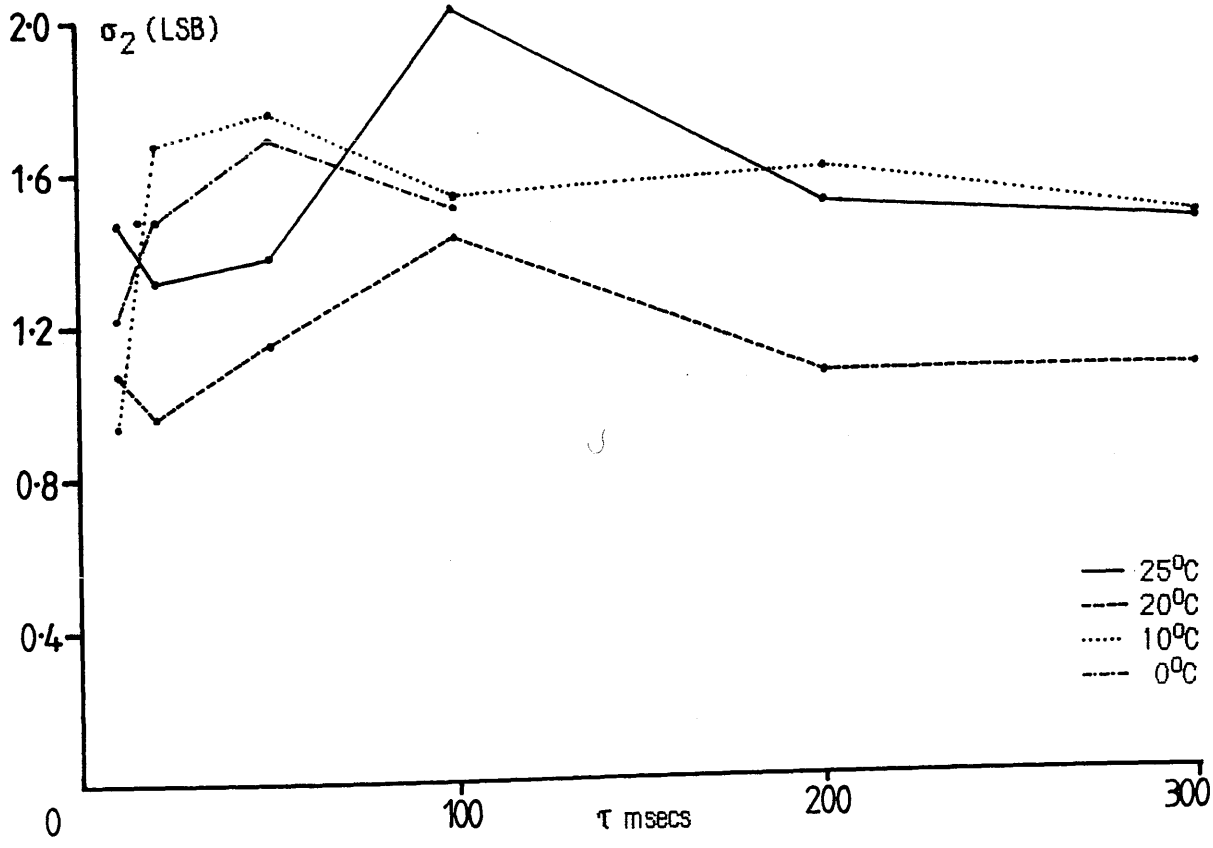

Figure 7.8a Mean Value S Of Difference Scans
Reticon 1 On Preamp Board

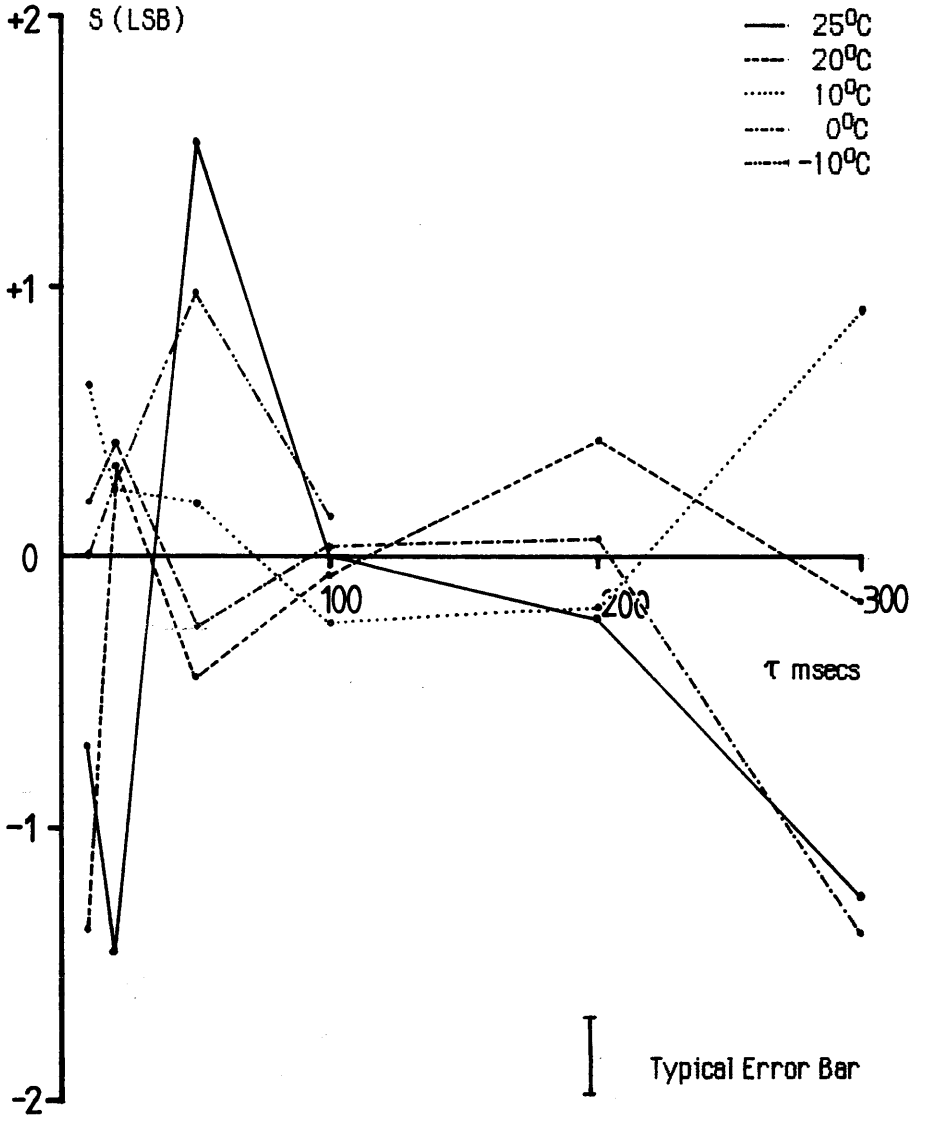

Figure 7.8b Mean Value S Of Difference Scans
Reticon 2 On Preamp Board

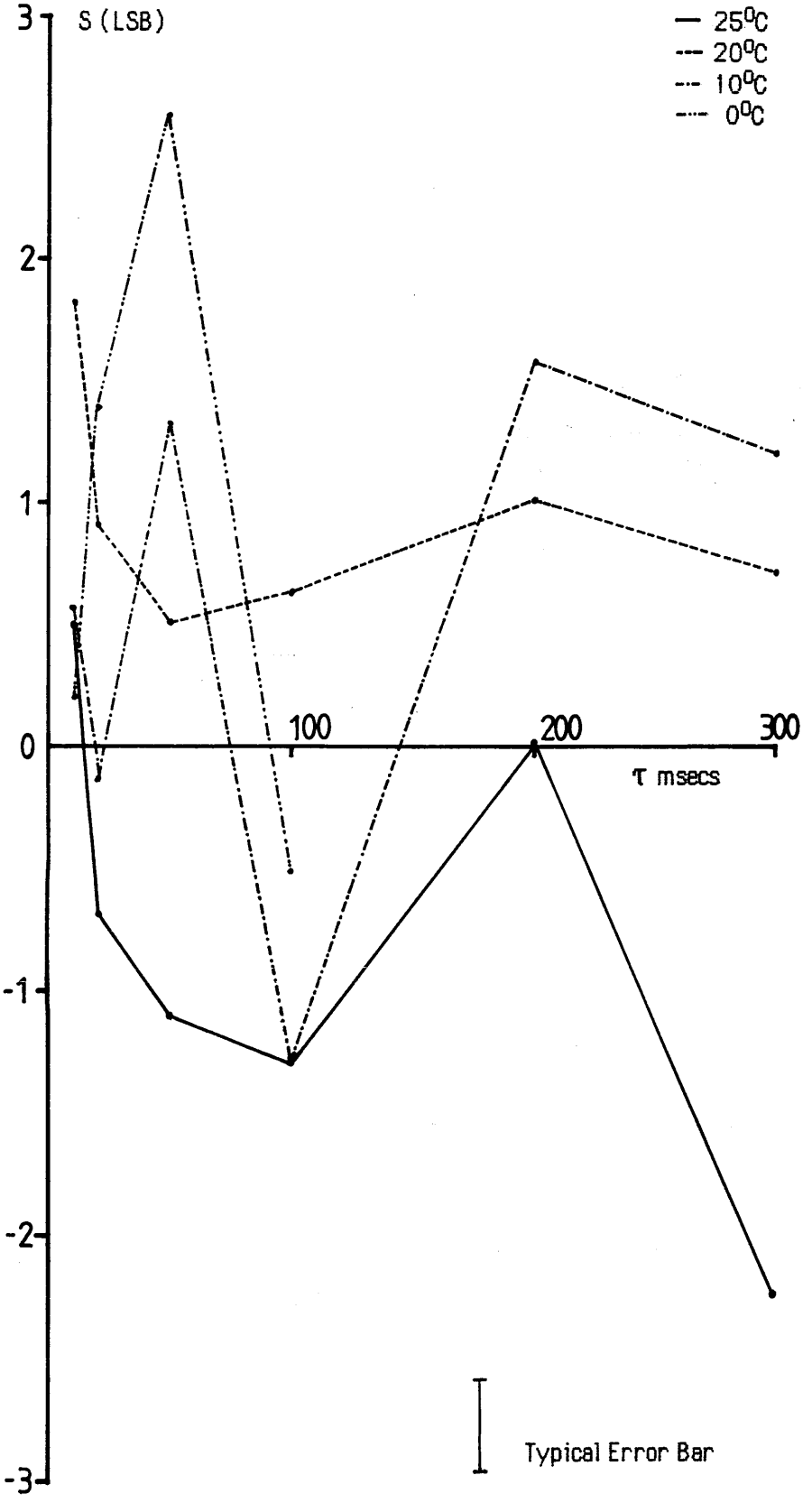

Non-zero values of S greater than this level indicate the presence of flicker noise. To find the statistical uncertainty in the averaged value of each difference scan, assume that the readout noise level is the same in each scan and is uncorrelated, and that distribution of noise is similar to figure 7.7a. Thus, the statistical error ΔS in the average value of each difference scan is $\sim \sqrt{2}\sigma_{av}/\sqrt{n}$, where n is the number of elements in the array, and σ_{av} is the average standard deviation of each dark scan. Using the typical values of $\sigma_1 \sim 1.1$LSB and $\sigma_2 \sim 1.5$ LSB from figures 7.7b and 7.7c gives $\Delta S_1 \sim \pm 0.14$ LSB, and $\Delta S_2 \sim \pm 0.19$ LSB for Reticon 1 and Reticon 2 respectively.

Figures 7.8a and 7.8b graph the corresponding mean values of each difference scan S, as a function of integration time. As can be seen, the magnitude of S extends well beyond the limits imposed by uncertainties ΔS_1 and ΔS_2 in each case, indicating the presence of flicker noise. The flicker noise on Reticon 1 lies in the range of $\sim \pm 1$ LSB, whilst that of Reticon 2 is $\sim \pm 1.5$ LSB. There is possibly a slight decrease in the flicker with decreasing temperature for Reticon 1, but the same effect is not obvious for Reticon 2. Again, no apparent connection between integration time and flicker noise can be deduced from either figure at any temperature. The implications of the above results are examined in section 7.4.

7.3 DARK CURRENT AND NOISE EXPERIMENTS : S2304-512F array

The experiments described in the previous sections were applied to the Hamamatsu S2304-512F array, and the results are presented below.

7.3.1 Variation of dark current : Hamamatsu S2304-512F

Figure 7.9a illustrates a dark scan obtained from the Hamamatsu S2304-512F array at 26°C, with an integration time of 2 secs. The peak to peak nonuniformity in the dark pattern is ~2% of the saturation output; very much better than that of the Reticon diodes. In the case of this array the dark current saturation time at 26°C is ~14 secs.

Figure 7.10 shows the average dark signal as a function of integration time, at various operating temperatures. In contrast to the Reticon arrays, the dark current is linear at longer integration times, and becomes non-linear as the integration time is decreased, particularly at lower temperatures. The reason for this behaviour is apparent upon examination of figures 7.9b and 7.9c. Figure 7.9b is a dark scan taken at 30°C with an integration time of 50 msecs, whilst figure 7.9c is a similar scan at -10°C, with an integration time of 5 secs. The

Figure 7.9a Hamamatsu S2304-512F Dark Scan τ=2secs

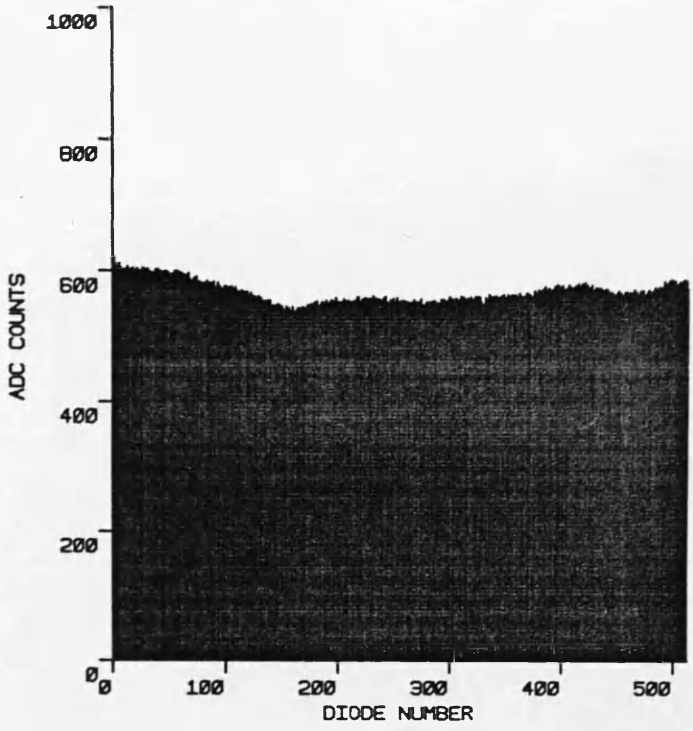

Hamamatsu Diode 26° C

Figure 7.9b Hamamatsu Dark Scan

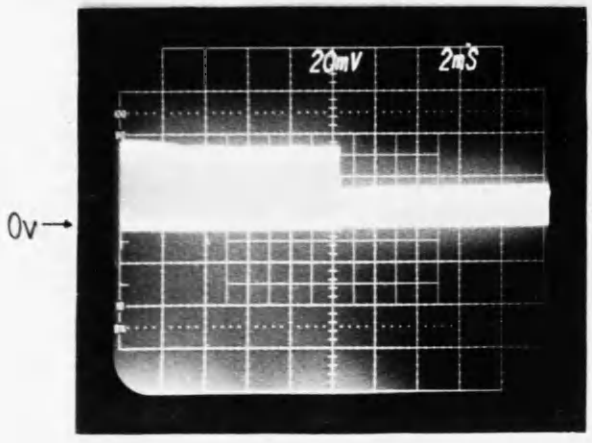

(τ=50msec, T= 30°C)

Figure 7.9c Hamamatsu Dark Scan

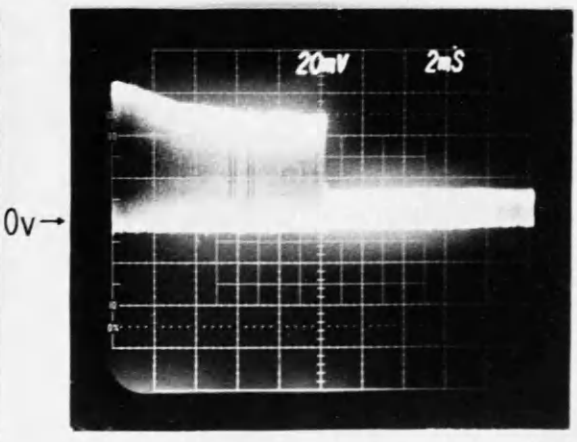

(τ= 5sec, T= -10°C)

Figure 7.10 Average Dark Signal v Integration Time
Hamamatsu S2304-512F

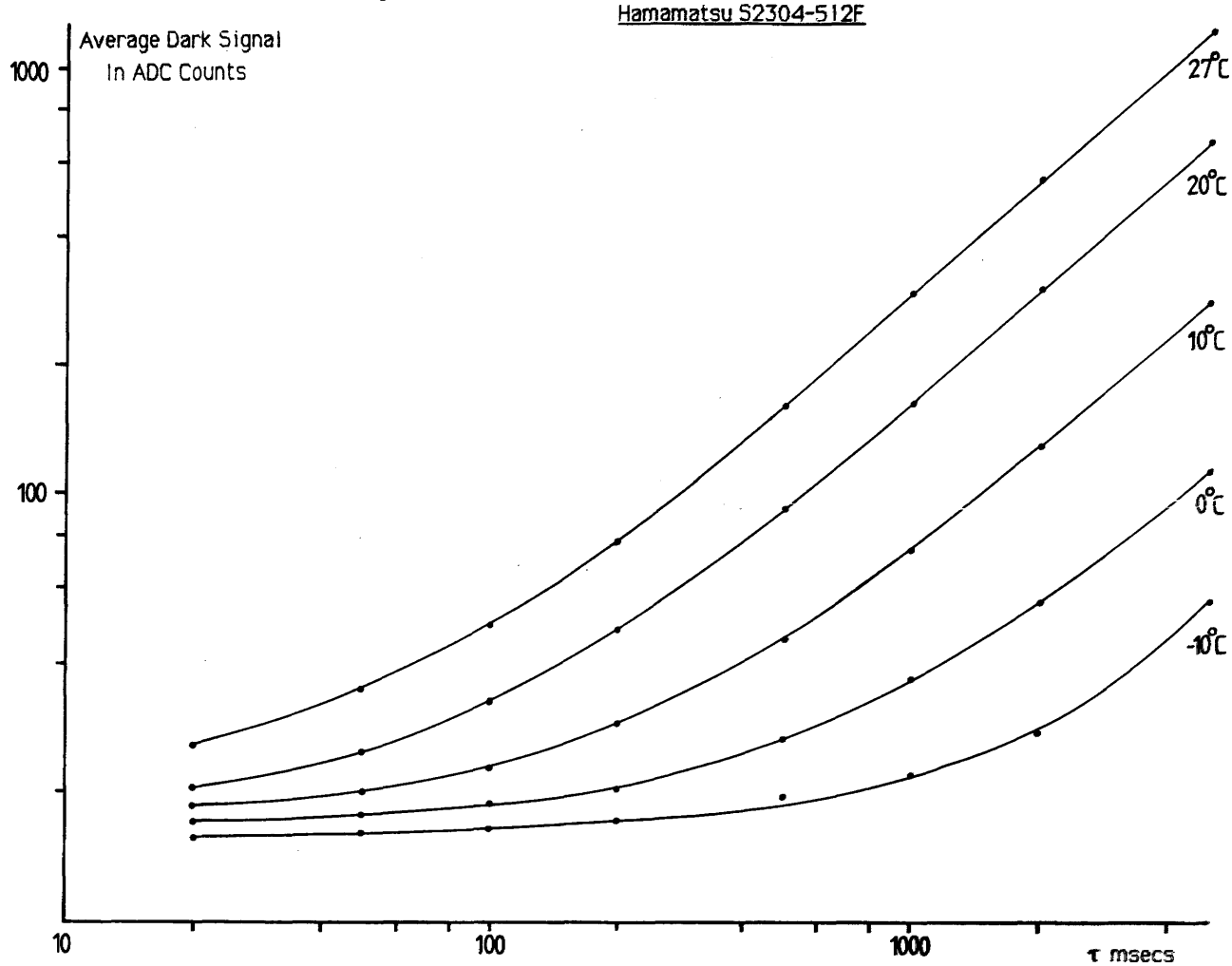

Figure 7.11 Average Dark Current v Temperature
Hamamatsu S2304-512F

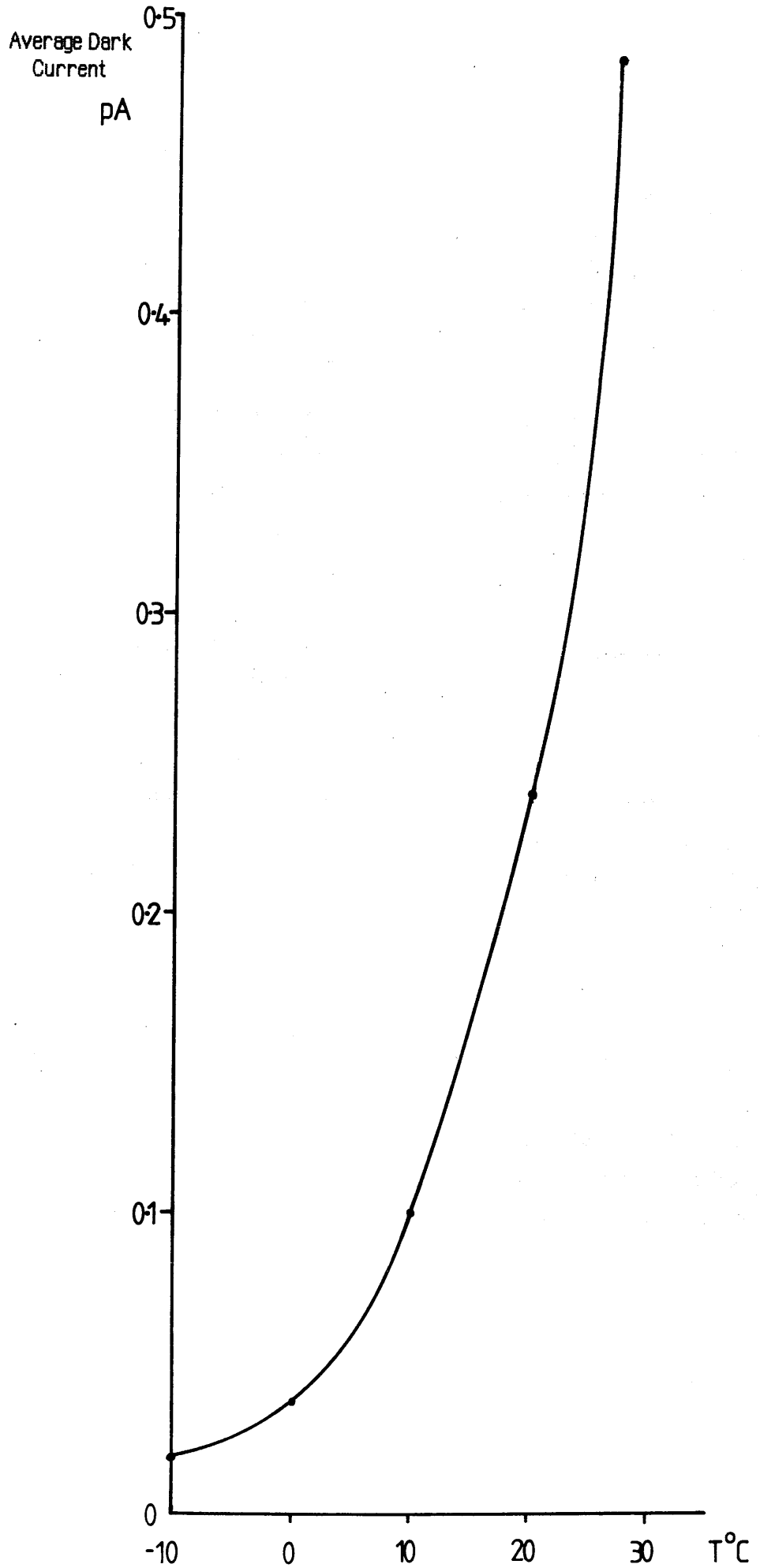

retrace blank level of both scans is not a d.c. signal as it should be, but contains an a.c. component of ~ 15mV at the same frequency as the video signal. This spurious signal must also be present in the video output, as no amount of cooling or reduction in integration time could reduce the video signal to below this level, hence the behaviour of figure 7.10. The artefact was found to be constant under all possible operating conditions, and could not be traced to any external source of interference. One possibility is that of crosstalk in the connector cable, from the digital leads onto the video line, but this could not be proved either way. As this signal varies with the same frequency and phase as the video signal itself, the only effect it has is to introduce an effectively constant d.c. offset to the output voltage.

Figure 7.11 shows the average dark current i_d as a function of temperature. The values plotted were obtained using the gradients of the linear regions of the curves of figure 7.10. When compared with the Reticon arrays, the dark current is almost an order of magnitude lower, so that at 0^oC the maximum integration time for this array is ~203 secs, compared with 36 secs for the best Reticon device.

7.3.2 Dark current noise : Hamamatsu S2304-512F

The technique of dark scan subtraction was used to obtain information on the noise levels in this array, as a function of temperature and integration time. Figure 7.12a shows the normalised distribution of ADC counts in a difference scan taken at 20^oC, with an integration time of 200 msecs. As in the case of the Reticon arrays, the distribution is Gaussian, with a mean value of -0.05 LSB, and a standard deviation about this mean σ = 1.18 LSB. Figure 7.12b shows σ values of difference scans taken at various operating temperatures, as a function of integration time. The range of σ lies between ~0.9 LSB and 1.3 LSB; again there is no clear connection between values of readout noise and temperature or integration time.

From figure 7.12b the average value of σ is ~ 1.1 LSB, which gives a value for ΔS of ~ $\pm$ 0.07 LSB. Figure 7.12c plots the average value S of each difference scan, as a function of integration time. It can be seen that S typically lies in the range $\pm$ 0.10 LSB, and at no time does S exceed $\pm$ 0.16 LSB, indicating that the flicker noise present is negligible. As before there does not seem to be any correlation between the magnitude of the flicker noise and temperature or integration time.

Figure 7.12a Normalised Distribution Of Conversion Values In Difference Scan

Hamamatsu S2304-512F T=20°C τ=200 msecs

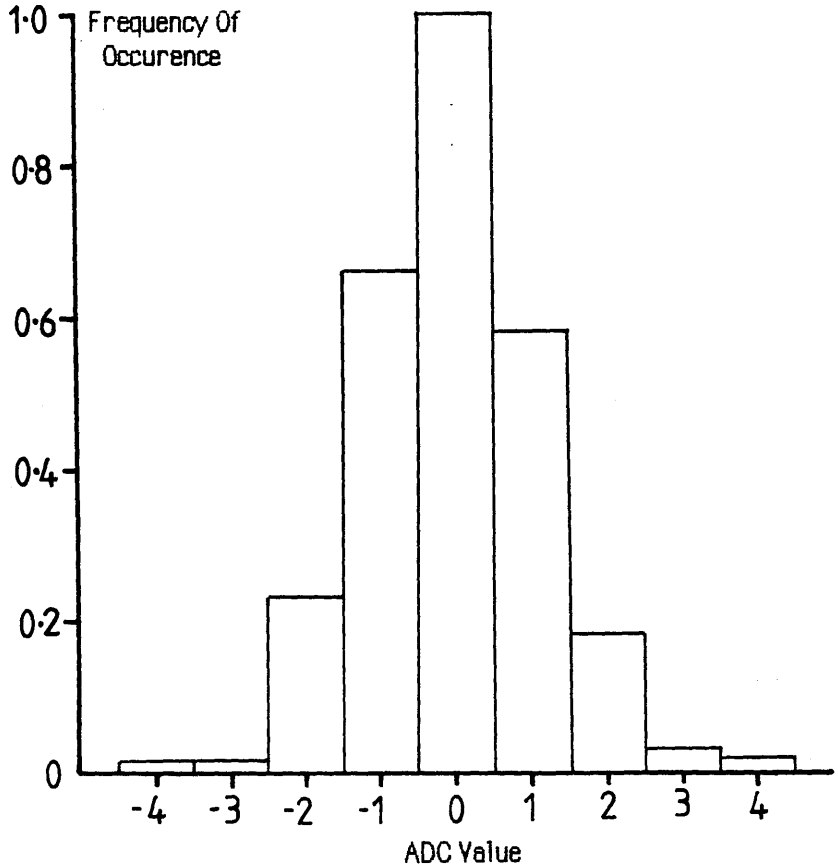

Figure 7.12b Standard Deviation In Difference Scans

Hamamatsu S2304-512F

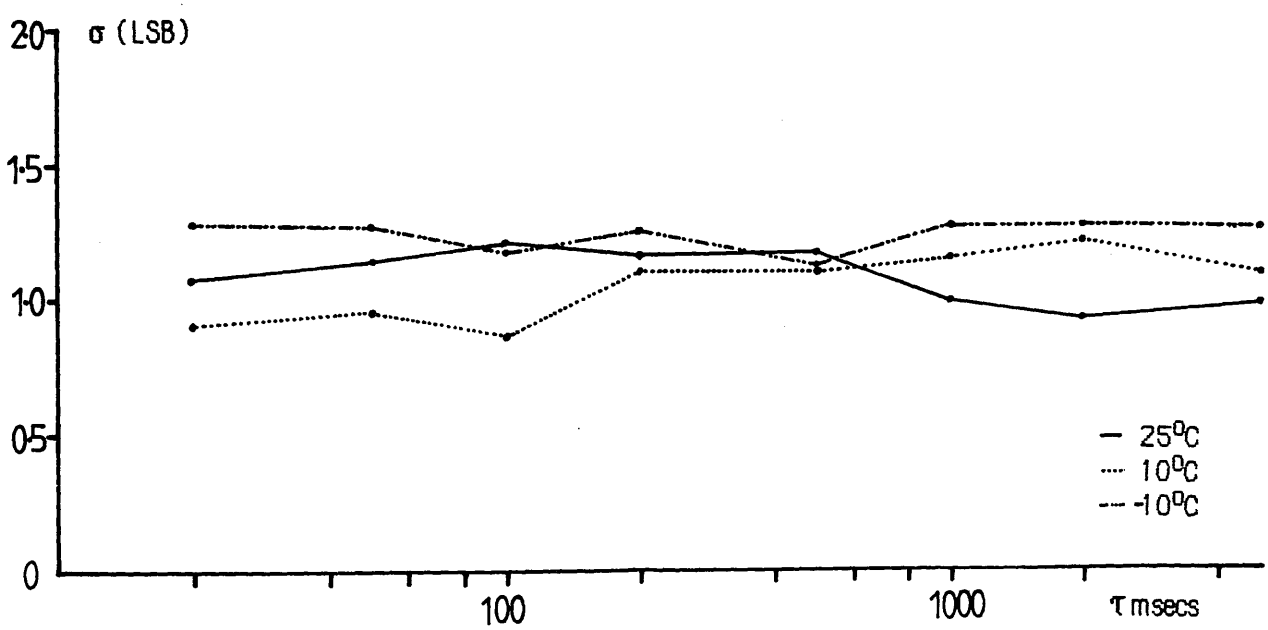

7.4 SUMMARY OF DARK SCAN EXPERIMENTS

The next few sections attempt to summarise the electrical performance of the Hamamatsu and Reticon arrays in the dark. No consideration is given to the signal artefacts mentioned previously, as these do not seem to introduce any extra noise into the system, merely causing a non-linear response of dark signal, which can be removed by subtraction of the appropriate dark scan from the scan containing the information of interest. It is important to realise however, that dark scan subtraction must be done under identical conditions of temperature and integration time, due to the non-linear response.

7.4.1 Dark current production and uniformity

A comparison of the average dark current values i_d, as a function of array temperature (figures 7.6 and 7.11) clearly demonstrates the superiority of the Hamamatsu device in this area, with a dark current production almost an order of magnitude lower than that of the Reticon arrays. Given the fact that the signal capacity of the Reticon photodiodes is approximately twice that of the Hamamatsu array, the maximum integration time that can be used, at a given temperature, is five times longer for the Hamamatsu device. An examination of figures 7.2a,b and 7.9a also reveals the much more uniform dark response of the Hamamatsu array. The non-uniformity in dark current is clearly less than for the Reticon arrays, especially Reticon 2. This, along with the lower dark current production, would tend to indicate that the fabrication processes are better controlled in the Hamamatsu device. The fact that two seemingly identical devices from Reticon show such differing dark patterns also tends to support this hypothesis.

7.4.2 Flicker noise

Turning to the question of noise performance, figures 7.8a and 7.8b show that the Reticon arrays suffer from flicker noise, particularly Reticon 2. This effect has been noted by Talmi and Simpson [1980], who suspected the cause to be flicker noise in the MOS-FET multiplex switches. Flicker noise does not limit the absolute dynamic range of the signal, but is detrimental to any form of digital signal processing:- for example procedures such as dark scan subtraction and digital response correction are subject to this uncertainty. Signal averaging (i.e. averaging the results of many identical scans) can help to improve the signal to noise range, but is obviously limited by the extent of the flicker noise.

Using the information of figures 7.8a and 7.8b, the flicker noise for Reticon 1 lies in a range of ~ ± 1 LSB, corresponding to ~ 21000 signal electrons. This limits the maximum dynamic

range of any (non-averaging) signal processing procedure to 4095 : 1. The flicker noise figure for Reticon 2 is ~ ±1.5 LSB, which corresponds to ~ 32000 signal electrons, giving a dynamic limit of 2731:1. Figure 7.12c shows that the Hamamatsu array has a very much better performance, and does not possess any detectable flicker noise.

7.4.3 Readout noise

The magnitude of other sources of random noise can be estimated from figures 7.7b,c and figure 7.12b. The readout noise levels of Reticon 1 and the Hamamatsu array are comparable at ~ ±1.1 LSB, corresponding to ~19000 signal electrons for the Reticon device and ~12100 signal electrons for the Hamamatsu device. Reticon 2 is again slightly worse at ~ ±1.5 LSB or ~32000 signal electrons. These figures limit the dynamic range of the Hamamatsu device to ~ 3722:1, and Reticon 1 and Reticon 2 to ~ 3722:1 and ~ 2731:1 respectively. The absence of any obvious relationship between these figures and operating temperature or integration time tends to suggest that most of the readout noise is composed of digitisation, reset, and preamplifier noise, plus an unknown contribution from electrical noise introduced external to the photodiodes. The Gaussian distribution of figures 7.7a and 7.12a implies that digitisation noise (± 1/2 LSB) is not the principle source of the random signal. Signal averaging should improve the signal to noise ratio of the Hamamatsu array, and a slight improvement may be possible for the Reticon arrays, subject to the flicker noise described previously.

7.5 OPTICAL RESPONSE OF PHOTODIODE ARRAYS

Having examined the electrical properties of the photodiode arrays in darkness, the next experiments involved evaluating their response to uniform illumination. Important factors such as linearity and uniformity of response as functions of temperature, integration time, and incident intensity are discussed below. The effectiveness of digital response correction procedures is also reported, while other factors such as resolution and detection efficiency are discussed in chapter 8. Measuring the direct response of photodiode arrays to varying illumination levels is difficult, principally due to the problems involved in quantifying the incident photon flux. For this reason the following experiments used an indirect measurement technique, using a scintillator to convert an incident electron distribution into a photon flux.

7.5.1 Description of experiments

The following experiments were carried out with the photodiode arrays in the vacuum chamber of figure 6.15, attached to the JEM 100C TEM. Uniform illumination was provided by electron irradiation of a 1mm thick slice of single crystal cerium doped yttrium aluminium garnet (YAG), whose properties are discussed more fully in chapter 8. The crystal was cut from a 20mm disk, and measured 9mm across by 20mm at its widest part as shown in figure 8.2. The YAG was glued onto the back of a 1mm thick aluminium shield using 'Loctite Glass Bond' UV sensitive adhesive. A rectangular slot measuring 17mm x 6mm had previously been cut in the shield allowing electrons to penetrate the scintillator. The edges of the slot were bevelled, and the whole top surface, including the YAG, was coated with ~ 500 Å of aluminium, to prevent charging. The entire assembly was mounted on the electronics board (see fig 6.15) above the photodiode array, in such a way that the height and position of the scintillator could be varied, relative to the photodiodes. The aluminium shield served to protect the electronic boards from electron irradiation, and was earthed to the vacuum chamber. Opening the camera shutter plate in the microscope viewing chamber allowed the passage of electrons through the camera chamber to the scintillator. By defocussing the electron beam (no specimen present) the illumination could be made uniform, and the intensity controlled by the degree of defocus introduced to the beam.

7.5.2 Beam current measurement - Faraday Cup

In order to give some measure of the electron beam current density in the viewing chamber, a Faraday cup was made. The cup consisted of a circular copper disk 19mm in diameter, with a 5mm diameter central hole allowing passage of the electrons into a copper cup 8mm deep and 15mm in diameter. The inside of the cup was painted with carbon dag, reducing the backscattering coefficient for 100keV electrons to ~ 6%, and the entire assembly was supported by a copper rod attached to a rotatable metal to glass seal so that it could be swung in and out of the beam. The top surface of the copper disk was coated with a layer of P47 phosphor, to enable easy location of the electron beam. A Keithley model 616 digital electrometer was used to monitor the current reading.

The Faraday cup could only give an accurate current reading for electron beam diameters less than 5mm, so that all the particles entered the cup. For defocussed illumination, the current reading (now a measure of the current density rather than the total current) was obviously a function of the position and angle of the cup relative to the beam, as well as the number of electrons intercepted by the supporting copper rod. In order to maintain a consistent sensitivity, the Faraday cup was placed in as near to possible an identical position for each

current measurement, by aligning its shadow image with marks on the viewing screen. The area of the copper support rod exposed to the beam was kept constant by defining a constant illuminated area using a selected area aperture. Tests showed that this procedure allowed consistent measurements of beam current densities with an repeatability of better than ± 5%.

7.6 OPTICAL RESPONSE : Reticon RL128S arrays

The following sections describe the response of the Reticon photodiode arrays to uniform illumination, provided by the single crystal YAG screen which was centred over the photosensitive elements and mounted approximately 1mm above the quartz window of the arrays. Figure 7.13 shows the saturation output of Reticon 2 under constant illumination. The maximum video voltage was initially set up outside the vacuum system to be 3V, but the saturation value was reduced to 2.8V (ie 3822 ADC counts) once the vacuum chamber was attached to the microscope, probably due to the sensitivity of diode alignment to movements of the external connector cables. The saturation output voltage was not sensitive to changes in operating temperature, integration time or readout rate and was the same for both Reticon 1 and Reticon 2. In principle, changing the gain of the op-amp input to the sample and hold amplifier should restore the full scale value although this was not done in practice.

7.6.1 Linearity of response - Reticon RL128S arrays

Figure 7.14 is a plot of the response of Reticon 1 to constant illumination as a function of integration time, at an operating temperature of $0^{o}C$. On the vertical axis is plotted the average value of each scan, after subtraction of the dark signal component. As expected the relationship is seen to be linear to within experimental error. This experiment was repeated at various temperatures between $+25^{o}C$ and $-10^{o}C$ with no effect on the results. The response of Reticon 2 under identical operating conditions was very similar and is not shown.

Figure 7.15a shows the relationship between the photodiode response and incident illumination level for Reticon 1 at an operating temperature of $0^{o}C$ and integration time of 50msec. Again the vertical axis plots the average value of each scan after subtraction of the dark signal component, while the horizontal axis is calibrated in terms of the beam current reading from the Faraday cup. This is not an absolute value as the beam was defocussed, however the main concern in this experiment was to measure the relative intensity of the illumination which is correct to within an error of ~± 5%. As can be seen from figure 7.15a the relationship is linear up to the maximum beam current which could be achieved while

Figure 7.13 Saturation Output Of Reticon RL128S

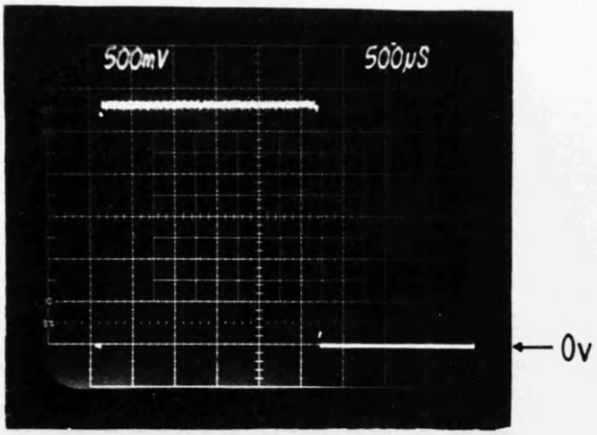

Figure 7.14 Response Of Reticon 1 To Constant Illumination As A Function Of Integration Time T=0°C

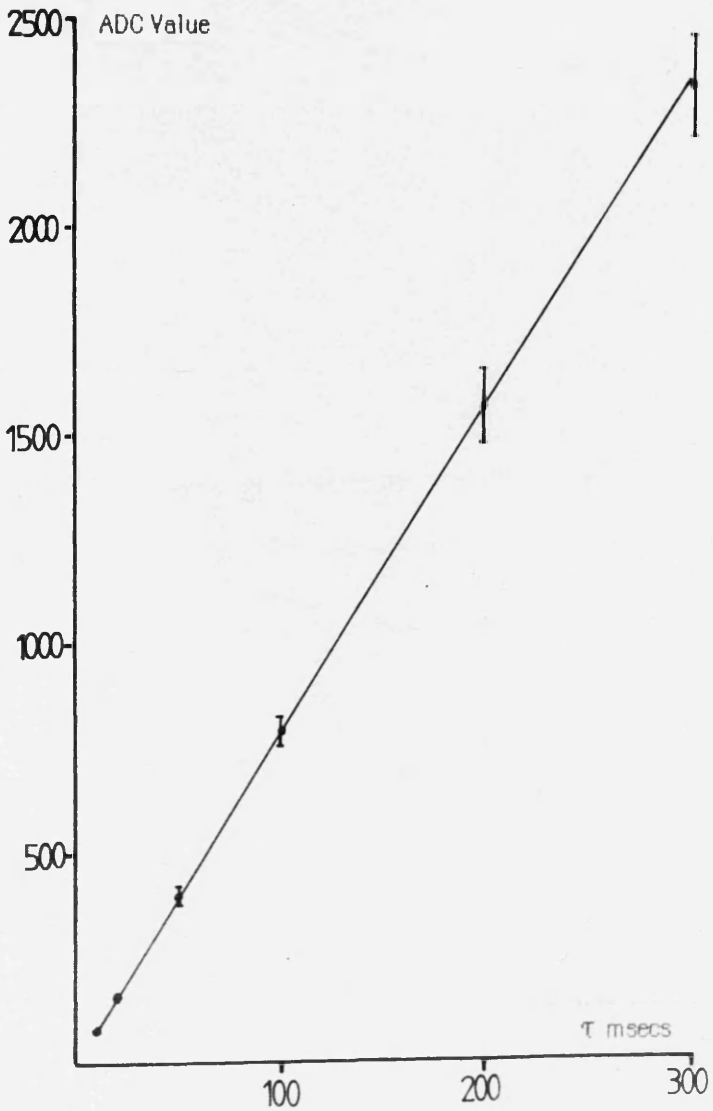

Figure 7.15a Response Of Reticon 1 To Varying Illumination Level
$T = 0^{o}C$ $\tau = 50$ msec

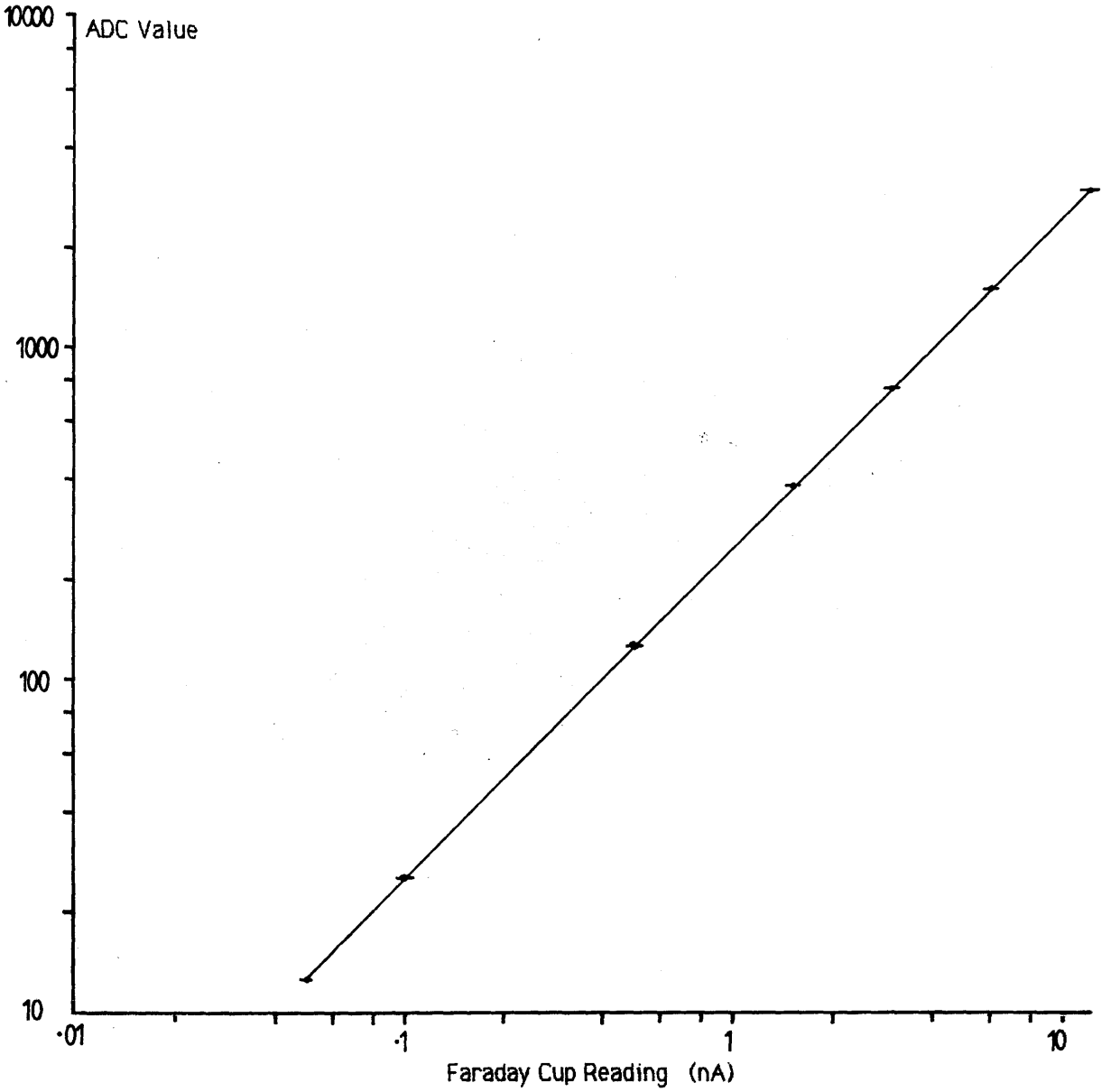

Figure 7.15b Response Of Reticon 2 To Varying Illumination Level
T = 0°C

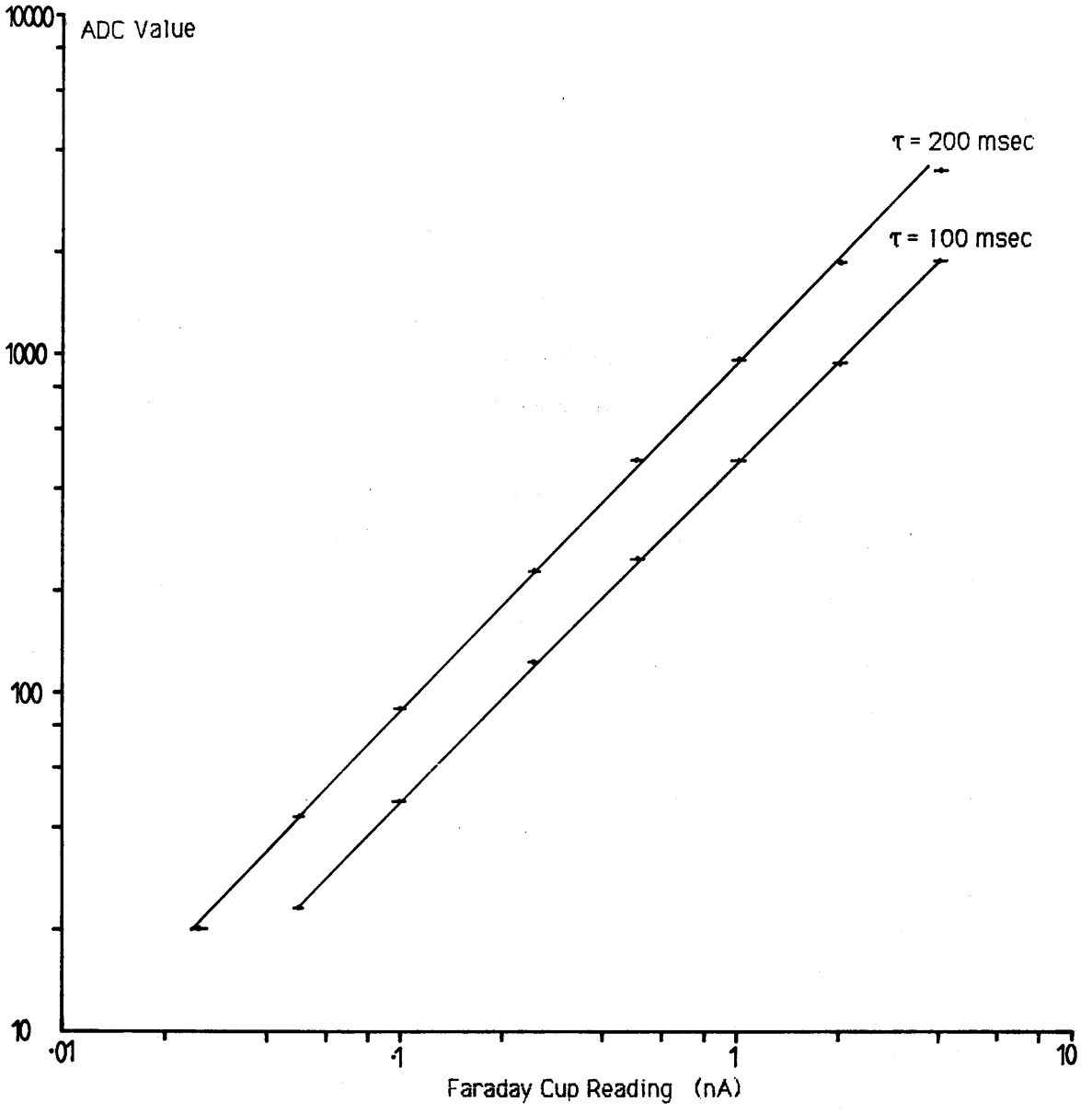

maintaining uniform illumination. A similar experiment was carried out using Reticon 2 with increased integration times of 100 msec and 200 msec, again at 0^{o}C. Figure 7.15b shows that the response using the shorter integration time is linear to within experimental error, while that using the longer integration time appears to fall off slightly as the array reaches saturation. This effect cannot be due to saturation of the scintillator as the current density of the electron beam is no greater than that used in the shorter integration time. From figure 7.4b the integrated dark current could only amount to ~30 ADC counts, so that this could not be the cause. Similar behaviour was exhibited by Reticon 1 under identical conditions, suggesting that some kind of saturation process is occurring in the photodiodes.

7.6.2 Uniformity of response and digital correction- Reticon RL128S

A measure of the non-uniformity of response of the Reticon diodes was obtained by examination of a uniformly illuminated scan after subtraction of the dark signal component. A figure for the percentage non-uniformity was calculated by dividing the differences of the most and least sensitive elements by the average value of the diodes along the array. Naturally, this figure contains some contribution from non-uniform components present in either the electron illumination or luminescent screen; however the technique of digital response correction described later can compensate for this, at least in part.

Reticon specify the non-uniformity of response for the S-series PDAs, measured at 50% of saturation, to be $<\pm 10\%$ at 25^{o}C. Measurements on the two diodes using the YAG screen gave experimental values of $\sim\pm 1.8\%$ for Reticon 1 and $\sim\pm 2.5\%$ for Reticon 2 (ignoring diode 1)under these conditions - well within the specified response figure.

After subtraction of the dark signal any non-random variation in the output signal from photodiodes under ideal uniform illumination is due to differences in the diode to diode sensitivity along the array, plus any component of signal dependent fixed pattern noise not common to the dark signal. Subject to the limitations imposed by flicker noise, the non-uniform response can be corrected to first order by multiplying the video data by a digital mask stored in memory. This is known as digital response correction. In practice the technique is only capable of correcting variations caused by linear effects, i.e. if the individual photodiode sensitivities are not constant but vary as a function of signal level, then simple correction is not possible.

Best results using this technique were obtained using digital masks made by uniformly illuminating the array with the maximum signal intensity to be recorded, subtracting off the

dark signal component and dividing the resultant scan by the average value of all the diodes. In practice, it was found that if the initial scan and the dark scan were produced by averaging the results of 10 identical consecutive scans the effects of flicker noise and spurious interference signals could be reduced, so that better correction was obtained.

Figure 7.16 shows the advantages of digital response correction for the Reticon 1 array operated at $0^{o}C$ with an integration time of 50 msec. The array was uniformly illuminated at various intensities over a range of three orders of magnitude, and the corresponding average signal value (after dark scan subtraction) is plotted along the horizontal axis in terms of ADC counts. The vertical axis is scaled as ±% non-uniformity in the recorded scans. This value is not a simple 'highest-lowest' type estimate as before, but is calculated from three times the standard deviation about the mean (3σ level) of each uniform scan. The reasons for choosing this generally more conservative criterion are; firstly that spurious single channel effects are averaged out, and secondly it gives a better representation of the improvement in response that can be achieved using digital response correction.

The top curve of figure 7.16 represents the unprocessed data after dark scan subtraction, while the lower curve is the same data after multiplication by a digital response correction mask generated in the manner described previously. The upper straight line is the limit to signal uniformity imposed by the readout noise (3σ level ~ 3.3LSB) whilst the remaining line represents the fundamental uniformity limit imposed by the 12 bit digitisation.

At low signal levels, the non-uniformity is dominated by the readout noise described in section 7.2 and digital response correction has no effect. As the signal level increases the effect of random noise decreases, and the corrected scan begins to show some clear improvement in uniformity remaining close to the readout noise limit. The 3σ level drops to below 1% for average signal outputs ≥500 ADC counts, while at midrange the non-uniformity is reduced to below ±0.4%. Comparison of the corrected scan with the uniformity limit imposed by readout noise shows that perfect correction is not achieved - the limiting factors are most likely flicker noise and non-linear sensitivity effects.

Figure 7.17 shows the results of digital response correction when the incident illumination was held constant and the diode integration time was varied at an operating temperature of $0^{o}C$. In this case the correction mask was made at the longest integration time of 300msecs, where the average value of the scan was 2344 ADC counts. The graph illustrates the effectiveness of the technique and again shows non-uniformity of response corrected to

Figure 7.16 Digital Response Correction For Varying Illumination Levels

Reticon 1 $T = 0^{0}C$ $\tau = 50$ msec

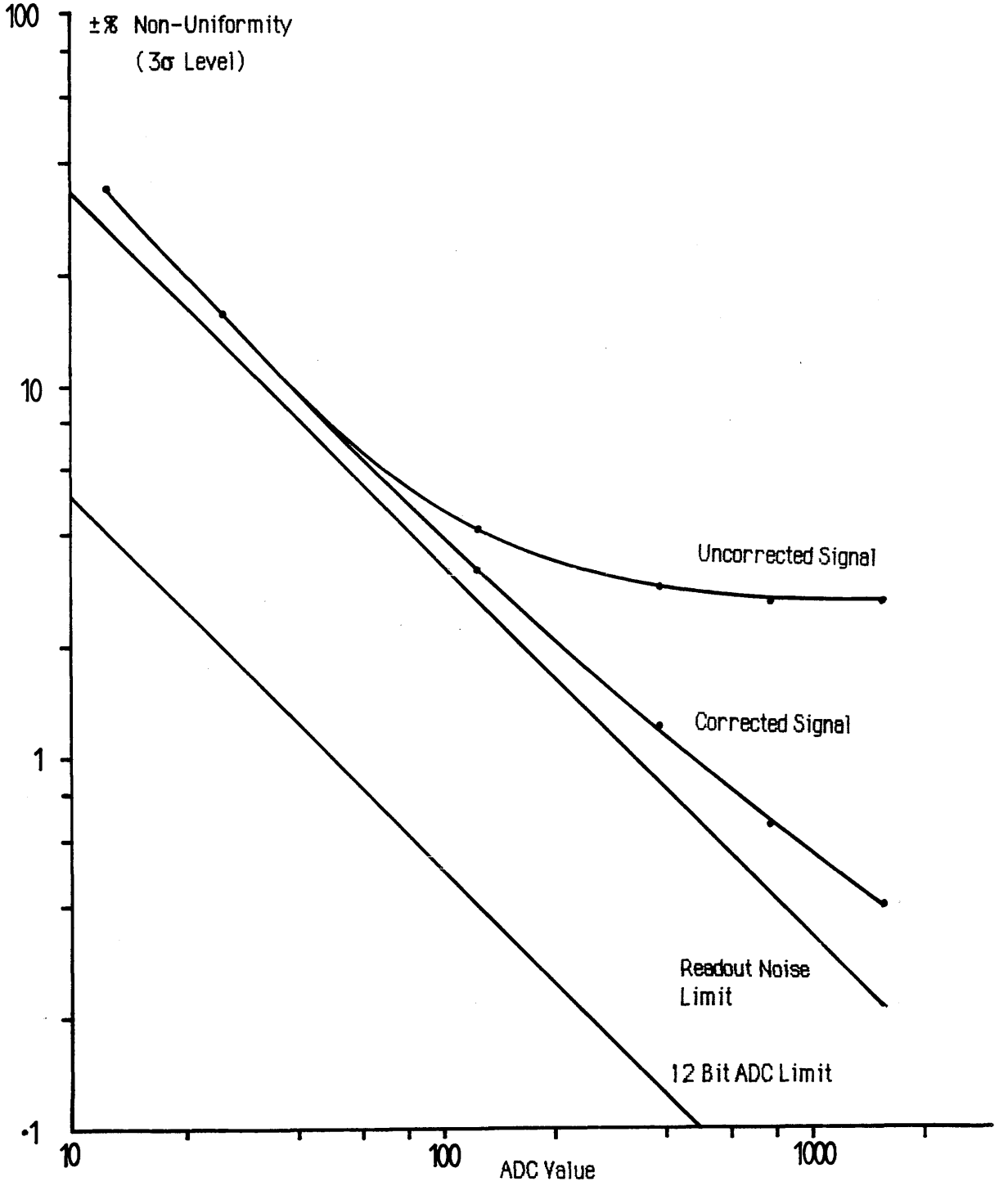

Figure 7.17 Digital Response Correction For Varying Integration Times - Reticon 1 T=0°C

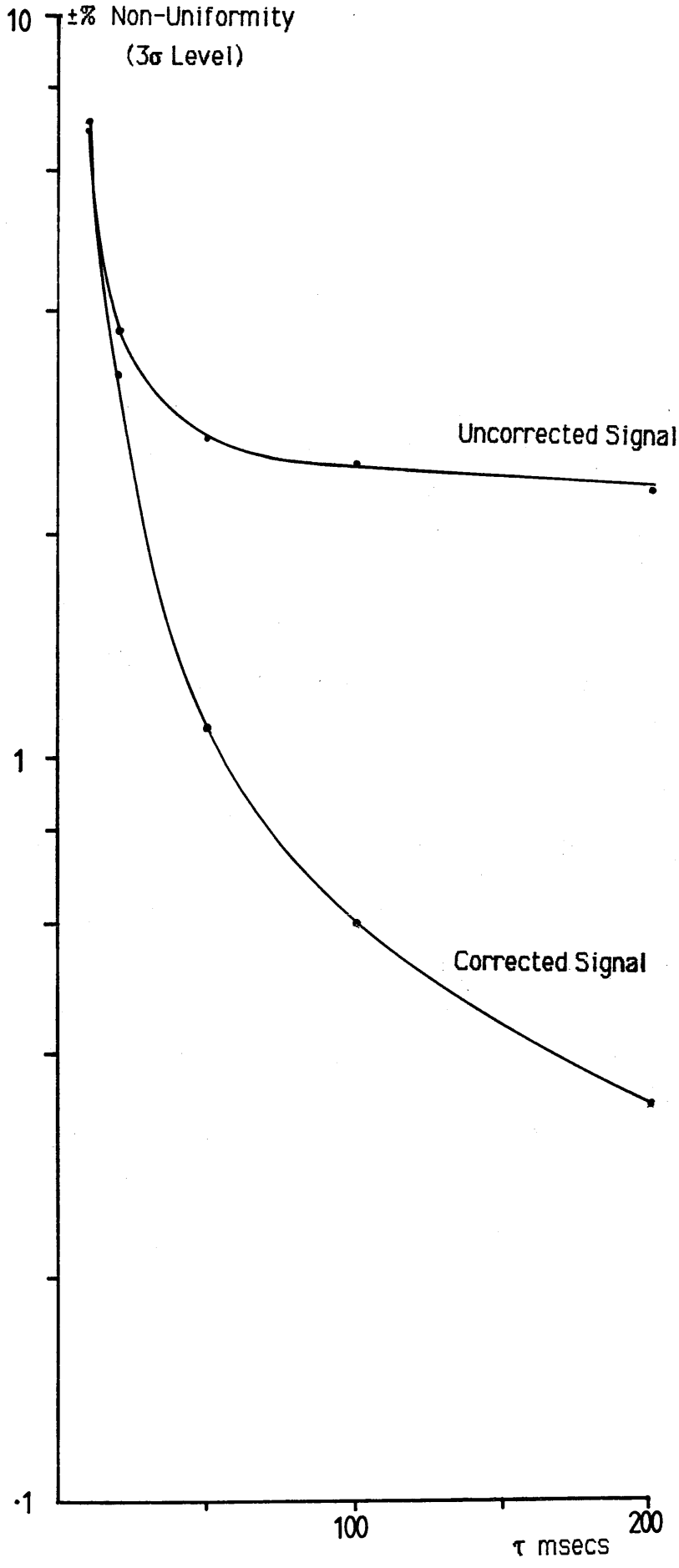

<±0.4% for midrange signals. The above experiments were also carried out using Reticon 2 and the results were very similar. The significance of these figures is discussed more fully in section 7.8.

7.7 OPTICAL RESPONSE : Hamamatsu S2304-512F array

The video output signal of the Hamamatsu photodiode array just before saturation is shown in figure 7.18a, using a 20 msec integration time at 0°C. Figure 7.18b shows the output when the illumination is increased so that the photodiodes were over-saturated. The saturation video voltage is 2.8 volts, corresponding to ~3820 ADC counts. It was found that this value was dependent upon the reference clock frequency applied to the C2325 driver/amplifier board, and hence the diode sampling rate. At lower frequencies than the 50 kHz sample rate used for all these experiments the saturation video voltage reached 3V, suggesting some form of bandwidth limitation in the video amplifier section.

The rounded response shown in figure 7.18a is due to some non-uniformity in the incident illumination rather than the array itself. The shape of the response could be altered by small shifts in the position of the defocussed electron beam, suggesting that there was some variance in the current density applied to the YAG screen over the 12.8mm active length of the array. The effect was probably not apparent when using the Reticon arrays because of their much shorter active lengths of 3.2mm.

7.7.1 Linearity of response: Hamamatsu S2304-512F array

Figure 7.19 graphs the response of the Hamamatsu photodiode array to constant illumination as a function of integration time at a temperature of 0°C. The vertical axis plots the average value of each scan after subtraction of the dark signal component. The relationship is linear to within experimental error, under all operating temperatures from -10°C to +30°C. The associated relationship between photodiode response and incident illumination level is plotted in figure 7.20 using an integration time of 1sec at 0°C. Again the beam current reading on the horizontal axis is only relative as the illumination was defocussed, however the response is seen to be linear within experimental error.

7.7.2 Uniformity of response+digital correction:Hamamatsu S2304-512F

The non-uniformity of response of the Hamamatsu photodiode array is specified to be <±5% at half saturation at 25°C. A true experimental value could not be obtained using the YAG screen because of the non-uniform illumination produced, however later experiments using

Figure 7.18a Hamamatsu Photodiode Just Before Saturation

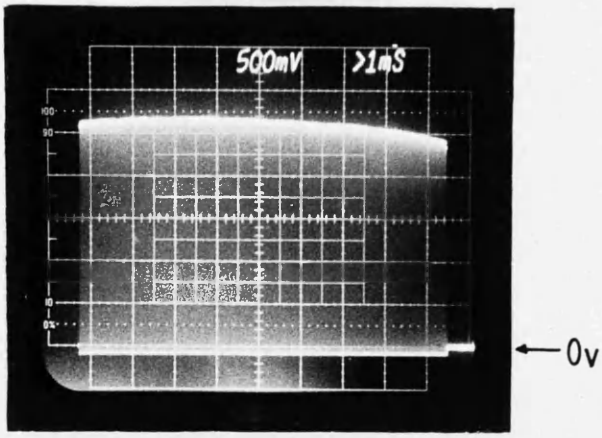

Figure 7.18b Hamamatsu Photodiode Oversaturated

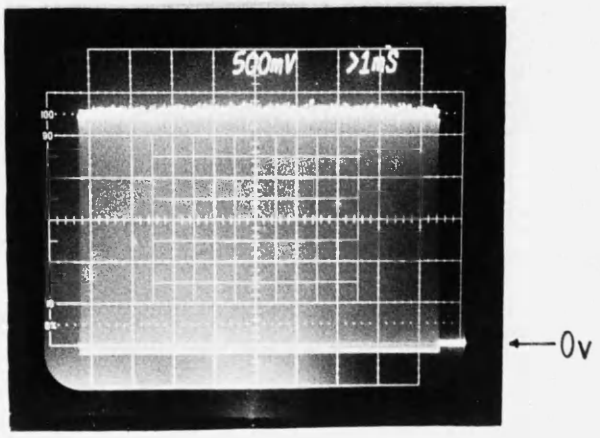

Figure 7.19 Response Of Hamamatsu S2304-512F To Constant Illumination As A Function Of Integration Time T=0°C

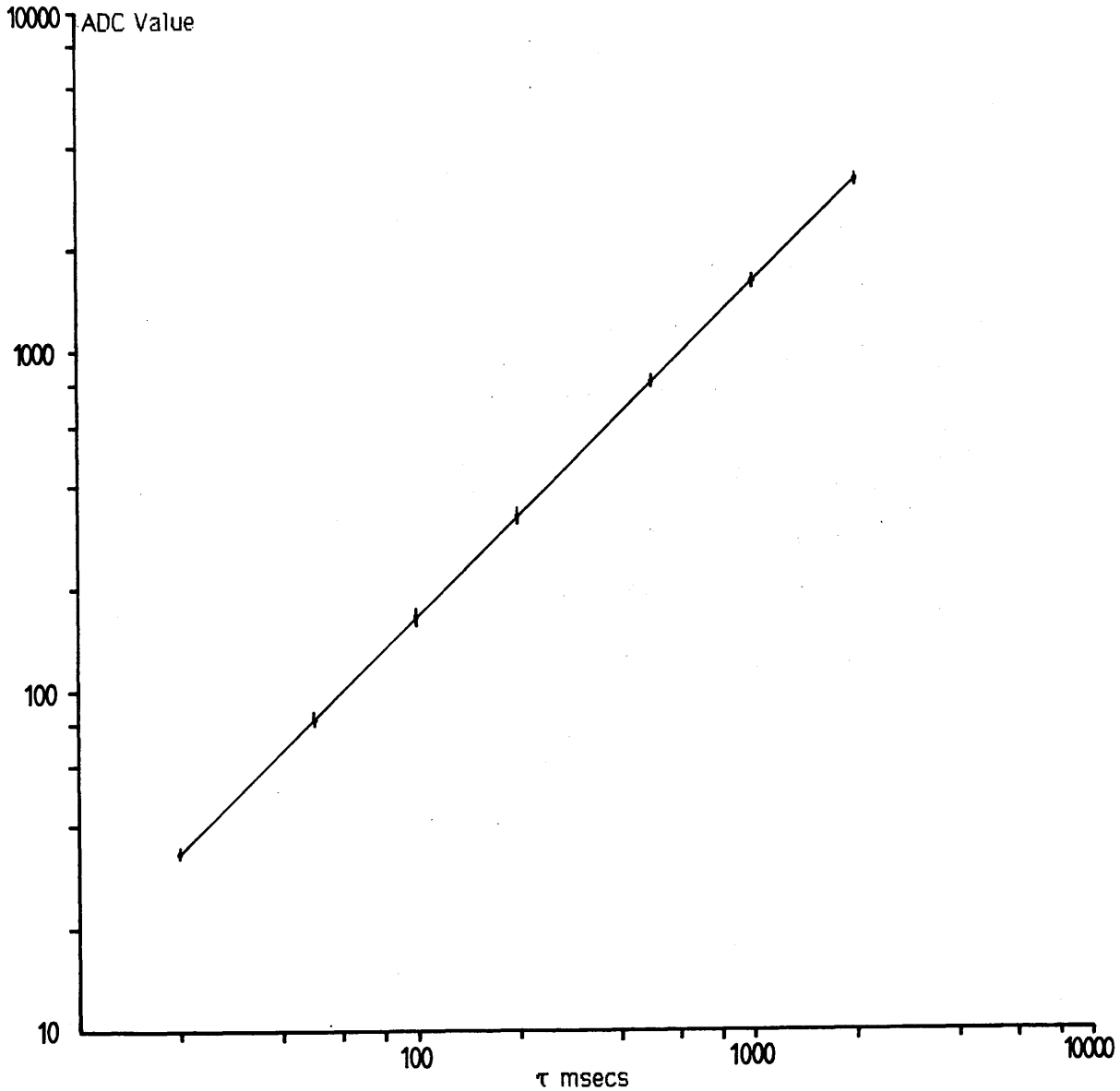

Figure 7.20 Response Of Hamamatsu S2304-512F To Varying Illumination Level $T = 0^{0}C$ $\tau = 1$ sec

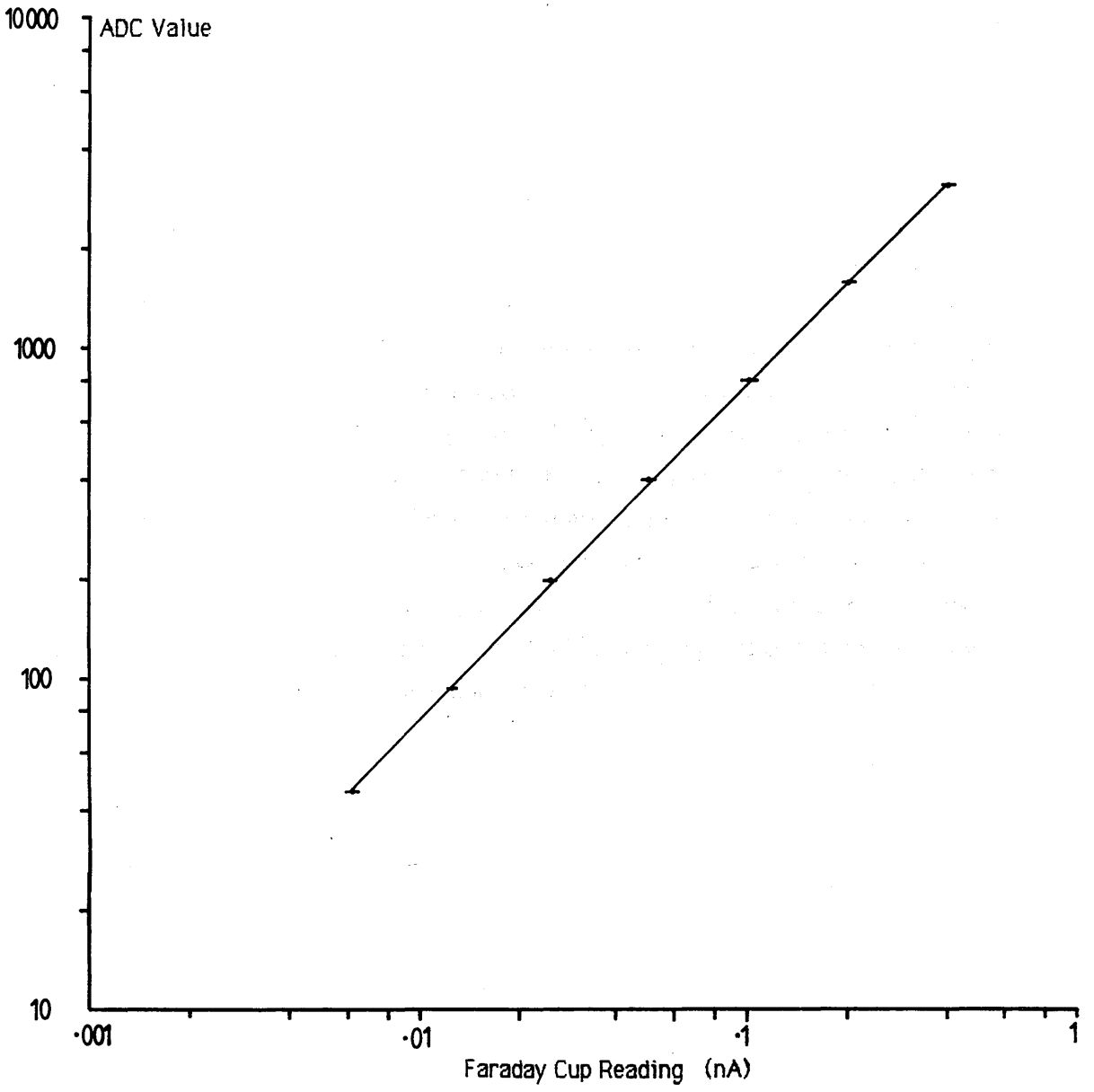

the Terbium doped scintillator faceplate described in chapter 8 seemed to produce a more uniform response (see figure 8.7a), and an experimental value for the non-uniformity of response (based on a 'highest-lowest' calculation) of ±1.2% was measured, exclusive of the first and last diodes in the scan. The only plausible explanation for this is that somehow the microscope parameters were altered in the time between the two sets of experiments, so that the illumination became more uniform.

Figure 7.21 shows the effect of digital response correction on the Hamamatsu array when illuminated using the Terbium screen. The integration time was 1 sec and the operating temperature was 0^{o}C. As before the non-uniformity is plotted as a ±% obtained from the 3σ level of each uniformly illuminated scan. The unprocessed data shows a 3σ non-uniformity ~±2% at midrange values. In comparison, the non-uniformity of the digitally corrected scan drops below ±1% at ADC values ≥ 500 counts, and seems to be reduced to <±0.5% for ADC counts >1000. A comparison with the limiting uniformity line, calculated on the basis of ±3.3 LSB readout noise (3σ level) shows that again perfect correction is not obtained; the performance is similar to that of the Reticon arrays. The Hamamatsu array does not possess any measurable flicker noise, so that the limitation to perfect correction must be non-linear sensitivity effects in the individual photodiodes.

Figure 7.22 shows the results of digital response correction when the incident intensity is held constant and the diode integration time is varied at a constant temperature of 0^{o}C. This experiment was carried out using the YAG screen, as the incident electron current was not altered during the measurements hence the non-uniformity in illumination was constant and could be corrected. The required digital correction mask was made at an integration time of 2 secs, which corresponded to an average ADC value of 3196. Again the correction is seen to be very effective.

7.8 SUMMARY OF OPTICAL RESPONSE EXPERIMENTS

The results of the optical response experiments described previously are briefly summarised in the next two sections, and the performances of the Reticon and Hamamatsu photodiode arrays are compared.

7.8.1 Linearity of response

An examination of figures 7.13 and 7.18b shows that the saturation video voltage levels of both the Hamamatsu and Reticon arrays are ~2.8V instead of 3V under the prescribed

Figure 7.21 Digital Response Correction For Varying Illumination Levels

Hamamatsu S2304-512F T = 0°C τ = 1 sec - Terbium Screen

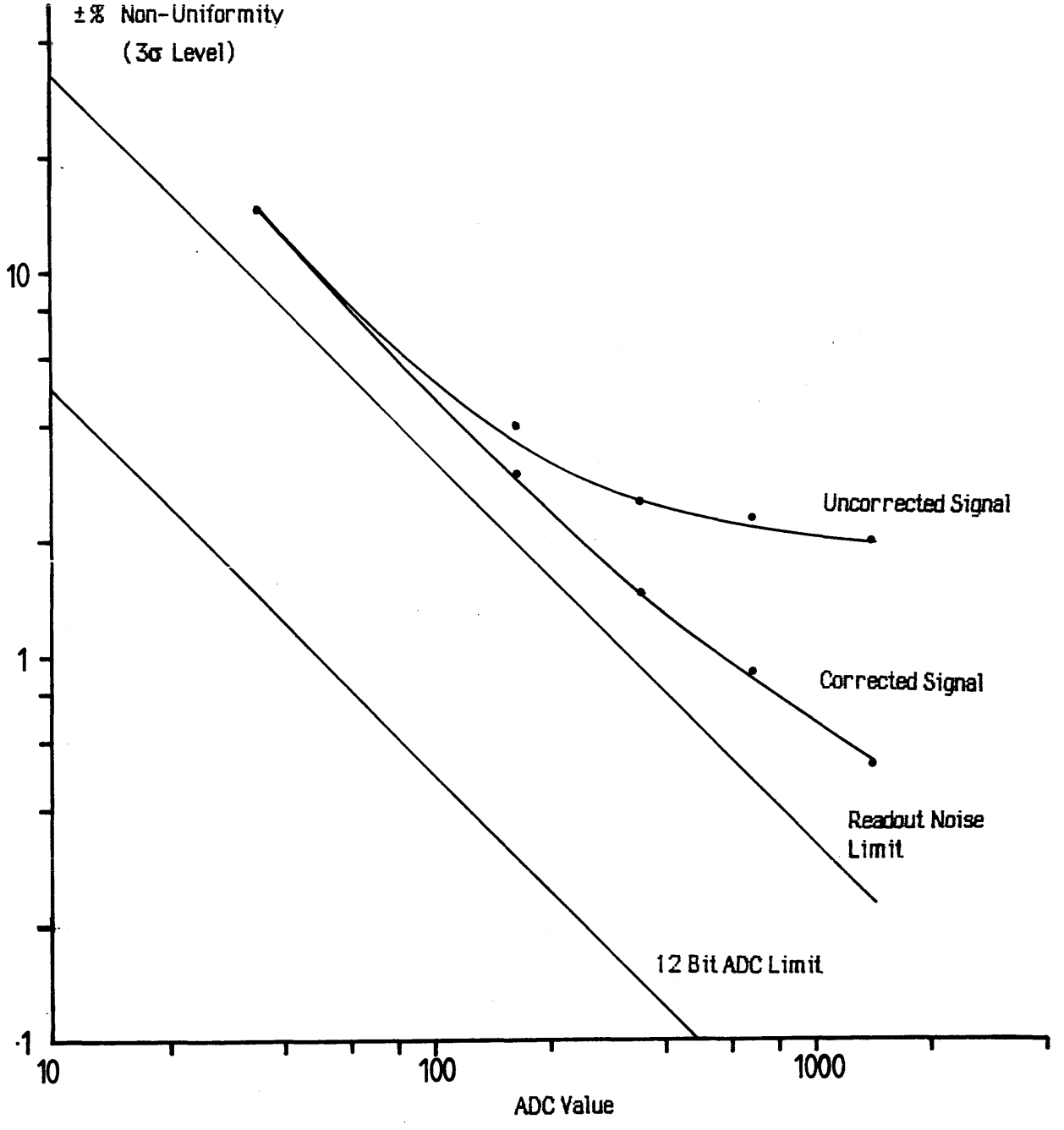

Figure 7.22 Digital Response Correction For Varying Integration Times
Hamamatsu S2304-512F T=0°C YAG Screen

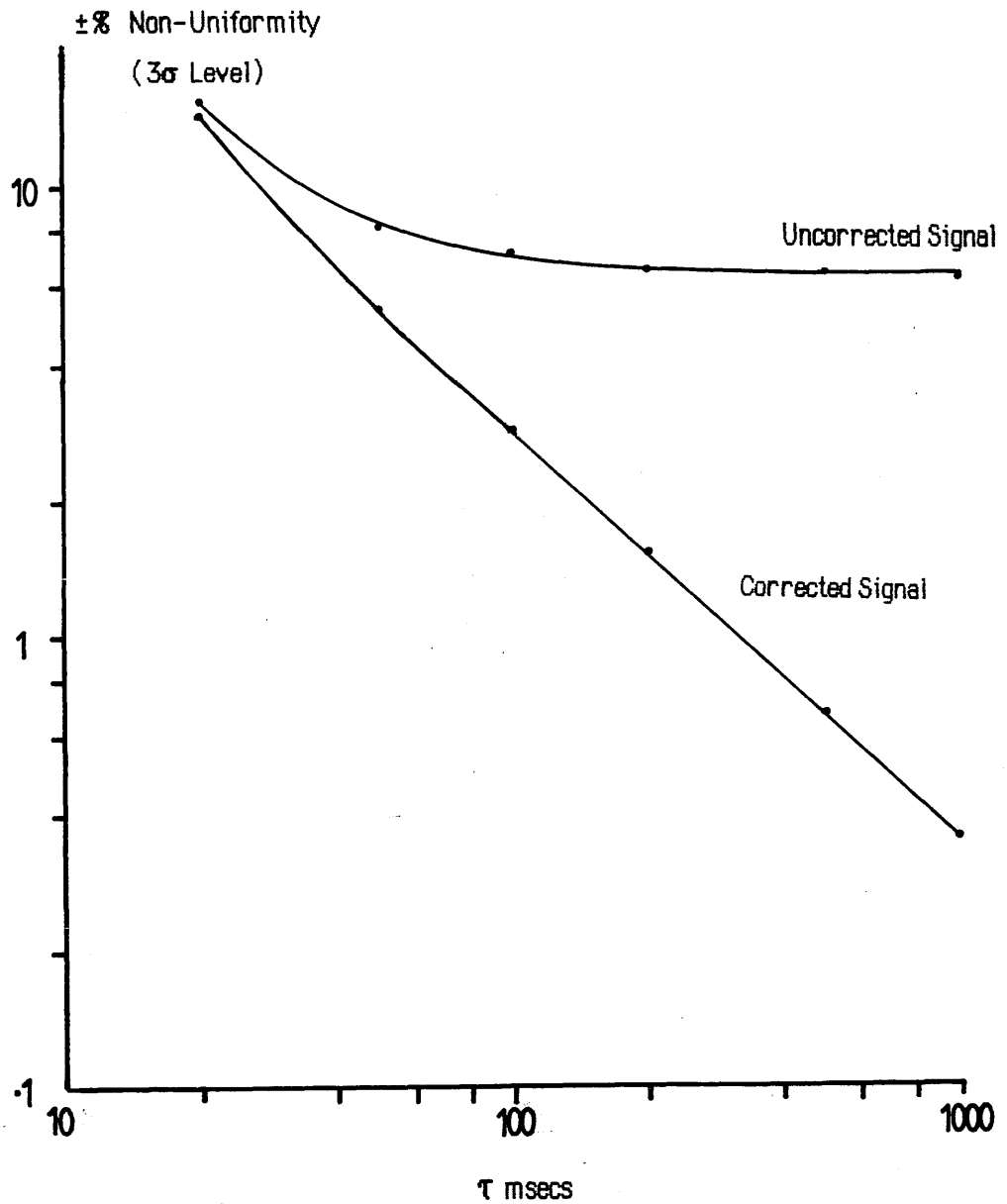

operating conditions. Possible causes of these effects have been discussed in the relevant sections, and a slight increase in the gain applied to the video signal prior to digitisation should restore the full dynamic range.

As regards linearity of response to uniform illumination both devices responded well, except when close to saturation. Figure 7.15b illustrates a slight non-linearity in response of the Reticon array as the signal level increases towards saturation. Any similar such non-linearity in the response of the Hamamatsu array was small enough to be hidden by the uncertainty in beam current measurement as shown in figure 7.20.

7.8.2 Uniformity of response and digital response correction

Values for the non-uniformity of response of the two Reticon arrays, based on the difference of the most and least sensitive elements, were found to be ~±1.8% and ~± 2.5% at half saturation for Reticon 1 and Reticon 2 respectively, using the YAG screen. Both figures are considerably better than the ±10% uniformity specified by the manufacturers. In comparison, the corresponding uniformity figure for the Hamamatsu array was found to be ±1.2%, measured using the terbium fibre-optic screen. Again this figure is better than the manufacturers specification of ±5%

These figures are influenced to some extent by the degree of uniformity present in both the illumination and the luminescent screens. Unfortunately, time prevented the investigation of the Reticon response when illuminated using the terbium screen, however later experiments on the uniformity of various types of screen (section 8.2.3) suggests that the difference would not be large.

The improvement in uniformity of response obtained by digital response correction is clearly illustrated for both types of photodiode in figures 7.16 and 7.21. The degree of correction obtained for both photodiodes is similar; - the figures show that the non-uniformity of response can be reduced to ≤±0.4% at half saturation for both types of array. This level of correction does not quite approach the uniformity limit imposed by the readout noise, suggesting that there are some non-linear sensitivity effects occurring in both the Reticon and Hamamatsu photodiodes. However, it is most likely that a reduction in readout noise levels would result in a corresponding improvement in the uniformity of response levels that can be achieved in both types of array.

CHAPTER 8

Electron-photon conversion and Detective Quantum Efficiency

Introduction

The examination of the properties of two commercial photodiode arrays carried out in the previous chapter illustrated the superiority of the Hamamatsu S2304-512F device for use as a parallel detector in EELS. However, the performance of indirect detection systems based around this or any other detector depends crucially upon the properties of the electron-photon conversion medium. The most important parameters to be considered are: efficiency of photon production, linearity and uniformity of response, resistance to radiation damage, spatial resolution, spectral response and decay time. This chapter describes experimental measurements of the above properties for various luminescent screens, referenced to those of a commercial high resolution Zn Cd S: Ag (P20) phosphor screen manufactured by Mullard for use as an image intensifier faceplate. The screens examined include: P46 cerium doped yttrium aluminate powder phosphor screens in three different particle sizes supplied by Derby Luminescents Ltd, two single crystal YAG screens thinned by different polishing techniques and a novel terbium doped fibre optic faceplate scintillator developed by Collimated Holes Inc. Results are presented for these screens, and the detective quantum efficiency of a complete detector assembly consisting of the Hamamatsu photodiode array fibre-optically coupled to the screen with the most favourable qualities is evaluated. Unfortunately it was not possible to test the detector by recording an actual EELS spectrum because of the lack of a suitable spectrometer, but a line image through the spot diffraction pattern of a single crystal gold specimen was recorded in the JEM 100C microscope. The dynamic range of such a pattern is comparable to that found in EELS spectra. Finally, the diffraction line scan was compared to one serially recorded from the HB5 using the same specimen, in order to estimate the degree of spreading in the image.

8.1 LUMINESCENT SCREENS AND COUPLING OPTICS

The amount of data published concerning the fabrication and properties of luminescent screens is almost overwhelming, dating right back to the invention of the cathode ray tube. Frequently the information presented is confusing or even contradictory because of the large effects that minute differences in phosphor composition, purity, and deposition can introduce. No attempt will be made here to discuss the complex mechanisms of photon

production in the myriads of compounds which exhibit cathodoluminescence, a standard reference being the book by Leverenz [1950] or the review by Garlick [1966]. A useful investigation of the performance of some scintillators commonly used in electron microscopy is given by Pawley [1974]. The properties required of an ideal conversion screen are discussed, and a brief description of some of the types of luminescent materials which could be considered is given. The particular compounds thought to be most promising for use in this application are highlighted, and investigated further in later sections. The most appropriate form of optical coupling between the luminescent screen and the photodiode array is via a fibre-optic plate; some of the advantages this method offers over conventional lens optics are also mentioned.

8.1.1 Electron-photon conversion and image transfer

When a 100keV electron strikes a solid scintillator it gradually loses energy in a series of scattering processes. The fraction of this energy converted to light is known as the scintillator conversion efficiency. Assuming, on average, an energy of ~2.5eV is required to create one photon, then a scintillator with a 5% conversion efficiency would produce ~2000 photons per incident electron. This figure assumes that all the electron energy is deposited in the scintillator, if there is a large amount of backscattering or the screen thickness is less than the electron range the number of photons produced will be reduced.

The photons emitted by the luminescent centres in any scintillator propagate in all directions, so that only a fraction find their way to the exit surface. The addition of a thin reflecting layer of aluminium at the input surface helps to retain light which would otherwise be lost, at some cost to the spatial resolution. The aluminium screen fulfills the dual role of providing a conducting path to ground, which is most important for transmission screens fabricated on insulating transparent media such as quartz or glass. Photons which have to travel a long path distance in the scintillator may well be reabsorbed, particulary in thick screens of opaque powder phosphors. In the case of transparent single crystal scintillators light which strikes the polished input and output faces at angles greater than the critical angle is totally internally reflected and piped out to the edges of the crystal, or dissipated at surface defects such as scratches, pits or burrs. Shauer and Autrata [1979] have shown that matt finishing the output surface of bulk single crystal YAG scintillators can increase the light output by 30% due to the suppression of light piping. Autrata [1978] also suggests that the corresponding increase in the light output of thinned scintillators is likely to be up to ~60%, but the effect on screen resolution and uniformity is not clear.

The light produced by a luminescent screen can most efficiently be coupled into the photodiode array using fibre-optic plates, as large numerical apertures can easily be obtained over a wide area without distortion, allowing more efficient transfer of the light than conventional lens optics. Another advantage of fibre-optic technology is that the screens are strong enough to be made into vacuum windows, so that the scintillator inside the vacuum system can be laid directly onto a fibre-optic vacuum seal; - the output face of which is in contact with the fibre-optic window of the photodiode array in air (if the array is cooled then it should be in a roughing vacuum to prevent condensation). The complete optical system is then very robust and compact, needing no setting up once in operation. The transfer efficiency of the fibre-optics depends upon the numerical aperture, open area, and transmittance of the individual fibres at the wavelengths of interest. The small size of fibre repeat distances (<10μm) available in current faceplates means that the spatial resolution of the system will be limited by the screen itself rather than the coupling optics.

Not all the photons which eventually reach the photodiode array are ultimately recorded. Some of the light is absorbed in the SiO_2 layer at the diode surfaces, particularly the blue wavelengths. The transmission of the PDA fibre-optic input window is also a function of wavelength, tending towards a maximum in the red end of the spectrum. These factors determine the quantum efficiency of the array, which describes the percentage of incident photons which are recorded as a function of wavelength. Figures taken from the standard Hamamatsu data sheets indicate that the S2304 series Hamamatsu arrays with a quartz input window have a spectral response peak at ~600nm where the quantum efficiency is 71%. With a fibre-optic input window the peak shifts to ~750nm with a quantum efficiency of ~52% and the quantum efficiency at 600nm is reduced to ~44%.

8.1.2 Performance requirements of an ideal scintillator

The high dynamic range of a typical EELS spectrum means that the electron beam current incident upon the scintillator in a parallel recording system will vary over a range of $\sim 10^{-5} A/cm^2$ to $\sim 10^{-11} A/cm^2$, although much higher current densities may occur during alignment. It is most important that the light production of the luminescent screen is linear over this range, and that it does not suffer from radiation damage caused by prolonged exposure to the higher intensities. The efficiency of photon production should be high enough so that low level signals can be detected above the photodiode readout noise, and the spatial resolution should ideally match that of the photodiode array i.e. 20 line pairs/mm. The principal decay time should be reasonably short <1μsec, and more importantly there should be no long secondary time constants to produce low intensity afterglow effects which

could cause artefacts to occur at the low current range of the spectrum. The spectral output of the scintillator should provide a reasonable match for the Hamamatsu array with a fibre-optic input window, so that scintillators which emit in the blue region are not suitable. The final requirements are that the screen should be mechanically robust, UHV compatible and preferably able to be vacuum baked to 200°C.

8.1.3 Scintillator materials

Compounds exhibiting cathodoluminescence can be categorised into 5 groups determined by their physical structure and chemical composition. The basic categories are listed below along with a brief discussion of their important properties.

A) Inorganic Powder Phosphors

These are the most common types of luminescent screens and have been extensively investigated for use in television, radar and general display devices. The materials consist of a polycrystalline powder deposited (usually by liquid sedimentation methods) on a glass or other suitable substrate. Much early work on high efficiency, fast decay phosphors was carried out by Bril and Klasens [1952a,1952b] who found that compounds of zinc sulphide activated by silver (ZnS: Ag)had the highest absolute conversion efficiencies of any scintillator at ~25%. Unfortunately the decay times of the most efficient phosphors are usually rather long. The strongest candidates in this class for recording EELS spectra are cerium doped yttrium aluminate phosphors (P46). Figures published by Autrata et al [1983a] indicate that the conversion efficiency of this phosphor is ~4%, decay time is ~200nsec to 10%, the spectral response peak occurs at ~560nm, and resistance to radiation damage is extremely good. There is no commercially available phosphor with a longer wavelength emission which can match the speed and linearity of this compound [Hill 1985].

B) Inorganic Single Crystals

This class of scintillators consists of blocks of single crystal usually grown from a melt. The conversion efficiencies are generally less than that of ZnS: Ag with thallium activated sodium iodide (NaI:Tl) being the most efficient at ~13%. Other single crystal scintillators available include caesium iodide (CsI:Na) and calcium fluoride (CaF_2:Eu), but the most useful of all for microscopy are the single crystal forms of cerium activated yttrium aluminium perovskite or YAP (Y Al O_3) and yttrium aluminium garnet or YAG (Y_3 Al_5 O_{12}).

Of the two the latter has the more suitable spectral emission for coupling to photodiode arrays. Autrata et al. [1983b] measured the conversion efficiency of YAG to be ~4% with a decay time similar to that of P46, and found that the material was almost unaffected by radiation damage. These properties, together with the uniformity of response and mechanical strength advantages inherent in the single crystal structure, make single crystal YAG a leading contender for this application.

C) Glass Scintillators

Certain types of lithium activated glasses (e.g. NE901) fluoresce with the required short time constant and are reasonably resistant to radiation damage. Unfortunately the light emission tends to occur in the blue region of the spectrum and the efficiency of production is not high. An interesting new scintillator material developed by Collimated Holes Inc. uses glass fibres activated with terbium oxide. The fibres are formed into a fibre-optic faceplate which can be made into a scintillating vacuum seal. A pre-production sample of this scintillator was made available for testing for general use in electron microscopy and EELS in particular.

D) Organic Single Crystals

Luminescent single crystals of organic compounds such as anthracine and naphthalene can be grown from the melt and have been applied to electron microscopy. Decay times are suitably short, but the spectral response tends to be unsuitable for coupling to photodiode arrays, and the vapour pressure of these compounds tends to be too high for UHV applications. Also the resistance to radiation damage of these materials is not high enough for EELS.

E) Plastic Scintillators

Plastic scintillators such as NE102A have very fast decay times and are reasonably efficient. The main drawback, as reported by Pawley [1974], is an extreme sensitivity to radiation damage which renders this class of materials almost unusable for EELS.

8.1.4 Preparation of luminescent screens

All the screens examined (except the terbium faceplate) were prepared on fibre-optic faceplates supplied by Mullard Ltd. Figure 8.1a is a photograph of one of these plates. The

Figure 8.1a Mullard Fibre Optic Faceplate

Figure 8.1b Optical Micrograph of Fibre Plate

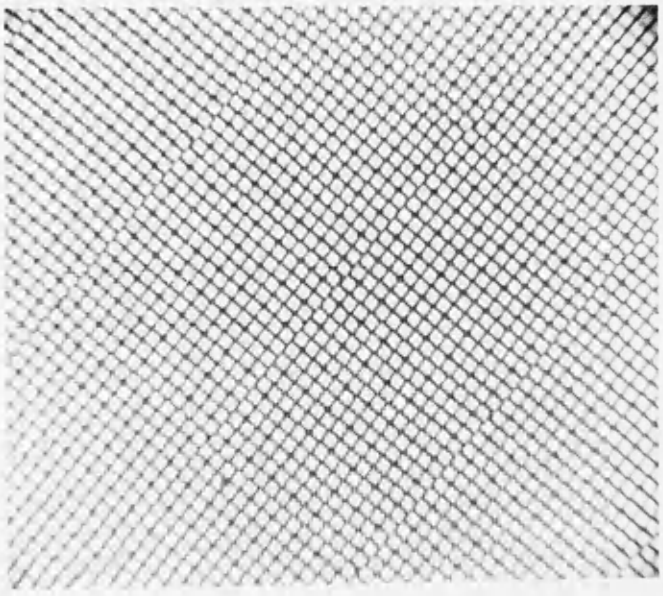

Repeat distance = 5.5µm

diameter of the central circle which contains the fibres is ~20mm, and the plate is ~4mm thick. Figure 8.1b is an optical transmission micrograph showing the regular construction of the fibre bundles. The light areas are the fibre cores which make up ~90% of the total area and the dark lines are the optically inactive fibre cladding. The diamond shaped area at the intersection of each group of four fibres is an extra-mural absorber which helps to reduce cross-talk between fibres. The fibre repeat distance in figure 8.1b is ~5.5μm and Mullard specify the numerical aperture in air and the optical transmission to be 1.0 and 60% respectively. The methods of luminescent screen production used are described in the following subsections.

A) P46 Powder Screens

The P46 powder was obtained from Derby Luminescents Ltd. in three different grades: YAG69M, YAG69MM and YAG69MF, corresponding to mean particle sizes of 8-9μm, 6μm, and 3μm respectively. The actual fabrication method used was the standard sedimentation method described below, the only difference being that it was found to be necessary to add a few drops of collodion binder to ensure good screen adhesion of the 3μm grade phosphor. The method was as follows:

1) First of all the fibre optic plate and all glassware used in the procedure were thoroughly cleaned in the following manner:

   a) Wash in quadralene solution, rubbing surfaces vigo rously with a clean cloth.
   b) Ultrasonic for 5 mins in fresh quadralene solution.
   c) Rinse in de-ionised water.
   d) Ultrasonic for 5 mins in acetone.
   e) Ultrasonic for 5 mins in absolute alchohol.
   f) Blow dry using inert gas e.g. dry nitrogen.

2) Approximately 1g of phosphor powder was weighed out and added to 100ml of acetone [at this point a few drops of collodion binder were added to the 3μm suspension]. The solution was agitated in an ultrasonic bath for 5 minutes then quickly decanted into the settling dish containing the fibre optic plate. It was found to be best if the fibre optic was immersed in ~50ml of acetone prior to the introduction of the phosphor suspension. The top of the dish was covered to prevent dust contamination and the solution left overnight or until such time as all the phosphor had settled out. After the required settling time the drain tap on the settling dish was opened to allow

the remaining acetone to escape slowly, without disturbing the screen.

3) The finished screen was carefully removed from the settling dish and the excess phosphor removed using a fine point artist's brush and an air-jet. A conductive coating of ~50nm of aluminium was then evaporated onto the top surface, and the screen was ready for use.

The limited quantities of phosphor powder available meant that the scope for experimentation with screen weights was very limited, as it often took several tries to produce an acceptable screen. In the end the screens tested had weights of 35mg/cm^2 for the 8-9μm grain size, 18mg/cm^2 for the 6μm grain size and 15mg/cm^2 for the 3μm grain size. The first screen weight is really too heavy for imaging 100keV electrons, however it was the best available at the time.

B) Single Crystal YAG Screens

A disk of single crystal YAG 1mm thick and 20mm in diameter was purchased from Agar Aids Ltd. One side of the crystal was polished and the other had a matt finish to reduce total internal reflection effects. This disk was cut into three portions as shown in figure 8.2, and the central part was used to provide uniform illumination for the photodiode array experiments described in the previous chapter. The two remaining sectors were made into thinned screens, in the following manner:

1) The YAG crystals and fibre optic faceplates were cleaned using the method described previously.

2) The bulk crystals were bonded polished side down to the fibre plates using Loctite 'Glass Bond' UV sensitive adhesive. A small drop of glue was applied to the surface of the fibre plate and the YAG carefully positioned in the center. Once the position was correct the YAG was weighted down for 12 hours, so that the compressive action tended to force excess adhesive out from under the crystal. After this time the glue was hardened using an ultra-violet lamp. Experiments showed that a uniform layer of adhesive <5μm thick could be achieved using this method.

3) The fibre-optic plates were clamped in a lapping machine and the bulk YAG samples were then ground down roughly, using 600 grade silicon carbide powder on a brass lapping plate.

Figure 8.2 Segmentation of YAG Disk

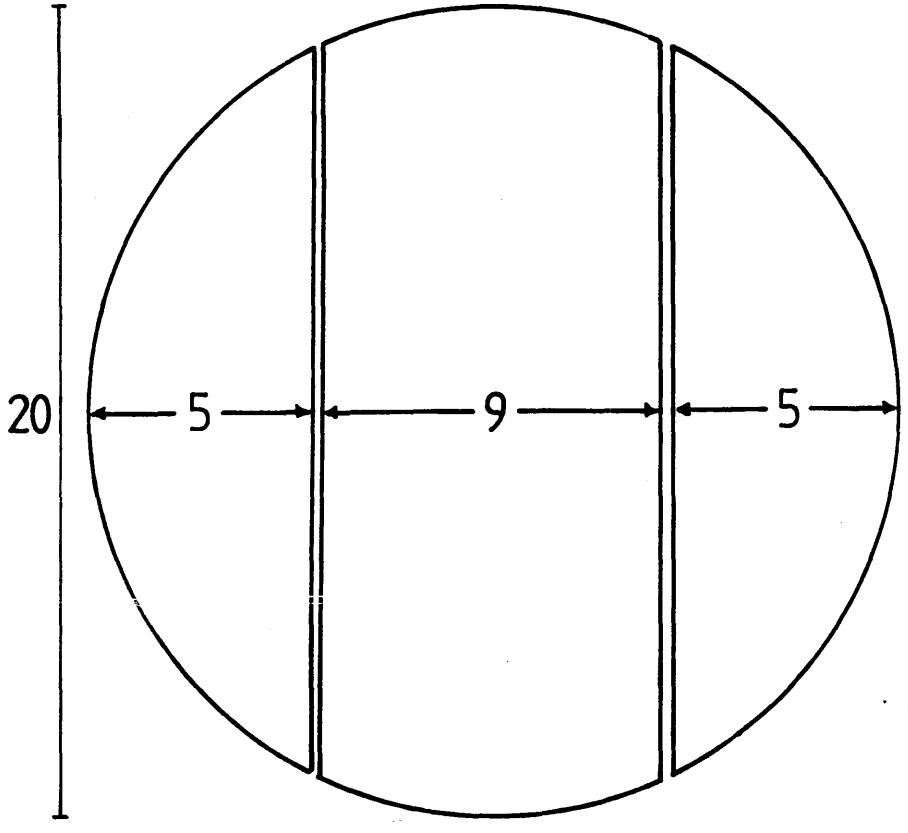

(all dimensions millimetres)

4) One sample, known as screen A, was mechanically fine polished using 1μm grade diamond paste on a solder lapping plate. This method gives good thickness control, however the surface finish tends to contain scratches. The second sample, screen B, was finished using SYTON W15 colloidal silica polish on an expanded polyurethane lapping plate. The silica polish is less abrasive than the diamond paste, and gives a much smoother surface finish. However, the control achievable over the screen thickness and uniformity is much less.

5) The finished screens were coated with a conducting layer of ~50nm of aluminium to prevent charging and increase light output.

From the Monte-Carlo studies reported in section 8.3, the optimum thickness of single crystal YAG for imaging 100keV electrons is ~30μm. The purpose of using two different finishing polishes on the YAG was to see which gave the best overall properties. Measurements carried out on the two screens using a micrometer dial gauge showed that the thickness of screen A varied between 30μm and 35μm over its whole area, and that of screen B varied between 52μm and 58μm. Screen B could not safely be thinned any more using the silica polish. The thickness of both screens was most uniform around the center, and tended to decrease slightly towards the edges.

Figures 8.3a and b are optical micrographs of screen A showing the boundary between the edge of the YAG and the fibre plate. The boundary layer between the YAG and the glass is hardened glue. In figure 8.3a the fibre-optic plate is focussed while in figure 8.3b the top surface of the scintillator is in focus. The dark scratches which can be seen on the surface of the YAG are caused by the diamond polish. Figures 8.3c and 8.3d are equivalent micrographs of screen B. In this case the boundary glue layer is very much wider, probably due to the less abrasive polishing method, and the YAG thickness is seen to be greater as the fibre-optic surface is not visible through the crystal. The surface finish is much better, unfortunately the photograph is marred slightly by blemishes on the negative which gave rise to the white scratch lines.

C) Terbium Faceplate

This screen was supplied as a rectangular fibre-optic plate measuring 25mm x 17mm x 3.2 mm thick. Figure 8.4 is an optical micrograph showing the arrangement of the fibre bundles. Most fibres are hexagonal in cross-section, with a mean diameter of 25μm. No EMA is provided on this sample, although the manufacturers include this as an option. The

Figure 8.3a Optical Micrograph of YAG Screen A (30µm)

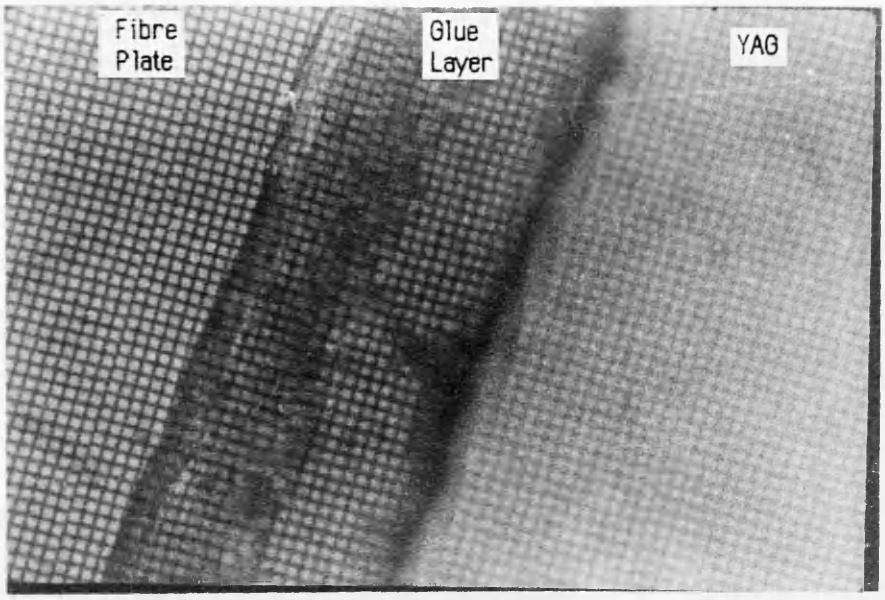

Focus on Fibre Plate

Figure 8.3b Optical Micrograph of YAG Screen A (30µm)

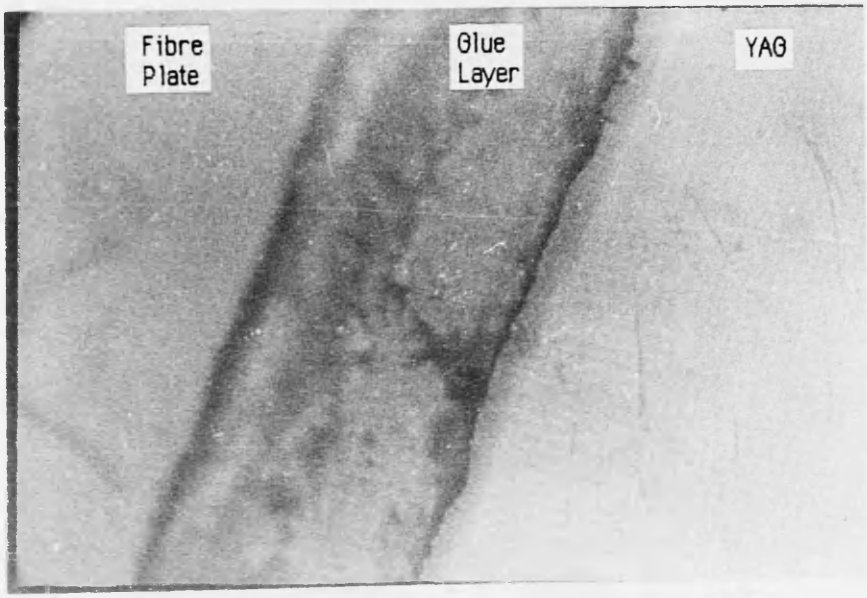

Focus on YAG Surface

Figure 8.3c Optical Micrograph of YAG Screen B (50µm)

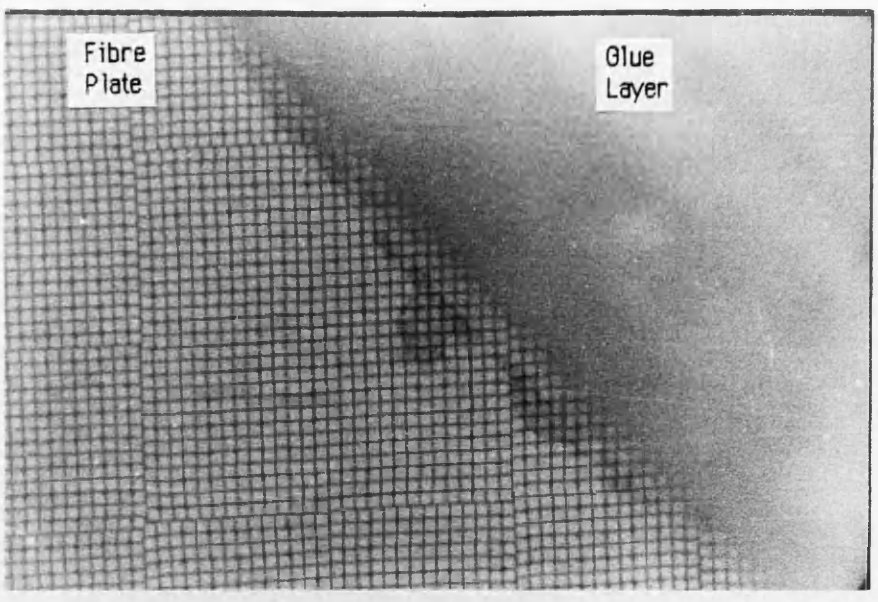

Focus on Fibre Plate

Figure 8.3d Optical Micrograph of YAG Screen B (50µm)

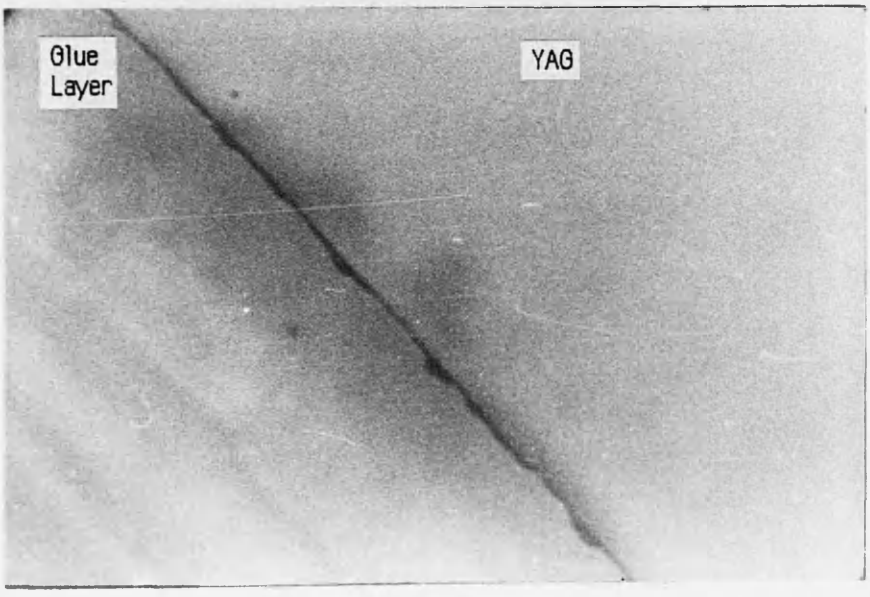

Focus on YAG Surface

Figure 8.4 Optical Micrograph of Terbium Doped Fibre Optic Faceplate

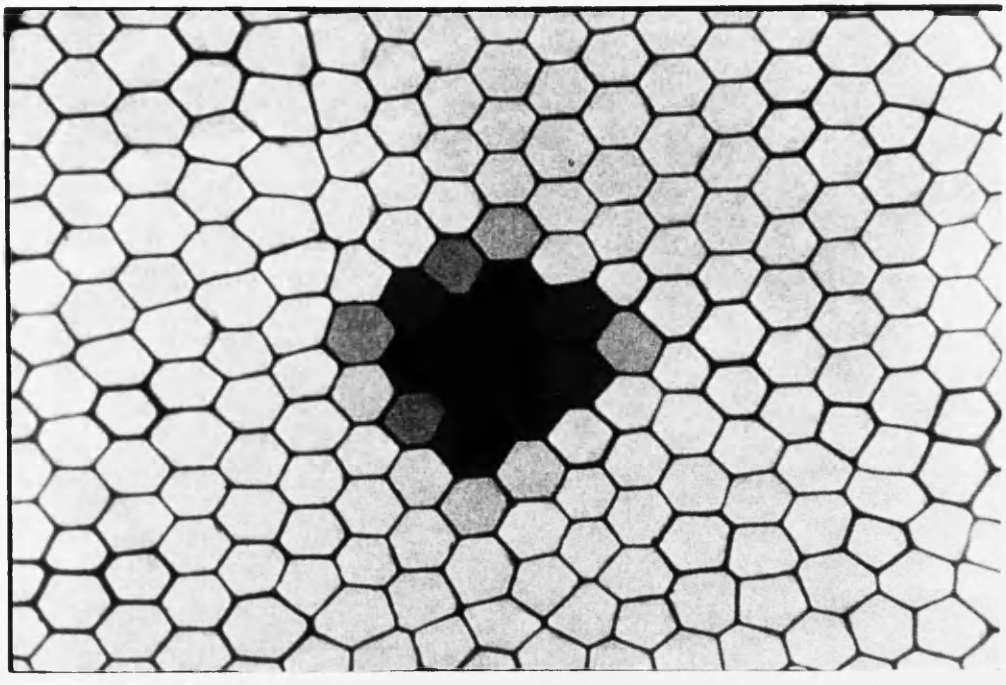

Repeat Distance ~25µm

numerical aperture is less than that of the Mullard plates at 0.4. An examination of the fibre plate under the optical microscope revealed some evidence of 'dead' fibres, i.e. those where the optical transmission is very low, as seen in the centre of figure 8.4. All that was required to make the plate usable was to evaporate ~50nm of aluminium as a conducting coating on the top surface.

D) Mullard P20 Screen

The Mullard screen used as a reference was designed to be used as the faceplate of an image intensifier and as such is optimised for 10keV electrons. The screen weight is therefore much too low for efficient detection of 100keV electrons, however the high conversion efficiency of the P20 phosphor helps to improve the performance. The screen was supplied on a fibre-optic plate with a coating of aluminium already applied.

8.2 EVALUATION OF SCINTILLATOR SCREEN PERFORMANCE

The results of a series of experiments designed to determine the imaging properties of the various scintillator screens under consideration are given. In the cases where absolute quantitation is not possible the measured parameter is referenced to that of the commercial P20 image intensifier faceplate supplied by Mullard. All of the experiments, except those which measured the principal decay times, were carried out in the vacuum chamber attached to the JEM 100C microscope. An aluminium shield similar to that described in section 7.5 was constructed to hold the fibre-optic plates above the Hamamatsu photodiode array. The screens were positioned centrally above the photodiodes so that the fibre-optic window of the array was in contact with the output side of the fibre-optic faceplates.

8.2.1 Linearity and efficiency of photon production

Measurements of the response of the various scintillators to changes in the incident electron intensity were carried out in an identical manner to those described in chapter 7. The only difference was that the thinned single crystal YAG screens were not large enough in area to cover the whole array, so to ensure uniform illumination of a reasonable fraction of the 512 available photodiode elements the YAG screens were positioned across the array, such that their long axes were at right angles to the pitch of the diodes (see figures 8.7 b, c).

Figures 8.5 a-e show plots of the response of the screens under investigation to variations in the incident electron current, over the range accessible in the JEM 100C microscope.

Unfortunately this range is not wide compared to that likely to be found in an EELS spectrum, because of the necessity to keep the illumination uniform over the area of the array. As before the beam current measurements plotted along the horizontal axes are not absolute, because the illumination was defocussed. All the results of figure 8.5 were obtained using an integration time of 1 sec at an operating temperature of $0^{o}C$. In each case the response of the screens was found to be linear within experimental error. The response of the bulk YAG used in the previous chapter is included for comparison in figure 8.5c.

Some information on the relative detection efficiency of each scintillator can be deduced from the graphs of figure 8.5. This detection efficiency is not the same as the phosphor conversion efficiency discussed previously as it represents the number of photons recorded by the photodiode array per incident 100keV electron, which is subject to many other factors such as the coupling efficiency of the fibre-optics and the degree of spectral matching between the phosphor and the photodiode array. Values of detection efficiency normalised to that of the Mullard P20 screen are listed in table 8.1.

A more quantitative measure of scintillator efficiency was made by recording the signal produced by a small circular electron probe of diameter < 2.4mm. The probe was produced at a microscope magnification of 1600x using a 20μm selected area aperture, and the probe current was accurately measured using the Faraday cup. An oscilloscope was used to monitor the video output of the photodiode array, enabling the probe to be positioned so that the output signal was a maximum i.e. the incident beam was directly over the photodiodes. Figures 8.6 a-g show the recorded signals after subtraction of the dark signal. The integration times and probe currents are listed in table 8.2, as well as the integrated counts under each peak. The number of ADC counts can be converted to the number of recorded photons using the fact that the full well capacity of the Hamamatsu array is 4.7×10^{7} electrons (section 7.6.3) and the saturation video voltage is 2.8V (figure 7.18a). Each ADC count corresponds to 11474 diode electrons or 11474 recorded photons, assuming each recorded photon produces one diode electron-hole pair.

A comparison of the number of photons recorded per incident 100keV electron, normalised to that of the P20 screen gives reasonable agreement with table 8.1, except in the case of the Terbium screen. A glance at figure 8.6g shows the reason for the discrepancy is that the spreading of the light signal in this scintillator means that a non-negligible fraction of the photons are incident beyond the 2.5mm width of the array elements, and are therefore not recorded. A corrected signal based on the relative efficiency figure of table 8.1 is included in

Figure 8.5a Response of Mullard P20 Screen

to Variations in Incident Electron Intensity

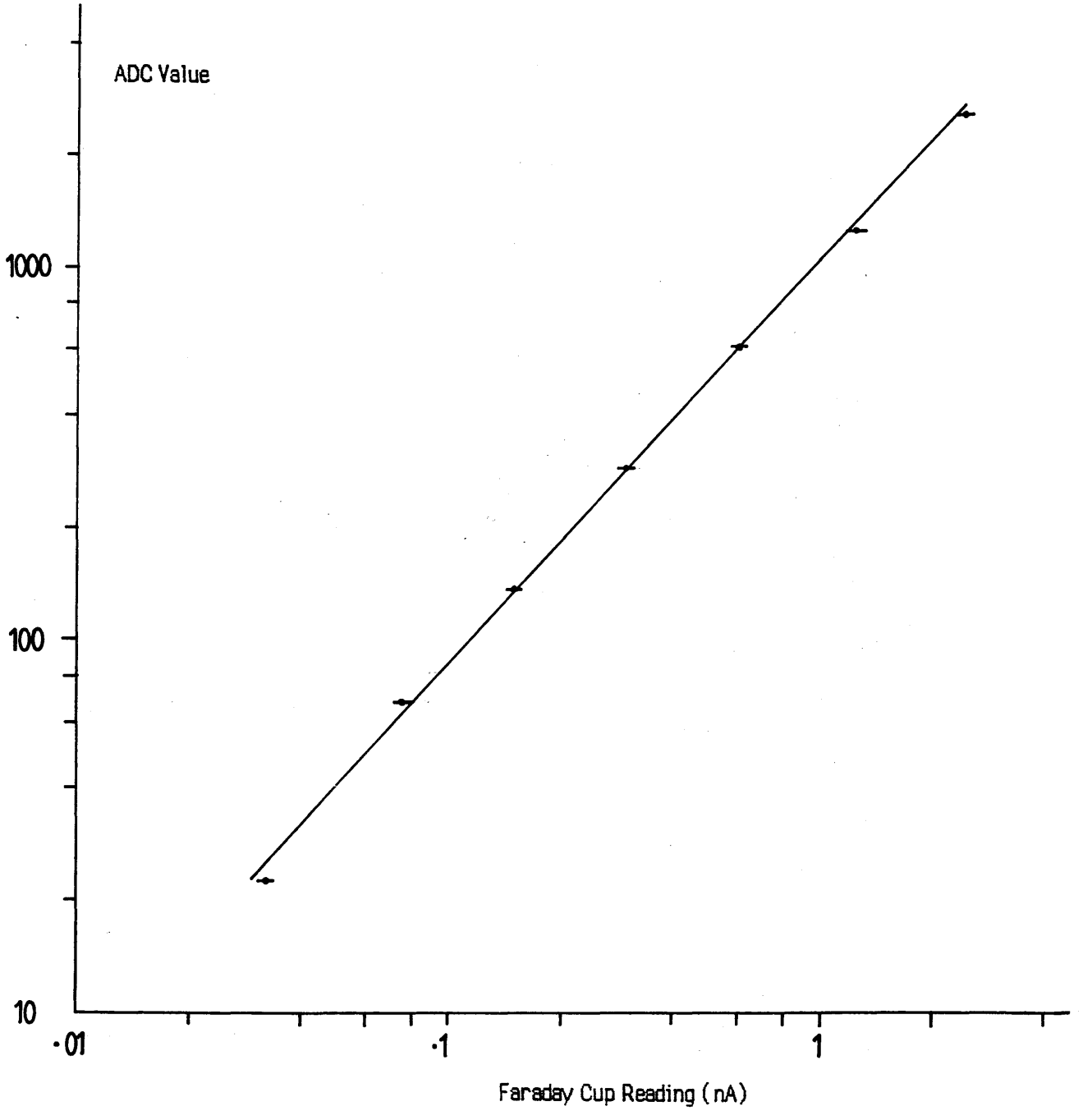

Figure 8.5b Response of Single Crystal YAG Screen B (50μm)

to Variations in Incident Electron Intensity

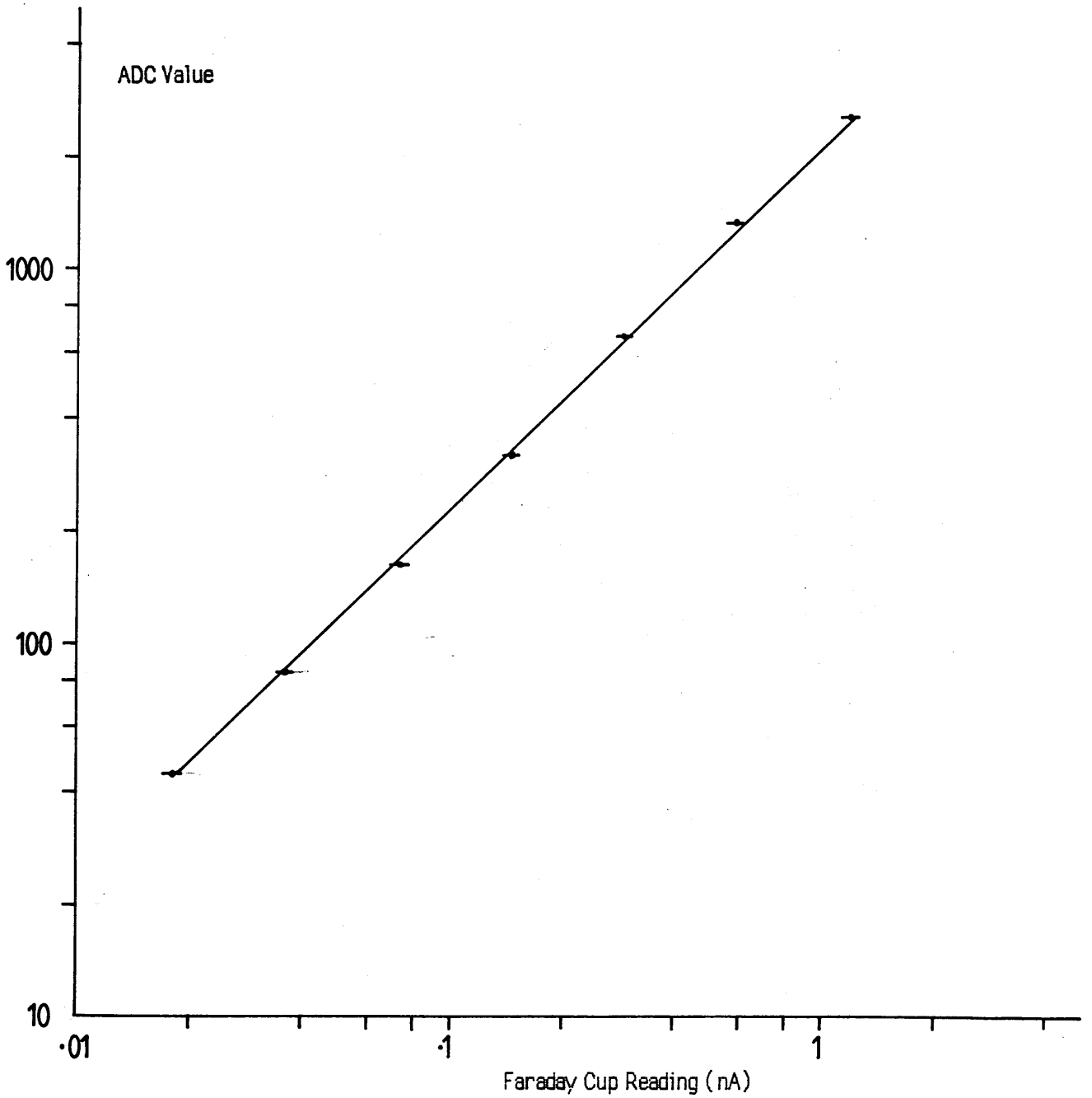

Figure 8.5c Response of Single Crystal YAG Screen A (30μm)

to Variations in Incident Electron Intensity

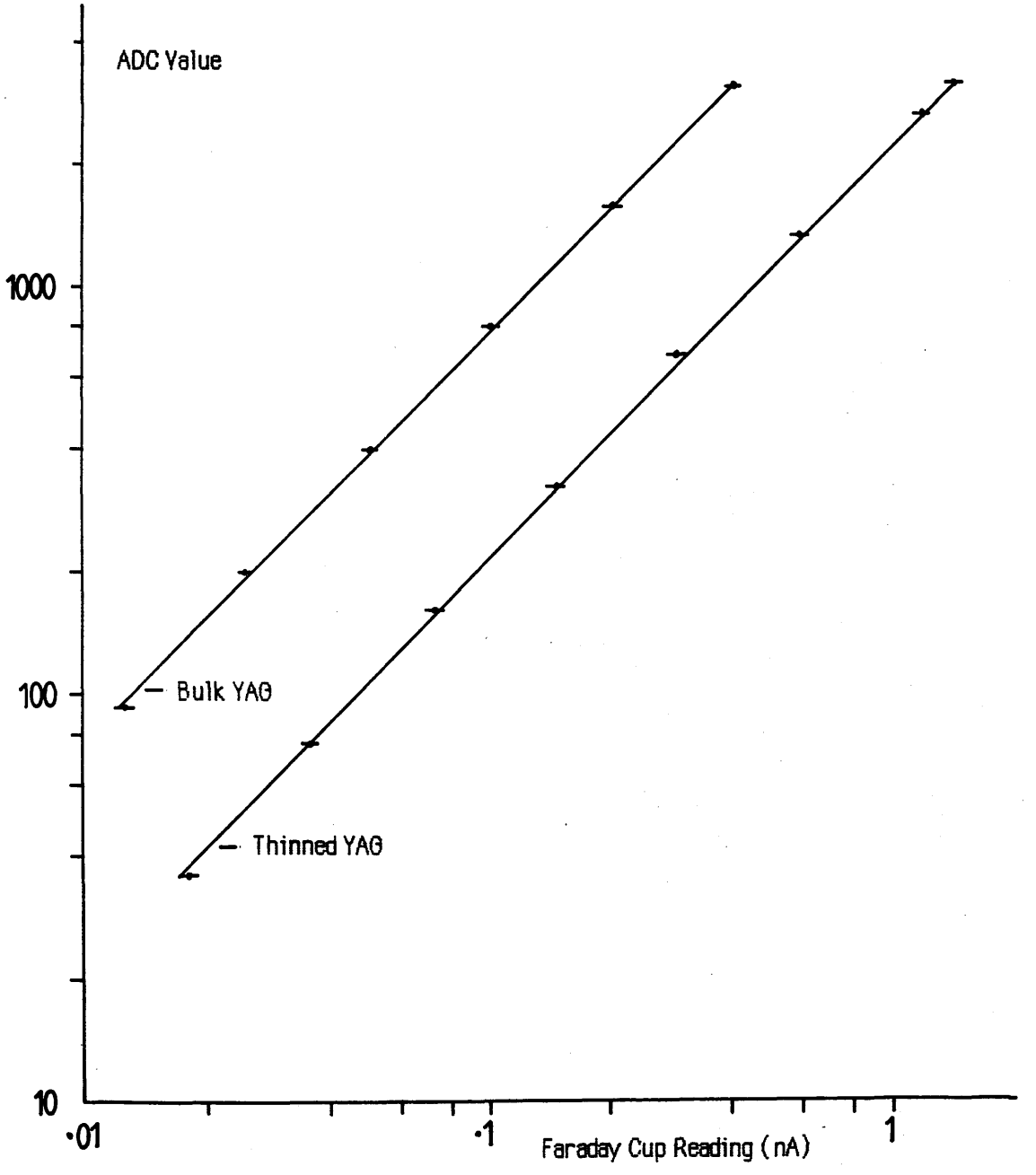

Figure 8.5d Response of Mullard P46 Powder Phosphor Screens to Variations in Incident Electron Intensity

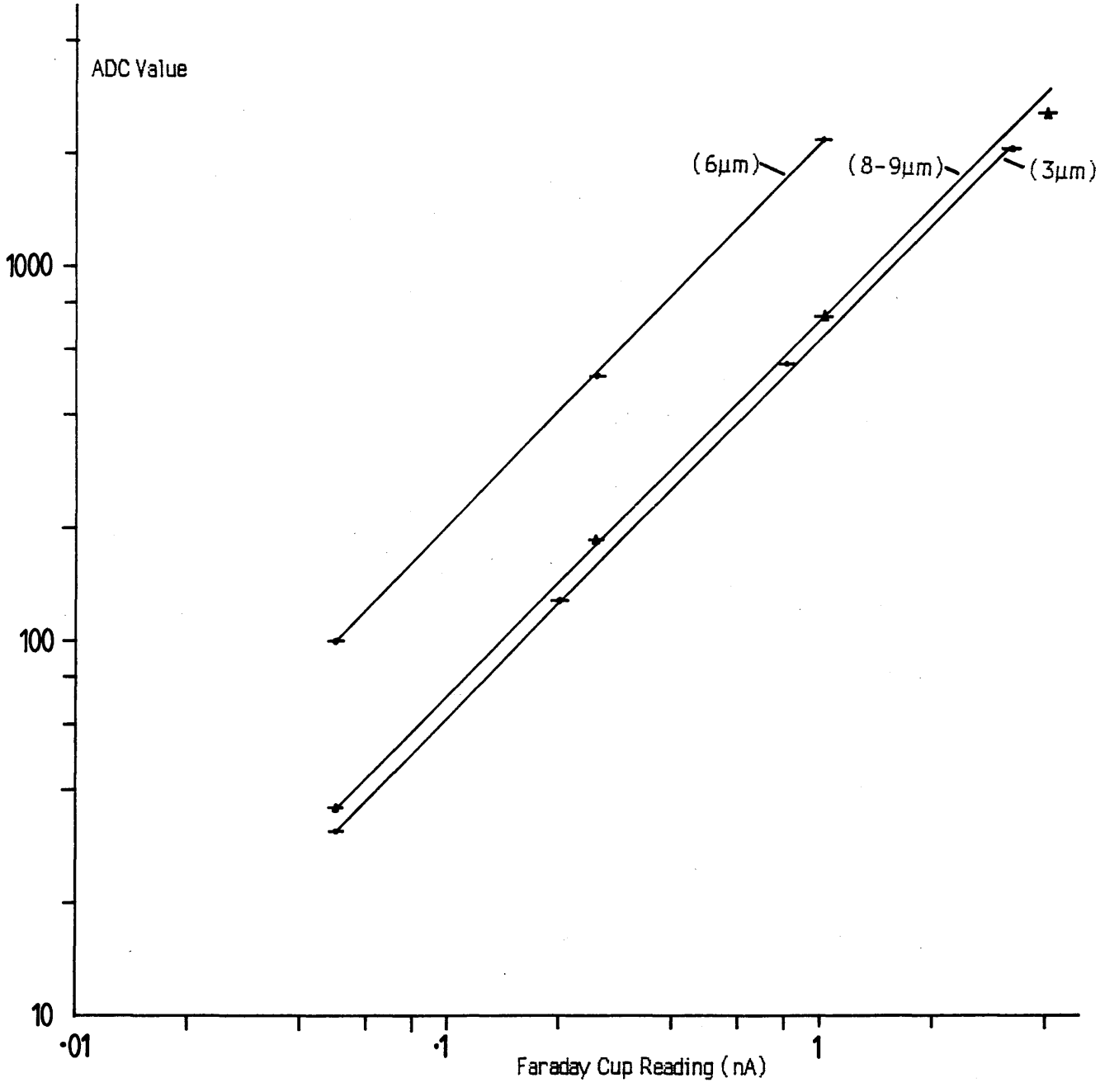

Figure 8.5e Response of Terbium Doped Fibre Optic Faceplate to Variations in Incident Electron Intensity

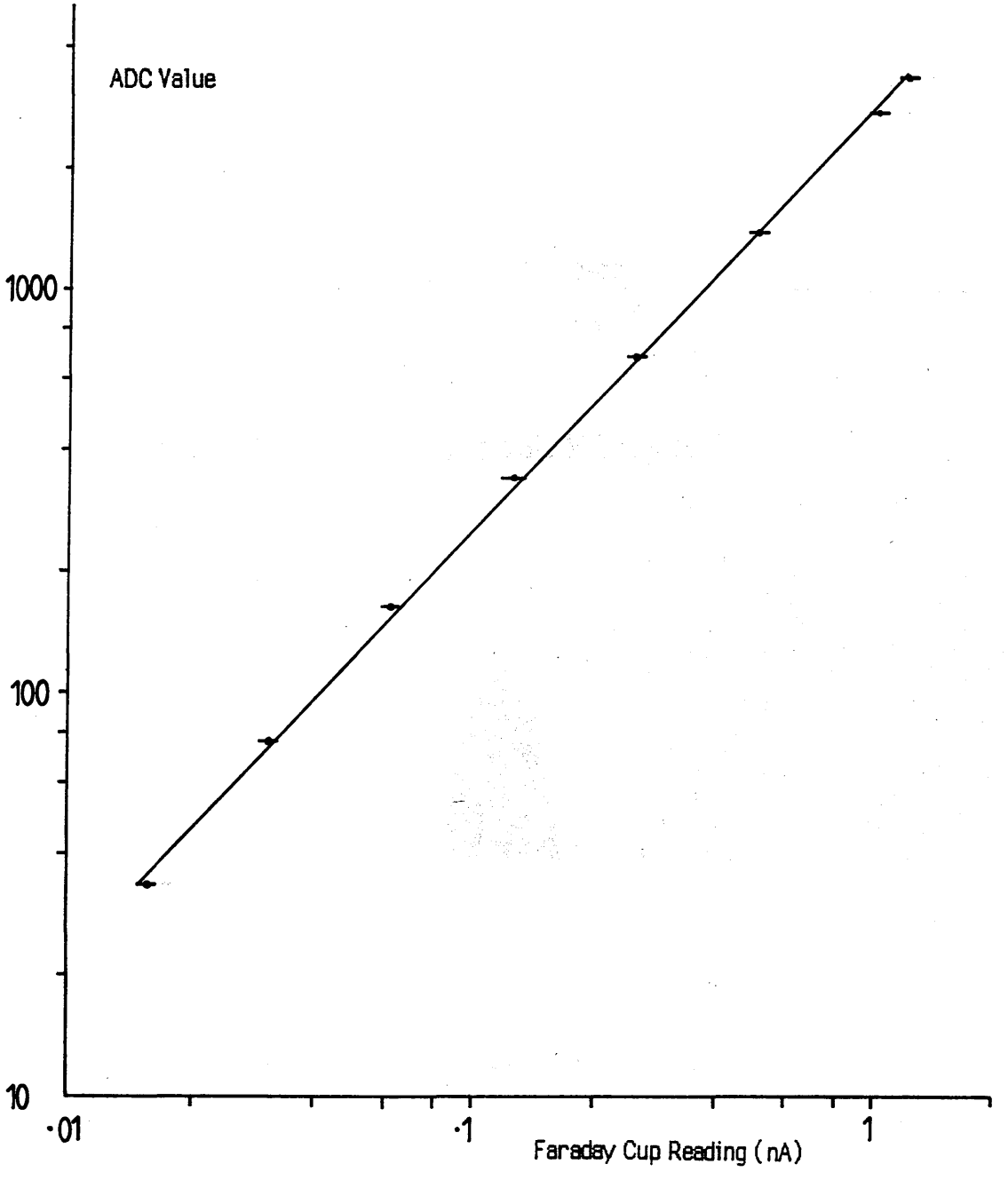

Figure 8.6a Mullard P20 Phosphor Screen

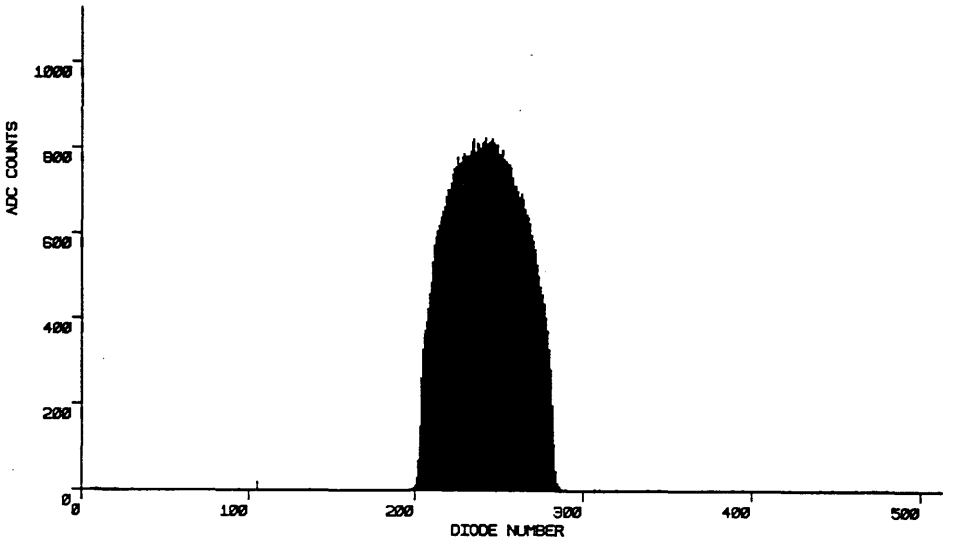

Figure 8.6b Single Crystal YAG Screen B (50µm)

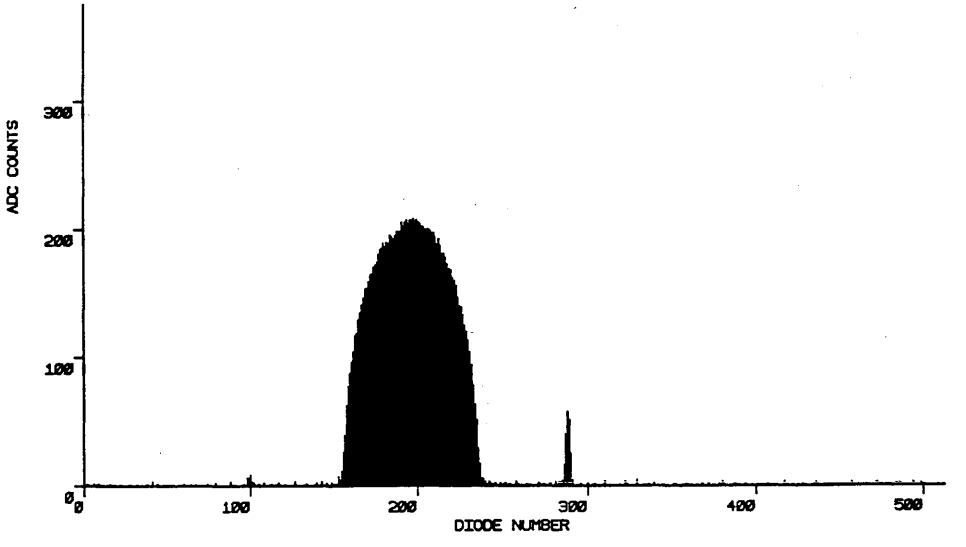

Figure 8.6c Single Crystal YAG Screen A (30µm)

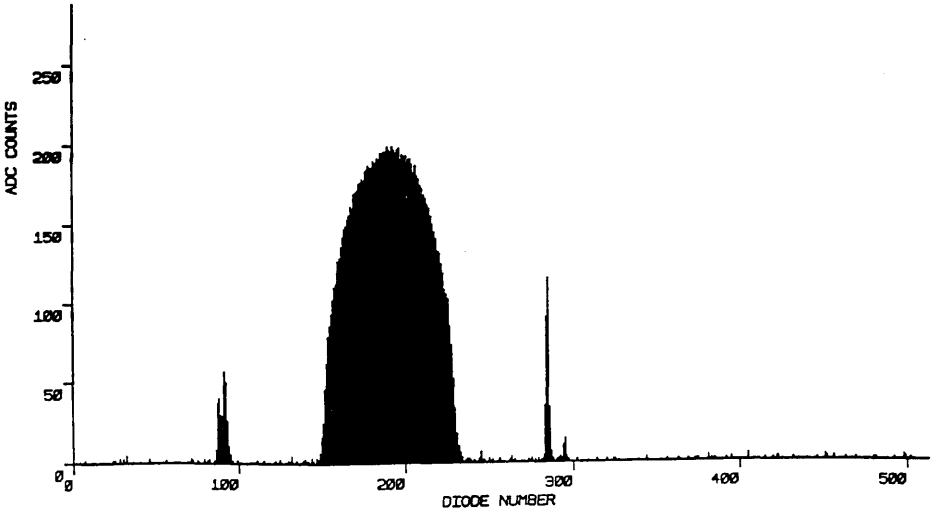

Figure 8.6d P46 Powder Phosphor Screen (8-9µm Grade)

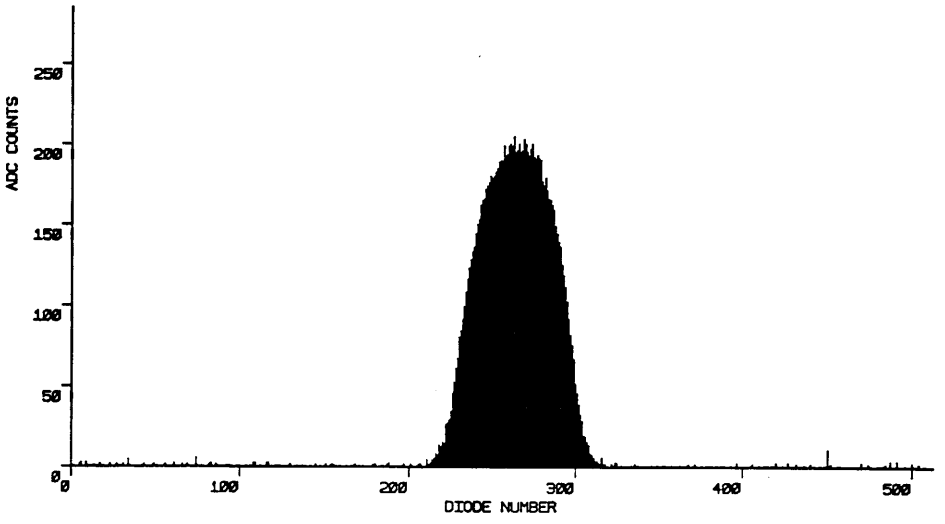

Figure 8.6e P46 Powder Phosphor Screen (6µm Grade)

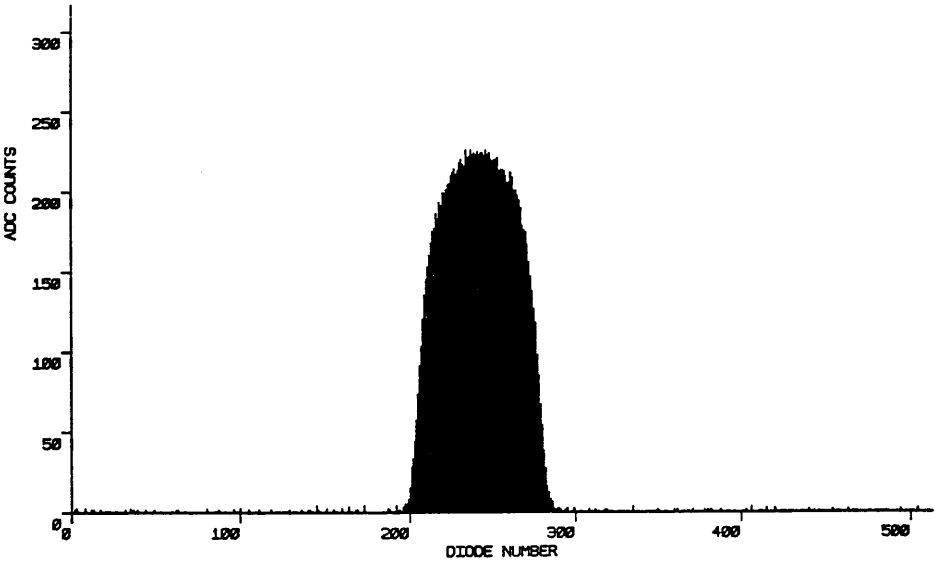

Figure 8.6f P46 Powder Phosphor Screen (3µm Grade)

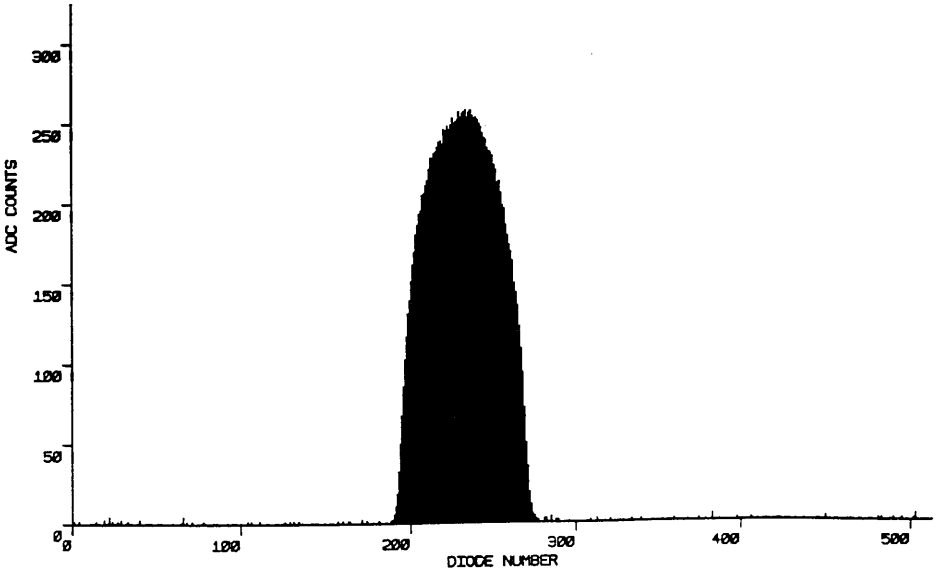

Figure 8.6g Terbium Doped Fibre Optic Faceplate

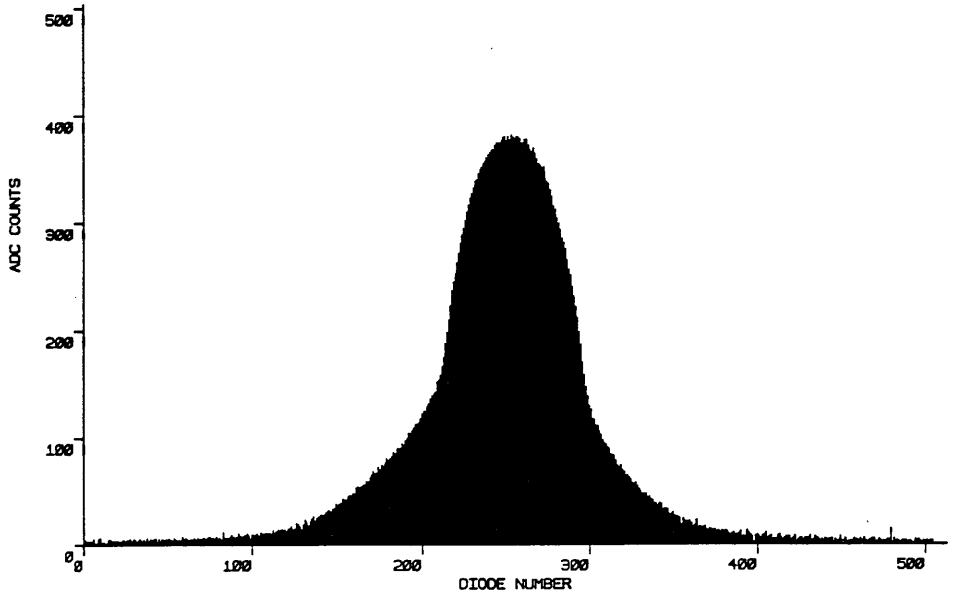

Table 8.1

Screen	Relative Efficiency	Non-Uniformity of Response
P20	1.0	±8.4%
P46 8-9μm	0.7	±4.7%
P46 6μm	2.0	±3.1%
P46 3μm	0.6	±17 %
YAG 30μm	2.2	±1.4%
YAG 50μm	2.2	±1.5%
YAG Bulk	7.7	-
Terbium	2.7	±1.2%

Table 8.2

Screen	Beam Current	Integration Time t	Total no. electrons	Integrated ADC Counts	Photons per e-	Relative Efficiency
P20	.00488nA	500msec	1.53×10^7	52804	40	1.00
P46 8-9μm	.01526nA	50msec	4.77×10^6	12085	29	0.73
P46 6μm	.00760nA	50msec	2.38×10^6	14707	71	1.78
P46 3μm	.02250nA	50msec	7.03×10^6	15470	26	0.65
YAG 30μm	.00615nA	50msec	1.92×10^6	12515	75	1.88
YAG 30μm*	.00615nA	50msec	1.92×10^6	12515	79	1.98
YAG 50μm	.00591nA	50msec	1.85×10^6	13147	82	2.05
YAG 50μm*	.00591nA	50msec	1.85×10^6	13147	83	2.08
Terbium	.04460nA	20msec	5.58×10^6	39139	81	2.03
Terbium**	.04460nA	20msec	5.58×10^6	39139	108	2.70
YAG Bulk**	-	-	-	-	308	7.70

* Including internally reflected light peaks

** Estimated from table 8.1

table 8.2.

There are two sets of figures for the YAG screens, the first are simply the integrated counts under the image peak and the second include the counts recorded at the edges of the crystal. Even these second figures are somewhat lower than expected, because most of the internally reflected light is piped out to edges of the crystal not imaged by the detector, and is therefore not recorded.

8.2.2 Linearity and efficiency of photon production:- discussion

The graphs of figure 8.5 establish that there are no obvious non-linear effects occurring in any of the screens that were tested, within the current range investigated. There is, however, a wide variation in the efficiency of the screens as a whole. By far the most efficient screen was the bulk single crystal YAG used in the previous chapter, at an estimated 308 photons recorded per incident 100keV electron. This higher figure is due mostly to the fact that the YAG screen was directly coupled to the fibre-optic window of the photodiode array and the matt output surface reduced total internal reflection effects.

The next highest performer was the terbium doped fibre-optic with a corrected figure of 108 photons/ e^-(100keV), reflecting the advantage of having the scintillator integral with the fibre-optic plate so that light loss is restricted to the boundary between the scintillator and the photodiode window.

The two thinned YAG screens showed very similar efficiencies of 79 and 83 photons/ e^-(100keV) for the 30μm and 50μm thicknesses respectively. The closeness of the two figures suggests that the optimum depth of 30μm which is calculated in section 8.3 is reasonable. Assuming that each incident electron produces ~1600 photons (see section 8.3.2) then the Mullard faceplate will couple ~960 of these to the photodiode input window. If losses at the interface are ignored, and the transmission of the Hamamatsu fibre optic window is also ~60%, then ~576 of these photons reach the photodiodes. The quantum efficiency of the Hamamatsu array is ~44% at the spectral response peak of YAG, giving a theoretical efficiency of 253 photons recorded per incident 100keV electron.

The fact that the experimental efficiency is so much less than the theoretical efficiency (and that of bulk YAG) is most likely due to internal reflections in the YAG discussed earlier, and possibly losses at the interface of the fibre plates. By comparison, figures published by Egerton and Crozier [1986] show an efficiency of ~250 photons recorded per 100keV

electron when using a 65 μm thick YAG screen fibre-optically coupled to a Reticon RL1024 SF photodiode array. The YAG had its output face matt finished to reduce total internal reflections, and the junction of the fibre-optic plate and the fibre-optic photodiode window was filled with a thin layer of silicon oil to reduce reflections at this interface. A resolution of 70μm was quoted (but not the contrast), and there was no measure of screen uniformity.

Of the P46 powder phosphors only one screen approached the efficiency of the single crystals and this was the 6μm grade, with a screen weight of 18mg/cm^2, which produced 71 photons/e$^-$(100keV). This was superior to the screens produced using the 3μm and 8-9μm grades of P46 which gave efficiencies of 26 photons/e$^-$(100keV) and 29 photons/e$^-$(100keV) respectively. The screen weight of the 3μm grade phosphor was 15mg/cm^2, and the reason for its comparative inefficiency when compared to the similar weight 6μm screen is the fact that light output from powder phosphors is known to decrease as the mean particle size falls below ~4μm. This phenomenon has been noted by Hill [1985] and McGee et al. [1966] among others. The result obtained for the 8-9μm grade screen reflects the fact that the weight of 35mg/cm^2 is too heavy to image 100keV electrons, and results in a thick inefficient screen with considerable self-absorption.

The P20 phosphor screen manufactured by Mullard gave an efficiency of 40 photons/e$^-$(100keV) which compares favourably with that of the less efficient P46 screens. The reason is of course that the screen weight is optimised for high resolution imaging of 10keV electrons and is therefore too thin to efficiently record 100keV electrons. The fact that it performs better than some heavier P46 screens is because the phosphor conversion efficiency is very much higher.

8.2.3 Uniformity of response and digital response correction

Figures 8.7 a-g show uniform illumination recordings after dark scan subtraction taken at approximately half scale using the different screens. Again all the data was recorded using a 1sec integration time at 0^{o}C. The percentage non-uniformity of response of each screen was calculated as in chapter 7 (using the 'highest-lowest' criterion) and is included in table 8.1. It can be seen that in general the powder screens show more variation, with finer grained screens giving more even diode-to-diode response, although the bulk thickness is more difficult to control (figure 8.7 f).

The terbium faceplate (figure 8.7 g) has the best response over the whole array length with a non-uniformity value of ~±1.2%. The two thinned YAG screens show almost as good

Figure 8.7a Response of Mullard P20 Phosphor Screen to Uniform Illumination

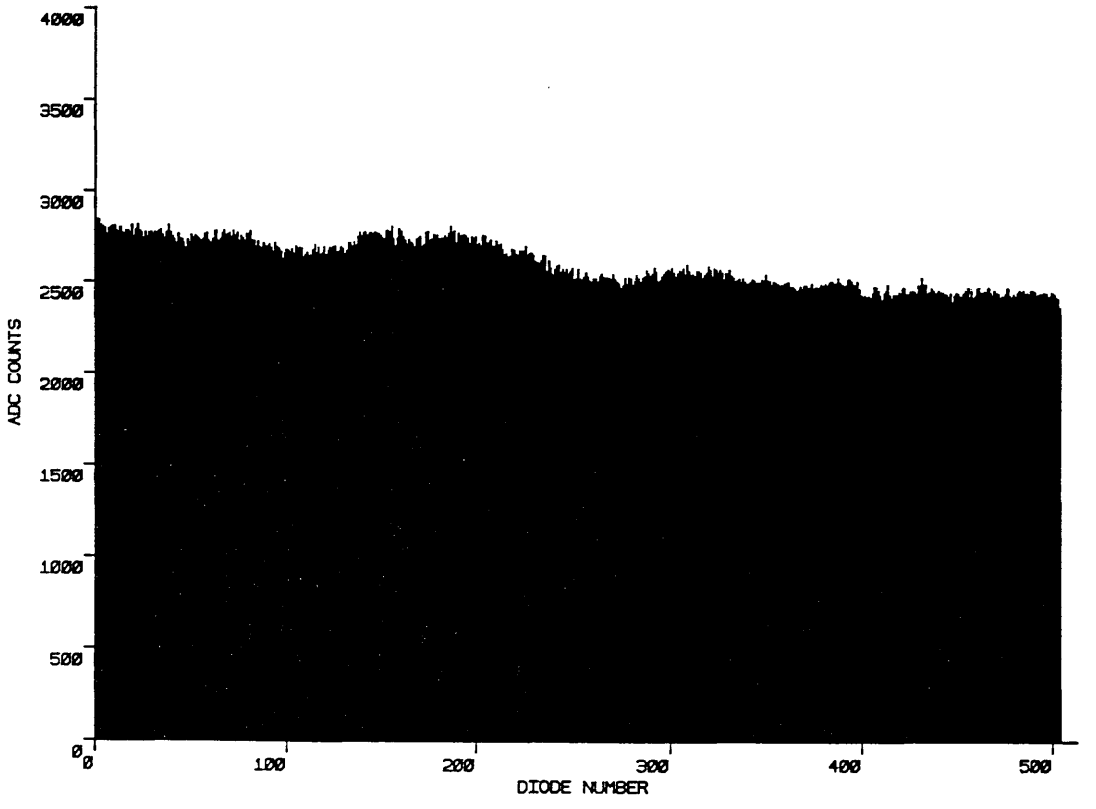

Figure 8.7b Response of Single Crystal YAG Screen B (50µm) to Uniform Illumination

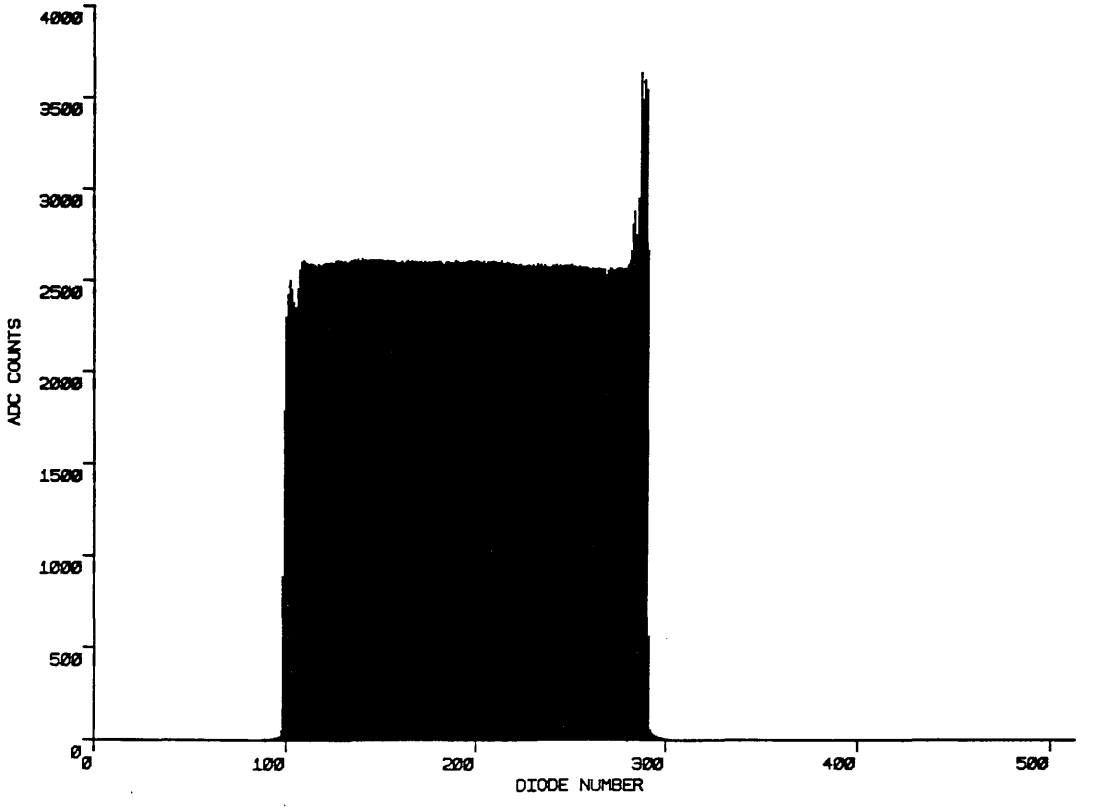

Figure 8.7c Response of Single Crystal YAG Screen A (30µm)

to Uniform Illumination

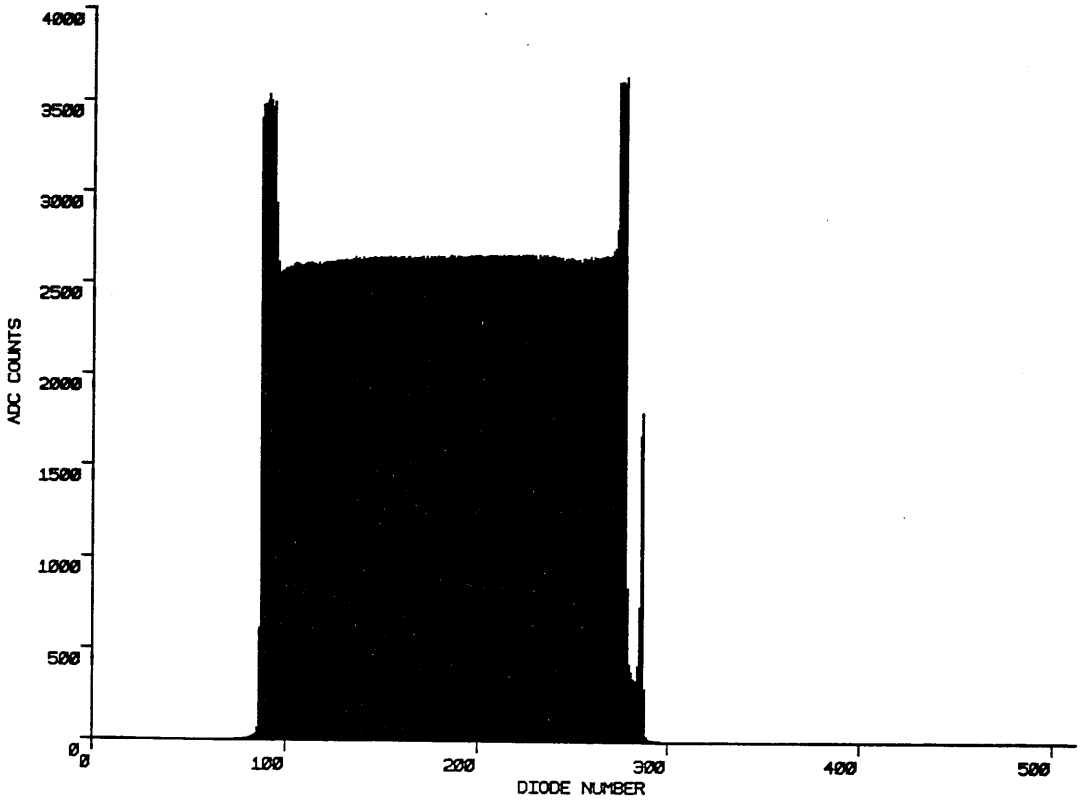

Figure 8.7d Response of P46 Powder Phosphor Screen (8-9µm Grade)

to Uniform Illumination

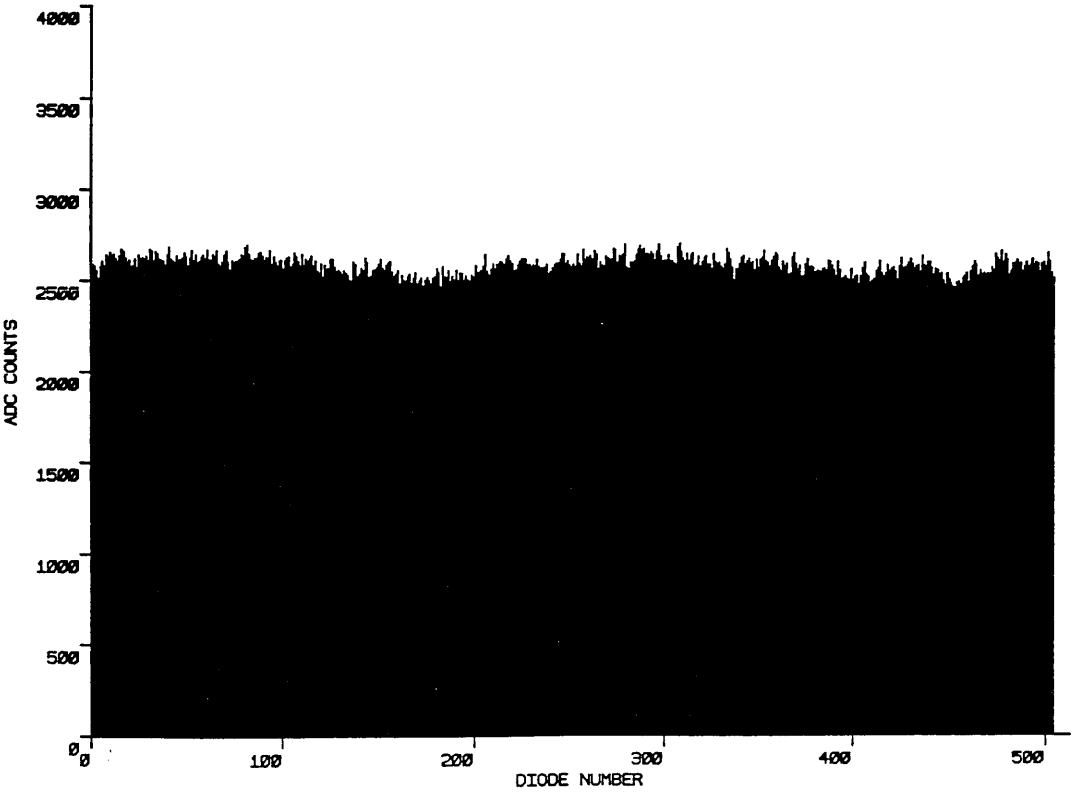

Figure 8.7e Response of P46 Powder Phosphor Screen (6µm Grade) to Uniform Illumination

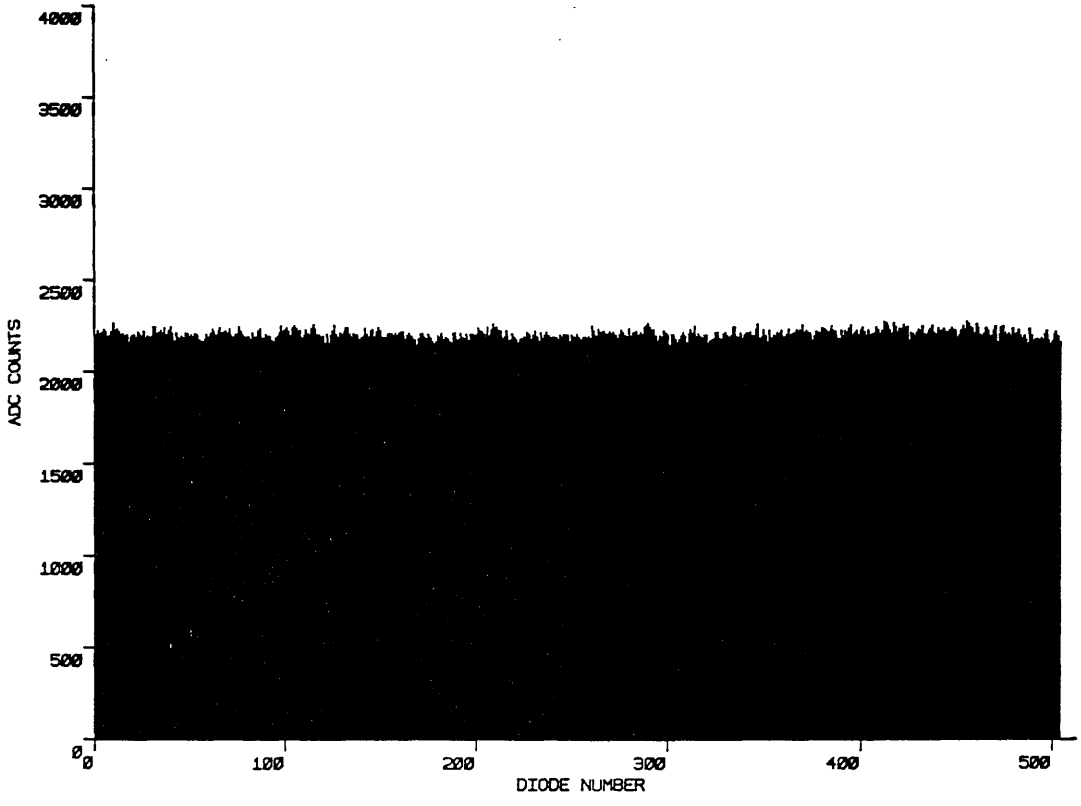

Figure 8.7f Response of P46 Powder Phosphor Screen (3µm Grade) to Uniform Illumination

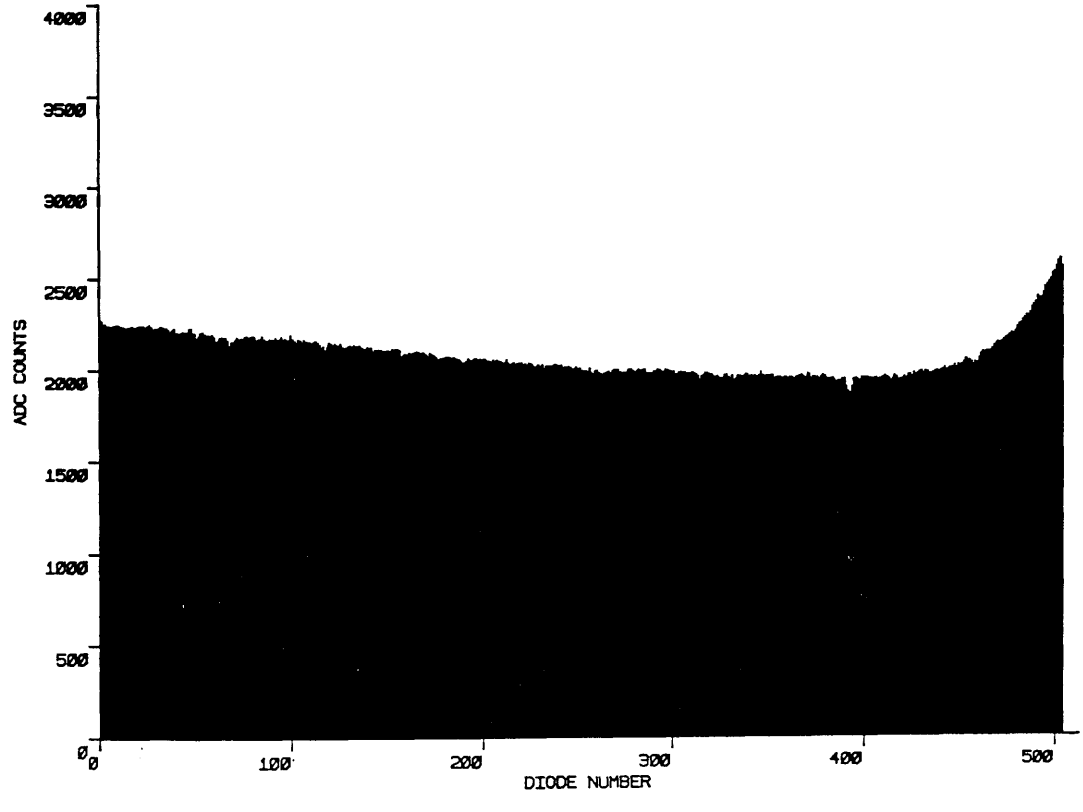

Figure 8.7g Response of Terbium Doped Fibre Optic Faceplate to Uniform Illumination

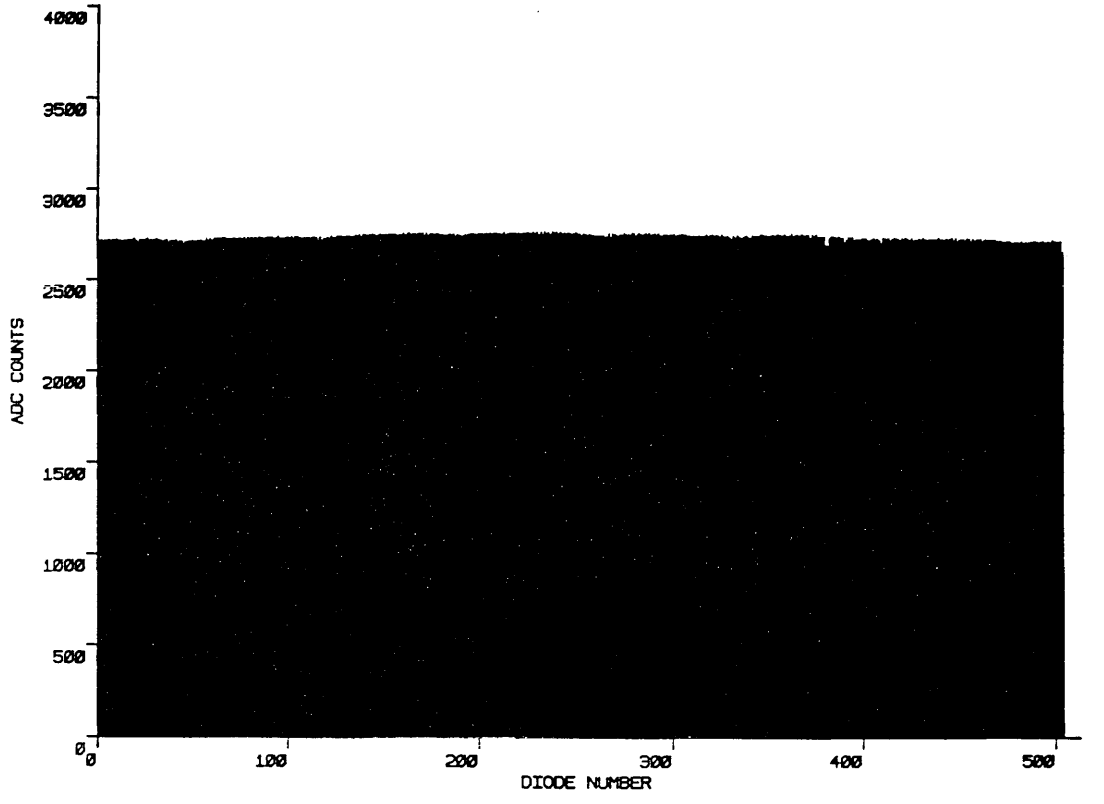

performance over their central area, but suffer markedly from the effects of 'light piping' at the edges (figures 8.7 b,c) due to total internal reflection. The thinner 30μm screen (screen A) seems to show this effect to a greater extent than the other (see also figs 8.6 b,c). It is not clear why one edge of the 50μm screen (screen B) should display the effect so much more than the other, unless it has something to do with the thickness or shape of the boundary glue layer. In practice an operational screen would be larger in area than the array elements, so that the edge effects would not be recorded. As mentioned previously a matt finish on the exit surface of the YAG reduces the internal reflections, but might possibly impair the uniformity of response.

The method of digital response correction described in chapter 7 was applied to all of the screens, and it was found that the 3σ non-uniformity of response for the thinned single crystal YAG screens and the Terbium screen could be reduced to below ±0.4% at half scale, while that of the powder screens was reduced to between ±0.5% and ±1% at mid-range.

8.2.4 Spatial resolution

The ultimate spatial resolution of the detector is limited to 20 line pairs (lp)/mm by the 25μm pitch of the photodiode elements. The resolution of each screen is determined by the degree of electron scatter and light spreading in the scintillator. The former is controlled by the average atomic number and density of the phosphor, and the latter mainly depends upon the screen thickness.

A measure of the resolution of each screen was obtained by projecting the shadow image of a 1000 mesh copper foil (~39 lp/mm) down onto the screen at very low magnification and recording the image produced. The square grid pattern of the foil had an aspect ratio of ~2:1 i.e. the distance between two adjacent copper grid lines was twice the thickness of each grid line. The foil was held in a tilt and rotate specimen holder, allowing the grid lines to be accurately aligned with the diode elements. By monitoring the video output from the array on an oscilloscope, the shadow image could be positioned and rotated so that the signal showed the greatest contrast.

In order to obtain sufficiently low magnifications the JEM 100C microscope was operated in free lens controller mode with the objective and second intermediate lenses switched off. The projector lens was run at a constant current of 139mA, and the magnification was varied using the first intermediate lens. The condenser control was turned fully anticlockwise, the spot size selected was 1 and condenser aperture 1 (400μm) was inserted. In this way

magnifications of < 3x could be achieved with minimum distortion. To maintain a relatively constant illumination it was found to be necessary to reduce the gun bias as the magnification was decreased.

The factors which limit the highest spatial frequencies and image contrast that can be achieved using this method are electron optical image distortions incurred in the projection lenses. As the magnification is decreased the image aberrations tend to increase causing the shadow image axes to depart from orthogonality. Thus precise alignment of the grid lines with the photodiode elements becomes impossible, and the image contrast is decreased.

Figure 8.8a is an enlargement of a micrograph taken at a magnification of ~2.6x. The fine mesh is 2000 lines per inch, and the spatial frequency of the micrograph is ~30 lp/mm. At this low magnification there is some evidence of 'pincushion' type distortion in the image, resulting in a slight curvature of the fine mesh lines especially near the edges. It can be seen that the contrast of the coarse grid is very much better than that of the fine mesh; this is due to a combination of microscope aberrations degrading the actual image at the film plane, electron spread in the film, and optical limitations imposed by the enlarging process. For the actual experiment a 1000 mesh foil was supported over a 1 x 2mm slot so that the coarse grid bars of figure 8.8a were not imaged.

Figures 8.9 a-c are signals recorded from the Mullard P20 screen at spatial frequencies of 3.2, 8, and 13 lp/mm respectively. The area of array illuminated decreases at the higher spatial frequencies because the size of the shadow image was unavoidably reduced at the lower magnifications. The degree of contrast varies from >90% at 3.2 lp/mm, to 67% at 8 lp/mm, to >20% at 13 lp/mm. At the higher spatial frequencies the shading effect seen in the diode scans could be due to variations in the spatial frequency of the image caused by the aberrations described previously. It is also quite possible that some aliasing is taking place as the spatial frequency in the image approaches the Nyquist limit for the detector (20 lp/mm) resulting in a reduction in contrast of the recorded scan.

Results using the 50μm YAG screen (screen B) are presented in figures 8.10a-c and similar data obtained from the 30μm YAG (screen A) is displayed in figures 8.11 a-c. Screen B gives a contrast of 80% at 3.6 lp/mm, falling to 50% at 7.3 lp/mm and 30% at 10 lp/mm. In comparison screen A gives contrasts of 90% at 2.8 lp/mm, 50% at 8 lp/mm and 40% at 10 lp/mm.

Figure 8.8a Shadow Electron Image Of 2000 Mesh Cu Foil

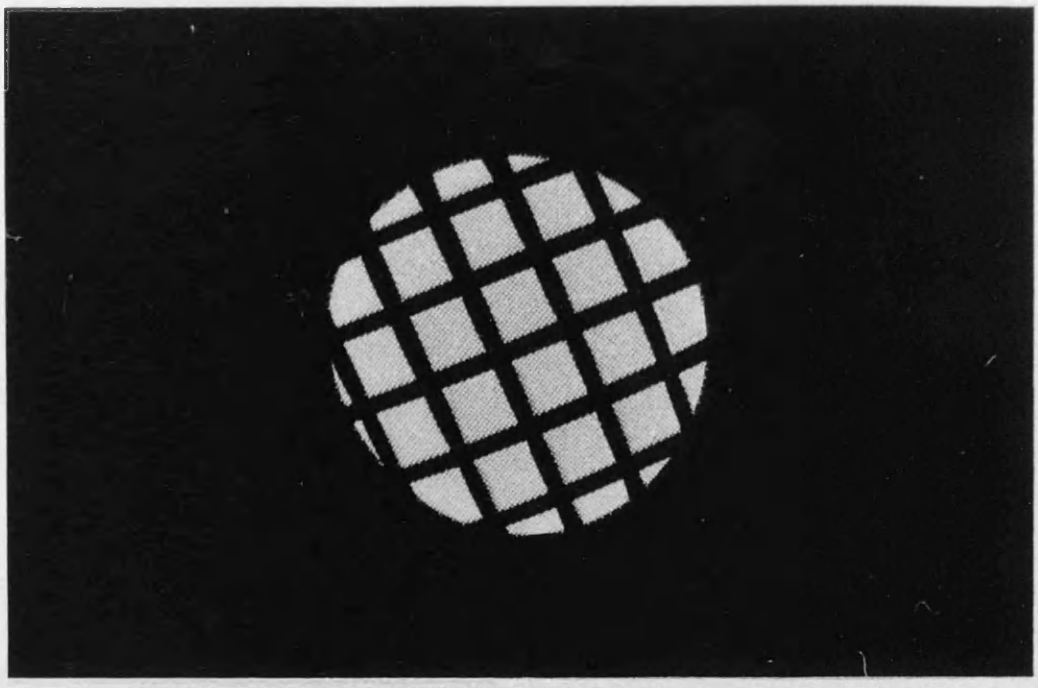

Spatial frequency of micrograph = ~30 lp/mm

Figure 8.9 a,b,c Spatial Resolution of Mullard P20 Phosphor Screen

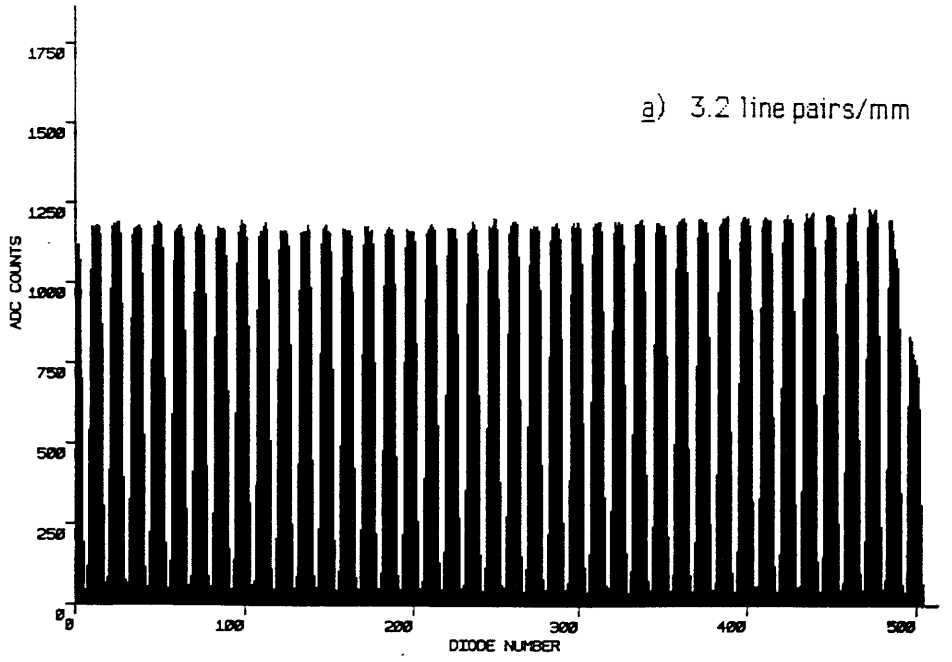

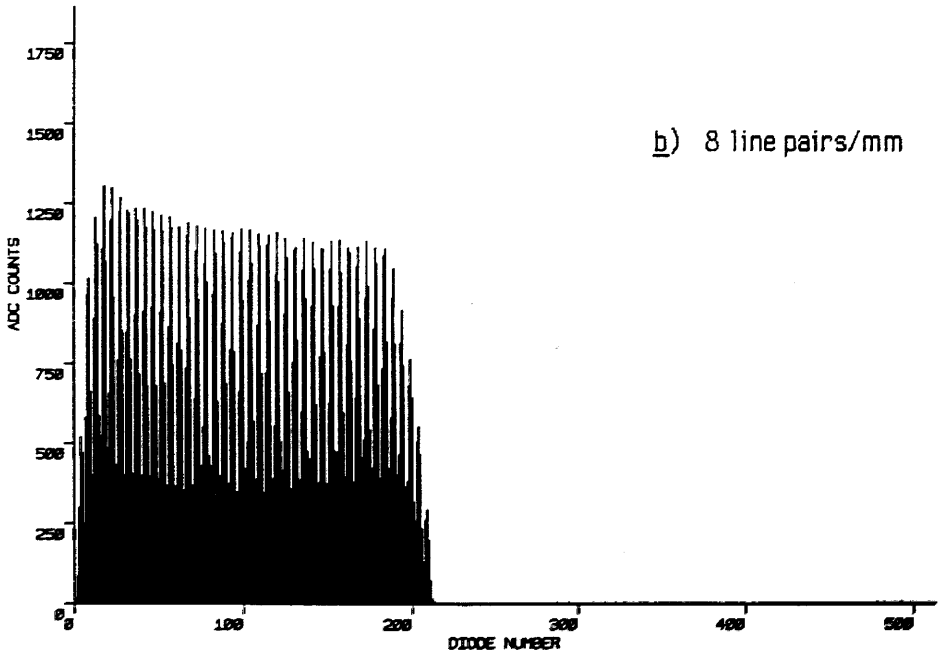

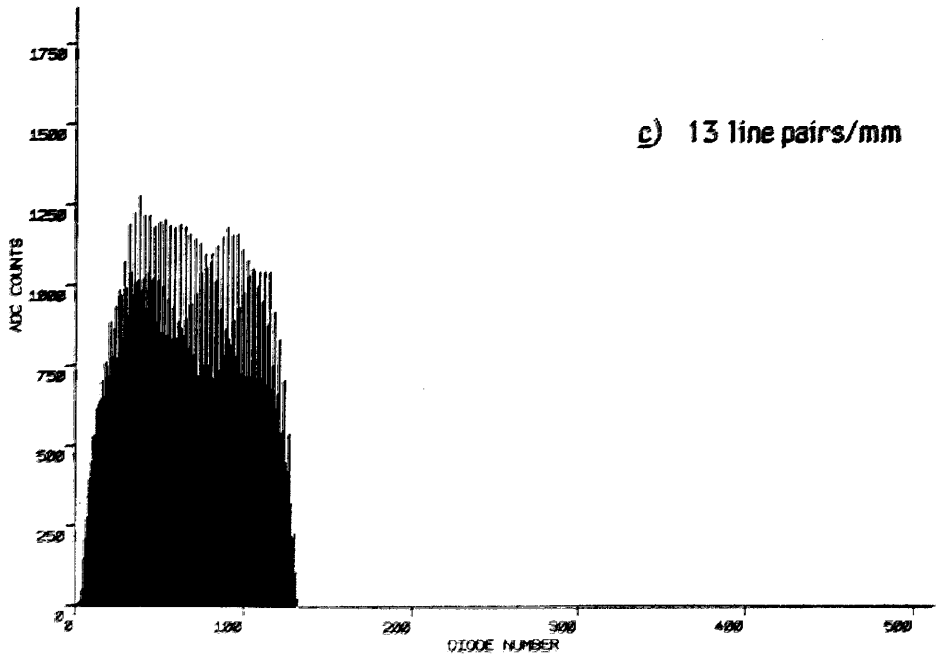

Figure 8.10 a,b,c Spatial Resolution of Single Crystal YAG Screen B (50µm)

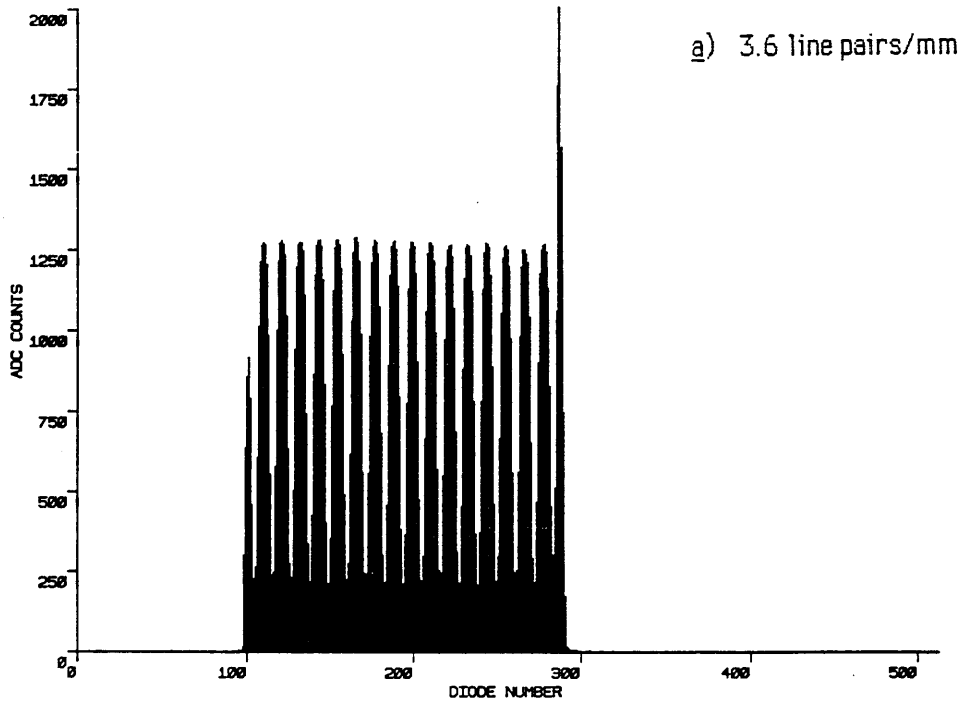

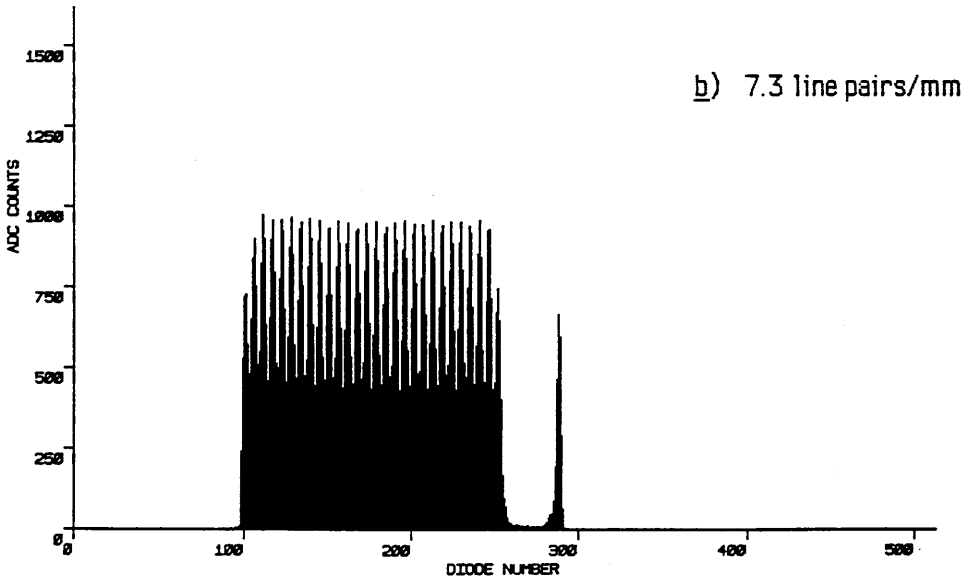

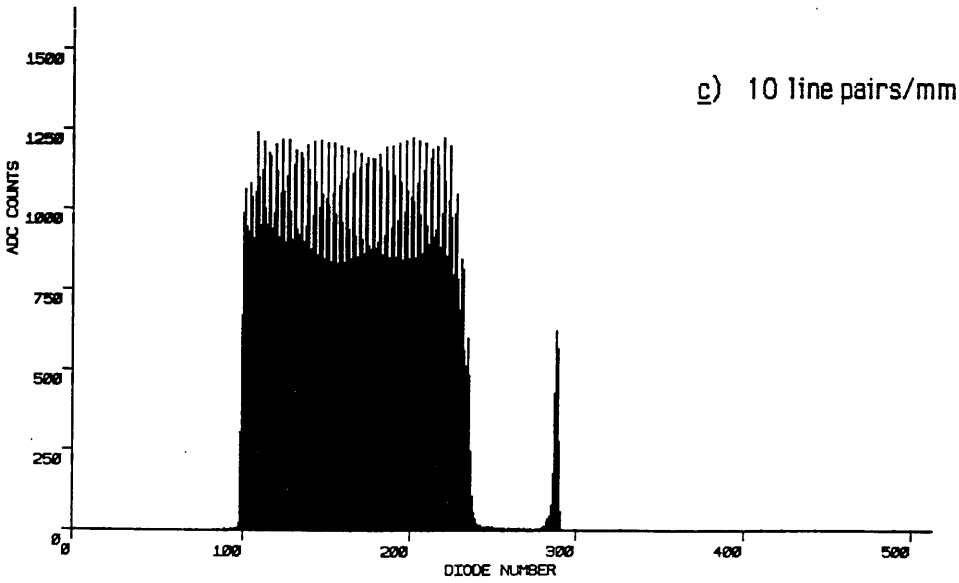

Figure 8.11 a,b,c Spatial Resolution of Single Crystal YAG Screen A (30μm)

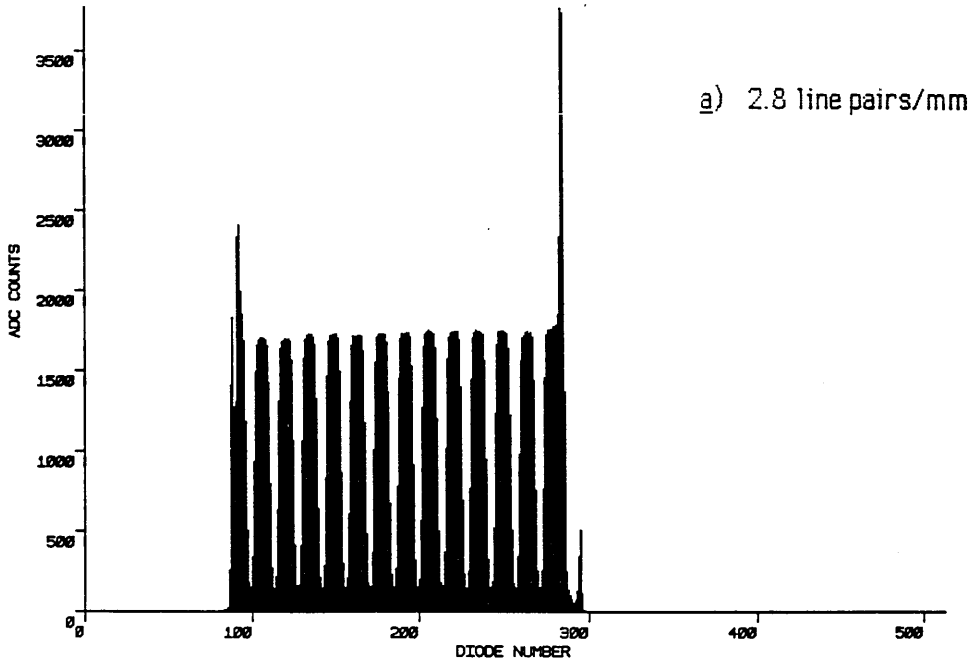

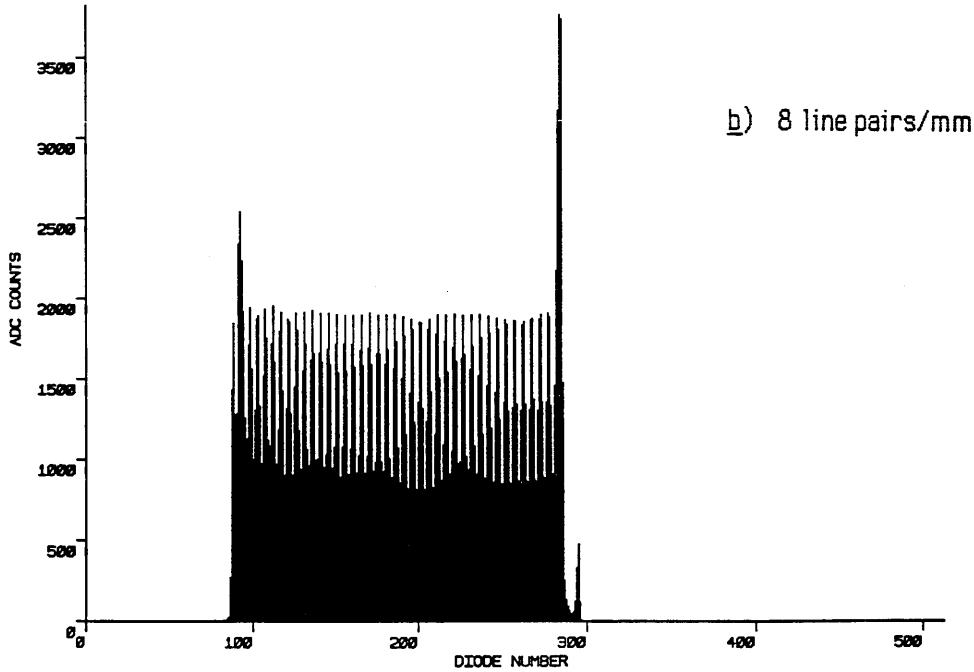

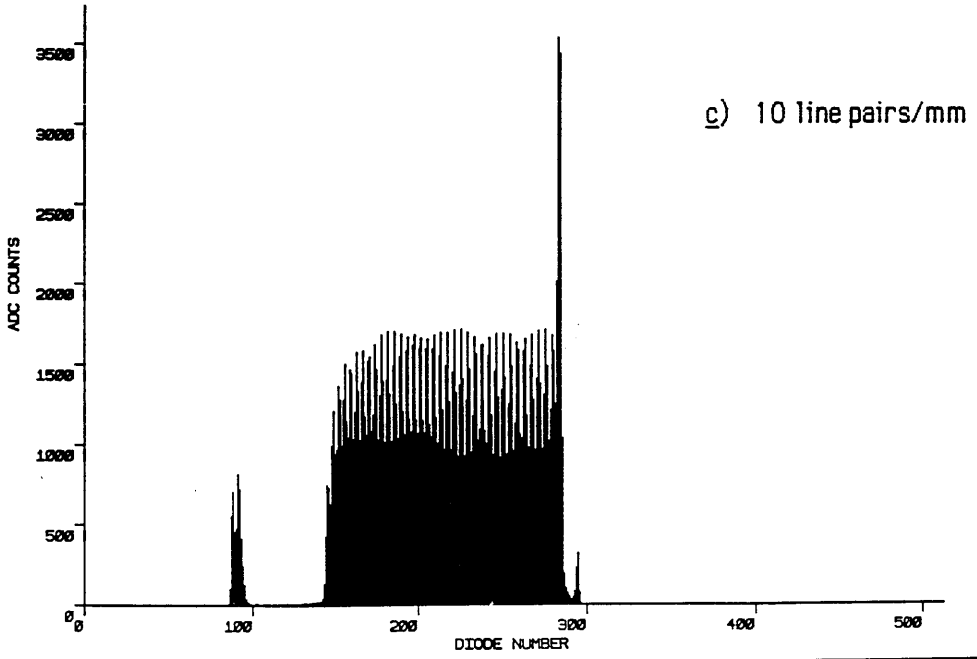

Figure 8.12 a,b,c Spatial Resolution of P46 Powder Phosphor Screens

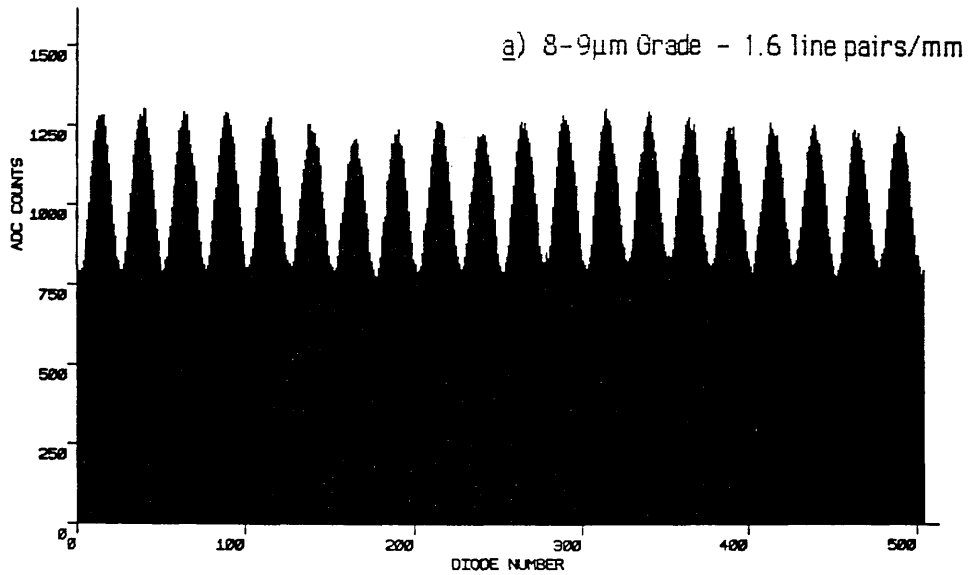

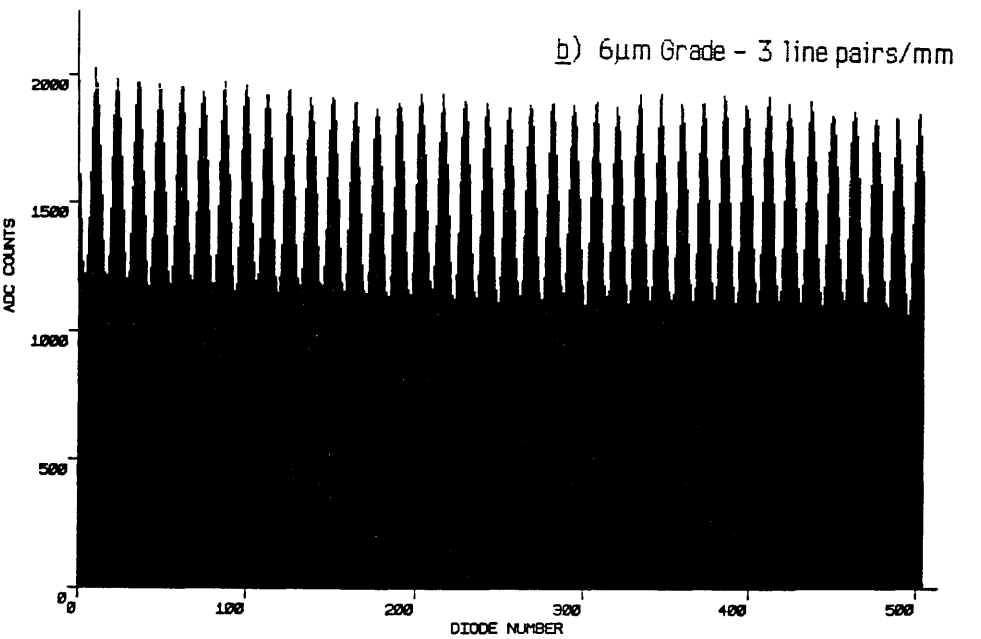

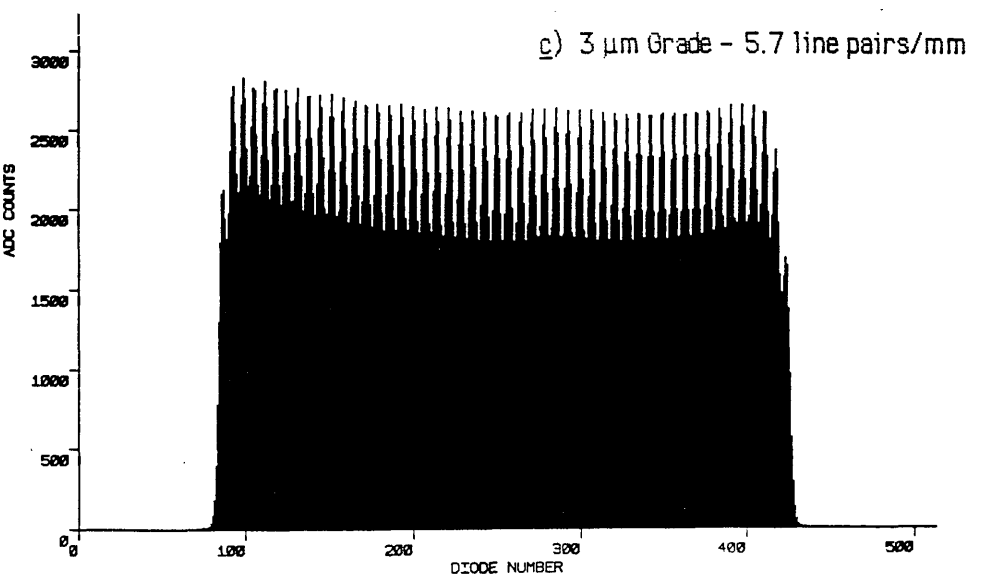

Figure 8.12 d Spatial Resolution of Terbium Doped Fibre Optic Faceplate

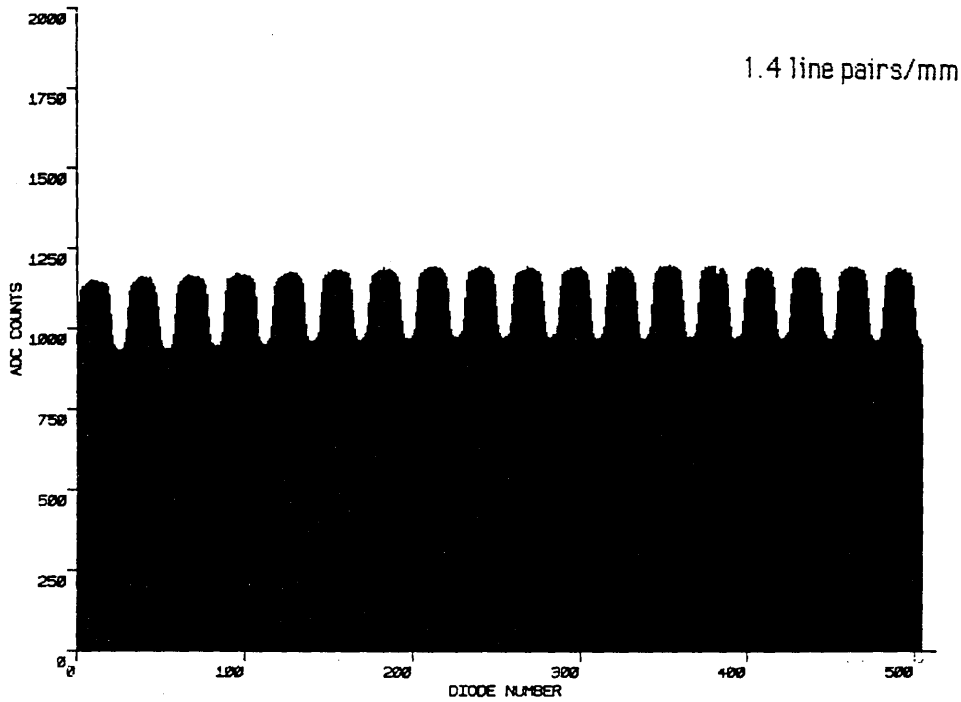

Figures 8.12 a,b,c are scans taken using the powder P46 screens of 8-9μm, 6μm and 3μm grades respectively. The contrast for the 8-9μm grade phosphor shown in figure 8.11a is 35% at a spatial frequency of 1.6 lp/mm. The 6μm grade P46 displays 47% contrast at 3 lp/mm in figure 8.12b, and the finest 3μm grade has a 30% contrast at 5.7 lp/mm in figure 8.12c. The terbium doped fibre optic plate gave a contrast of less than 20% at 1.4 lp/mm as illustrated in figure 8.12d.

As expected, the best resolution was obtained using the Mullard P20 screen with its thin layer of phosphor, however the performance of the single crystal YAG screens was not very much inferior, with the 30μm screen being predictably the better of the two. The resolution of the P46 powder phosphor screens is directly proportional to screen thickness (hence screen weight) and also tends to increase as the particle size decreases as shown in figure 8.12a-c. It can be seen that, for the screen weights tested, the contrast is limited by light scatter in the phosphor layers to give resolution levels much poorer than the P20 or thinned YAG screens.

Predictably, from figure 8.6g, the poorest resolution of all was found in the terbium doped fibre-optic plate. It was noted that varying the electron accelerating voltage between 20 and 100keV produced no substantial change in the image contrast or resolution, suggesting that it is light and not electron scatter within the plate which is the limiting factor. The particular sample investigated did not contain any form of extra-mural absorption (EMA), which would help to reduce the light spreading illustrated in figure 8.12d and also in figure 8.6g. It can only be concluded that, unless the screen is mechanically thinned like the YAG specimens, the resolution without EMA is much poorer than other luminescent screens commonly used in electron microscopy.

8.2.5 Measurements of principal decay times

Precise measurements of the decay times of fast scintillators requires carefully controlled experimental conditions and specialised high speed electronics- none of which were available at the time of these experiments. However, if absolute measurements could not readily be carried out then certainly comparative results could be obtained, and upper limits placed upon the principal decay times of each of the phosphors examined.

The experimental apparatus was set up as in figure 8.13. A special vacuum flange for the JEM 100C microscope was designed and constructed to allow the fibre-optic plates carrying the luminescent screens to act as vacuum windows. This flange replaced the STEM detector

Figure 8.13 Measurement of Principal Decay Times

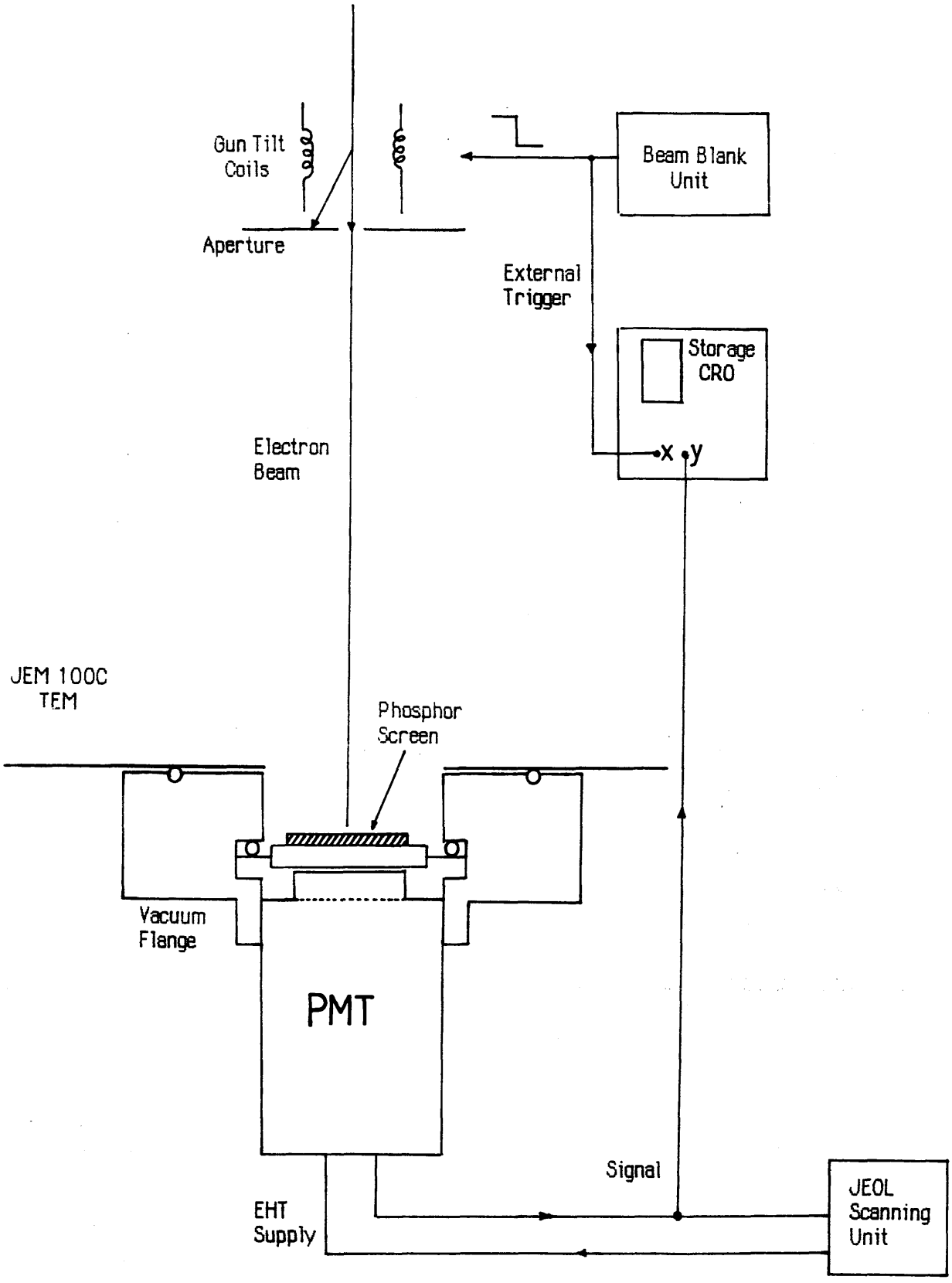

unit beneath the camera chamber of the microscope. A modified photomultiplier screw fitting was attached to the outside of the flange enabling a standard JEOL photomultiplier tube (PMT) to be directly coupled to the output face of the fibre-optic plates.

The microscope was operated in scanning mode with the scanning unit set to spot mode, i.e. the scan coils were disabled. The beam was instead deflected using a beam blank unit which automatically applied a current pulse to the microscope tilt coils causing the beam to be shifted onto the condenser aperture mechanism. The output voltage from the PMT (0v to ~-7v max) was applied to the Y input of a Tektronix storage oscilloscope, and the X triggering was taken directly from the beam blank unit. Thus deflection of the electron beam from the phosphor screen triggered the oscilloscope to store and display the voltage output from the PMT, the rate of decay of which was proportional to the scintillator time constants.

Clearly the time resolution of this apparatus was limited mainly by the speed of the beam deflecting electronics and the bandwidth of the oscilloscope input amplifier. The voltage risetime of the blanking signal applied to the microscope tilt coils was measured to be ~2μsec and the corresponding current risetime, which is the important quantity, is likely to be much slower due to the inductance of the coils. Taking this into account, the input bandwidth of the oscilloscope was set at 1MHz in order to suppress any signals faster than the beam blank action.

Figure 8.14a shows the initial decay of the Mullard P20 screen to be quite fast, the output drops by 50% in <1msec. This figure agrees well with the published specification (Mullard data sheets) which is 0.5msec to the 1/e (37%) point. After the fast primary decrease in output intensity a slower decay phase becomes dominant, the output is still ~16% of the initial value at 19msecs after removal of the beam. Figure 8.14b is taken using a slower timebase indicating that the output falls below 1% after ~500 msecs.

The principal decay time of YAG in P46 or single crystal form has been measured by Autrata et al [1983a] to be ~80nsec to 37% which is far too fast for this system to resolve. Figure 8.15a is the decay curve recorded for the 3μm grade P46 phosphor showing a drop to 50% in ~100μsecs, which is 3 orders of magnitude longer than the above specification. Obviously the rate of decay is limited by the blanking system rather than the YAG decay time, and no sensible information about the principal decay time, other than it is less than 100μsecs, can be derived from the figure. All the other YAG screens measured displayed curves of similar form.

Figure 8.14a Initial Decay of Mullard P20 Screen

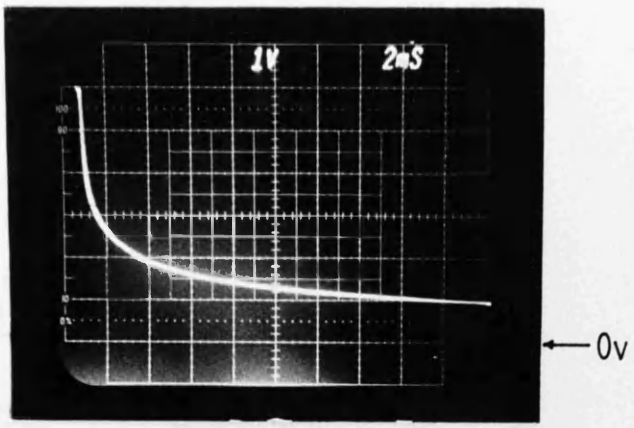

Figure 8.14b Secondary Decay of Mullard P20 Screen

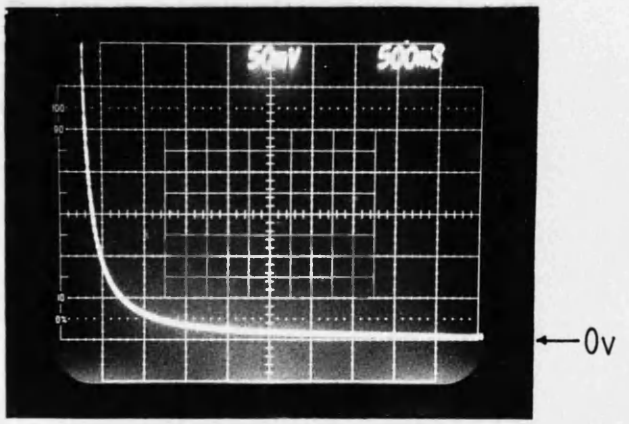

Figure 8.15a Initial Decay of 3µm Grade P46 Powder Phosphor Screen

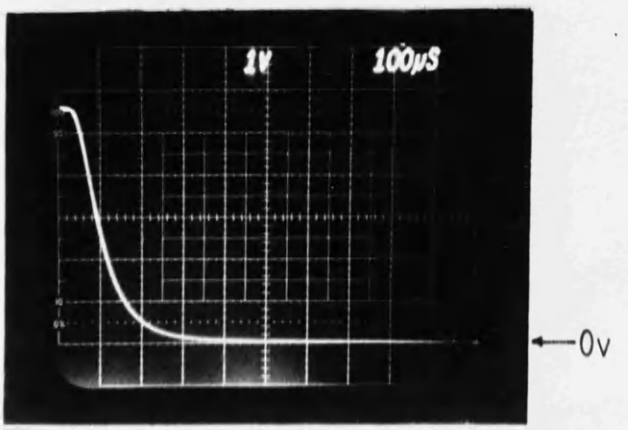

Figure 8.15b Secondary Decay of 3µm Grade Powder Phosphor Screen

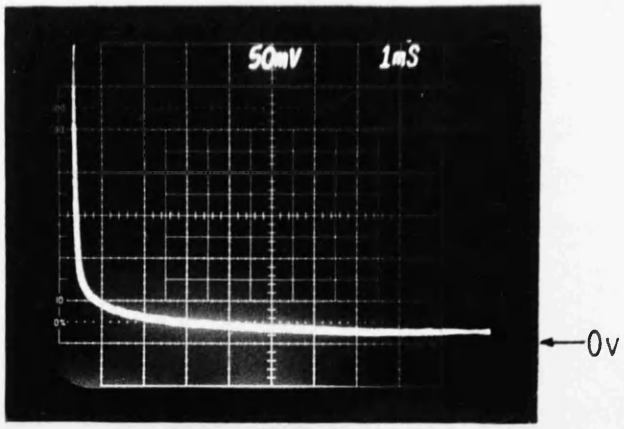

Figure 8.15c Secondary Decay of Single Crystal YAG Screen A

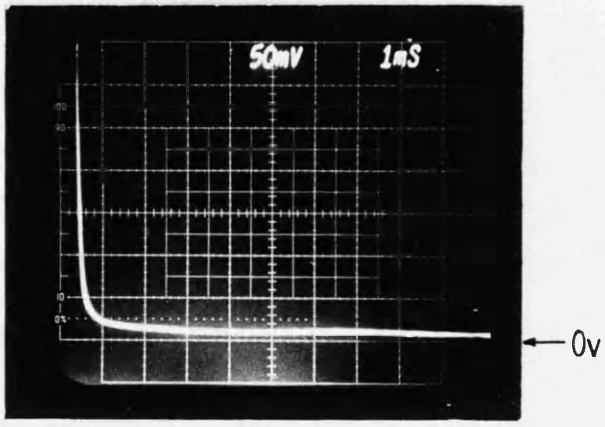

Figure 8.16 Initial Decay of Terbium Doped Fibre Optic Faceplate

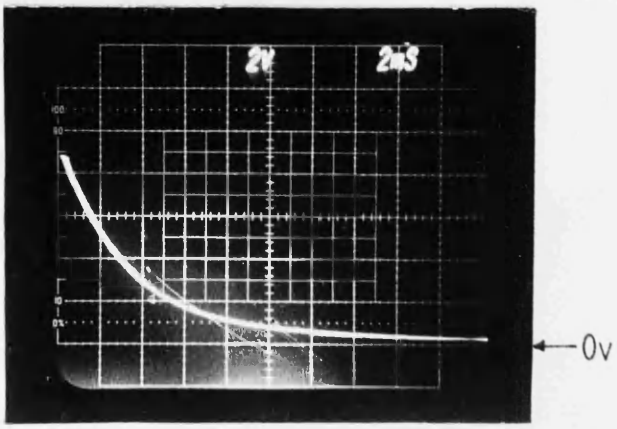

Figure 8.15b and 8.15c are recordings of the decay curves of 3μm grade P46 phosphor and the thinned single crystal YAG screen A respectively, captured using a longer timebase. Interestingly, the initial decay is very fast as expected, but there exists a comparatively long-lived secondary effect at around 0.005% of the initial intensity. The gradient of this secondary decay seems to be slightly greater for the powder phosphor. A close examination of the 'tail' of figure 8.15c seems to show the light output actually increasing at one point which is clearly impossible- it must be assumed that this effect is due to some external electrical interference, possibly mains frequency interference.

The principal responses of the other YAG based screens were found to be very similar, and the secondary effects are investigated in more detail in the next section. The final trace, figure 8.16, displays the decay curve of the terbium scintillator which exhibits a slow principal decay, reaching 50% in ~2msecs and 10% at ~10 msecs. The presence of any long term decay constant for this screen is also discussed in the next section.

8.2.6 Examination of secondary time constants

Most phosphors exhibit decay characteristics with more than one time constant, generally because their light production involves more than one radiative process, each different mechanism having its own associated decay time. Usually there is a comparatively fast primary decay constant, such as those illustrated previously, and one or more slower secondary time constants at lower intensities. These secondary time constants can cause a long-lived afterglow or 'ghost' image to be retained. Obviously this kind of effect is undesirable for parallel EELS as it may introduce artefacts into the data, particularly when recording a low-level signal soon after an intense signal.

Figure 8.17a is a dark scan taken using an integration time of 5 secs at a temperature of $0^{o}C$, ~10 secs after uniformly irradiating the single crystal YAG screen A for 1 minute at a high current density (7.5nA Faraday cup reading). There is a clear ghost image superimposed upon the dark signal, and figures 8.17b-f illustrate the decay of this image at five minute intervals, showing that the signal is just about detectable 25 minutes after the original irradiation. Similar results were obtained for the other single crystal YAG screen. Figure 8.18 is a graph of the integrated counts in each scan (after subtraction of the dark signal) as a function of time. The uncertainties are due to errors incurred in the dark signal subtraction. It appears that there are many time constants involved in this decay process, as the points lie on a smooth curve, however it is clear that these decay constants are of the order of several minutes.

Figure 8.17 a-f Dark Scan Single Crystal YAG Screen A

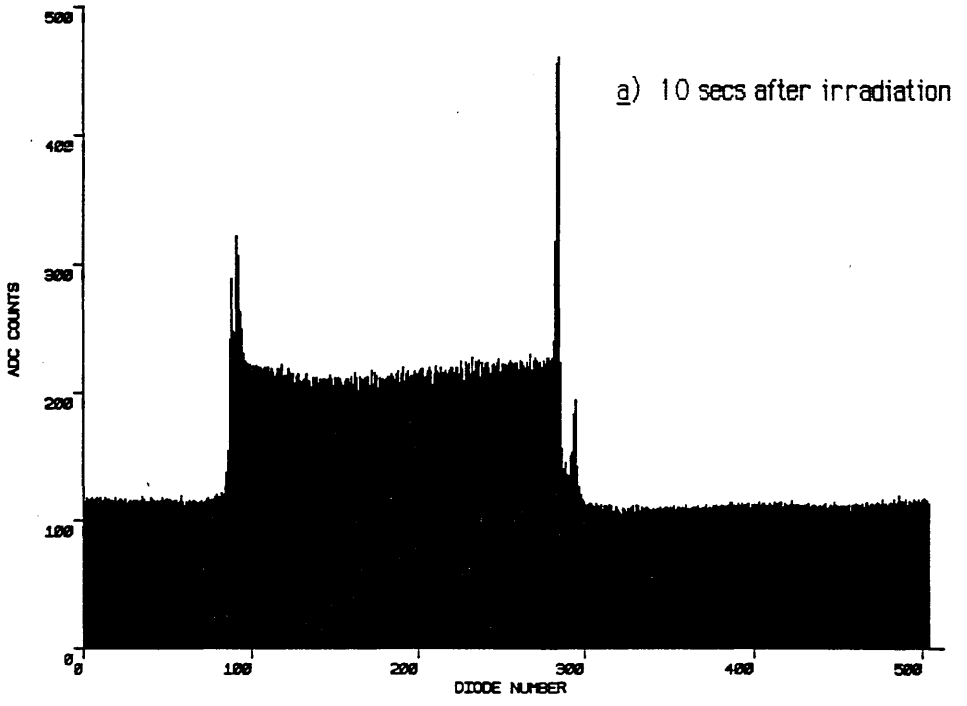

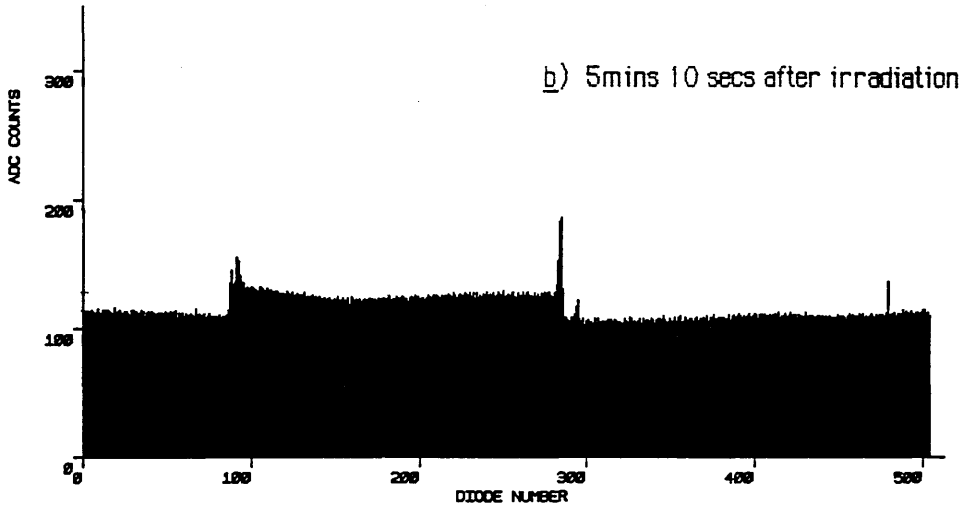

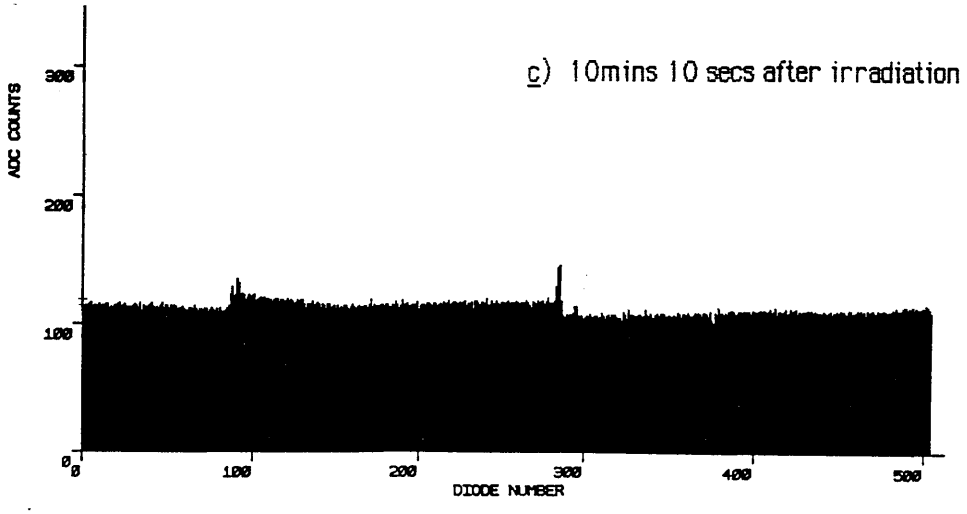

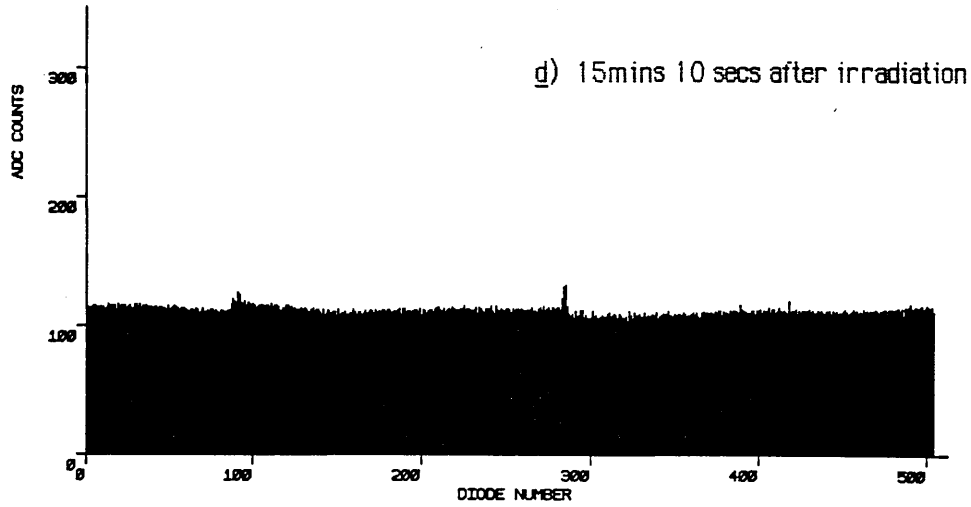
d) 15mins 10 secs after irradiation
ADC COUNTS
300
200
100
0
0
100
200
300
400
500
DIODE NUMBER

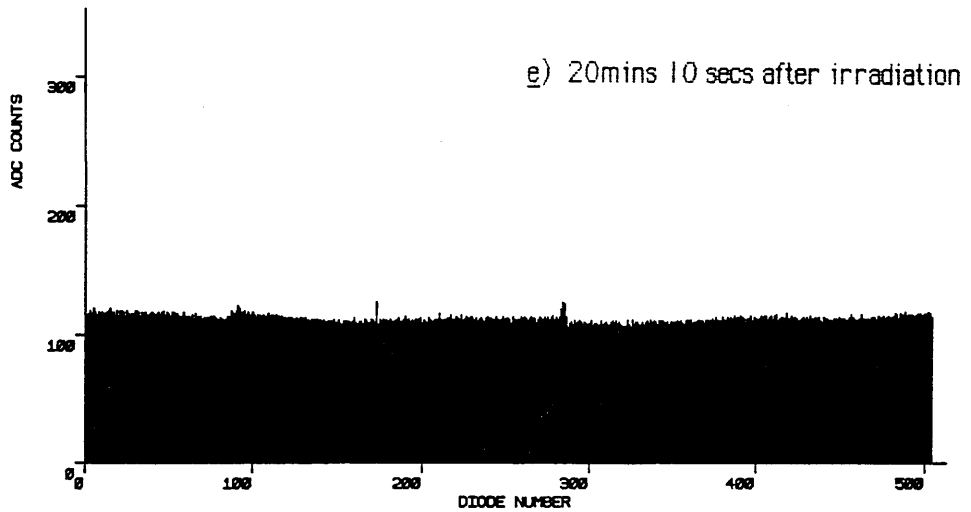
e) 20mins 10 secs after irradiation
ADC COUNTS
300
200
100
0
0
100
200
300
400
500
DIODE NUMBER

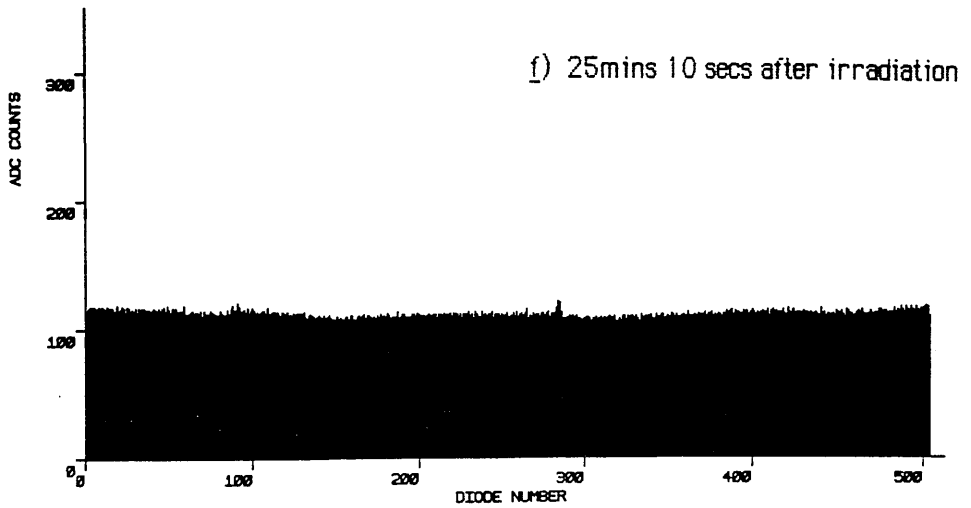
f) 25mins 10 secs after irradiation
ADC COUNTS
300
200
100
0
0
100
200
300
400
500
DIODE NUMBER

Figure 8.18 Variation of Integrated Counts In 'Ghost' Image With Time

Single Crystal YAG Screen A

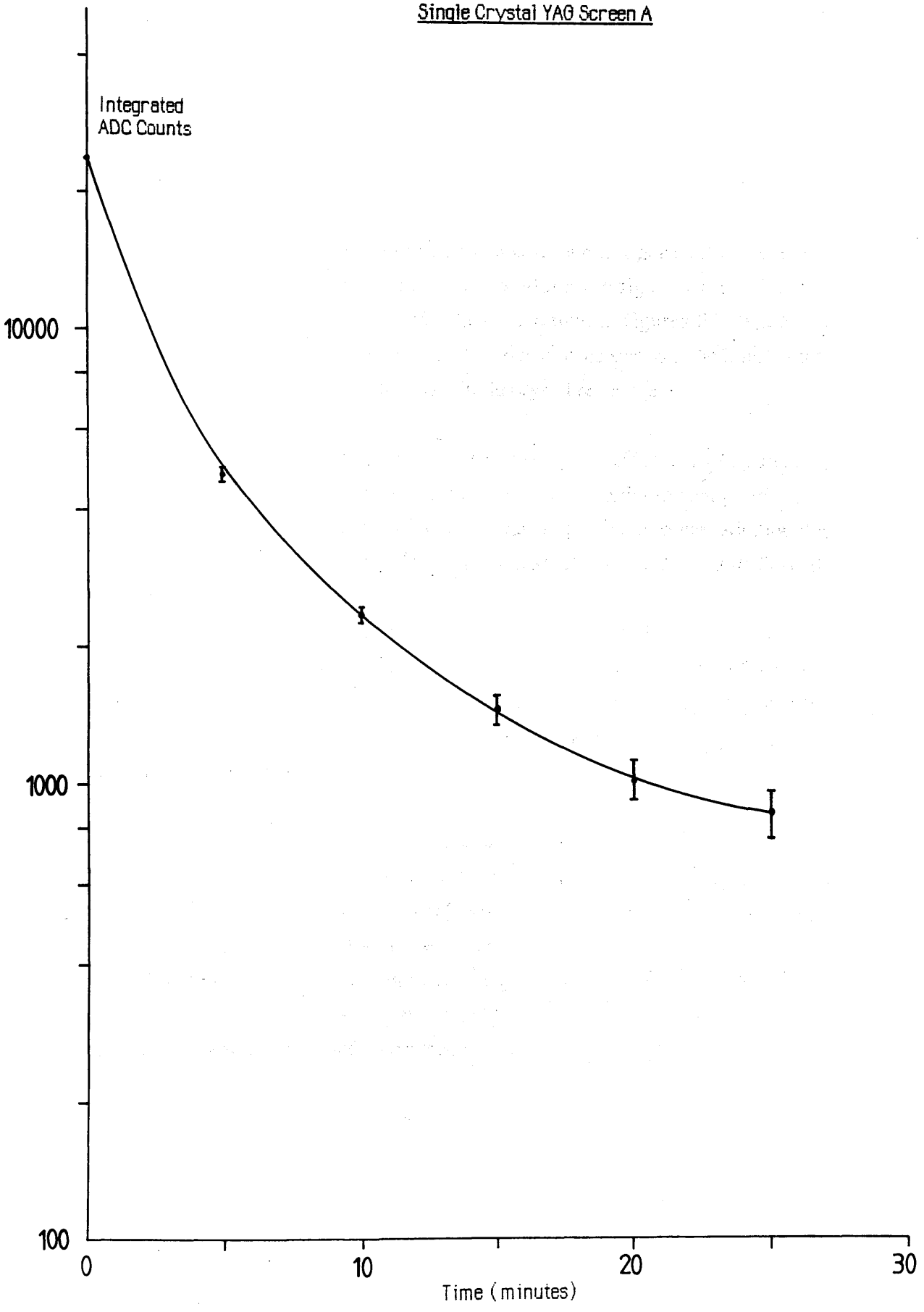

Figure 8.19a is a dark scan taken 10 secs after exposing the 6μm grade P46 powder screen to a high intensity electron probe for ~2 minutes. Again a ghost image of the probe is superimposed upon the dark signal, but the decay is much faster as evidenced by figure 8.19b which is an identical scan acquired 4 minutes later. The 3μm grade phosphor displayed very similar characteristics, but the largest grade (8-9μm) did not show any significant afterglow at all. This latter observation is unexplained, the cause may possibly be due to some difference in the preparation of the different phosphor grades.

The response of the terbium fibre-optic screen is shown in figure 8.20a which is a dark scan taken 20 secs after irradiation using identical conditions to figure 8.19a. The ghost image of the probe can clearly be seen, and the decay is shown in figures 8.20b and c which were taken at four minute intervals. The secondary decay time seems to be longer than that of the powder P46 screens but shorter than the single crystal response.

The afterglow effect is most pronounced in the single crystal YAG screens, where the secondary decay constants have been shown to be of the order of many minutes. In practice it seemed that the level of afterglow detected was proportional to the radiation dose received by the YAG, up to a saturation limit which was of the order of 0.01% of the incident intensity. No explicit experiments were carried out to determine the exact correlation between radiation dose and afterglow levels, but certainly with the maximum beam currents available in the TEM significant 'ghosting' required constant exposure times of the order of tens of seconds. Current densities present in parallel recording of EELS spectra are likely to be at least 100x greater than those used in these experiments, so that a corresponding decrease in the exposure time should be anticipated.

Decay times of the order of minutes as measured above would be disastrous for parallel EELS detection if the signal intensities involved were comparable with those of the spectrum to be recorded. Fortunately, the intensities of these afterglow effects lie at around the 0.005% level (which is much less than 1 LSB in a 12 bit system), and can only be easily detected by integrating the dark signal for long periods. Another helpful factor is that with such slow decay rates, the afterglow could effectively be removed from a spectrum by subtracting a dark scan recorded immediately before the signal of interest.

When recording EELS spectra using scintillators with long secondary time constants, such as single crystal YAG, several precautions should be adopted in order to reduce the risk of spurious images corrupting the data. It seems sensible to try to avoid as much as possible

Figure 8.19 a,b Dark Scan 6µm Grade P46 Powder Phosphor Screen

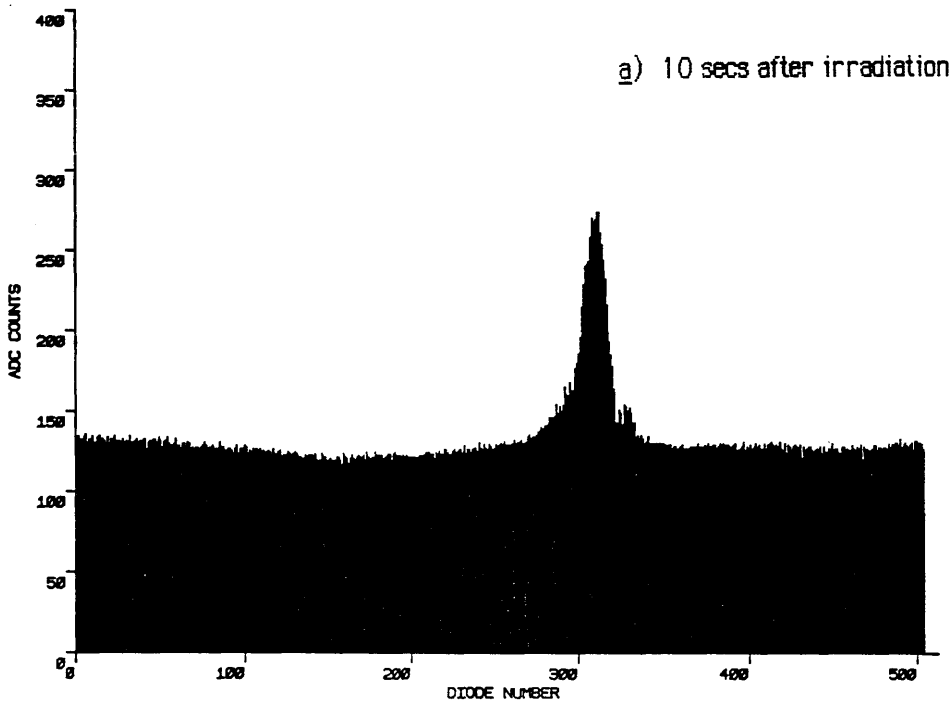

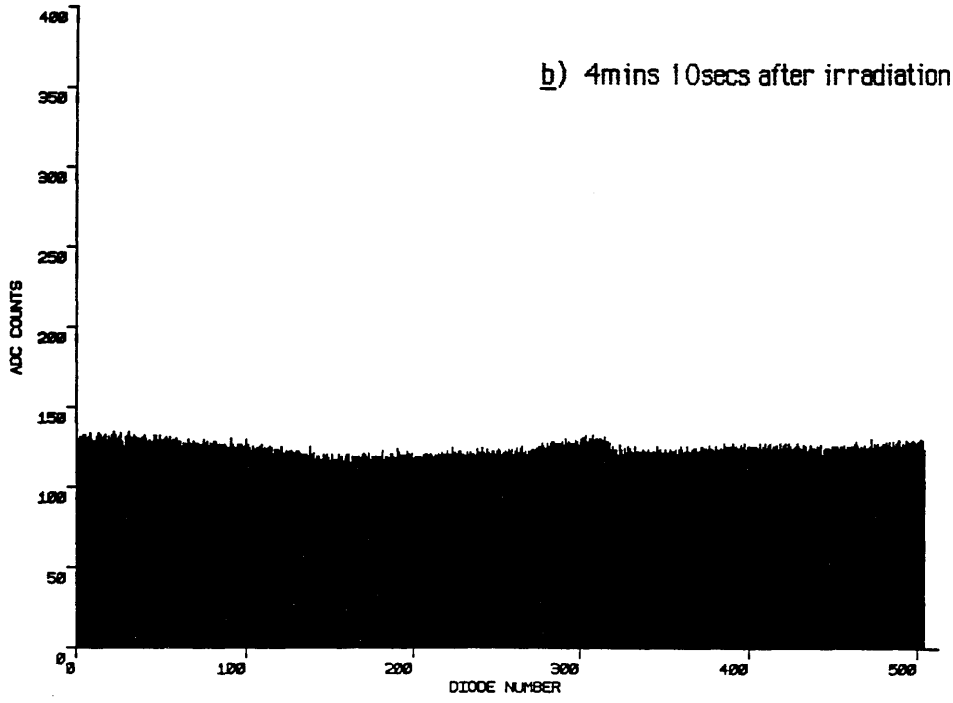

Figure 8.20 a,b,c Dark Scan Terbium Doped Fibre Optic Faceplate

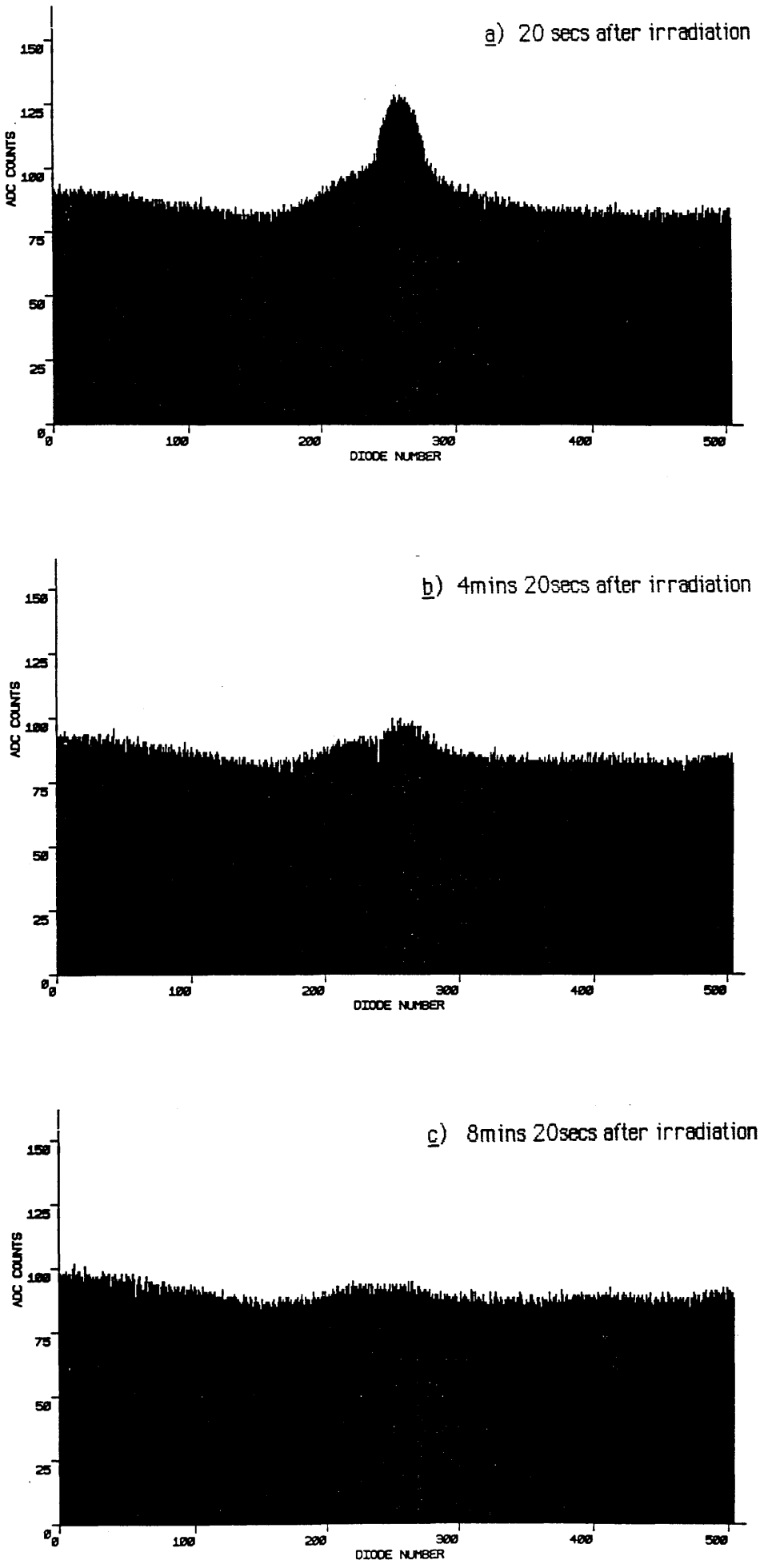

prolonged exposure of the scintillator to intense signals such as the zero loss beam, both in order to reduce the ghosting effect and also to help minimise radiation damage. Secondly, when recording whole spectra in discrete sections the less intense regions (i.e. the far energy loss) should be recorded first and the highest (zero loss) last. If the scintillator is exposed to intense irradiation for a length of time greater than a few seconds then it would be advisable to wait for at least 5 minutes before recording any more data, by which time the ghost image should have decayed to a negligible level. With care and attention to the above details there should be no difficulty in successfully recording wide dynamic range spectra using these scintillators.

8.2.7 Summary of luminescent screen performance

The results of the previous experiments are used to consider the overall suitability of each scintillator for use as an electron-photon conversion screen in a parallel EELS detector, and thus select the screen which best meets the requirements listed in section 8.1.2.

Mullard P20 screen

This commercially produced screen was used as a performance reference for the others. It has the highest spatial resolution of any of the screens tested, showing >20% contrast at a spatial frequency of 13 lp/mm, but consequently suffers in the areas of efficiency and uniformity of light production. Apart from this, the main drawback for its use in parallel EELS is the relatively slow principal decay time which is of the order of 0.5 msec to 50%, and an even slower secondary time constant which means that the light output takes ~500 msec to decay to 1% of the initial value.

P46 powder phosphor screens

The performance of these screens was in most cases below that of the thinned single crystal screens. Admittedly many of the parameters measured depend to a large extent upon the thickness and uniformity of the phosphor layer, which is difficult to control with any degree of accuracy due to the nature of the settling technique. Of the three screens tested the 6μm grade gave by far the highest levels of efficiency at 71 photons recorded per 100keV electron, and was also the most uniform. The principal decay times are very fast, and secondary time constants are shorter than those of single crystal YAG. Spatial resolution is dependent upon the screen thickness and upon the mean phosphor particle size; unfortunately the efficiency of photon production is inversely proportional to these factors so that a compromise must be made. Generally the P46 screens offer no real advantage over single crystal YAG and in fact suffer from several defects commonly associated with particulate

screens.

Terbium doped fibre plate

This novel scintillator has several attractive properties- it is was the most efficient screen measured (apart from bulk YAG) giving >100 recorded photons/e^-(100keV) and displayed the best uniformity of response of any screen at ±1.2%. The fibre plate construction is mechanically robust allowing the screen to be formed into an integral vacuum window, and resistance to radiation damage should be good as in other glass scintillators. Unfortunately the spatial resolution of this sample was the poorest of any of the screens tested, due to light spreading in the fibre array. The introduction of EMA should improve the performance, at the risk of reducing the active area and hence efficiency. The principal decay time is fairly slow, reaching the 10% level in ~10msecs, and there is a low level secondary decay constant which is longer than that of P46 but less than single crystal YAG. Overall the scintillator is potentially very useful for general use in microscopy, if the resolution can be improved, but the slow decay times make it unsuitable for EELS recording.

Single crystal YAG screens

The thinned single crystal YAG screens performed well in the areas of efficiency and uniformity of response, and were second only to the Mullard P20 screen in terms of spatial resolution. The principal decay time is very fast but there does exist a very long term secondary time constant which may cause problems when recording very faint signals immediately after an intense signal. The radiation damage resistance of single crystal YAG is known to be extremely good, and the favourable mechanical properties of the single crystal structure are well suited to parallel EELS recording. The main disadvantage of this scintillator is the reduction in efficiency caused by total internal reflections between the polished surfaces. It should be possible to substantially increase the light output of thinned YAG by matt finishing the output side of the crystal, but the effect on resolution and uniformity of response would have to be carefully examined.

8.2.8 Conclusions

Taking all the above factors into account the most suitable screen for use in a parallel EELS detector is clearly thinned single crystal YAG. Of the two YAG screens tested the 30μm thick screen A showed the better resolution, giving 40% contrast at 10 lp/mm, but seemed to suffer slightly more from light piping. Consequently the thinner screen produced 79 recorded photons/e^-(100keV) as against 83 recorded photons/e^-(100keV) for the 50μm thick screen. The rougher surface finish of screen A does not seem to cause any problems, as

evidenced by the similar uniformity of light production from both screens. It seems that the diamond paste polishing method which was used to finish screen A is more useful than the silica polish used on screen B, as it allows the thickness of the screen to approach the optimum value (as discussed in the next section) without any serious decrease in efficiency or uniformity of light production.

8.3 MONTE CARLO SIMULATION IN YAG

For a given incident electron energy, the optimum thickness of a single crystal YAG screen is that thickness in which all of the energy of the electrons is just absorbed, screens that are thinner than this lose efficiency and thicker screens lose resolution because of increased light spreading. Obviously the optimum thickness is therefore determined by the incident electron energy. A Monte Carlo study was made of the scattering process of 100keV electrons in bulk single crystal YAG in order to determine the most suitable practical depth of scintillator. The original Monte Carlo program was written to model the behaviour of electrons incident upon a thin poly-methyl-methacrylate (PMMA) resist upon a bulk substrate as used in electron beam lithography, but was modified to simulate a layer of single crystal YAG on a glass substrate.

8.3.1 Theoretical outline

A detailed description of the physical model used in the Monte Carlo simulation is contained in 'The Resist Exposure and Development Suite' guide available from Dr Steve Beaumont of the Department of Electrical Engineering at Glasgow University, and a listing of the modified Fortran code along with information on running the program is contained in appendix 6.

The Monte Carlo model simulates real electron trajectories by the assembly of straight line steps of finite length. The progress of a simulated electron is illustrated in figure 8.21 where each step represents the distance between elastic collisions with nuclei or inelastic collisions with other electrons. It is assumed that elastic collisions involve no dissipation of energy but cause angular scattering of the electrons and inelastic collisions involve dissipation of energy without angular deviation. The mean free path λ_{tot} between collisions is a combination of the mean free paths for elastic scattering and inelastic scattering:

$$\frac{1}{\lambda_{tot}} = \frac{1}{\lambda_{elastic}} + \frac{1}{\lambda_{inelastic}} \qquad (8.1)$$

and the actual step length computed is determined, on the basis of a Poisson distribution

Figure 8.21 Monte Carlo Simulation Of Electron Scattering

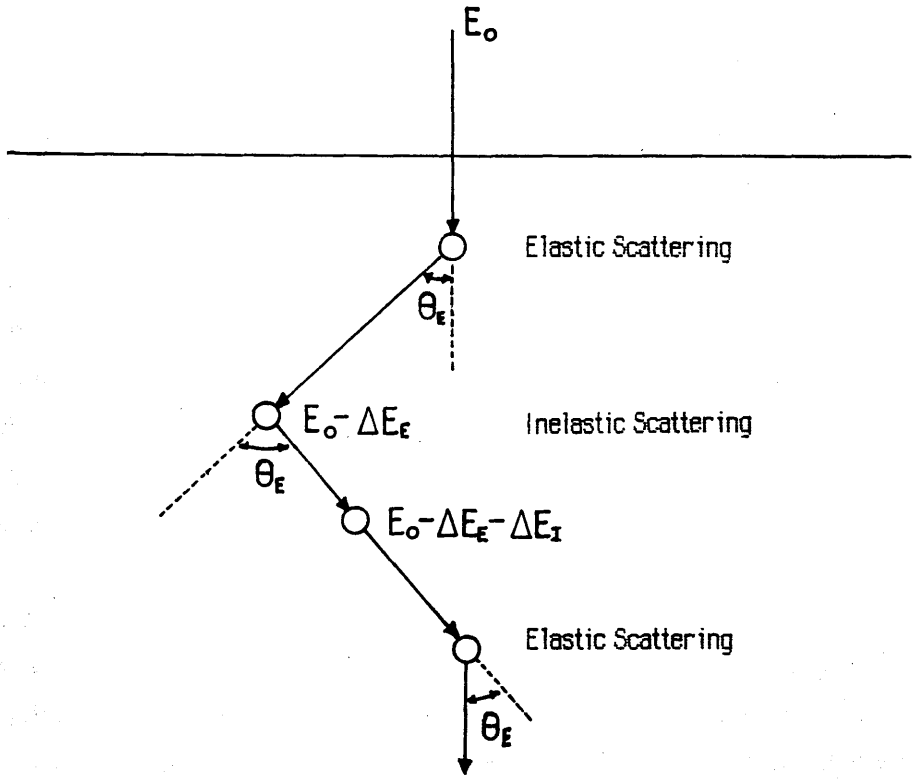

about λ_{tot}, by a uniformly distributed random number. The mean free path for elastic scattering is derived from the screened Rutherford scattering model as is the inelastic scattering angle θ_E, while an expression for the mean free path for inelastic scattering, derived from the Bethe energy loss equation, is given by Shimizu et al [1975].

Selection of an inelastic or elastic event is decided by a random number- if the collision is elastic then the scattering angle θ_E is determined using the Rutherford model, and the energy lost by the electron in travelling to the next collision site ΔE_E is calculated using an approximate analytic solution to the Bethe energy loss equation (also known as the Bethe continuous slowing down approximation) derived by Greeneich and Van Duzer [1973]. The energy dissipated is attributed to the elastic collision point at the start of the current path element, which in the case of the first path element is assumed to be the origin (although no angular scattering takes place at the origin).

The energy lost in an inelastic collision ΔE_I is selected by a random number according to a Poisson distribution about the mean excitation energy for electron loss in the solid I, which appears in the Bethe energy loss equation. This energy is attributed to the inelastic collision site. After each collision the energy lost by the electron is decremented from the original energy, and the next collision is calculated. The trajectory stops when the electron is either absorbed or leaves the YAG.

The angular distribution of the scattered electrons is determined by the elastic scattering events, and is a function of the atomic number of the atom involved in each collision. For YAG scintillator this atom might be yttrium, oxygen, aluminium or cerium. For simplicity the latter is discounted as it makes up only 1 atomic percent of the available atoms. The probability that any one type of atom is involved in a collision depends upon the scattering cross section of that atom and what percentage of the total number of atoms it makes up. The Monte Carlo program selects the collision atom type using a random function weighted with the above probabilities.

8.3.2 Results

Figure 8.22a shows the trajectories of 1000 100keV electrons in 30μm of YAG (density 4.56 g/cm^3). The incident energy of the electrons is relativistically corrected to 109780 eV. Each electron enters the YAG at coordinates Y=X=0 travelling in the Z direction, and the resultant trajectories have all been projected down onto the Y-Z plane. As can be seen, only one electron actually manages to enter the glass substrate.

Figure 8.22a Monte Carlo Simulation Of Electron Scattering in 30μm YAG

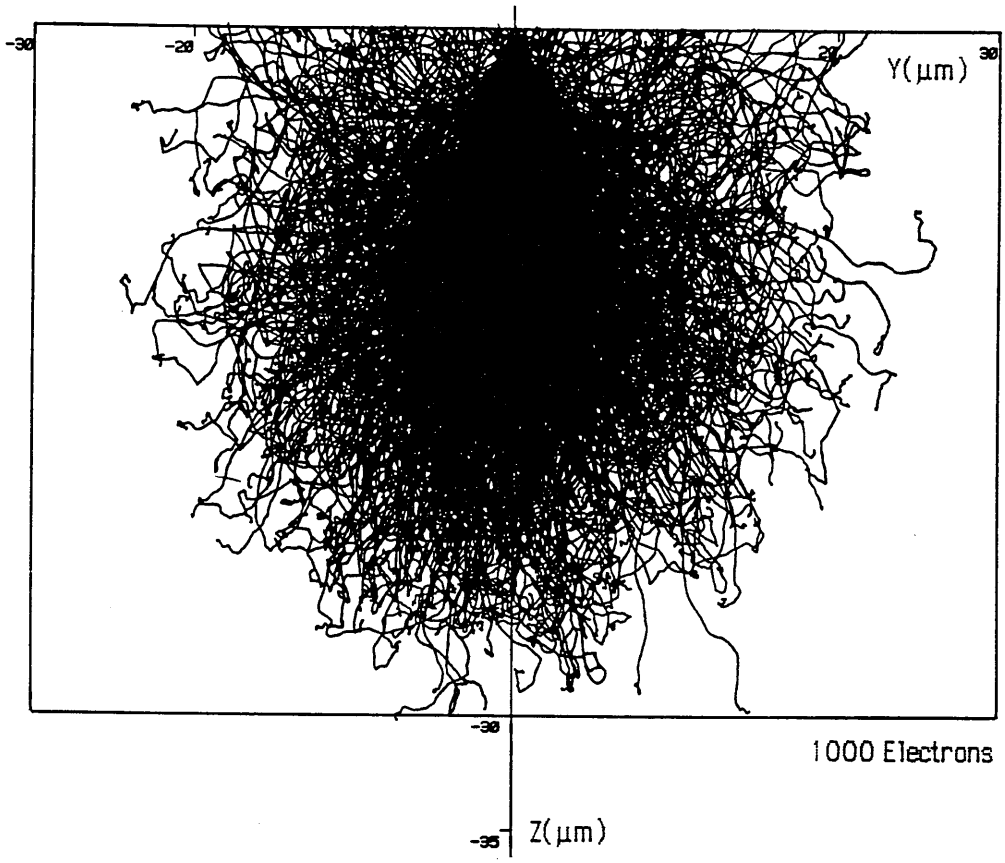

Figure 8.22b Integrated Energy Deposited in YAG

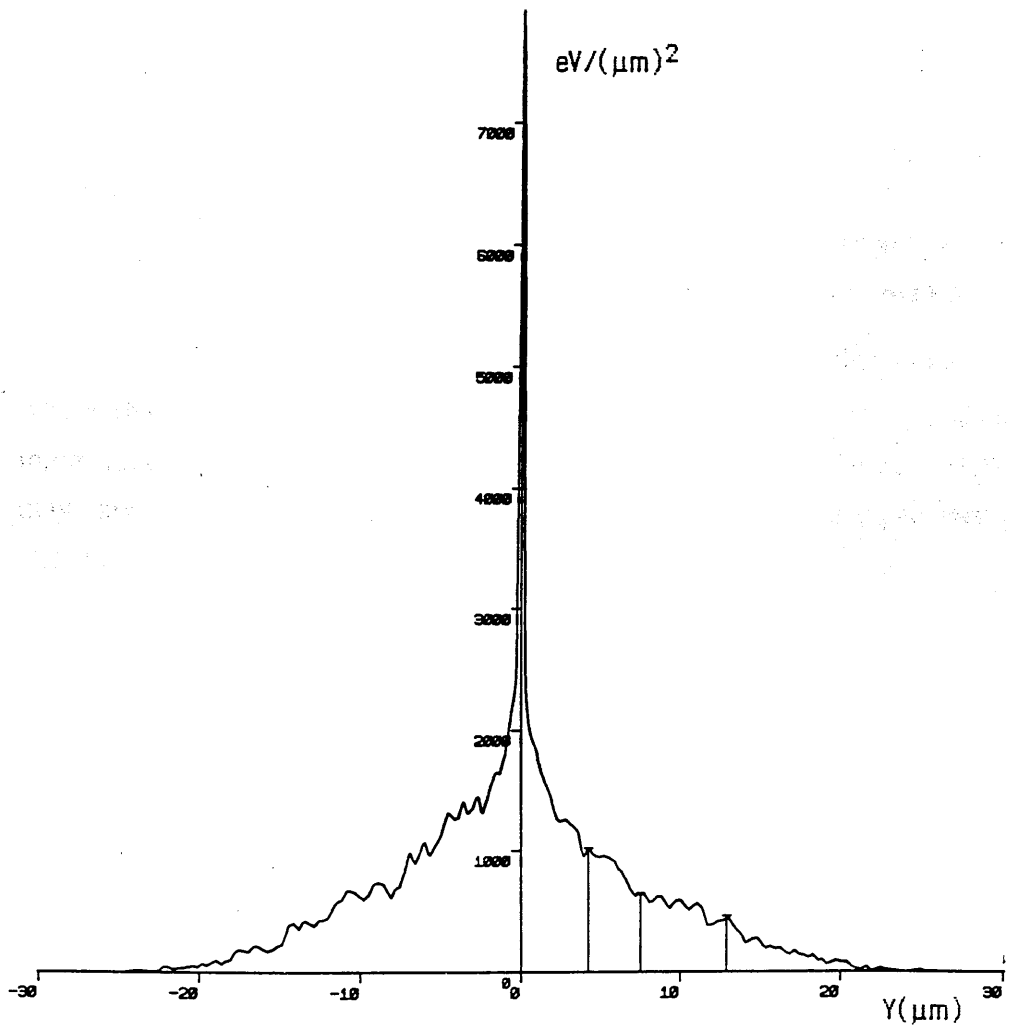

Calculations show that almost 93 % of the total incident electron energy is deposited in the YAG, while the other 7% is backscattered. Thus, assuming an average photon energy of 2.5eV, and a conversion efficiency of 4% each incident electron should produce ~1600 photons. Thinner substrates result in less energy being deposited in the YAG and are correspondingly less efficient; for example similar calculations have shown that a 20μm thick YAG screen absorbs only 83% of the total incident electron energy, while a 10 μm thick screen absorbs only 40%. Figure 8.22b shows the integrated energy deposited in $eV/\mu m^2$ in a series X-Z slices taken through the plane of figure 8.22a. The 50, 70 and 90% boundaries of energy deposition are clearly marked. As can be seen, at the 90% point the maximum lateral spread of the electrons is ~26μm, indicating that this is the minimum point to point resolution which can be achieved using 30μm of YAG to image 100keV electrons. Of course this spread function corresponds to an infinitely narrow electron beam, for real probes the response function would have to be convoluted with the probe shape.

8.4 EVALUATION OF DETECTIVE QUANTUM EFFICIENCY

The experiments of this and the previous chapter have suggested that a successful detector for a parallel recording system for 100keV EELS could be constructed using a 30μm thick single crystal YAG screen fibre-optically coupled to a Hamamatsu S2304-512F photodiode array. This section attempts to evaluate the detective quantum efficiency (DQE) of such a system over a range of electron intensities, using the experimental data of chapters 7 and 8.

8.4.1 Definition of DQE

The efficiency of any electron detector can most usefully be expressed in terms of it s DQE, specified over some range of input intensities. For a linear detector the DQE is defined as:

$$DQE = (\text{SNR of output signal})^2 \; / \; (\text{SNR of input signal})^2$$

where SNR is the signal to noise ratio. Thus a perfect detector which adds no noise to the input signal has a DQE of unity. Real detectors are not perfect but have DQE values which may approach unity over a limited intensity range, gradually falling to zero outside of this region.

For a 30μm single crystal YAG screen the figure of 79 recorded photons per incident 100keV electron was found. The maximum diode capacity of the Hamamatsu S2304-512F array is 4.7×10^7 electrons, so that each individual diode is saturated after receiving a dose of

~5.9×10^5 incident electrons. Thus, electron doses beyond this range cannot be recorded, and the DQE must fall due to saturation effects. At the other end of the scale low input signal levels are masked by the detector readout and digitisation noise, which is approximately 12100 photodiode electrons (section 7.4.3) corresponding to an input noise of ~153 incident 100keV electrons. The DQE is therefore very low for electron doses less than this value.

8.4.2 Calculation of the DQE

The DQE of the detector is calculated in the following section subject to two assumptions: the first is that the input signal SNR is shot noise limited and instrumental variations can be ignored. According to Poisson statistics the input noise n_i is equal to $\sqrt{N_i}$, where N_i is the number of incident electrons per diode element. Thus the input signal SNR_i is just $N_i/n_i=\sqrt{N_i}$. The second assumption is that the influence of the dark current shot noise upon the output SNR of the array can be made negligible by suitable cooling. The output noise per element can be expressed as:

$$n_o = \left[(\eta\sqrt{N_i})^2 + n_t^2 + (\eta\varepsilon N_i)^2 \right]^{\frac{1}{2}} \qquad (8.2)$$

where η is the number of photons recorded per incident electron, n_t is the total readout noise of the array as defined in section 7.1.3 but including digitisation noise, and ε is the fractional non-uniformity in channel to channel response for the whole detector. Equation (8.2) can be re-expressed in terms of an equivalent input noise to give:

$$n_o^* = \left[N_i + (\frac{n_t}{\eta})^2 + (\varepsilon N_i)^2 \right]^{\frac{1}{2}} \qquad (8.3)$$

The output SNR_o can be written in terms of the input signal as:

$$SNR_o^* = N_i \; / \left[N_i + (\frac{n_t}{\eta})^2 + (\varepsilon N_i)^2 \right]^{\frac{1}{2}} \qquad (8.4)$$

and the DQE is therefore just:

$$DQE = N_i \; / \left[N_i + (\frac{n_t}{\eta})^2 + (\varepsilon N_i)^2 \right] \qquad (8.5)$$

This is plotted in figure 8.23 for values of ε of $\pm 1.4\%$ which is the non-uniformity figure for the 30μm YAG screen, and also $\varepsilon = \pm 0.4\%$ which is the value that can be obtained using digital correction methods.

Figure 8.23 DQE of Parallel Detection System

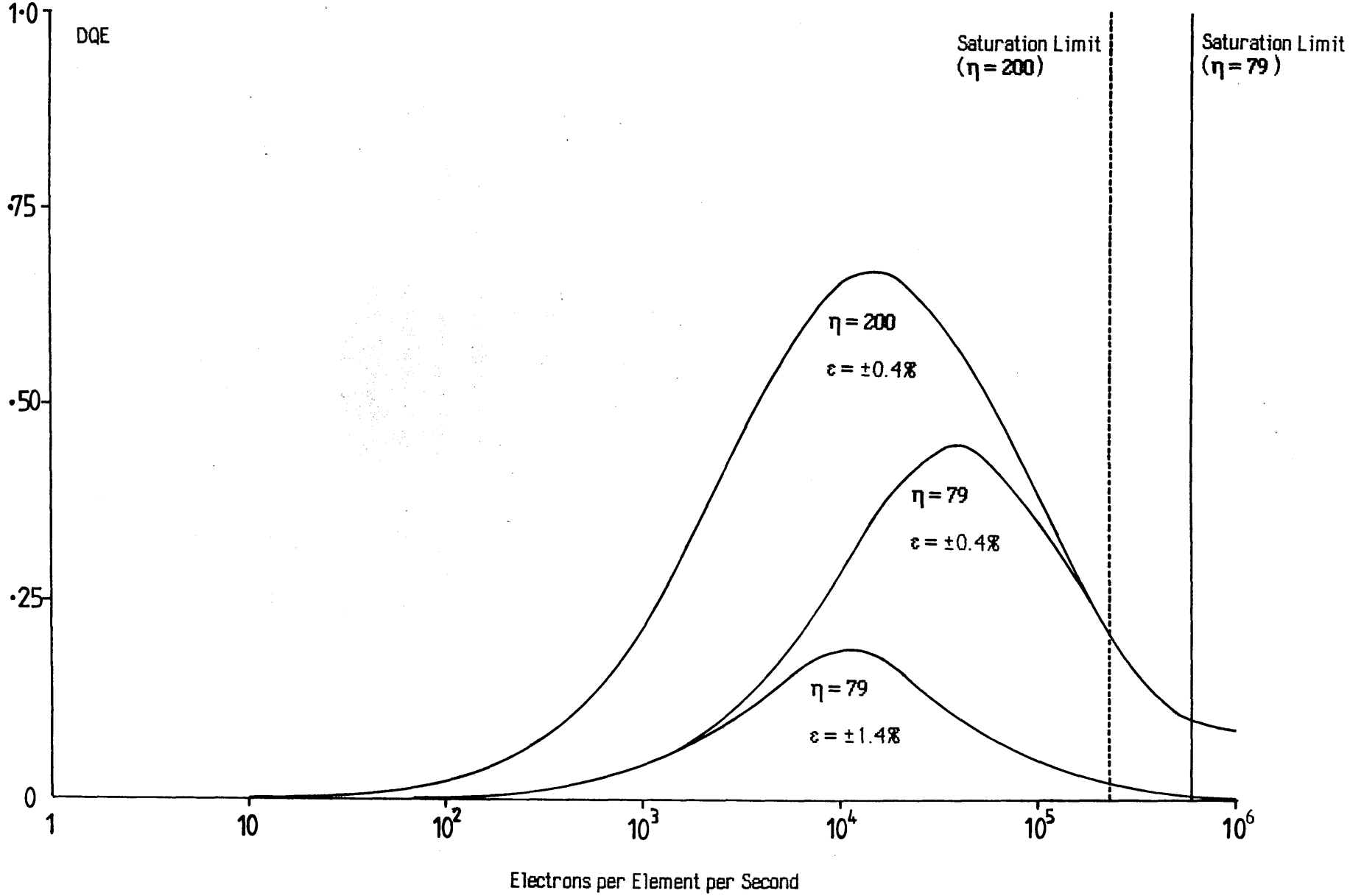

At electron doses of less than 2000 electrons / element the DQE is the same in both cases, being dominated by the large readout noise factor n_t. The DQE values then increase as the dose rises well above the readout noise level, but the corrected curve increases faster because of its much lower non-uniformity value ε, ultimately reaching a DQE of 0.45 at a dose of $4x10^4$ electrons/element. The uncorrected signal peaks at a DQE of <0.2 at a dose of $1x10^4$ electrons/element. Above the maxima the DQE is dominated by the level of non-uniformity of response in the detector, which causes the response to fall off towards the saturation limit.

8.4.3 Discussion of the DQE response

Figure 8.23 clearly demonstrates the advantages of digital response correction especially at higher dose rates. The detector DQE response can only be extended at the high dose region by improving further the value of ε. The non-uniformity of response of the photodiode array itself is probably the limiting factor, rather than any non-uniformities in the scintillator screen. As it is, the value of ε for the complete detector of $\pm 1.4\%$ is well below the specified maximum value of $\pm 5\%$ for the Hamamatsu array alone, so that further gains here will probably have to come from improvements in the manufacture of the photodiode arrays. It may be possible to improve the digital response correction technique to give a lower value for the corrected non-uniformity, for instance by correcting for non-linear response in each diode element, but this would require very careful characterisation of each array and large computational overheads and would possibly change with time.

The rather poor DQE response at lower doses is mainly due to the large value of the readout noise $(n_t / \eta)^2$. Any reduction in this figure would greatly improve the performance for very low doses, and increase the maximum DQE attainable. The best way to do this would be to reduce the levels of readout noise - possibly by giving more care to the electronic layout and connections for the photodiode array, and by increasing the precision of the ADC so that the digitisation noise was reduced. In addition to this, the value of η could be increased at the cost of lowering the saturation limit of the array. A third DQE trace shows the theoretical DQE (assuming $\varepsilon = \pm 0.4\%$) if η was increased to 200 photons per incident electron, as achieved by Egerton and Crozier [1987]. Clearly the DQE is much improved at lower electron doses, being above 0.25 for over 2 decades, however the saturation limit is decreased from $5.9x10^5$ electrons/element to $2.3x10^5$ electrons/element.

As it stands, the DQE in a single scan (with digital response correction) is above 0.25 for a range of input electron doses covering ~1.5 decades. However, the range of electron intensities which can be detected at this level is greatly increased by varying the photodiode

integration time. The shortest integration time that can be used is determined by the diode readout rate, which is limited to 20msec using the Hamamatsu C2325 evaluation board, whereas the longest useful integration time is determined by the dark signal accumulation. At $-10^{o}C$ the dark current is ~20fA (figure 7.11) so that the array would be half filled in approximately 180 seconds and the shot noise in the dark current would be ~4743 electrons which is equivalent to an input noise of 60 fast electrons. Thus the range of useful integration times is of the order of 10^4, and the range of incident beam intensities per detector element which can be recorded with DQE>0.25 is from ~40 e^-/(channel sec) to ~$1x10^7$ e^-/(channel sec).

If the value of η could be increased to 200 there would be an improvement in the detectability of low level signals, where the DQE would be above 0.25 from ~7 e^-/(channel sec). The high level response is dominated by the array non-uniformity of response and so is not improved by increasing η. A further increase in the sensor dynamic range is made possible by varying the magnification of the spectrum at the YAG surface. For example, assuming a spectrometer dispersion of 2μm/eV, the magnification system described in chapter 5 could vary the dispersion at the YAG screen from ~2.5eV/channel to ~0.14eV/channel, giving an almost twenty-fold decrease in the intensity of the spectrum at the detector. This would effectively extend the dynamic range at high intensities (at the cost of reducing the energy range which could be recorded simultaneously to ~72eV) by another order of magnitude, allowing electron doses of between ~40 e^-/(channel sec) to $>10^8$ e^-/(channel sec) to be recorded with a DQE of greater than 0.25.

This range is sufficient to record all the signals of interest in a typical EELS spectrum except possibly the zero loss peak, which could be detected using a Faraday cup placed somewhere in the detector plane or, better still, the higher intensities could be recorded by effectively decreasing the array integration time using a fast beam blanking system. Such a system would have to be synchronised to the diode scans, and the blanking action should preferably be carried out before the specimen. As it stands, a spectrum with a dynamic range of 10^7 would have to be recorded in 5 separate sections to maintain a DQE >0.25 at all intensities. If the DQE response could be improved as shown in figure 8.23 then a dynamic range of 10^8 could be recorded in 4 sections and it may be possible, with reductions in the readout noise levels, to improve the DQE further thus reducing this value to 3 sections.

8.5 RECORDING A DIFFRACTION PATTERN

As mentioned previously it was not possible to test the detector by recording an EELS spectrum because no suitable spectrometer / magnification system was available. It seemed reasonable instead to record a line scan through a spot diffraction pattern in the JEM 100C TEM, because the dynamic range of such a pattern is similar to that observed in EELS spectra and also because recording TEM diffraction patterns is one possible use for a parallel detection system, albeit 2 dimensional. The parallel image obtained in the TEM is then compared with a similar pattern obtained serially in the HB5 STEM using the rocking beam diffraction mode.

8.5.1 The gold foil diffraction pattern

Figure 8.24 is a micrograph of a selected area diffraction pattern from a thin single crystal gold foil taken in the TEM using a camera length of 20cm. This diffraction pattern was projected down onto the 30μm YAG screen, which was repositioned to have it s long axis parallel to the photodiode pitch, allowing two diffraction spots to be recorded simultaneously. The images of the five diffraction spots indicated were recorded in pairs using integration times from 20 msec to 1 sec. Positioning of the required spots relative to the array was accomplished by mechanically moving the final projector lens of the microscope while the video output was displayed on an oscilloscope.

The resultant images, after dark signal subtraction and digital response correction, are shown in figures 8.25a-d. The dynamic range of the five spots is ~2000:1, and it can be seen that the detector can cope with this easily. The background of figure 8.25d is not due to dark current but to thermal diffuse electron scattering. The fact that single channel peak values of each spot are clearly distinguished indicates that the point to point resolution of the detector cannot be much worse than 25μm.

Figure 8.26a is the central spot of figure 8.25a magnified to show the fine detail. The spikes on the tail sections are due to the edge effects illustrated in figure 8.26b, which displays the response of the YAG screen to constant illumination. The poor uniformity arises from the fact that the thinned screen was not large enough in area to illuminate all of the array, and the alignment was such that some of the light piped to the edge of the crystal was recorded. Digital response correction techniques cannot completely eliminate edge effects, as the relative intensities in the spikes vary slightly with the position of the beam on the scintillator. In a production detector the area of YAG would be greater than the array area, so that edge

Figure 8.24 Gold Diffraction Pattern From TEM

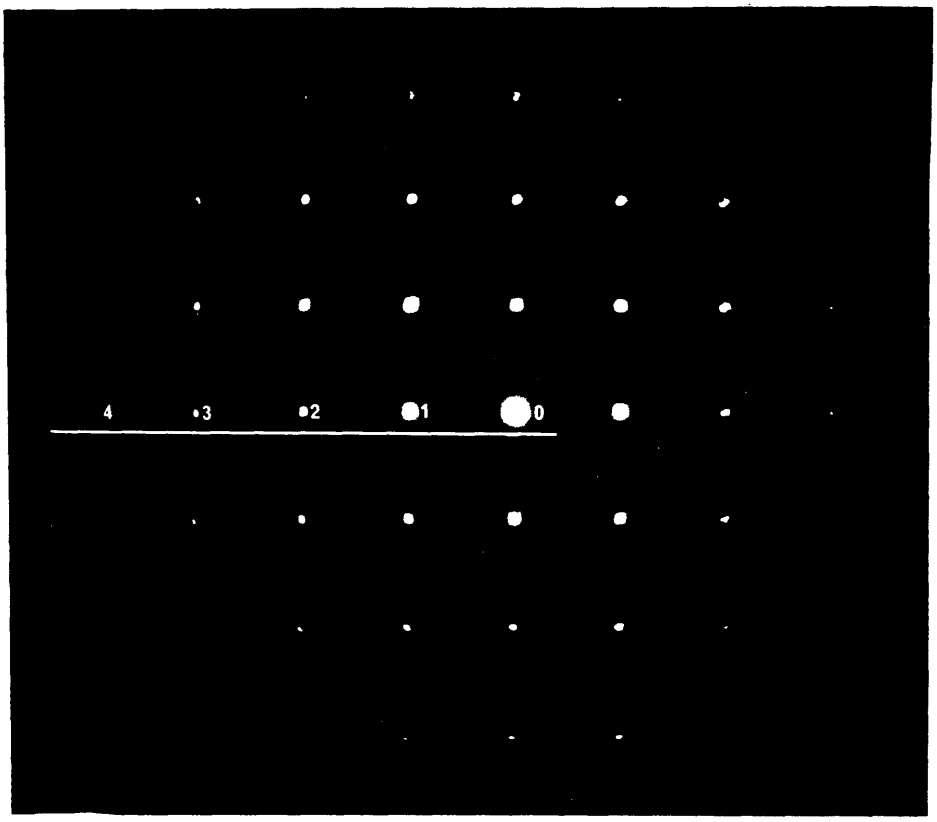

Figure 8.25a-d Line Image of Gold Diffraction Pattern

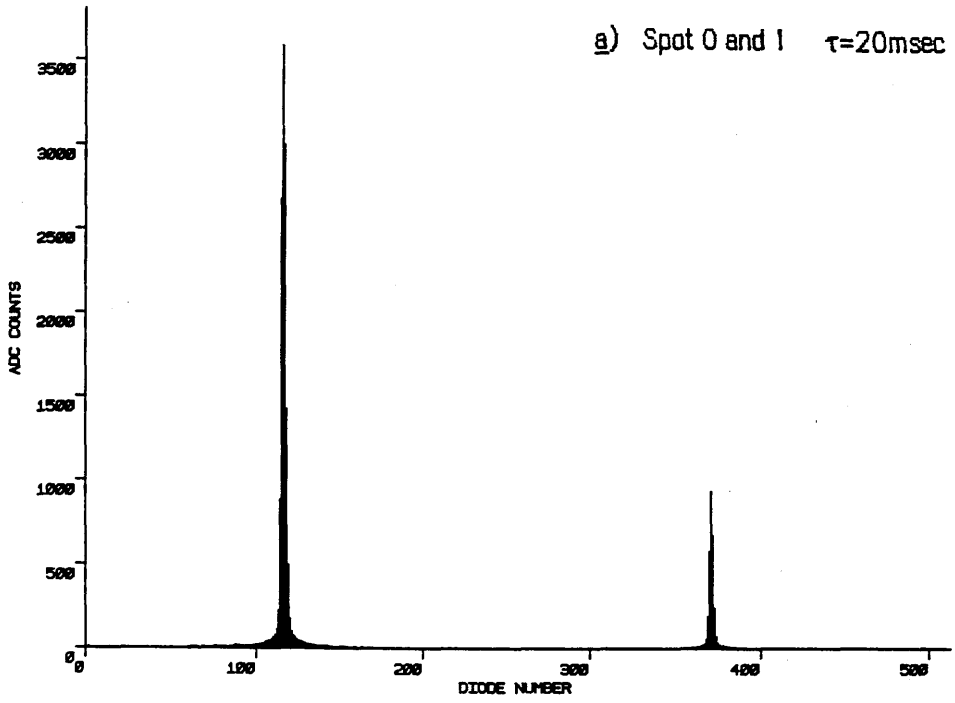

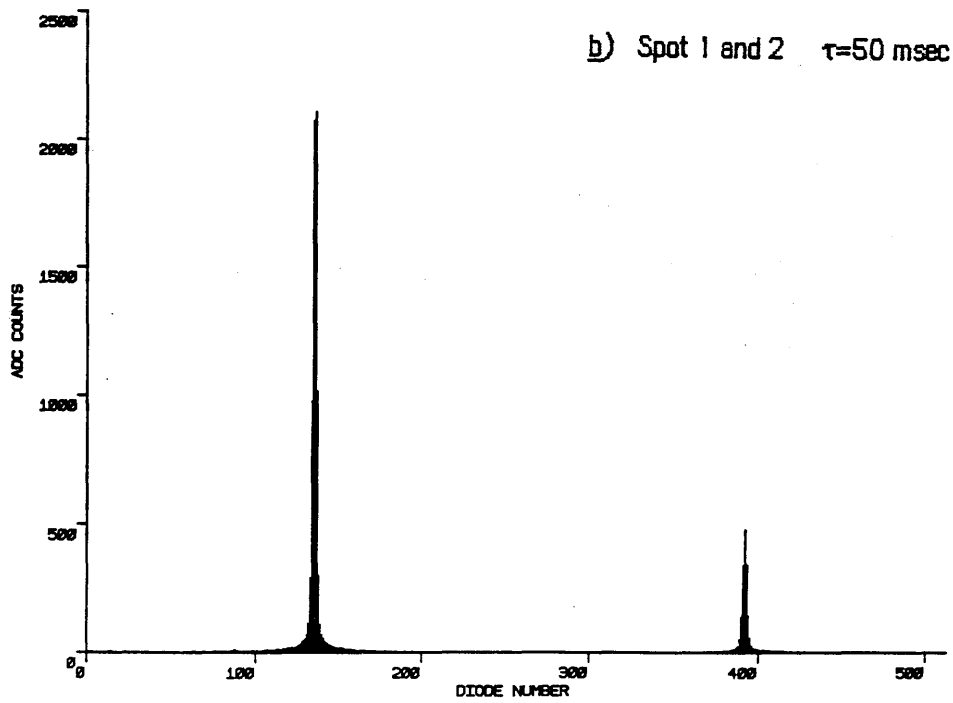

c) Spot 2 and 3 τ=200msec

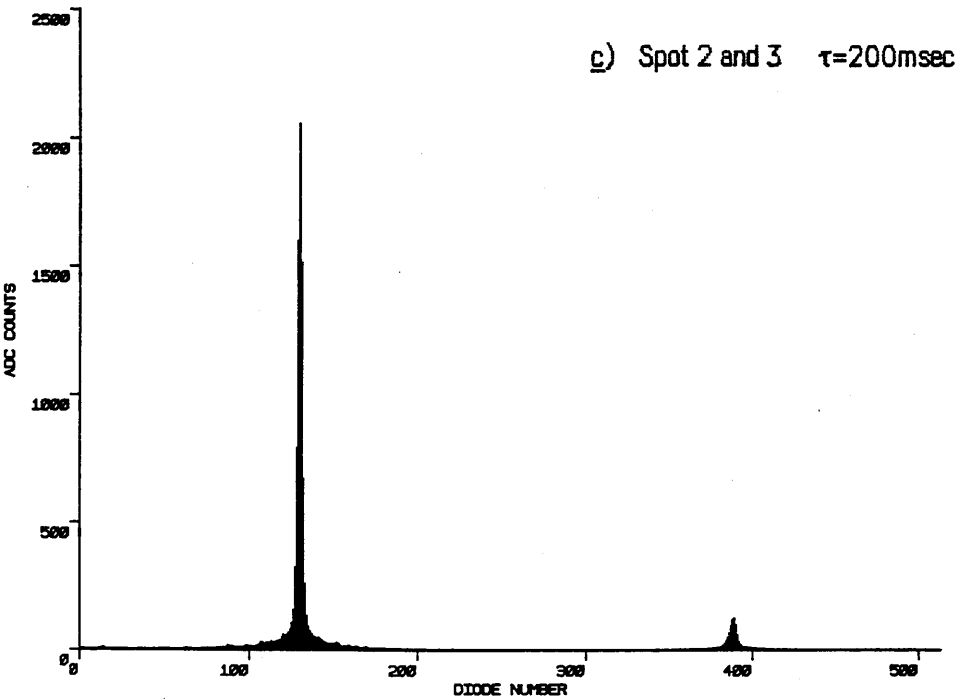

d) Spot 3 and 4 τ=1000 msec

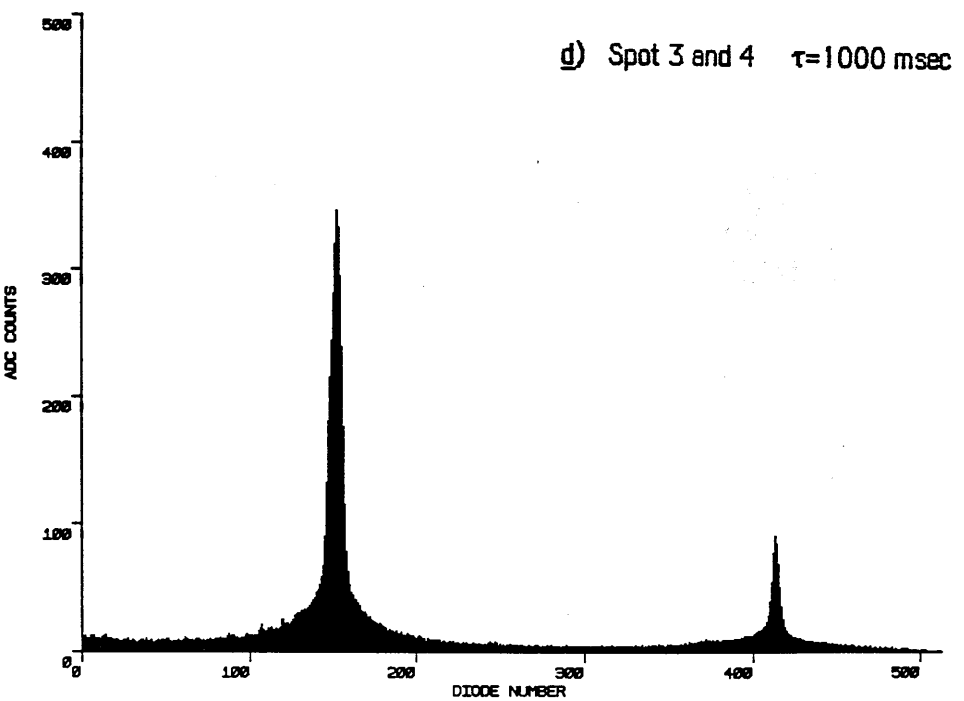

Figure 8.26a Magnified Image of Central Diffraction Spot

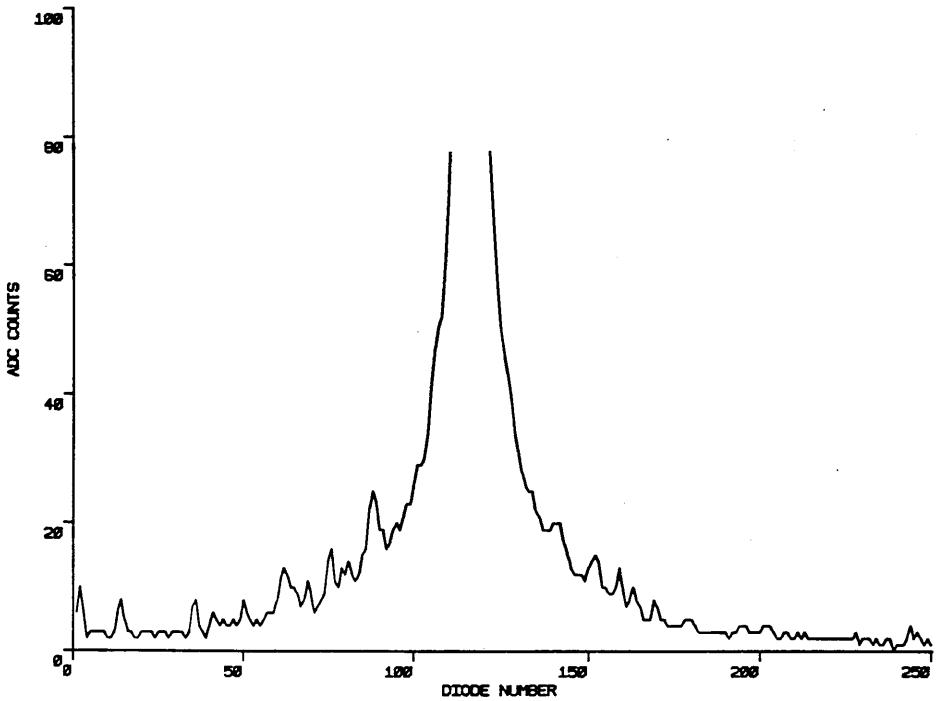

Figure 8.26b Response of YAG Screen A to Uniform Illumination

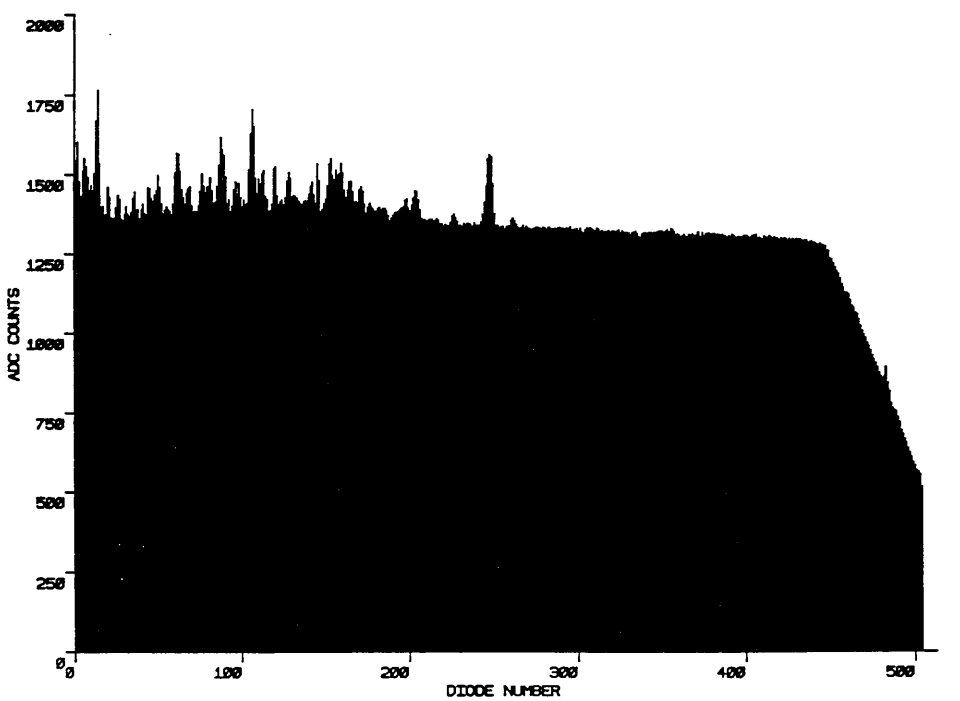

Figure 8.27a Rocking Beam Diffraction Pattern Line Scan From HB5

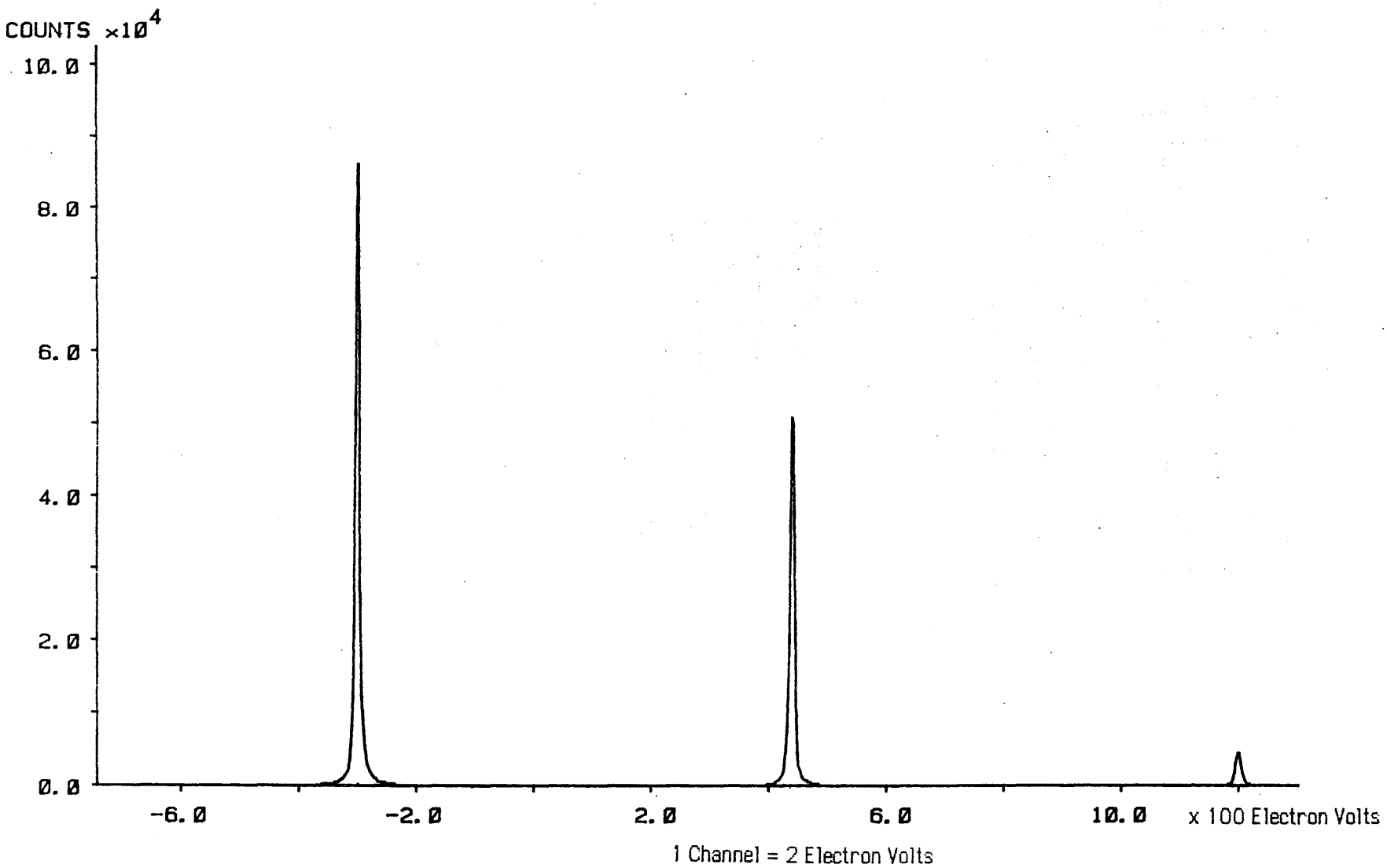

Figure 8.27b Comparison of Full Widths of Central Diffraction Spot

For Parallel and Serial Detection

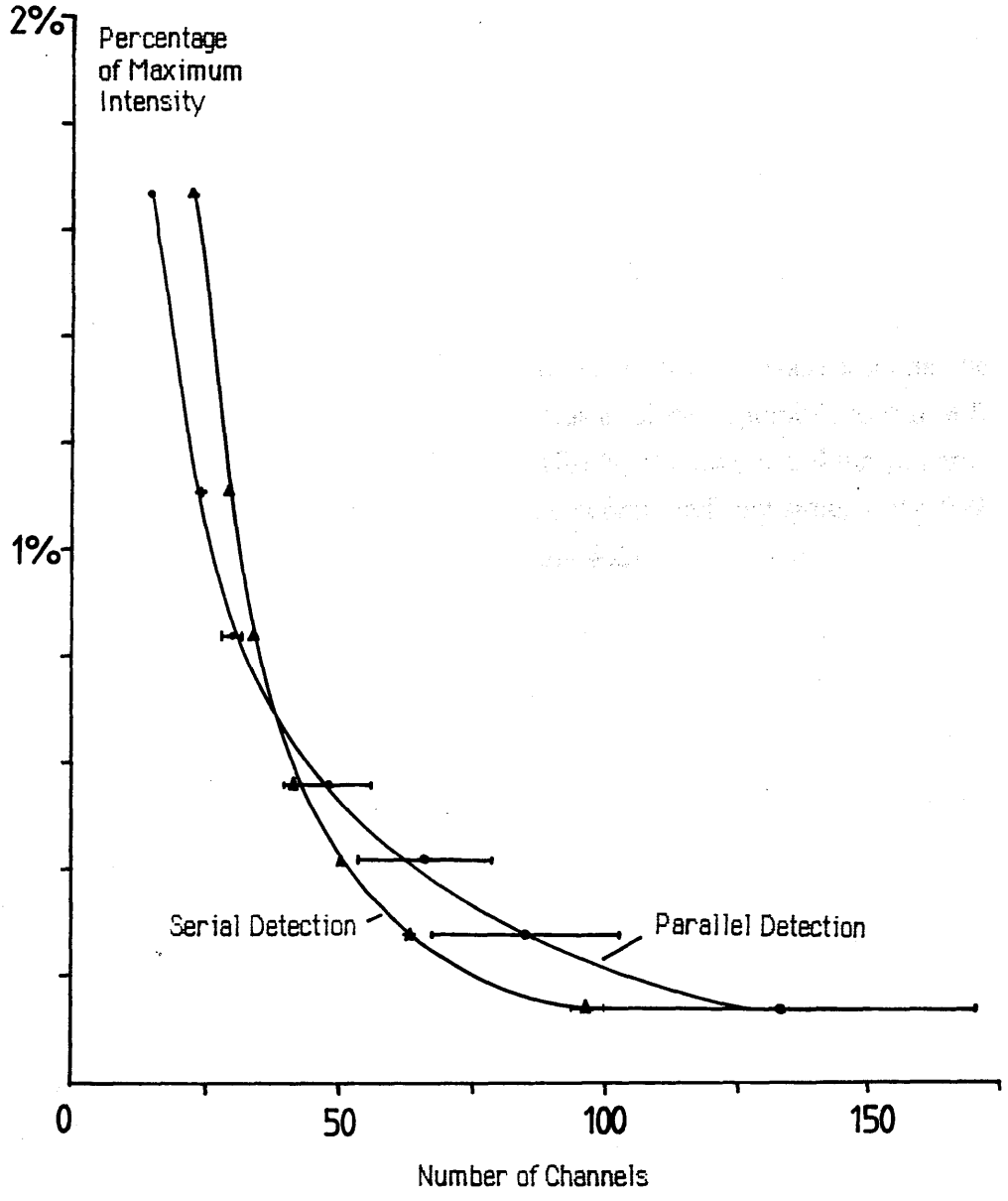

effects could be neglected.

However, even ignoring the edge effects there do exist definite low intensity tails on each of the recorded diffraction spots. In order to determine whether these tails were due to genuine signal or a detector artefact, a rocking beam diffraction pattern from the same specimen was serially recorded in the HB5 STEM. A line scan from this pattern is shown in figure 8.27a. Of course it was not possible to recreate the exact recording conditions of figure 8.25a, but it can be seen that there also exist tails on the serially recorded pattern which were definitely due to a real signal and not an artefact. The HB5 channel width was set so that the full width at half maximum (FWHM) of the central spot was as close as possible to that of figure 8.25a (4 channels FWHM in HB5 v 3 channels FWHM figure 8.25a), and the camera length was set so that the ratio of the distance between the central and first spots to the FWHM of the central peak were the same in both cases (within ~8%).

Figure 8.27b is a graph showing the full width of the central diffraction spot against intensity level, for the parallel and serial images. With such a crude comparison it is difficult to draw any definite conclusions, essentially since like is not compared with like and instrumental effects must play a part. However, it does seem that the degree of spreading is slightly greater in the parallel detector at the lowest intensities. This may be due to the fact that the points plotted on figure 8.27b are influenced by the noise present in the recorded signals, and the fact that the statistics of the serially recorded data are in this case very much better will have an effect on the comparison. Also the non-uniformity of response of the particular area of YAG screen used tends to increase the uncertainties involved. The information from the serial scan does however indicate that most of the tailing effect recorded by the parallel detector is due to a genuine signal.

It is interesting to note that figure 8.27a was recorded with a dwell time of 100msec per channel, and took over 100secs to record the 1024 channels in the image, whereas the 512 channels of figure 8.25a were recorded in 20msecs. To get similar statistics in the parallel scan, the integration time would have to be increased to around 0.5 secs which is still 200 times more efficient than the serial detector.

CHAPTER 9

Conclusions and suggestions for further work

Introduction

In this thesis the results of an investigation into the design of a parallel recording system for EELS were presented. The results described in this work are generally applicable to any transmission electron microscope equipped with a suitable spectrometer, and in particular the Glasgow University HB5 STEM. Interest in the parallel recording technique derives from the much improved detection efficiency which can be achieved using this method, as compared with that of the more common serial recording systems - such as the one presently installed on the HB5. Parallel recording is especially useful in areas such as high spatial resolution EELS where specimen drift and contamination can be problematic, investigations of radiation sensitive materials such as biological specimens, and the study of EXELFS information where the signal to noise ratio is critical. At the time of writing one commercial parallel recording system is entering the early stages of production, with further development currently in progress. It is clear that the optimum design of such a system is a complex task involving many variables - hopefully this thesis provides the framework on which an operational system could be based.

9.1 THE PARALLEL RECORDING SYSTEM

The proposed parallel detection system consists of many separate components all of which interact to a greater or lesser degree. The following sections summarise the essential parts of the design and discuss the performance of the various individual elements which make up the detector.

9.1.1 The nature of the energy loss spectrum

The operational specifications of any detection system are determined by the nature of the signal to be recorded. In the case of EELS the signal of interest can vary from ~10^9 electrons/sec at the most intense part of the spectrum down to ~100 electrons/sec for the far energy loss events. The first part of this work involved gaining an understanding of the nature of this intensity distribution, since this obviously influences the choice of detector used to record the spectrum.

It seems clear that, at the present time, the most suitable type of spectrometer for use in parallel EELS is a second order aberration corrected homogeneous field magnetic sector spectrometer, since the theoretical and practical development of these analysers is much more complete than that of any other kind currently in use. In general the energy resolution limiting second order aberrations of the median plane are corrected by the use of curved entrance and exit faces, along with external multipole corrector lenses. However the second order vertical plane aberrations are not eliminated, and while these are relatively unimportant for serial detection they do have an influence on parallel recording.

A computer program was written to calculate values for the residual median plane aberration coefficients and uncorrected vertical plane aberration coefficients of any spectrometer of this type, using the analytical expressions of Enge [1967], Brown [1967], and the fringe field approximations derived by Heighway [1975]. Knowledge of the aberration coefficients allows the spatial distribution of the spectrum formed at the spectrometer dispersion plane to be determined.

Studies of two well known spectrometers, designed by Scheinfein and Isaacson [1984] and Shuman [1983], were carried out. The Scheinfein and Isaacson spectrometer is of special interest to this project as it is commercially available for the HB5. Results of the analysis revealed that both spectrometers produced good theoretical energy resolutions, as expected from second order corrected designs: 0.55eV for the Scheinfein and Isaacson design and 0.2eV for the Shuman spectrometer, and that the aberration which causes tilting of the dispersion plane had been eliminated, which is most important for parallel recording.

There was however, a considerable defocus with energy loss in the non-dispersive direction for both designs, caused by one of the uncorrected vertical plane aberrations. The magnitude of the defocus was found to be 0.2μm/eV for the Scheinfein and Isaacson design and 0.31μm/eV for the Shuman analyser, broadening the non-dispersive width of a full 2000eV spectrum to ~200μm and ~310μm respectively at the extremities. It seems that this defocus is a general property of sector spectrometers having a negative exit poleface curvature coupled with positive poleface tilts, which is the most common configuration used in second order corrected designs. Obviously the type of detector chosen should be wider than the maximum defocus, so that the whole signal can be accommodated.

9.1.2 Post spectrometer magnification

The dispersion of a typical magnetic sector spectrometer is ~2μm/eV. When a 100keV electron hits the solid surface of, for example, a silicon detector it spreads laterally by ~30μm, thus reducing the energy resolution of a silicon device placed directly at the dispersion plane to an unacceptably low 15eV.

In order to overcome this difficulty a post spectrometer magnification system consisting of four quadrupole lenses was designed. The major advantage of using four quadrupoles as opposed to a more conventional round lens system is the fact that the magnifications in the dispersive and non-dispersive directions can be made virtually independent, allowing the dispersion to be increased without changing the width of the spectrum. The predicted range of magnifications in the dispersion direction (assuming a maximum excitation of 200 amp-turns per pole) lies between 5x and 97x at 100keV, corresponding to a dispersion range of ~10μm/eV to ~194μm/eV, which is more than adequate for general purposes.

The magnification system was designed using a real as opposed to a virtual object configuration, as this allows independent alignment of the spectrometer, ease of elimination of stray scattering, and also retains the option of using serial scanning where necessary. Both the central lenses of the quadruplet are designed to run at fixed excitations, with the magnification and focus of the spectrum being controlled by varying the strengths of the outer quadrupoles. In this manner, the whole range of magnifications can be accessed using a simple double control system. As far as the electron-optical aberrations of the system are concerned the main considerations with quadrupole lenses are the effects of the four second order chromatic aberration coefficients, which were computed in a sharp cut-off fringe field (SCOFF) approximation, and shown to be negligible over the useful range of operating conditions.

The major disadvantage of using a real object as opposed to a virtual object configuration is the associated extension of the electron flight path, and the corresponding increase in susceptibility to external a.c. magnetic fields. The proposed magnification system would extend the flight path 22.5cm beyond the spectrometer dispersion plane. In order to estimate the loss in resolution incurred, a calculation (using a thin lens approximation) of the defocus produced by an external a.c. field of 1milligauss was carried out, assuming a point source at the entrance plane of the magnification system. The reduction in energy resolution over the whole magnification range was found to be < 0.5eV. Indeed, it was shown that this figure is less than the resolution loss that would be incurred in the drift space between the exit face

and dispersion plane of the Scheinfein and Isaacson spectrometer alone, subject to a similar a.c. field.

9.1.3 The choice of electron detector and detection mode

In choosing a suitable multielement detector for EELS there are many factors to be considered - the first decision to be made is whether to detect the spectrum directly, by allowing the 100keV electrons to strike the surface of a solid state device, or whether to use an indirect detection method whereby the electron signal is converted to a photon flux in a scintillator, and the resultant light signal recorded. The former method offers very good sensitivity at low electron rates, but is generally unsuitable for EELS because the high signal intensities involved in a typical spectrum tend to saturate the detector, and very likely degrade its performance over a period of time due to radiation damage effects.

Two types of solid state detector were considered - area CCD arrays and wide aperture linear photodiode arrays. CCD arrays offer better noise performance than photodiode arrays, but the limited cell capacity of these devices means that saturation effects are very much a problem when recording the more intense regions of EELS spectra. Furthermore, the small cell size of a CCD array (typically 25μmx25μm) means that the non-dispersive defocus described previously would spread the spectrum over many rows of cells, the contents of which would then have to be summed electronically. It seems that the higher cell capacity, larger cell size and simpler application of the wide aperture photodiode arrays outweighs the disadvantage of their higher noise levels for this application.

Two different wide aperture photodiode arrays were investigated, the RL128S array manufactured by Reticon, and the S2304-512F array manufactured by Hamamatsu. Both these devices have sensor elements 2.5mm wide on a 25μm pitch, so that the defocus of the spectrum in the non-dispersive direction can be easily accommodated. A comparison of the electrical and optical properties of both arrays revealed the superiority of the Hamamatsu device in the areas of uniformity and linearity of response, dark current, and readout noise. This, together with the more compact drive circuitry and lower cost of the Hamamatsu device, indicated that the S2304-512F array was the more suitable device for this application.

9.1.4 Choice of scintillator screen and optical coupling mode

Indirect detection methods depend crucially upon the properties of the electron-photon conversion medium and the efficiency of the optical coupling between the screen and the detector. Fibre-optic plates offer several advantages over conventional lens optics in the

latter respect, allowing a larger fraction of the available light to be recorded. Several types of luminescent screen were fabricated on Mullard fibre-optic faceplates for evaluation purposes. The output surface of the fibre-optic faceplates was in direct contact with the fibre-optic input window of the Hamamatsu array, allowing an estimated 36% of the available light to reach the array.

The luminescent screens were tested for linearity and efficiency of photon production, uniformity of response, spatial resolution and decay times. The screen which performed consistently well in all these areas was thinned single crystal YAG, which has the added advantage of possessing exceptional resistance to radiation damage. Monte Carlo studies suggested that the optimum screen thickness was 30μm, where the combination of spatial resolution and photon production efficiency was at a maximum. Calculations suggested that, in theory, ~1600 photons should be produced by every 100keV electron, of which ~250 should be recorded by the array. In practice only ~80 photons were recorded for every incident 100keV electron; - this loss of efficiency was attributed to internal reflection effects in the YAG causing light to be piped out to the edges of the crystal, and losses at the fibre-optic interface. The only disadvantage of single crystal YAG is the presence of some very long decay constants at low intensity levels. With care this latter effect should not cause any serious problems when recording spectra.

9.1.5 Performance of the detector

Assuming an efficiency of 80 photons recorded per incident 100keV electron, the Hamamatsu array saturates for electron doses greater than 5.9×10^5 electrons/channel. The combined readout and digitisation noise of the current detection system is equivalent to an input noise of 153 fast electrons, so that single electron detection is not possible. The DQE of the detector is strongly influenced by the latter figure at low electron dose rates, and by the channel to channel non-uniformity of response at higher dose rates. A figure of ±1.4% non-uniformity of response was found using the 30μm YAG screen, but this was reduced to ±0.4% using digital response correction techniques. The DQE of the detector in a single scan is above 0.25 for a range of input electron doses covering ~1.5 decades (with digital response correction); however by varying the integration time of the array and the dispersion of the spectrum, a range of ~40e^-/channel sec to $>10^8$ e-/channel sec can be recorded with the same efficiency.

Unfortunately it was not possible to test the detector by recording an EELS spectrum because of the lack of a suitable spectrometer/magnification system. However, it was possible to

demonstrate the capabilities of the system by recording a line scan through the spot diffraction pattern produced by a single crystal gold foil in the JEM 100C TEM. The data obtained from the parallel detector was compared to that obtained from a serially recorded line scan of a rocking beam diffraction pattern from the same specimen in the HB5 STEM, revealing a detection efficiency ~200 times greater for the parallel system.

9.2 IMPROVING THE DETECTION SYSTEM

The prototype detection system described in this thesis functions satisfactorily within certain limitations - it is clear that some straightforward improvements can be made to improve both the DQE and the overall performance.

9.2.1 Improving the DQE

At low signal intensities the DQE response is limited by the high readout and digitisation noise associated with the photodiode array and its drive electronics. The most obvious way to reduce this figure is to employ a higher precision (14 or 15 bit) ADC, in order to reduce the contribution made by digitisation errors. Secondly, more attention should be paid to suppressing external noise picked up on signal leads etc, by shortening signal paths and using shielding wherever possible.

An immediate DQE benefit could be obtained by increasing the number of photons recorded per incident electron as discussed in chapter 8. This could be done by matt finishing the output face of the YAG scintillator to reduce internal reflection effects, although care is required to ensure that the spatial resolution and uniformity of response of the screen are not significantly degraded.

At higher dose rates the DQE is determined by the channel to channel non-uniformity of response of the detector, and saturation effects of the photodiode array. The latter could be improved by replacing the Hamamatsu S2304 class sensor with an S2301 series device, which has an identical construction except that the photodiode element pitch is increased from 25μm to 50μm, resulting in a cell capacity which is more than doubled. The non-uniformity of response of the detector is readout noise limited, as illustrated in chapter 8, so that the previous suggestions for reducing the readout noise should also help in this area. Implementation of a more sophisticated digital response correction technique such as the gain averaging procedure described by Shuman [1985] is certainly possible, however these

methods generally require the acquisition of multiple spectra, thus reducing the detection efficiency advantage that is the whole purpose behind parallel recording. Ultimately it is the non-linear component of the channel to channel response of the photodiode array itself which determines the limit to uniformity of response, and this can only be reduced by improvements in the manufacture of the devices.

9.2.2 General improvements in the acquisition system

The electronics designed and built to acquire, store and process the data from the photodiode arrays functioned successfully and reliably during these experiments. However several modifications could be made to improve the performance. It would be useful (and necessary in an operational detector) to interface the photodiode drive electronics to the microprocessor acquisition system, allowing electronic control of the array integration time. The incorporation of a direct memory access (DMA) circuit for storage of the diode video data, and a parallel data transfer interface between this and the VME minicomputer would speed up the data acquisition throughput considerably. Also the stability of the Peltier cooling system could be improved if the diode temperature was monitored and regulated by the microprocessor.

9.2.3 Towards an operational system - future work

The successful implementation of a parallel recording system on the HB5 STEM requires the installation of a suitable second order aberration corrected spectrometer. It would be relatively simple to convert the analysis program of chapter 3 to actually design a spectrometer, however it would be more efficient to utilise an existing design which is commercially available such as the Scheinfein and Isaacson analyser. The construction and testing of a post spectrometer magnification system, of the design described in chapter 5, would have to be undertaken, along with the preparation of a full size 30μm thick single crystal YAG screen.

As regards the detector itself, even if all the improvements to the DQE mentioned previously could be achieved, it is unlikely that the zero loss signal could be recorded without saturating the detector. Either the diode integration time would have to be reduced by speeding up the clocking signals (and accepting the associated decrease in performance), or else some form of fast beam blanking system installed in the microscope and synchronised to the photodiode scan.

Appendix 1

Focussing coefficients of homogeneous field magnetic sector spectrometers

After Enge [1967]

First Order Coefficients - Median Plane

(y/y)	$\cos(\phi - \alpha) / \cos\alpha$
(y/y')	$\sin\phi$
(y/δ)	$1 - \cos\phi$
(y'/y)	$-\sin(\phi - \alpha - \beta) / \cos\alpha\cos\beta$
(y'/y')	$\cos(\phi - \beta) / \cos\beta$
(y'/δ)	$\sin\phi + (1 - \cos\phi)\tan\beta$

First Order Coefficients -Vertical Plane

(x/x)	$1 - \phi\tan\alpha_v$
(x/x')	ϕ
(x'/x)	$-\tan\alpha_v - \tan\beta_v + \phi\tan\alpha_v\tan\beta_v$
(x'/x')	$1 - \phi\tan\beta_v$

Second Order Coefficients - Median Plane

(y/y^2)	$1/2\,[(y'/y)\sin\phi_{-\beta\alpha} + C_1\sin\phi]$
(y/yy')	$(y/y)\tan\alpha + \sin\phi_\alpha\sec^2\beta\cos\phi + \tan\alpha\tan^2\beta$
(y/y'2)	$1/2\,[\cos\phi - (y'/y')\cos\phi_{-\beta}]$
(y/yδ)	$1 + (y/y)(\tan^2\beta - \sec^2\beta\cos\phi)$
(y/y'δ)	$(y/\delta)\sec^2\beta\sin\phi$
(y/δ^2)	$1/2\,[(y/\delta)^2\tan^2\beta - \sin^2\phi]$
(y'/y^2)	$1/2\,[-(y'/y)^2\tan\beta + C_1(y'/y') + C_2(y/y)^2]$
(y'/yy')	$(y'/y)\,[\tan\alpha - (y'/y')\tan\beta] + C_2(y/y)\sin\phi$
(y'/y'^2)	$1/2\,[-\sin\phi_\beta - (y'/y')^2\tan\beta + C_2\sin^2\phi]$
(y'/yδ)	$-(y'/y)(\sec^2\beta + \sin\phi_\beta\tan\beta) + C_2(y/y)(y/\delta)$
(y'/y'δ)	$-(y'/y')(y'/\delta)\tan\beta + C_2(y/\delta)\sin\phi$
(y'/δ^2)	$1/2\,[-(y'/\delta)(2 + (y'/\delta)\tan\beta) + C_2(y/\delta)^2]$

Second Order Coefficients - Cross Terms

(y/x^2) $\quad 1/2\,[(y/y)\sec^2\alpha + \sin\phi\tan^3\alpha - (y/\delta)\tan^2\alpha - (x/x)^2\sec^2\beta - C_1\sin\phi]$

(y/xx') $\quad (y/\delta)\tan\alpha - (y/y')\tan^2\alpha - (x/x)(x/x')\sec^2\beta$

(y/x'^2) $\quad -1/2\,[(y/\delta) + (x/x')^2\sec^2\beta]$

(y'/x^2) $\quad 1/2\,[(y'/y)\sec^2\alpha + (y'/y')\tan^3\alpha - (y'/\delta)\tan^2\alpha + 2(x/x)(x'/x)\tan^2\beta$
$+ (x/x)^2\tan^3\beta - C_1(y'/y) + C_2(x/x)^2]$

(y'/xx') $\quad (y'/\delta)\tan\alpha - (y'/y')\tan^2\alpha + [(x/x')(x'/x) + (x/x)(x'/x')]\tan^2\beta$
$+ (x/x)(x/x')\tan^3\beta - C_2(x/x)(x/x')$

(y'/x'^2) $\quad 1/2\,[(x/x')^2\tan^3\beta + 2(x/x')(x'/x')\tan^2\beta - (y'/\delta) - C_2(x/x')^2]$

Second Order Coefficients - Vertical Plane

(x/yx) $\quad (y'/y)\tan\alpha + (y/y)(x'/x)\tan\beta - C_1\phi$

(x/yx') $\quad (x/x)\tan\alpha + (y/y)(x'/x')\tan\beta - (y'/y)$

$(x/y'x)$ $\quad -\phi\sec^2\alpha - [1 - (y'/y')]\tan\alpha + (y/y')(x'/x)\tan\beta$

$(x/y'x')$ $\quad 1 - (y'/y') + (y/y')(x'/x')\tan\beta$

$(x/\delta x)$ $\quad (y'/\delta)\tan\alpha + (y/\delta)(x'/x)\tan\beta$

$(x/\delta x')$ $\quad \phi - (y'/\delta) + (y/\delta)(x'/x')\tan\beta$

(x'/yx) $\quad (y'/y)\ [(x/x)\sec^2\beta - \tan\alpha\tan\beta\,] - C_1(x'/x') - C_2(y/y)(x/x)$

(x'/yx') $\quad (y'/y)\ [\phi\sec^2\beta + \tan\beta\,] + (x'/x)\tan\alpha - C_2\phi(y/y)$

$(x'/y'x)$ $\quad (y'/y')(x/x)\sec^2\beta - (x'/x')\sec^2\alpha + [1 - (y'/y')]\tan\alpha\tan\beta - C_2(x/x)\sin\phi$

$(x'/y'x')$ $\quad (y'/y')\ [\phi\sec^2\beta + \tan\beta\,] - \tan\beta - C_2\phi\sin\phi$

$(x'/\delta x)$ $\quad (y'/\delta)\ [(x/x)\sec^2\beta - \tan\alpha\tan\beta] - (x'/x) - C_2(x/x)(y/\delta)$

$(x'/\delta x')$ $\quad (y'/\delta)\ [\phi\sec^2\beta + \tan\beta\,] - C_2\phi(y/\delta)$

Where: $\quad C_1 = R / R_1\cos^3\alpha \qquad C_2 = R / R_2\cos^3\beta$

$\sin\phi_{-\beta\alpha} = \sin(\phi - \alpha + \beta) / \cos\alpha\cos\beta \qquad \cos\phi_{-\beta} = \cos(\phi + \beta) / \cos\beta$

$\sin\phi_{\alpha} = \sin(\phi - \alpha) / \cos\alpha \qquad \sin\phi_{\beta} = \sin(\phi - \beta) / \cos\beta$

Appendix 2

Spectrometer Analysis Programs

Complete listings of programs FSPECT and SPECTRUM are given along with example data files for each. The programs are self-contained except for the plotting routines which call subroutines from the 'SIMPLEPLOT' library.

Program FSPECT expects the input parameters to be those of the spectrometer virtual field boundaries. If only the mechanical boundaries are known, then the integer parameter IV should be set to 1. The program will calculate the displacement between the polefaces and the virtual field boundaries (assuming a value for the fringe field coefficient I_2 is given or can be calculated) but otherwise runs as normal. For more accurate results the input parameters PHI, R1, R2, AOBJ and BIM should be referenced to the position of the virtual field boundaries and the program rerun.

Program SPECTRUM is straightforward to use. Parameters DTHETA and DPHI are concerned with the number and angular separation of the trajectories from the point source and should be kept within the limits specified in the program header. ELIMIT and ELOSS determine the energy range and energy increment of the incident electrons - the output spectrum is formed symmetrically about the central ray within an energy range $\pm$ ELIMIT.

```
C                                                                       FSP00010
C     PROGRAM FSPECT                                                    FSP00020
C                                                                       FSP00030
C     This program computes transfer matrix coefficients and            FSP00040
C     optical properties for homogeneous magnetic field sector          FSP00050
C     magnets using the fringing field approximations of ENGE           FSP00060
C     and HEIGHWAY. It is assumed that the sector parameters            FSP00070
C     given are referenced to the virtual field boundaries. If          FSP00080
C     not, the displacement of the effective edges from the             FSP00090
C     mechanical boundaries can be calculated, thus allowing            FSP00100
C     recalculation of the other parameters (by hand!).                 FSP00110
C                                                                       FSP00120
C     The principle variables are defined as follows-                   FSP00130
C     PHI    = Bending angle of central ray in degrees.                 FSP00140
C     R0     = Bending radius of central ray in millimetres.            FSP00150
C     R1     = Radius of curvature of entrance poleface (mm).           FSP00160
C     R2     = Radius of curvature of exit poleface (mm).               FSP00170
C     R1     = 0.0 for straight entrance poleface.                      FSP00180
C     R2     = 0.0 for straight exit poleface.                          FSP00190
C     Alpha  = Tilt angle of entrance poleface in degrees.              FSP00200
C     Beta   = Tilt angle of exit poleface in degrees.                  FSP00210
C     Alphae= Effective tilt angle of entrance poleface due to          FSP00220
C             fringing field effects (vertical transfer matrix only).FSP00230
C     Betae  = Effective tilt angle of exit poleface due to             FSP00240
C             fringing field effects (vertical transfer matrix only).FSP00250
C     Aobj   = Object distance from entrance poleface in millimetres.   FSP00260
C     Bim    = Image distance from exit poleface in millimetres.        FSP00270
C     U      = Object distance normalised to bending radius.            FSP00280
C     V      = Image distance normalised to bending radius.             FSP00290
C     Gap    = Polepiece separation in millimetres.                     FSP00300
C     IFC    = Integer parameter describing fringe field clamping.      FSP00310
C     IFC    = 1 No field clamps used.                                  FSP00320
C     IFC    = 2 Entrance field clamp only.                             FSP00330
C     IFC    = 3 Exit field clamp only.                                 FSP00340
C     IFC    = 4 Entrance and exit field clamps used.                   FSP00350
C     DFC1   = Distance from field clamp to entrance poleface.          FSP00360
C     DFC2   = Distance from exit poleface to field clamp.              FSP00370
C     DFC1/2= 0.0 If no field clamp is used.                            FSP00380
C     I2     = Value of ENGE integral coefficient for fringe field.     FSP00390
C              If I2=0.0 an empirical value is calculated (HEIGHWAY)    FSP00400
C     IV     = Parameter determining the reference of above values.     FSP00410
C     IV     = 0 If parameters referenced to virtual field boundaries.FSP00420
C     IV     = 1 If parameters referenced to mechanical boundaries.     FSP00430
C     Y      = Horizontal transfer matrix.                              FSP00440
C     X      = Vertical transfer matrix.                                FSP00450
C     TY     = Total horizontal transfer matrix.                        FSP00460
C     TX     = Total vertical transfer matrix.                          FSP00470
C     HMAG   = Horizontal magnification at horizontal focus.            FSP00480
C     VMAG   = Vertical magnification at vertical focus.                FSP00490
C     DISP   = Horizontal dispersion at horizontal focus.               FSP00500
C                                                                       FSP00510
      IMPLICIT REAL*8(A-H,O-Z)                                          FSP00520
      DIMENSION Y(12,3),X(8,2),TY(12,3),TX(8,2)                         FSP00530
      DIMENSION TITLE(20)                                               FSP00540
      REAL*8 I2                                                         FSP00550
C                                                                       FSP00560
C     Read title of up to 80 characters from unit 1                     FSP00570
      READ(1,1)(TITLE(I),I=1,20)                                        FSP00580
    1 FORMAT(20A4)                                                      FSP00590
C                                                                       FSP00600
C     Read a blank line from unit 1                                     FSP00610
      READ(1,2)                                                         FSP00620
    2 FORMAT(1X)                                                        FSP00630
C                                                                       FSP00640
C     Read first order parameters from unit 1                           FSP00650
C                                                                       FSP00660
      READ(1,5) PHI,R0,ALPHA,BETA,AOBJ,BIM                              FSP00670
      READ(1,2)                                                         FSP00680
C                                                                       FSP00690
C     Read second order and fringe field parameters from unit 1         FSP00700
C                                                                       FSP00710
      READ(1,6) R1,R2,GAP,IFC,DFC1,DFC2                                 FSP00720
```

```
      READ(1,2)                                                          FSP00730
      READ(1,7) I2,IV                                                    FSP00740
5     FORMAT(5X,6F10.4)                                                  FSP00750
6     FORMAT(5X,3F10.4,I10,2F10.4)                                       FSP00760
7     FORMAT(5X,F10.4,I10)                                               FSP00770
C                                                                        FSP00780
C       Write title and headings on unit 2                               FSP00790
C                                                                        FSP00800
      CALL HEAD(PHI,R0,ALPHA,BETA,AOBJ,R1,R2,GAP,IFC,DFC1,DFC2,TITLE,IV)FSP00810
C                                                                        FSP00820
C       Convert from degrees to radians                                  FSP00830
C                                                                        FSP00840
      PHIR=(3.1415926*2*PHI)/360                                         FSP00850
      ALPHAR=(3.1415926*2*ALPHA)/360                                     FSP00860
      BETAR=(3.1415926*BETA*2)/360                                       FSP00870
C                                                                        FSP00880
C       Divide AOBJ and BIM by R0 to make equations non-dimensional      FSP00890
C                                                                        FSP00900
      U=AOBJ/R0                                                          FSP00910
      V=BIM/R0                                                           FSP00920
C                                                                        FSP00930
C       Call subroutine to calculate effective vertical entrance         FSP00940
C       and exit tilts. If the sector parameters given are those of      FSP00950
C       the mechanical boundaries (IV = 1) then the displacement of      FSP00960
C       virtual field boundary from the poleface is calculated.          FSP00970
C                                                                        FSP00980
      CALL FRINGE(GAP,IFC,DFC1,ALPHAR,R0,R1,ALPHAE,1,I2,IV)              FSP00990
      CALL FRINGE(GAP,IFC,DFC2,BETAR,R0,R2,BETAE,2,I2,IV)                FSP01000
C                                                                        FSP01010
C       Call subroutine to calculate transfer matrices                   FSP01020
C                                                                        FSP01030
99    CALL TRANS(PHIR,ALPHAR,BETAR,ALPHAE,BETAE,R0,R1,R2,Y,X)            FSP01040
C                                                                        FSP01050
C       Call subroutine to print out transfer matrices.                  FSP01060
C                                                                        FSP01070
      CALL MATRIX(Y,X,1)                                                 FSP01080
C                                                                        FSP01090
C       Call subroutine to calculate total transfer matrices             FSP01100
C                                                                        FSP01110
      CALL TTRANS(Y,X,U,V,TY,TX)                                         FSP01120
C                                                                        FSP01130
C       Call subroutine to print out total transfer matrices             FSP01140
C                                                                        FSP01150
      CALL MATRIX(TY,TX,2)                                               FSP01160
C                                                                        FSP01170
C       Check if system is double focussing and calculate optical        FSP01180
C       properties. If not, calculate horizontal and vertical image      FSP01190
C       positions and optical properties at these positions.             FSP01200
C                                                                        FSP01210
      IF(DABS(TY(2,1)).GT.0.01) GOTO 10                                  FSP01220
      IF(DABS(TX(2,1)).GT.0.01) GOTO 10                                  FSP01230
      HMAG=TY(1,1)                                                       FSP01240
      VMAG=TX(1,1)                                                       FSP01250
      DISP=TY(3,1)                                                       FSP01260
      VY=V                                                               FSP01270
      VX=V                                                               FSP01280
      WRITE(2,30) AOBJ                                                   FSP01290
      GOTO 16                                                            FSP01300
C                                                                        FSP01310
C       Not double focussing so calculate new image positions            FSP01320
C                                                                        FSP01330
10    WRITE(2,31) AOBJ                                                   FSP01340
      VY=-(Y(1,1)*U+Y(2,1))/(Y(1,2)*U+Y(2,2))                            FSP01350
      VX=-(X(1,1)*U+X(2,1))/(X(1,2)*U+X(2,2))                            FSP01360
      HMAG=Y(1,1)+(VY*Y(1,2))                                            FSP01370
      VMAG=X(1,1)+(VX*X(1,2))                                            FSP01380
      DISP=Y(3,1)+(VY*Y(3,2))                                            FSP01390
C                                                                        FSP01400
C       Output optical properties                                        FSP01410
C                                                                        FSP01420
16    WRITE(2,40) HMAG,VY*R0                                             FSP01430
      WRITE(2,50) VMAG,VX*R0                                             FSP01440
```

```
      WRITE(2,60) DISP                                                  FSP01450
30    FORMAT(//1X,'SPECTROMETER IS DOUBLE FOCUSSING AT OBJECT',         FSP01460
     -     ' POSITION ',F8.2,' mm')                                     FSP01470
31    FORMAT(//1X,'SPECTROMETER IS NOT DOUBLE FOCUSSING AT OBJECT',     FSP01480
     -     ' POSITION ',F8.2,' mm')                                     FSP01490
40    FORMAT(/1X,'HORIZONTAL MAGNIFICATION = ',F8.4,3X,'AT IMAGE',      FSP01500
     -     ' POSITION = ',F8.4,' mm')                                   FSP01510
50    FORMAT(/1X,'VERTICAL MAGNIFICATION = ',F8.4,3X,'AT IMAGE',        FSP01520
     -     ' POSITION = ',F8.4,' mm')                                   FSP01530
60    FORMAT(/1X,'DISPERSION = ',F8.4,3X,'AT HORIZONTAL IMAGE POSITION')FSP01540
      STOP                                                              FSP01550
      END                                                               FSP01560
C                                                                       FSP01570
C       Subroutine Trans                                                FSP01580
C                                                                       FSP01590
C       This subroutine calculates the horizontal                       FSP01600
C       and vertical transfer matrices.                                 FSP01610
C                                                                       FSP01620
      SUBROUTINE TRANS(PHI,A,B,AE,BE,R0,R1,R2,Y,X)                      FSP01630
      IMPLICIT REAL*8(A-H,O-Z)                                          FSP01640
      DIMENSION Y(12,3),X(8,2)                                          FSP01650
C                                                                       FSP01660
C       Set up various constants                                        FSP01670
C                                                                       FSP01680
      IF(R1.EQ.0.0.OR.R2.EQ.0.0) GOTO 5                                 FSP01690
      C1=R0/(R1*(DCOS(A)**3))                                           FSP01700
      C2=R0/(R2*(DCOS(B)**3))                                           FSP01710
5     SEC2A=1.0/(DCOS(A)**2)                                            FSP01720
      SEC2B=1.0/(DCOS(B)**2)                                            FSP01730
      SPHIBA=DSIN(PHI-A+B)/(DCOS(A)*DCOS(B))                            FSP01740
      CPHIB=DCOS(PHI+B)/DCOS(B)                                         FSP01750
      SPHIA=DSIN(PHI-A)/DCOS(A)                                         FSP01760
      SPHIB=DSIN(PHI-B)/DCOS(B)                                         FSP01770
C                                                                       FSP01780
C       Initialise Y and X arrays to zero                               FSP01790
C                                                                       FSP01800
      DO 20 I=1,12                                                      FSP01810
      DO 10 J=1,3                                                       FSP01820
      Y(I,J)=0.0                                                        FSP01830
10    CONTINUE                                                          FSP01840
20    CONTINUE                                                          FSP01850
      DO 40 I=1,8                                                       FSP01860
      DO 30 J=1,2                                                       FSP01870
      X(I,J)=0.0                                                        FSP01880
30    CONTINUE                                                          FSP01890
40    CONTINUE                                                          FSP01900
C                                                                       FSP01910
C       Calculate first order horizontal coefficients                   FSP01920
C                                                                       FSP01930
      Y(1,1)=DCOS(PHI-A)/DCOS(A)                                        FSP01940
      Y(2,1)=DSIN(PHI)                                                  FSP01950
      Y(3,1)=(1.0-DCOS(PHI))                                            FSP01960
      Y(1,2)=-(DSIN(PHI-A-B)/(DCOS(A)*DCOS(B)))                         FSP01970
      Y(2,2)=DCOS(PHI-B)/DCOS(B)                                        FSP01980
      Y(3,2)=DSIN(PHI)+((1.0-DCOS(PHI))*DTAN(B))                        FSP01990
      Y(3,3)=1.0                                                        FSP02000
C                                                                       FSP02010
C       Calculate first order vertical coefficients                     FSP02020
C                                                                       FSP02030
      X(1,1)=1.0-(PHI*DTAN(AE))                                         FSP02040
      X(2,1)=PHI                                                        FSP02050
      X(1,2)=((PHI*DTAN(AE))*DTAN(BE))-DTAN(AE)-DTAN(BE)                FSP02060
      X(2,2)=1.0-(PHI*DTAN(BE))                                         FSP02070
C                                                                       FSP02080
C       Calculate second order horizontal elements (row 1)              FSP02090
C                                                                       FSP02100
      Y(4,1) =0.5*(DCOS(PHI)-(Y(2,2)*CPHIB))                            FSP02110
      Y(5,1) =-0.5*(Y(3,1)+((X(2,1)**2)*SEC2B))                         FSP02120
      Y(6,1) =0.5*((Y(3,1)**2)*(DTAN(B)**2)-(DSIN(PHI)**2))             FSP02130
      Y(7,1) =Y(3,1)*SEC2B*DSIN(PHI)                                    FSP02140
      Y(8,1) =0.5*(Y(1,2)*SPHIBA+(C1*DSIN(PHI)))                        FSP02150
      Y(9,1) =0.5*(Y(1,1)*SEC2A+(DSIN(PHI)*(DTAN(A)**3))-(Y(3,1)*       FSP02160
```

```
     -       (DTAN(AE)**2))-((X(1,1)**2)*SEC2B)-(C1*DSIN(PHI)))          FSP02170
      Y(10,1)=(Y(1,1)*DTAN(A))+(SPHIA*SEC2B*DCOS(PHI))+(DTAN(A)*         FSP02180
     -       (DTAN(B)**2))                                               FSP02190
      Y(11,1)=(Y(3,1)*DTAN(AE))-(Y(2,1)*(DTAN(A)**2))-(X(1,1)*X(2,1)*    FSP02200
     -       SEC2B)                                                      FSP02210
      Y(12,1)=1.0+(Y(1,1)*((DTAN(B)**2)-(SEC2B*DCOS(PHI))))              FSP02220
C                                                                        FSP02230
C        Calculate second order horizontal elements (row 2)              FSP02240
C                                                                        FSP02250
      Y(4,2) =0.5*(-SPHIB-((Y(2,2)**2)*DTAN(B))+(C2*(DSIN(PHI)**2)))     FSP02260
      Y(5,2) =0.5*((X(2,1)**2)*(DTAN(B)**3)+(2.0*X(2,1)*X(2,2)*          FSP02270
     -       (DTAN(B)**2))-Y(3,2)-(C2*(X(2,1)**2)))                      FSP02280
      Y(6,2) =0.5*(-Y(3,2)*(2.0+(Y(3,2)*DTAN(B)))+(C2*(Y(3,1)**2)))      FSP02290
      Y(7,2) =-(Y(2,2)*Y(3,2)*DTAN(B))+(C2*Y(3,1)*DSIN(PHI))             FSP02300
      Y(8,2) =0.5*(-((Y(1,2)**2)*DTAN(B))+(C1*Y(2,2))+(C2*(Y(1,1)**2)))  FSP02310
      Y(9,2) =0.5*((Y(1,2)*SEC2A)+(Y(2,2)*(DTAN(A)**3))-(Y(3,2)*(DTAN    FSP02320
     -       (AE)**2))+(2.0*X(1,1)*X(1,2)*(DTAN(B)**2))+((X(1,1)**2)*    FSP02330
     -       (DTAN(B)**3))-(C1*Y(2,2))-(C2*(X(1,1)**2)))                 FSP02340
      Y(10,2)=Y(1,2)*(DTAN(A)-(Y(2,2)*DTAN(B)))+(C2*Y(1,1)*DSIN(PHI))    FSP02350
      Y(11,2)=(Y(3,2)*DTAN(AE))-(Y(2,2)*(DTAN(A)**2))+((DTAN(B)**2)*     FSP02360
     -       (X(2,1)*X(1,2)+X(1,1)*X(2,2)))+(X(1,1)*X(2,1)*(DTAN(B)**3)FSP02370
     -       )-(C2*X(1,1)*X(2,1))                                        FSP02380
      Y(12,2)=-Y(1,2)*(SEC2B+(SPHIB*DTAN(B)))+(C2*Y(1,1)*Y(3,1))         FSP02390
C                                                                        FSP02400
C        Calculate second order vertical elements (row 1)                FSP02410
C                                                                        FSP02420
      X(3,1)=1.0-Y(2,2)+(Y(2,1)*X(2,2)*DTAN(B))                          FSP02430
      X(4,1)=PHI-Y(3,2)+(Y(3,1)*X(2,2)*DTAN(B))                          FSP02440
      X(5,1)=(Y(1,2)*DTAN(A))+(Y(1,1)*X(1,2)*DTAN(B))-(C1*PHI)           FSP02450
      X(6,1)=-(PHI*SEC2A)-((1.0-Y(2,2))*DTAN(A))+(Y(2,1)*X(1,2)*DTAN(B))FSP02460
      X(7,1)=(Y(3,2)*DTAN(A))+(Y(3,1)*X(1,2)*DTAN(B))                    FSP02470
      X(8,1)=(X(1,1)*DTAN(A))+(Y(1,1)*X(2,2)*DTAN(B))-Y(1,2)             FSP02480
C                                                                        FSP02490
C        Calculate second order vertical elements (row 2)                FSP02500
C                                                                        FSP02510
      X(3,2)=Y(2,2)*((PHI*SEC2B)+DTAN(B))-DTAN(B)-(C2*PHI*DSIN(PHI))     FSP02520
      X(4,2)=Y(3,2)*((PHI*SEC2B)+DTAN(B))-(C2*PHI*Y(3,1))                FSP02530
      X(5,2)=Y(1,2)*((X(1,1)*SEC2B)-(DTAN(A)*DTAN(B)))-(C1*X(2,2))-      FSP02540
     -       (C2*Y(1,1)*X(1,1))                                          FSP02550
      X(6,2)=(Y(2,2)*X(1,1)*SEC2B)-(X(2,2)*SEC2A)+((1.0-Y(2,2))*DTAN(A)) FSP02560
     -       *DTAN(B))-(C2*X(1,1)*DSIN(PHI))                             FSP02570
      X(7,2)=Y(3,2)*((X(1,1)*SEC2B)-(DTAN(A)*DTAN(B)))-(C2*X(1,1)*Y(3,1)FSP02580
     -       )-X(1,2)                                                    FSP02590
      X(8,2)=Y(1,2)*((PHI*SEC2B)+DTAN(B))+(X(1,2)*DTAN(A))-(C2*PHI*      FSP02600
     -       Y(1,1))                                                     FSP02610
      RETURN                                                             FSP02620
      END                                                                FSP02630
C                                                                        FSP02640
C                                                                        FSP02650
C        Subroutine Ttrans                                               FSP02660
C                                                                        FSP02670
C        This subroutine calculates the total vertical                   FSP02680
C        and horizontal transfer matrices.                               FSP02690
C                                                                        FSP02700
      SUBROUTINE TTRANS(Y,X,U,V,TY,TX)                                   FSP02710
      IMPLICIT REAL*8(A-H,O-Z)                                           FSP02720
      DIMENSION Y(12,3),TY(12,3),X(8,2),TX(8,2)                          FSP02730
C                                                                        FSP02740
C        INITIALISE TY AND TZ ARRAYS TO ZERO                             FSP02750
C                                                                        FSP02760
      DO 20 I=1,12                                                       FSP02770
      DO 10 J=1,3                                                        FSP02780
      TY(I,J)=0.0                                                        FSP02790
10    CONTINUE                                                           FSP02800
20    CONTINUE                                                           FSP02810
      DO 40 I=1,8                                                        FSP02820
      DO 30 J=1,2                                                        FSP02830
      TX(I,J)=0.0                                                        FSP02840
30    CONTINUE                                                           FSP02850
40    CONTINUE                                                           FSP02860
C                                                                        FSP02870
C        Calculate total horizontal matrix elements                      FSP02880
```

```
C
      TY(1,1) =Y(1,1)+(V*Y(1,2))                                        FSP02890
      TY(2,1) =U*(Y(1,1)+(V*Y(1,2)))+Y(2,1)+(V*Y(2,2))                  FSP02900
      TY(3,1) =Y(3,1)+(V*Y(3,2))                                        FSP02910
      TY(4,1) =(U*U*(Y(8,1)+(V*Y(8,2))))+(U*(Y(10,1)+(V*Y(10,2))))+     FSP02920
     -         Y(4,1)+(V*Y(4,2))                                        FSP02930
      TY(5,1) =(U*U*(Y(9,1)+(V*Y(9,2))))+(U*(Y(11,1)+(V*Y(11,2))))+     FSP02940
     -         Y(5,1)+(V*Y(5,2))                                        FSP02950
      TY(6,1) =Y(6,1)+(V*Y(6,2))                                        FSP02960
      TY(7,1) =(U*(Y(12,1)+(V*Y(12,2))))+Y(7,1)+(V*Y(7,2))              FSP02970
      TY(8,1) =Y(8,1)+(V*Y(8,2))                                        FSP02980
      TY(9,1) =Y(9,1)+(V*Y(9,2))                                        FSP02990
      TY(10,1)=(2.0*U*(Y(8,1)+(V*Y(8,2))))+(Y(10,1)+(V*Y(10,2)))        FSP03000
      TY(11,1)=(2.0*U*(Y(9,1)+(V*Y(9,2))))+(Y(11,1)+(V*Y(11,2)))        FSP03010
      TY(12,1)=Y(12,1)+(V*Y(12,2))                                      FSP03020
      TY(1,2) =Y(1,2)                                                   FSP03030
      TY(2,2) =(U*Y(1,2))+Y(2,2)                                        FSP03040
      TY(3,2) =Y(3,2)                                                   FSP03050
      TY(4,2) =(U*U*Y(8,2))+(U*(Y(10,2)+Y(4,2)))                        FSP03060
      TY(5,2) =(U*U*Y(9,2))+(U*(Y(11,2)+Y(5,2)))                        FSP03070
      TY(6,2) =Y(6,2)                                                   FSP03080
      TY(7,2) =(U*Y(12,2))+Y(7,2)                                       FSP03090
      TY(8,2) =Y(8,2)                                                   FSP03100
      TY(9,2) =Y(9,2)                                                   FSP03110
      TY(10,2)=(2.0*U*Y(8,2))+Y(10,2)                                   FSP03120
      TY(11,2)=(2.0*U*Y(9,2))+Y(11,2)                                   FSP03130
      TY(12,2)=Y(12,2)                                                  FSP03140
      TY(3,3) =1.0                                                      FSP03150
C                                                                       FSP03160
C       Calculate total vertical matrix elements                        FSP03170
C                                                                       FSP03180
      TX(1,1) =X(1,1)+(V*X(1,2))                                        FSP03190
      TX(2,1) =U*(X(1,1)+(V*X(1,2)))+X(2,1)+(V*X(2,2))                  FSP03200
      TX(3,1) =(U*U*X(5,1))+U*(X(6,1)+X(8,1))+X(3,1)+V*(X(3,2)+(U*(     FSP03210
     -         X(6,2)+X(8,2)))+(U*U*X(5,2)))                            FSP03220
      TX(4,1) =(U*X(7,1))+X(4,1)+V*(X(4,2)+(U*X(7,2)))                  FSP03230
      TX(5,1) =X(5,1)+(V*X(5,2))                                        FSP03240
      TX(6,1) =(U*X(5,1))+X(6,1)+V*(X(6,2)+(U*X(5,2)))                  FSP03250
      TX(7,1) =X(7,1)+(V*X(7,2))                                        FSP03260
      TX(8,1) =(U*X(5,1))+X(8,1)+V*(X(8,2)+(U*X(5,2)))                  FSP03270
      TX(1,2) =X(1,2)                                                   FSP03280
      TX(2,2) =(U*X(1,2))+X(2,2)                                        FSP03290
      TX(3,2) =(U*U*X(5,2))+U*(X(6,2)+X(8,2))+X(3,2)                    FSP03300
      TX(4,2) =X(4,2)+(U*X(7,2))                                        FSP03310
      TX(5,2) =X(5,2)                                                   FSP03320
      TX(6,2) =X(6,2)+(U*X(5,2))                                        FSP03330
      TX(7,2) =X(7,2)                                                   FSP03340
      TX(8,2) =X(8,2)+(U*X(5,2))                                        FSP03350
      RETURN                                                            FSP03360
      END                                                               FSP03370
C                                                                       FSP03380
C                                                                       FSP03390
C                                                                       FSP03400
C       Subroutine Matrix                                               FSP03410
C                                                                       FSP03420
C       This subroutine prints out the transfer matrices on             FSP03430
C       unit 2. The parameter ORDER defines the type of matrix          FSP03440
C       ORDER = 1 Transfer matrix                                       FSP03450
C       ORDER = 2 Total transfer matrix                                 FSP03460
C                                                                       FSP03470
      SUBROUTINE MATRIX(Y,X,ORDER)                                      FSP03480
      IMPLICIT REAL*8(A-H,O-Z)                                          FSP03490
      INTEGER ORDER                                                     FSP03500
      DIMENSION Y(12,3),X(8,2)                                          FSP03510
      IF(ORDER.EQ.1) WRITE(2,10)                                        FSP03520
      IF(ORDER.EQ.2) WRITE(2,80)                                        FSP03530
      WRITE(2,91)                                                       FSP03540
      WRITE(2,50)(Y(J,1),J=1,6)                                         FSP03550
      WRITE(2,50)(Y(J,2),J=1,6)                                         FSP03560
      WRITE(2,50)(Y(J,3),J=1,6)                                         FSP03570
      WRITE(2,92)                                                       FSP03580
      WRITE(2,50)(Y(J,1),J=7,12)                                        FSP03590
      WRITE(2,50)(Y(J,2),J=7,12)                                        FSP03600
```

```
      WRITE(2,50)(Y(J,3),J=7,12)                                        FSP03610
      IF(ORDER.EQ.1) WRITE(2,60)                                        FSP03620
      IF(ORDER.EQ.2) WRITE(2,90)                                        FSP03630
      WRITE(2,93)                                                       FSP03640
      WRITE(2,61)(X(J,1),J=1,4)                                         FSP03650
      WRITE(2,61)(X(J,2),J=1,4)                                         FSP03660
      WRITE(2,94)                                                       FSP03670
      WRITE(2,61)(X(J,1),J=5,8)                                         FSP03680
      WRITE(2,61)(X(J,2),J=5,8)                                         FSP03690
      RETURN                                                            FSP03700
10    FORMAT(//1X,'ELEMENTS OF HORIZONTAL TRANSFER MATRIX',/)           FSP03710
60    FORMAT(//1X,'ELEMENTS OF VERTICAL TRANSFER MATRIX',/)             FSP03720
80    FORMAT(//1X,'ELEMENTS OF THE TOTAL HORIZONTAL TRANSFER MATRIX',/) FSP03730
90    FORMAT(//1X,'ELEMENTS OF THE TOTAL VERTICAL TRANSFER MATRIX',/)   FSP03740
91    FORMAT(10X,'y/y',7X,4Hy/y',6X,'y/d',5X,5Hy/y'2,5X,5Hy/x'2,6X,     FSP03750
     -       4Hy/d2)                                                    FSP03760
92    FORMAT(/8X,5Hy/y'd,6X,4Hy/y2,6X,4Hy/x2,6X,5Hy/yy',5X,5Hy/xx',     FSP03770
     -       5X,4Hy/yd)                                                 FSP03780
93    FORMAT(10X,'x/x',7X,4Hx/x',4X,6Hx/y'x',4X,5Hx/x'd)                FSP03790
94    FORMAT(/9X,'x/yx',5X,5Hx/y'x,6X,4Hx/xd,6X,5Hx/yx')                FSP03800
50    FORMAT(1X,'| ',6F10.4,' |')                                       FSP03810
61    FORMAT(1X,'| ',4F10.4,' |')                                       FSP03820
      END                                                               FSP03830
C                                                                       FSP03840
C                                                                       FSP03850
C       Subroutine Head                                                 FSP03860
C                                                                       FSP03870
C       This subroutine writes out titles and headings on unit 2.       FSP03880
C                                                                       FSP03890
      SUBROUTINE HEAD(PHI,R0,AL,BET,AOBJ,R1,R2,GAP,IFC,DFC1,DFC2,T,IV)  FSP03900
      IMPLICIT REAL*8(A-H,O-Z)                                          FSP03910
      DIMENSION T(20)                                                   FSP03920
      WRITE(2,5)                                                        FSP03930
      WRITE(2,7)(T(I),I=1,20)                                           FSP03940
      IF(IV.EQ.0) THEN                                                  FSP03950
      WRITE(2,8)                                                        FSP03960
      ELSE                                                              FSP03970
      WRITE(2,9)                                                        FSP03980
      END IF                                                            FSP03990
      WRITE(2,10) PHI                                                   FSP04000
      WRITE(2,15) R0                                                    FSP04010
      WRITE(2,20) AL                                                    FSP04020
      WRITE(2,25) BET                                                   FSP04030
      WRITE(2,30) AOBJ                                                  FSP04040
      WRITE(2,35) GAP                                                   FSP04050
      IF(R1.NE.0.0) WRITE(2,40) R1                                      FSP04060
      IF(R2.NE.0.0) WRITE(2,45) R2                                      FSP04070
      GOTO(50,55,60,65)IFC                                              FSP04080
50    RETURN                                                            FSP04090
55    WRITE(2,75) DFC1                                                  FSP04100
      WRITE(2,80)                                                       FSP04110
      RETURN                                                            FSP04120
60    WRITE(2,90)                                                       FSP04130
      WRITE(2,85) DFC2                                                  FSP04140
      RETURN                                                            FSP04150
65    WRITE(2,75) DFC1                                                  FSP04160
      WRITE(2,85) DFC2                                                  FSP04170
      RETURN                                                            FSP04180
5     FORMAT(//1X,'OPTICAL PROPERTIES OF HOMOGENOUS MAGNETIC FIELD',/,  FSP04190
     -       ' SECTOR MAGNET USING FRINGING FIELD APPROXIMATION.'//)     FSP04200
7     FORMAT(20A4)                                                      FSP04210
8     FORMAT(/1X,'VIRTUAL FIELD BOUNDARIES')                            FSP04220
9     FORMAT(/1X,'MECHANICAL BOUNDARIES')                               FSP04230
10    FORMAT(//1X,'BENDING ANGLE OF CENTRAL RAY = ',F8.2,' Degrees')    FSP04240
15    FORMAT(/1X,'BENDING RADIUS OF CENTRAL RAY = ',F8.2,' mm.')        FSP04250
20    FORMAT(/1X,'ENTRANCE POLEFACE TILT = ',F8.3,' Degrees')           FSP04260
25    FORMAT(/1X,'EXIT POLEFACE TILT = ',F8.3,' Degrees')               FSP04270
30    FORMAT(/1X,'OBJECT POSITION = ',F8.2,' mm.')                      FSP04280
35    FORMAT(/1X,'POLEPIECE SEPARATION = ',F8.2,' mm.')                 FSP04290
40    FORMAT(/1X,'ENTRANCE FIELD RADIUS OF CURVATURE = ',F8.2,' mm.')   FSP04300
45    FORMAT(/1X,'EXIT FACE RADIUS OF CURVATURE = ',F8.2,' mm.')        FSP04310
70    FORMAT(/1X,'NO FIELD CLAMPS USED.')                               FSP04320
```

```
75    FORMAT(/1X,'DISTANCE FROM ENTRANCE CLAMP TO POLE = ',F6.2,' mm.') FSP04330
80    FORMAT(/1X,'NO EXIT FIELD CLAMP')                                 FSP04340
85    FORMAT(/1X,'DISTANCE FROM EXIT CLAMP TO POLE = ',F6.2,' mm.')     FSP04350
90    FORMAT(/1X,'NO ENTRANCE FIELD CLAMP')                             FSP04360
      END                                                               FSP04370
C                                                                       FSP04380
C                                                                       FSP04390
C       Subroutine Fringe                                               FSP04400
C                                                                       FSP04410
C       This subroutine calculates the effective poleface tilts         FSP04420
C       using the semi-empirical formulae of ENGE and HEIGHWAY.         FSP04430
C       If the parameters given are not referenced to the virtual fieldFSP04440
C       boundaries then the virtual field boundary displacement from    FSP04450
C       the mechanical edge can be calculated.                          FSP04460
C                                                                       FSP04470
C       The principle variables are defined as follows:                 FSP04480
C       GAP   = Polepiece separation.                                   FSP04490
C       D     = Polepiece separation normalised to bending radius.      FSP04500
C       IFC   = Integer parameter describing fringe field clamping.     FSP04510
C       DFC   = Distance of field clamp from poleface.                  FSP04520
C       T     = Distance of clamp from poleface normalised to GAP       FSP04530
C       A     = Mechanical poleface tilt.                               FSP04540
C       R0    = Bending radius.                                         FSP04550
C       R     = Radius of curvature of poleface.                        FSP04560
C       ANGLE = Effective poleface tilt.                                FSP04570
C       ISIDE = Integer parameter.                                      FSP04580
C       ISIDE = 1 Entrance poleface.                                    FSP04590
C       ISIDE = 2 Exit poleface.                                        FSP04600
C       I2    = Integral coefficient from ENGE. If I2=0.0 then an       FSP04610
C               empirical value is calculated from HEIGHWAY.            FSP04620
C       K     = Equivalent empirical value for I2 (HEIGHWAY)            FSP04630
C       C     = Correction coefficient C (HEIGHWAY)                     FSP04640
C       DELTA = Poleface tilt correction angle.                         FSP04650
C       E     = Distance of virtual field boundary from poleface.       FSP04660
C                                                                       FSP04670
      SUBROUTINE FRINGE(GAP,IFC,DFC,A,R0,R,ANGLE,ISIDE,I2,IV)           FSP04680
      IMPLICIT REAL*8(A-H,O-Z)                                          FSP04690
      REAL*8 K,I2                                                       FSP04700
C                                                                       FSP04710
C       Set constants.                                                  FSP04720
C                                                                       FSP04730
      IF(GAP.NE.0.0) GOTO 3                                             FSP04740
      T = 0.0                                                           FSP04750
      GOTO 4                                                            FSP04760
3     T = DFC/GAP                                                       FSP04770
4     D = GAP/R0                                                        FSP04780
C                                                                       FSP04790
C       Entrance or exit poleface?                                      FSP04800
C                                                                       FSP04810
      GOTO(5,10) ISIDE                                                  FSP04820
5     WRITE(2,1)                                                        FSP04830
C                                                                       FSP04840
C       If I2 is given then use Enge expression for effective tilt.     FSP04850
C                                                                       FSP04860
      IF(I2.NE.0.0) GOTO 50                                             FSP04870
      GOTO 15                                                           FSP04880
C                                                                       FSP04890
C       If I2 is given then use Enge expression for effective tilt.     FSP04900
C                                                                       FSP04910
10    WRITE(2,2)                                                        FSP04920
      IF(I2.NE.0.0) GOTO 50                                             FSP04930
      GOTO 15                                                           FSP04940
C                                                                       FSP04950
C       Field is clamped so use HEIGHWAY expression for K               FSP04960
C                                                                       FSP04970
15    K = 0.1326+(0.0842*T)+(0.00805*T*T)                               FSP04980
C                                                                       FSP04990
C       Calculate HEIGHWAY correction coefficient C                     FSP05000
C                                                                       FSP05010
20    C = 1.015-(0.9226D-3*A)+(0.02794*D)-(0.4276D-2*A*D)-(0.1912*D*D*D)FSP05020
      C = C+(0.9153D-7*A*A*A)-(0.3320D-6*A*A*A*D)-(0.0232*K)            FSP05030
      C = C+(0.2834D-2*K*A)-(0.2621D-4*K*A*A)-(0.05834*K*A*D)           FSP05040
```

```
      C = C-(0.5473D-3*K*A*A*D*D)+(1.994*K*D*D*D)+(0.06623*K*A*D*D)      FSP05050
      C = C+(0.3968D-3*K*D*A*A)-(0.1698*K*A*D*D*D)                       FSP05060
      C = C+(0.4281D-2*K*A*A*D*D*D)-(0.3498D-4*K*A*A*A*D*D*D)            FSP05070
C                                                                        FSP05080
C        Calculate tilt correction angle and resultant effective tilt    FSP05090
C                                                                        FSP05100
      DELTA = C*K*D*(1.0+(DSIN(A)**2))/DCOS(A)                           FSP05110
      ANGLE = A-DELTA                                                    FSP05120
C                                                                        FSP05130
C        If the parameters are those of the mechanical boundaries        FSP05140
C        then calculate distance of virtual field from poleface.         FSP05150
C        Note - only valid for clamped fields.                           FSP05160
C        Is poleface straight or curved?                                 FSP05170
C                                                                        FSP05180
      IF(IV.GT.0) GOTO 29                                                FSP05190
      IF(R.NE.0.0) GOTO 25                                               FSP05200
      E = GAP*((0.386*T)-(0.0455*T*T))                                   FSP05210
      GOTO 29                                                            FSP05220
25    E = GAP*((0.386+(0.324*GAP/R))*T-(0.0455+(0.093*GAP/R))*T*T)       FSP05230
      GOTO 29                                                            FSP05240
C                                                                        FSP05250
C        Integral coefficient I2 has been given so calculate             FSP05260
C        correction angle based on ENGE expression.                      FSP05270
C                                                                        FSP05280
50    DELTA = I2*D*(1.0+(DSIN(A-(1.2*I2*D))**2))/(DCOS(A-(1.2*I2*D))**3)FSP05290
      ANGLE = DTAN(A)-DELTA                                              FSP05300
      ANGLE = DATAN(ANGLE)                                               FSP05310
C                                                                        FSP05320
C        Write out properties on unit 1                                  FSP05330
C                                                                        FSP05340
29    WRITE(2,30) K,C                                                    FSP05350
      WRITE(2,35)((ANGLE*360)/(2*3.1415926))                             FSP05360
      IF(IV.GT.0) WRITE(2,40) E                                          FSP05370
      RETURN                                                             FSP05380
1     FORMAT(//1X,'ENTRANCE FRINGING FIELD PROPERTIES.')                 FSP05390
2     FORMAT(//1X,'EXIT FRINGING FIELD PROPERTIES.')                     FSP05400
30    FORMAT(/1X,'INTEGRAL COEFFICIENT K = ',F12.4,//,                   FSP05410
     -     ' CORRECTION COEFFICIENT C = ',F10.4)                         FSP05420
35    FORMAT(/1X,'EFFECTIVE VERTICAL POLEFACE TILT = ',F10.4,' Degrees')FSP05430
40    FORMAT(/1X,'EFFECTIVE EDGE DISPLACEMENT = ',F10.4,' mm.')          FSP05440
      END                                                                FSP05450
```

```
C       PROGRAM SPECTRUM                                                SPE00010
C                                                                       SPE00020
C       This program uses the total first and second order transfer     SPE00030
C       coefficients from FSPECT to produce an intensity distribution   SPE00040
C       plot of the spectrometer dispersion plane for a  point source   SPE00050
C       with a circular collector aperture. The central ray is assumed  SPE00060
C       to be the zero energy loss beam. For serial collection systems  SPE00070
C       an alignment figure can also be produced.                       SPE00080
C                                                                       SPE00090
C       The principle variables are defined as follows:                 SPE00100
C                                                                       SPE00110
C       TY     = 1st and 2nd order median plane transfer coefficients   SPE00120
C       TZ     = 1st and 2nd order vertical plane transfer coefficients SPE00130
C       R0     = Bending radius of spectrometer (mm).                   SPE00140
C       EEV    = Electron energy (eV).                                  SPE00150
C       ELOSS  = Electron energy loss step (eV).                        SPE00160
C       ELIMIT = Maximum energy loss (eV).                              SPE00170
C       BETA   = Acceptance half angle of spectrometer (mrad).          SPE00180
C       DTHETA = Increment in azimuthal angle of the point source       SPE00190
C                (1 < dtheta < 90) degrees.                             SPE00200
C       DPHI   = Increment in polar angle of the point source           SPE00210
C                (dphi > beta/21) mrads.                                SPE00220
C       SLIT   = Width of energy selecting slit in microns.             SPE00230
C       DSLIT  = Distance of lower edge of the slit from the optic axis SPE00240
C                (measured in the +y direction) in um.                  SPE00250
C       YDASH  = Array containing median plane gradient component       SPE00260
C                of each ray.                                           SPE00270
C       ZDASH  = Array containing vertical plane gradient component     SPE00280
C                of each ray.                                           SPE00290
C       RMAX   = Maximum gradient                                       SPE00300
C       IPOINT = Number of rays between (0.0 < PHI < BETA)              SPE00310
C       ILINE  = Number of lines of rays between (0.0 < THETA < 90.0)   SPE00320
C       IEND   = Last column of YDASH and ZDASH containing a gradient   SPE00330
C       ILOOP  = Loop counter (Maximum energy loss/energy loss step)    SPE00340
C       DV     = Energy increment                                       SPE00350
C       YSCALE = Length of dispersion (median) axis (um)                SPE00360
C       ZSCALE = Length of vertical axis (um)                           SPE00370
C       DELTA  = Fractional change in momentum from central ray         SPE00380
C       YIM    = Y coordinate of image point (um)                       SPE00390
C       ZIM    = Z coordinate of image point (um)                       SPE00400
C                                                                       SPE00410
C                                                                       SPE00420
      DIMENSION YDASH(94,84),ZDASH(94,84),TY(6,1),TZ(3,1)               SPE00430
      DIMENSION YIM(94,84),ZIM(94,84),AZ1(2),AY1(2),AY2(2)              SPE00440
      DATA EEV/100000./                                                 SPE00450
C                                                                       SPE00460
C       Read input parameters from unit 1                               SPE00470
C                                                                       SPE00480
      READ(1,1) BETA,DTHETA,DPHI                                        SPE00490
    1 FORMAT(/5X,3F10.4)                                                SPE00500
      READ(1,1) R0,ELIMIT,ELOSS                                         SPE00510
C                                                                       SPE00520
C       Read array elements from unit 1                                 SPE00530
C                                                                       SPE00540
      READ(1,3) TY                                                      SPE00550
    3 FORMAT(/5X,6F10.4)                                                SPE00560
      READ(1,4) TZ                                                      SPE00570
    4 FORMAT(/5X,3F10.4)                                                SPE00580
C                                                                       SPE00590
C     Read data on slits                                                SPE00600
C                                                                       SPE00610
      READ(1,5) SLIT,DSLIT                                              SPE00620
    5 FORMAT(/5X,2F10.4)                                                SPE00630
C                                                                       SPE00640
C       Convert from milliradians to radians                            SPE00650
C                                                                       SPE00660
      BETA = BETA*0.001                                                 SPE00670
      DPHI = DPHI*0.001                                                 SPE00680
C                                                                       SPE00690
C       Convert from radians to gradients                               SPE00700
C                                                                       SPE00710
      RMAX = TAN(BETA)                                                  SPE00720
```

```
      DPHI = TAN(DPHI)                                                  SPE00730
C                                                                       SPE00740
C        Calculate loop counters and convert DTHETA to radians          SPE00750
C                                                                       SPE00760
      IPOINT = IFIX(RMAX/DPHI)+1                                        SPE00770
      IEND=IPOINT*4                                                     SPE00780
      ILINE = IFIX(90.0/DTHETA)+1                                       SPE00790
      DTHETA = DTHETA*2*3.1415926/360                                   SPE00800
      ANGLE = 0.0                                                       SPE00810
C                                                                       SPE00820
C        Do loop to assign median plane and vertical plane              SPE00830
C        gradients of each ray in all four quadrants.                   SPE00840
C                                                                       SPE00850
      DO 10 I = 1,ILINE                                                 SPE00860
      R = 0.0                                                           SPE00870
      DO 20 J = 1,IPOINT                                                SPE00880
      YDASH(I,J) = R*COS(ANGLE)                                         SPE00890
      ZDASH(I,J) = R*SIN(ANGLE)                                         SPE00900
      R = R+DPHI                                                        SPE00910
20    CONTINUE                                                          SPE00920
      ANGLE = ANGLE+DTHETA                                              SPE00930
10    CONTINUE                                                          SPE00940
      DO 30 I = 1,ILINE                                                 SPE00950
      DO 40 J = 1,IPOINT                                                SPE00960
      K = J+IPOINT                                                      SPE00970
      YDASH(I,K) = -YDASH(I,J)                                          SPE00980
      ZDASH(I,K) = ZDASH(I,J)                                           SPE00990
      L = K+IPOINT                                                      SPE01000
      YDASH(I,L) = -YDASH(I,J)                                          SPE01010
      ZDASH(I,L) = -ZDASH(I,J)                                          SPE01020
      M = L+IPOINT                                                      SPE01030
      YDASH(I,M) = YDASH(I,J)                                           SPE01040
      ZDASH(I,M) = -ZDASH(I,J)                                          SPE01050
40    CONTINUE                                                          SPE01060
30    CONTINUE                                                          SPE01070
C                                                                       SPE01080
C        Calculate energy loss loop counter                             SPE01090
C                                                                       SPE01100
      ILOOP = IFIX(ELIMIT/ELOSS)+1                                      SPE01110
C                                                                       SPE01120
C        Calculate vertical (median) and horizontal scales              SPE01130
C        for dispersion plane plot.                                     SPE01140
C                                                                       SPE01150
      YSCALE=(ABS(TY(1,1)*RMAX)+ABS(TY(2,1)*0.5*ELIMIT/EEV)+ABS(TY(3,1) SPE01160
     -       *(RMAX**2))+ABS(TY(4,1)*(RMAX**2))+ABS(TY(5,1)*0.25*ELIMIT SPE01170
     -       *ELIMIT/(EEV**2)))*R0*1000*1.1                             SPE01180
      ZSCALE=(ABS(TZ(1,1)*RMAX)+ABS(TZ(2,1)*RMAX*0.5*RMAX)+             SPE01190
     -       (ABS(TZ(3,1)*RMAX*(0.5*ELIMIT/EEV))))*R0*1000*1.1          SPE01200
      YNEG=YSCALE                                                       SPE01210
C     IF(ELIMIT.NE.0.0) YNEG=YSCALE/20                                  SPE01220
C                                                                       SPE01230
C        Set up graphical outputs                                       SPE01240
C                                                                       SPE01250
C     CALL PAGE(20.0,29.0)                                              SPE01260
C     CALL PACK IN(14.0,28.0)                                           SPE01270
      CALL NEWPLT(-ZSCALE,ZSCALE,12.0,-YNEG,YSCALE,12.0)                SPE01280
      CALL DRAW AX('um',2,0.0,0.0)                                      SPE01290
      CALL DRAW AX('um',2,0.0,90.0)                                     SPE01300
C     CALL TITLE('T   ','L   ','SCHEINFEIN ZERO LOSS 5.0 MR',27)        SPE01310
C     AZ1(1)=-ZSCALE                                                    SPE01320
C     AZ1(2)=ZSCALE                                                     SPE01330
C     AY1(1)=-DSLIT                                                     SPE01340
C     AY1(2)=-DSLIT                                                     SPE01350
C     AY2(1)=SLIT-DSLIT                                                 SPE01360
C     AY2(2)=SLIT-DSLIT                                                 SPE01370
C     CALL BRKN CV(AZ1,AY1,2,-1)                                        SPE01380
C     CALL BRKN CV(AZ1,AY2,2,-1)                                        SPE01390
C                                                                       SPE01400
C        Calculate aberration pattern                                   SPE01410
C                                                                       SPE01420
      DO 100 L=1,2                                                      SPE01430
      DV=0.0                                                            SPE01440
```

```
      DO 90 I=1,ILOOP                                                   SPE01450
      IF(L.EQ.1) THEN                                                   SPE01460
      DELTA=0.5*DV/EEV                                                  SPE01470
      ELSE                                                              SPE01480
      DELTA=-0.5*DV/EEV                                                 SPE01490
      END IF                                                            SPE01500
      DO 80 J=1,ILINE                                                   SPE01510
      DO 70 K=1,IEND                                                    SPE01520
      YIN=(TY(1,1)*YDASH(J,K))+(TY(2,1)*DELTA)+(TY(3,1)*(YDASH(J,K)**2))SPE01530
     -    +(TY(4,1)*(ZDASH(J,K)**2))+(TY(5,1)*(DELTA**2))+(TY(6,1)*DELTASPE01540
     -    *YDASH(J,K))                                                 SPE01550
      YIM(J,K)=YIN*R0*1000                                              SPE01560
      ZIN=(TZ(1,1)*ZDASH(J,K))+(TZ(2,1)*ZDASH(J,K)*YDASH(J,K))+(TZ(3,1)*SPE01570
     -    ZDASH(J,K)*DELTA)                                            SPE01580
      ZIM(J,K)=ZIN*R0*1000                                              SPE01590
      CALL JOIN PT(ZIM(J,K),YIM(J,K))                                   SPE01600
      CALL JOIN PT(ZIM(J,K),YIM(J,K))                                   SPE01610
      CALL BREAK                                                        SPE01620
70    CONTINUE                                                          SPE01630
80    CONTINUE                                                          SPE01640
      DV=DV+ELOSS                                                       SPE01650
90    CONTINUE                                                          SPE01660
100   CONTINUE                                                          SPE01670
C                                                                       SPE01680
C       Calculate alignment figure                                      SPE01690
C                                                                       SPE01700
      SCALE=(BETA*1000)+0.5                                             SPE01710
      CALL NEWPLT(-SCALE,SCALE,12.0,-SCALE,SCALE,12.0)                  SPE01720
      CALL DRAW AX(' ',1,0.0,0.0)                                       SPE01730
      CALL DRAW AX(' ',1,0.0,90.0)                                      SPE01740
      CALL TITLE('T   ','L   ','YPRIME V ZPRIME',15)                    SPE01750
C                                                                       SPE01760
C     Does the trajectory pass through the slits?                       SPE01770
C                                                                       SPE01780
      DO 50 I=1,ILINE                                                   SPE01790
      DO 60 J=1,IEND                                                    SPE01800
      Z = ZDASH(I,J)*1000                                               SPE01810
      Y = YDASH(I,J)*1000                                               SPE01820
      IF(YIM(I,J).GE.-DSLIT.AND.YIM(I,J).LE.(SLIT-DSLIT)) THEN          SPE01830
      CALL MARK PT(Z,Y,3)                                               SPE01840
      END IF                                                            SPE01850
60    CONTINUE                                                          SPE01860
50    CONTINUE                                                          SPE01870
      CALL END PLT                                                      SPE01880
      STOP                                                              SPE01890
      END                                                               SPE01900
```

Example data files for FSPECT and SPECDAT. The parameters given refer to the Shuman spectrometer described in chapter 3.

```
FILE: FSPECT    DATA      A    GLASGOW HEP CMS/SP V 4.19

 SHUMAN SPECTROMETER VIRTUAL FIELD BOUNDARIES.
          PHI      RADIUS       ALPHA        BETA        AOBJ         BIM
      70.0000     165.100     11.7440     28.7850    594.3600    393.598
           R1          R2         GAP         IFC        DFC1        DFC2
      116.726     -99.555     22.6770           4      10.669      10.669
           I2          IV
         0.00           0
```

```
FILE: SPECTRUM DATA      A    GLASGOW HEP CMS/SP V 4.19

         BETA     DTHETA       DPHI
          5.0        1.0      0.250
           R0     ELIMIT       STEP
        165.1     1000.0      100.0
         y/y'        y/d      y/y'2       y/x'2       y/d2      y/y'd
      -0.0003     3.7600    -0.0266      0.0542    -5.8583    -0.0031
         x/x'     x/y'x'       x/x'd
       0.0005    -0.0593    37.4568
        SLIT       DSLIT
        1.00       0.500
```

Appendix 3

First and second order focussing coefficients for quadrupole lenses

Convergent Plane		Divergent Plane	
(y/y)	$\cos \sqrt{q}\, z$	(x/x)	$\cosh \sqrt{q}\, z$
(y/y')	$(1 / \sqrt{q}) \sin \sqrt{q}\, z$	(x/x')	$(1 / \sqrt{q}) \sinh \sqrt{q}\, z$
(y'/y)	$-\sqrt{q} \sin \sqrt{q}\, z$	(x'/x)	$\sqrt{q} \sinh \sqrt{q}\, z$
(y'/y')	$\cos \sqrt{q}\, z$	(x'/x')	$\cosh \sqrt{q}\, z$
(y/yδ)	$1/2\, q\, z\, (y/y')$	(x/xδ)	$-1/2\, q\, z\, (x/x')$
(y/y'δ)	$1/2\, [(y/y') - z\, (y/y)]$	(x/x'δ)	$1/2\, [(x/x') - z\, (x/x)]$
(y'/yδ)	$1/2\, q\, [z\, (y/y) + (y/y')]$	(x'/xδ)	$-1/2\, q\, [z\, (x/x) + (x/x')]$
(y'/y'δ)	$1/2 \sqrt{q}\, z \sin \sqrt{q}\, z$	(x'/x'δ)	$-1/2 \sqrt{q}\, z \sinh \sqrt{q}\, z$

After Nakabushi and Matsuo [1982]

Appendix 4

Quadrupole Analysis Programs

Listings of programs QPAIR, QTRIP4 and QQUAD are given along with example data files. Again the programs are self-contained except for the plotting routines which use the SIMPLEPLOT library. QTRIP4 and QQUAD are set up to analyse the 'high mag mode' described in chapter 5. 'Low mag' or any other configuration can be simulated by making the appropriate changes in the order of the parameters in the calls to subroutine QCOMB. Changing the configuration will also affect the iteration procedure in QQUAD, and lines 161 and 165 may have to be altered - the correct sense can be determined from the output of QTRIP4.

```
C                                                                       QPA00010
C       PROGRAM QPAIR                                                   QPA00020
C                                                                       QPA00030
C       This program computes the universal curves and                  QPA00040
C       magnifications of quadrupole pairs over a given                 QPA00050
C       range of lens excitations                                       QPA00060
C                                                                       QPA00070
C       The principle variables are defined as follows-                 QPA00080
C                                                                       QPA00090
C       Lenth1 - Effective length of first quadrupole Q1                QPA00100
C       Lenth2 - Effective length of second quadrupole Q2               QPA00110
C       Rtqz1  - Excitation (theta1) of first quadrupole Q1             QPA00120
C       Rtqz2  - Excitation (theta2) of second quadrupole Q2            QPA00130
C       Delqz1 - Increment in Q1 excitation                             QPA00140
C       Delqz2 - Increment in Q2 excitation                             QPA00150
C       Nk1    - Number of increments in Q1 excitation (<=10)           QPA00160
C       Nk2    - Number of increments in Q2 excitation (<=10)           QPA00170
C       Ratio  - Ratio of image positions (W/V)                         QPA00180
C       D      - Gap between lenses (mm)                                QPA00190
C       Y1     - First order convergent transfer matrix Q1              QPA00200
C       Y2     - First order convergent transfer matrix Q2              QPA00210
C       YCD    - Combined transfer matrix - vertical plane              QPA00220
C       XDC    - Combined transfer matrix - horizontal plane            QPA00230
C       TY     - Total transfer matrix - vertical plane                 QPA00240
C       TX     - Total transfer matrix - horizontal plane               QPA00250
C       Ustig  - Calculated object position giving desired ratio of     QPA00260
C                image positions                                        QPA00270
C       Vstig  - Calculated image position - vertical plane             QPA00280
C       Wstig  - Calculated image position - horizontal plane           QPA00290
C       Conmag - Vertical plane magnification at focus                  QPA00300
C       Divmag - Horizontal plane magnification at focus                QPA00310
C                                                                       QPA00320
C                                                                       QPA00330
      IMPLICIT REAL*8(A-H,O-Z)                                          QPA00340
      REAL*4 OBJ(10,10),IMG(10,10),MAG(10,10),EXITN(10,10)              QPA00350
      DIMENSION Y1(2,2),X1(2,2),TY(2,2),TX(2,2)                         QPA00360
      DIMENSION Y2(2,2),X2(2,2),YCD(2,2),XDC(2,2)                       QPA00370
      DIMENSION TITLE(20)                                               QPA00380
      REAL*8 LENTH1,LENTH2                                              QPA00390
C                                                                       QPA00400
C       Read title of up to 80 characters from unit 1                   QPA00410
      READ(1,1)(TITLE(I),I=1,20)                                        QPA00420
C                                                                       QPA00430
C       Read a blank line from unit 1                                   QPA00440
      READ(1,2)                                                         QPA00450
C                                                                       QPA00460
C       Read first quadrupole parameters from unit 1                    QPA00470
C                                                                       QPA00480
      READ(1,7) LENTH1,RTQZ1,DELQZ1,NK1                                 QPA00490
C                                                                       QPA00500
C       Read another blank line then second quadrupole parameters       QPA00510
C                                                                       QPA00520
      READ(1,2)                                                         QPA00530
      READ(1,7) LENTH2,RTQZ2,DELQZ2,NK2                                 QPA00540
C                                                                       QPA00550
C       Read a blank line then first order imaging properties           QPA00560
C                                                                       QPA00570
      READ(1,2)                                                         QPA00580
      READ(1,6) RATIO,D                                                 QPA00590
C                                                                       QPA00600
1     FORMAT(20A4)                                                      QPA00610
2     FORMAT(1X)                                                        QPA00620
6     FORMAT(5X,2F10.4)                                                 QPA00630
7     FORMAT(5X,3F10.4,I10)                                             QPA00640
C                                                                       QPA00650
C       Convert from millimetres to metres                              QPA00660
C                                                                       QPA00670
      D=D*0.001                                                         QPA00680
      LENTH1=LENTH1*0.001                                               QPA00690
      LENTH2=LENTH2*0.001                                               QPA00700
C                                                                       QPA00710
C       Write title and headings on unit 2                              QPA00720
```

```
C                                                                       QPA00730
      CALL FHEAD(LENTH1,LENTH2,RTQZ1,RTQZ2,U,RATIO,D,TITLE)             QPA00740
C                                                                       QPA00750
C     Start to loop through all the desired excitations                 QPA00760
C                                                                       QPA00770
      DO 1001 J = 1,NK2                                                 QPA00780
      DO 1000 I = 1,NK1                                                 QPA00790
C                                                                       QPA00800
C        Call subroutine to calculate first quadrupole transfer matrix  QPA00810
C                                                                       QPA00820
      CALL QTRANS(LENTH1,RTQZ1,Y1,X1)                                   QPA00830
C                                                                       QPA00840
C        Call subroutine to calculate second quadrupole transfer matrix QPA00850
C                                                                       QPA00860
      CALL QTRANS(LENTH2,RTQZ2,Y2,X2)                                   QPA00870
C                                                                       QPA00880
C        Call subroutine to calculate the combined transfer matrices    QPA00890
C                                                                       QPA00900
      CALL QCOMB(Y1,X1,Y2,X2,D,YCD,XDC)                                 QPA00910
C                                                                       QPA00920
C        Calculate correct object position to give the required         QPA00930
C        ratio of horizontal to vertical image distances. A ratio       QPA00940
C        of 1 corresponds to psuedo-stigmatic double focussing.         QPA00950
C                                                                       QPA00960
      A=RATIO*(YCD(1,1)*XDC(1,2))-(YCD(1,2)*XDC(1,1))                   QPA00970
      B=(RATIO*((YCD(1,1)*XDC(2,2))+(YCD(2,1)*XDC(1,2)))-               QPA00980
     +  (YCD(2,2)*XDC(1,1))-(YCD(1,2)*XDC(2,1)))/A                      QPA00990
      C=RATIO*(YCD(2,1)*XDC(2,2))-(YCD(2,2)*XDC(2,1))                   QPA01000
      ROOT=(B**2)-(4*(C/A))                                             QPA01010
      IF(ROOT.GT.0.0) THEN                                              QPA01020
      GOTO 100                                                          QPA01030
      ELSE                                                              QPA01040
      WRITE(2,110)                                                      QPA01050
      USTIG=0.0                                                         QPA01060
      VSTIG=0.0                                                         QPA01070
      WSTIG=0.0                                                         QPA01080
      CONMAG=0.0                                                        QPA01090
      GOTO 999                                                          QPA01100
      END IF                                                            QPA01110
100   USTIG=0.5*(-B+DSQRT(ROOT))                                        QPA01120
      VSTIG=-1.0*((YCD(1,1)*USTIG)+YCD(2,1))/((YCD(1,2)*USTIG)+YCD(2,2))QPA01130
      WSTIG=-1.0*((XDC(1,1)*USTIG)+XDC(2,1))/((XDC(1,2)*USTIG)+XDC(2,2))QPA01140
      CONMAG=YCD(1,1)+(VSTIG*YCD(1,2))                                  QPA01150
      DIVMAG=XDC(1,1)+(WSTIG*XDC(1,2))                                  QPA01160
      WRITE(2,101) USTIG/LENTH1                                         QPA01170
C                                                                       QPA01180
C        Output optical properties                                      QPA01190
C                                                                       QPA01200
16    WRITE(2,40) CONMAG,VSTIG/LENTH1                                   QPA01210
      WRITE(2,50) DIVMAG,WSTIG/LENTH1                                   QPA01220
C                                                                       QPA01230
C     Store results for graphical output                                QPA01240
C                                                                       QPA01250
999   OBJ(I,J)=SNGL(USTIG/LENTH1)                                       QPA01260
      IMG(I,J)=SNGL(VSTIG/LENTH1)                                       QPA01270
      MAG(I,J)=CONMAG                                                   QPA01280
      EXITN(I,J)=RTQZ1                                                  QPA01290
C                                                                       QPA01300
      RTQZ1=RTQZ1+DELQZ1                                                QPA01310
1000  CONTINUE                                                          QPA01320
      RTQZ2=RTQZ2+DELQZ2                                                QPA01330
      RTQZ1=RTQZ1-(NK1*DELQZ1)                                          QPA01340
1001  CONTINUE                                                          QPA01350
C                                                                       QPA01360
C     Call subroutine to draw graph                                     QPA01370
C                                                                       QPA01380
      CALL GRAPH(OBJ,IMG,MAG,EXITN)                                     QPA01390
C                                                                       QPA01400
40    FORMAT(1X,'CONV-DIV MAGNIFICATION = ',F8.4,3X,'AT IMAGE',         QPA01410
     -     ' POSITION = ',F8.4)                                         QPA01420
50    FORMAT(1X,'DIV-CONV MAGNIFICATION = ',F8.4,3X,'AT IMAGE',         QPA01430
     -     ' POSITION = ',F8.4)                                         QPA01440
```

```
101   FORMAT(/1X,'CORRECT OBJECT POSITION FOR REQUIRED IMAGE RATIO = ', QPA01450
     -       D12.6)                                                    QPA01460
110   FORMAT(/1X,'ERROR IN CALCULATION OF ASTIGMATIC OBJECT DISTANCE.') QPA01470
120   STOP                                                            QPA01480
      END                                                             QPA01490
C                                                                     QPA01500
C                                                                     QPA01510
C       Subroutine Qtrans                                             QPA01520
C                                                                     QPA01530
C       This subroutine calculates the first order                    QPA01540
C       convergent and divergent transfer matrices.                   QPA01550
C                                                                     QPA01560
      SUBROUTINE QTRANS(LENGTH,ROOTQZ,Y,X)                            QPA01570
      IMPLICIT REAL*8(A-H,O-Z)                                        QPA01580
      DIMENSION Y(2,2),X(2,2)                                         QPA01590
      REAL*8 LENGTH                                                   QPA01600
      ROOTQ=ROOTQZ/LENGTH                                             QPA01610
      WRITE(2,6) ROOTQZ                                               QPA01620
6     FORMAT(/1X,'Quadrupole angle theta = ',F8.4,' (Dimensionless)') QPA01630
C                                                                     QPA01640
C       Initialise Y and X arrays to zero                             QPA01650
C                                                                     QPA01660
      DO 20 I=1,2                                                     QPA01670
      DO 10 J=1,2                                                     QPA01680
      Y(I,J)=0.0                                                      QPA01690
      X(I,J)=0.0                                                      QPA01700
10    CONTINUE                                                        QPA01710
20    CONTINUE                                                        QPA01720
C                                                                     QPA01730
C       Calculate first order convergent coefficients                 QPA01740
C                                                                     QPA01750
      Y(1,1)=DCOS(ROOTQZ)                                             QPA01760
      Y(2,1)=(1.0/ROOTQ)*DSIN(ROOTQZ)                                 QPA01770
      Y(1,2)=-ROOTQ*DSIN(ROOTQZ)                                      QPA01780
      Y(2,2)=DCOS(ROOTQZ)                                             QPA01790
C                                                                     QPA01800
C       Calculate first order divergent coefficients                  QPA01810
C                                                                     QPA01820
      X(1,1)=DCOSH(ROOTQZ)                                            QPA01830
      X(2,1)=(1.0/ROOTQ)*DSINH(ROOTQZ)                                QPA01840
      X(1,2)=ROOTQ*DSINH(ROOTQZ)                                      QPA01850
      X(2,2)=DCOSH(ROOTQZ)                                            QPA01860
      RETURN                                                          QPA01870
      END                                                             QPA01880
C                                                                     QPA01890
C                                                                     QPA01900
C       Subroutine Qcomb                                              QPA01910
C                                                                     QPA01920
C       This subroutine calculates the combined horizontal            QPA01930
C       and vertical transfer matrices.                               QPA01940
C                                                                     QPA01950
      SUBROUTINE QCOMB(Y1,X1,Y2,X2,D,YCD,XDC)                         QPA01960
      IMPLICIT REAL*8(A-H,O-Z)                                        QPA01970
      DIMENSION Y1(2,2),X1(2,2),Y2(2,2),X2(2,2),YCD(2,2),XDC(2,2)     QPA01980
C                                                                     QPA01990
C       Initialise YCD and XDC arrays to zero                         QPA02000
C                                                                     QPA02010
      DO 10 I=1,2                                                     QPA02020
      DO 10 J=1,2                                                     QPA02030
      YCD(I,J)=0.0                                                    QPA02040
      XDC(I,J)=0.0                                                    QPA02050
10    CONTINUE                                                        QPA02060
C                                                                     QPA02070
C       Calculate convergent-divergent transfer matrix                QPA02080
C                                                                     QPA02090
      YCD(1,1)=Y1(1,1)*X2(1,1)+(Y1(1,2)*(D*X2(1,1)+X2(2,1)))          QPA02100
      YCD(2,1)=Y1(2,1)*X2(1,1)+(Y1(2,2)*(D*X2(1,1)+X2(2,1)))          QPA02110
      YCD(1,2)=Y1(1,1)*X2(1,2)+(Y1(1,2)*(D*X2(1,2)+X2(2,2)))          QPA02120
      YCD(2,2)=Y1(2,1)*X2(1,2)+(Y1(2,2)*(D*X2(1,2)+X2(2,2)))          QPA02130
C                                                                     QPA02140
C       Calculate divergent-convergent matrix                         QPA02150
C                                                                     QPA02160
```

```
      XDC(1,1)=X1(1,1)*Y2(1,1)+(X1(1,2)*(D*Y2(1,1)+Y2(2,1)))            QPA02170
      XDC(2,1)=X1(2,1)*Y2(1,1)+(X1(2,2)*(D*Y2(1,1)+Y2(2,1)))            QPA02180
      XDC(1,2)=X1(1,1)*Y2(1,2)+(X1(1,2)*(D*Y2(1,2)+Y2(2,2)))            QPA02190
      XDC(2,2)=X1(2,1)*Y2(1,2)+(X1(2,2)*(D*Y2(1,2)+Y2(2,2)))            QPA02200
      RETURN                                                            QPA02210
      END                                                               QPA02220
C                                                                       QPA02230
C                                                                       QPA02240
C        Subroutine Fhead                                               QPA02250
C                                                                       QPA02260
C        This subroutine writes out titles and headings on unit 2.      QPA02270
C                                                                       QPA02280
      SUBROUTINE FHEAD(LENTH1,LENTH2,RTQZ1,RTQZ2,U,RATIO,D,TITL)        QPA02290
      IMPLICIT REAL*8(A-H,O-Z)                                          QPA02300
      DIMENSION TITL(20)                                                QPA02310
      REAL*8 LENTH1,LENTH2                                              QPA02320
      WRITE(2,5)                                                        QPA02330
      WRITE(2,7)(TITL(I),I=1,20)                                        QPA02340
      WRITE(2,15) LENTH1*1000                                           QPA02350
      WRITE(2,16) LENTH2*1000                                           QPA02360
      WRITE(2,20) RTQZ1                                                 QPA02370
      WRITE(2,21) RTQZ2                                                 QPA02380
      WRITE(2,30) U*1000                                                QPA02390
      WRITE(2,35) RATIO                                                 QPA02400
      WRITE(2,40) D*1000                                                QPA02410
      RETURN                                                            QPA02420
 5    FORMAT(//1X,'OPTICAL PROPERTIES OF MAGNETIC QUADRUPOLE PAIRS.'//) QPA02430
 7    FORMAT(20A4)                                                      QPA02440
 15   FORMAT(/1X,'LENGTH OF FIRST LENS              = ',F8.2,' mm.')    QPA02450
 16   FORMAT(/1X,'LENGTH OF SECOND LENS             = ',F8.2,' mm.')    QPA02460
 20   FORMAT(/1X,'QUADRUPOLE1 ANGLE THETA           = ',F8.2)           QPA02470
 21   FORMAT(/1X,'QUADRUPOLE2 ANGLE THETA           = ',F8.2)           QPA02480
 30   FORMAT(/1X,'OBJECT POSITION = ',F8.2,' mm.')                      QPA02490
 35   FORMAT(/1X,'RATIO OF HORIZONTAL-VERTICAL IMAGE POSITIONS= ',F8.2) QPA02500
 40   FORMAT(/1X,'LENS SEPARATION = ',F8.2,' mm.'//)                    QPA02510
      END                                                               QPA02520
C                                                                       QPA02530
C                                                                       QPA02540
C        Subroutine Graph                                               QPA02550
C                                                                       QPA02560
C        This subroutine does the plotting                              QPA02570
C                                                                       QPA02580
      SUBROUTINE GRAPH(OBJ,IMG,MAG,EXITN)                               QPA02590
      REAL*4 OBJ(10,10),IMG(10,10),MAG(10,10),EXITN(10,10)              QPA02600
      REAL*4 AX(2),AY(2),BX(2),BY(2),CX(2),CY(2),DX(2),DY(2)            QPA02610
      AX(1)=1.00                                                        QPA02620
      AX(2)=1.00                                                        QPA02630
      AY(1)=0.0                                                         QPA02640
      AY(2)=5.0                                                         QPA02650
      BX(1)=0.0                                                         QPA02660
      BX(2)=4.0                                                         QPA02670
      BY(1)=1.0                                                         QPA02680
      BY(2)=1.0                                                         QPA02690
      CX(1)=-11.05                                                      QPA02700
      CX(2)=-11.05                                                      QPA02710
      CY(1)=0.80                                                        QPA02720
      CY(2)=1.651                                                       QPA02730
      DX(1)=-11.05                                                      QPA02740
      DX(2)=0.0                                                         QPA02750
      DY(1)=1.651                                                       QPA02760
      DY(2)=1.651                                                       QPA02770
C     CALL PAGE(20.0,22.0)                                              QPA02780
      CALL NEWPLT(0.0,5.0,10.0,0.0,5.0,12.0)                            QPA02790
      CALL DRAW AX('Normalised Object Distance U',28,0.0,0.0)           QPA02800
      CALL DRAW AX('Normalsied Image Distance V',27,0.0,90.0)           QPA02810
      CALL BRKN CV(AX,AY,2,-1)                                          QPA02820
      CALL BRKN CV(BX,BY,2,-1)                                          QPA02830
C     CALL TITLE('H   ','C   ','QUADRUPOLE PAIR W/V RATIO = 0.25',32)   QPA02840
C     CALL TITLE('L   ','C   ','QUADRUPOLE SEPARATION = L/2',27)        QPA02850
      DO 10 I=1,10                                                      QPA02860
      DO 20 J=1,10                                                      QPA02870
      IF(OBJ(I,J).GT.5.0.OR.IMG(I,J).GT.5.0) GOTO 20                    QPA02880
```

```
      IF(OBJ(I,J).LE.0.0.OR.IMG(I,J).LE.0.0) GOTO 20                    QPA02890
      CALL JOIN PT(OBJ(I,J),IMG(I,J))                                   QPA02900
20    CONTINUE                                                          QPA02910
      CALL BREAK                                                        QPA02920
10    CONTINUE                                                          QPA02930
      DO 30 J=1,10                                                      QPA02940
      DO 40 I=1,10                                                      QPA02950
      IF(OBJ(I,J).GT.5.0.OR.IMG(I,J).GT.5.0) GOTO 40                    QPA02960
      IF(OBJ(I,J).LE.0.0.OR.IMG(I,J).LE.0.0) GOTO 40                    QPA02970
      CALL JOIN PT(OBJ(I,J),IMG(I,J))                                   QPA02980
40    CONTINUE                                                          QPA02990
      CALL BREAK                                                        QPA03000
30    CONTINUE                                                          QPA03010
C                                                                       QPA03020
C       Draw the magnification graph                                    QPA03030
C                                                                       QPA03040
      CALL NEWPLT(-25.0,0.0,10.0,0.8,1.7,12.0)                          QPA03050
      CALL DRAW AX('Divergent-Convergent Magnification',34,0.8,0.0)     QPA03060
      CALL DRAW AX(' ',1,0.0,90.0)                                      QPA03070
      CALL BRKN CV(CX,CY,2,-1)                                          QPA03080
      CALL BRKN CV(DX,DY,2,-1)                                          QPA03090
C     CALL TITLE('H   ','C   ','QUADRUPOLE PAIR VERTICAL MAGNIFICATION',QPA03100
C    +           38)                                                   QPA03110
C     CALL TITLE('L   ','C   ','QUADRUPOLE SEPARATION = L/2',27)       QPA03120
      DO 50 J=1,10                                                      QPA03130
      DO 60 I=1,10                                                      QPA03140
      IF(MAG(I,J).LT.-25.0.OR.MAG(I,J).GE.0.0) THEN                     QPA03150
      CALL BREAK                                                        QPA03160
      GOTO 60                                                           QPA03170
      END IF                                                            QPA03180
      CALL JOIN PT(MAG(I,J),EXITN(I,J))                                 QPA03190
60    CONTINUE                                                          QPA03200
      CALL BREAK                                                        QPA03210
50    CONTINUE                                                          QPA03220
      CALL END PLT                                                      QPA03230
      RETURN                                                            QPA03240
      END                                                               QPA03250
```

```
C                                                                       QTR00010
C       PROGRAM QTRIP4                                                  QTR00020
C                                                                       QTR00030
C       This program calculates the optical properties of a             QTR00040
C       quadrupole quadruplet given a specified object position.        QTR00050
C       By changing the relevant parameters in the code any two lenses  QTR00060
C       can be varied while the other two run at fixed excitation. The  QTR00070
C       normal case is that the central lenses (Q1,Q2) are held fixed   QTR00080
C       while the outer two (Q0,Q1) are varied. The lens configuration  QTR00090
C       (high mag mode or low mag made) is controlled by the order of   QTR00100
C       the parameters in the call to subroutine QCOMB                  QTR00110
C                                                                       QTR00120
C       The principle variables are defined as follows-                 QTR00130
C                                                                       QTR00140
C       Lenth0   Effective length of first quadrupole Q0 (mm)           QTR00150
C       Lenth1   Effective length of second quadrupole Q1 (mm)          QTR00160
C       Lenth2   Effective length of third quadrupole Q2 (mm)           QTR00170
C       Lenth3   Effective length of fourth quadrupole Q3 (mm)          QTR00180
C       Rtqz0-4  Excitation (theta) of respective quadrupole            QTR00190
C       Delqz0   Increment in Q0 excitation                             QTR00200
C       Delqz3   Increment in Q3 excitation                             QTR00210
C       Nk0      Number of increments in Q0 excitation (<=5)            QTR00220
C       Nk3      Number of increments in Q3 excitation (<=20)           QTR00230
C       D0       Gap between lenses Q0,Q1 (mm)                          QTR00240
C       D1       Gap between lenses Q1,Q2 (mm)                          QTR00250
C       D2       Gap between lenses Q2,Q3 (mm)                          QTR00260
C       U        Object position referenced to entrance of Q0 (mm)      QTR00270
C       Y0-Y3    Second order convergent transfer matrix of relevant    QTR00280
C                quadrupole lens.                                       QTR00290
C       X0-X3    Second order divergent transfer matrix of relevant     QTR00300
C                quadrupole lens.                                       QTR00310
C       YCD      Combined transfer matrix (Q2,Q3) - vertical plane      QTR00320
C       XDC      Combined transfer matrix (Q2,Q3) - horizontal plane    QTR00330
C       YCDC     Combined transfer matrix (Q1,Q2,Q3) - vertical plane   QTR00340
C       XDCD     Combined transfer matrix (Q1,Q2,Q3) - horizontal planeQTR00350
C       YDCDC    Combined transfer matrix (Q0,Q1,Q2,Q3) - vertical      QTR00360
C       XCDCD    Combined transfer matrix (Q0,Q1,Q2,Q3) - horizontal    QTR00370
C       TY       Total second order transfer matrix - vertical plane    QTR00380
C       TX       Total second order transfer matrix - horizontal plane QTR00390
C       Hastig   Calculated image position - vertical plane             QTR00400
C       Dastig   Calculated image position - horizontal plane           QTR00410
C       Conmag   Vertical plane magnification at focus                  QTR00420
C       Divmag   Horizontal plane magnification at focus                QTR00430
C                                                                       QTR00440
      IMPLICIT REAL*8(A-H,O-Z)                                          QTR00450
      DIMENSION Y0(4,4),X0(4,4),YDCDC(4,4),XCDCD(4,4)                   QTR00460
      DIMENSION Y1(4,4),X1(4,4),TY(4,4),TX(4,4)                         QTR00470
      DIMENSION Y2(4,4),X2(4,4),YCD(4,4),XDC(4,4)                       QTR00480
      DIMENSION Y3(4,4),X3(4,4),YCDC(4,4),XDCD(4,4)                     QTR00490
      DIMENSION TITLE(20)                                               QTR00500
      REAL*4 OBJ(20,5,10),HIMAG(20,5,10),DIMAG(20,5,10)                 QTR00510
      REAL*4 CDCMAG(20,5,10),DCDMAG(20,5,10),EXITN(20),Q3EX(10)         QTR00520
      REAL*8 LENTH0,LENTH1,LENTH2,LENTH3                                QTR00530
C                                                                       QTR00540
C       Read title of up to 80 characters from unit 1                   QTR00550
      READ(1,1)(TITLE(I),I=1,20)                                        QTR00560
C                                                                       QTR00570
C       Read focussing quadrupole paramaters                            QTR00580
C                                                                       QTR00590
      READ(1,2)                                                         QTR00600
      READ(1,7) LENTH0,RTQZ0,DELQZ0,NK0                                 QTR00610
C                                                                       QTR00620
C       Read first quadrupole parameters from unit 1                    QTR00630
C                                                                       QTR00640
      READ(1,2)                                                         QTR00650
      READ(1,7) LENTH1,RTQZ1,DELQZ1,NK1                                 QTR00660
C                                                                       QTR00670
C       Read another blank line then second quadrupole parameters       QTR00680
C                                                                       QTR00690
      READ(1,2)                                                         QTR00700
      READ(1,7) LENTH2,RTQZ2,DELQZ2,NK2                                 QTR00710
C                                                                       QTR00720
```

```
C       Read another blank line then third quadrupole parameters        QTR00730
C                                                                       QTR00740
      READ(1,2)                                                         QTR00750
      READ(1,7) LENTH3,RTQZ3,DELQZ3,NK3                                 QTR00760
C                                                                       QTR00770
C       Read a blank line then first order imaging properties           QTR00780
C                                                                       QTR00790
      READ(1,2)                                                         QTR00800
      READ(1,6) U,D0,D1,D2                                              QTR00810
C                                                                       QTR00820
1     FORMAT(20A4)                                                      QTR00830
2     FORMAT(1X)                                                        QTR00840
6     FORMAT(5X,4F10.0)                                                 QTR00850
7     FORMAT(5X,3F10.4,I10)                                             QTR00860
C                                                                       QTR00870
C       Convert from millimetres to metres                              QTR00880
C                                                                       QTR00890
      LENTH0=LENTH0*0.001                                               QTR00900
      LENTH1=LENTH1*0.001                                               QTR00910
      LENTH2=LENTH2*0.001                                               QTR00920
      LENTH3=LENTH3*0.001                                               QTR00930
      U=U*0.001                                                         QTR00940
      D0=D0*0.001                                                       QTR00950
      D1=D1*0.001                                                       QTR00960
      D2=D2*0.001                                                       QTR00970
C                                                                       QTR00980
C       Write title and headings on unit 2                              QTR00990
C                                                                       QTR01000
      CALL FHEAD(LENTH0,LENTH1,LENTH2,LENTH3,RTQZ0,RTQZ1,RTQZ2,RTQZ3,   QTR01010
     -           U,D0,D1,D2,TITLE)                                      QTR01020
C                                                                       QTR01030
C       Start looping excitations                                       QTR01040
C                                                                       QTR01050
      DO 1002 L=1,NK1                                                   QTR01060
      DO 1001 N=1,NK0                                                   QTR01070
      DO 1000 I=1,NK3                                                   QTR01080
C                                                                       QTR01090
C       Call subroutine to calculate focus quadrupole transfer matrix   QTR01100
C                                                                       QTR01110
      CALL QTRANS(LENTH0,RTQZ0,Y0,X0)                                   QTR01120
C                                                                       QTR01130
C       Call subroutine to calculate first quadrupole transfer matrix   QTR01140
C                                                                       QTR01150
      CALL QTRANS(LENTH1,RTQZ1,Y1,X1)                                   QTR01160
C                                                                       QTR01170
C       Call subroutine to calculate second quadrupole transfer matrix  QTR01180
C                                                                       QTR01190
      CALL QTRANS(LENTH2,RTQZ2,Y2,X2)                                   QTR01200
C                                                                       QTR01210
C       Call subroutine to calculate third quadrupole transfer matrix   QTR01220
C                                                                       QTR01230
      CALL QTRANS(LENTH3,RTQZ3,Y3,X3)                                   QTR01240
C                                                                       QTR01250
C       Call subroutine to calculate the Q2/Q3 transfer matrices        QTR01260
C                                                                       QTR01270
      CALL QCOMB(X2,Y2,Y3,X3,D2,YCD,XDC)                                QTR01280
C                                                                       QTR01290
C       Call subroutine to calculate the Q1/Q2/Q3 transfer matrices     QTR01300
C                                                                       QTR01310
      CALL QCOMB(Y1,X1,XDC,YCD,D1,YCDC,XDCD)                            QTR01320
C                                                                       QTR01330
C       Call subroutine to calculate the Q0/Q1/Q2/Q3 transfer matrices  QTR01340
C                                                                       QTR01350
      CALL QCOMB(Y0,X0,XDCD,YCDC,D0,YDCDC,XCDCD)                        QTR01360
C                                                                       QTR01370
C       Object position is given so calculate non-stigmatic             QTR01380
C       image positions.                                                QTR01390
C                                                                       QTR01400
      CALL ASTIG(YDCDC,XCDCD,U,DASTIG,HASTIG,CONMAG,DIVMAG)             QTR01410
C                                                                       QTR01420
C       Output optical properties                                       QTR01430
C                                                                       QTR01440
```

```
      WRITE(2,101) U/LENTH2                                              QTR01450
      WRITE(2,40) CONMAG,HASTIG/LENTH2                                   QTR01460
      WRITE(2,50) DIVMAG,DASTIG/LENTH2                                   QTR01470
C                                                                        QTR01480
C        Set up arrays for graphical output                              QTR01490
C                                                                        QTR01500
      EXITN(I)=SNGL(RTQZ3)                                               QTR01510
      OBJ(I,N,L)=SNGL((U+LENTH0+D0)/LENTH2)                              QTR01520
      IF(OBJ(I,N,L).GT.5.0.OR.OBJ(I,N,L).LT.0.0) OBJ(I,N,L)=0.0          QTR01530
      HIMAG(I,N,L)=SNGL(HASTIG/LENTH2)                                   QTR01540
      DIMAG(I,N,L)=SNGL(DASTIG/LENTH2)                                   QTR01550
      IF(HIMAG(I,N,L).GT.4.0.OR.HIMAG(I,N,L).LT.0.0) HIMAG(I,N,L)=0.0    QTR01560
      IF(DIMAG(I,N,L).GT.4.0.OR.DIMAG(I,N,L).LT.-1.) DIMAG(I,N,L)=0.0    QTR01570
C                                                                        QTR01580
C     Reference the image positions to the central quadrupole pair       QTR01590
C                                                                        QTR01600
      IF(HIMAG(I,N,L).NE.0.0) THEN                                       QTR01610
      HIMAG(I,N,L)=SNGL((HASTIG+LENTH3+D2)/LENTH2)                       QTR01620
      END IF                                                             QTR01630
      IF(DIMAG(I,N,L).NE.0.0) THEN                                       QTR01640
      DIMAG(I,N,L)=SNGL((DASTIG+LENTH3+D2)/LENTH2)                       QTR01650
      END IF                                                             QTR01660
      CDCMAG(I,N,L)=SNGL(CONMAG)                                         QTR01670
      DCDMAG(I,N,L)=SNGL(DIVMAG)                                         QTR01680
      IF(CDCMAG(I,N,L).LT.-70.0.OR.CDCMAG(I,N,L).GT.0.0)                 QTR01690
     +   CDCMAG(I,N,L)=0.0                                               QTR01700
      IF(DCDMAG(I,N,L).LT.-70.0.OR.DCDMAG(I,N,L).GT.0.0)                 QTR01710
     +   DCDMAG(I,N,L)=0.0                                               QTR01720
      RTQZ3=RTQZ3+DELQZ3                                                 QTR01730
1000  CONTINUE                                                           QTR01740
      RTQZ3=RTQZ3-(NK3*DELQZ3)                                           QTR01750
      RTQZ0=RTQZ0+DELQZ0                                                 QTR01760
1001  CONTINUE                                                           QTR01770
      RTQZ0=RTQZ0-(NK0*DELQZ0)                                           QTR01780
      Q3EX(L)=SNGL(RTQZ1)                                                QTR01790
      RTQZ0=RTQZ0+DELQZ0                                                 QTR01800
1002  CONTINUE                                                           QTR01810
C                                                                        QTR01820
C        Call plotting subroutine                                        QTR01830
C                                                                        QTR01840
      IF(NK1.LE.1) THEN                                                  QTR01850
      CALL GRAPH1(OBJ,HIMAG,DIMAG,CDCMAG,DCDMAG,EXITN,NK3,NK0)           QTR01860
      ELSE                                                               QTR01870
      CALL GRAPH2(OBJ,HIMAG,DIMAG,CDCMAG,DCDMAG,Q3EX,NK3)                QTR01880
      END IF                                                             QTR01890
C                                                                        QTR01900
40    FORMAT(/1X,'CONV-DIV-CONV MAG = ',D10.4,3X,'AT IMAGE',             QTR01910
     -     ' POSITION = ',D12.6)                                         QTR01920
50    FORMAT(/1X,'DIV-CONV-DIV  MAG = ',D10.4,3X,'AT IMAGE',             QTR01930
     -     ' POSITION = ',D12.6)                                         QTR01940
101   FORMAT(/1X,'OBJECT POSITION = ',D10.4,' mm.')                      QTR01950
      STOP                                                               QTR01960
      END                                                                QTR01970
C                                                                        QTR01980
C                                                                        QTR01990
C        Subroutine Qtrans                                               QTR02000
C                                                                        QTR02010
C        This subroutine calculates the convergent                       QTR02020
C        and divergent transfer matrices.                                QTR02030
C                                                                        QTR02040
      SUBROUTINE QTRANS(LENGTH,ROOTQZ,Y,X)                               QTR02050
      IMPLICIT REAL*8(A-H,O-Z)                                           QTR02060
      DIMENSION Y(4,4),X(4,4)                                            QTR02070
      REAL*8 LENGTH                                                      QTR02080
C                                                                        QTR02090
C        Set up various constants                                        QTR02100
C                                                                        QTR02110
      ROOTQ=ROOTQZ/LENGTH                                                QTR02120
      Q=ROOTQ**2                                                         QTR02130
      WRITE(2,6) ROOTQZ                                                  QTR02140
6     FORMAT(/1X,'Quadrupole angle theta = ',F8.4,' (Dimensionless)')    QTR02150
C                                                                        QTR02160
```

```
C       Initialise Y and X arrays to zero                                QTR02170
C                                                                        QTR02180
      DO 20 I=1,4                                                        QTR02190
      DO 10 J=1,4                                                        QTR02200
      Y(I,J)=0.0                                                         QTR02210
      X(I,J)=0.0                                                         QTR02220
10    CONTINUE                                                           QTR02230
20    CONTINUE                                                           QTR02240
C                                                                        QTR02250
C       Calculate first and second order convergent coefficients         QTR02260
C                                                                        QTR02270
      Y(1,1)=DCOS(ROOTQZ)                                                QTR02280
      Y(2,1)=(1.0/ROOTQ)*DSIN(ROOTQZ)                                    QTR02290
      Y(3,1)=0.5*Q*LENGTH*Y(2,1)                                         QTR02300
      Y(4,1)=0.5*(Y(2,1)-(LENGTH*Y(1,1)))                                QTR02310
      Y(1,2)=-ROOTQ*DSIN(ROOTQZ)                                         QTR02320
      Y(2,2)=DCOS(ROOTQZ)                                                QTR02330
      Y(3,2)=0.5*Q*((LENGTH*Y(1,1))+Y(2,1))                              QTR02340
      Y(4,2)=0.5*ROOTQZ*DSIN(ROOTQZ)                                     QTR02350
      Y(3,3)=Y(1,1)                                                      QTR02360
      Y(4,3)=Y(2,1)                                                      QTR02370
      Y(3,4)=Y(1,2)                                                      QTR02380
      Y(4,4)=Y(2,2)                                                      QTR02390
C                                                                        QTR02400
C       Calculate first and second order divergent coefficients          QTR02410
C                                                                        QTR02420
      X(1,1)=DCOSH(ROOTQZ)                                               QTR02430
      X(2,1)=(1.0/ROOTQ)*DSINH(ROOTQZ)                                   QTR02440
      X(3,1)=-0.5*ROOTQZ*DSINH(ROOTQZ)                                   QTR02450
      X(4,1)=0.5*(X(2,1)-(LENGTH*X(1,1)))                                QTR02460
      X(1,2)=ROOTQ*DSINH(ROOTQZ)                                         QTR02470
      X(2,2)=DCOSH(ROOTQZ)                                               QTR02480
      X(3,2)=-0.5*Q*((LENGTH*X(1,1))+X(2,1))                             QTR02490
      X(4,2)=-0.5*ROOTQZ*DSINH(ROOTQZ)                                   QTR02500
      X(3,3)=X(1,1)                                                      QTR02510
      X(4,3)=X(2,1)                                                      QTR02520
      X(3,4)=X(1,2)                                                      QTR02530
      X(4,4)=X(2,2)                                                      QTR02540
      RETURN                                                             QTR02550
      END                                                                QTR02560
C                                                                        QTR02570
C                                                                        QTR02580
C       Subroutine Qcomb                                                 QTR02590
C                                                                        QTR02600
C       This subroutine calculates the combined horizontal               QTR02610
C       and vertical transfer matrices.                                  QTR02620
C                                                                        QTR02630
      SUBROUTINE QCOMB(Y1,X1,Y2,X2,D,YCD,XDC)                            QTR02640
      IMPLICIT REAL*8(A-H,O-Z)                                           QTR02650
      DIMENSION Y1(4,4),X1(4,4),Y2(4,4),X2(4,4),YCD(4,4),XDC(4,4)        QTR02660
C                                                                        QTR02670
C       Initialise YCD and XDC arrays to zero                            QTR02680
C                                                                        QTR02690
      DO 10 I=1,4                                                        QTR02700
      DO 10 J=1,4                                                        QTR02710
      YCD(I,J)=0.0                                                       QTR02720
      XDC(I,J)=0.0                                                       QTR02730
10    CONTINUE                                                           QTR02740
C                                                                        QTR02750
C       Calculate convergent-divergent transfer matrix                   QTR02760
C                                                                        QTR02770
      YCD(1,1)=Y1(1,1)*X2(1,1)+(Y1(1,2)*(D*X2(1,1)+X2(2,1)))             QTR02780
      YCD(2,1)=Y1(2,1)*X2(1,1)+(Y1(2,2)*(D*X2(1,1)+X2(2,1)))             QTR02790
      YCD(3,1)=Y1(3,1)*X2(1,1)+(Y1(3,2)*(D*X2(1,1)+X2(2,1)))+            QTR02800
     -         Y1(3,3)*X2(3,1)+(Y1(3,4)*(D*X2(3,1)+X2(4,1)))             QTR02810
      YCD(4,1)=Y1(4,1)*X2(1,1)+(Y1(4,2)*(D*X2(1,1)+X2(2,1)))+            QTR02820
     -         Y1(4,3)*X2(3,1)+(Y1(4,4)*(D*X2(3,1)+X2(4,1)))             QTR02830
      YCD(1,2)=Y1(1,1)*X2(1,2)+(Y1(1,2)*(D*X2(1,2)+X2(2,2)))             QTR02840
      YCD(2,2)=Y1(2,1)*X2(1,2)+(Y1(2,2)*(D*X2(1,2)+X2(2,2)))             QTR02850
      YCD(3,2)=Y1(3,1)*X2(1,2)+(Y1(3,2)*(D*X2(1,2)+X2(2,2)))+            QTR02860
     -         Y1(3,3)*X2(3,2)+(Y1(3,4)*(D*X2(3,2)+X2(4,2)))             QTR02870
      YCD(4,2)=Y1(4,1)*X2(1,2)+(Y1(4,2)*(D*X2(1,2)+X2(2,2)))+            QTR02880
```

```
      TX(4,3) =U*(X(3,3)+(V*X(3,4)))+X(4,3)+(V*X(4,4))                  QTR03610
      TX(3,4) =X(3,4)                                                   QTR03620
      TX(4,4) =(U*X(3,4))+X(4,4)                                        QTR03630
      RETURN                                                            QTR03640
      END                                                               QTR03650
C                                                                       QTR03660
C                                                                       QTR03670
C        Subroutine Astig                                               QTR03680
C                                                                       QTR03690
C        This subroutine calculates the object plane distances          QTR03700
C        given the image plane distance and the transfer matrices.      QTR03710
C                                                                       QTR03720
      SUBROUTINE ASTIG(YCDC,XDCD,U,DASTIG,HASTIG,CONMAG,DIVMAG)         QTR03730
      IMPLICIT REAL*8 (A-H,O-Z)                                         QTR03740
      DIMENSION YCDC(4,4),XDCD(4,4)                                     QTR03750
      DASTIG=-(XDCD(1,1)*U+XDCD(2,1))/(XDCD(1,2)*U+XDCD(2,2))           QTR03760
      DIVMAG=XDCD(1,1)+(DASTIG*XDCD(1,2))                               QTR03770
      HASTIG=-(YCDC(1,1)*U+YCDC(2,1))/(YCDC(1,2)*U+YCDC(2,2))           QTR03780
      CONMAG=YCDC(1,1)+(HASTIG*YCDC(1,2))                               QTR03790
      RETURN                                                            QTR03800
      END                                                               QTR03810
C                                                                       QTR03820
C                                                                       QTR03830
C        Subroutine Fhead                                               QTR03840
C                                                                       QTR03850
C        This subroutine writes out titles and headings on unit 2.      QTR03860
C                                                                       QTR03870
      SUBROUTINE FHEAD(LENTH0,LENTH1,LENTH2,LENTH3,RTQZ0,RTQZ1,         QTR03880
     +                 RTQZ2,RTQZ3,U,D0,D1,D2,TITLE)                    QTR03890
      IMPLICIT REAL*8 (A-H,O-Z)                                         QTR03900
      DIMENSION TITLE(20)                                               QTR03910
      REAL*8 LENTH0,LENTH1,LENTH2,LENTH3                                QTR03920
      WRITE(2,5)                                                        QTR03930
      WRITE(2,7)(TITLE(I),I=1,20)                                       QTR03940
      WRITE(2,14) LENTH0*1000                                           QTR03950
      WRITE(2,19) RTQZ0                                                 QTR03960
      WRITE(2,15) LENTH1*1000                                           QTR03970
      WRITE(2,20) RTQZ1                                                 QTR03980
      WRITE(2,16) LENTH2*1000                                           QTR03990
      WRITE(2,21) RTQZ2                                                 QTR04000
      WRITE(2,17) LENTH3*1000                                           QTR04010
      WRITE(2,22) RTQZ3                                                 QTR04020
      WRITE(2,30) U*1000                                                QTR04030
      WRITE(2,35) D0*1000                                               QTR04040
      WRITE(2,40) D1*1000                                               QTR04050
      WRITE(2,45) D2*1000                                               QTR04060
      RETURN                                                            QTR04070
 5    FORMAT(//1X,'OPTICAL PROPERTIES OF MAGNETIC QUADRUPOLE PAIRS.'//) QTR04080
 7    FORMAT(20A4)                                                      QTR04090
 14   FORMAT(/1X,'LENGTH OF FIRST LENS              = ',F8.2,'mm.')     QTR04100
 15   FORMAT(/1X,'LENGTH OF SECOND LENS             = ',F8.2,'mm.')     QTR04110
 16   FORMAT(/1X,'LENGTH OF THIRD LENS              = ',F8.2,'mm.')     QTR04120
 17   FORMAT(/1X,'LENGTH OF FOURTH LENS             = ',F8.2,'mm.')     QTR04130
 19   FORMAT(/1X,'First quadrupole strength         = ',F8.2)           QTR04140
 20   FORMAT(/1X,'Second quadrupole strength        = ',F8.2)           QTR04150
 21   FORMAT(/1X,'Third quadrupole strength         = ',F8.2)           QTR04160
 22   FORMAT(/1X,'Fourth quadrupole strength        = ',F8.2)           QTR04170
 30   FORMAT(/1X,'OBJECT POSITION = ',F8.2,' mm.')                      QTR04180
 35   FORMAT(/1X,'LENS 1-2 SEPARATION = ',F8.2,' mm.')                  QTR04190
 40   FORMAT(/1X,'LENS 2-3 SEPARATION = ',F8.2,' mm.')                  QTR04200
 45   FORMAT(/1X,'LENS 3-4 SEPARATION = ',F8.2,' mm.')                  QTR04210
      END                                                               QTR04220
C                                                                       QTR04230
C                                                                       QTR04240
C        SUBROUTINE GRAPH1                                              QTR04250
C                                                                       QTR04260
C        This subroutine plots out the optical properties               QTR04270
C        using the simpleplot library routines                          QTR04280
C                                                                       QTR04290
      SUBROUTINE GRAPH1(OBJ,HIMAG,DIMAG,CDCMAG,DCDMAG,EXITN,NK1,NK2)    QTR04300
      REAL*4 OBJ(20,5,10),HIMAG(20,5,10),DIMAG(20,5,10)                 QTR04310
      REAL*4 CDCMAG(20,5,10),DCDMAG(20,5,10),EXITN(20)                  QTR04320
```

```
      REAL*4 OBJIM(20,15),COMMAG(20,10)                                 QTR04330
      DO 10 I=1,NK1                                                     QTR04340
      OBJIM(I,1)=(OBJ(I,1,1))                                           QTR04350
      OBJIM(I,2)=(HIMAG(I,1,1))                                         QTR04360
      OBJIM(I,3)=(DIMAG(I,1,1))                                         QTR04370
      OBJIM(I,4)=(OBJ(I,2,1))                                           QTR04380
      OBJIM(I,5)=(HIMAG(I,2,1))                                         QTR04390
      OBJIM(I,6)=(DIMAG(I,2,1))                                         QTR04400
      OBJIM(I,7)=(OBJ(I,3,1))                                           QTR04410
      OBJIM(I,8)=(HIMAG(I,3,1))                                         QTR04420
      OBJIM(I,9)=(DIMAG(I,3,1))                                         QTR04430
      OBJIM(I,10)=(OBJ(I,4,1))                                          QTR04440
      OBJIM(I,11)=(HIMAG(I,4,1))                                        QTR04450
      OBJIM(I,12)=(DIMAG(I,4,1))                                        QTR04460
      OBJIM(I,13)=(OBJ(I,5,1))                                          QTR04470
      OBJIM(I,14)=(HIMAG(I,5,1))                                        QTR04480
      OBJIM(I,15)=(DIMAG(I,5,1))                                        QTR04490
      COMMAG(I,1)=(CDCMAG(I,1,1))                                       QTR04500
      COMMAG(I,2)=(DCDMAG(I,1,1))                                       QTR04510
      COMMAG(I,3)=(CDCMAG(I,2,1))                                       QTR04520
      COMMAG(I,4)=(DCDMAG(I,2,1))                                       QTR04530
      COMMAG(I,5)=(CDCMAG(I,3,1))                                       QTR04540
      COMMAG(I,6)=(DCDMAG(I,3,1))                                       QTR04550
      COMMAG(I,7)=(CDCMAG(I,4,1))                                       QTR04560
      COMMAG(I,8)=(DCDMAG(I,4,1))                                       QTR04570
      COMMAG(I,9)=(CDCMAG(I,5,1))                                       QTR04580
      COMMAG(I,10)=(DCDMAG(I,5,1))                                      QTR04590
10    CONTINUE                                                          QTR04600
      OBJIM(1,1)=0.0                                                    QTR04610
      CALL PAGE(18.0,22.0)                                              QTR04620
      CALL PACK IN(14.0,20.0)                                           QTR04630
      CALL JBAXES(OBJIM,300,12.0,'Normalised Object and Image Positions'QTR04640
     +           ,37,EXITN,20,8.0,' ',1)                                QTR04650
      ITEMP1=1                                                          QTR04660
      ITEMP2=2                                                          QTR04670
      ITEMP3=3                                                          QTR04680
      DO 21 K=1,NK2*3                                                   QTR04690
      IF((K-ITEMP1).EQ.0) LINE=3                                        QTR04700
      IF((K-ITEMP2).EQ.0) LINE=2                                        QTR04710
      IF((K-ITEMP3).EQ.0) THEN                                          QTR04720
      LINE=0                                                            QTR04730
      ITEMP1=ITEMP1+3                                                   QTR04740
      ITEMP2=ITEMP2+3                                                   QTR04750
      ITEMP3=ITEMP3+3                                                   QTR04760
      ELSE                                                              QTR04770
      GOTO 19                                                           QTR04780
      END IF                                                            QTR04790
19    DO 20 L=1,NK1                                                     QTR04800
      IF(ABS(OBJIM(L,K)).GT.0.0) THEN                                   QTR04810
      CALL JOIN PT(OBJIM(L,K),EXITN(L))                                 QTR04820
      CALL MARK PT(OBJIM(L,K),EXITN(L),LINE)                            QTR04830
      END IF                                                            QTR04840
20    CONTINUE                                                          QTR04850
      CALL BREAK                                                        QTR04860
21    CONTINUE                                                          QTR04870
      CALL SET KY('T   ','R   ',3,12)                                   QTR04880
      CALL MARK KY(3,'OBJECT  POSN ',13)                                QTR04890
      CALL MARK KY(2,'V IMAGE POSN ',13)                                QTR04900
      CALL MARK KY(0,'W IMAGE POSN ',13)                                QTR04910
      CALL JBAXES(COMMAG,200,12.0,'Magnification',13,                   QTR04920
     +           EXITN,20,8.0,'  ',2)                                   QTR04930
      DO 31 M=1,NK2*2                                                   QTR04940
      TEMP=M/2.0                                                        QTR04950
      TEMP=TEMP-INT(TEMP)                                               QTR04960
      IF(ABS(TEMP).GT.0.001) THEN                                       QTR04970
      LINE=2                                                            QTR04980
      ELSE                                                              QTR04990
      LINE=0                                                            QTR05000
      END IF                                                            QTR05010
      DO 30 N=1,NK1                                                     QTR05020
      IF(COMMAG(N,M).LT.0.0) THEN                                       QTR05030
      CALL JOIN PT(COMMAG(N,M),EXITN(N))                                QTR05040
```

```
      CALL MARK PT(COMMAG(N,M),EXITN(N),LINE)                          QTR05050
      END IF                                                           QTR05060
30    CONTINUE                                                         QTR05070
      CALL BREAK                                                       QTR05080
31    CONTINUE                                                         QTR05090
      CALL SET KY('T   ','L   ',2,8)                                   QTR05100
      CALL MARK KY(2,'DCDC MAG ',9)                                    QTR05110
      CALL MARK KY(0,'CDCD MAG ',9)                                    QTR05120
      CALL END PLT                                                     QTR05130
      STOP                                                             QTR05140
      END                                                              QTR05150
C                                                                      QTR05160
C                                                                      QTR05170
C        SUBROUTINE GRAPH2                                             QTR05180
C                                                                      QTR05190
C        This subroutine does the plotting if q3                       QTR05200
C        is the quadrupole which is varied while                       QTR05210
C        q1 and q2 are held constant.                                  QTR05220
C                                                                      QTR05230
      SUBROUTINE GRAPH2(OBJ,HIMAG,DIMAG,CDCMAG,DCDMAG,Q3EX,NK3)        QTR05240
      REAL*4 OBJ(20,5,10),HIMAG(20,5,10),DIMAG(20,5,10)                QTR05250
      REAL*4 CDCMAG(20,5,10),DCDMAG(20,5,10),Q3EX(10)                  QTR05260
      REAL*4 OBJIM(10,3),COMMAG(10,2)                                  QTR05270
      DO 10 I=1,10                                                     QTR05280
      OBJIM(I,1)=OBJ(1,1,I)                                            QTR05290
      OBJIM(I,2)=HIMAG(1,1,I)                                          QTR05300
      OBJIM(I,3)=DIMAG(1,1,I)                                          QTR05310
      COMMAG(I,1)=CDCMAG(1,1,I)                                        QTR05320
      COMMAG(I,2)=DCDMAG(1,1,I)                                        QTR05330
10    CONTINUE                                                         QTR05340
      CALL PAGE(25.0,25.0)                                             QTR05350
      CALL PACK IN(14.0,22.0)                                          QTR05360
      CALL JBAXES(OBJIM,30,15.0,'M',1,Q3EX,10,10.0,' ',1)              QTR05370
      DO 20 K=1,3                                                      QTR05380
      DO 20 L=1,NK3                                                    QTR05390
      LINE=K                                                           QTR05400
20    CALL MARK PT(OBJIM(L,K),Q3EX(L),LINE)                            QTR05410
      CALL SET KY('B   ','L   ',3,12)                                  QTR05420
      CALL MARK KY(1,' OBJECT POSN',12)                                QTR05430
      CALL MARK KY(2,' HIMAGE POSN',12)                                QTR05440
      CALL MARK KY(3,' DIMAGE POSN',12)                                QTR05450
      CALL TITLE('T   ','L   ','QUADRUPOLE TRIPLET OPTICS',25)         QTR05460
      CALL JBAXES(COMMAG,20,15.0,'MAG',3,Q3EX,10,10.0,'K3',2)          QTR05470
      DO 30 M=1,2                                                      QTR05480
      DO 30 N=1,NK3                                                    QTR05490
      LINE=M                                                           QTR05500
30    CALL MARK PT(COMMAG(N,M),Q3EX(N),LINE)                           QTR05510
      CALL SET KY('B   ','L   ',2,8)                                   QTR05520
      CALL MARK KY(1,' CDC MAG',8)                                     QTR05530
      CALL MARK KY(2,' DCD MAG',8)                                     QTR05540
      CALL TITLE('T   ','L   ','QUADRUPOLE TRIPLET OPTICS',25)         QTR05550
      CALL END PLT                                                     QTR05560
      STOP                                                             QTR05570
      END                                                              QTR05580
```

```
C                                                                       QQU00010
C       PROGRAM QQUAD                                                   QQU00020
C                                                                       QQU00030
C       This program calculates the required excitations of the         QQU00040
C       Q0 and Q3 quadrupole lenses in a quadruplet to give a fixed     QQU00050
C       object and vertical image position, assuming that Q1 and Q2     QQU00060
C       are held constant. The lens configuration is controlled         QQU00070
C       by the order of parameters in the call to subroutine QCOMB.     QQU00080
C       Also changing from say high mag to low mag mode requires        QQU00090
C       adjustment of the sign of the lens increments - the correct     QQU00100
C       sense can be obtained by running QTRIP4 for the same optical    QQU00110
C       configuration.                                                  QQU00120
C                                                                       QQU00130
C       The principle variables are defined as follows-                 QQU00140
C                                                                       QQU00150
C       Lenth0   Effective length of first quadrupole Q0 (mm)           QQU00160
C       Lenth1   Effective length of second quadrupole Q1 (mm)          QQU00170
C       Lenth2   Effective length of third quadrupole Q2 (mm)           QQU00180
C       Lenth3   Effective length of fourth quadrupole Q3 (mm)          QQU00190
C       Rtqz0-4  Excitation (theta) of respective quadrupole            QQU00200
C       Delqz0   Increment in Q0 excitation                             QQU00210
C       Delqz3   Increment in Q3 excitation                             QQU00220
C       Nk3      Number of increments in Q3 excitation (<=20)           QQU00230
C       D0       Gap between lenses Q0,Q1 (mm)                          QQU00240
C       D1       Gap between lenses Q1,Q2 (mm)                          QQU00250
C       D2       Gap between lenses Q2,Q3 (mm)                          QQU00260
C       U        Required object position ref. to entrance of Q0 (mm)   QQU00270
C       V        Required vertical image position referenced to the     QQU00280
C                exit of Q3 - normalised to length of Q1 (LENTH2)       QQU00290
C       Y0-Y3    Second order convergent transfer matrix of relevant    QQU00300
C                quadrupole lens.                                       QQU00310
C       X0-X3    Second order divergent transfer matrix of relevant     QQU00320
C                quadrupole lens.                                       QQU00330
C       YCD      Combined transfer matrix (Q2,Q3) - vertical plane      QQU00340
C       XDC      Combined transfer matrix (Q2,Q3) - horizontal plane    QQU00350
C       YCDC     Combined transfer matrix (Q1,Q2,Q3) - vertical plane   QQU00360
C       XDCD     Combined transfer matrix (Q1,Q2,Q3) - horizontal planeQQU00370
C       YDCDC    Combined transfer matrix (Q0,Q1,Q2,Q3) - vertical      QQU00380
C       XCDCD    Combined transfer matrix (Q0,Q1,Q2,Q3) - horizontal    QQU00390
C       TY       Total second order transfer matrix - vertical plane    QQU00400
C       TX       Total second order transfer matrix - horizontal plane QQU00410
C       Hastig   Calculated image position - vertical plane             QQU00420
C       Dastig   Calculated image position - horizontal plane           QQU00430
C       Conmag   Vertical plane magnification at focus                  QQU00440
C       Divmag   Horizontal plane magnification at focus                QQU00450
C                                                                       QQU00460
      IMPLICIT REAL*8(A-H,O-Z)                                          QQU00470
      DIMENSION Y0(4,4),X0(4,4),YDCDC(4,4),XCDCD(4,4)                   QQU00480
      DIMENSION Y1(4,4),X1(4,4),TY(4,4),TX(4,4)                         QQU00490
      DIMENSION Y2(4,4),X2(4,4),YCD(4,4),XDC(4,4)                       QQU00500
      DIMENSION Y3(4,4),X3(4,4),YCDC(4,4),XDCD(4,4)                     QQU00510
      DIMENSION TITLE(20)                                               QQU00520
      REAL*4 CDCMAG(40),DCDMAG(40),Q0EX(40),Q3EX(40)                    QQU00530
      REAL*8 LENTH0,LENTH1,LENTH2,LENTH3                                QQU00540
C                                                                       QQU00550
C        Read title of up to 80 characters from unit 1                  QQU00560
      READ(1,1)(TITLE(I),I=1,20)                                        QQU00570
C                                                                       QQU00580
C        Read focussing quadrupole paramaters                           QQU00590
C                                                                       QQU00600
      READ(1,2)                                                         QQU00610
      READ(1,7) LENTH0,RTQZ0,DELQZ0                                     QQU00620
C                                                                       QQU00630
C        Read first quadrupole parameters from unit 1                   QQU00640
C                                                                       QQU00650
      READ(1,2)                                                         QQU00660
      READ(1,5) LENTH1,RTQZ1                                            QQU00670
C                                                                       QQU00680
C        Read another blank line then second quadrupole parameters      QQU00690
C                                                                       QQU00700
      READ(1,2)                                                         QQU00710
      READ(1,5) LENTH2,RTQZ2                                            QQU00720
```

```
C                                                                       QQU00730
C       Read another blank line then third quadrupole parameters        QQU00740
C                                                                       QQU00750
      READ(1,2)                                                         QQU00760
      READ(1,8) LENTH3,RTQZ3,DELQZ3,NK3                                 QQU00770
C                                                                       QQU00780
C       Read a blank line then first order imaging properties           QQU00790
C                                                                       QQU00800
      READ(1,2)                                                         QQU00810
      READ(1,6) U,V,D0,D1,D2                                            QQU00820
C                                                                       QQU00830
1     FORMAT(20A4)                                                      QQU00840
2     FORMAT(1X)                                                        QQU00850
5     FORMAT(5X,2F10.0)                                                 QQU00860
6     FORMAT(5X,5F10.0)                                                 QQU00870
7     FORMAT(5X,3F10.0)                                                 QQU00880
8     FORMAT(5X,3F10.0,I10)                                             QQU00890
C                                                                       QQU00900
C       Convert from millimetres to metres                              QQU00910
C                                                                       QQU00920
      LENTH0=LENTH0*0.001                                               QQU00930
      LENTH1=LENTH1*0.001                                               QQU00940
      LENTH2=LENTH2*0.001                                               QQU00950
      LENTH3=LENTH3*0.001                                               QQU00960
      U=U*0.001                                                         QQU00970
      D0=D0*0.001                                                       QQU00980
      D1=D1*0.001                                                       QQU00990
      D2=D2*0.001                                                       QQU01000
C                                                                       QQU01010
C       Write title and headings on unit 2                              QQU01020
C                                                                       QQU01030
      CALL FHEAD(LENTH0,LENTH1,LENTH2,LENTH3,RTQZ0,RTQZ1,RTQZ2,RTQZ3,   QQU01040
     -           U,V,D0,D1,D2,TITLE)                                    QQU01050
C                                                                       QQU01060
C       Call subroutine to calculate first quadrupole transfer matrix   QQU01070
C                                                                       QQU01080
      CALL QTRANS(LENTH1,RTQZ1,Y1,X1)                                   QQU01090
C                                                                       QQU01100
C       Call subroutine to calculate second quadrupole transfer matrix  QQU01110
C                                                                       QQU01120
      CALL QTRANS(LENTH2,RTQZ2,Y2,X2)                                   QQU01130
      ICOUNT=0                                                          QQU01140
C                                                                       QQU01150
C       Start looping excitations - if the correct excitation of Q0     QQU01160
C       is beyond 2000xDELQZ0 then the calculation stops and the next   QQU01170
C       value of RTQZ3 is examined.                                     QQU01180
C                                                                       QQU01190
      DO 1000 I=1,NK3                                                   QQU01200
C                                                                       QQU01210
10    IF(ICOUNT.GT.2000) THEN                                           QQU01220
      Q3EX(I)=RTQZ3                                                     QQU01230
      Q0EX(I)=RTQZ0                                                     QQU01240
      WRITE(2,89)                                                       QQU01250
      GOTO 995                                                          QQU01260
      END IF                                                            QQU01270
C                                                                       QQU01280
C       Call subroutine to calculate focus quadrupole transfer matrix   QQU01290
C                                                                       QQU01300
      CALL QTRANS(LENTH0,RTQZ0,Y0,X0)                                   QQU01310
C                                                                       QQU01320
C       Call subroutine to calculate third quadrupole transfer matrix   QQU01330
C                                                                       QQU01340
      CALL QTRANS(LENTH3,RTQZ3,Y3,X3)                                   QQU01350
C                                                                       QQU01360
C       Call subroutine to calculate the Q2/Q3 transfer matrices        QQU01370
C                                                                       QQU01380
      CALL QCOMB(X2,Y2,Y3,X3,D2,YCD,XDC)                                QQU01390
C                                                                       QQU01400
C       Call subroutine to calculate the Q1/Q2/Q3 transfer matrices     QQU01410
C                                                                       QQU01420
      CALL QCOMB(Y1,X1,XDC,YCD,D1,YCDC,XDCD)                            QQU01430
C                                                                       QQU01440
```

```
C       Call subroutine to calculate the Q0/Q1/Q2/Q3 transfer matrices QQU01450
C                                                                     QQU01460
      CALL QCOMB(Y0,X0,XDCD,YCDC,D0,YDCDC,XCDCD)                      QQU01470
C                                                                     QQU01480
C       Object position is given so calculate non-stigmatic          QQU01490
C       image positions.                                              QQU01500
C                                                                     QQU01510
      CALL ASTIG(YDCDC,XCDCD,U,DASTIG,HASTIG,CONMAG,DIVMAG)           QQU01520
C                                                                     QQU01530
C       Check to see if the vertical image position is within        QQU01540
C       a given range of the required position. If it is then        QQU01550
C       store the results else increment Q0 exitation approp-        QQU01560
C       riately.                                                      QQU01570
C                                                                     QQU01580
      TEMP=(HASTIG/LENTH2)-V                                          QQU01590
      IF(DABS(TEMP).LE.0.005) GOTO 990                                QQU01600
      IF(TEMP.GT.0.005.OR.RTQZ0.LE.0.0) THEN                          QQU01610
      RTQZ0=RTQZ0+DELQZ0                                              QQU01620
      ICOUNT=ICOUNT+1                                                 QQU01630
      END IF                                                          QQU01640
      IF(TEMP.LT.-0.005.AND.RTQZ0.GT.0.0) THEN                        QQU01650
      RTQZ0=RTQZ0-DELQZ0                                              QQU01660
      ICOUNT=ICOUNT+1                                                 QQU01670
      END IF                                                          QQU01680
      GOTO 10                                                         QQU01690
C                                                                     QQU01700
C       Vertical image correct - output optical properties           QQU01710
C                                                                     QQU01720
990   Q3EX(I)=SNGL(RTQZ3)                                             QQU01730
      Q0EX(I)=SNGL(RTQZ0)                                             QQU01740
995   WRITE(2,60) RTQZ0,RTQZ3                                         QQU01750
      WRITE(2,101) U/LENTH2                                           QQU01760
      WRITE(2,40) CONMAG,HASTIG/LENTH2                                QQU01770
      WRITE(2,50) DIVMAG,DASTIG/LENTH2                                QQU01780
C                                                                     QQU01790
C       Set up arrays for graphical output                           QQU01800
C                                                                     QQU01810
      CDCMAG(I)=SNGL(CONMAG)                                          QQU01820
      DCDMAG(I)=SNGL(DIVMAG)                                          QQU01830
      IF(CDCMAG(I).LT.-100.0.OR.CDCMAG(I).GT.0.0)                     QQU01840
     +   CDCMAG(I)=0.0                                                QQU01850
      IF(DCDMAG(I).LT.-100.0.OR.DCDMAG(I).GT.0.0)                     QQU01860
     +   DCDMAG(I)=0.0                                                QQU01870
      RTQZ3=RTQZ3+DELQZ3                                              QQU01880
      ICOUNT=0                                                        QQU01890
1000  CONTINUE                                                        QQU01900
C                                                                     QQU01910
C       Call plotting subroutine                                     QQU01920
C                                                                     QQU01930
      CALL GRAPH(Q3EX,Q0EX,CDCMAG,DCDMAG,NK3)                         QQU01940
                                                                      QQU01950
40    FORMAT(/1X,'CONV-DIV-CONV MAG = ',F10.5,3X,'AT IMAGE',          QQU01960
     -     ' POSITION = ',F10.5,' mm.')                               QQU01970
50    FORMAT(/1X,'DIV-CONV-DIV  MAG = ',F10.5,3X,'AT IMAGE',          QQU01980
     -     ' POSITION = ',F10.5,' mm.')                               QQU01990
60    FORMAT(/1X,'RTQZ0=',F10.5,2X,'RTQZ3=',F10.5)                    QQU02000
89    FORMAT(/1X,'Q0 EXITATION NOT CONVERGED TO OBJECT POSITION')     QQU02010
101   FORMAT(/1X,'OBJECT POSITION = ',F10.5,' mm.')                   QQU02020
      STOP                                                            QQU02030
      END                                                             QQU02040
C                                                                     QQU02050
C                                                                     QQU02060
C       Subroutine Qtrans                                            QQU02070
C                                                                     QQU02080
C       This subroutine calculates the convergent                    QQU02090
C       and divergent transfer matrices.                              QQU02100
C                                                                     QQU02110
      SUBROUTINE QTRANS(LENGTH,ROOTQZ,Y,X)                            QQU02120
      IMPLICIT REAL*8(A-H,O-Z)                                        QQU02130
      DIMENSION Y(4,4),X(4,4)                                         QQU02140
      REAL*8 LENGTH                                                   QQU02150
C                                                                     QQU02160
```

Appendix 4

Quadrupole Analysis Programs

Listings of programs QPAIR, QTRIP4 and QQUAD are given along with example data files. Again the programs are self-contained except for the plotting routines which use the SIMPLEPLOT library. QTRIP4 and QQUAD are set up to analyse the 'high mag mode' described in chapter 5. 'Low mag' or any other configuration can be simulated by making the appropriate changes in the order of the parameters in the calls to subroutine QCOMB. Changing the configuration will also affect the iteration procedure in QQUAD, and lines 161 and 165 may have to be altered - the correct sense can be determined from the output of QTRIP4.

```
C                                                                       QPA00010
C       PROGRAM QPAIR                                                   QPA00020
C                                                                       QPA00030
C       This program computes the universal curves and                  QPA00040
C       magnifications of quadrupole pairs over a given                 QPA00050
C       range of lens excitations                                       QPA00060
C                                                                       QPA00070
C       The principle variables are defined as follows-                 QPA00080
C                                                                       QPA00090
C       Lenth1 - Effective length of first quadrupole Q1                QPA00100
C       Lenth2 - Effective length of second quadrupole Q2               QPA00110
C       Rtqz1  - Excitation (theta1) of first quadrupole Q1             QPA00120
C       Rtqz2  - Excitation (theta2) of second quadrupole Q2            QPA00130
C       Delqz1 - Increment in Q1 excitation                             QPA00140
C       Delqz2 - Increment in Q2 excitation                             QPA00150
C       Nk1    - Number of increments in Q1 excitation (<=10)           QPA00160
C       Nk2    - Number of increments in Q2 excitation (<=10)           QPA00170
C       Ratio  - Ratio of image positions (W/V)                         QPA00180
C       D      - Gap between lenses (mm)                                QPA00190
C       Y1     - First order convergent transfer matrix Q1              QPA00200
C       Y2     - First order convergent transfer matrix Q2              QPA00210
C       YCD    - Combined transfer matrix - vertical plane              QPA00220
C       XDC    - Combined transfer matrix - horizontal plane            QPA00230
C       TY     - Total transfer matrix - vertical plane                 QPA00240
C       TX     - Total transfer matrix - horizontal plane               QPA00250
C       Ustig  - Calculated object position giving desired ratio of     QPA00260
C                image positions                                        QPA00270
C       Vstig  - Calculated image position - vertical plane             QPA00280
C       Wstig  - Calculated image position - horizontal plane           QPA00290
C       Conmag - Vertical plane magnification at focus                  QPA00300
C       Divmag - Horizontal plane magnification at focus                QPA00310
C                                                                       QPA00320
C                                                                       QPA00330
      IMPLICIT REAL*8(A-H,O-Z)                                          QPA00340
      REAL*4 OBJ(10,10),IMG(10,10),MAG(10,10),EXITN(10,10)              QPA00350
      DIMENSION Y1(2,2),X1(2,2),TY(2,2),TX(2,2)                         QPA00360
      DIMENSION Y2(2,2),X2(2,2),YCD(2,2),XDC(2,2)                       QPA00370
      DIMENSION TITLE(20)                                               QPA00380
      REAL*8 LENTH1,LENTH2                                              QPA00390
C                                                                       QPA00400
C       Read title of up to 80 characters from unit 1                   QPA00410
      READ(1,1)(TITLE(I),I=1,20)                                        QPA00420
C                                                                       QPA00430
C       Read a blank line from unit 1                                   QPA00440
      READ(1,2)                                                         QPA00450
C                                                                       QPA00460
C       Read first quadrupole parameters from unit 1                    QPA00470
C                                                                       QPA00480
      READ(1,7) LENTH1,RTQZ1,DELQZ1,NK1                                 QPA00490
C                                                                       QPA00500
C       Read another blank line then second quadrupole parameters       QPA00510
C                                                                       QPA00520
      READ(1,2)                                                         QPA00530
      READ(1,7) LENTH2,RTQZ2,DELQZ2,NK2                                 QPA00540
C                                                                       QPA00550
C       Read a blank line then first order imaging properties           QPA00560
C                                                                       QPA00570
      READ(1,2)                                                         QPA00580
      READ(1,6) RATIO,D                                                 QPA00590
C                                                                       QPA00600
1     FORMAT(20A4)                                                      QPA00610
2     FORMAT(1X)                                                        QPA00620
6     FORMAT(5X,2F10.4)                                                 QPA00630
7     FORMAT(5X,3F10.4,I10)                                             QPA00640
C                                                                       QPA00650
C       Convert from millimetres to metres                              QPA00660
C                                                                       QPA00670
      D=D*0.001                                                         QPA00680
      LENTH1=LENTH1*0.001                                               QPA00690
      LENTH2=LENTH2*0.001                                               QPA00700
C                                                                       QPA00710
C       Write title and headings on unit 2                              QPA00720
```

```
C                                                                       QPA00730
      CALL FHEAD(LENTH1,LENTH2,RTQZ1,RTQZ2,U,RATIO,D,TITLE)             QPA00740
C                                                                       QPA00750
C     Start to loop through all the desired excitations                 QPA00760
C                                                                       QPA00770
      DO 1001 J = 1,NK2                                                 QPA00780
      DO 1000 I = 1,NK1                                                 QPA00790
C                                                                       QPA00800
C        Call subroutine to calculate first quadrupole transfer matrix  QPA00810
C                                                                       QPA00820
      CALL QTRANS(LENTH1,RTQZ1,Y1,X1)                                   QPA00830
C                                                                       QPA00840
C        Call subroutine to calculate second quadrupole transfer matrix QPA00850
C                                                                       QPA00860
      CALL QTRANS(LENTH2,RTQZ2,Y2,X2)                                   QPA00870
C                                                                       QPA00880
C        Call subroutine to calculate the combined transfer matrices    QPA00890
C                                                                       QPA00900
      CALL QCOMB(Y1,X1,Y2,X2,D,YCD,XDC)                                 QPA00910
C                                                                       QPA00920
C        Calculate correct object position to give the required         QPA00930
C        ratio of horizontal to vertical image distances. A ratio       QPA00940
C        of 1 corresponds to psuedo-stigmatic double focussing.         QPA00950
C                                                                       QPA00960
      A=RATIO*(YCD(1,1)*XDC(1,2))-(YCD(1,2)*XDC(1,1))                   QPA00970
      B=(RATIO*((YCD(1,1)*XDC(2,2))+(YCD(2,1)*XDC(1,2)))-               QPA00980
     +  (YCD(2,2)*XDC(1,1))-(YCD(1,2)*XDC(2,1)))/A                      QPA00990
      C=RATIO*(YCD(2,1)*XDC(2,2))-(YCD(2,2)*XDC(2,1))                   QPA01000
      ROOT=(B**2)-(4*(C/A))                                             QPA01010
      IF(ROOT.GT.0.0) THEN                                              QPA01020
      GOTO 100                                                          QPA01030
      ELSE                                                              QPA01040
      WRITE(2,110)                                                      QPA01050
      USTIG=0.0                                                         QPA01060
      VSTIG=0.0                                                         QPA01070
      WSTIG=0.0                                                         QPA01080
      CONMAG=0.0                                                        QPA01090
      GOTO 999                                                          QPA01100
      END IF                                                            QPA01110
100   USTIG=0.5*(-B+DSQRT(ROOT))                                        QPA01120
      VSTIG=-1.0*((YCD(1,1)*USTIG)+YCD(2,1))/((YCD(1,2)*USTIG)+YCD(2,2))QPA01130
      WSTIG=-1.0*((XDC(1,1)*USTIG)+XDC(2,1))/((XDC(1,2)*USTIG)+XDC(2,2))QPA01140
      CONMAG=YCD(1,1)+(VSTIG*YCD(1,2))                                  QPA01150
      DIVMAG=XDC(1,1)+(WSTIG*XDC(1,2))                                  QPA01160
      WRITE(2,101) USTIG/LENTH1                                         QPA01170
C                                                                       QPA01180
C        Output optical properties                                      QPA01190
C                                                                       QPA01200
16    WRITE(2,40) CONMAG,VSTIG/LENTH1                                   QPA01210
      WRITE(2,50) DIVMAG,WSTIG/LENTH1                                   QPA01220
C                                                                       QPA01230
C     Store results for graphical output                                QPA01240
C                                                                       QPA01250
999   OBJ(I,J)=SNGL(USTIG/LENTH1)                                       QPA01260
      IMG(I,J)=SNGL(VSTIG/LENTH1)                                       QPA01270
      MAG(I,J)=CONMAG                                                   QPA01280
      EXITN(I,J)=RTQZ1                                                  QPA01290
C                                                                       QPA01300
      RTQZ1=RTQZ1+DELQZ1                                                QPA01310
1000  CONTINUE                                                          QPA01320
      RTQZ2=RTQZ2+DELQZ2                                                QPA01330
      RTQZ1=RTQZ1-(NK1*DELQZ1)                                          QPA01340
1001  CONTINUE                                                          QPA01350
C                                                                       QPA01360
C     Call subroutine to draw graph                                     QPA01370
C                                                                       QPA01380
      CALL GRAPH(OBJ,IMG,MAG,EXITN)                                     QPA01390
C                                                                       QPA01400
40    FORMAT(1X,'CONV-DIV MAGNIFICATION = ',F8.4,3X,'AT IMAGE',         QPA01410
     -      ' POSITION = ',F8.4)                                        QPA01420
50    FORMAT(1X,'DIV-CONV MAGNIFICATION = ',F8.4,3X,'AT IMAGE',         QPA01430
     -      ' POSITION = ',F8.4)                                        QPA01440
```

```
101   FORMAT(/1X,'CORRECT OBJECT POSITION FOR REQUIRED IMAGE RATIO = ', QPA01450
     -       D12.6)                                                    QPA01460
110   FORMAT(/1X,'ERROR IN CALCULATION OF ASTIGMATIC OBJECT DISTANCE.') QPA01470
120   STOP                                                            QPA01480
      END                                                             QPA01490
C                                                                     QPA01500
C                                                                     QPA01510
C        Subroutine Qtrans                                            QPA01520
C                                                                     QPA01530
C        This subroutine calculates the first order                   QPA01540
C        convergent and divergent transfer matrices.                  QPA01550
C                                                                     QPA01560
      SUBROUTINE QTRANS(LENGTH,ROOTQZ,Y,X)                            QPA01570
      IMPLICIT REAL*8(A-H,O-Z)                                        QPA01580
      DIMENSION Y(2,2),X(2,2)                                         QPA01590
      REAL*8 LENGTH                                                   QPA01600
      ROOTQ=ROOTQZ/LENGTH                                             QPA01610
      WRITE(2,6) ROOTQZ                                               QPA01620
6     FORMAT(/1X,'Quadrupole angle theta = ',F8.4,' (Dimensionless)') QPA01630
C                                                                     QPA01640
C        Initialise Y and X arrays to zero                            QPA01650
C                                                                     QPA01660
      DO 20 I=1,2                                                     QPA01670
      DO 10 J=1,2                                                     QPA01680
      Y(I,J)=0.0                                                      QPA01690
      X(I,J)=0.0                                                      QPA01700
10    CONTINUE                                                        QPA01710
20    CONTINUE                                                        QPA01720
C                                                                     QPA01730
C        Calculate first order convergent coefficients                QPA01740
C                                                                     QPA01750
      Y(1,1)=DCOS(ROOTQZ)                                             QPA01760
      Y(2,1)=(1.0/ROOTQ)*DSIN(ROOTQZ)                                 QPA01770
      Y(1,2)=-ROOTQ*DSIN(ROOTQZ)                                      QPA01780
      Y(2,2)=DCOS(ROOTQZ)                                             QPA01790
C                                                                     QPA01800
C        Calculate first order divergent coefficients                 QPA01810
C                                                                     QPA01820
      X(1,1)=DCOSH(ROOTQZ)                                            QPA01830
      X(2,1)=(1.0/ROOTQ)*DSINH(ROOTQZ)                                QPA01840
      X(1,2)=ROOTQ*DSINH(ROOTQZ)                                      QPA01850
      X(2,2)=DCOSH(ROOTQZ)                                            QPA01860
      RETURN                                                          QPA01870
      END                                                             QPA01880
C                                                                     QPA01890
C                                                                     QPA01900
C        Subroutine Qcomb                                             QPA01910
C                                                                     QPA01920
C        This subroutine calculates the combined horizontal           QPA01930
C        and vertical transfer matrices.                              QPA01940
C                                                                     QPA01950
      SUBROUTINE QCOMB(Y1,X1,Y2,X2,D,YCD,XDC)                         QPA01960
      IMPLICIT REAL*8(A-H,O-Z)                                        QPA01970
      DIMENSION Y1(2,2),X1(2,2),Y2(2,2),X2(2,2),YCD(2,2),XDC(2,2)     QPA01980
C                                                                     QPA01990
C        Initialise YCD and XDC arrays to zero                        QPA02000
C                                                                     QPA02010
      DO 10 I=1,2                                                     QPA02020
      DO 10 J=1,2                                                     QPA02030
      YCD(I,J)=0.0                                                    QPA02040
      XDC(I,J)=0.0                                                    QPA02050
10    CONTINUE                                                        QPA02060
C                                                                     QPA02070
C        Calculate convergent-divergent transfer matrix               QPA02080
C                                                                     QPA02090
      YCD(1,1)=Y1(1,1)*X2(1,1)+(Y1(1,2)*(D*X2(1,1)+X2(2,1)))          QPA02100
      YCD(2,1)=Y1(2,1)*X2(1,1)+(Y1(2,2)*(D*X2(1,1)+X2(2,1)))          QPA02110
      YCD(1,2)=Y1(1,1)*X2(1,2)+(Y1(1,2)*(D*X2(1,2)+X2(2,2)))          QPA02120
      YCD(2,2)=Y1(2,1)*X2(1,2)+(Y1(2,2)*(D*X2(1,2)+X2(2,2)))          QPA02130
C                                                                     QPA02140
C        Calculate divergent-convergent matrix                        QPA02150
C                                                                     QPA02160
```

```
      XDC(1,1)=X1(1,1)*Y2(1,1)+(X1(1,2)*(D*Y2(1,1)+Y2(2,1)))          QPA02170
      XDC(2,1)=X1(2,1)*Y2(1,1)+(X1(2,2)*(D*Y2(1,1)+Y2(2,1)))          QPA02180
      XDC(1,2)=X1(1,1)*Y2(1,2)+(X1(1,2)*(D*Y2(1,2)+Y2(2,2)))          QPA02190
      XDC(2,2)=X1(2,1)*Y2(1,2)+(X1(2,2)*(D*Y2(1,2)+Y2(2,2)))          QPA02200
      RETURN                                                          QPA02210
      END                                                             QPA02220
C                                                                     QPA02230
C                                                                     QPA02240
C        Subroutine Fhead                                             QPA02250
C                                                                     QPA02260
C        This subroutine writes out titles and headings on unit 2.    QPA02270
C                                                                     QPA02280
      SUBROUTINE FHEAD(LENTH1,LENTH2,RTQZ1,RTQZ2,U,RATIO,D,TITL)      QPA02290
      IMPLICIT REAL*8(A-H,O-Z)                                        QPA02300
      DIMENSION TITL(20)                                              QPA02310
      REAL*8 LENTH1,LENTH2                                            QPA02320
      WRITE(2,5)                                                      QPA02330
      WRITE(2,7)(TITL(I),I=1,20)                                      QPA02340
      WRITE(2,15) LENTH1*1000                                         QPA02350
      WRITE(2,16) LENTH2*1000                                         QPA02360
      WRITE(2,20) RTQZ1                                               QPA02370
      WRITE(2,21) RTQZ2                                               QPA02380
      WRITE(2,30) U*1000                                              QPA02390
      WRITE(2,35) RATIO                                               QPA02400
      WRITE(2,40) D*1000                                              QPA02410
      RETURN                                                          QPA02420
5     FORMAT(//1X,'OPTICAL PROPERTIES OF MAGNETIC QUADRUPOLE PAIRS.'//) QPA02430
7     FORMAT(20A4)                                                    QPA02440
15    FORMAT(/1X,'LENGTH OF FIRST LENS              = ',F8.2,' mm.')  QPA02450
16    FORMAT(/1X,'LENGTH OF SECOND LENS             = ',F8.2,' mm.')  QPA02460
20    FORMAT(/1X,'QUADRUPOLE1 ANGLE THETA           = ',F8.2)         QPA02470
21    FORMAT(/1X,'QUADRUPOLE2 ANGLE THETA           = ',F8.2)         QPA02480
30    FORMAT(/1X,'OBJECT POSITION = ',F8.2,' mm.')                    QPA02490
35    FORMAT(/1X,'RATIO OF HORIZONTAL-VERTICAL IMAGE POSITIONS= ',F8.2) QPA02500
40    FORMAT(/1X,'LENS SEPARATION = ',F8.2,' mm.'//)                  QPA02510
      END                                                             QPA02520
C                                                                     QPA02530
C                                                                     QPA02540
C        Subroutine Graph                                             QPA02550
C                                                                     QPA02560
C        This subroutine does the plotting                            QPA02570
C                                                                     QPA02580
      SUBROUTINE GRAPH(OBJ,IMG,MAG,EXITN)                             QPA02590
      REAL*4 OBJ(10,10),IMG(10,10),MAG(10,10),EXITN(10,10)            QPA02600
      REAL*4 AX(2),AY(2),BX(2),BY(2),CX(2),CY(2),DX(2),DY(2)          QPA02610
      AX(1)=1.00                                                      QPA02620
      AX(2)=1.00                                                      QPA02630
      AY(1)=0.0                                                       QPA02640
      AY(2)=5.0                                                       QPA02650
      BX(1)=0.0                                                       QPA02660
      BX(2)=4.0                                                       QPA02670
      BY(1)=1.0                                                       QPA02680
      BY(2)=1.0                                                       QPA02690
      CX(1)=-11.05                                                    QPA02700
      CX(2)=-11.05                                                    QPA02710
      CY(1)=0.80                                                      QPA02720
      CY(2)=1.651                                                     QPA02730
      DX(1)=-11.05                                                    QPA02740
      DX(2)=0.0                                                       QPA02750
      DY(1)=1.651                                                     QPA02760
      DY(2)=1.651                                                     QPA02770
C     CALL PAGE(20.0,22.0)                                            QPA02780
      CALL NEWPLT(0.0,5.0,10.0,0.0,5.0,12.0)                          QPA02790
      CALL DRAW AX('Normalised Object Distance U',28,0.0,0.0)         QPA02800
      CALL DRAW AX('Normalsied Image Distance V',27,0.0,90.0)         QPA02810
      CALL BRKN CV(AX,AY,2,-1)                                        QPA02820
      CALL BRKN CV(BX,BY,2,-1)                                        QPA02830
C     CALL TITLE('H   ','C   ','QUADRUPOLE PAIR W/V RATIO = 0.25',32) QPA02840
C     CALL TITLE('L   ','C   ','QUADRUPOLE SEPARATION = L/2',27)     QPA02850
      DO 10 I=1,10                                                    QPA02860
      DO 20 J=1,10                                                    QPA02870
      IF(OBJ(I,J).GT.5.0.OR.IMG(I,J).GT.5.0) GOTO 20                  QPA02880
```

```
      IF(OBJ(I,J).LE.0.0.OR.IMG(I,J).LE.0.0) GOTO 20                    QPA02890
      CALL JOIN PT(OBJ(I,J),IMG(I,J))                                   QPA02900
20    CONTINUE                                                          QPA02910
      CALL BREAK                                                        QPA02920
10    CONTINUE                                                          QPA02930
      DO 30 J=1,10                                                      QPA02940
      DO 40 I=1,10                                                      QPA02950
      IF(OBJ(I,J).GT.5.0.OR.IMG(I,J).GT.5.0) GOTO 40                    QPA02960
      IF(OBJ(I,J).LE.0.0.OR.IMG(I,J).LE.0.0) GOTO 40                    QPA02970
      CALL JOIN PT(OBJ(I,J),IMG(I,J))                                   QPA02980
40    CONTINUE                                                          QPA02990
      CALL BREAK                                                        QPA03000
30    CONTINUE                                                          QPA03010
C                                                                       QPA03020
C        Draw the magnification graph                                   QPA03030
C                                                                       QPA03040
      CALL NEWPLT(-25.0,0.0,10.0,0.8,1.7,12.0)                          QPA03050
      CALL DRAW AX('Divergent-Convergent Magnification',34,0.8,0.0)     QPA03060
      CALL DRAW AX(' ',1,0.0,90.0)                                      QPA03070
      CALL BRKN CV(CX,CY,2,-1)                                          QPA03080
      CALL BRKN CV(DX,DY,2,-1)                                          QPA03090
C     CALL TITLE('H   ','C   ','QUADRUPOLE PAIR VERTICAL MAGNIFICATION',QPA03100
C    +           38)                                                   QPA03110
C     CALL TITLE('L   ','C   ','QUADRUPOLE SEPARATION = L/2',27)       QPA03120
      DO 50 J=1,10                                                      QPA03130
      DO 60 I=1,10                                                      QPA03140
      IF(MAG(I,J).LT.-25.0.OR.MAG(I,J).GE.0.0) THEN                     QPA03150
      CALL BREAK                                                        QPA03160
      GOTO 60                                                           QPA03170
      END IF                                                            QPA03180
      CALL JOIN PT(MAG(I,J),EXITN(I,J))                                 QPA03190
60    CONTINUE                                                          QPA03200
      CALL BREAK                                                        QPA03210
50    CONTINUE                                                          QPA03220
      CALL END PLT                                                      QPA03230
      RETURN                                                            QPA03240
      END                                                               QPA03250
```

```
C                                                                       QTR00010
C       PROGRAM QTRIP4                                                  QTR00020
C                                                                       QTR00030
C       This program calculates the optical properties of a             QTR00040
C       quadrupole quadruplet given a specified object position.        QTR00050
C       By changing the relevant parameters in the code any two lenses  QTR00060
C       can be varied while the other two run at fixed excitation. The  QTR00070
C       normal case is that the central lenses (Q1,Q2) are held fixed   QTR00080
C       while the outer two (Q0,Q1) are varied. The lens configuration  QTR00090
C       (high mag mode or low mag made) is controlled by the order of   QTR00100
C       the parameters in the call to subroutine QCOMB                  QTR00110
C                                                                       QTR00120
C       The principle variables are defined as follows-                 QTR00130
C                                                                       QTR00140
C       Lenth0   Effective length of first quadrupole Q0 (mm)           QTR00150
C       Lenth1   Effective length of second quadrupole Q1 (mm)          QTR00160
C       Lenth2   Effective length of third quadrupole Q2 (mm)           QTR00170
C       Lenth3   Effective length of fourth quadrupole Q3 (mm)          QTR00180
C       Rtqz0-4  Excitation (theta) of respective quadrupole            QTR00190
C       Delqz0   Increment in Q0 excitation                             QTR00200
C       Delqz3   Increment in Q3 excitation                             QTR00210
C       Nk0      Number of increments in Q0 excitation (<=5)            QTR00220
C       Nk3      Number of increments in Q3 excitation (<=20)           QTR00230
C       D0       Gap between lenses Q0,Q1 (mm)                          QTR00240
C       D1       Gap between lenses Q1,Q2 (mm)                          QTR00250
C       D2       Gap between lenses Q2,Q3 (mm)                          QTR00260
C       U        Object position referenced to entrance of Q0 (mm)      QTR00270
C       Y0-Y3    Second order convergent transfer matrix of relevant    QTR00280
C                quadrupole lens.                                       QTR00290
C       X0-X3    Second order divergent transfer matrix of relevant     QTR00300
C                quadrupole lens.                                       QTR00310
C       YCD      Combined transfer matrix (Q2,Q3) - vertical plane      QTR00320
C       XDC      Combined transfer matrix (Q2,Q3) - horizontal plane    QTR00330
C       YCDC     Combined transfer matrix (Q1,Q2,Q3) - vertical plane   QTR00340
C       XDCD     Combined transfer matrix (Q1,Q2,Q3) - horizontal planeQTR00350
C       YDCDC    Combined transfer matrix (Q0,Q1,Q2,Q3) - vertical      QTR00360
C       XCDCD    Combined transfer matrix (Q0,Q1,Q2,Q3) - horizontal    QTR00370
C       TY       Total second order transfer matrix - vertical plane    QTR00380
C       TX       Total second order transfer matrix - horizontal plane QTR00390
C       Hastig   Calculated image position - vertical plane             QTR00400
C       Dastig   Calculated image position - horizontal plane           QTR00410
C       Conmag   Vertical plane magnification at focus                  QTR00420
C       Divmag   Horizontal plane magnification at focus                QTR00430
C                                                                       QTR00440
      IMPLICIT REAL*8(A-H,O-Z)                                          QTR00450
      DIMENSION Y0(4,4),X0(4,4),YDCDC(4,4),XCDCD(4,4)                   QTR00460
      DIMENSION Y1(4,4),X1(4,4),TY(4,4),TX(4,4)                         QTR00470
      DIMENSION Y2(4,4),X2(4,4),YCD(4,4),XDC(4,4)                       QTR00480
      DIMENSION Y3(4,4),X3(4,4),YCDC(4,4),XDCD(4,4)                     QTR00490
      DIMENSION TITLE(20)                                               QTR00500
      REAL*4 OBJ(20,5,10),HIMAG(20,5,10),DIMAG(20,5,10)                 QTR00510
      REAL*4 CDCMAG(20,5,10),DCDMAG(20,5,10),EXITN(20),Q3EX(10)         QTR00520
      REAL*8 LENTH0,LENTH1,LENTH2,LENTH3                                QTR00530
C                                                                       QTR00540
C        Read title of up to 80 characters from unit 1                  QTR00550
      READ(1,1)(TITLE(I),I=1,20)                                        QTR00560
C                                                                       QTR00570
C        Read focussing quadrupole paramaters                           QTR00580
C                                                                       QTR00590
      READ(1,2)                                                         QTR00600
      READ(1,7) LENTH0,RTQZ0,DELQZ0,NK0                                 QTR00610
C                                                                       QTR00620
C        Read first quadrupole parameters from unit 1                   QTR00630
C                                                                       QTR00640
      READ(1,2)                                                         QTR00650
      READ(1,7) LENTH1,RTQZ1,DELQZ1,NK1                                 QTR00660
C                                                                       QTR00670
C        Read another blank line then second quadrupole parameters      QTR00680
C                                                                       QTR00690
      READ(1,2)                                                         QTR00700
      READ(1,7) LENTH2,RTQZ2,DELQZ2,NK2                                 QTR00710
C                                                                       QTR00720
```

```
C       Read another blank line then third quadrupole parameters       QTR00730
C                                                                      QTR00740
      READ(1,2)                                                        QTR00750
      READ(1,7) LENTH3,RTQZ3,DELQZ3,NK3                                QTR00760
C                                                                      QTR00770
C       Read a blank line then first order imaging properties          QTR00780
C                                                                      QTR00790
      READ(1,2)                                                        QTR00800
      READ(1,6) U,D0,D1,D2                                             QTR00810
C                                                                      QTR00820
1     FORMAT(20A4)                                                     QTR00830
2     FORMAT(1X)                                                       QTR00840
6     FORMAT(5X,4F10.0)                                                QTR00850
7     FORMAT(5X,3F10.4,I10)                                            QTR00860
C                                                                      QTR00870
C       Convert from millimetres to metres                             QTR00880
C                                                                      QTR00890
      LENTH0=LENTH0*0.001                                              QTR00900
      LENTH1=LENTH1*0.001                                              QTR00910
      LENTH2=LENTH2*0.001                                              QTR00920
      LENTH3=LENTH3*0.001                                              QTR00930
      U=U*0.001                                                        QTR00940
      D0=D0*0.001                                                      QTR00950
      D1=D1*0.001                                                      QTR00960
      D2=D2*0.001                                                      QTR00970
C                                                                      QTR00980
C       Write title and headings on unit 2                             QTR00990
C                                                                      QTR01000
      CALL FHEAD(LENTH0,LENTH1,LENTH2,LENTH3,RTQZ0,RTQZ1,RTQZ2,RTQZ3,  QTR01010
     -           U,D0,D1,D2,TITLE)                                     QTR01020
C                                                                      QTR01030
C       Start looping excitations                                      QTR01040
C                                                                      QTR01050
      DO 1002 L=1,NK1                                                  QTR01060
      DO 1001 N=1,NK0                                                  QTR01070
      DO 1000 I=1,NK3                                                  QTR01080
C                                                                      QTR01090
C       Call subroutine to calculate focus quadrupole transfer matrix  QTR01100
C                                                                      QTR01110
      CALL QTRANS(LENTH0,RTQZ0,Y0,X0)                                  QTR01120
C                                                                      QTR01130
C       Call subroutine to calculate first quadrupole transfer matrix  QTR01140
C                                                                      QTR01150
      CALL QTRANS(LENTH1,RTQZ1,Y1,X1)                                  QTR01160
C                                                                      QTR01170
C       Call subroutine to calculate second quadrupole transfer matrix QTR01180
C                                                                      QTR01190
      CALL QTRANS(LENTH2,RTQZ2,Y2,X2)                                  QTR01200
C                                                                      QTR01210
C       Call subroutine to calculate third quadrupole transfer matrix  QTR01220
C                                                                      QTR01230
      CALL QTRANS(LENTH3,RTQZ3,Y3,X3)                                  QTR01240
C                                                                      QTR01250
C       Call subroutine to calculate the Q2/Q3 transfer matrices       QTR01260
C                                                                      QTR01270
      CALL QCOMB(X2,Y2,Y3,X3,D2,YCD,XDC)                               QTR01280
C                                                                      QTR01290
C       Call subroutine to calculate the Q1/Q2/Q3 transfer matrices    QTR01300
C                                                                      QTR01310
      CALL QCOMB(Y1,X1,XDC,YCD,D1,YCDC,XDCD)                           QTR01320
C                                                                      QTR01330
C       Call subroutine to calculate the Q0/Q1/Q2/Q3 transfer matrices QTR01340
C                                                                      QTR01350
      CALL QCOMB(Y0,X0,XDCD,YCDC,D0,YDCDC,XCDCD)                       QTR01360
C                                                                      QTR01370
C       Object position is given so calculate non-stigmatic            QTR01380
C       image positions.                                               QTR01390
C                                                                      QTR01400
      CALL ASTIG(YDCDC,XCDCD,U,DASTIG,HASTIG,CONMAG,DIVMAG)            QTR01410
C                                                                      QTR01420
C       Output optical properties                                      QTR01430
C                                                                      QTR01440
```

```
      WRITE(2,101) U/LENTH2                                              QTR01450
      WRITE(2,40) CONMAG,HASTIG/LENTH2                                   QTR01460
      WRITE(2,50) DIVMAG,DASTIG/LENTH2                                   QTR01470
C                                                                        QTR01480
C        Set up arrays for graphical output                              QTR01490
C                                                                        QTR01500
      EXITN(I)=SNGL(RTQZ3)                                               QTR01510
      OBJ(I,N,L)=SNGL((U+LENTH0+D0)/LENTH2)                              QTR01520
      IF(OBJ(I,N,L).GT.5.0.OR.OBJ(I,N,L).LT.0.0) OBJ(I,N,L)=0.0          QTR01530
      HIMAG(I,N,L)=SNGL(HASTIG/LENTH2)                                   QTR01540
      DIMAG(I,N,L)=SNGL(DASTIG/LENTH2)                                   QTR01550
      IF(HIMAG(I,N,L).GT.4.0.OR.HIMAG(I,N,L).LT.0.0) HIMAG(I,N,L)=0.0    QTR01560
      IF(DIMAG(I,N,L).GT.4.0.OR.DIMAG(I,N,L).LT.-1.) DIMAG(I,N,L)=0.0    QTR01570
C                                                                        QTR01580
C     Reference the image positions to the central quadrupole pair       QTR01590
C                                                                        QTR01600
      IF(HIMAG(I,N,L).NE.0.0) THEN                                       QTR01610
      HIMAG(I,N,L)=SNGL((HASTIG+LENTH3+D2)/LENTH2)                       QTR01620
      END IF                                                             QTR01630
      IF(DIMAG(I,N,L).NE.0.0) THEN                                       QTR01640
      DIMAG(I,N,L)=SNGL((DASTIG+LENTH3+D2)/LENTH2)                       QTR01650
      END IF                                                             QTR01660
      CDCMAG(I,N,L)=SNGL(CONMAG)                                         QTR01670
      DCDMAG(I,N,L)=SNGL(DIVMAG)                                         QTR01680
      IF(CDCMAG(I,N,L).LT.-70.0.OR.CDCMAG(I,N,L).GT.0.0)                 QTR01690
     +   CDCMAG(I,N,L)=0.0                                               QTR01700
      IF(DCDMAG(I,N,L).LT.-70.0.OR.DCDMAG(I,N,L).GT.0.0)                 QTR01710
     +   DCDMAG(I,N,L)=0.0                                               QTR01720
      RTQZ3=RTQZ3+DELQZ3                                                 QTR01730
1000  CONTINUE                                                           QTR01740
      RTQZ3=RTQZ3-(NK3*DELQZ3)                                           QTR01750
      RTQZ0=RTQZ0+DELQZ0                                                 QTR01760
1001  CONTINUE                                                           QTR01770
      RTQZ0=RTQZ0-(NK0*DELQZ0)                                           QTR01780
      Q3EX(L)=SNGL(RTQZ1)                                                QTR01790
      RTQZ0=RTQZ0+DELQZ0                                                 QTR01800
1002  CONTINUE                                                           QTR01810
C                                                                        QTR01820
C        Call plotting subroutine                                        QTR01830
C                                                                        QTR01840
      IF(NK1.LE.1) THEN                                                  QTR01850
      CALL GRAPH1(OBJ,HIMAG,DIMAG,CDCMAG,DCDMAG,EXITN,NK3,NK0)           QTR01860
      ELSE                                                               QTR01870
      CALL GRAPH2(OBJ,HIMAG,DIMAG,CDCMAG,DCDMAG,Q3EX,NK3)                QTR01880
      END IF                                                             QTR01890
C                                                                        QTR01900
40    FORMAT(/1X,'CONV-DIV-CONV MAG = ',D10.4,3X,'AT IMAGE',             QTR01910
     -     ' POSITION = ',D12.6)                                         QTR01920
50    FORMAT(/1X,'DIV-CONV-DIV  MAG = ',D10.4,3X,'AT IMAGE',             QTR01930
     -     ' POSITION = ',D12.6)                                         QTR01940
101   FORMAT(/1X,'OBJECT POSITION = ',D10.4,' mm.')                      QTR01950
      STOP                                                               QTR01960
      END                                                                QTR01970
C                                                                        QTR01980
C                                                                        QTR01990
C        Subroutine Qtrans                                               QTR02000
C                                                                        QTR02010
C        This subroutine calculates the convergent                       QTR02020
C        and divergent transfer matrices.                                QTR02030
C                                                                        QTR02040
      SUBROUTINE QTRANS(LENGTH,ROOTQZ,Y,X)                               QTR02050
      IMPLICIT REAL*8(A-H,O-Z)                                           QTR02060
      DIMENSION Y(4,4),X(4,4)                                            QTR02070
      REAL*8 LENGTH                                                      QTR02080
C                                                                        QTR02090
C        Set up various constants                                        QTR02100
C                                                                        QTR02110
      ROOTQ=ROOTQZ/LENGTH                                                QTR02120
      Q=ROOTQ**2                                                         QTR02130
      WRITE(2,6) ROOTQZ                                                  QTR02140
6     FORMAT(/1X,'Quadrupole angle theta = ',F8.4,' (Dimensionless)')    QTR02150
C                                                                        QTR02160
```

```
C       Initialise Y and X arrays to zero                                QTR02170
C                                                                        QTR02180
      DO 20 I=1,4                                                        QTR02190
      DO 10 J=1,4                                                        QTR02200
      Y(I,J)=0.0                                                         QTR02210
      X(I,J)=0.0                                                         QTR02220
10    CONTINUE                                                           QTR02230
20    CONTINUE                                                           QTR02240
C                                                                        QTR02250
C       Calculate first and second order convergent coefficients         QTR02260
C                                                                        QTR02270
      Y(1,1)=DCOS(ROOTQZ)                                                QTR02280
      Y(2,1)=(1.0/ROOTQ)*DSIN(ROOTQZ)                                    QTR02290
      Y(3,1)=0.5*Q*LENGTH*Y(2,1)                                         QTR02300
      Y(4,1)=0.5*(Y(2,1)-(LENGTH*Y(1,1)))                                QTR02310
      Y(1,2)=-ROOTQ*DSIN(ROOTQZ)                                         QTR02320
      Y(2,2)=DCOS(ROOTQZ)                                                QTR02330
      Y(3,2)=0.5*Q*((LENGTH*Y(1,1))+Y(2,1))                              QTR02340
      Y(4,2)=0.5*ROOTQZ*DSIN(ROOTQZ)                                     QTR02350
      Y(3,3)=Y(1,1)                                                      QTR02360
      Y(4,3)=Y(2,1)                                                      QTR02370
      Y(3,4)=Y(1,2)                                                      QTR02380
      Y(4,4)=Y(2,2)                                                      QTR02390
C                                                                        QTR02400
C       Calculate first and second order divergent coefficients          QTR02410
C                                                                        QTR02420
      X(1,1)=DCOSH(ROOTQZ)                                               QTR02430
      X(2,1)=(1.0/ROOTQ)*DSINH(ROOTQZ)                                   QTR02440
      X(3,1)=-0.5*ROOTQZ*DSINH(ROOTQZ)                                   QTR02450
      X(4,1)=0.5*(X(2,1)-(LENGTH*X(1,1)))                                QTR02460
      X(1,2)=ROOTQ*DSINH(ROOTQZ)                                         QTR02470
      X(2,2)=DCOSH(ROOTQZ)                                               QTR02480
      X(3,2)=-0.5*Q*((LENGTH*X(1,1))+X(2,1))                             QTR02490
      X(4,2)=-0.5*ROOTQZ*DSINH(ROOTQZ)                                   QTR02500
      X(3,3)=X(1,1)                                                      QTR02510
      X(4,3)=X(2,1)                                                      QTR02520
      X(3,4)=X(1,2)                                                      QTR02530
      X(4,4)=X(2,2)                                                      QTR02540
      RETURN                                                             QTR02550
      END                                                                QTR02560
C                                                                        QTR02570
C                                                                        QTR02580
C       Subroutine Qcomb                                                 QTR02590
C                                                                        QTR02600
C       This subroutine calculates the combined horizontal               QTR02610
C       and vertical transfer matrices.                                  QTR02620
C                                                                        QTR02630
      SUBROUTINE QCOMB(Y1,X1,Y2,X2,D,YCD,XDC)                            QTR02640
      IMPLICIT REAL*8(A-H,O-Z)                                           QTR02650
      DIMENSION Y1(4,4),X1(4,4),Y2(4,4),X2(4,4),YCD(4,4),XDC(4,4)        QTR02660
C                                                                        QTR02670
C       Initialise YCD and XDC arrays to zero                            QTR02680
C                                                                        QTR02690
      DO 10 I=1,4                                                        QTR02700
      DO 10 J=1,4                                                        QTR02710
      YCD(I,J)=0.0                                                       QTR02720
      XDC(I,J)=0.0                                                       QTR02730
10    CONTINUE                                                           QTR02740
C                                                                        QTR02750
C       Calculate convergent-divergent transfer matrix                   QTR02760
C                                                                        QTR02770
      YCD(1,1)=Y1(1,1)*X2(1,1)+(Y1(1,2)*(D*X2(1,1)+X2(2,1)))             QTR02780
      YCD(2,1)=Y1(2,1)*X2(1,1)+(Y1(2,2)*(D*X2(1,1)+X2(2,1)))             QTR02790
      YCD(3,1)=Y1(3,1)*X2(1,1)+(Y1(3,2)*(D*X2(1,1)+X2(2,1)))+            QTR02800
     -         Y1(3,3)*X2(3,1)+(Y1(3,4)*(D*X2(3,1)+X2(4,1)))             QTR02810
      YCD(4,1)=Y1(4,1)*X2(1,1)+(Y1(4,2)*(D*X2(1,1)+X2(2,1)))+            QTR02820
     -         Y1(4,3)*X2(3,1)+(Y1(4,4)*(D*X2(3,1)+X2(4,1)))             QTR02830
      YCD(1,2)=Y1(1,1)*X2(1,2)+(Y1(1,2)*(D*X2(1,2)+X2(2,2)))             QTR02840
      YCD(2,2)=Y1(2,1)*X2(1,2)+(Y1(2,2)*(D*X2(1,2)+X2(2,2)))             QTR02850
      YCD(3,2)=Y1(3,1)*X2(1,2)+(Y1(3,2)*(D*X2(1,2)+X2(2,2)))+            QTR02860
     -         Y1(3,3)*X2(3,2)+(Y1(3,4)*(D*X2(3,2)+X2(4,2)))             QTR02870
      YCD(4,2)=Y1(4,1)*X2(1,2)+(Y1(4,2)*(D*X2(1,2)+X2(2,2)))+            QTR02880
```

```
     -         Y1(4,3)*X2(3,2)+(Y1(4,4)*(D*X2(3,2)+X2(4,2)))          QTR02890
      YCD(3,3)=Y1(3,3)*X2(3,3)+(Y1(3,4)*(D*X2(3,3)+X2(4,3)))        QTR02900
      YCD(4,3)=Y1(4,3)*X2(3,3)+(Y1(4,4)*(D*X2(3,3)+X2(4,3)))        QTR02910
      YCD(3,4)=Y1(3,3)*X2(3,4)+(Y1(3,4)*(D*X2(3,4)+X2(4,4)))        QTR02920
      YCD(4,4)=Y1(4,3)*X2(3,4)+(Y1(4,4)*(D*X2(3,4)+X2(4,4)))        QTR02930
C                                                                   QTR02940
C        Calculate divergent-convergent matrix                      QTR02950
C                                                                   QTR02960
      XDC(1,1)=X1(1,1)*Y2(1,1)+(X1(1,2)*(D*Y2(1,1)+Y2(2,1)))        QTR02970
      XDC(2,1)=X1(2,1)*Y2(1,1)+(X1(2,2)*(D*Y2(1,1)+Y2(2,1)))        QTR02980
      XDC(3,1)=X1(3,1)*Y2(1,1)+(X1(3,2)*(D*Y2(1,1)+Y2(2,1)))+       QTR02990
     -         X1(3,3)*Y2(3,1)+(X1(3,4)*(D*Y2(3,1)+Y2(4,1)))        QTR03000
      XDC(4,1)=X1(4,1)*Y2(1,1)+(X1(4,2)*(D*Y2(1,1)+Y2(2,1)))+       QTR03010
     -         X1(4,3)*Y2(3,1)+(X1(4,4)*(D*Y2(3,1)+Y2(4,1)))        QTR03020
      XDC(1,2)=X1(1,1)*Y2(1,2)+(X1(1,2)*(D*Y2(1,2)+Y2(2,2)))        QTR03030
      XDC(2,2)=X1(2,1)*Y2(1,2)+(X1(2,2)*(D*Y2(1,2)+Y2(2,2)))        QTR03040
      XDC(3,2)=X1(3,1)*Y2(1,2)+(X1(3,2)*(D*Y2(1,2)+Y2(2,2)))+       QTR03050
     -         X1(3,3)*Y2(3,2)+(X1(3,4)*(D*Y2(3,2)+Y2(4,2)))        QTR03060
      XDC(4,2)=X1(4,1)*Y2(1,2)+(X1(4,2)*(D*Y2(1,2)+Y2(2,2)))+       QTR03070
     -         X1(4,3)*Y2(3,2)+(X1(4,4)*(D*Y2(3,2)+Y2(4,2)))        QTR03080
      XDC(3,3)=X1(3,3)*Y2(3,3)+(X1(3,4)*(D*Y2(3,3)+Y2(4,3)))        QTR03090
      XDC(4,3)=X1(4,3)*Y2(3,3)+(X1(4,4)*(D*Y2(3,3)+Y2(4,3)))        QTR03100
      XDC(3,4)=X1(3,3)*Y2(3,4)+(X1(3,4)*(D*Y2(3,4)+Y2(4,4)))        QTR03110
      XDC(4,4)=X1(4,3)*Y2(3,4)+(X1(4,4)*(D*Y2(3,4)+Y2(4,4)))        QTR03120
      RETURN                                                        QTR03130
      END                                                           QTR03140
C                                                                   QTR03150
C                                                                   QTR03160
C        Subroutine Qttran                                          QTR03170
C                                                                   QTR03180
C        This subroutine calculates the total vertical              QTR03190
C        and horizontal transfer matrices.                          QTR03200
C                                                                   QTR03210
      SUBROUTINE QTTRAN(Y,X,U,V,TY,TX)                              QTR03220
      IMPLICIT REAL*8(A-H,O-Z)                                      QTR03230
      DIMENSION Y(4,4),TY(4,4),X(4,4),TX(4,4)                       QTR03240
C                                                                   QTR03250
C        Initialise TY and TX arrays to zero                        QTR03260
C                                                                   QTR03270
      DO 20 I=1,4                                                   QTR03280
      DO 10 J=1,4                                                   QTR03290
      TY(I,J)=0.0                                                   QTR03300
      TX(I,J)=0.0                                                   QTR03310
10    CONTINUE                                                      QTR03320
20    CONTINUE                                                      QTR03330
C                                                                   QTR03340
C        Calculate total horizontal matrix elements                 QTR03350
C                                                                   QTR03360
      TY(1,1) =Y(1,1)+(V*Y(1,2))                                    QTR03370
      TY(2,1) =U*(Y(1,1)+(V*Y(1,2)))+Y(2,1)+(V*Y(2,2))              QTR03380
      TY(3,1) =Y(3,1)+(V*Y(3,2))                                    QTR03390
      TY(4,1) =U*(Y(3,1)+V*Y(3,2))+Y(4,1)+(V*Y(4,2))                QTR03400
      TY(1,2) =Y(1,2)                                               QTR03410
      TY(2,2) =(U*Y(1,2))+Y(2,2)                                    QTR03420
      TY(3,2) =Y(3,2)                                               QTR03430
      TY(4,2) =Y(4,2)+(U*Y(3,2))                                    QTR03440
      TY(3,3) =Y(3,3)+(V*Y(3,4))                                    QTR03450
      TY(4,3) =U*(Y(3,3)+(V*Y(3,4)))+Y(4,3)+(V*Y(4,4))              QTR03460
      TY(3,4) =Y(3,4)                                               QTR03470
      TY(4,4) =(U*Y(3,4))+Y(4,4)                                    QTR03480
C                                                                   QTR03490
C        Calculate total vertical matrix elements                   QTR03500
C                                                                   QTR03510
      TX(1,1) =X(1,1)+(V*X(1,2))                                    QTR03520
      TX(2,1) =U*(X(1,1)+(V*X(1,2)))+X(2,1)+(V*X(2,2))              QTR03530
      TX(3,1) =X(3,1)+(V*X(3,2))                                    QTR03540
      TX(4,1) =U*(X(3,1)+V*X(3,2))+X(4,1)+(V*X(4,2))                QTR03550
      TX(1,2) =X(1,2)                                               QTR03560
      TX(2,2) =(U*X(1,2))+X(2,2)                                    QTR03570
      TX(3,2) =X(3,2)                                               QTR03580
      TX(4,2) =X(4,2)+(U*X(3,2))                                    QTR03590
      TX(3,3) =X(3,3)+(V*X(3,4))                                    QTR03600
```

```
      TX(4,3) =U*(X(3,3)+(V*X(3,4)))+X(4,3)+(V*X(4,4))                  QTR03610
      TX(3,4) =X(3,4)                                                   QTR03620
      TX(4,4) =(U*X(3,4))+X(4,4)                                        QTR03630
      RETURN                                                            QTR03640
      END                                                               QTR03650
C                                                                       QTR03660
C                                                                       QTR03670
C        Subroutine Astig                                               QTR03680
C                                                                       QTR03690
C        This subroutine calculates the object plane distances          QTR03700
C        given the image plane distance and the transfer matrices.      QTR03710
C                                                                       QTR03720
      SUBROUTINE ASTIG(YCDC,XDCD,U,DASTIG,HASTIG,CONMAG,DIVMAG)         QTR03730
      IMPLICIT REAL*8 (A-H,O-Z)                                         QTR03740
      DIMENSION YCDC(4,4),XDCD(4,4)                                     QTR03750
      DASTIG=-(XDCD(1,1)*U+XDCD(2,1))/(XDCD(1,2)*U+XDCD(2,2))           QTR03760
      DIVMAG=XDCD(1,1)+(DASTIG*XDCD(1,2))                               QTR03770
      HASTIG=-(YCDC(1,1)*U+YCDC(2,1))/(YCDC(1,2)*U+YCDC(2,2))           QTR03780
      CONMAG=YCDC(1,1)+(HASTIG*YCDC(1,2))                               QTR03790
      RETURN                                                            QTR03800
      END                                                               QTR03810
C                                                                       QTR03820
C                                                                       QTR03830
C        Subroutine Fhead                                               QTR03840
C                                                                       QTR03850
C        This subroutine writes out titles and headings on unit 2.      QTR03860
C                                                                       QTR03870
      SUBROUTINE FHEAD(LENTH0,LENTH1,LENTH2,LENTH3,RTQZ0,RTQZ1,         QTR03880
     +                 RTQZ2,RTQZ3,U,D0,D1,D2,TITLE)                    QTR03890
      IMPLICIT REAL*8 (A-H,O-Z)                                         QTR03900
      DIMENSION TITLE(20)                                               QTR03910
      REAL*8 LENTH0,LENTH1,LENTH2,LENTH3                                QTR03920
      WRITE(2,5)                                                        QTR03930
      WRITE(2,7)(TITLE(I),I=1,20)                                       QTR03940
      WRITE(2,14) LENTH0*1000                                           QTR03950
      WRITE(2,19) RTQZ0                                                 QTR03960
      WRITE(2,15) LENTH1*1000                                           QTR03970
      WRITE(2,20) RTQZ1                                                 QTR03980
      WRITE(2,16) LENTH2*1000                                           QTR03990
      WRITE(2,21) RTQZ2                                                 QTR04000
      WRITE(2,17) LENTH3*1000                                           QTR04010
      WRITE(2,22) RTQZ3                                                 QTR04020
      WRITE(2,30) U*1000                                                QTR04030
      WRITE(2,35) D0*1000                                               QTR04040
      WRITE(2,40) D1*1000                                               QTR04050
      WRITE(2,45) D2*1000                                               QTR04060
      RETURN                                                            QTR04070
5     FORMAT(//1X,'OPTICAL PROPERTIES OF MAGNETIC QUADRUPOLE PAIRS.'//) QTR04080
7     FORMAT(20A4)                                                      QTR04090
14    FORMAT(/1X,'LENGTH OF FIRST LENS              = ',F8.2,'mm.')     QTR04100
15    FORMAT(/1X,'LENGTH OF SECOND LENS             = ',F8.2,'mm.')     QTR04110
16    FORMAT(/1X,'LENGTH OF THIRD LENS              = ',F8.2,'mm.')     QTR04120
17    FORMAT(/1X,'LENGTH OF FOURTH LENS             = ',F8.2,'mm.')     QTR04130
19    FORMAT(/1X,'First quadrupole strength         = ',F8.2)           QTR04140
20    FORMAT(/1X,'Second quadrupole strength        = ',F8.2)           QTR04150
21    FORMAT(/1X,'Third quadrupole strength         = ',F8.2)           QTR04160
22    FORMAT(/1X,'Fourth quadrupole strength        = ',F8.2)           QTR04170
30    FORMAT(/1X,'OBJECT POSITION = ',F8.2,' mm.')                      QTR04180
35    FORMAT(/1X,'LENS 1-2 SEPARATION = ',F8.2,' mm.')                  QTR04190
40    FORMAT(/1X,'LENS 2-3 SEPARATION = ',F8.2,' mm.')                  QTR04200
45    FORMAT(/1X,'LENS 3-4 SEPARATION = ',F8.2,' mm.')                  QTR04210
      END                                                               QTR04220
C                                                                       QTR04230
C                                                                       QTR04240
C        SUBROUTINE GRAPH1                                              QTR04250
C                                                                       QTR04260
C        This subroutine plots out the optical properties               QTR04270
C        using the simpleplot library routines                          QTR04280
C                                                                       QTR04290
      SUBROUTINE GRAPH1(OBJ,HIMAG,DIMAG,CDCMAG,DCDMAG,EXITN,NK1,NK2)    QTR04300
      REAL*4 OBJ(20,5,10),HIMAG(20,5,10),DIMAG(20,5,10)                 QTR04310
      REAL*4 CDCMAG(20,5,10),DCDMAG(20,5,10),EXITN(20)                  QTR04320
```

```
      REAL*4 OBJIM(20,15),COMMAG(20,10)                                 QTR04330
      DO 10 I=1,NK1                                                     QTR04340
      OBJIM(I,1)=(OBJ(I,1,1))                                           QTR04350
      OBJIM(I,2)=(HIMAG(I,1,1))                                         QTR04360
      OBJIM(I,3)=(DIMAG(I,1,1))                                         QTR04370
      OBJIM(I,4)=(OBJ(I,2,1))                                           QTR04380
      OBJIM(I,5)=(HIMAG(I,2,1))                                         QTR04390
      OBJIM(I,6)=(DIMAG(I,2,1))                                         QTR04400
      OBJIM(I,7)=(OBJ(I,3,1))                                           QTR04410
      OBJIM(I,8)=(HIMAG(I,3,1))                                         QTR04420
      OBJIM(I,9)=(DIMAG(I,3,1))                                         QTR04430
      OBJIM(I,10)=(OBJ(I,4,1))                                          QTR04440
      OBJIM(I,11)=(HIMAG(I,4,1))                                        QTR04450
      OBJIM(I,12)=(DIMAG(I,4,1))                                        QTR04460
      OBJIM(I,13)=(OBJ(I,5,1))                                          QTR04470
      OBJIM(I,14)=(HIMAG(I,5,1))                                        QTR04480
      OBJIM(I,15)=(DIMAG(I,5,1))                                        QTR04490
      COMMAG(I,1)=(CDCMAG(I,1,1))                                       QTR04500
      COMMAG(I,2)=(DCDMAG(I,1,1))                                       QTR04510
      COMMAG(I,3)=(CDCMAG(I,2,1))                                       QTR04520
      COMMAG(I,4)=(DCDMAG(I,2,1))                                       QTR04530
      COMMAG(I,5)=(CDCMAG(I,3,1))                                       QTR04540
      COMMAG(I,6)=(DCDMAG(I,3,1))                                       QTR04550
      COMMAG(I,7)=(CDCMAG(I,4,1))                                       QTR04560
      COMMAG(I,8)=(DCDMAG(I,4,1))                                       QTR04570
      COMMAG(I,9)=(CDCMAG(I,5,1))                                       QTR04580
      COMMAG(I,10)=(DCDMAG(I,5,1))                                      QTR04590
10    CONTINUE                                                          QTR04600
      OBJIM(1,1)=0.0                                                    QTR04610
      CALL PAGE(18.0,22.0)                                              QTR04620
      CALL PACK IN(14.0,20.0)                                           QTR04630
      CALL JBAXES(OBJIM,300,12.0,'Normalised Object and Image Positions'QTR04640
     +           ,37,EXITN,20,8.0,' ',1)                                QTR04650
      ITEMP1=1                                                          QTR04660
      ITEMP2=2                                                          QTR04670
      ITEMP3=3                                                          QTR04680
      DO 21 K=1,NK2*3                                                   QTR04690
      IF((K-ITEMP1).EQ.0) LINE=3                                        QTR04700
      IF((K-ITEMP2).EQ.0) LINE=2                                        QTR04710
      IF((K-ITEMP3).EQ.0) THEN                                          QTR04720
      LINE=0                                                            QTR04730
      ITEMP1=ITEMP1+3                                                   QTR04740
      ITEMP2=ITEMP2+3                                                   QTR04750
      ITEMP3=ITEMP3+3                                                   QTR04760
      ELSE                                                              QTR04770
      GOTO 19                                                           QTR04780
      END IF                                                            QTR04790
19    DO 20 L=1,NK1                                                     QTR04800
      IF(ABS(OBJIM(L,K)).GT.0.0) THEN                                   QTR04810
      CALL JOIN PT(OBJIM(L,K),EXITN(L))                                 QTR04820
      CALL MARK PT(OBJIM(L,K),EXITN(L),LINE)                            QTR04830
      END IF                                                            QTR04840
20    CONTINUE                                                          QTR04850
      CALL BREAK                                                        QTR04860
21    CONTINUE                                                          QTR04870
      CALL SET KY('T   ','R   ',3,12)                                   QTR04880
      CALL MARK KY(3,'OBJECT  POSN ',13)                                QTR04890
      CALL MARK KY(2,'V IMAGE POSN ',13)                                QTR04900
      CALL MARK KY(0,'W IMAGE POSN ',13)                                QTR04910
      CALL JBAXES(COMMAG,200,12.0,'Magnification',13,                   QTR04920
     +            EXITN,20,8.0,'  ',2)                                  QTR04930
      DO 31 M=1,NK2*2                                                   QTR04940
      TEMP=M/2.0                                                        QTR04950
      TEMP=TEMP-INT(TEMP)                                               QTR04960
      IF(ABS(TEMP).GT.0.001) THEN                                       QTR04970
      LINE=2                                                            QTR04980
      ELSE                                                              QTR04990
      LINE=0                                                            QTR05000
      END IF                                                            QTR05010
      DO 30 N=1,NK1                                                     QTR05020
      IF(COMMAG(N,M).LT.0.0) THEN                                       QTR05030
      CALL JOIN PT(COMMAG(N,M),EXITN(N))                                QTR05040
```

```
      CALL MARK PT(COMMAG(N,M),EXITN(N),LINE)                          QTR05050
      END IF                                                           QTR05060
30    CONTINUE                                                         QTR05070
      CALL BREAK                                                       QTR05080
31    CONTINUE                                                         QTR05090
      CALL SET KY('T    ','L    ',2,8)                                 QTR05100
      CALL MARK KY(2,'DCDC MAG ',9)                                    QTR05110
      CALL MARK KY(0,'CDCD MAG ',9)                                    QTR05120
      CALL END PLT                                                     QTR05130
      STOP                                                             QTR05140
      END                                                              QTR05150
C                                                                      QTR05160
C                                                                      QTR05170
C        SUBROUTINE GRAPH2                                             QTR05180
C                                                                      QTR05190
C        This subroutine does the plotting if q3                       QTR05200
C        is the quadrupole which is varied while                       QTR05210
C        q1 and q2 are held constant.                                  QTR05220
C                                                                      QTR05230
      SUBROUTINE GRAPH2(OBJ,HIMAG,DIMAG,CDCMAG,DCDMAG,Q3EX,NK3)        QTR05240
      REAL*4 OBJ(20,5,10),HIMAG(20,5,10),DIMAG(20,5,10)                QTR05250
      REAL*4 CDCMAG(20,5,10),DCDMAG(20,5,10),Q3EX(10)                  QTR05260
      REAL*4 OBJIM(10,3),COMMAG(10,2)                                  QTR05270
      DO 10 I=1,10                                                     QTR05280
      OBJIM(I,1)=OBJ(1,1,I)                                            QTR05290
      OBJIM(I,2)=HIMAG(1,1,I)                                          QTR05300
      OBJIM(I,3)=DIMAG(1,1,I)                                          QTR05310
      COMMAG(I,1)=CDCMAG(1,1,I)                                        QTR05320
      COMMAG(I,2)=DCDMAG(1,1,I)                                        QTR05330
10    CONTINUE                                                         QTR05340
      CALL PAGE(25.0,25.0)                                             QTR05350
      CALL PACK IN(14.0,22.0)                                          QTR05360
      CALL JBAXES(OBJIM,30,15.0,'M',1,Q3EX,10,10.0,' ',1)              QTR05370
      DO 20 K=1,3                                                      QTR05380
      DO 20 L=1,NK3                                                    QTR05390
      LINE=K                                                           QTR05400
20    CALL MARK PT(OBJIM(L,K),Q3EX(L),LINE)                            QTR05410
      CALL SET KY('B    ','L    ',3,12)                                QTR05420
      CALL MARK KY(1,' OBJECT POSN',12)                                QTR05430
      CALL MARK KY(2,' HIMAGE POSN',12)                                QTR05440
      CALL MARK KY(3,' DIMAGE POSN',12)                                QTR05450
      CALL TITLE('T    ','L    ','QUADRUPOLE TRIPLET OPTICS',25)       QTR05460
      CALL JBAXES(COMMAG,20,15.0,'MAG',3,Q3EX,10,10.0,'K3',2)          QTR05470
      DO 30 M=1,2                                                      QTR05480
      DO 30 N=1,NK3                                                    QTR05490
      LINE=M                                                           QTR05500
30    CALL MARK PT(COMMAG(N,M),Q3EX(N),LINE)                           QTR05510
      CALL SET KY('B    ','L    ',2,8)                                 QTR05520
      CALL MARK KY(1,' CDC MAG',8)                                     QTR05530
      CALL MARK KY(2,' DCD MAG',8)                                     QTR05540
      CALL TITLE('T    ','L    ','QUADRUPOLE TRIPLET OPTICS',25)       QTR05550
      CALL END PLT                                                     QTR05560
      STOP                                                             QTR05570
      END                                                              QTR05580
```

```
C                                                                       QQU00010
C       PROGRAM QQUAD                                                   QQU00020
C                                                                       QQU00030
C       This program calculates the required excitations of the         QQU00040
C       Q0 and Q3 quadrupole lenses in a quadruplet to give a fixed     QQU00050
C       object and vertical image position, assuming that Q1 and Q2     QQU00060
C       are held constant. The lens configuration is controlled         QQU00070
C       by the order of parameters in the call to subroutine QCOMB.     QQU00080
C       Also changing from say high mag to low mag mode requires        QQU00090
C       adjustment of the sign of the lens increments - the correct     QQU00100
C       sense can be obtained by running QTRIP4 for the same optical    QQU00110
C       configuration.                                                  QQU00120
C                                                                       QQU00130
C       The principle variables are defined as follows-                 QQU00140
C                                                                       QQU00150
C       Lenth0   Effective length of first quadrupole Q0 (mm)           QQU00160
C       Lenth1   Effective length of second quadrupole Q1 (mm)          QQU00170
C       Lenth2   Effective length of third quadrupole Q2 (mm)           QQU00180
C       Lenth3   Effective length of fourth quadrupole Q3 (mm)          QQU00190
C       Rtqz0-4  Excitation (theta) of respective quadrupole            QQU00200
C       Delqz0   Increment in Q0 excitation                             QQU00210
C       Delqz3   Increment in Q3 excitation                             QQU00220
C       Nk3      Number of increments in Q3 excitation (<=20)           QQU00230
C       D0       Gap between lenses Q0,Q1 (mm)                          QQU00240
C       D1       Gap between lenses Q1,Q2 (mm)                          QQU00250
C       D2       Gap between lenses Q2,Q3 (mm)                          QQU00260
C       U        Required object position ref. to entrance of Q0 (mm)   QQU00270
C       V        Required vertical image position referenced to the     QQU00280
C                exit of Q3 - normalised to length of Q1 (LENTH2)       QQU00290
C       Y0-Y3    Second order convergent transfer matrix of relevant    QQU00300
C                quadrupole lens.                                       QQU00310
C       X0-X3    Second order divergent transfer matrix of relevant     QQU00320
C                quadrupole lens.                                       QQU00330
C       YCD      Combined transfer matrix (Q2,Q3) - vertical plane      QQU00340
C       XDC      Combined transfer matrix (Q2,Q3) - horizontal plane    QQU00350
C       YCDC     Combined transfer matrix (Q1,Q2,Q3) - vertical plane   QQU00360
C       XDCD     Combined transfer matrix (Q1,Q2,Q3) - horizontal planeQQU00370
C       YDCDC    Combined transfer matrix (Q0,Q1,Q2,Q3) - vertical      QQU00380
C       XCDCD    Combined transfer matrix (Q0,Q1,Q2,Q3) - horizontal    QQU00390
C       TY       Total second order transfer matrix - vertical plane    QQU00400
C       TX       Total second order transfer matrix - horizontal plane QQU00410
C       Hastig   Calculated image position - vertical plane             QQU00420
C       Dastig   Calculated image position - horizontal plane           QQU00430
C       Conmag   Vertical plane magnification at focus                  QQU00440
C       Divmag   Horizontal plane magnification at focus                QQU00450
C                                                                       QQU00460
      IMPLICIT REAL*8(A-H,O-Z)                                          QQU00470
      DIMENSION Y0(4,4),X0(4,4),YDCDC(4,4),XCDCD(4,4)                   QQU00480
      DIMENSION Y1(4,4),X1(4,4),TY(4,4),TX(4,4)                         QQU00490
      DIMENSION Y2(4,4),X2(4,4),YCD(4,4),XDC(4,4)                       QQU00500
      DIMENSION Y3(4,4),X3(4,4),YCDC(4,4),XDCD(4,4)                     QQU00510
      DIMENSION TITLE(20)                                               QQU00520
      REAL*4 CDCMAG(40),DCDMAG(40),Q0EX(40),Q3EX(40)                    QQU00530
      REAL*8 LENTH0,LENTH1,LENTH2,LENTH3                                QQU00540
C                                                                       QQU00550
C        Read title of up to 80 characters from unit 1                  QQU00560
      READ(1,1)(TITLE(I),I=1,20)                                        QQU00570
C                                                                       QQU00580
C        Read focussing quadrupole paramaters                           QQU00590
C                                                                       QQU00600
      READ(1,2)                                                         QQU00610
      READ(1,7) LENTH0,RTQZ0,DELQZ0                                     QQU00620
C                                                                       QQU00630
C        Read first quadrupole parameters from unit 1                   QQU00640
C                                                                       QQU00650
      READ(1,2)                                                         QQU00660
      READ(1,5) LENTH1,RTQZ1                                            QQU00670
C                                                                       QQU00680
C        Read another blank line then second quadrupole parameters      QQU00690
C                                                                       QQU00700
      READ(1,2)                                                         QQU00710
      READ(1,5) LENTH2,RTQZ2                                            QQU00720
```

```
C                                                                       QQU00730
C       Read another blank line then third quadrupole parameters        QQU00740
C                                                                       QQU00750
      READ(1,2)                                                         QQU00760
      READ(1,8) LENTH3,RTQZ3,DELQZ3,NK3                                 QQU00770
C                                                                       QQU00780
C       Read a blank line then first order imaging properties           QQU00790
C                                                                       QQU00800
      READ(1,2)                                                         QQU00810
      READ(1,6) U,V,D0,D1,D2                                            QQU00820
C                                                                       QQU00830
1     FORMAT(20A4)                                                      QQU00840
2     FORMAT(1X)                                                        QQU00850
5     FORMAT(5X,2F10.0)                                                 QQU00860
6     FORMAT(5X,5F10.0)                                                 QQU00870
7     FORMAT(5X,3F10.0)                                                 QQU00880
8     FORMAT(5X,3F10.0,I10)                                             QQU00890
C                                                                       QQU00900
C       Convert from millimetres to metres                              QQU00910
C                                                                       QQU00920
      LENTH0=LENTH0*0.001                                               QQU00930
      LENTH1=LENTH1*0.001                                               QQU00940
      LENTH2=LENTH2*0.001                                               QQU00950
      LENTH3=LENTH3*0.001                                               QQU00960
      U=U*0.001                                                         QQU00970
      D0=D0*0.001                                                       QQU00980
      D1=D1*0.001                                                       QQU00990
      D2=D2*0.001                                                       QQU01000
C                                                                       QQU01010
C       Write title and headings on unit 2                              QQU01020
C                                                                       QQU01030
      CALL FHEAD(LENTH0,LENTH1,LENTH2,LENTH3,RTQZ0,RTQZ1,RTQZ2,RTQZ3,   QQU01040
     -           U,V,D0,D1,D2,TITLE)                                    QQU01050
C                                                                       QQU01060
C       Call subroutine to calculate first quadrupole transfer matrix   QQU01070
C                                                                       QQU01080
      CALL QTRANS(LENTH1,RTQZ1,Y1,X1)                                   QQU01090
C                                                                       QQU01100
C       Call subroutine to calculate second quadrupole transfer matrix  QQU01110
C                                                                       QQU01120
      CALL QTRANS(LENTH2,RTQZ2,Y2,X2)                                   QQU01130
      ICOUNT=0                                                          QQU01140
C                                                                       QQU01150
C       Start looping excitations - if the correct excitation of Q0     QQU01160
C       is beyond 2000xDELQZ0 then the calculation stops and the next   QQU01170
C       value of RTQZ3 is examined.                                     QQU01180
C                                                                       QQU01190
      DO 1000 I=1,NK3                                                   QQU01200
C                                                                       QQU01210
10    IF(ICOUNT.GT.2000) THEN                                           QQU01220
      Q3EX(I)=RTQZ3                                                     QQU01230
      Q0EX(I)=RTQZ0                                                     QQU01240
      WRITE(2,89)                                                       QQU01250
      GOTO 995                                                          QQU01260
      END IF                                                            QQU01270
C                                                                       QQU01280
C       Call subroutine to calculate focus quadrupole transfer matrix   QQU01290
C                                                                       QQU01300
      CALL QTRANS(LENTH0,RTQZ0,Y0,X0)                                   QQU01310
C                                                                       QQU01320
C       Call subroutine to calculate third quadrupole transfer matrix   QQU01330
C                                                                       QQU01340
      CALL QTRANS(LENTH3,RTQZ3,Y3,X3)                                   QQU01350
C                                                                       QQU01360
C       Call subroutine to calculate the Q2/Q3 transfer matrices        QQU01370
C                                                                       QQU01380
      CALL QCOMB(X2,Y2,Y3,X3,D2,YCD,XDC)                                QQU01390
C                                                                       QQU01400
C       Call subroutine to calculate the Q1/Q2/Q3 transfer matrices     QQU01410
C                                                                       QQU01420
      CALL QCOMB(Y1,X1,XDC,YCD,D1,YCDC,XDCD)                            QQU01430
C                                                                       QQU01440
```

```
C       Call subroutine to calculate the Q0/Q1/Q2/Q3 transfer matrices QQU01450
C                                                                     QQU01460
      CALL QCOMB(Y0,X0,XDCD,YCDC,D0,YDCDC,XCDCD)                      QQU01470
C                                                                     QQU01480
C       Object position is given so calculate non-stigmatic          QQU01490
C       image positions.                                              QQU01500
C                                                                     QQU01510
      CALL ASTIG(YDCDC,XCDCD,U,DASTIG,HASTIG,CONMAG,DIVMAG)           QQU01520
C                                                                     QQU01530
C       Check to see if the vertical image position is within        QQU01540
C       a given range of the required position. If it is then        QQU01550
C       store the results else increment Q0 exitation approp-        QQU01560
C       riately.                                                      QQU01570
C                                                                     QQU01580
      TEMP=(HASTIG/LENTH2)-V                                          QQU01590
      IF(DABS(TEMP).LE.0.005) GOTO 990                                QQU01600
      IF(TEMP.GT.0.005.OR.RTQZ0.LE.0.0) THEN                          QQU01610
      RTQZ0=RTQZ0+DELQZ0                                              QQU01620
      ICOUNT=ICOUNT+1                                                 QQU01630
      END IF                                                          QQU01640
      IF(TEMP.LT.-0.005.AND.RTQZ0.GT.0.0) THEN                        QQU01650
      RTQZ0=RTQZ0-DELQZ0                                              QQU01660
      ICOUNT=ICOUNT+1                                                 QQU01670
      END IF                                                          QQU01680
      GOTO 10                                                         QQU01690
C                                                                     QQU01700
C       Vertical image correct - output optical properties           QQU01710
C                                                                     QQU01720
990   Q3EX(I)=SNGL(RTQZ3)                                             QQU01730
      Q0EX(I)=SNGL(RTQZ0)                                             QQU01740
995   WRITE(2,60) RTQZ0,RTQZ3                                         QQU01750
      WRITE(2,101) U/LENTH2                                           QQU01760
      WRITE(2,40) CONMAG,HASTIG/LENTH2                                QQU01770
      WRITE(2,50) DIVMAG,DASTIG/LENTH2                                QQU01780
C                                                                     QQU01790
C       Set up arrays for graphical output                           QQU01800
C                                                                     QQU01810
      CDCMAG(I)=SNGL(CONMAG)                                          QQU01820
      DCDMAG(I)=SNGL(DIVMAG)                                          QQU01830
      IF(CDCMAG(I).LT.-100.0.OR.CDCMAG(I).GT.0.0)                     QQU01840
     +   CDCMAG(I)=0.0                                                QQU01850
      IF(DCDMAG(I).LT.-100.0.OR.DCDMAG(I).GT.0.0)                     QQU01860
     +   DCDMAG(I)=0.0                                                QQU01870
      RTQZ3=RTQZ3+DELQZ3                                              QQU01880
      ICOUNT=0                                                        QQU01890
1000  CONTINUE                                                        QQU01900
C                                                                     QQU01910
C       Call plotting subroutine                                     QQU01920
C                                                                     QQU01930
      CALL GRAPH(Q3EX,Q0EX,CDCMAG,DCDMAG,NK3)                         QQU01940
                                                                      QQU01950
40    FORMAT(/1X,'CONV-DIV-CONV MAG = ',F10.5,3X,'AT IMAGE',          QQU01960
     -      ' POSITION = ',F10.5,' mm.')                             QQU01970
50    FORMAT(/1X,'DIV-CONV-DIV  MAG = ',F10.5,3X,'AT IMAGE',          QQU01980
     -      ' POSITION = ',F10.5,' mm.')                             QQU01990
60    FORMAT(/1X,'RTQZ0=',F10.5,2X,'RTQZ3=',F10.5)                    QQU02000
89    FORMAT(/1X,'Q0 EXITATION NOT CONVERGED TO OBJECT POSITION')     QQU02010
101   FORMAT(/1X,'OBJECT POSITION = ',F10.5,' mm.')                   QQU02020
      STOP                                                            QQU02030
      END                                                             QQU02040
C                                                                     QQU02050
C                                                                     QQU02060
C       Subroutine Qtrans                                            QQU02070
C                                                                     QQU02080
C       This subroutine calculates the convergent                    QQU02090
C       and divergent transfer matrices.                             QQU02100
C                                                                     QQU02110
      SUBROUTINE QTRANS(LENGTH,ROOTQZ,Y,X)                            QQU02120
      IMPLICIT REAL*8(A-H,O-Z)                                        QQU02130
      DIMENSION Y(4,4),X(4,4)                                         QQU02140
      REAL*8 LENGTH                                                   QQU02150
C                                                                     QQU02160
```

```
C       Set up various constants                                        QQU02170
C                                                                       QQU02180
      ROOTQ=ROOTQZ/LENGTH                                               QQU02190
      Q=ROOTQ**2                                                        QQU02200
C                                                                       QQU02210
C       Initialise Y and X arrays to zero                               QQU02220
C                                                                       QQU02230
      DO 20 I=1,4                                                       QQU02240
      DO 10 J=1,4                                                       QQU02250
      Y(I,J)=0.0                                                        QQU02260
      X(I,J)=0.0                                                        QQU02270
10    CONTINUE                                                          QQU02280
20    CONTINUE                                                          QQU02290
C                                                                       QQU02300
C       Calculate first and second order convergent coefficients        QQU02310
C                                                                       QQU02320
      Y(1,1)=DCOS(ROOTQZ)                                               QQU02330
      Y(2,1)=(1.0/ROOTQ)*DSIN(ROOTQZ)                                   QQU02340
      Y(3,1)=0.5*Q*LENGTH*Y(2,1)                                        QQU02350
      Y(4,1)=0.5*(Y(2,1)-(LENGTH*Y(1,1)))                               QQU02360
      Y(1,2)=-ROOTQ*DSIN(ROOTQZ)                                        QQU02370
      Y(2,2)=DCOS(ROOTQZ)                                               QQU02380
      Y(3,2)=0.5*Q*((LENGTH*Y(1,1))+Y(2,1))                             QQU02390
      Y(4,2)=0.5*ROOTQZ*DSIN(ROOTQZ)                                    QQU02400
      Y(3,3)=Y(1,1)                                                     QQU02410
      Y(4,3)=Y(2,1)                                                     QQU02420
      Y(3,4)=Y(1,2)                                                     QQU02430
      Y(4,4)=Y(2,2)                                                     QQU02440
C                                                                       QQU02450
C       Calculate first and second order divergent coefficients         QQU02460
C                                                                       QQU02470
      X(1,1)=DCOSH(ROOTQZ)                                              QQU02480
      X(2,1)=(1.0/ROOTQ)*DSINH(ROOTQZ)                                  QQU02490
      X(3,1)=-0.5*ROOTQZ*DSINH(ROOTQZ)                                  QQU02500
      X(4,1)=0.5*(X(2,1)-(LENGTH*X(1,1)))                               QQU02510
      X(1,2)=ROOTQ*DSINH(ROOTQZ)                                        QQU02520
      X(2,2)=DCOSH(ROOTQZ)                                              QQU02530
      X(3,2)=-0.5*Q*((LENGTH*X(1,1))+X(2,1))                            QQU02540
      X(4,2)=-0.5*ROOTQZ*DSINH(ROOTQZ)                                  QQU02550
      X(3,3)=X(1,1)                                                     QQU02560
      X(4,3)=X(2,1)                                                     QQU02570
      X(3,4)=X(1,2)                                                     QQU02580
      X(4,4)=X(2,2)                                                     QQU02590
      RETURN                                                            QQU02600
      END                                                               QQU02610
C                                                                       QQU02620
C                                                                       QQU02630
C       Subroutine Qcomb                                                QQU02640
C                                                                       QQU02650
C       This subroutine calculates the combined horizontal              QQU02660
C       and vertical transfer matrices.                                 QQU02670
C                                                                       QQU02680
      SUBROUTINE QCOMB(Y1,X1,Y2,X2,D,YCD,XDC)                           QQU02690
      IMPLICIT REAL*8(A-H,O-Z)                                          QQU02700
      DIMENSION Y1(4,4),X1(4,4),Y2(4,4),X2(4,4),YCD(4,4),XDC(4,4)       QQU02710
C                                                                       QQU02720
C       Initialise YCD and XDC arrays to zero                           QQU02730
C                                                                       QQU02740
      DO 10 I=1,4                                                       QQU02750
      DO 10 J=1,4                                                       QQU02760
      YCD(I,J)=0.0                                                      QQU02770
      XDC(I,J)=0.0                                                      QQU02780
10    CONTINUE                                                          QQU02790
C                                                                       QQU02800
C       Calculate convergent-divergent transfer matrix                  QQU02810
C                                                                       QQU02820
      YCD(1,1)=Y1(1,1)*X2(1,1)+(Y1(1,2)*(D*X2(1,1)+X2(2,1)))            QQU02830
      YCD(2,1)=Y1(2,1)*X2(1,1)+(Y1(2,2)*(D*X2(1,1)+X2(2,1)))            QQU02840
      YCD(3,1)=Y1(3,1)*X2(1,1)+(Y1(3,2)*(D*X2(1,1)+X2(2,1)))+           QQU02850
     -         Y1(3,3)*X2(3,1)+(Y1(3,4)*(D*X2(3,1)+X2(4,1)))            QQU02860
      YCD(4,1)=Y1(4,1)*X2(1,1)+(Y1(4,2)*(D*X2(1,1)+X2(2,1)))+           QQU02870
     -         Y1(4,3)*X2(3,1)+(Y1(4,4)*(D*X2(3,1)+X2(4,1)))            QQU02880
```

```
      YCD(1,2)=Y1(1,1)*X2(1,2)+(Y1(1,2)*(D*X2(1,2)+X2(2,2)))              QQU02890
      YCD(2,2)=Y1(2,1)*X2(1,2)+(Y1(2,2)*(D*X2(1,2)+X2(2,2)))              QQU02900
      YCD(3,2)=Y1(3,1)*X2(1,2)+(Y1(3,2)*(D*X2(1,2)+X2(2,2)))+             QQU02910
     -         Y1(3,3)*X2(3,2)+(Y1(3,4)*(D*X2(3,2)+X2(4,2)))              QQU02920
      YCD(4,2)=Y1(4,1)*X2(1,2)+(Y1(4,2)*(D*X2(1,2)+X2(2,2)))+             QQU02930
     -         Y1(4,3)*X2(3,2)+(Y1(4,4)*(D*X2(3,2)+X2(4,2)))              QQU02940
      YCD(3,3)=Y1(3,3)*X2(3,3)+(Y1(3,4)*(D*X2(3,3)+X2(4,3)))              QQU02950
      YCD(4,3)=Y1(4,3)*X2(3,3)+(Y1(4,4)*(D*X2(3,3)+X2(4,3)))              QQU02960
      YCD(3,4)=Y1(3,3)*X2(3,4)+(Y1(3,4)*(D*X2(3,4)+X2(4,4)))              QQU02970
      YCD(4,4)=Y1(4,3)*X2(3,4)+(Y1(4,4)*(D*X2(3,4)+X2(4,4)))              QQU02980
C                                                                         QQU02990
C        Calculate divergent-convergent matrix                            QQU03000
C                                                                         QQU03010
      XDC(1,1)=X1(1,1)*Y2(1,1)+(X1(1,2)*(D*Y2(1,1)+Y2(2,1)))              QQU03020
      XDC(2,1)=X1(2,1)*Y2(1,1)+(X1(2,2)*(D*Y2(1,1)+Y2(2,1)))              QQU03030
      XDC(3,1)=X1(3,1)*Y2(1,1)+(X1(3,2)*(D*Y2(1,1)+Y2(2,1)))+             QQU03040
     -         X1(3,3)*Y2(3,1)+(X1(3,4)*(D*Y2(3,1)+Y2(4,1)))              QQU03050
      XDC(4,1)=X1(4,1)*Y2(1,1)+(X1(4,2)*(D*Y2(1,1)+Y2(2,1)))+             QQU03060
     -         X1(4,3)*Y2(3,1)+(X1(4,4)*(D*Y2(3,1)+Y2(4,1)))              QQU03070
      XDC(1,2)=X1(1,1)*Y2(1,2)+(X1(1,2)*(D*Y2(1,2)+Y2(2,2)))              QQU03080
      XDC(2,2)=X1(2,1)*Y2(1,2)+(X1(2,2)*(D*Y2(1,2)+Y2(2,2)))              QQU03090
      XDC(3,2)=X1(3,1)*Y2(1,2)+(X1(3,2)*(D*Y2(1,2)+Y2(2,2)))+             QQU03100
     -         X1(3,3)*Y2(3,2)+(X1(3,4)*(D*Y2(3,2)+Y2(4,2)))              QQU03110
      XDC(4,2)=X1(4,1)*Y2(1,2)+(X1(4,2)*(D*Y2(1,2)+Y2(2,2)))+             QQU03120
     -         X1(4,3)*Y2(3,2)+(X1(4,4)*(D*Y2(3,2)+Y2(4,2)))              QQU03130
      XDC(3,3)=X1(3,3)*Y2(3,3)+(X1(3,4)*(D*Y2(3,3)+Y2(4,3)))              QQU03140
      XDC(4,3)=X1(4,3)*Y2(3,3)+(X1(4,4)*(D*Y2(3,3)+Y2(4,3)))              QQU03150
      XDC(3,4)=X1(3,3)*Y2(3,4)+(X1(3,4)*(D*Y2(3,4)+Y2(4,4)))              QQU03160
      XDC(4,4)=X1(4,3)*Y2(3,4)+(X1(4,4)*(D*Y2(3,4)+Y2(4,4)))              QQU03170
      RETURN                                                              QQU03180
      END                                                                 QQU03190
C                                                                         QQU03200
C                                                                         QQU03210
C        Subroutine Qttran                                                QQU03220
C                                                                         QQU03230
C        This subroutine calculates the total vertical                    QQU03240
C        and horizontal transfer matrices.                                QQU03250
C                                                                         QQU03260
      SUBROUTINE QTTRAN(Y,X,U,V,TY,TX)                                    QQU03270
      IMPLICIT REAL*8(A-H,O-Z)                                            QQU03280
      DIMENSION Y(4,4),TY(4,4),X(4,4),TX(4,4)                             QQU03290
C                                                                         QQU03300
C        Initialise TY and TX arrays to zero                              QQU03310
C                                                                         QQU03320
      DO 20 I=1,4                                                         QQU03330
      DO 10 J=1,4                                                         QQU03340
      TY(I,J)=0.0                                                         QQU03350
      TX(I,J)=0.0                                                         QQU03360
10    CONTINUE                                                            QQU03370
20    CONTINUE                                                            QQU03380
C                                                                         QQU03390
C        Calculate total horizontal matrix elements                       QQU03400
C                                                                         QQU03410
      TY(1,1) =Y(1,1)+(V*Y(1,2))                                          QQU03420
      TY(2,1) =U*(Y(1,1)+(V*Y(1,2)))+Y(2,1)+(V*Y(2,2))                    QQU03430
      TY(3,1) =Y(3,1)+(V*Y(3,2))                                          QQU03440
      TY(4,1) =U*(Y(3,1)+V*Y(3,2))+Y(4,1)+(V*Y(4,2))                      QQU03450
      TY(1,2) =Y(1,2)                                                     QQU03460
      TY(2,2) =(U*Y(1,2))+Y(2,2)                                          QQU03470
      TY(3,2) =Y(3,2)                                                     QQU03480
      TY(4,2) =Y(4,2)+(U*Y(3,2))                                          QQU03490
      TY(3,3) =Y(3,3)+(V*Y(3,4))                                          QQU03500
      TY(4,3) =U*(Y(3,3)+(V*Y(3,4)))+Y(4,3)+(V*Y(4,4))                    QQU03510
      TY(3,4) =Y(3,4)                                                     QQU03520
      TY(4,4) =(U*Y(3,4))+Y(4,4)                                          QQU03530
C                                                                         QQU03540
C        Calculate total vertical matrix elements                         QQU03550
C                                                                         QQU03560
      TX(1,1) =X(1,1)+(V*X(1,2))                                          QQU03570
      TX(2,1) =U*(X(1,1)+(V*X(1,2)))+X(2,1)+(V*X(2,2))                    QQU03580
      TX(3,1) =X(3,1)+(V*X(3,2))                                          QQU03590
      TX(4,1) =U*(X(3,1)+V*X(3,2))+X(4,1)+(V*X(4,2))                      QQU03600
```

```
      TX(1,2) =X(1,2)                                                   QQU03610
      TX(2,2) =(U*X(1,2))+X(2,2)                                        QQU03620
      TX(3,2) =X(3,2)                                                   QQU03630
      TX(4,2) =X(4,2)+(U*X(3,2))                                        QQU03640
      TX(3,3) =X(3,3)+(V*X(3,4))                                        QQU03650
      TX(4,3) =U*(X(3,3)+(V*X(3,4)))+X(4,3)+(V*X(4,4))                  QQU03660
      TX(3,4) =X(3,4)                                                   QQU03670
      TX(4,4) =(U*X(3,4))+X(4,4)                                        QQU03680
      RETURN                                                            QQU03690
      END                                                               QQU03700
C                                                                       QQU03710
C                                                                       QQU03720
C        Subroutine Astig                                               QQU03730
C                                                                       QQU03740
C        This subroutine calculates the object plane distances          QQU03750
C        given the image plane distance and the transfer matrices.      QQU03760
C                                                                       QQU03770
      SUBROUTINE ASTIG(YCDC,XDCD,U,DASTIG,HASTIG,CONMAG,DIVMAG)         QQU03780
      IMPLICIT REAL*8 (A-H,O-Z)                                         QQU03790
      DIMENSION YCDC(4,4),XDCD(4,4)                                     QQU03800
      DASTIG=-(XDCD(1,1)*U+XDCD(2,1))/(XDCD(1,2)*U+XDCD(2,2))           QQU03810
      DIVMAG=XDCD(1,1)+(DASTIG*XDCD(1,2))                               QQU03820
      HASTIG=-(YCDC(1,1)*U+YCDC(2,1))/(YCDC(1,2)*U+YCDC(2,2))           QQU03830
      CONMAG=YCDC(1,1)+(HASTIG*YCDC(1,2))                               QQU03840
      RETURN                                                            QQU03850
      END                                                               QQU03860
C                                                                       QQU03870
C                                                                       QQU03880
C        Subroutine Fhead                                               QQU03890
C                                                                       QQU03900
C        This subroutine writes out titles and headings on unit 2.      QQU03910
C                                                                       QQU03920
      SUBROUTINE FHEAD(LENTH0,LENTH1,LENTH2,LENTH3,RTQZ0,RTQZ1,         QQU03930
     +                 RTQZ2,RTQZ3,U,V,D0,D1,D2,TITLE)                  QQU03940
      IMPLICIT REAL*8 (A-H,O-Z)                                         QQU03950
      DIMENSION TITLE(20)                                               QQU03960
      REAL*8 LENTH0,LENTH1,LENTH2,LENTH3                                QQU03970
      WRITE(2,5)                                                        QQU03980
      WRITE(2,7)(TITLE(I),I=1,20)                                       QQU03990
      WRITE(2,14) LENTH0*1000                                           QQU04000
      WRITE(2,19) RTQZ0                                                 QQU04010
      WRITE(2,15) LENTH1*1000                                           QQU04020
      WRITE(2,20) RTQZ1                                                 QQU04030
      WRITE(2,16) LENTH2*1000                                           QQU04040
      WRITE(2,21) RTQZ2                                                 QQU04050
      WRITE(2,17) LENTH3*1000                                           QQU04060
      WRITE(2,22) RTQZ3                                                 QQU04070
      WRITE(2,30) U*1000                                                QQU04080
      WRITE(2,31) V                                                     QQU04090
      WRITE(2,35) D0*1000                                               QQU04100
      WRITE(2,40) D1*1000                                               QQU04110
      WRITE(2,45) D2*1000                                               QQU04120
      RETURN                                                            QQU04130
5     FORMAT(//1X,'OPTICAL PROPERTIES OF MAGNETIC QUADRUPOLE PAIRS.'//) QQU04140
7     FORMAT(20A4)                                                      QQU04150
14    FORMAT(/1X,'LENGTH OF FIRST LENS             = ',F8.2,'mm.')      QQU04160
15    FORMAT(/1X,'LENGTH OF SECOND LENS            = ',F8.2,'mm.')      QQU04170
16    FORMAT(/1X,'LENGTH OF THIRD LENS             = ',F8.2,'mm.')      QQU04180
17    FORMAT(/1X,'LENGTH OF FOURTH LENS            = ',F8.2,'mm.')      QQU04190
19    FORMAT(/1X,'First quadrupole strength        = ',F8.2)            QQU04200
20    FORMAT(/1X,'Second quadrupole strength       = ',F8.2)            QQU04210
21    FORMAT(/1X,'Third quadrupole strength        = ',F8.2)            QQU04220
22    FORMAT(/1X,'Fourth quadrupole strength       = ',F8.2)            QQU04230
30    FORMAT(/1X,'OBJECT POSITION = ',F8.2,' mm.')                      QQU04240
31    FORMAT(/1X,'NORMALISED IMAGE POSITION = ',F8.2)                   QQU04250
35    FORMAT(/1X,'LENS 1-2 SEPARATION = ',F8.2,' mm.')                  QQU04260
40    FORMAT(/1X,'LENS 2-3 SEPARATION = ',F8.2,' mm.')                  QQU04270
45    FORMAT(/1X,'LENS 3-4 SEPARATION = ',F8.2,' mm.')                  QQU04280
      END                                                               QQU04290
C                                                                       QQU04300
C                                                                       QQU04310
C                                                                       QQU04320
```

```
C       SUBROUTINE GRAPH                                                    QQU04330
C                                                                           QQU04340
C       This subroutine does the plotting                                   QQU04350
C                                                                           QQU04360
      SUBROUTINE GRAPH(Q3EX,Q0EX,CDCMAG,DCDMAG,NK3)                         QQU04370
      REAL*4 CDCMAG(40),DCDMAG(40),COMMAG(40,2),Q3EX(40),Q0EX(40)           QQU04380
      DO 10 I=1,NK3                                                         QQU04390
      COMMAG(I,1)=CDCMAG(I)                                                 QQU04400
10    COMMAG(I,2)=DCDMAG(I)                                                 QQU04410
      CALL PAGE(18.0,22.0)                                                  QQU04420
      CALL PACK IN(14.0,20.0)                                               QQU04430
      CALL JBAXES(Q0EX,40,12.0,'  ',2,Q3EX,40,8.0,'  ',2)                   QQU04440
      DO 20 L=1,NK3                                                         QQU04450
      IF(Q0EX(L).GT.0.0) THEN                                               QQU04460
      CALL JOIN PT(Q0EX(L),Q3EX(L))                                         QQU04470
      END IF                                                                QQU04480
20    CONTINUE                                                              QQU04490
C20    CALL MARK PT(Q0EX(L),Q3EX(L),3)                                      QQU04500
      CALL BREAK                                                            QQU04510
      CALL JBAXES(COMMAG,80,12.0,'Magnification',13,Q3EX,40,8.0,'  ',2)     QQU04520
      DO 40 M=1,2                                                           QQU04530
      DO 30 N=1,NK3                                                         QQU04540
      LINE=M                                                                QQU04550
      CALL JOIN PT(COMMAG(N,M),Q3EX(N))                                     QQU04560
30    CONTINUE                                                              QQU04570
C30    CALL MARK PT(COMMAG(N,M),Q3EX(N),LINE)                               QQU04580
      CALL BREAK                                                            QQU04590
40    CONTINUE                                                              QQU04600
C      CALL SET KY('B   ','L   ',2,8)                                       QQU04610
C      CALL MARK KY(1,'DCDC MAG',8)                                         QQU04620
C      CALL MARK KY(2,'CDCD MAG',8)                                         QQU04630
C     CALL TITLE('T   ','L   ','QUADRUPLET OPTICS',17)                      QQU04640
      CALL END PLT                                                          QQU04650
      STOP                                                                  QQU04660
      END                                                                   QQU04670
```

Example data files for QPAIR, QTRIP4 and QQUAD

```
FILE: QPAIR     DATA      A    GLASGOW HEP CMS/SP V 4.19


Central quadrupole pair from quadruplet system
        LENGTH1    ROOTQZ1     DELQZ1        NK1
           50.0     1.0000     0.1000          8
        LENGTH2    ROOTQZ2     DELQZ2        NK2
           50.0     1.1000     0.1000          7
          RATIO          D
           0.50       25.0
```

```
FILE: QTRIP4    DATA      A    GLASGOW HEP CMS/SP V 4.19


 Quadrupole quadruplet high magnification mode
        LENGTH0    ROOTQZ0     DELQZ0        NK0
           15.00   0.00000      0.075          5
        LENGTH1    ROOTQZ1     DELQZ1        NK1
           50.00    1.6510      0.010          1
        LENGTH2    ROOTQZ2     DELQZ2        NK2
           50.00    1.4860      0.001          1
        LENGTH3    ROOTQZ3     DELQZ3        NK3
           25.00    0.0000     0.0500         20
          OBJECT       GAP0       GAP1       GAP2
          -7.500     5.0100      25.00      12.50
```

```
FILE: QQUAD     DATA      A    GLASGOW HEP CMS/SP V 4.19


 QUADRUPOLE QUADRUPLET HIGH MAG MODE
        LENGTH0    ROOTQZ0     DELQZ0
           15.00   0.09001    0.00005
        LENGTH1    ROOTQZ1
           50.00    1.6510
        LENGTH2    ROOTQZ2
           50.00    1.4860
        LENGTH3    ROOTQZ3     DELQZ3        NK3
           25.00    0.7500      0.030         33
          OBJECT     IMAGE       GAP0       GAP1       GAP2
         -7.5000    1.0000       5.01      25.00     12.500
```

Appendix 5

Data acquisition program.

A listing of the assembly language program written to acquire the digital data from the ADC is given. All the memory locations, traps etc. are specific to the Motorola KDM 68000 monoboard computer.

```
* PROGRAM TO READ MULTIPLE SCANS OF DATA FROM AN ADC *
*
DATA      EQU    $2000
BLOCK     EQU    $5000
STACK     EQU    $8000
VECTOR2   EQU    $68
VECTOR3   EQU    $6C
NSCANS    EQU    10
*
DDRA1     EQU    $3FF41
PDRA1     EQU    $3FF41
CRA1      EQU    $3FF45
DDRA2     EQU    $3FF40
PDRA2     EQU    $3FF40
CRA2      EQU    $3FF44
*
*SET UP STATUS REGISTER,LOAD AUTOVECTORS,STACK POINTER AND SCAN COUNTER*
*
          MOVE.W #$2700,SR         *MASK INTERRUPTS TO LEVEL 7
          MOVE.L #STACK,A7         *SET STACK POINTER
          MOVE.L #SERVICE,VECTOR2 *LOAD AUTOVECTOR POINTERS
          MOVE.L #SERVICE,VECTOR3
          MOVE.W #NSCANS,D0        *SCAN COUNTER
          MOVE.L #DATA,A0          *START ADDRESS OF DATA BLOCK
*
* CLEAR BLOCK OF MEMORY FOR DATA STORAGE OF UP TO TEN SCANS *
*
          LEA    DATA,A1           *START ADDRESS OF DATA BLOCK
CLEAR     CLR    (A1)+             *ZERO MEMORY LOCATION
          CMP    #BLOCK,A1         *FINISHED YET?
          BLT.S  CLEAR             *IF NOT CONTINUE
*
* SET UP PIA'S AND ENABLE PROCESSOR INTERRUPTS AT LEVEL 6 OR ABOVE *
*
          RESET
          MOVE.B #0,CRA1           *ACCESS DATA DIR REG A OF PIA1
          MOVE.B #0,DDRA1          *MAKE ALL LINES INPUTS
          MOVE.B #%00000100,CRA1   *ACCESS PER DATA REG OF PIA1
*                                  *CA1 INTERRUPT ON FALLING EDGE MASKED
          MOVE.B #0,CRA2           *ACCESS DATA DIR REG A OF PIA2
          MOVE.B #%00010000,DDRA2 *MAKE A0-A3 I/P,A4 O/P,A5-A7 NOT USED
          MOVE.B #%00000111,CRA2   *ACCESS PER DATA REG OF PIA2
*                                  *CA1 INTERRUPT ON RISING EDGE UNMASKED
          MOVE.W #$2500,SR         *ENABLE PROCESSOR INTERRUPT AT LEVEL 5
*
* MAIN PROGRAM POLLS CA1 OF PIA1 EXITING ON INTERRUPT FROM CA1 OF PIA2 *
*
PROGRAM   SUBQ.B #1,D0             *DECREMENT SCAN COUNTER
          BMI.S  ENDJOB            *IF SCANS COMPLETE THEN EXIT
*
          MOVE.B #00010000,PDRA2   *SEND OUT INITIALISATION RESET PULSE
          CLR.B  PDRA2             *CLEAR PULSE
*
LOOP      MOVE.B CRA1,D3           *ANY DATA YET?
          BPL.S  LOOP              *IF NOT REPEAT TEST
          MOVE.W PDRA2,(A0)+       *16 BIT READ, PIA2 LINE A3 HAS MSB
          BRA.S  LOOP              *REPEAT UNTIL INTERRUPT
*
ENDJOB    TRAP   #15               *FINISHED NOW SO ESCAPE TO MONITOR
          DC.W   0
*
* INTERRUPT SERVICE ROUTINE CLEARS 16 BYTES OF MEMORY BETWEEN SCANS *
*
SERVICE   ADD.W  #32,A0            *MOVE DATA BLOCK POINTER ALONG
          MOVE.L #PROGRAM,2(A7)    *CHANGE ADDRESS ON STACKED PROGRAM
*                                  *COUNTER TO SET UP NEXT SCAN
          MOVE.W PDRA2,A2          *DUMMY READ TO CLEAR INTERRUPT
          RTE                      *RETURN TO CORRECT START POINT
          END
```

Appendix 6

Monte Carlo Simulation

A listing of the Monte Carlo routine is given along with an example data file. The program allows simulation of electron scatter in a layer of YAG on top of a glass (silicon) substrate, although any combination of elements can be used by recalculating the appropriate parameters and constants. This version of the program allows the placement of a rectangular array of vertical gold pixellation walls throughout the YAG. The size and spacing of these walls is controlled by parameters XWALL, YWALL and WIDTH. Alignment of the gold walls with respect to the incident electron beam (at the origin) is controlled by the parameter OFFSET. If OFFSET = 0 the beam hits the YAG in the x-y plane in the centre of a rectangle (square) bounded by four gold walls. If OFFSET = 1 the beam hits the centre of a y-direction gold wall, and if OFFSET=2 the beam hits the centre of both y and x direction walls; i.e. in the centre of the gold cross formed at the intersection of two walls. If pixellation is not desired set parameter OFFSET = 0 and make XWALL and YWALL larger than YAX.

Methods of calculating the various constants used in the program are described in 'The resist exposure and development suite user guide' available from Dr. Steve Beaumont of Glasgow University Electrical Engineering Department. The input parameters not defined in the program header are:

Ncode	Parameter determining the form of the output plot.
Ncode = 0	Produces a y-z plot as shown in chapter 8.
Ncode = 1	Produces an x-y slice with the trajectories followed between two z limits.
Ztop	Upper z axis limit for x-y display (μm).
Zbot	Lower z axis limit for x-y display (μm).
Xwall	Half spacing of gold walls in x direction (μm).
Ywall	Half spacing of gold walls in y direction (μm).
Offset	Parameter controlling position of gold walls relative to the origin.
Offset = 0	Walls equidistant about origin in x and y directions.
Offset = 1	Origin coincides with the centre of a y direction gold wall, x direction walls equidistant about the origin.
Offset = 2	Origin coincides with centre of gold wall in both x and y directions.

```
C                                                                       MON00010
C     MONTE CARLO PROGRAM                                               MON00020
C                                                                       MON00030
C     THE PRINCIPAL VARIABLES ARE DEFINED AS FOLLOWS:                   MON00040
C                                                                       MON00050
C     CO1 = ARRAY OF X,Y,Z CO-ORDS IN CM                                MON00060
C     A1 = TRANSFORMATION MATRIX TO CONVERT TO MAIN COORDS              MON00070
C     TETA = ANGLE OF DEFLECTION IN RADIANS                             MON00080
C     FIE = AZIMUTHAL ANGLE IN RADIANS                                  MON00090
C     STEP = STEP LENGTH IN CM                                          MON00100
C     EEV = CURRENT ENERGY OF ELECTRON IN ELECTRON VOLTS                MON00110
C     ALPHAS = VALUE OF ALPHA FOR THE SCATTERING ATOM                   MON00120
C     YFL = RANDOM NUMBER GENERATOR VARIABLE                            MON00130
C     IX,IY = RANDOM NUMBER GENERATOR VARIABLES                         MON00140
C     NCODE = DATA CODE - DETERMINES FORM OF OUTPUT                     MON00150
C     NMODE = INDICATION OF THE STATE OF THE ELECTRON                   MON00160
C             NMODE = 1 ELECTRON IS IN YAG                              MON00170
C             NMODE = 2 ELECTRON HAS BEEN REFLECTED                     MON00180
C             NMODE = 3 ELECTRON IS IN THE SUBSTRATE (GLASS)            MON00190
C             NMODE = 4 ELECTRON IS IN THE GOLD BARRIERS                MON00200
C     EEV0 = INITIAL ENERGY OF ELECTRONS IN ELECTRON VOLTS              MON00210
C     FILM = THICKNESS OF YAG FILM IN MICRONS                           MON00220
C     SUBSTR = THICKNESS OF SUBSTRATE FILM IN MICRONS                   MON00230
C     ZFILM = THICKNESS OF YAG FILM IN CM                               MON00240
C     ZSUPP = THICKNESS OF SUBSTRATE FILM IN CM                         MON00250
C     NEVT = NUMBER OF ELECTRONS TO BE SIMULATED                        MON00260
C     NEVTX,NEVT1 = ELECTRON COUNTER                                    MON00270
C     NT = NUMBER OF ELECTRONS TRANSMITTED                              MON00280
C     NR = NUMBER OF ELECTRONS REFLECTED                                MON00290
C     NP = NUMBER OF ELECTRONS REMAINING IN YAG                         MON00300
C     NB = NUMBER OF ELECTRONS BACKSCATTERED FROM SUBSTRATE             MON00310
C     NTS = NUMBER OF ELECTRONS TRANSMITTED THROUGH ENTIRE FILM         MON00320
C     FT = FRACTION OF ELECTRONS TRANSMITTED                            MON00330
C     FR = FRACTION OF ELECTRONS REFLECTED                              MON00340
C     FP = FRACTION OF ELECTRONS IN YAG                                 MON00350
C     FB = FRACTION OF ELECTRONS BACKSCATTERED INTO YAG AT LEAST ONCE   MON00360
C     FNTS = FRACTION OF ELECTRONS TRANSMITTED THROUGH SUPPORT FILM     MON00370
C     EEV1 = ELECTRON ENERGY BEFORE SCATTERING EVENT                    MON00380
C     EEVL = ELECTRON ENERGY LOSS IN ELECTRON VOLTS                     MON00390
C     IY = DISTANCE OF SCATTERING CENTRE FROM ORIGIONAL DIRECTION OF    MON00400
C          ENTRY MEASURED IN THE Y DIRECTION IN CM.                     MON00410
C     RTIME = TIME REMAINING UNTIL JOB ENDS IN SECONDS                  MON00420
C     NEVT1 = TOTAL NUMBER OF ELECTRONS SIMULATED                       MON00430
C     NEVTS = DO LOOP COUNTER FOR ELECTRONS                             MON00440
C     RANGE = RANGE OF ELECTRONS IN CM.                                 MON00450
C     DIST = DISTANCE OF ELECTRON FROM YAG                              MON00460
C     EYAGN = NORMALISED INITIAL ENERGY IN YAG                          MON00470
C     RYAG = NORMALISED INITIAL RANGE IN YAG                            MON00480
C     GYAG = CONSTANT FOR GREENEICH AND VAN DUZER APPROXIMATION         MON00490
C     ACONST = VALUE OF DSQRT(E/2)                                      MON00500
C     AIYAG = EXCITATION ENERGY OF YAG IN EV                            MON00510
C     AISI = EXCITATION ENERGY OF SI IN EV                              MON00520
C     ESIN = NORMALISED INITIAL ENERGY IN SILICON                       MON00530
C     GSI = ANOTHER CONSTANT FOR GREENEICH AND VAN DUZER APPROXIMATION  MON00540
C                                                                       MON00550
C                                                                       MON00560
      IMPLICIT REAL*8(A-H,O-Z)                                          MON00570
      DIMENSION CO1(3),CSTART(3),A1(3,3),TITL(20)                       MON00580
      REAL*4 RTIME,YFL,AEV(201),AY(201),AEVXY(201,201),YW(4),XW(4)      MON00590
      COMMON CO1,A1,TETA,FIE,STEP,EEV,EEVL,ALPHAS,RANGE,INEL,NCODE      MON00600
      COMMON /RAN/YFL,IX,IY                                             MON00610
      COMMON /SUB/EYAGN,RYAG,GYAG                                       MON00620
      COMMON /SUB1/ESIN,RSI,GSI                                         MON00630
      COMMON /WALL/EAUN,RAU,GAU                                         MON00640
      COMMON /PLOT/AMY,AEV                                              MON00650
      COMMON /PLOT2/EEVT                                                MON00660
      COMMON /PLOT3/AEVXY                                               MON00670
      DATA ACONST/1.1658/                                               MON00680
      DATA AIYAG/171.32586/,AISI/172.25/,AIAU/796.675/                  MON00690
      DATA NT/0/,NR/0/,NTS/0/,NGTOY/0/,NAUTOY/0/,NYAG/0/,NAU/0/,NGLAS/0/MON00700
      DATA YAGEN/0.0/,GLASEN/0.0/,AUEN/0.0/,REN/0.0/,TEN/0.0/           MON00710
      DATA RTIME/0.0/                                                   MON00720
```

```
      IX = 1722371299                                                   MON00730
C                                                                       MON00740
C     Set up random number generator                                    MON00750
C                                                                       MON00760
C     CALL G05CCF                                                       MON00770
      CALL G05CBF(1)                                                    MON00780
      CALL ABN322                                                       MON00790
C                                                                       MON00800
C     Read input data                                                   MON00810
C                                                                       MON00820
      READ(3,20) (TITL(I),I=1,20)                                       MON00830
20    FORMAT(20A4)                                                      MON00840
      READ(3,21)NCODE,EEV0,FILM,SUBSTR,NEVT                             MON00850
      READ(3,22)RYAG,RSI,RAU,YAX,OFFSET                                 MON00860
      READ(3,23)ZTOP,ZBOT,XWALL,YWALL,WIDTH                             MON00870
21    FORMAT(/5X,I10,3F10.2,I10)                                        MON00880
22    FORMAT(/5X,4F10.0,I10)                                            MON00890
23    FORMAT(/5X,5F10.0)                                                MON00900
C                                                                       MON00910
C     Calculate normalised incident energy in YAG, EYAGN                MON00920
C                                                                       MON00930
      EYAGN=ACONST*EEV0/AIYAG                                           MON00940
C                                                                       MON00950
C     Calculate normalsied incident energy in SI, ESIN                  MON00960
C                                                                       MON00970
      ESIN=ACONST*EEV0/AISI                                             MON00980
C                                                                       MON00990
C     Calculate normalised incident energy in AU, EAUN                  MON01000
C                                                                       MON01010
      EAUN=ACONST*EEV0/AIAU                                             MON01020
C                                                                       MON01030
C     Calculate gammas                                                  MON01040
C                                                                       MON01050
      GYAG=1.0-DEXP(DSQRT((DLOG(EYAGN)**2)-2.                           MON01060
     -*(EYAGN**2)/RYAG)-DLOG(EYAGN))                                    MON01070
C                                                                       MON01080
      GSI=1.0-DEXP(DSQRT((DLOG(ESIN)**2)-2.                             MON01090
     -*(ESIN**2)/RSI)-DLOG(ESIN))                                       MON01100
C                                                                       MON01110
      GAU=1.0-DEXP(DSQRT((DLOG(EAUN)**2)-2.                             MON01120
     -*(EAUN**2)/RAU)-DLOG(EAUN))                                       MON01130
C                                                                       MON01140
C     Convert film and substrate thickness to cm                        MON01150
C                                                                       MON01160
      ZFILM=FILM*1.0E-4                                                 MON01170
      ZSUPP=SUBSTR*1.0E-4                                               MON01180
C                                                                       MON01190
C     Initialise arrays for graph plotting routines                     MON01200
      AMY=YAX/100.0                                                     MON01210
      AEV(1)=0.0                                                        MON01220
      AY(1)=-YAX                                                        MON01230
      EEVT=0.0                                                          MON01240
      DO 30 I=2,201                                                     MON01250
      AEV(I)=0.0                                                        MON01260
      AY(I)=AY(I-1)+AMY                                                 MON01270
30    CONTINUE                                                          MON01280
      DO 31 I=1,201                                                     MON01290
      DO 31 J=1,201                                                     MON01300
      AEVXY(I,J)=0.0                                                    MON01310
31    CONTINUE                                                          MON01320
C                                                                       MON01330
C     Set up coordinates of AU wall boundaries in X and Y directions.   MON01340
C     Geometry is controlled by parameter OFFSET.                       MON01350
C                                                                       MON01360
      YOFFST=0.0                                                        MON01370
      XOFFST=0.0                                                        MON01380
      IF(OFFSET.GT.0) YOFFST=YWALL+(WIDTH/2.0)                          MON01390
      IF(OFFSET.EQ.2) XOFFST=XWALL+(WIDTH/2.0)                          MON01400
      XW(1)=XWALL-XOFFST                                                MON01410
      XW(2)=XWALL+WIDTH-XOFFST                                          MON01420
      XW(3)=(3*XWALL)+WIDTH-XOFFST                                      MON01430
      XW(4)=(3*XWALL)+(2*WIDTH)-XOFFST                                  MON01440
```

```
      YW(1)=YWALL-YOFFST                                                MON01450
      YW(2)=YWALL+WIDTH-YOFFST                                          MON01460
      YW(3)=(3*YWALL)+WIDTH-YOFFST                                      MON01470
      YW(4)=(3*YWALL)+(2*WIDTH)-YOFFST                                  MON01480
C                                                                       MON01490
C     Set up plotting routines                                          MON01500
C                                                                       MON01510
      IF(NCODE.NE.0) GOTO 24                                            MON01520
      CALL SETYZ(FILM,SUBSTR,YW,YAX)                                    MON01530
      GOTO 25                                                           MON01540
24    CALL SETXY(FILM,SUBSTR,XW,YW,YAX)                                 MON01550
C                                                                       MON01560
C     Convert wall dimensions to centimetres                            MON01570
C                                                                       MON01580
25    DO 26 I=1,4                                                       MON01590
      XW(I)=XW(I)*1.0E-4                                                MON01600
      YW(I)=YW(I)*1.0E-4                                                MON01610
26    CONTINUE                                                          MON01620
      WIDTH=WIDTH*1.0E-4                                                MON01630
C                                                                       MON01640
C     Set up do loop for electrons                                      MON01650
C                                                                       MON01660
      DO 185 NEVTS=1,NEVT                                               MON01670
C                                                                       MON01680
      CALL JOIN PT(0.0,0.0)                                             MON01690
C                                                                       MON01700
C     Initialise electron energy,CO1,CSTART,A1,MMODE,TETA,FIE           MON01710
C                                                                       MON01720
      EEV=EEV0                                                          MON01730
      DO 50 I=1,3                                                       MON01740
      CSTART(I)=0.0                                                     MON01750
50    CO1(I)=0.0                                                        MON01760
      DO 51 I=1,3                                                       MON01770
      DO 52 J=1,3                                                       MON01780
52    A1(I,J)=0.0                                                       MON01790
51    A1(I,I)=1.0                                                       MON01800
      TETA=0.0                                                          MON01810
      FIE=0.0                                                           MON01820
      MMODE=1                                                           MON01830
C                                                                       MON01840
C     Branch to appropriate subroutine for first scattering event       MON01850
C                                                                       MON01860
      IF(DABS(CO1(2)).GE.YW(1).AND.DABS(CO1(2)).LE.YW(2)) GOTO 300      MON01870
      IF(DABS(CO1(2)).GE.YW(3).AND.DABS(CO1(2)).LE.YW(4)) GOTO 300      MON01880
C                                                                       MON01890
C***********************************************************************MON01900
C ELECTRON IS IN YAG REGION                                             MON01910
C***********************************************************************MON01920
C                                                                       MON01930
C     Store electron energy and position prior to collision             MON01940
C     and establish position of next scattering centre                  MON01950
C                                                                       MON01960
100   EEV1=EEV                                                          MON01970
      DO 101 I=1,3                                                      MON01980
      CSTART(I)=CO1(I)                                                  MON01990
101   CONTINUE                                                          MON02000
      CALL YAG                                                          MON02010
      IF(INEL.EQ.1) GOTO 500                                            MON02020
      CALL ANGLE                                                        MON02030
      CALL CORD(ZTOP,ZBOT)                                              MON02040
      GOTO 530                                                          MON02050
500   TETA=0.0                                                          MON02060
      FIE=0.0                                                           MON02070
      CALL CORD(ZTOP,ZBOT)                                              MON02080
C                                                                       MON02090
C     Has electron been reflected out of top surface?                   MON02100
C                                                                       MON02110
530   IF(CO1(3).GT.0.0) GOTO 90                                         MON02120
      NR=NR+1                                                           MON02130
      REN=REN+EEV                                                       MON02140
      MMODE=2                                                           MON02150
C                                                                       MON02160
```

```
C     Is electron still above substrate interface?                    MON02170
C                                                                     MON02180
90    IF(CO1(3).GE.ZFILM) MMODE=3                                     MON02190
C                                                                     MON02200
C     Is electron inside gold barriers?                               MON02210
C                                                                     MON02220
      IF(MMODE.EQ.2.OR.MMODE.EQ.3)GOTO 91                             MON02230
      IF(DABS(CO1(1)).GT.XW(1).AND.DABS(CO1(1)).LT.XW(2)) MMODE=4     MON02240
      IF(DABS(CO1(1)).GT.XW(3).AND.DABS(CO1(1)).LT.XW(4)) MMODE=4     MON02250
      IF(DABS(CO1(2)).GT.YW(1).AND.DABS(CO1(2)).LT.YW(2)) MMODE=4     MON02260
      IF(DABS(CO1(2)).GT.YW(3).AND.DABS(CO1(2)).LT.YW(4)) MMODE=4     MON02270
C                                                                     MON02280
C     Add energy loss to total lost in YAG. Terminate trajectory      MON02290
C     if electron energy less than mean ionisation energy in YAG      MON02300
C     Branch to appropriate subroutine for next scattering event      MON02310
C                                                                     MON02320
91    IF(EEV.LT.AIYAG.AND.MMODE.NE.2.AND.MMODE.NE.3) GOTO 116         MON02330
      YAGEN=YAGEN+EEVL                                                MON02340
      CALL ARRAY(CSTART(1),CSTART(2),EEVL)                            MON02350
      GOTO(100,180,110,300) MMODE                                     MON02360
116   YAGEN=YAGEN+EEV1                                                MON02370
      CALL ARRAY(CSTART(1),CSTART(2),EEV1)                            MON02380
      NYAG=NYAG+1                                                     MON02390
      GOTO 180                                                        MON02400
C                                                                     MON02410
C*********************************************************************MON02420
C ELECTRON IS IN THE SUBSTRATE (GLASS) REGION                         MON02430
C*********************************************************************MON02440
C                                                                     MON02450
C     Electron heas entered the glass (silicon) substrate-           MON02460
C     store energy prior to next collision.                           MON02470
C                                                                     MON02480
110   NT=NT+1                                                         MON02490
111   EEV1=EEV                                                        MON02500
C                                                                     MON02510
C     Establish position of next scattering centre (silicon)          MON02520
      CALL SI                                                         MON02530
      IF(INEL.EQ.1) GOTO 510                                          MON02540
      CALL ANGLE                                                      MON02550
      CALL CORD(ZTOP,ZBOT)                                            MON02560
      GOTO 520                                                        MON02570
510   TETA=0.0                                                        MON02580
      FIE=0.0                                                         MON02590
      CALL CORD(ZTOP,ZBOT)                                            MON02600
C                                                                     MON02610
C     Is electron above or below YAG/GLASS interface?                 MON02620
C                                                                     MON02630
520   IF(CO1(3).GE.ZFILM) GOTO 140                                    MON02640
C                                                                     MON02650
C     Electron has left substrate - has it been reflected?            MON02660
C                                                                     MON02670
      IF(CO1(3).GT.0.0) GOTO 150                                      MON02680
C                                                                     MON02690
C     Electron has been reflected through YAG - Terminate trajectory  MON02700
C                                                                     MON02710
      GLASEN = GLASEN+EEVL                                            MON02720
      REN=REN+EEV                                                     MON02730
      NR=NR+1                                                         MON02740
      GOTO 180                                                        MON02750
C                                                                     MON02760
C     Electtron is either in YAG or GOLD, which?                      MON02770
C                                                                     MON02780
150   IF(DABS(CO1(1)).GT.XW(1).AND.DABS(CO1(1)).LT.XW(2)) GOTO 152    MON02790
      IF(DABS(CO1(1)).GT.XW(3).AND.DABS(CO1(1)).LT.XW(4)) GOTO 152    MON02800
      IF(DABS(CO1(2)).GT.YW(1).AND.DABS(CO1(2)).LT.YW(2)) GOTO 152    MON02810
      IF(DABS(CO1(2)).GT.YW(3).AND.DABS(CO1(2)).LT.YW(4)) GOTO 152    MON02820
C                                                                     MON02830
C     Electron has been backscattered into YAG                        MON02840
C                                                                     MON02850
151   NGTOY=NGTOY+1                                                   MON02860
      MMODE=1                                                         MON02870
      GOTO 299                                                        MON02880
```

```
C                                                                       MON02890
C     Electron has been backscattered into GOLD                         MON02900
C                                                                       MON02910
152   MMODE=4                                                           MON02920
      GOTO 299                                                          MON02930
C                                                                       MON02940
C     Electron is below YAG/GLASS interface- has it been transmitted?   MON02950
C                                                                       MON02960
140   IF(CO1(3).LT.(ZFILM+ZSUPP)) GOTO 145                              MON02970
      GLASEN=GLASEN+EEVL                                                MON02980
      TEN=TEN+EEV                                                       MON02990
      NTS=NTS+1                                                         MON03000
      GOTO 180                                                          MON03010
C                                                                       MON03020
C     Electron is still in glass -  can it return to YAG. Terminate     MON03030
C     if not or if energy < mean ionisation energy in glass             MON03040
C                                                                       MON03050
145   IF(RANGE.LT.(CO1(3)-ZFILM).OR.EEV.LT.AISI) GOTO 146               MON03060
      GOTO 299                                                          MON03070
146   GLASEN=GLASEN+EEV1                                                MON03080
      NGLAS=NGLAS+1                                                     MON03090
      GOTO 180                                                          MON03100
C                                                                       MON03110
C     Add energy loss into total lost in glass and branch to required   MON03120
C     scattering subroutine                                             MON03130
C                                                                       MON03140
299   GLASEN=GLASEN+EEVL                                                MON03150
      GOTO(100,180,111,300) MMODE                                       MON03160
C                                                                       MON03170
C***********************************************************************MON03180
C ELECTRON IS IN GOLD REGION                                            MON03190
C***********************************************************************MON03200
C                                                                       MON03210
C     Electron is in gold barrier                                       MON03220
C     Establish position of next scattering event (GOLD)                MON03230
C     Store electron energy and position prior to scattering            MON03240
C                                                                       MON03250
300   EEV1=EEV                                                          MON03260
      DO 301 I=1,3                                                      MON03270
      CSTART(I)=CO1(I)                                                  MON03280
301   CONTINUE                                                          MON03290
      CALL GOLD                                                         MON03300
      IF(INEL.EQ.1) GOTO 330                                            MON03310
      CALL ANGLE                                                        MON03320
      CALL CORD(ZTOP,ZBOT)                                              MON03330
      GOTO 335                                                          MON03340
330   TETA=0.0                                                          MON03350
      FIE=0.0                                                           MON03360
      CALL CORD(ZTOP,ZBOT)                                              MON03370
C                                                                       MON03380
C     Is electron above or below interface?                             MON03390
C                                                                       MON03400
335   IF(CO1(3).GE.ZFILM) GOTO 340                                      MON03410
C                                                                       MON03420
C     Electron is above glass - has it been reflected?                  MON03430
C                                                                       MON03440
      IF(CO1(3).GT.0.0) GOTO 350                                        MON03450
C                                                                       MON03460
C     Electron has been reflected - terminate trajectory                MON03470
      AUEN=AUEN+EEVL                                                    MON03480
      REN=REN+EEV                                                       MON03490
      NR=NR+1                                                           MON03500
      GOTO 180                                                          MON03510
C                                                                       MON03520
C     Electron is in YAG or GOLD - which?                               MON03530
C                                                                       MON03540
350   IF(DABS(CO1(1)).GT.XW(1).AND.DABS(CO1(1)).LT.XW(2)) GOTO 351      MON03550
      IF(DABS(CO1(1)).GT.XW(3).AND.DABS(CO1(1)).LT.XW(4)) GOTO 351      MON03560
      IF(DABS(CO1(2)).GT.YW(1).AND.DABS(CO1(2)).LT.YW(2)) GOTO 351      MON03570
      IF(DABS(CO1(2)).GT.YW(3).AND.DABS(CO1(2)).LT.YW(4)) GOTO 351      MON03580
C                                                                       MON03590
C     Electron has been backscattered into YAG                          MON03600
```

```
C                                                                       MON03610
      NAUTOY=NAUTOY+1                                                   MON03620
      MMODE=1                                                           MON03630
      GOTO 399                                                          MON03640
C                                                                       MON03650
C     Electron is still in gold - can it return to YAG? Terminate       MON03660
C     if not or if energy < mean ionisation energy in GOLD              MON03670
C                                                                       MON03680
351   IF(EEV.LE.AIAU.OR.RANGE.LE.(WIDTH/SQRT(2.0))) GOTO 380            MON03690
      GOTO 381                                                          MON03700
380   AUEN=AUEN+EEV1                                                    MON03710
      NAU=NAU+1                                                         MON03720
      GOTO 180                                                          MON03730
381   MMODE=4                                                           MON03740
      GOTO 399                                                          MON03750
C                                                                       MON03760
C     Electron is below YAG/GOLD layer - has it been transmitted?       MON03770
C                                                                       MON03780
340   IF(CO1(3).LT.(ZFILM+ZSUPP)) GOTO 370                              MON03790
      NTS=NTS+1                                                         MON03800
      AUEN=AUEN+EEVL                                                    MON03810
      TEN=TEN+EEV                                                       MON03820
      GOTO 180                                                          MON03830
C                                                                       MON03840
C     Electron has been backscattered into the substrate (GLASS)        MON03850
C                                                                       MON03860
370   MMODE=3                                                           MON03870
C                                                                       MON03880
C     Add energy loss into total lost in the substrate and              MON03890
C     branch to the appropriate scattering routine.                     MON03900
C                                                                       MON03910
399   AUEN=AUEN+EEVL                                                    MON03920
      GOTO(100,180,110,300) MMODE                                       MON03930
C                                                                       MON03940
C*********************************************************************** MON03950
C START NEW ELECTRON AFTER TIME CHECK                                   MON03960
C*********************************************************************** MON03970
C                                                                       MON03980
180   NEVTX=NEVTS                                                       MON03990
      CALL TIMEL(RTIME)                                                 MON04000
      IF(RTIME.LE.20.0) GOTO 186                                        MON04010
      CALL BREAK                                                        MON04020
      CALL JOIN PT(0.0,0.0)                                             MON04030
185   CONTINUE                                                          MON04040
186   CALL BREAK                                                        MON04050
C                                                                       MON04060
C*************************************************************************MON04070
C CALCULATE FRACTIONS AND PRINT RESULTS                                 MON04080
C*************************************************************************MON04090
C                                                                       MON04100
C     CALCULATE PERCENTAGES                                             MON04110
      TOTEV=EEV0*NEVTX                                                  MON04120
      FYAGEN=(YAGEN/TOTEV)*100                                          MON04130
      FGLASE=(GLASEN/TOTEV)*100                                         MON04140
      FAUEN=(AUEN/TOTEV)*100                                            MON04150
      FREN=(REN/TOTEV)*100                                              MON04160
      FTEN=(TEN/TOTEV)*100                                              MON04170
      FNYAG=(DFLOAT(NYAG)/DFLOAT(NEVTX))*100                            MON04180
      FNGLAS=(DFLOAT(NGLAS)/DFLOAT(NEVTX))*100                          MON04190
      FNAU=(DFLOAT(NAU)/DFLOAT(NEVTX))*100                              MON04200
      FNR=(DFLOAT(NR)/DFLOAT(NEVTX))*100                                MON04210
      FNTS=(DFLOAT(NTS)/DFLOAT(NEVTX))*100                              MON04220
      FNT=(DFLOAT(NT)/DFLOAT(NEVTX))*100                                MON04230
      FNGTOY=(DFLOAT(NGTOY)/DFLOAT(NEVTX))*100                          MON04240
      FAUTOY=(DFLOAT(NAUTOY)/DFLOAT(NEVTX))*100                         MON04250
C                                                                       MON04260
C     CALCULATE 50,70 AND 90% RANGES FOR ENERGY GRAPH                   MON04270
      NPERC=EEVT*(9.0/10.0)                                             MON04280
      SPERC=EEVT*(7.0/10.0)                                             MON04290
      FPERC=EEVT*(5.0/10.0)                                             MON04300
      SUM1=AEV(101)                                                     MON04310
      SUM2=0.0                                                          MON04320
```

```
      DO 600 I=1,100                                                    MON04330
      SUM1=SUM1+AEV(101+I)                                              MON04340
      SUM2=SUM2+AEV(101-I)                                              MON04350
      IF((SUM1+SUM2).LE.FPERC) IFPERC=I                                 MON04360
      IF((SUM1+SUM2).LE.SPERC) ISPERC=I                                 MON04370
      IF((SUM1+SUM2).LE.NPERC) INPERC=I                                 MON04380
600   CONTINUE                                                          MON04390
C                                                                       MON04400
C*************                                                          MON04410
CPRINT RESULTS                                                          MON04420
C*************                                                          MON04430
C                                                                       MON04440
      WRITE(4,192)(TITL(I),I=1,20)                                      MON04450
192   FORMAT(///20A4)                                                   MON04460
      WRITE(4,193) EEV0                                                 MON04470
193   FORMAT(F10.0,' = RELATIVISTIC ENERGY OF ELECTRONS IN eV')         MON04480
      WRITE(4,194) FILM                                                 MON04490
194   FORMAT(F10.4,' = THICKNESS OF YAG FILM IN MICRONS')               MON04500
      WRITE(4,195) SUBSTR                                               MON04510
195   FORMAT(F10.4,' = THICKNESS OF SUBSTRATE FILM IN MICRONS')         MON04520
      WRITE(4,196) XWALL*2.0                                            MON04530
196   FORMAT(F10.4,' = DISTANCE BETWEEN AU WALLS (X DIRN.) IN MICRONS') MON04540
      WRITE(4,197) YWALL*2.0                                            MON04550
197   FORMAT(F10.4,' = DISTANCE BETWEEN AU WALLS (Y DIRN.) IN MICRONS') MON04560
      WRITE(4,216) WIDTH*1.0E4                                          MON04570
216   FORMAT(F10.4,' = WIDTH OF GOLD WALLS IN MICRONS')                 MON04580
      WRITE(4,198) RYAG                                                 MON04590
198   FORMAT(F10.3,' = NORMALISED RANGE IN YAG')                        MON04600
      WRITE(4,199) RSI                                                  MON04610
199   FORMAT(F10.3,' = NORMALISED RANGE IN SILICON')                    MON04620
      WRITE(4,200) RAU                                                  MON04630
200   FORMAT(F10.3,' = NORMALISED RANGE IN GOLD')                       MON04640
      WRITE(4,201) NEVTX                                                MON04650
201   FORMAT(I10,' = NUMBER OF ELECTRONS SIMULATED')                    MON04660
      WRITE(4,202)                                                      MON04670
202   FORMAT(//1X,'NUMBER OF ELECTRONS :',/)                            MON04680
      WRITE(4,203) NYAG,FNYAG                                           MON04690
203   FORMAT(1X,'ABSORBED IN YAG                  = ',I6,5X,F6.2,' %')  MON04700
      WRITE(4,204) NAU,FNAU                                             MON04710
204   FORMAT(1X,'ABSORBED IN GOLD                 = ',I6,5X,F6.2,' %')  MON04720
      WRITE(4,205) NGLAS,FNGLAS                                         MON04730
205   FORMAT(1X,'ABSORBED IN GLASS                = ',I6,5X,F6.2,' %')  MON04740
      WRITE(4,206) NR,FNR                                               MON04750
206   FORMAT(1X,'REFLECTED BACK OUT               = ',I6,5X,F6.2,' %')  MON04760
      WRITE(4,207) NTS,FNTS                                             MON04770
207   FORMAT(1X,'TRANSMITTED THROUGH BULK         = ',I6,5X,F6.2,' %')  MON04780
      WRITE(4,208) NT,FNT                                               MON04790
208   FORMAT(1X,'CROSSING INTO SUBSTRATE          = ',I6,5X,F6.2,' %')  MON04800
      WRITE(4,209) NAUTOY,FAUTOY                                        MON04810
209   FORMAT(1X,'BACKSCATTERED FROM GOLD TO YAG   = ',I6,5X,F6.2,' %')  MON04820
      WRITE(4,210) NGTOY,FNGTOY                                         MON04830
210   FORMAT(1X,'BACKSCATTERED FROM GLASS TO YAG = ',I6,5X,F6.2,' %')   MON04840
      WRITE(4,211) FYAGEN                                               MON04850
211   FORMAT(//1X,'FRACTION OF INCIDENT ENERGY DEPOSITED IN YAG   = ',  MON04860
     -F6.2,' %')                                                        MON04870
      WRITE(4,212) FAUEN                                                MON04880
212   FORMAT(1X,'FRACTION OF INCIDENT ENERGY DEPOSITED IN GOLD  = ',    MON04890
     -F6.2,' %')                                                        MON04900
      WRITE(4,213) FGLASE                                               MON04910
213   FORMAT(1X,'FRACTION OF INCIDENT ENERGY DEPOSITED IN GLASS = ',    MON04920
     -F6.2,' %')                                                        MON04930
      WRITE(4,214) FREN                                                 MON04940
214   FORMAT(1X,'FRACTION OF INCIDENT ENERGY REFLECTED          = ',    MON04950
     -F6.2,' %')                                                        MON04960
      WRITE(4,215) FTEN                                                 MON04970
215   FORMAT(1X,'FRACTION OF INCIDENT ENERGY TRANSMITTED        = ',    MON04980
     -F6.2,' %')                                                        MON04990
      WRITE(4,218)                                                      MON05000
218   FORMAT(/////)                                                     MON05010
      WRITE(4,217)(AEV(I),I=1,201)                                      MON05020
217   FORMAT(1X,5F10.0)                                                 MON05030
C                                                                       MON05040
```

```
C************                                                          MON05050
C DRAW GRAPH                                                          MON05060
C************                                                          MON05070
C                                                                     MON05080
      CALL JBAXES(AY,201,22.5,'MICRONS',7,AEV,201,22.5,'ELECTRON VOLTS' MON05090
     -,14)                                                            MON05100
      CALL DRAW CV(AY,AEV,201)                                        MON05110
      CALL YRANGE(AY(IFPERC+101),0.0,AEV(IFPERC+101))                 MON05120
      CALL YRANGE(AY(ISPERC+101),0.0,AEV(ISPERC+101))                 MON05130
      CALL YRANGE(AY(INPERC+101),0.0,AEV(INPERC+101))                 MON05140
      CALL TITLE('B    ','C    ','100 keV ELECTRONS 30 um YAG',27)    MON05150
      CALL SKETCH(AEVXY,201,201,22.5,15.0)                            MON05160
C     CALL SOLID(AEVXY,201,201,22.5,15.0)                             MON05170
      CALL END PLT                                                    MON05180
      STOP                                                            MON05190
      END                                                             MON05200
C                                                                     MON05210
C*********************************************************************MON05220
C SUBROUTINE YAG                                                      MON05230
C*********************************************************************MON05240
C                                                                     MON05250
C     This subroutine calculates the step length, final energy,       MON05260
C     and range in YAG for the scattering event                       MON05270
C                                                                     MON05280
C     The principle variables are defined as follows:                 MON05290
C                                                                     MON05300
C     DENY = DENSITY OF YTTRIUM ATOMS IN YAG                          MON05310
C     DENAL = DENSITY OF ALUMINIUM ATOMS IN YAG                       MON05320
C     DENO = DENSITY OF OXYGEN ATOMS IN YAG                           MON05330
C     ALPHAY = VALUE OF ALPHA FOR YTTRIUM                             MON05340
C     ALPHAL = VALUE OF ALPHA FOR ALUMINIUM                           MON05350
C     ALPHAO = VALUE OF ALPHA FOR OXYGEN                              MON05360
C     ALPHAS = VALUE OF ALPHA FOR THE SCATTERING ATOM                 MON05370
C     ALAMDA = MEAN FREE PATH IN CM.                                  MON05380
C     VEL = VELOCITY OF ELECTRONS IN CM/SEC                           MON05390
C     SIGMAY = SCATTERING CROSS SECTION OF YTTRIUM                    MON05400
C     SIGMAL = SCATTERING CROSS SECTION OF ALUMINIUM                  MON05410
C     SIGMAO = SCATTERING CROSS SECTION OF OXYGEN                     MON05420
C     R1,R2 = RANDOM NUMBERS BETWEEN 0 AND 1                          MON05430
C     STEPN = NORMALISED STEP LENGTH                                  MON05440
C     RANGE = ELECTRON RANGE IN CM                                    MON05450
C     RANGEN = NORMALISED RANGE                                       MON05460
C     STEP = STEP LENGTH IN CM                                        MON05470
C     PY = PROBABILITY THAT YTTRIUM IS THE SCATTERER                  MON05480
C     PA = PROBABILITY THAT ALUMINIUM IS THE SCATTERER                MON05490
C     PO = PROBABILITY THAT OXYGEN IS THE SCATTERER                   MON05500
C     EYAGN = NORMALISED INITIAL ENERGY IN YAG                        MON05510
C     RYAG = NORMALISED INITIAL RANGE IN YAG                          MON05520
C     GYAG = CONSTANT IN GREENEICH AND VAN DUZER EQUATION             MON05530
C     CONST = DENORMALISING FACTOR FOR RANGES                         MON05540
C     DENSTY = DENSITY OF YAG IN GM/CM                                MON05550
C     AIYAG = EXCITATION ENERGY OF YAG IN EV                          MON05560
C                                                                     MON05570
      SUBROUTINE YAG                                                  MON05580
      IMPLICIT REAL*8(A-H,O-Z)                                        MON05590
      DIMENSION CO1(3),A1(3,3)                                        MON05600
      COMMON CO1,A1,TETA,FIE,STEP,EEV,EEVL,ALPHAS,RANGE,INEL          MON05610
      COMMON /RAN/YFL,IX,IY                                           MON05620
      COMMON /SUB/EYAGN,RYAG,GYAG                                     MON05630
      DATA DENY/1.39156D22/,DENAL/2.31928D22/                         MON05640
      DATA DENO/5.56627D22/,CONST/5.86182D-7/                         MON05650
      DATA DENSTY/4.56/                                               MON05660
      DATA C1/7.9015225/,C2/5.4786098/,C3/4.66/                       MON05670
      DATA C4/3.5176094D15/,C5/3.13612D20/                            MON05680
      DATA C6/3.6588D19/,C7/1.44743D19/                               MON05690
      DATA C8/2.31928D22/,C9/1.39156D22/                              MON05700
      DATA C10/1.68009D11/,C11/6.80457D-3/                            MON05710
      DATA ACONST/1.1658/,AIYAG/171.32586/                            MON05720
      Z=DSQRT(EEV)                                                    MON05730
      ALPHAY=C1/Z                                                     MON05740
      ALPHAL=C2/Z                                                     MON05750
      ALPHAO=C3/Z                                                     MON05760
```

```
C                                                                       MON05770
C     Calculate elastic mean free path.                                 MON05780
C                                                                       MON05790
      VEL=DSQRT(C4*EEV)                                                 MON05800
      Z=VEL**4                                                          MON05810
      SIGMAY=C5/(Z*(ALPHAY**2)*(ALPHAY**2+1.0))                         MON05820
      SIGMAL=C6/(Z*(ALPHAL**2)*(ALPHAL**2+1.0))                         MON05830
      SIGMAO=C7/(Z*(ALPHAO**2)*(ALPHAO**2+1.0))                         MON05840
      AMFPE=1.0/((DENY*SIGMAY)+(DENAL*SIGMAL)+(DENO*SIGMAO))            MON05850
C                                                                       MON05860
C     Calculate inelastic mean free path                                MON05870
C                                                                       MON05880
      AMFPI=(AIYAG)/(C10*DLOG(C11*EEV)/EEV)                             MON05890
C                                                                       MON05900
C     Calculate the total mean free path                                MON05910
C                                                                       MON05920
      AMFPT=AMFPI*AMFPE/(AMFPI+AMFPE)                                   MON05930
C                                                                       MON05940
C     Step length is mean free path * random number                     MON05950
C                                                                       MON05960
      CALL RAND                                                         MON05970
      R1=DBLE(YFL)                                                      MON05980
      IX=IY                                                             MON05990
      STEP=-AMFPT*DLOG(R1)                                              MON06000
C                                                                       MON06010
C     Decide whether scattering event is elastic or inelastic.          MON06020
C                                                                       MON06030
      CALL RAND                                                         MON06040
      R1=DBLE(YFL)                                                      MON06050
      IX=IY                                                             MON06060
      IF(R1.LE.(AMFPT/AMFPI)) GOTO 20                                   MON06070
C                                                                       MON06080
C     Elastic collision; determine which atom has scattered the electronMON06090
C                                                                       MON06100
      INEL=0                                                            MON06110
      EETEMP=EEV                                                        MON06120
      PA=C8*SIGMAL*AMFPE                                                MON06130
      PY=C9*SIGMAY*AMFPE                                                MON06140
      CALL RAND                                                         MON06150
      R2=DBLE(YFL)                                                      MON06160
      IX=IY                                                             MON06170
      IF(R2.LT.PA)GOTO 100                                              MON06180
      Z=PA+PY                                                           MON06190
      IF(R2.LE.Z)GOTO 101                                               MON06200
      ALPHAS=ALPHAO                                                     MON06210
      GOTO 30                                                           MON06220
100   ALPHAS=ALPHAL                                                    MON06230
      GOTO 30                                                           MON06240
101   ALPHAS=ALPHAY                                                     MON06250
      GOTO 30                                                           MON06260
C                                                                       MON06270
C     Inelastic collision; determine the energy loss                    MON06280
C                                                                       MON06290
20    INEL=1                                                            MON06300
      CALL RAND                                                         MON06310
      R1=DBLE(YFL)                                                      MON06320
      IX=IY                                                             MON06330
      EEVL=-(AIYAG*DLOG(R1))                                            MON06340
      EEV=EEV-EEVL                                                      MON06350
C                                                                       MON06360
C     Calculate Bethe energy loss and range                             MON06370
C                                                                       MON06380
30    STEPN=DENSTY*STEP/CONST                                           MON06390
      EEVN=EEV*ACONST/AIYAG                                             MON06400
      RANGEN=(RYAG/GYAG)*((GYAG-1.0)+(1.0/EYAGN)*                       MON06410
     -DEXP(DSQRT((DLOG(EYAGN))**2-2.0*EYAGN*(EYAGN-EEVN)/RYAG)))        MON06420
      RANGEN=RANGEN-STEPN                                               MON06430
      IF(INEL.EQ.1) GOTO 35                                             MON06440
      EEVN=EYAGN+(0.5*RYAG/EYAGN)*((DLOG(EYAGN*                         MON06450
     -(1.0-GYAG*(RYAG-RANGEN)/RYAG)))**2-(DLOG(EYAGN)**2))              MON06460
      EEV=AIYAG*EEVN/ACONST                                             MON06470
      EEVL=EETEMP-EEV                                                   MON06480
```

```
35    RANGE=CONST*RANGEN/DENSTY                                          MON06490
      RETURN                                                             MON06500
      END                                                                MON06510
C                                                                        MON06520
C*************************************************************************MON06530
C SUBROUTINE CORD                                                        MON06540
C*************************************************************************MON06550
C                                                                        MON06560
C     This subroutine calculates the position of the next                MON06570
C     scattering event                                                   MON06580
C                                                                        MON06590
      SUBROUTINE CORD(ZTOP,ZBOT)                                         MON06600
      IMPLICIT REAL*8(A-H,O-Z)                                           MON06610
      DIMENSION CO(3),COA(3),CO1(3)                                      MON06620
      DIMENSION A1(3,3),A2(3,3),A3(3,3)                                  MON06630
      COMMON CO1,A1,TETA,FIE,STEP,EEV,EEVL,ALPHAS,RANGE,INEL,NCODE       MON06640
C                                                                        MON06650
C     Calculate the coordinates of the next scattering position          MON06660
C                                                                        MON06670
      STETA=DSIN(TETA)                                                   MON06680
      CTETA=DCOS(TETA)                                                   MON06690
      SFIE=DSIN(FIE)                                                     MON06700
      CFIE=DCOS(FIE)                                                     MON06710
      CO(1)=STETA*CFIE*STEP                                              MON06720
      CO(2)=STETA*SFIE*STEP                                              MON06730
      CO(3)=CTETA*STEP                                                   MON06740
C                                                                        MON06750
C     Calculate coordinates relative to unrotated main coordinates       MON06760
C                                                                        MON06770
      DO 53 I=1,3                                                        MON06780
      COA(I)=0.0                                                         MON06790
      DO 54 J=1,3                                                        MON06800
54    COA(I)=COA(I)+A1(I,J)*CO(J)                                        MON06810
53    CO1(I)=CO1(I)+COA(I)                                               MON06820
C                                                                        MON06830
      IF(NCODE.NE.0)GOTO 10                                              MON06840
      CALL PLOTYZ                                                        MON06850
      GOTO 20                                                            MON06860
10    CALL PLOTXY(ZTOP,ZBOT)                                             MON06870
C                                                                        MON06880
C     Set members of A2 for coordinate transformation                    MON06890
C     of next scattering event                                           MON06900
C                                                                        MON06910
20    A2(1,1)=CTETA*CFIE                                                 MON06920
      A2(1,2)=-1.0*SFIE                                                  MON06930
      A2(1,3)=STETA*CFIE                                                 MON06940
      A2(2,1)=CTETA*SFIE                                                 MON06950
      A2(2,2)=CFIE                                                       MON06960
      A2(2,3)=STETA*SFIE                                                 MON06970
      A2(3,1)=-1.0*STETA                                                 MON06980
      A2(3,2)=0.0                                                        MON06990
      A2(3,3)=CTETA                                                      MON07000
C                                                                        MON07010
C     Multiply A2 to A1 for use in next scattering event                 MON07020
C                                                                        MON07030
      DO 55 I=1,3                                                        MON07040
      A3(I,1)=0.0                                                        MON07050
      A3(I,2)=0.0                                                        MON07060
      A3(I,3)=0.0                                                        MON07070
      DO 56 J=1,3                                                        MON07080
      A3(I,1)=A3(I,1)+A1(I,J)*A2(J,1)                                    MON07090
      A3(I,2)=A3(I,2)+A1(I,J)*A2(J,2)                                    MON07100
56    A3(I,3)=A3(I,3)+A1(I,J)*A2(J,3)                                    MON07110
55    CONTINUE                                                           MON07120
      DO 57 I=1,3                                                        MON07130
      DO 58 J=1,3                                                        MON07140
58    A1(I,J)=A3(I,J)                                                    MON07150
57    CONTINUE                                                           MON07160
      RETURN                                                             MON07170
      END                                                                MON07180
C                                                                        MON07190
C*************************************************************************MON07200
```

```
C SUBROUTINE ANGLE                                                      MON07210
C***********************************************************************MON07220
C                                                                       MON07230
C     This subroutine calculates scattering angles TETA and FIE         MON07240
C                                                                       MON07250
      SUBROUTINE ANGLE                                                  MON07260
      IMPLICIT REAL*8(A-H,O-Z)                                          MON07270
      DIMENSION CO1(3),A1(3,3)                                          MON07280
      COMMON CO1,A1,TETA,FIE,STEP,EEV,EEVL,ALPHAS,RANGE                 MON07290
      COMMON /RAN/YFL,IX,IY                                             MON07300
      CALL RAND                                                         MON07310
      R3=DBLE(YFL)                                                      MON07320
      IX=IY                                                             MON07330
      Z1=ALPHAS*ALPHAS                                                  MON07340
      Z3=R3                                                             MON07350
      Z2=(Z3*(1.0+(2.0*Z1))-Z1)/(Z3+Z1)                                 MON07360
      TETA=DACOS(Z2)                                                    MON07370
      CALL RAND                                                         MON07380
      R4=DBLE(YFL)                                                      MON07390
      IX=IY                                                             MON07400
      FIE=2.0*3.1415927*R4                                              MON07410
      RETURN                                                            MON07420
      END                                                               MON07430
C                                                                       MON07440
C***********************************************************************MON07450
C SUBROUTINE RAND                                                       MON07460
C***********************************************************************MON07470
C                                                                       MON07480
C     This subroutine generates a uniform random                        MON07490
C     number between 0 and 1 (obtained from G05CAF)                     MON07500
C                                                                       MON07510
      SUBROUTINE RAND                                                   MON07520
      REAL*4 G05CAF                                                     MON07530
      COMMON /RAN/YFL,IX,IY                                             MON07540
      YFL=G05CAF(YFL)                                                   MON07550
      RETURN                                                            MON07560
      END                                                               MON07570
C                                                                       MON07580
C***********************************************************************MON07590
C SUBROUTINE SI                                                         MON07600
C***********************************************************************MON07610
C                                                                       MON07620
C     This subroutine calculates the step length                        MON07630
C     and energy loss in SILICON (Glass substitute)                     MON07640
C                                                                       MON07650
C     The principle variables are defined as follows:                   MON07660
C                                                                       MON07670
C     ALPHAS = VALUE OF ALPHA FOR SILICON                               MON07680
C     ALAMDA = MEAN FREE PATH IN CM.                                    MON07690
C     SIGMAS = VALUE OF SIGMA IN CM(2)                                  MON07700
C     ESIN = NORMALISED INITIAL ENERGY IN SILICON                       MON07710
C     RSI = NORMALISED INITIAL RANGE IN SILICON                         MON07720
C     CONST = DENORMALISING FACTOR FOR RANGES                           MON07730
C     DENSTY = DENSITY OF SILICON IN GM/CC                              MON07740
C     STEPN = NORMALISED STEP LENGTH                                    MON07750
C     EEVN = NORMALISED ELECTRON ENERGY                                 MON07760
C     RANGEN = NORMALISED ELECTRON RANGE                                MON07770
C     AISI = EXCITATION ENERGY OF SILICON IN EV                         MON07780
C                                                                       MON07790
C                                                                       MON07800
      SUBROUTINE SI                                                     MON07810
      IMPLICIT REAL*8(A-H,O-Z)                                          MON07820
      DIMENSION CO1(3),A1(3,3)                                          MON07830
      COMMON CO1,A1,TETA,FIE,STEP,EEV,EEVL,ALPHAS,RANGE,INEL            MON07840
      COMMON /RAN/YFL,IX,IY                                             MON07850
      COMMON /SUB1/ESIN,RSI,GSI                                         MON07860
      DATA CONST/5.5820694D-7/,DENSTY/2.33/                             MON07870
      DATA ACONST/1.1658/,AISI/172.25/                                  MON07880
      DATA C1/5.61563/,C2/3.5176094D15/                                 MON07890
      DATA C3/4.231734D19/,C4/4.99586D22/                               MON07900
      DATA C10/9.140519D10/,C11/6.76806D-3/                             MON07910
C                                                                       MON07920
```

```
C     Calculate the elastic mean free path                              MON07930
C                                                                       MON07940
      ALPHAS=C1/(DSQRT(EEV))                                            MON07950
      Z=ALPHAS*ALPHAS                                                   MON07960
      VEL=DSQRT(C2*EEV)                                                 MON07970
      SIGMAS=C3/((VEL**4)*Z*(Z+1.0))                                    MON07980
      AMFPE=1.0/(C4*SIGMAS)                                             MON07990
C                                                                       MON08000
C     Calculate the inelastic mean free path                            MON08010
C                                                                       MON08020
      AMFPI=AISI/(C10*DLOG(C11*EEV)/EEV)                                MON08030
C                                                                       MON08040
C     Calculate the total mean free path                                MON08050
C                                                                       MON08060
      AMFPT=AMFPI*AMFPE/(AMFPI+AMFPE)                                   MON08070
C                                                                       MON08080
C     Step length = total mean free path * random number                MON08090
C                                                                       MON08100
      CALL RAND                                                         MON08110
      R1=DBLE(YFL)                                                      MON08120
      IX=IY                                                             MON08130
      STEP=-AMFPT*DLOG(R1)                                              MON08140
C                                                                       MON08150
C     Decide whether event is elastic or inelastic                      MON08160
C                                                                       MON08170
      CALL RAND                                                         MON08180
      R1=DBLE(YFL)                                                      MON08190
      IX=IY                                                             MON08200
      IF(R1.LE.(AMFPT/AMFPI)) GOTO 20                                   MON08210
C                                                                       MON08220
C     Elastic collision                                                 MON08230
C                                                                       MON08240
      INEL=0                                                            MON08250
      EETEMP=EEV                                                        MON08260
      GOTO 30                                                           MON08270
C                                                                       MON08280
C     Inelastic collision - determine energy loss                       MON08290
C                                                                       MON08300
20    INEL=1                                                            MON08310
      CALL RAND                                                         MON08320
      R1=DBLE(YFL)                                                      MON08330
      IX=IY                                                             MON08340
      EEVL=-(AISI*DLOG(R1))                                             MON08350
      EEV=EEV-EEVL                                                      MON08360
C                                                                       MON08370
C     Calculate Bethe energy loss and range                             MON08380
C                                                                       MON08390
30    STEPN=DENSTY*STEP/CONST                                           MON08400
      EEVN=EEV*ACONST/AISI                                              MON08410
      RANGEN=(RSI/GSI)*((GSI-1.0)+(1.0/ESIN)*DEXP(DSQRT((DLOG(ESIN))**2-MON08420
     -2.0*ESIN*(ESIN-EEVN)/RSI)))                                       MON08430
      RANGEN=RANGEN-STEPN                                               MON08440
      IF(INEL.EQ.1) GOTO 35                                             MON08450
      EEVN=ESIN+(0.5*RSI/ESIN)*((DLOG(ESIN*(1.0-GSI*(RSI-RANGEN)/       MON08460
     -RSI)))**2-(DLOG(ESIN)**2))                                        MON08470
      EEV=AISI*EEVN/ACONST                                              MON08480
      EEVL=EETEMP-EEV                                                   MON08490
35    RANGE=RANGEN*CONST/DENSTY                                         MON08500
      RETURN                                                            MON08510
      END                                                               MON08520
C                                                                       MON08530
C***********************************************************************MON08540
C SUBROUTINE GOLD                                                       MON08550
C***********************************************************************MON08560
C                                                                       MON08570
C     This subroutine calculates the step length                        MON08580
C     and energy loss in gold                                           MON08590
C                                                                       MON08600
C     The principle variables are defined as follows:                   MON08610
C                                                                       MON08620
C     ALPHAS = VALUE OF ALPHA FOR GOLD                                  MON08630
C     ALAMDA = MEAN FREE PATH IN CM.                                    MON08640
```

```
C     SIGMAG = VALUE OF SIGMA IN CM(2)                                  MON08650
C     EAUN = NORMALISED INITIAL ENERGY IN GOLD                          MON08660
C     RAU = NORMALISED INITIAL RANGE IN GOLD                            MON08670
C     CONST = DENORMALISING FACTOR FOR RANGES                           MON08680
C     DENSTY = DENSITY OF GOLD IN GM/CC                                 MON08690
C     STEPN = NORMALISED STEP LENGTH                                    MON08700
C     EEVN = NORMALISED ELECTRON ENERGY                                 MON08710
C     RANGEN = NORMALISED ELECTRON RANGE                                MON08720
C     AIAU = EXCITATION ENERGY OF GOLD IN EV                            MON08730
C                                                                       MON08740
C                                                                       MON08750
      SUBROUTINE GOLD                                                   MON08760
      IMPLICIT REAL*8(A-H,O-Z)                                          MON08770
      DIMENSION CO1(3),A1(3,3)                                          MON08780
      COMMON CO1,A1,TETA,FIE,STEP,EEV,EEVL,ALPHAS,RANGE,INEL            MON08790
      COMMON /RAN/YFL,IX,IY                                             MON08800
      COMMON /WALL/EAUN,RAU,GAU                                         MON08810
      DATA CONST/1.484D-5/,DENSTY/19.32/                                MON08820
      DATA ACONST/1.1658/,AIAU/796.675/                                 MON08830
      DATA C1/9.9977/,C2/3.5176094D15/                                  MON08840
      DATA C3/1.27052D21/,C4/5.90684D22/                                MON08850
      DATA C10/3.77935D12/,C11/1.463D-3/                                MON08860
C                                                                       MON08870
C     Calculate the elastic mean free path                              MON08880
C                                                                       MON08890
      ALPHAS=C1/(DSQRT(EEV))                                            MON08900
      Z=ALPHAS*ALPHAS                                                   MON08910
      VEL=DSQRT(C2*EEV)                                                 MON08920
      SIGMAG=C3/((VEL**4)*Z*(Z+1.0))                                    MON08930
      AMFPE=1.0/(C4*SIGMAG)                                             MON08940
C                                                                       MON08950
C     Calculate the inelastic mean free path                            MON08960
C                                                                       MON08970
      AMFPI=AIAU/(C10*DLOG(C11*EEV)/EEV)                                MON08980
C                                                                       MON08990
C     Total mean free path                                              MON09000
C                                                                       MON09010
      AMFPT=AMFPI*AMFPE/(AMFPI+AMFPE)                                   MON09020
C                                                                       MON09030
C     Step length = total mean free path * random number                MON09040
C                                                                       MON09050
      CALL RAND                                                         MON09060
      R1=DBLE(YFL)                                                      MON09070
      IX=IY                                                             MON09080
      STEP=-AMFPT*DLOG(R1)                                              MON09090
C                                                                       MON09100
C     Decide whether event is elastic or inelastic                      MON09110
C                                                                       MON09120
      CALL RAND                                                         MON09130
      R1=DBLE(YFL)                                                      MON09140
      IX=IY                                                             MON09150
      IF(R1.LE.(AMFPT/AMFPI)) GOTO 20                                   MON09160
C                                                                       MON09170
C     Elastic collision                                                 MON09180
C                                                                       MON09190
      INEL=0                                                            MON09200
      EETEMP=EEV                                                        MON09210
      GOTO 30                                                           MON09220
C                                                                       MON09230
C     Inelastic collision - determine energy loss                       MON09240
C                                                                       MON09250
20    INEL=1                                                            MON09260
      CALL RAND                                                         MON09270
      R1=DBLE(YFL)                                                      MON09280
      IX=IY                                                             MON09290
      EEVL=-(AIAU*DLOG(R1))                                             MON09300
      EEV=EEV-EEVL                                                      MON09310
C                                                                       MON09320
C     Calculate Bethe energy loss and range                             MON09330
C                                                                       MON09340
30    STEPN=DENSTY*STEP/CONST                                           MON09350
      EEVN=EEV*ACONST/AIAU                                              MON09360
```

```
      RANGEN=(RAU/GAU)*((GAU-1.0)+(1.0/EAUN)*DEXP(DSQRT((DLOG(EAUN))**2-MON09370
     -2.0*EAUN*(EAUN-EEVN)/RAU)))                                       MON09380
      RANGEN=RANGEN-STEPN                                               MON09390
      IF(INEL.EQ.1) GOTO 35                                             MON09400
      EEVN=EAUN+(0.5*RAU/EAUN)*((DLOG(EAUN*(1.0-GAU*(RAU-RANGEN)/       MON09410
     -RAU)))**2-(DLOG(EAUN)**2))                                        MON09420
      EEV=AIAU*EEVN/ACONST                                              MON09430
      EEVL=EETEMP-EEV                                                   MON09440
35    RANGE=RANGEN*CONST/DENSTY                                         MON09450
      RETURN                                                            MON09460
      END                                                               MON09470
C                                                                       MON09480
C***********************************************************************MON09490
C SUBROUTINE ARRAY                                                      MON09500
C***********************************************************************MON09510
C                                                                       MON09520
C     This subroutine assigns the relevant energy lost by the           MON09530
C     electron to the appropriate element of the energy loss            MON09540
C     array                                                             MON09550
C                                                                       MON09560
      SUBROUTINE ARRAY(X,Y,EEV2,NEVTS)                                  MON09570
      IMPLICIT REAL*8(A-H,O-Z)                                          MON09580
      REAL*4 AEV(201),AEVXY(201,201)                                    MON09590
      COMMON /PLOT/AMY,AEV                                              MON09600
      COMMON /PLOT2/EEVT                                                MON09610
      COMMON /PLOT3/AEVXY                                               MON09620
      IX=IDINT((X*1.0E4)/AMY)                                           MON09630
      IY=IDINT((Y*1.0E4)/AMY)                                           MON09640
      IF(ABS(IX).GT.100.OR.ABS(IY).GT.100) RETURN                       MON09650
      AEV(IY+101)=AEV(IY+101)+EEV2                                      MON09660
      AEVXY(IX+101,IY+101)=AEVXY(IX+101,IY+101)+EEV2                    MON09670
      EEVT=EEVT+EEV2                                                    MON09680
      RETURN                                                            MON09690
      END                                                               MON09700
C                                                                       MON09710
C***********************************************************************MON09720
C SUBROUTINE SETYZ                                                      MON09730
C***********************************************************************MON09740
C                                                                       MON09750
C     This subroutine produces a y-z plot of the electron               MON09760
C     scattering volume. Subroutine PLOTYZ does the actual              MON09770
C     plotting                                                          MON09780
C                                                                       MON09790
      SUBROUTINE SETYZ(FILM,SUBSTR,YW,YAX)                              MON09800
      IMPLICIT REAL*8(A-H,O-Z)                                          MON09810
      REAL*4 SZAX,SFILM,SSUBST,SYAX,YW(4)                               MON09820
      SFILM=SNGL(FILM)                                                  MON09830
      SSUBST=SNGL(SUBSTR)                                               MON09840
      SYAX=SNGL(YAX)                                                    MON09850
      SZAX=SFILM+SSUBST                                                 MON09860
      CALL NEW PLT(-SYAX,SYAX,15.0,-SZAX,2.00,15.0)                     MON09870
      CALL DRAW AX(' ',1,0.0,0.0)                                       MON09880
      CALL DRAW AX(' ',1,0.0,90.0)                                      MON09890
      CALL XRANGE(-SYAX,SYAX,-SFILM)                                    MON09900
      CALL XRANGE(-SYAX,SYAX,-SZAX)                                     MON09910
      CALL YRANGE(YW(1),-SFILM,0.0)                                     MON09920
      CALL YRANGE(-YW(1),-SFILM,0.0)                                    MON09930
      CALL YRANGE(YW(2),-SFILM,0.0)                                     MON09940
      CALL YRANGE(-YW(2),-SFILM,0.0)                                    MON09950
      CALL YRANGE(YW(3),-SFILM,0.0)                                     MON09960
      CALL YRANGE(-YW(3),-SFILM,0.0)                                    MON09970
      CALL YRANGE(YW(4),-SFILM,0.0)                                     MON09980
      CALL YRANGE(-YW(4),-SFILM,0.0)                                    MON09990
C     CALL TITLE('T   ','L   ','100KEV ELECTRONS YAG DEN=4.56 G/CM3',35)MON10000
      CALL JOIN PT(0.0,0.0)                                             MON10010
      RETURN                                                            MON10020
      END                                                               MON10030
C                                                                       MON10040
C***********************************************************************MON10050
C SUBROUTINE SETXY                                                      MON10060
C***********************************************************************MON10070
C                                                                       MON10080
```

```
C     This subroutine produces an XY slice of the electron              MON10090
C     scattering volume at any depth in the YAG or GLASS                MON10100
C     Subroutine PLOTXY does the actual plotting                        MON10110
C                                                                       MON10120
      SUBROUTINE SETXY(FILM,SUBSTR,XW,YW,YAX)                           MON10130
      IMPLICIT REAL*8(A-H,O-Z)                                          MON10140
      REAL*4 SFILM,SSUBST,XW(4),YW(4),SYAX,SXAX                         MON10150
      SFILM=SNGL(FILM)                                                  MON10160
      SSUBST=SNGL(SUBSTR)                                               MON10170
      SYAX=SNGL(YAX)                                                    MON10180
      SXAX=SYAX                                                         MON10190
      CALL NEW PLT(-SXAX,SXAX,22.0,-SYAX,SYAX,22.0)                     MON10200
      CALL DRAW AX('                                    UM ',35,0.0,0.0)  MON10210
      CALL DRAW AX('                                     UM',35,0.0,90.0)  MON10220
      CALL XRANGE(-XW(1),XW(1),YW(1))                                   MON10230
      CALL XRANGE(-XW(1),XW(1),-YW(1))                                  MON10240
      CALL XRANGE(-XW(2),XW(2),YW(2))                                   MON10250
      CALL XRANGE(-XW(2),XW(2),-YW(2))                                  MON10260
      CALL YRANGE(XW(1),-YW(1),YW(1))                                   MON10270
      CALL YRANGE(-XW(1),-YW(1),YW(1))                                  MON10280
      CALL YRANGE(XW(2),-YW(2),YW(2))                                   MON10290
      CALL YRANGE(-XW(2),-YW(2),YW(2))                                  MON10300
      CALL TITLE('T   ','L   ','100KV ELECTRONS YAG DEN=4.56',28)       MON10310
      RETURN                                                            MON10320
      END                                                               MON10330
C                                                                       MON10340
C***********************************************************************MON10350
C SUBROUTINE PLOTYZ                                                     MON10360
C***********************************************************************MON10370
C                                                                       MON10380
      SUBROUTINE PLOTYZ                                                 MON10390
      IMPLICIT REAL*8(A-H,O-Z)                                          MON10400
      DIMENSION CO1(3),A1(3,3)                                          MON10410
      REAL*4 YPT,ZPT                                                    MON10420
      COMMON CO1,A1,TETA,FIE,STEP,EEV,ALPHAS,RANGE                      MON10430
      YPT=SNGL(CO1(2)*1.0E4)                                            MON10440
      ZPT=SNGL(CO1(3)*1.0E4)                                            MON10450
      CALL JOIN PT(YPT,-ZPT)                                            MON10460
      RETURN                                                            MON10470
      END                                                               MON10480
C                                                                       MON10490
C***********************************************************************MON10500
C SUBROUTINE PLOTXY                                                     MON10510
C***********************************************************************MON10520
C                                                                       MON10530
      SUBROUTINE PLOTXY(ZTOP,ZBOT)                                      MON10540
      IMPLICIT REAL*8(A-H,O-Z)                                          MON10550
      DIMENSION CO1(3),A1(3,3)                                          MON10560
      REAL*4 SZTOP,SZBOT,XPT,YPT                                        MON10570
      COMMON CO1,A1,TETA,FIE,STEP,EEV,ALPHAS,RANGE                      MON10580
      SZTOP=SNGL(ZTOP)                                                  MON10590
      SZBOT=SNGL(ZBOT)                                                  MON10600
      XPT=SNGL(CO1(1)*1.0E4)                                            MON10610
      YPT=SNGL(CO1(2)*1.0E4)                                            MON10620
      ZPT=SNGL(CO1(3)*1.0E4)                                            MON10630
      IF(ZPT.LE.SZTOP.OR.ZPT.GT.SZBOT)GOTO 10                           MON10640
      IF(ABS(SZTOP-SZBOT).GT.1.0) GOTO 5                                MON10650
      CALL MARK PT(XPT,YPT,3)                                           MON10660
      GOTO 10                                                           MON10670
5     CALL JOIN PT(XPT,YPT)                                             MON10680
10    RETURN                                                            MON10690
      END                                                               MON10700
```

Example data file for the Monte Carlo simulation shown in chapter 8.

```
FILE: MONTDAT  DATA     A   GLASGOW HEP CMS/SP V 4.19

 100kV electrons in 30 microns YAG density 4.56 gm/cm**3
        Ncode       EEV0       Film     Substr       Nevt
            0  109780.0       30.0       10.0       1000
         Ryag        Rsi        Rau        Yax     Offset
      44258.0    43950.0  2870.268       30.0          0
         Ztop       Zbot      Xwall      Ywall      Width
       0.0000     30.000      50.00      50.00       1.00
```

References

R Autrata, P Schauer, J Kvapil, J Kvapil (1978), J. Phys. E (II), 707

R Autrata, P Schauer, J Kvapil, J Kvapil (1983a), Scanning Electron Microscopy (II), 489

R Autrata, P Schauer, J Kvapil, J Kvapil (1983b), Scanning 5, 91

A Bril, H A Klasens (1952a), Philips Res. Rep. 7, 401

A Bril, H A Klasens (1952b), Philips Res. Rep. 7, 421

A J Bourdillon et al. (1985), EMAG 85, Inst. Phys. Conf. Ser. 78 (ed. G J Tatlock), 169

C M Braams (1964), Nucl. Inst. and Methods 26, 83

K L Brown, R Belbeoch, P Bounin (1964), Rev. Sci. Inst. 35 (4), 481

K L Brown (1967), SLAC Report 75

K L Brown (1980), CERN Report 80-04

T W Buggy, A J Craven (1981), EMAG 81, Inst. Phys. Conf. Ser. 61 (ed. M J Goringe), 169

J N Chapman, J D Steele, J H Paterson, J M Titchmarsh (1985) EMAG 85, Inst. Phys. Conf. Ser. 78 (ed. G J Tatlock), 177

A J Craven, T W Buggy (1984), J. Microsc. 136 (II), 227

A V Crewe et al. (1967) J. Appl. Phys. 38, 4257

A V Crewe, M Isaacson, D Johnson (1971), Rev. Sci. Inst. 42 (4), 411

R F Egerton (1980), Optik 57 (2), 229

R F Egerton (1981), Ultramicroscopy 6, 93

R F Egerton (1982), Phil. Trans. R. Soc. London A 305, 521

R F Egerton (1984), J. Elec. Microsc. Tech. 1, 37

R F Egerton, P A Crozier (1986), Proc. XIth ICEM (ed. T Imura, S Maruse, T Suzuki), Jap. Soc. of Elec. Microsc. Tokyo, Vol 1, 525

R F Egerton, P A Crozier (1987), J. Microsc. 148, 157

H A Enge (1964), Rev. Sci. Inst. 35 (3), 278

H A Enge (1967), Focussing of Charged Particles Vol 2 (ed. A Septier) Academic Press, 203

Y Fujita, H Matsuda, T Matsuo (1977), Nucl. Inst. Meth. 144, 279

G F J Garlick (1966), Luminescence of Inorganic Solids (ed. Goldberg) Academic Press, 685

J S Greeneich, T Van Duzer (1973), IEEE Trans. Elect. Devices, 598

P Grivet (1972), Electron Optics I (2nd ed.) Pergamon Press, 293

Hamamatsu Photonics (1986), PCD Linear Image Sensors (data sheet)
P W Hawkes (1970), Quadrupoles in Electron Lens Design, Adv. Elect. Elect. Phys. Supp. 7
E A Heighway (1975), Nucl. Inst. Meth. 123, 413
G Hill (1985), Private Communication
H Hubner, H Wollnik (1970), Nucl. Inst. Meth. 86, 141
M Isaacson (1978), Scanning Elect. Microsc. 1, 763
C Jeanguillame, O Krivanek, C Colliex (1981), EMAG 81 Inst. Phys. Conf. Series 61 (ed. M J Goringe) 189
L Kerwin (1949), Rev. Sci. Inst. 20, 36
O L Krivanek, P R Swann (1981), Quantitative Microanalysis with High Spatial Resolution (eds G W Lorimer, M H Jacobs, P Doig), The Metals Society London, 136
O L Krivanek, C C Ahn, R B Keeney (1987), Ultramicroscopy 22, 103
P Kruit, H Shuman (1985), J. Elect. Microsc. Techn. 2, 167
G E Lee-Whiting (1970), Nucl. Inst. Meth. 83, 232
H W Leverenz (1950), Introduction to the Luminescence of Solids, Wiley NY.
H Matsuda, H Wollnik (1970), Nucl. Inst. Meth. 77, 40
H Matsuda, H Wollnik (1972), Nucl. Inst. Meth. 103, 117
J D McGee, M Aslam, R W Airey (1966), Adv. Elect. Electr. Phys. 22A, 407
D McMullan, B G Williams, T Sparrow (1985), EMAG 85 Inst. Phys. Conf. Series 78 (ed. G J Tatlock), 169
K L Monson, D E Johnson, S Csillag (1982), Scanning Electr. Microsc. IV, 1411
E Munro (1973), Image Processing and Computer Aided Design in Electron Optics (ed. P W Hawkes) Academic Press, 234
H Nakabushi, T Matsuo (1982), Nucl. Inst. Meth. 198, 207
J B Pawley (1974), Scanning Elect. Microsc. 27
H T Pearce-Percy (1978), Scanning Elect. Microsc. 1, 41
S Penner (1961), Rev. Sci. Ins. 32 (II), 150
Reticon Corporation (1978) S Series Solid State Line Scanners (data sheet)
P T E Roberts (1980), PhD Thesis, University of Glasgow.
P Schagen (1975), J. Phys. E 8 (3), 153
P Schauer, R Autrata (1979), J. Microsc. Spectrosc. Electron. 4, 633
M Scheinfein, M Isaacson (1984), Scanning Elect. Microsc. IV, 1681

R Shimizu et al. (1976), J. Phys. D, 101
H Shuman (1980), Ultramicroscopy 5, 45
H Shuman (1981), Ultramicroscopy 6, 163
H Shuman et al (1983), Scanning Elect. Microsc. II, 737
H Shuman, P Kruit (1985), Rev. Sci. Inst. 56 (2), 231
H Shuman, C-F Chang, A P Somlyo (1986) Ultramicroscopy 19, 121
R W Simpson (1979), Rev. Sci. Inst. 50 (6), 730
D L Smith (1970), Nucl. Inst. Meth. 83, 232
K G Steffen (1965) High Energy Beam Optics
(Interscience Publishers Vol XVII), 90
M G Strauss, I Naday, I F Sherman, N J Zaluzec (1987), Ultramicroscopy 22, 117
Y Talmi, R W Simpson (1980), Applied Optics 19, 203
T T Tang (1981), Ultramicroscopy 7, 305
T T Tang (1982), Scanning Elect. Microsc. I, 39
G A H Walker, R Johnson, S Yang (1985) Adv. Elect. Electr. Phys. 64A, 213
R F Egerton (1986) Electron Energy Loss Spectroscopy in
The Electron Microscope, Plenum Press
New York and London.
J B Le Poole (1983) Quantitative Electron Microscopy
(eds J N Chapman and A J Craven)
SUSSP publications, 97
H Shuman (1986) Private Communication
Sherzer (1947) Optik 2, 114